0.4 Abbreviations

Aa	amino acid
Abu	aminobutyric acid
Ac_2O	acetic anhydride
AcOH	acetic acid
Ala	alanine
$AlaN_3$	azidoalanine
APCs	antigen presenting cells
ASGPR	asialoglycoprotein receptor
BME	β-mercaptoethanol
Boc	*tert*-butyloxycarbonyl
BSA	bovine serum albumin
CRD	carbohydrate recognition domain
CTLA4	cytotoxic T–lymphocytes–associated protein 4
CuAAC	Cu(I)–catalysed Huisgen azide–alkyne cycloaddition
DC	dendritic cell
DCM	dichloromethane
Dde	*N*-(1-(4,4-dimethyl-2,6-dioxocyclohexylidene)ethyl
DIC	diisopropylcarbodiimide
DIPEA	*N*,*N*-diisopropylethylamine
DMC	2-chloro-1,3-dimethylimidazolinium
DMF	dimethylformamide
DMSO	dimethyl sulfoxide
DODT	3,6-Dioxa-1,8-octanedithiol
DSF	differential scanning fluorimetry
E. coli	*Escherichia coli*
EDTA·4Na	tetrasodium ethylenediaminetetraacetic acid
eq	equivalents
ERK1,2	extracellular signal-regulated kinase 1,2
EtOAc	ethyl acetate
EWG	electron withdrawing group
FACS	fluorescence-activated cell sorting
Fmoc	fluorenylmethyloxycarbonyl
GalNAc	α-*N*-acetylgalactosamine
GlcNAc	*N*-acetylglucosamine
GMSCF	granulocyte monocyte colony stimulating factor
h	hours

HATU	2-(1*H*-7-azabenzotriazol-1-yl)-1,1,3,3-tetramethyluronium hexafluorophosphate
HBTU	*O*-(1*H*-benzotriazole-1-yl)-*N*,*N*,*N'*,*N'*-tetramethyluronium hexafluorophosphate
HCTU	2-(6-chloro-1*H*-benzotriazole-1-yl)-1,1,3,3-tetramethylaminium hexafluorophosphate
HOBt	1-hydroxy-1*H*-benzotriazole
HMPP	2-hydroxy-2-methyl-l-phenyl-propan-l-one
HPA	*Helix pomatia* agglutinin
HPLC	high performance liquid chromatography
IL–4	interleukin 4
IPTG	isopropyl β–**D**–1–thiogalactopyranoside
KLH	keyhole limpet hemocyanin
LC	liquid chromatography
LCMS	liquid chromatography mass spectrometry
Lys	lysine
M	molar
MAG	multiple antigenic glycopeptide
MAP	multiple antigen peptide
MeCN	acetonitrile
MeOH	methanol
MFI	mean fluorescence intensity
MGL	macrophage galatose–type lectin
MHC	major histocompatibility complex
min	minutes
mini–PEG	8-amino-3,6-dioxaoctanoic acid
MoDC	monocyte dendritic cell
MS	mass spectrometry
Mtt	4-methyltrityl
MUC	mucin
NaAsc	sodium ascorbate
NF–KB	nuclear factor–KB
NMR	Nuclear magnetic resonance
Nu	nucleophile
OSA	ovine serum albumin
Ova	ovalbumin
OvaPADRE	ovalbumin pan dr epitope
PADRE	pan dr epitope
PAGE	polyacrylamide gel electrophoresis
Pam_3Cys	tripalmitoyl–*S*–glyceryl–cysteinyl–serine

PBMC	peripheral blood mononucleated cells
PMEDTA	*N*,*N*,*N*,*N*,*N*–pentamethyldiethylenetriamine
PRR	pattern recognition receptor
Pra	propargyl glycine
PV	polio virus
PS	polystyrene
RAFT	regioselectivity addressable functionalised template
R_F	retardation factor
RT	room temperature
SDS	sodium dodecyl sulfate
SEA	soluble egg antigen
SEC–MALS	size exclusion chromatography multi–angle laser light scattering
Ser	serine
SPPS	solid phase peptide synthesis
TACA	tumour associated carbohydrate antigen
TBA	*tert*-butanol
TBTA	tris[(1-benzyl-1H-1,2,3-triazol-4-yl)methyl]amine
TCEP	tris(2–carboxyethyl)phosphine
TFA	trifluoroacetic acid
TfN_3	triflic azide
T_H	T–helper cells
THF	tetrahydrofuran
Thr	threonine
TIPS	triisopropylsilane
TLC	thin layer chromatography
TT	tetanus toxoid

Contents

Chapter 1

Introduction

1.1 Targeting dendritic cells

Most synthetic vaccines which have been approved consist of a pathogen protein combined with an adjuvant (an agent which enhances the efficacy of the vaccine). This type of vaccine typically results in the induction of antibodies targeted against the infectious agent.[1] The aim of prophylactic vaccination is to prevent the development of disease by producing antibodies, whereas therapeutic vaccines stimulate cytotoxic T–lymphocytes. Effective therapeutic vaccines need to elicit a strong and durable cytotoxic T–lymphocyte response against intracellular pathogens and cancer. One approach which may be able to achieve this goal is the targeting of dendritic cell (DCs). Researchers are currently trying to optimise T–cells' responses to attack pathogens. As DCs are the most potent antigen presenting cells (APC) for activating T–cells, they are therefore an important target for therapeutic vaccines.[1]

One of the most widely studied approaches to T–cell activation involves the targeting of DC–specific endocytic receptors by linking the relevant antigens to antibodies or ligands.[1] One method that is being used is the linking of proteins to pattern recognition receptor (PRR) ligands to create antigen–PRR ligand conjugate vaccines. The advantage of this approach is that it can both target an antigen to the DCs while simultaneously stimulating an immune response from the same DC.[1] Many different *in vitro* studies with human DCs have suggested that how the DCs are targeted can influence both the extent and quality of the T–cell response.[1]

1.1.1 Role of T–cells

T–cells are a population of lymphocytes which are able to destroy cells infected with pathogens and cancer cells.[2] Naive T–cells are activated by APCs which have travelled to lymph nodes. T–cells mature in the thymus, and will express either CD8 or CD4 surface proteins.[2] CD4+ and CD8+ T–cells distinguish peptides bound to major histocompatibility complex (MHC) molecules presented by APC, such as dendritic cells. CD8+ T–cells recognise antigenic peptide fragments presented by MHC class I proteins whereas CD4+ T–cells recognise antigenic peptide fragments from MHC class II proteins. Controlled delivery of antigens to APC results in antigen presentation on the MHC complexes which reside on the APC surface. The APC can present the antigen on the MHC complex to T–cells, which could become activated towards that antigen. The T–cell will mature and then migrate to the site of infection so that it can selectively kill the antigen–expressing cells. Being able to initiate and control the T–cell response is a desirable goal for a therapeutic vaccine. Once a T–cell has been activated by an antigen it will proliferate into one of several different functional types of effector T–lymphocytes.[2]

T–lymphocytes which express CD8+ proteins are cytotoxic cells which destroy cells infected by pathogens or viruses.[2] CD8+ T–cells can recognise specific antigens presented on MHC class I proteins on the surface of tumour cells. Once attached the CD8+ T–cells produce cytotoxic granules which contain the proteins perforin and granulysins, as well as the enzyme granzymes to destroy the cancer cell.[2] Therapeutic vaccines based on MHC-I presented peptide epitopes could, theoretically, induce CD8+ T–cell responses that have tangible clinical impacts on tumour eradication and patient survival.[3]

T–lymphocytes which express CD4 proteins are Helper (T_H) T–cells and these provide signals to the immune system that activate antigen–stimulated B–cells.[2] The T_H produce cytokines which are small proteins that can improve the response of CD8+ T–cells and B–cells, resulting in a stronger and more robust immune response.[2] Both CD8+ T–cells and B–cells are involved in the destruction of cancer cells. CD4+ T–cells also are involved in the regulation of antibodies which are important for antibody directed cell cytotoxicity. The immune system selectively targets and lyses cells with membrane bound antibodies. CD4+ T–cells are also involved in complement dependent cytotoxicity, where cytokines are involved in the amplification and activation of membrane attack complex which lyses cells.

1.1.2 CD8+ T–cells and the immune checkpoints

Immune checkpoints are inhibitory pathways that are crucial for maintaining self tolerance and modulating the duration and amplitude of physiological immune responses.[4] For a T–cell immune response to be initiated, antigens need to be presented on a major histocompatibility complex (MHC) by an APC to a T–cell receptor. At the same time, the T–cell response is regulated by a balance of co–stimulatory and inhibitory signals which are referred to as immune checkpoints. These immune checkpoints are important for stopping autoimmunity, which can occur when the immune system reacts against self antigens expressed on healthy cells.[4] The T–cell will not respond to an immune checkpoint unless the T–cell receptor has recognised the cognate antigen. A selection of co-stimulatory and inhibitory interactions which regulate T–cell responses (immune checkpoints) are shown in Figure 1.1.

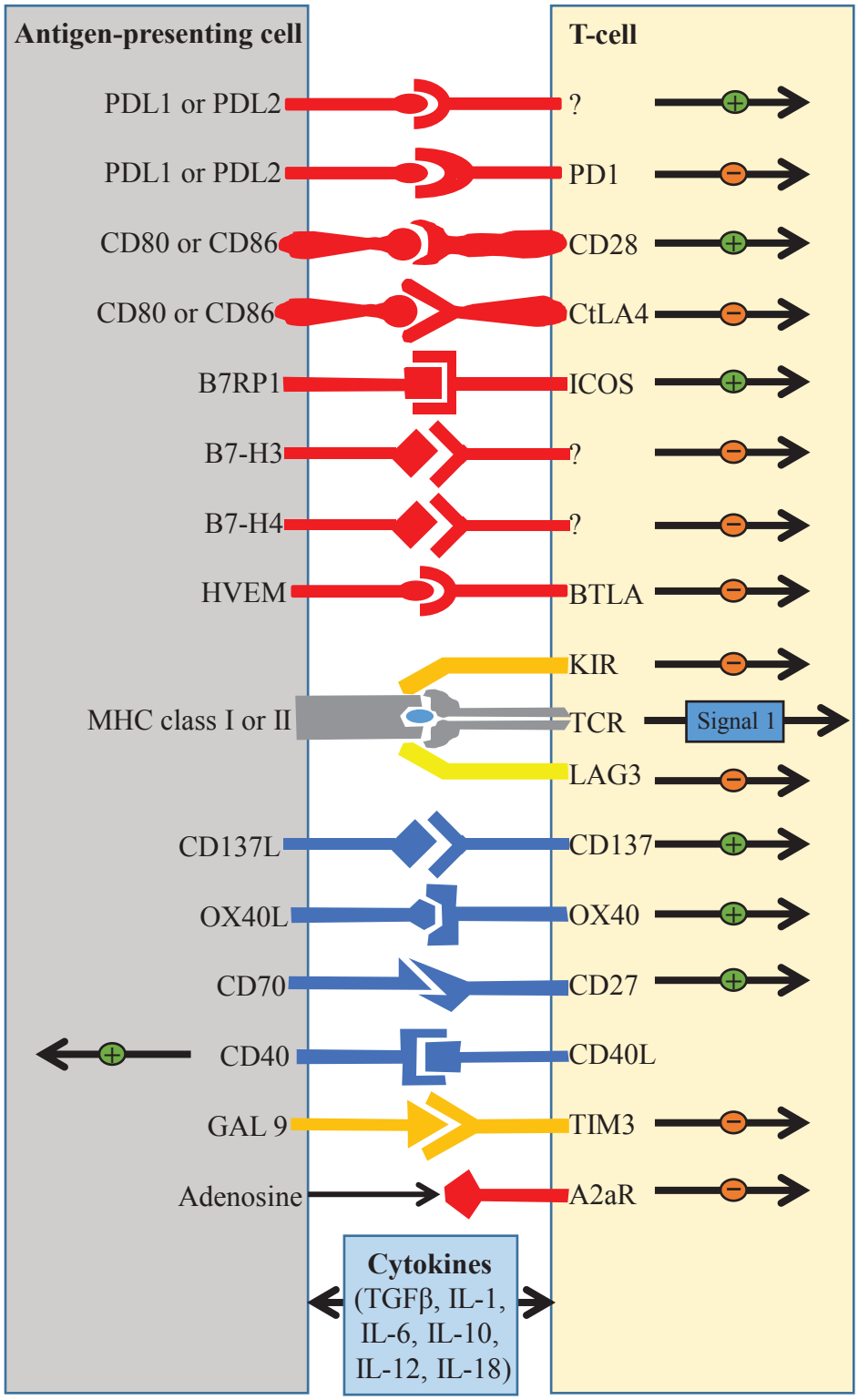

Figure 1.1: Multiple co–stimulatory (+) and inhibitory (-) interactions regulate T–cell response after interacting with an APC.[4]

Cancer research is making exciting developments focusing on the host's immune system and the microenvironment in which tumours grow.[5] Traditional anti–cancer drugs act directly on malig-

nant cells, whereas new immunotherapies are reactivating anti–tumour immune responses or making them strong enough to overcome tumour immunosuppression. Ipilimumab is a monoclonal antibody specific for the cytotoxic T lymphocyte–associated protein 4 (CTLA4).[5] It binds to CTLA4 which is an immune checkpoint that sends inhibitory signals to T–cells. The immune system responds by dampening the amplitude of their response towards tumours. After Ipilimumab binds CTLA4, it no longer sends the inhibitory signals to the cytotoxic T–cells which are then able to fight the cancer more effectively. Results from a clinical trial where cancer patients were treated with Ipilimumab showed this vaccine had a positive impact on survival statistics across all lines of therapy, treatment regimens and dose levels.[5] Immune checkpoints are therefore important for fighting cancer, and identification of receptors which are involved in this process will allow for new drugs to target different pathways for a tailored immune response. The development of therapeutic vaccines which target specific receptors in the immune system may lead to more effective cancer treatments.

Designing therapeutic vaccines which generate CD8+ T–cells is difficult, with the key process "the cross presentation pathway" not fully understood.[6] Therapeutic vaccines which succeed in generating a CD8+ T–cell response will struggle to be effective, since immune checkpoints will dampen the response, which results in an ineffective treatment. Despite the recent successes of drugs which target immune checkpoints, there are limits to what these drugs can achieve on their own. Figure 1.2 shows the scenarios where immune checkpoint drugs succeed and where they fail.[4] If the person with cancer has a T–cell response, the cancer will inhibit the T–cells unless an immune checkpoint drug can stop the inhibition. This results in the immune system being able to respond and fight the cancer effectively. But if the person has no T–cells, the immune checkpoint drug will not have any positive response.[4] This project is focused on the delivery system for a therapeutic vaccine which will target an APC receptor, which may lead to CD8+ T–cell responses that are an important initial step in generating the conditions for the immune checkpoint drugs to succeed.

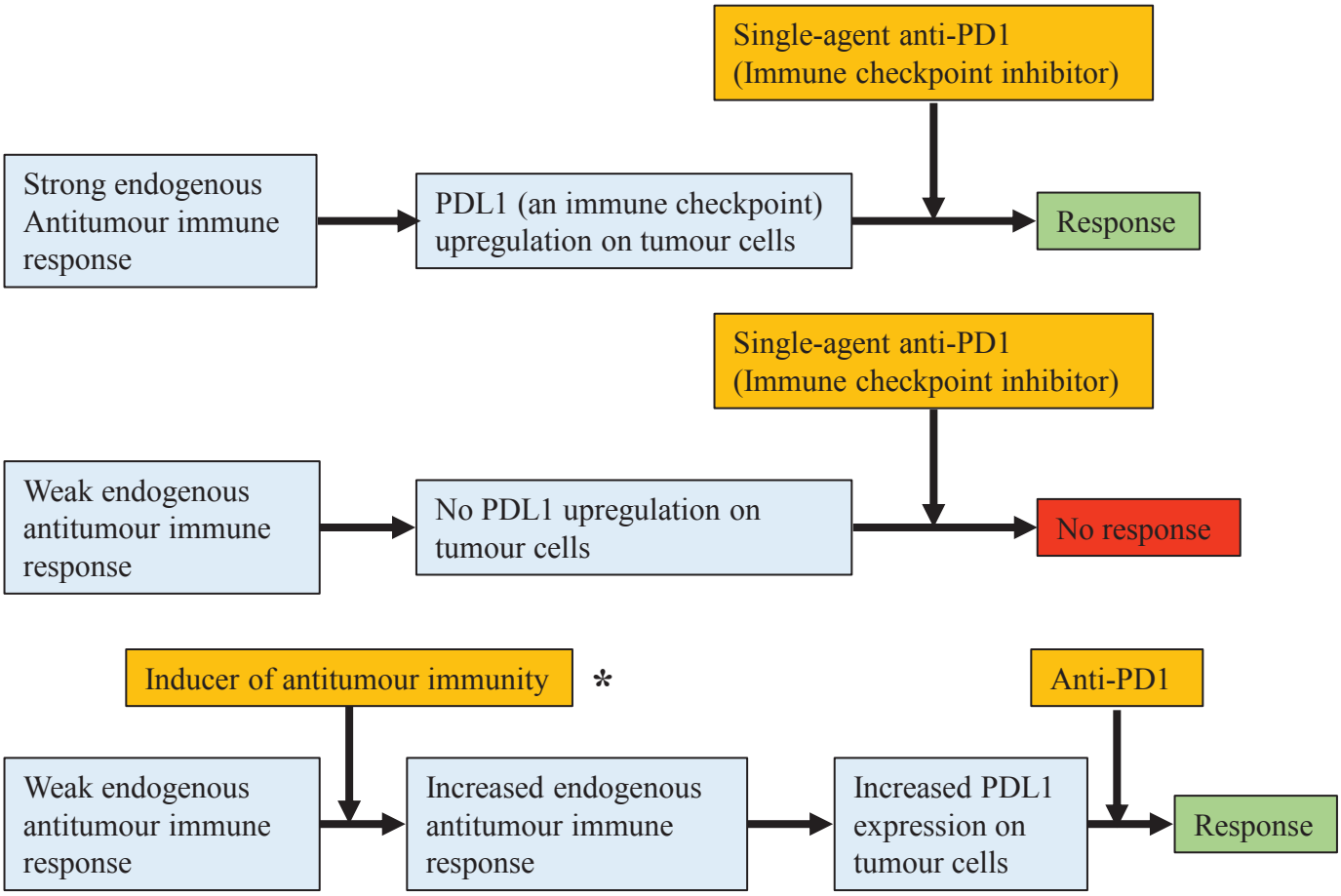

* The vaccines designed for this project are aimed to target APCs which induce CD8+ T-cells at this point in the process. The vaccines will hopefully be combined in the future with immune checkpoint inhibitors to treat cancer.

Figure 1.2: Implication of the adaptive immune resistance mechanism for combinatorial immunotherapy of cancer.[4]

1.1.3 Therapeutic vaccines for cancer

The need for effective cancer treatments is growing. Over fifteen hundred people were registered with a new primary malignant cancer in New Zealand in 2011 and this number increased by 3% in 2013.[7] Worldwide over eight million people died due to cancer in 2012. These numbers will most probably increase with growing life expectancies and populations.[8] In the UK 50% of people are predicted to survive cancer for ten or more years, but this number can drop dramatically with late diagnosis or specific types of cancer.[9] Current treatments look to treat or considerably prolong the life of patients and to ensure the best possible quality of life to cancer survivors.

Therapeutic vaccines need to be able to trigger an immune response which can be used to treat cancer. Diseases such as cancer are hard for the body to recognise due to the immunosupressive effects of tumours and its inability, due to the presence of self antigens, to recognise the pathogens. MGL is a known receptor on dendritic cells which are the most important APC. A glycopeptide delivery system which can reliably be used to deliver important cargoes such as CD8+ epitopes and stimulate the immune system via the MGL receptor may be a crucial tool for targeting APC. Inducing cytotoxic T–cell responses through therapeutic vacines in conjunction with control of immune checkpoints will be an important method for the treatment of cancer using the bodys own immune system.

1.2 C–type lectins

Pattern recognition receptors (PRR) can be involved in the internalisation of pathogens into cells by binding to specific antigens such as carbohydrates.[10] C–type lectins are proteins which are commonly found on dendritic cells and can function as PRR which recognize broad molecular patterns found on pathogens.[11] The C–type lectins are a family of proteins which require calcium as a cofactor to allow carbohydrates to bind. Examples of C–type lectins include DC-SIGN, asialoglycoprotein receptor (ASGPR), macrophage mannose receptor and macrophage galactose binding lectin (MGL).[10]

The C–type lectins share primary and secondary structural homology with their carbohydrate–recognition domains (CRDs).[10] Each C–type lectin has a fold with a highly variable protein sequence. These folds are compact domains of 110 to 130 amino acid residues in length, with a double–looped two–stranded antiparallel β–sheet formed by the amino–and carboxy–terminal residues connected by two α–helices and a three–stranded antiparallel β–sheet. The CRD of the C–type lectins contains two disulphide bonds and up to four sites which can incorporate Ca^{2+} for binding to carbohydrates.[10] The variance in protein sequence of C–type lectins results in the CRDs have different affinities for various glycans.[10]

C–type lectins commonly oligomerize into homodimers, homotrimers, and higher-ordered oligomers.[10] The oligomer structure of the C–type lectins makes these receptors have higher avidity to multivalent ligands such as oligosaccharides. The avidity of C–type lectins to specific carbohydrates are important for its involvement in adhesion and signalling in immune functions such as inflammation and immunity to tumour and virally infected cells.[10] Targeted binding to a C–type lectin is possible with carbohydrate ligands which are specific for the CRD, and this may be an important feature for future vaccines which target C–type lectin receptors.[10]

1.3 MGL

Macrophage galactose binding lectin (MGL) is a C–type lectin found on monocyte dendritic cells (MoDC) and some macrophages and dendritic cells (DC). MGL specifically binds to *N*–acetylgalactosamine.[12] These carbohydrates can be found on the surface of pathogens as part of the T_N antigen (Figure 1.3). Often associated with leukemia and leukopenia (Tn syndrome), the T_N antigen was originally found as a very rare blood-group antigen, detected by naturally occurring antibodies.[13]. The T_N antigen is expressed on 70% of lung, colon, and stomach carcinomas, while there is restricted expression on normal cells and tissues.[13]

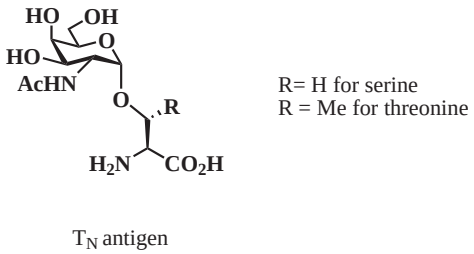

Figure 1.3: The structure of the T_N antigen.

MGL is a PRR which is involved in the internalisation of pathogens into the APC. MGL is thought to be involved in the mechanism of cross presentation. However, the process is not fully understood.[6] Cross presentation results in the introduction of extracellular antigens on the surface of the cell in complex with MHC class I proteins. CD8+ T–cells become primed by the MHC class I proteins, which then go on to kill cancerous, infected or damaged cells.[2] MGL is therefore a potential receptor for stimulation of CD8+ T–cells. Presentation of exogenous antigens in MHC–class I to CD8+ T-cells via cross presentation is important for anti–tumour vaccine development.[6]

1.3.1 Structure of MGL

MGL has been shown to be a homotrimeric cluster protein, and is thought to have a similar structure to the ASGPR.[14] There are five domains and a total of 316 amino acids in the MGL sequence. Figure 1.4 shows the sequence and positions of the domains.

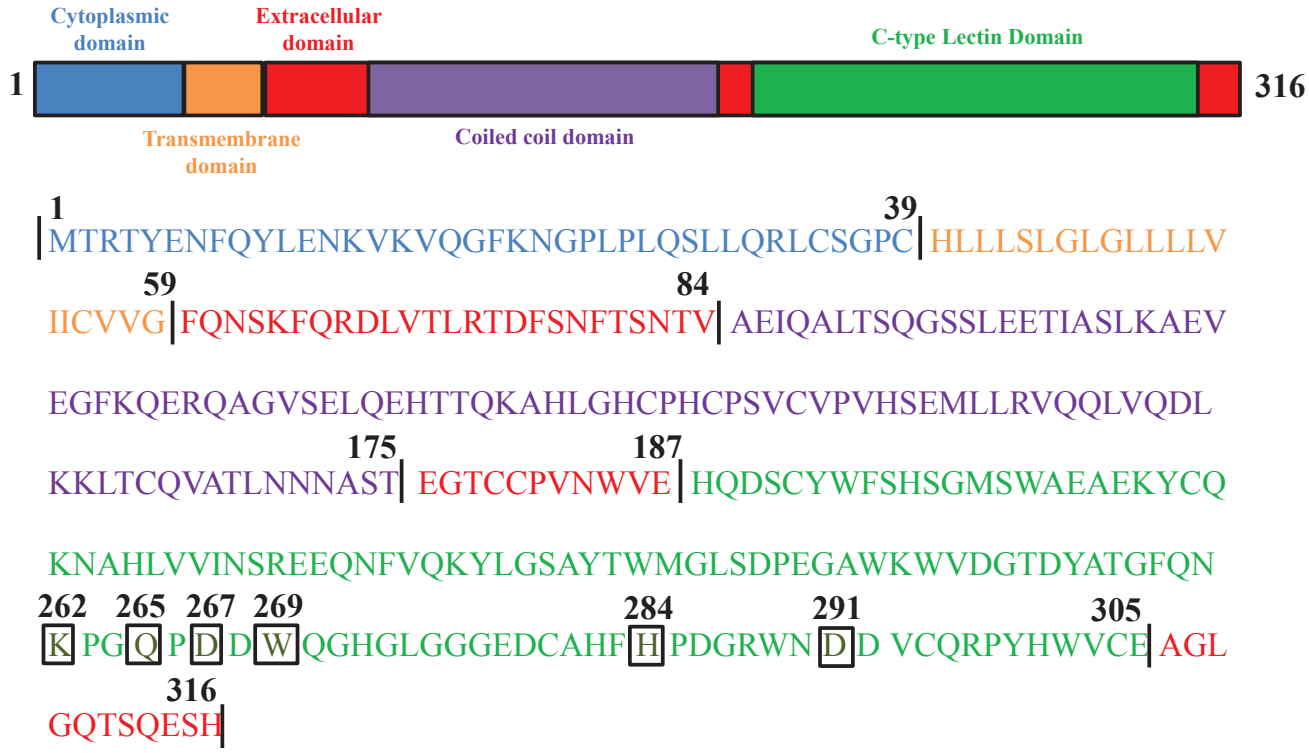

Figure 1.4: The full amino acid sequence of Macrophage Galactose binding Lectin (MGL). Amino acid residues at positions 265 (Q, glutamine), 267 (D, aspartic acid), 269 (W, tryptophan), and 291 (D, aspartic acid) of the MGL CRD are responsible for the GalNAc binding of MGL, while amino acid 262 (K, lysine) and 284 (H, histidine) make binding to other carbohydrates unfavourable.[15]

The first 39 amino acids make up the cytoplasmic domain which is found inside the cell. The role of the cytoplasmic domain is considered a key element in the regulation of uptake and intracellular trafficking of glycoproteins into the cell.[16]

Amino acids 40–59 make up the transmembrane domain which traverses the membrane of the cell. The role of the transmembrane domain is to span the cell membrane and anchor MGL in place.

Amino acids 60–84, 176–187, 306–316 are all part of the extracellular domain.

Amino acids 85–175 are part of the coiled coil domain. The coiled coil domain is important for forming the quaternary structure of the homotrimeric cluster. MGL is known to form trimeric structures through the interactions of the neck domain in a similar manner to that of ASGPR.[17] Investi-

gations showed that hetero–oligomer formation was not required for GalNAc recognition. However, MGL trimers cooperatively functioned to recognise and internalise extracellular molecules. This coiled coil domain creates distance between the cell membrane and the carbohydrate recognition domain.

Amino acids 188 to 305 are part of the carbohydrate recognition domain (or C-type lectin domain). The carbohydrate recognition domain is involved in the binding of GalNAc. The structure has a typical C–type lectin fold with two α helices and two antiparallel β sheets within the fold.[18] Part of this fold contains irregular loop structures which, along with Ca^{2+}, mediate monosaccharide binding.

Shimada *et al*. have studied the structure of various MGL proteins found in human and rodent DCs.[15] A site–directed mutagenesis study revealed amino acid residues at positions 265 (Q, glutamine), 267 (D, aspartic acid), 269 (W, tryptophan), and 291 (D, aspartic acid) of the MGL CRD are responsible for the GalNAc selectivity (Figure 1.6). The lysine group at 262 makes it unfavourable to bind to branched oligosaccharides which do not have terminal GalNAc residues (Figure 1.4).[15] The histidine at 284 in human MGL stops fucose binding due to its polar nature and also may bind to the oxygen of the acetyl group from GalNAc, whereas in mouse MGL1 a threonine is present at this position which cause a methyl group to generate a hydrophobic region promoting binding.

A homology model of the MGL CRD, kindly provided by Dr. Christopher Squire, is illustrated in Figure 1.5 and shows how GalNAc may fit into the sugar binding site. The model uses the structure PDB 1DV8 of the ASPGR protein which shares 85% amino acid identity with MGL. The 1DV8 crystal structure displays a number of water molecules in the sugar binding sites and these overlap closely with the GalNAc hydroxyl groups at C3, C4 and C6, as well as the oxygen in the ring and the acetyl group, suggesting the model is a valid description of GalNAc binding. In the model, the anomeric oxygen on the C1 projects into space away from the CRD and is therefore cannot be involved in binding.

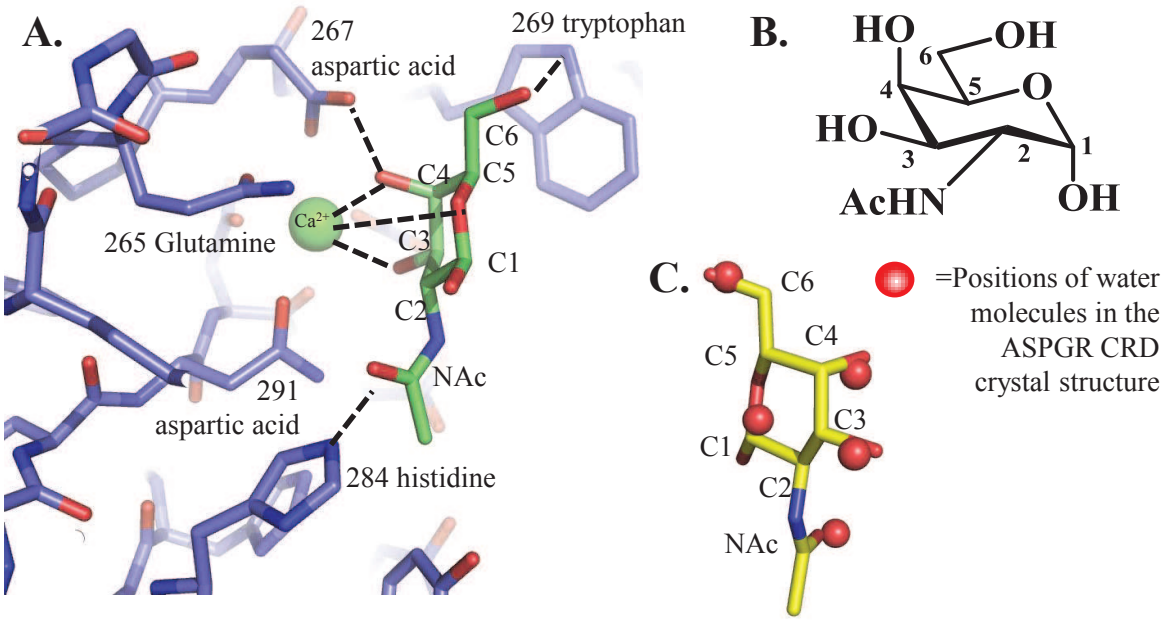

Figure 1.5: Homology model of GalNAc to MGL derived from the crystal structure PDB code 1DV8 of the ASPGR C–type lectin. A Predicted GalNAc binding to MGL highlighting binding interactions as dashed lines. B Chemical structure of GalNAc. C. The GalNAc model overlaid with the water molecules in the crystal structure of the ASPGR CRD that essentially validate the binding model.

Our homology model is supported by the work of Schimada *et al.* who used NMR combined with homology modeling to show the predicted similarity of the two structures.[15] An additional homology model provided by Dr Christopher Squire, predicts the quarternary structure of MGL as trimeric (Figure 1.6), modelled from the crystal structure PDB code 1FIH of a mannose–binding protein mutated specifically to bind GalNAc. MGL and 1FIH share around 75% sequence similarity and share greater sequence and presumably structural conservation in the sugar binding site. The model of MGL predicts the distances between adjacent sugar binding sites in the trimer of between 50 and 60 angstrom.

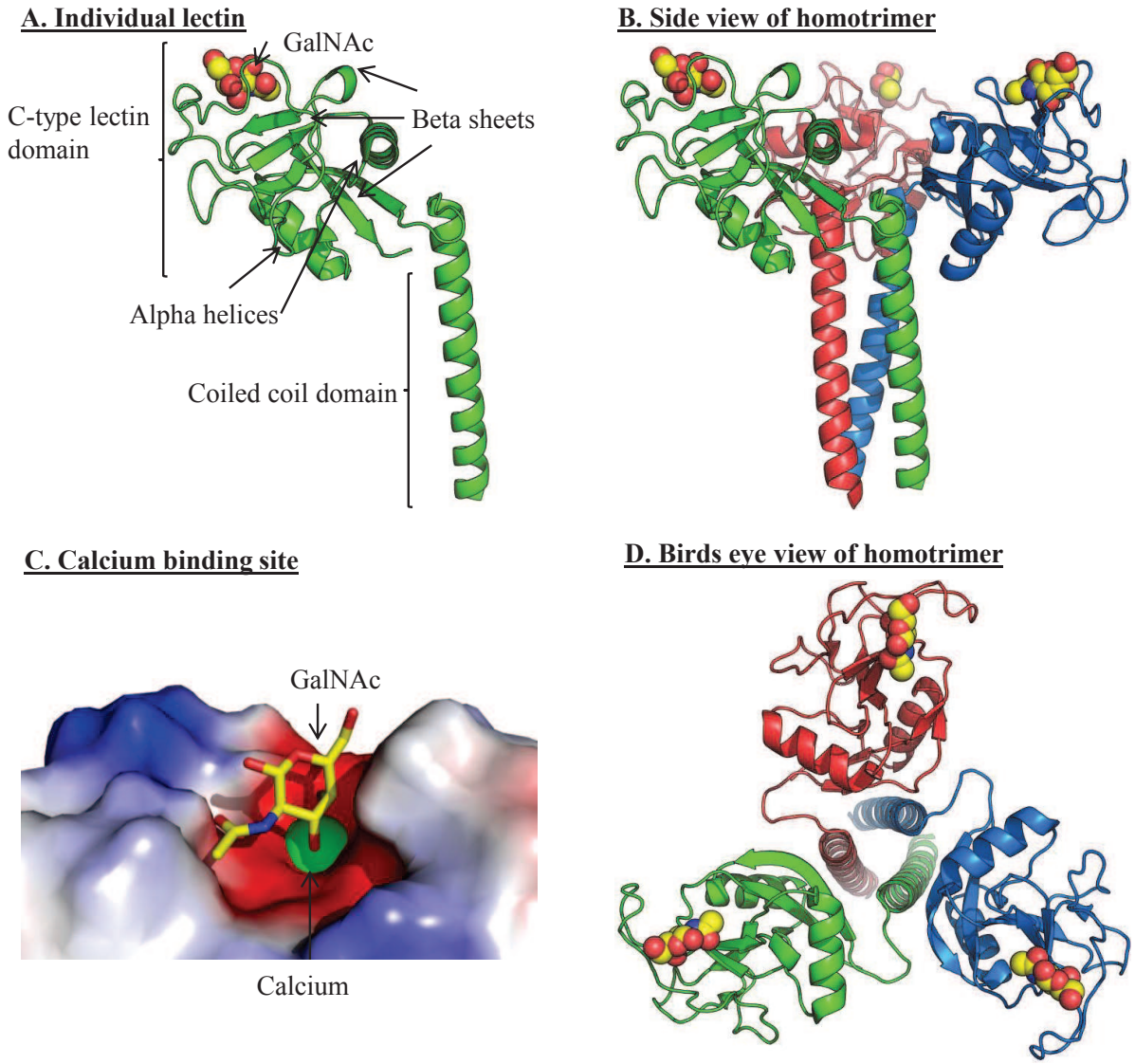

Figure 1.6: The structures of the C–type lectin 1fih mutated mannose binding protein, which was modified to specifically bind GalNAc to mimic MGL provided by Dr Chris Squire. A. The individual protein structure with the position for GalNAc binding; B. The side view of the 1fih homotrimer; C. The modified calcium binding site where GalNAc binds; D. The birds eye view of the 1fih homotrimer.

The sequence of MGL and structures of similar C–type lectins which could be crystalised reveal that the binding site is quite restrictive, which only allows carbohydrates with similar structures to GalNAc to bind. Our homology model suggest why galactose can also bind MGL, but not as strongly as GalNAc because, it doesn't bind as strongly because the hydroxyl group at C2 can't position itself to bind to the histidine at position 284 (unlike the carbonyl of the acetyl group for GalNAc).

1.4 The role of MGL in diseases

MGL has been implicated in a number of different diseases. By understanding the mechanisms by which MGL interacts with the immune system, appropriate targeting or suppression of the receptor may result in new vaccines for a variety of diseases.

1.4.1 The role of MGL in cancer

Van Kooyk *et al*. have shown that the amount of GalNAc (T_N–antigen) on a molecule may determine the immune response generated by the DCs after cross presentation through MGL, as this can determine the induction or inhibition of T–cell responses.[19] Immune responses specific to GalNAc–glycosylated MUC1 from MGL–expressing APC results in antibodies which evoke anti–tumour responses. These responses can be weak if the MUC1 sequence is heavily *O*–glycosylated, whereas the less glycosylated sequences can generate a stronger response.[19]

MGL research has been heavily associated with cancer. MUC1 is a highly *O*–glycosylated protein, which is over–expressed by tumour cells.[20] MUC1 expresses rare terminal GalNAc structures, to which MGL preferentially binds.[12] In breast cancer the MUC1 is glycosylated with shortened *O*–glycans such as GalNAcα1–*O*–Ser/Thr (otherwise known as the T_N antigen). 90% of all carcinomas had high levels of the T_N antigen expressed.[12] Tumour cells display aberrant glycosylation due to altered expression levels and activities of glycosyltransferases which results in abnormal expression of T_N antigens.

Mice contain two types of MGL (mMGL1 and mMGL2). mMGL1 was originally isolated from mouse ovarian cancer on metastatic tumour nodules, which express tumour–associated glycans such as the T_N antigen.[12] The APCs which expressed mMGL1 were shown to positively contribute to host defence against tumour metastasis.[21] Antigen targeting with GalNAc carbohydrates to mMGL1 and mMGL2 resulted in enhanced cross–presentation to antigen–specific CD8+ T–cells.[19, 22] While human and mouse MGL are different, it is still encouraging to see that CD8+ T–cells can be stimulated in mice and therefore there is potential for CD8+ T–cell stimulation through targeting human MGL.

mMGL2 interacts with tumour–associated antigen MUC1 in a similar fashion to human MGL, with the mMGL2 having been shown to uptake tumour–antigen MUC1 segments for intracellular processing and presentation resulting in the induction of cytotoxic T–lymphocyte responses.[23, 24] Human MGL may be involved through the preferential recognition of the tumour-associated MUC1.[20] Immature monocyte–derived DCs, which express MGL, bind the glycosylated MUC1 sequence but do not bind the unglycosylated peptide. In 2007 Van Kooyk *et al*. studied the in-

teraction of MUC1 expressed on colon cancer with MGL on DCs.[25] MGL bound specifically to MUC1–T_N in primary colon carcinoma but not to MUC1 from normal epithelial cells. It was also shown that MGL is highly expressed on tolerigenic APCs, which could lead to immunosuppressive effects.[23, 24] Specifically, heavily glycosylated MUC1 blocks MGL intracellular processing and presentation, which reduces CD8+ T–cell responses.[23, 24] This may have implications when designing therapeutic vaccines to target MGL, as a balance will need to be found between efficient delivery of molecules through glycan targeting and suppression of processing and presentation due to heavy glycosylation.

1.4.2 Targeting MGL with GalNAc ligands

The study of MGL may be important for the design of therapeutic vaccines for targeting cancers.[26, 27, 20, 28] MGL is a receptor which has been identified as a potential target for vaccine delivery, that can be specifically targeted and is known to bind GalNAc glycosylated structures.[20, 29, 30, 31] Van Kooyk has stated that tumour–associated GalNAc–modified antigens could lead to better cross presentation by MGL, which may have future implications for designing tumour vaccines.[19]

Tumour–associated carbohydrate antigens

Glycopeptides on the outer cell membrane are important for many biological processes such as:

- Immunodifferentiation
- Biological recognition
- Cell adhesion
- Cell differentiation
- Regulation of cell growth

The glycosylation of these proteins can effect their conformation, physiochemical properties and their susceptibility to proteolysis.[32] Glycoconjugates which are expressed predominantly on cancer cells are often referred to as tumour associated carbohydrate antigens (TACAs). Two of the most important groups of TACAs are the *O*–glycopeptides which are bound through the hydroxyl group of serine or threonine and the *N*–glycopeptides which are bound through asparagine.[32] The carbohydrates in these *O*–glycopeptides are becoming the focus of research in vaccines against cancer.[33] A problem for these vaccines is that the TACAs are 'self' antigens which are also found on healthy cells with which the body does not react immunologically.[34] This tolerance to 'self' antigens is an important reason why development of anticancer vaccines is more difficult compared to vaccines for infectious diseases.[35] Examples of some of the most important TACAs are shown in Figure 1.7.

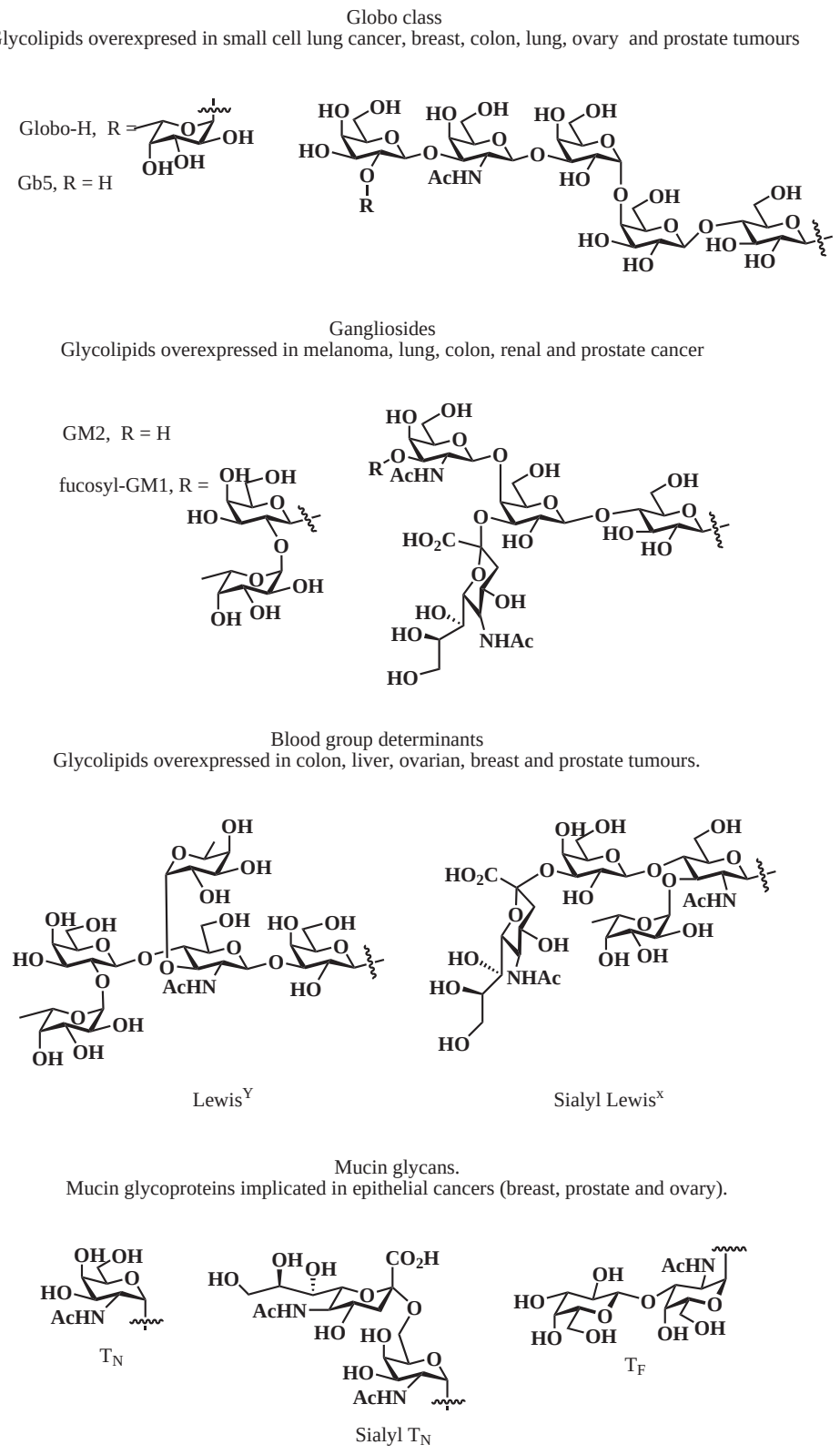

Figure 1.7: Carbohydrate moieties from representative members of the major TACAs classes.[36]

Cancer cells normally have altered cell surface glycosylation due to abnormal expression of glycosyltransferases which changes the typical glycan structures and/or their expression levels.[33, 34]

TACAs were first discovered in mucins, which normally contain GalNAc units α–*O*–linked to serine or threonine.[32] Mucins are normally over–expressed on cancer cells and these glycopeptides are normally incompletely glycosylated or have undergone premature sialylation. The incomplete glycosylation affects the conformation and physiochemical properties of the glycoprotein. The TACAs individually have weak immunogenicity, the immune response can be increased by clustering the TACAs.[32]

The first cancer vaccines were created based on TACAs in which the carbohydrates were conjugated to an immunogenic carrier protein (such as keyhole limpet hemocyanin (KLH), bovine serum albumin (BSA) or ovine serum albumin (OSA)).[32] These vaccines induced low levels of antibodies in their response against the TACAs and other irrelevant antibodies against the carrier protein. In order to enhance the initial response, the TACAs were then conjugated to dendrimeric lysine scaffolds. The scaffolds had defined chemical structures with reproducible purity and contain a high density of clustered antigens. These glycodendrimers were observed to elicit a strong specific antibody response.[32]

To study protein–carbohydrate interactions, chemists have designed synthetic oligosaccharides which overcome the low binding affinities of monovalent glycosides.[37] These oligosaccharides can be conjugated to multivalent scaffolds to facilitate the study of diverse biological phenomena and for vaccine development.

1.5 Peptide vaccines and drug delivery

The humoral immune system only reacts and recognises specific regions of pathogens.[38] Vaccines have been designed to incorporate subunits of the pathogen such as immunogenic polypeptides (like the polio virus (PV) epitope) or synthetic peptides that are in highly conserved regions, necessary for the pathogen's function. The aim is to develop vaccines with defined antigen structure in order to stimulate an effective immune response, while avoiding the potentially hazardous effects of the pathogen.[38]

Successful synthetic vaccines will contain both B and T–cell epitopes and a cytotoxic T lymphocyte inducing epitope.[38] For these vaccines to be effective they will need an appropriate delivery system to allow induction of specific immune responses, resulting in conferred protection.[38] This approach has been used for the design of peptide and polypeptide vaccines against viruses. Two examples of peptide vaccines for viral infections are Jackson's Influenza vaccine and Weinhold's HIV vaccine Figure 1.8.

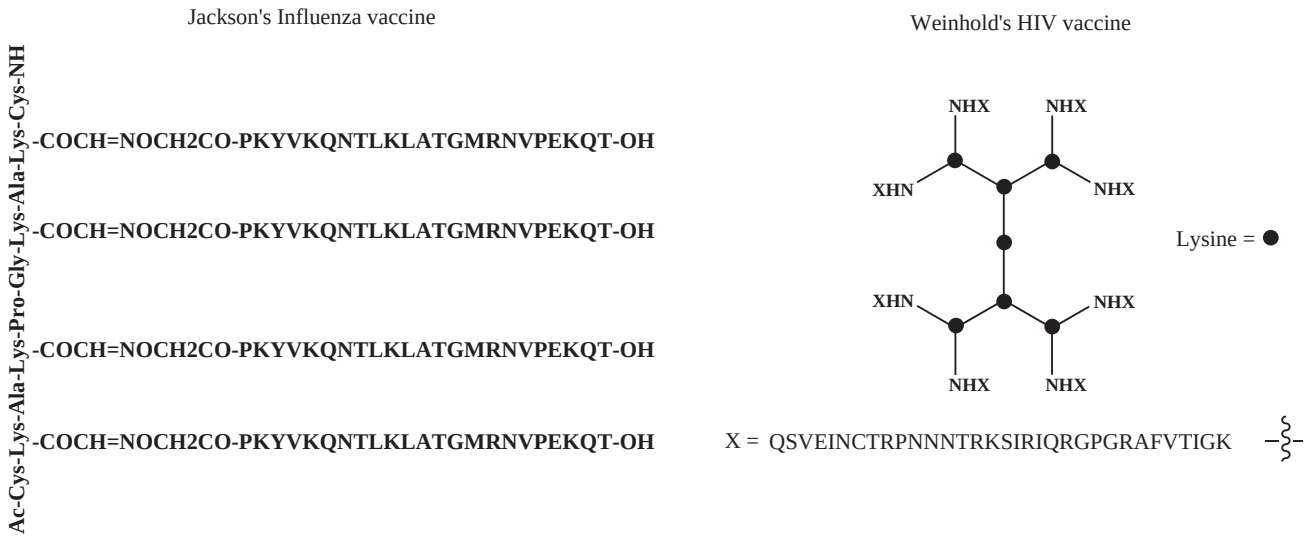

Figure 1.8: Jackson's Influenza vaccine and Weinhold's octavalent polylysine HIV vaccine.[39, 40]

Jackson *et al*. synthesised a tetraoxime artificial protein vaccine based on a peptide from the influenza virus haemagglutinin using Fmoc solid phase peptide synthesis (SPPS). This vaccine was able to invoke a specific T–cell immune response in mice.[39] Weinhold's branched peptide vaccine from the V3 loop region of HIV-1 gp120 was immunised into mice, which resulted in highly specific, long-term cytotoxic T–cell lymphocyte response. Following the success in the mouse model the peptide vaccine was tested in humans.[40] These two polylysine peptides are examples of how branched compounds can be used as delivery systems for epitope cargoes to the immune system.

1.5.1 Dendrimers

In 1978 Vögtle *et al*. developed small hyperbranched molecules which they called cascade polymers.[41] These would later be renamed 'dendrimers', derived from the Greek words *dendri*– meaning "Tree–like" and *meros* meaning "part of".[42] Peptide dendrimers are broadly defined as any dendrimer which contains peptide bonds. Dendrimers have many potential applications including delivery agents for drugs, modification of cell–cell interactions, vaccines against bacteria or viruses, inhibitors of inflammatory responses and autoimmune diseases.[43]

Dendrimers are well-defined multivalent, derivatisable and stable molecules which are ideal carriers of small antigens.[44] Dendrimers have seen limited use as carrier molecules to enhance immunogenicity of antigens for vaccine purposes. An exception to this is the lysine based multiple antigen peptide.[45]

Dendrimers can be synthesised in either a divergent or convergent fashion, as shown in Scheme 1.1. Divergent dendrimers are synthesised starting from the core of the molecule and

then branching outwards.[44] Each stage of the synthesis expands the molecule and the core is increasingly shielded by the outer shell of the molecule. Convergent dendrimers are synthesised by coupling branched entities together to form a bigger dendron.[44]

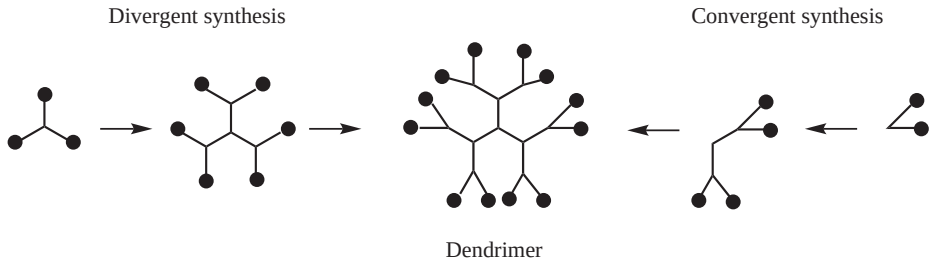

Scheme 1.1: Divergent and convergent styles of dendrimer synthesis.[44]

Dendrimers have a highly multivalent surface which can be used to gain increased ligand binding.[44] One dendrimer with multiple binding ligands at the end of each branch will bind in a stronger fashion to a receptor than the same number of individual ligands. This is known as the chelate effect. The dispersity of the dendrimer chains is dependent on the nature of the solvent they are in, with the dendrimer either extending or contracting its conformation.[44] The change in volume of the dendrimer can affect the multivalent binding as the surface area increases or decreases. The chemical composition of the dendrimer will determine how it reacts to the solvent system. The larger the dendrimer interior or core is, the more shielded from the solvent it will be. This means that the biological properties of the dendrimers are largely dependent on the properties of the surface groups.[44]

In 1988 Tam *et al*. synthesised the multiple antigen peptide (MAP) system, which used lysine as the monomer to grow the dendrimer (Figure 1.9).[45] The MAP was constructed with a divergent route using SPPS.

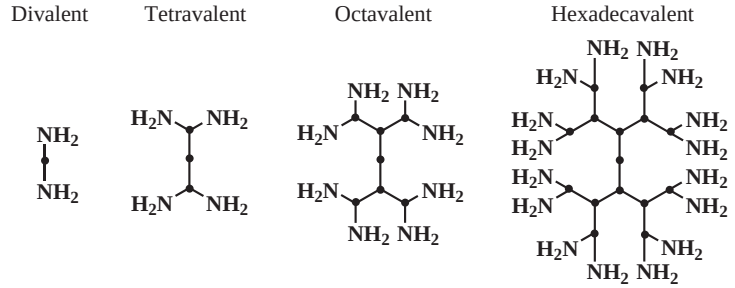

Figure 1.9: Schematic representation of Tam *et al*. multiple antigen peptide (MAP).[45]

MAP has several advantages over conventional carrier–antigen constructs:

- Orientation of the immunogen is well–defined, avoiding unnecessary epitopes which may be present in a conventional carrier.[38]
- MAP can be synthesised to carry any peptide epitope or antigen.[38]
- In model systems MAP vaccines have been shown to protect animals against malaria,[46] and to stimulate immune responses against HIV.[40]

1.5.2 Chemical glycosylation

A formidable challenge for chemists is the conjugation of polysaccharides and polypeptides.[47] Natural glycan–protein linkages are generally formed between *N*–(Asn) and *O*–(Ser/Thr).[48] Fully protected carbohydrates are commonly installed onto either individual amino acids or peptides and then deprotected post conjugation. Alternatives to the natural glycan—peptide linkage are unnatural glycan–peptide linkages. These linkers can allow alternative routes to peptides when conventional routes fail, or to make the glycosidic bond more resitant to degradation or to increase the distance between the sugar and the peptide.[48] Examples of unnatural linkages are shown in Figure 1.10.[48]

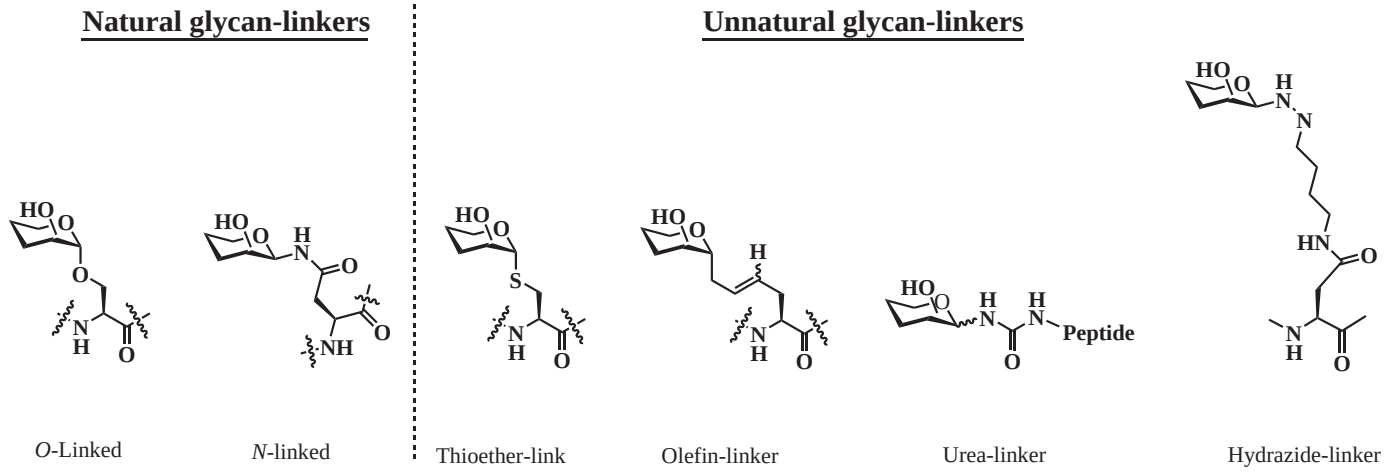

Figure 1.10: Examples of natural and unnatural glycan–peptide linkages.[48]

1.5.3 Glycopeptide drugs

Carbohydrate–based tumour antigens for cancer vaccines are hard to produce using cell cultures because cancer and normal cells show minimal levels of expression of TACAs.[49] It is very difficult to produce sufficient quantities of carbohydrate for clinical work by purification of these TACAs from cells. Synthetic organic chemistry can solve the issue of lack of homogeneous carbohydrate material.

Carbohydrate tumour antigens are generally poor immunogens and require an appropriate immunogenic carrier to achieve a significant response.[50] The optimal spacer–linker combinations for glycopeptides has not been fully established, so the aim is to produce carbohydrates conjugated to biocarriers that do not compromise the interaction with the receptor they bind to.[51]

The Danishefsky group have produced a preclinical vaccine programme which had the following goals in relation to glycopeptides:

- Total synthesis of the desired tumour–associated antigen, chemically rigorous proof of structure as well as homogeneity, and, when appropriate, synthesis of relevant truncated congeners as probes of epitope specificity.
- Incorporation of an appropriate spacer group so that the immunological integrity of the antigens is retained.
- Covalent contact with an immunostimulant or carrier protein to generate a fully functional vaccine.
- Mouse immunisation and follow–up evaluation of the immune response.[49]

These preclinical goals were applied with the synthesis and testing of several of the glycopeptides which Danishefsky *et al*. produced. One such example is the the Lewis^Y blood group determinant, which is an epitope for eliciting antibodies against colon and liver carcinomas and ovarian tumours.[52, 49] Starting from simple glycans, a complex pentasaccharide was synthesised and then conjugated (using a reductive amination) to proteins such as BSA and KLH (Figure 1.11). Mice were innoculated with these glycopeptides, and the Lewis^Y–KLH glycopeptide was found to be the most efficient for producing high titres of both IgG and IgM antibodies. The Lewis^Y–KLH glycopeptide was chosen for phase I trials using human patients with ovarian cancers.[53, 49] Danishefsky's glycopeptides are examples of how organic synthesis can produce a carbohydrate which can be incorporated into vaccines suitable for humans.

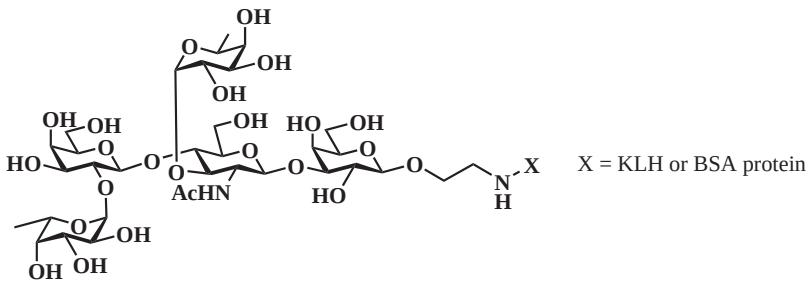

Figure 1.11: Danishefsky's glycopeptide vaccines: Lewis^Y–proteins.[52, 49]

1.6 Click chemistry

In 2001, Sharpless *et al*. published the highly prominent paper "Click chemistry: diverse chemical function from a few good reactions".[54] Sharpless *et al*. raised the agenda that "while truly brilliant organic chemistry is done to produce therapeutic agents, it would be better if it could be done in a cheaper, faster and more modular approach." Sharpless suggested that the synthesis should be less reliant on transformations that form carbon-carbon bonds with only small thermodynamic driving forces. Instead synthesis should be reliant on "spring–loaded" reactions which have a high thermodynamic driving force (>20 kcalmol^{-1}). Sharpless proclaimed that "Click chemistry must be modular, wide in scope, high yielding and generate only inoffensive by–products" with solvents that are "benign or easily removed". Their initial suggestions of reactions which fulfilled these conditions were:

- Cycloadditions of unsaturated species, especially 1,3-dipolar cycloaddition reactions, but also the Diels-Alder family of transformations.
- Nucleophilic substitution chemistry, particularly ring-opening reactions of strained heterocyclic electrophiles such as epoxides, aziridines, aziridinium ions and episulfonium ions.
- Carbonyl chemistry of the "non–aldol" type, such as formations of ureas, thioureas, aromatic heterocycles, oxime ethers, hydrazones and amides.
- Additions to carbon-carbon multiple bonds, especially oxidative cases such as epoxidation, dihydroxylation, aziridination and sulfenyl halide addition, but also Michael additions of nucleophilic–H reactants.

Examples of these reactions can be seen in Scheme 1.2.[55] Sharpless also briefly mentioned the Huisgen dipolar cycloaddition in this paper, claiming it to be a good example of a click reaction, but its use had thus far been limited due to the concern about the safety of azides.

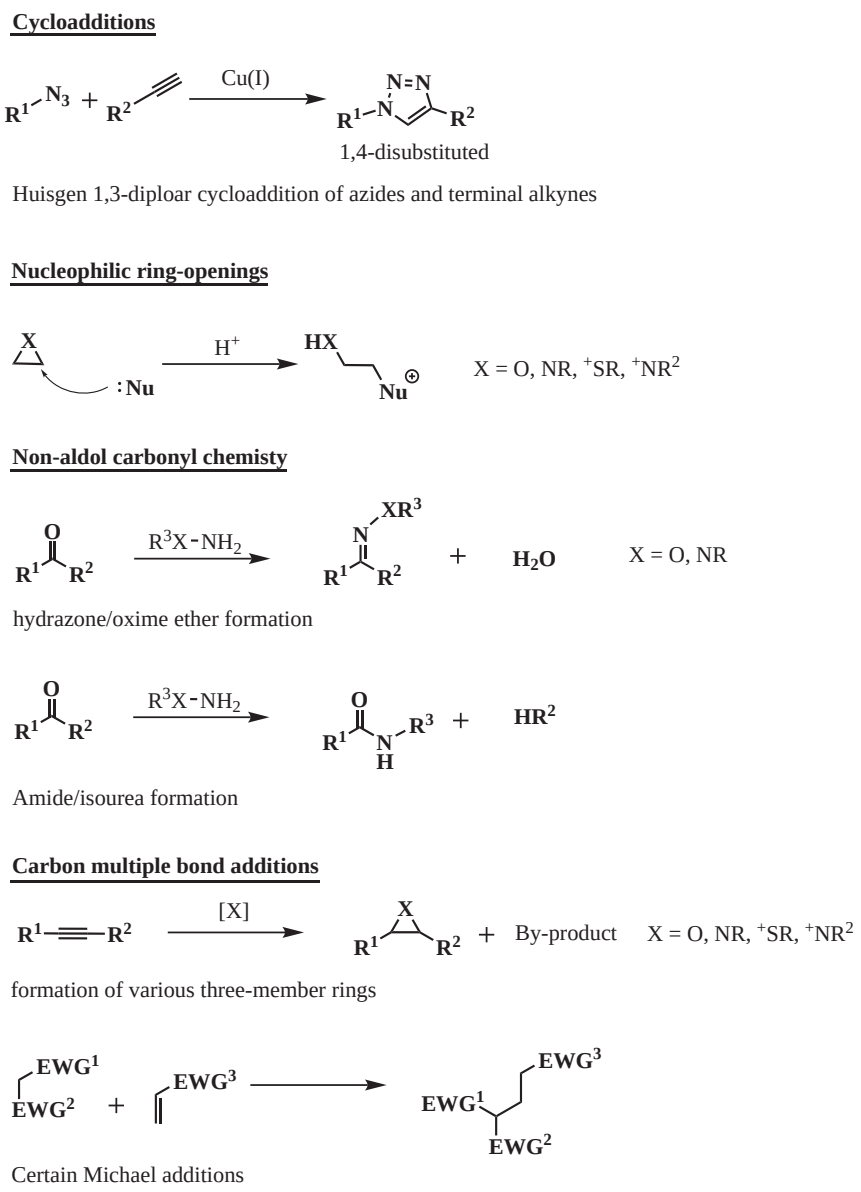

Scheme 1.2: Major classification of click chemistry reactions proposed by Sharpless *et al*. along with corresponding examples. Nu = nucleophile, EWG = electron withdrawing group.[55]

1.6.1 Cu(I)–catalysed Huisgen azide–alkyne cycloaddition reaction

One year after the seminal paper on "click" chemistry, there was still very little published on Huisgen's largely forgotten reaction. In 2002, both Medal[56] and Sharpless[57] showed that with the addition of catalytic amounts of Cu(I) there was a dramatic acceleration of reaction rate, with retention of regioselectivity for the Huisgen azide–alkyne cycloaddition (Scheme 1.3). Before 2002, there were four papers published on this reaction. Since then more than 1000 papers have been published in this area. Several key papers on the Cu(I)–catalysed Huisgen azide–alkyne cycloaddition (CuAAC) have been generated by scientists at the Scripps Research Institute, specifically Sharpless, Fokin and

Finn. The latter two were special guest editors for a whole issue of the Chemical Society Reviews dedicated to the CuAAC reaction.[58] The CuAAC has become a reliable and robust reaction, which has become an indispensable tool for linking two components together.

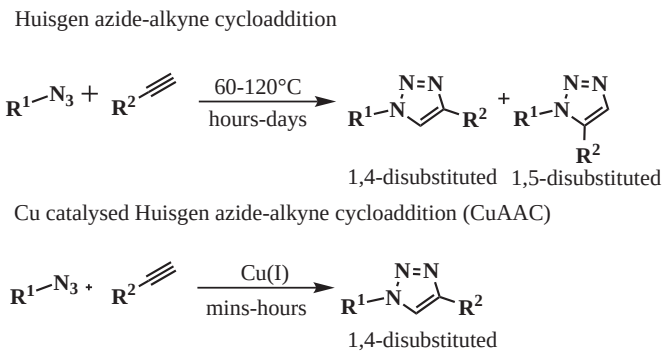

Scheme 1.3: Comparison of the Huisgen azide–alkyne cycloaddition and the Cu(I)-catalysed Huisgen azide-alkyne cycloaddition (CuAAC).

1.6.2 The triazole linker

There are several advantages of the CuAAC reaction, which include its orthogonality to a lot of other reactions and the ability to form triazoles with equimolar amounts of substrate. This allows the triazole linker to be installed with atom efficiency and without unwanted side reactions, while still producing high yields.[59] It has been shown that a 1,4–disubstituted triazole is similar to a peptide bond in geometry and distance between substituents, while retaining stability towards hydrolytic cleavage, oxidation and reduction (Figure 1.12).[60, 61] These are ideal properties when the ultimate goal is to develop a compound which is stable in the human body. The triazole itself is made up of three electronegative sp^2 hybridised nitrogens.[62] This leads to polarisation of the molecule which generates a five debye dipole with a co–linear axis to the C-H bond. The positive nature of the C-H bond and the negative nature of the nitrogen reinforces the dipole–monopole interactions of the triazole. The C–H bond is polarised by the electron deficient carbons in the ring, which makes this proton acidic. In the original Huisgen azide-alkyne cycloadditions a mixture of 1,4– and 1,5–disubstituted triazole products were isolated. This is no longer an issue due to the addition of Cu(I), which exclusively promotes the 1,4–disubstituted triazole product.[56, 57]

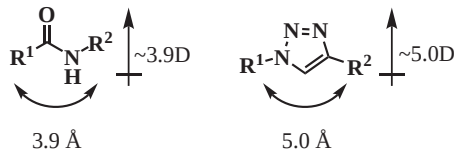

Figure 1.12: Comparison of the amide bond and a triazole linker.[62]

1.6.3 Mechanism of the CuAAC reaction

The uncatalysed Huisgen azide-alkyne cycloaddition reaction is a concerted reaction to form the triazole, with the lowest energy barrier being 25.7 kcal/mol.[63] Density functional theory calculations predict that the catalysed CuAAC reaction will proceed via a stepwise mechanism, as shown in Scheme 1.4.[57, 56, 64] The first stage of the catalytic cycle is the coordination of the alkyne to the Cu(I) species forming a π complex. The copper coordination lowers the pK_a of the alkyne C-H by up to 9.8 pH units. This allows the deprotonation of the copper–alkyne complex in aqueous systems with no need to use a base. The second stage is the formation of the copper–acetylide. From here, the third stage, a ligand is displaced and the azide functionality coordinates to the copper–catalyst to form a dimeric copper–species. The fourth stage is the cyclisation of the activated copper–acetylide–azide complex. Next in the cycle is the ring contraction to form the triazole–copper species. The final stage is the protonation of the triazole and dissociation of the labile copper complex. This results in the complete 1,4-disubstituted complex and the regenerated Cu(I) catalyst. In a DMSO:water solvent system the CuAAC reaction has been shown to be second order with respect to Cu(I) and first order with respect to the azide and the alkyne. The rate limiting step is the formation of the copper–acetylide complex. Therefore, the Cu(I) generation is an important part of the reaction.

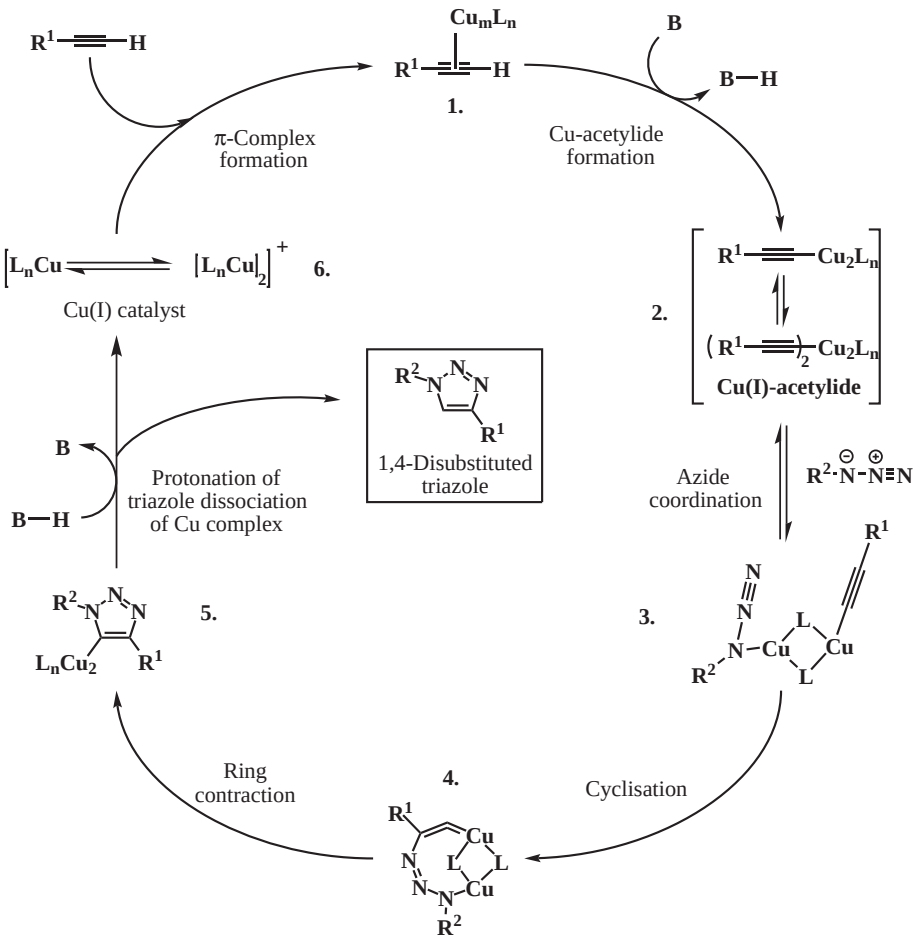

Scheme 1.4: The proposed mechanism for the CuAAC "click" reaction.[57, 56, 64]

1.6.4 Cu(I) generation and stabilisation

The CuAAC reaction is dependent on Cu(I) for catalysis, with each reaction commonly needing optimisation of solvents and source of Cu(I). Copper (II) sulphate and copper (I) halides (in particular the iodide and bromide) are prevalent sources of copper.[59] When copper (II) sulphate is chosen, it is typical to use sodium ascorbate as the reducing agent. Whereas the copper halides usually use tris(2–carboxyethyl)phosphine (TCEP) as the reducing agent. For the copper halides an amine base, ultrasonication or high temperature are vital to disrupt the copper lattice enough to form the copper–acetylide complex.[65, 66]

A variety of different solvents are tolerated by the CuAAC reaction, these include: tetrahydrofuran, acetonitrile, dimethylsulfoxide, water and certain alcohols. The CuAAC reaction has been shown to be robust, and generally be high yielding as long as the Cu(I) can be kept its reduced state, where it can perform catalysis. The CuAAC reaction has been shown to work with the Cu(I) in solution, in glassy states[67] or in aggregates.[68, 69] The common reasons for the reaction to fail or be

low yielding are: removal of the Cu(I) species from solution through chelation, disproportionation of the Cu(I) to Cu(0) and Cu(II) or oxidation of the Cu(I) to Cu(II).[59] A common solution to these problems is to use Cu(I) with an excess of reducing agent. This approach even allows the oxygen sensitive reaction to be performed in open air conditions. Another approach is to use some of the other ligands shown in Figure 1.13, which coordinate the Cu(I) and help maintain its oxidation state. The best ligands will preserve the Cu(I) oxidation state while promoting a fast reaction rate.[59] Tris[(1-benzyl-1H-1,2,3-triazol-4-yl)methyl]amine (TBTA)[70] and sulfonated bathophenanthroline (SBP) are primarily used for click reactions in organic synthesis, whereas *N*,*N*,*N*,*N*,*N*–pentamethyldiethylenetriamine (PMEDTA) is a popular choice for click polymerisation reactions.[71]

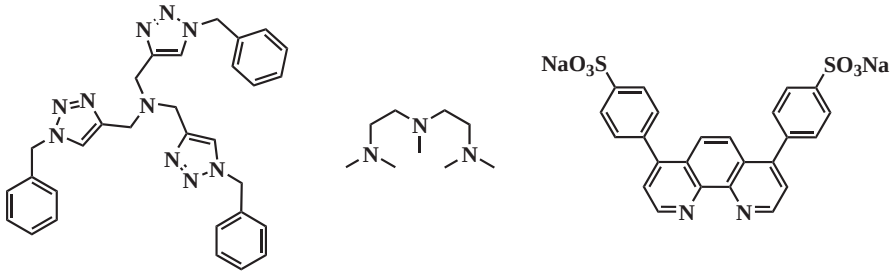

Figure 1.13: Three common CuAAC ligands.

1.6.5 Click carbohydrates

Biological systems are able to produce multivalent carbohydrate ligands with much greater inherent heterogeneity than organic chemistry currently can.[72] Peptides and dendrimers are two of many different scaffolds that can be used as supramolecular entities which display different saccharide motifs in a controlled fashion.

Individual carbohydrates tend to bind weakly to their complementary proteins. This can be overcome by multiple interactions of multivalent carbohydrates.[72] These circumstances can be attributed to the "cluster" or "multivalent" glycoside effect, which was first described by Lee *et al.*[73, 74] A strong glycoside cluster effect requires two partners: a lectin with clustered sugar binding sites and a multivalent ligand that can present sugars with the proper orientation and spacing.[73]

The CuAAC reaction has been used by a variety of groups to install sugar moieties onto scaffolds to create neoglycoconjugates.[72] Santoyo–González *et al.* produced a library of structurally diverse, multivalent, heterogeneous neoglycoconjugates, the general structure of which are shown in Figure 1.14.[75] The core of the structure is a pentaerythritol, which was protected on two of the chains using benzylidene. The two unprotected chains were then developed, allowing for controllable installation of azide and/or alkyne functionalities onto the scaffolds. The CuAAc reaction was

then used to install the desired acetyl protected sugars (mannose and glucosamine) which had been derivatised with the appropriate azide or alkyne handle. With the first two chains completed the benzylidene group was removed and the reaction repeated to produce dendrimers with the structure shown in Figure 1.14.

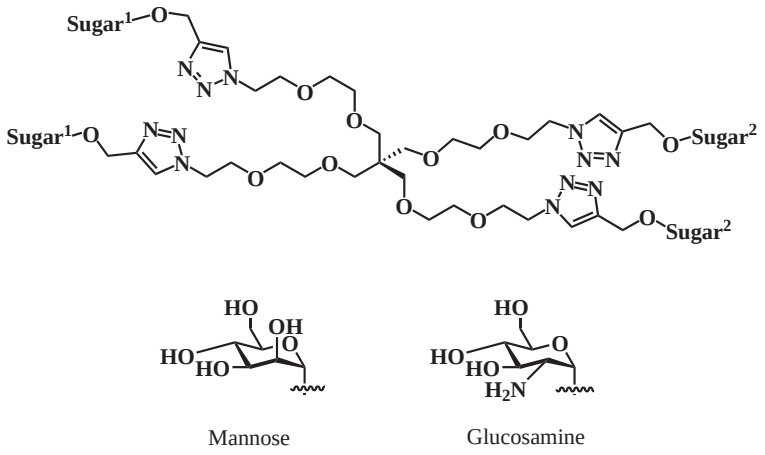

Figure 1.14: Neoglycoconjugate dendrimers synthsised by Santoyo–González *et al.*[75]

The dendrimers synthesised by Santoyo–González *et al.* were tested for binding to the natural carbohydrate binding lectin concanavalin A,[75] and were found to have inhibitory properties. The dendrimer with two α–mannose and two α–glucosamine units was found to be a superior binder to the four α–mannose system, even though concanavalin A is known to have a higher affinity for mannose monomers. The substitution pattern and distance between the sugars are thought to be the most important parameters for influencing the binding strength of the dendrimers to the lectin.[75]

The CuAAC reaction was used by Djedaïni–Pilard *et al.* to create a dendritic 'click' manno–oligomer, which mimics the high–mannose oligosaccharide Man_8 that binds the mannose–specific lectin concanavalin A.[76] A comparison of the two structures is shown in Figure 1.15. The triazole linkers act in a similar fashion to the C, E and G mannoses of Man_8, functioning as a spacer to branch the mannose moieties away from the core. The synthetic oligosaccharide was designed to preserve the overall length of oligomannosyl chains and the orientation of the external residues. Results of binding studies performed by Djedaïni–Pilard *et al.* show that binding to concanavalin A is preserved even when some of the mannopyranosidic units of the high mannose part of *N*–glycans have been replaced by triazole rings.[76]

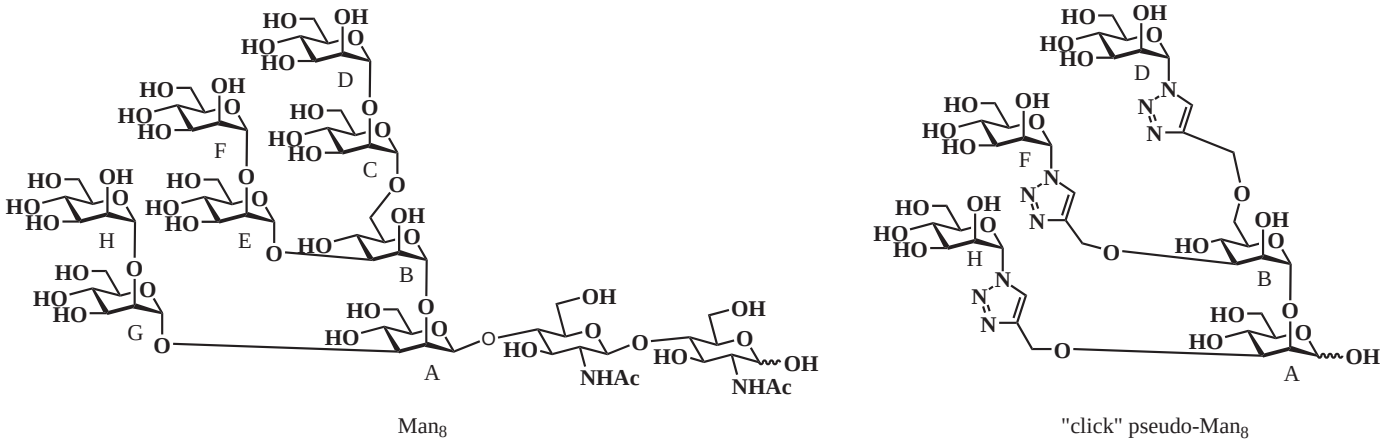

Figure 1.15: High–mannose oligosaccharide Man_8 (left) and "click" pseudo–Man_8 mimic (right) synthesised by Djedaïni–Pilard *et al.*[76]

Brimble *et al.* synthesised a multivalent MUC1 neoglycoconjugate using the CuAAC reaction.[77] The versatility and efficiency of the CuAAC reaction allowed a modular synthesis of the click multivalent neoglycoconjugates (Figure 1.16). The tetrasacharyl triazole cluster has a GlcNAc core, which orientates the other outer sugars. Figure 1.16 only shows the simplest carbohydrate from the library synthesised. However, the modular nature of the synthesis allows for three different carbohydrates to be glycosylated via sequential CuAAC reactions. The tetrasacharyl triazole cluster was even conjugated to the MUC1 sequence using click chemistry.[77] This approach allows either for broad targeting of different C–type lectins with just one carbohydrate cluster, or the straightforward synthesis of a sugar cluster which mimics complex carbohydrates.

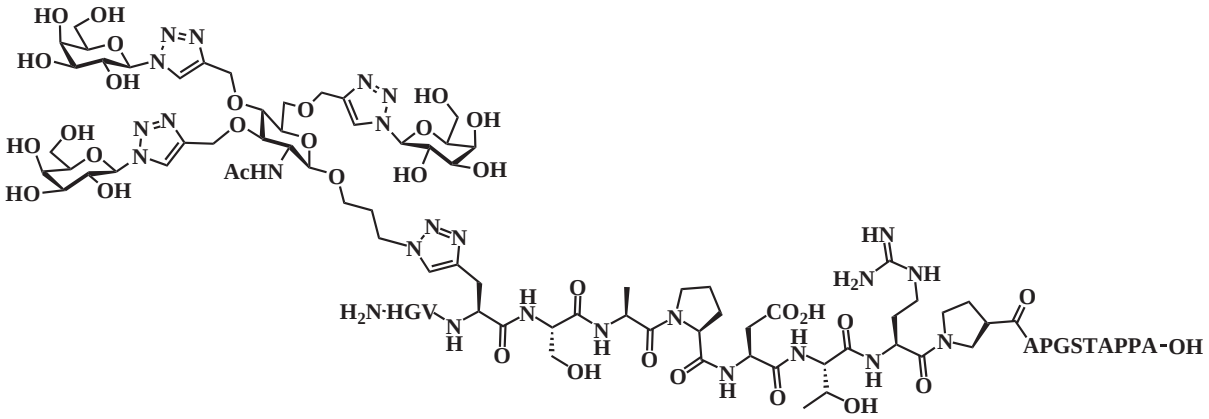

Figure 1.16: MUC1 click multivalent neoglycoconjugates synthesised by Brimble *et al.*[77]

Santoyo–González, Djedaïni–Pilard's and Brimble's glycopeptides are three examples where carbohydrates were installed through the CuAAC reaction, and also able to retain the ability to bind to the receptors they target.[75, 76] The triazole linker positioned the carbohydrates to make them available for binding in solution to the receptor. This is encouraging to observe as the CuAAC

reaction may provide a simpler route to neoglycopeptides which mimic more complex native glycopeptides while not losing the desired function.

1.7 Examples of T_N antigen vaccines

Previously, general examples of glycopeptides, dendrimers and 'click' sugars were given. Now these concepts have been introduced, the focus will be on examples such as the carbohydrates that bind specifically to MGL. The T_N antigen is specifically associated with epithelial cancers such as breast, colon, prostate and melanoma.[32] The following section will discuss vaccines which were designed to include T_N antigens and have later been shown to evoke an immune response. Most of these compounds were not tested for MGL binding and have been used to stimulate CD4+ T–cells and B cells rather than the CD8+ T–cells which this project focuses on. However, these scaffolds may have potential for targeting MGL as they contain the GalNAc necessary for selective MGL binding, and they could be modified to carry a cargo for CD8+ T–cell stimulation.

Danishefsky's "cassette" approach to synthesising T_N antigen

The difficult part of synthesising T_N antigens is the formation of the α–glycosidic linkage.[49, 78] Danishefsky's "cassette" approach builds a *N*–acetylgalactosamine synthon stereospecifically *O*–linked to a serine (or threonine) residue with a differentiable acceptor site on the GalNAc (Scheme 1.5).[78, 49] This building block acts as a general insert (referred to as a "cassette"). This strategy is reliant on orthogonal protecting groups and the successful coupling of bulky protected cassettes into the amino acid sequence. The "cassette" approach sacrifices a fully convergent approach for enhanced reliability of synthesis.[79] T_N antigen precursor building blocks are produced which can be included in larger oligosaccharides (Scheme 1.5).[79] The final step of each synthesis using a cassette is the reductive acetylation of the azide and deprotection of the protected hydroxyl groups.[78]

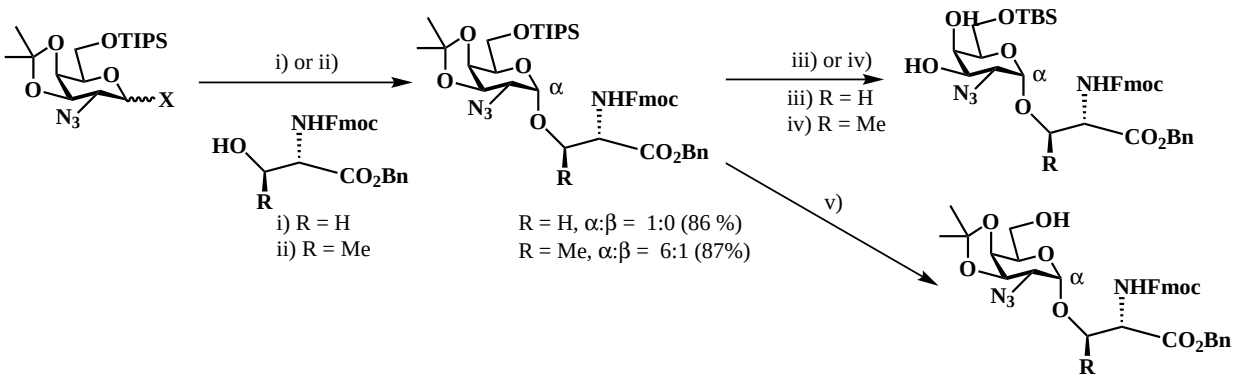

Reagents and conditions: (i) R = H: TMSOTf,THF, -78 ºC ; (ii) R = Me [CP_2ZrCl_2], AgOTf, CH_2Cl_2; (iii) I_2/MeOH (63-81 %); (iv) TBSCl, imidazole, DMF, (64-85 %); (v) TBAF, AcOH, THF, (94-100 %)

Scheme 1.5: Danishefsky's cassette approach to synthesise T_N antigen precursors.[49, 79, 78]

Danishefsky synthesised T_N antigen clustered conjugates using the cassette approach. These consisted of three consecutive T_N antigens conjugated to an immunological activator such as tripalmitoyl–*S*–glyceryl–cysteinyl–serine (Pam_3Cys) or immunogenic carriers such as KLH and BSA (Figure 1.17).[79, 78] All of these constructs proved to be immunogenic when tested in mice, generating IgM and IgG antibodies. Due to the quality of the results in mice, phase I and II human trials for prostate cancer were performed with a T_N antigen cluster conjugated through a linker to KLH.[49, 78]

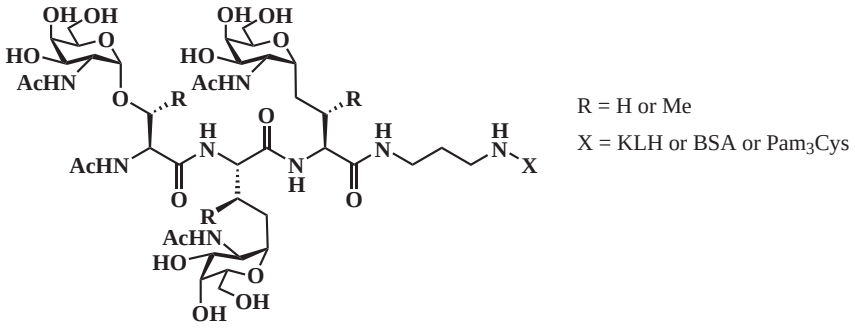

Figure 1.17: Danishefsky's T_N antigen clusters.[49, 79, 78]

Danishefsky's T_N antigen clusters are examples of linear glycopeptides which target the immune system. Linear peptides can be more straightforward to synthesise, but may be less effective at binding receptors with multiple CRD. The following examples involve alternative non–linear scaffolds which may be more effective for targeting the homotrimeric cluster of MGL.

Huang's T_N antigen block polymer

Huang *et al.* produced co–polymers which contained T_N antigens for anticancer vaccines (Scheme 1.6).[80] Huang chose polymers as his delivery system because they could carry multiple tumour associated carbohydrate antigens for avidity. The polymer contained two blocks: the first block contained ammonium moieties, while the second block contained methyl ester protecting groups. Once the polymer had been synthesised, the modified T_N antigens were coupled to the ammonium moieties using mild conditions. The methyl ester block was subsequently deprotected and an oligopeptide from PV could be coupled as a T–helper cell epitope.

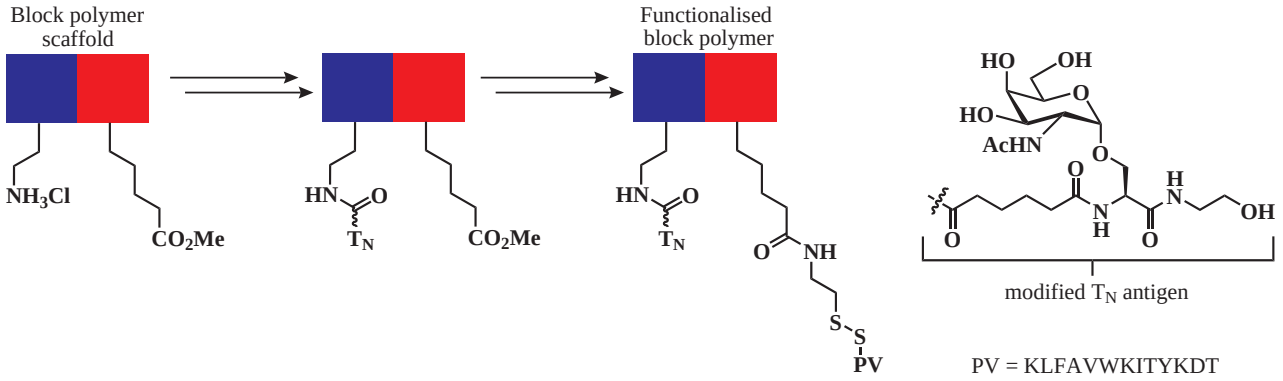

Scheme 1.6: Synthesis of water soluble block co–polymers containing T_N antigen and PV epitopes by Huang *et al.*[80]

Huang's polymer provides a platform which can incorporate both carbohydrate ligands for binding to lectins and epitopes for inducing an immune response. While this approach is able to produce a compound suitable for epitope delivery, there will always be doubts about the control of size and quality of the polymers synthesised. To avoid the huge variance in chain lengths which is dependent on synthesis method, alternatives such as peptide synthesis can produce defined structures through controlled chain growth.

Renaudet's T_N antigen mimic RAFT construct

Renaudet *et al*. produced fully–synthetic T_N antigen mimics which were conjugated to the regioselectively addressable functionalised template (RAFT) as shown in Figure 1.18. These were designed as therapeutic vaccines which would induce IgG/IgM antibody response to treat cancer.[81] The T_N antigen mimics were expected to be more resistant to enzymatic degradation, which would lead to increased bioavailability and therefore a stronger, longer–lasting immunogenicity and protective efficacy for the therapeutic vaccine.[81] The structure of the vaccine consisted of four T_N antigen mimics coupled to the lysine N^{ϵ} group of the RAFT scaffold on the upper face. Immunostimulant peptide epitope (OvaPADRE) was conjugated to the lower face of the RAFT scaffold through a disulphide bond.[81]

The fully–synthetic clustered T_N antigen mimic was tested on mice for *in vivo* safety, with no resulting adverse effects.[81] Significant levels of the IgG/IgM antibody were observed in the sera of mice ten days after the third immunisation with the vaccine. High levels of these two antibodies were also present 240 days later. Antibodies generated by the T_N mimetic–based vaccine recognised tumour cells expressing T_N antigens.[81] The immunotherapeutic was able to reduce the size of the tumour and keep seven out of ten mice alive over an eight week period, which was high compared to the control group where only one survived. The tumour protection was shown to be B–cell mediated.[81]

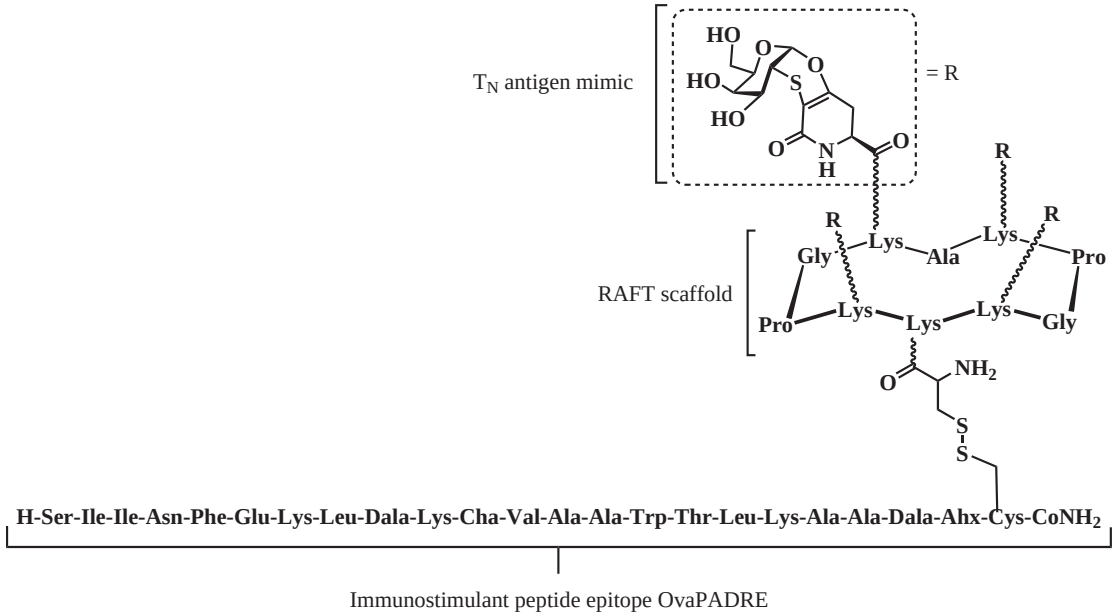

Figure 1.18: Renaudet's fully–synthetic clustered T_N antigen mimic.[81]

Renaudet's RAFT construct has already proved itself to be an effective immunotherapeutic, however it did not generate CD8+ T–cells. Maybe with a different peptide epitope this RAFT construct

could generate the desired T–cell immune response. Although targeting MGL with this T_N antigen mimic may be less successful due to the lack of an *N*–acetyl group at the carbohydrate C2 carbon.

Singhal's T_N antigen conjugates

Singhal *et al*. synthesised serine based T_N antigens which were incorporated into different peptide based constructs.[13] Singhal prepared Boc–protected T_N antigens for inclusion in SPPS. The glycosylation of Boc–protected serine with a protected glycosyl imidate predominantly formed the α anomer (5:1 α:β 72%). The azide protected building block anomers were near impossible to separate by chromatography, but could be separated after reduction of the azido groups and subsequent acetylation the two anomers. The acid–labile glycosidic bond was resistant to the condition of acidolysis (HCOOH, rt, 1 h) due to the stabilising effect of the *O*–acetyl groups in the GalNAc residue. This allowed the building blocks to be used in Boc SPPS, the process which would destroy the chiral integrity of other carbohydrates. The acetate groups were removed by saponification of the constructs with sodium methoxide at the end of the synthesis. A combination of mono–T_N, di–T_N and tri–T_N antigens with a spacer arm were conjugated to immunogens such as ovine serum albumin (OSA), fifth generation starburst dendrimers and Pam_3Cys (Scheme 1.7).[13, 82]

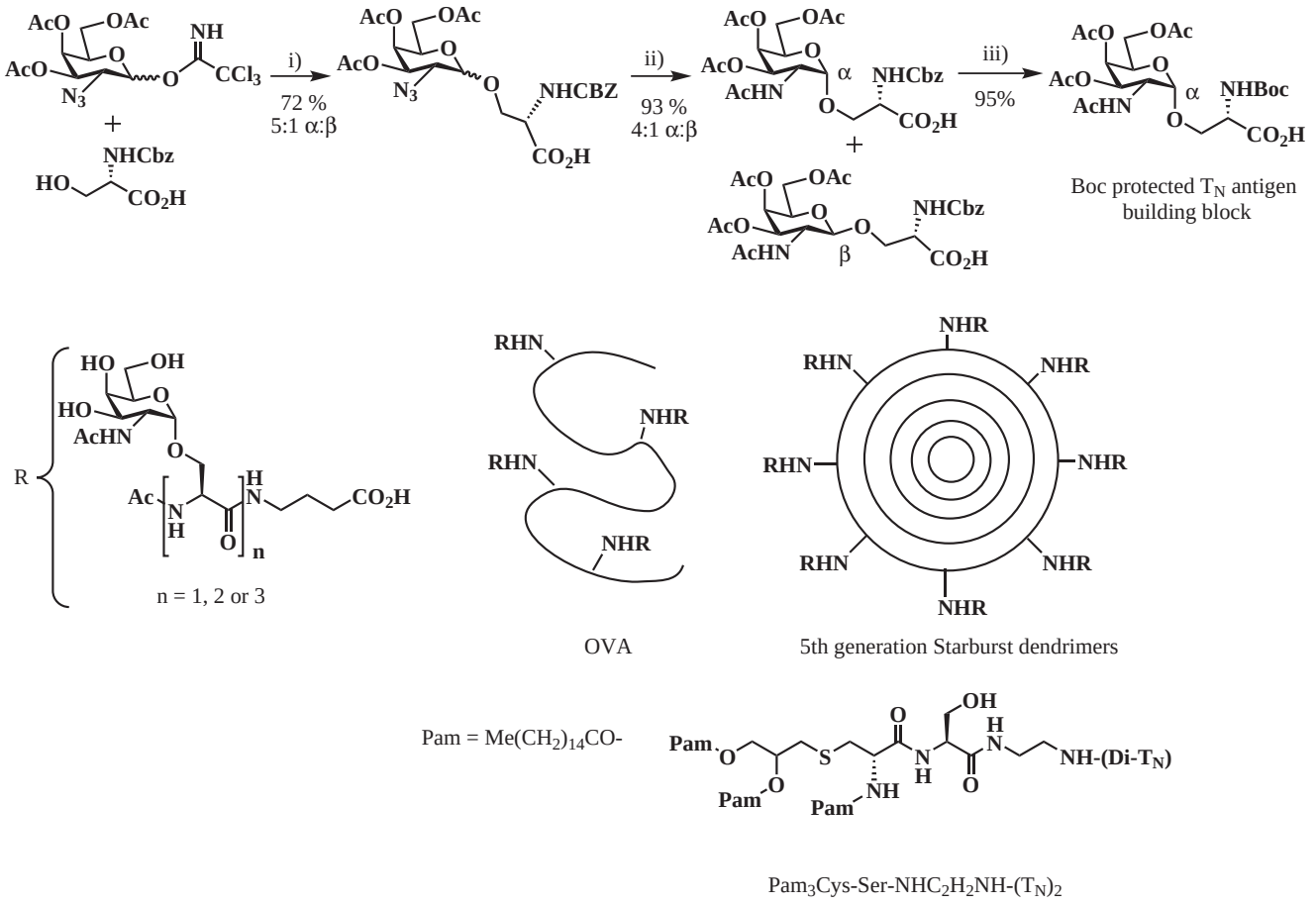

Reagents and conditions: (i) TMSOTf, CH_2Cl_2, -15ºC, 30 min; (ii) a. H_2S, pyridine:H_2O (2:1); b. Ac_2O, pyridine; (iii) a. H_2, 10% Pd/C, MeOH, 2 h ; b. Boc_2O, DIEA, MeOH, 1 h.

Scheme 1.7: Singhal's synthesis of Boc–protected T_N antigens, and schematics of the ovine serum albumin (OSA), fifth generation starburst dendrimers and Pam_3Cys T_N antigen scaffolds.[44]

The different conjugates in Scheme 1.7 were inoculated into mice, and the immune responses were measured.[13] Sera from the mice were measured for antibody titres. The OSA glycopeptides showed high–titre IgM response against T_N antigens, with the peptides bearing the di and tri–T_N antigen moieties also giving measurable IgG anti–Tn antibody responses.[13] No measurable T_N antibody response was observed for the starburst dendrimer, which may have been due to the non–immunogenic nature of the scaffold.[13, 82] Pam_3Cys conjugated to the di–T_N antigen generated more IgM and IgG antibodies than the OSA glycopeptides.[13] These results showed that the antibody response was specific to the T_N antigen but reliant on an immunogenic scaffold to generate the immune reaction.

Singhal produced a diverse selection of glycosylated compounds, none of which produced a CD8+ T–cell response. These compounds may bind selectively to MGL, with the branched starburst dendrimer most likely to be able to present the GalNAc residues to multiple CRDs at the same time.

However, the epitope would need to be changed if the desired activation of CD8+ T–cells was to be induced.

Ježek's resin–bound T_N antigenic glycopeptide dendrimers

Ježek *et al*. produced a library of T_N antigenic glycopeptide dendrimers which were bound to resin.[83] Biocompatible Tenta Gel resin beads were used as a non-detachable support for the multiple antigenic peptides because it was known from confocal laser microscopy and NMR spectroscopy studies that the structure of resin enables penetration of high molecular weight compounds to the core of the beads. The dendrimers consisted of a lysine core with aminobutyric acid (Abu) spacers connected to T_N antigens at the terminus of the chains. The T_N antigens were synthesised using Singhal's synthesis mentioned previously.[13] A selection of Ježek's resin–bound T_N antigenic glycopeptide dendrimers are shown in Figure 1.19.

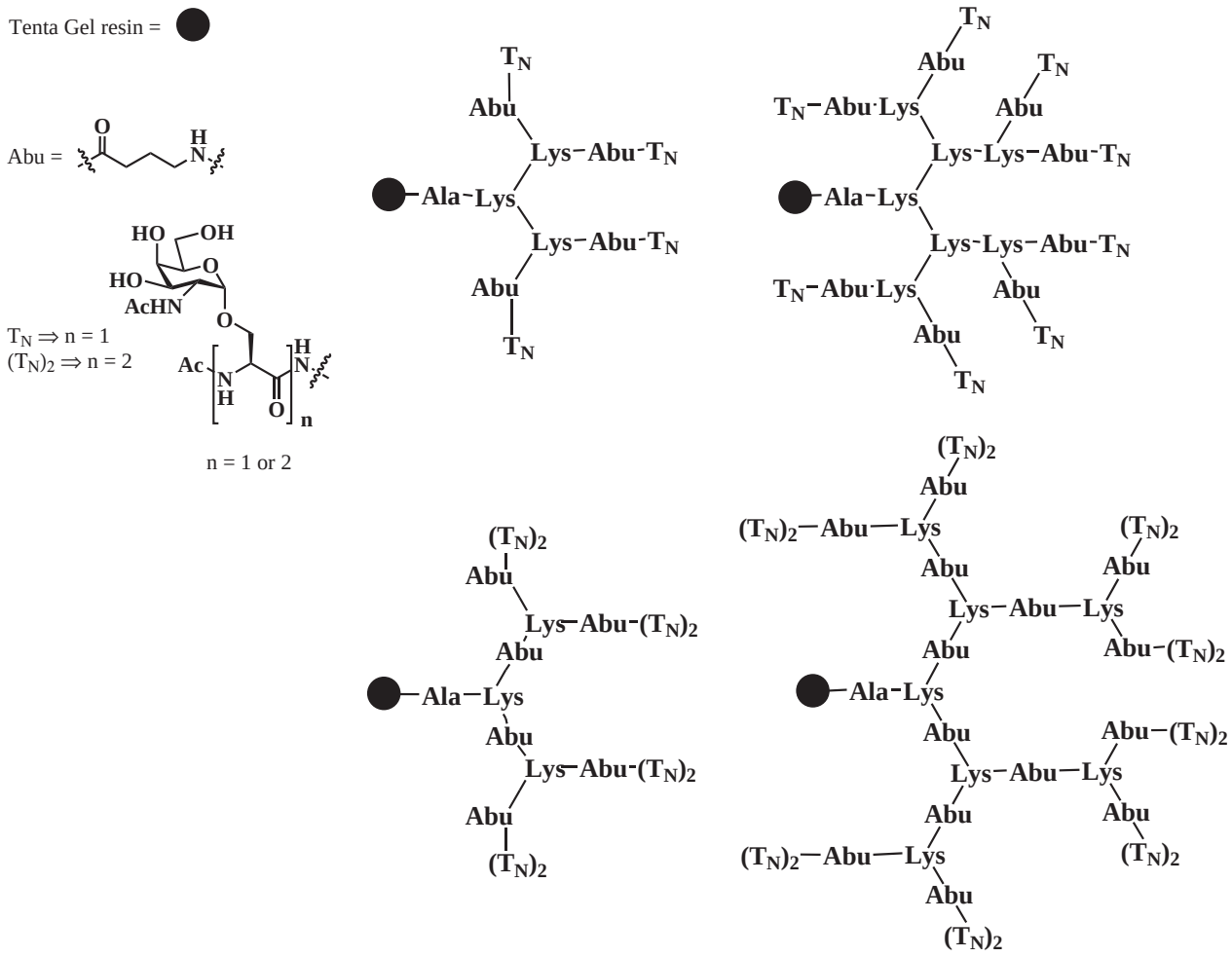

Figure 1.19: Ježek's Tenta Gel resin–bound T_N antigenic glycopeptide dendrimers.[83]

All four dendrimers shown were able to induce immune responses in mice. The dendrimers

which contained Abu were able to induce greater immune responses, however they were difficult to synthesise due to the tendency of the core to fold into more compact and less accessible structures.[83] The synthesis of these dendrimer constructs may have been made easier if Ježek *et al*. used a mini–PEG linker which is less hydrophobic and is known to spread out instead of the Abu linker.[84, 85]

Ježek's T_N antigen library was interesting because the dendrimers were prepared and biologically tested on resin. This approach allowed greater insight into the interactions of T_N antigen ligand binding through confocal laser microscopy and NMR spectroscopy studies. While production of resin–bound dendrimers are unlikely to have application as CD8+ T–cell stimulating therapeutic vaccines, it may generate useful information using these techniques for refining the binding of ligands to MGL.

Leclerc's multiple antigenic peptide

In 1997, Leclerc *et al*. synthesised fully synthetic carbohydrate–based constructs as immunogens which were able to induce a strong immune response based on the T_N antigen.[86] The dendrimers were multiple antigenic glycopeptides (MAG) consisting of four chains branching out from a poly–lysine core. Each chain was conjugated to a PV epitope and then glycosylated with the T_N antigen at the terminus as shown in Figure 1.20.

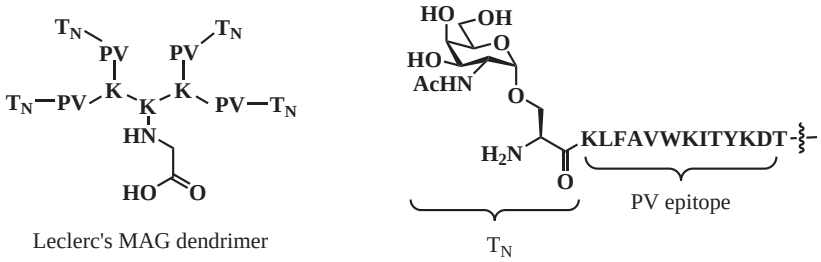

Figure 1.20: Leclerc's original multiple antigen glycopeptide (MAG) consisted of a polylysine core connected to a $CD4^+$ epitope from the PV and *N*–terminal T_N antigens.[87]

Leclerc *et al*. prepared Fmoc–protected T_N antigens for the synthesis of multiple antigenic glycopeptides. A Koenigs–Knorr reaction was performed with 3,4,6–tri–*O*–acetyl–2–azido-2-deoxy–β–D–galactopyranosyl chloride, to glycosylate the Fmoc–protected threonine or serine [86, 88, 89, 90] When the β–chloride was used the reaction predominantly produced the α–glycosylated product (8:1, α:β 70%).[86, 91, 92] Leclerc's synthesis afforded a much higher anomeric selectivity than Singhal's synthesis of the Boc–protected T_N antigens.[13]

The MAG was designed in a precise way with each component having an important function.

The lysine core was chosen as a non–immunogenic structure to facilitate branching. PV epitopes were chosen to enhance the T–cell dependent antibody response, as the T_N antigen alone is only weakly immunogenic and it is also known to activate the undesired B–cell response.[86] The MAG was synthesised by Fmoc SPPS on a Wang resin. The symmetrical nature of the MAG allowed each chain to have the PV epitope sequence incorporated in parallel. The final amino acid coupled to the dendrimer was the Fmoc–protected T_N antigen. After Fmoc deprotection, the MAG was cleaved from the resin to give the final product.[86]

The MAG was shown to induce anti–T_N IgG antibodies that recognised human tumour cell lines.[87] Two versions of this MAG were created: one version contained T_N antigens which were able to induce the specific antibody response. The second version only contained the branched core and the PV epitopes. The non–glycosylated dendrimer was not recognised by the antibodies and was ineffective at producing the desired T–cell response.[87]

Fully synthetic lipoglycopeptides with a dimeric T_N associated with a palmitoyl core were only able to invoke an IgM antibody response. However, no IgG antibody response was detected and this would be necessary for antibody dependent cellular cytotoxicity against cancer cells.[93] This problem could be overcome with a strong adjuvant, but the MAG was shown to produce this effect with a weak adjuvant such as alum. The combination of MAG with alum was able to cure 80% of tumour–bearing mice when it was administered in a therapeutic or prophylactic manner.[93]

Leclerc *et al*. synthesised a library of MAG derivatives, the components of which are shown in Figure 1.21.[94] The derivatives contain a polylysine core similar to the original MAG shown in Figure 1.20 but with different epitopes and antigen components. The epitope chain could be the PV epitope, the tetanus toxoid (TT) epitope or the synthetic pan dr epitope (PADRE). A selection of antigens based on the T_N and the sialyl T_N antigen were used to terminate the dendrimer chains. The effect of the aglycone of the antigen was also varied with serine, homoserine and threonine analogues of the T_N antigen being created. The number of antigen units was also varied, with both single and sequences of three antigens incorporated in the dendrimers (Figure 1.21).

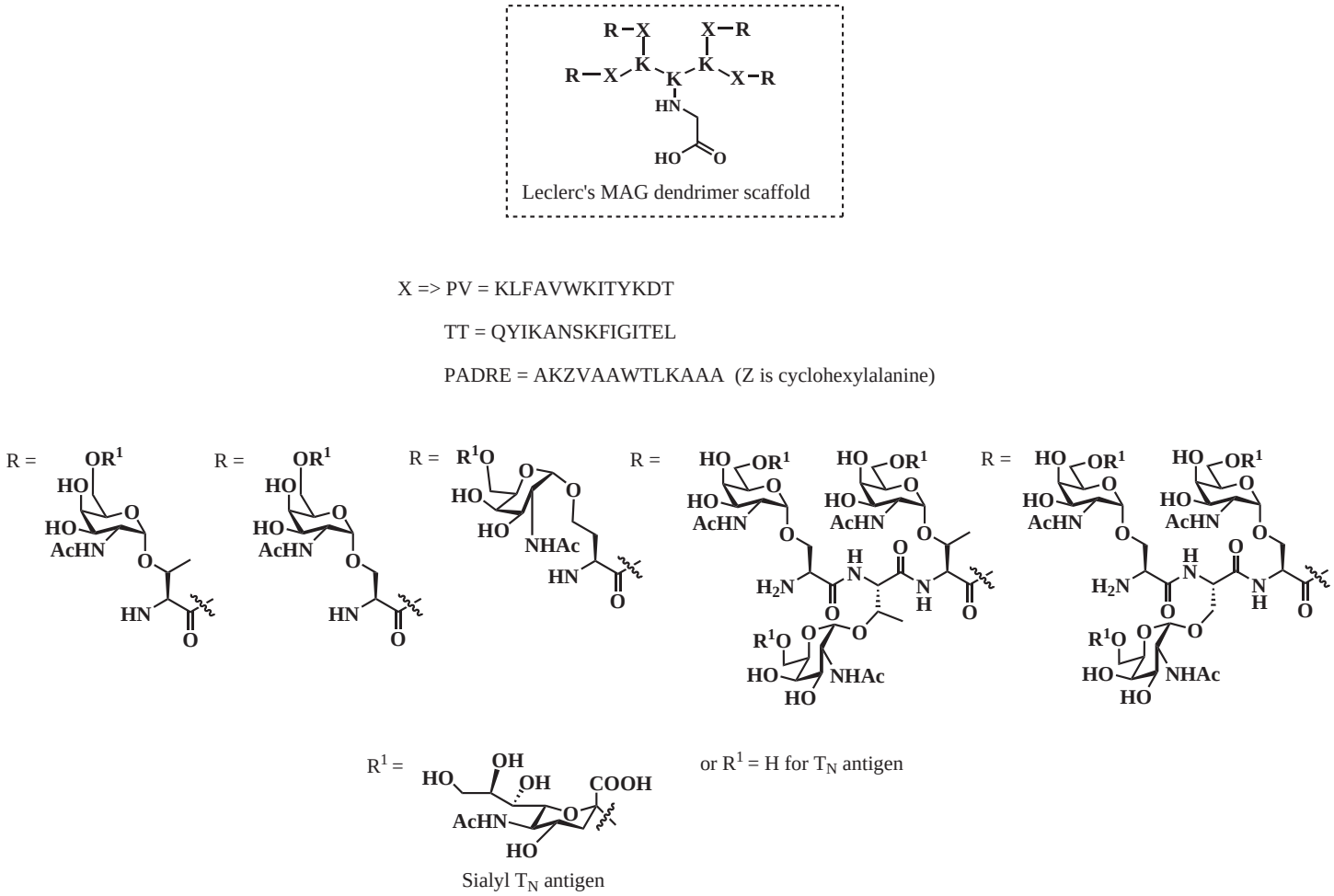

Figure 1.21: An overview of the multiple antigenic glycopeptides (MAG) library synthesised by Leclerc *et al*.[94]

Amino acid chains between the flanking T_N antigens have been shown to modulate antibody recognition.[94] Non–natural homoserine residues did not induce anti–T_N antibodies that recognise the native form of T_N. Antibodies induced by T_N clusters based on natural amino acids (Ser or Thr) failed to efficiently recognise the GalNAc residue on a homoserine backbone.[94] Monoclonal antibodies had exclusive specificity for Ser or Thr based MAG, with the serine–threonine-threonine cluster activating the largest array of monoclonal antibodies. Leclerc's MAGs have shown induction of anti–T_N antibodies in two non–human primate species with no adverse reaction observed in any animal.[94]

Leclerc's MAGs are examples of branched glycopeptide dendrimers, and are similar to what was envisioned for this project. The MAGs were not equipped with an epitope that was suitable for CD8+

T–cell stimulation. However, the general structure of the MAGs make them suitable epitope delivery systems to DCs via the MGL receptor. It is thought that with the correct epitope and incubation with MGL expressing cells, the MAG could stimulate a CD8+ T–cell response.

MUC1 sequences

The mucin MUC1 was introduced while discussing MGL earlier in Section 1.4.1. Mucins are common proteins associated with epithelial tissues and characterised by repeat domains and a dense *O*–glycosylation.[95, 96] These heavily glycosylated proteins are involved in the formation of gels, epithelial lubrication, cell signalling and can also act as efficient barriers against chemical aggressions.[95] The MUC1 sequence plays a major role in tumour progression and metastasis,[97] and is over–expressed by malignant cells in various types of cancers.[96, 98, 99, 100]

Vaccination against cancer is a very desirable goal, and MUC1 has been identified as an attractive target for immunotherapy.[19, 100] Antibodies stimulated from MUC1 interactions with the immune system are gaining interest as potential treatments for killing tumour cells via proliferation of cytotoxic T–cells.[101] Tumour–associated glycopeptides alone do not elicit a sufficiently robust immune reaction, so increased stimulation is needed to elicit a robust humoral response.[37] DCs incubated with glycan modified tumour antigen MUC1 can produce measurable antibody–responses and also produce cytotoxic T– lymphocytes. As stated earlier, generation of cytotoxic T lymphocytes is an important goal for a therapeutic vaccine for cancer.[6]

Several groups have synthesised different truncations of the MUC1 sequence. Of note is the synthesis by Kunz and Danishefsky which is not covered in this review.[102] While these syntheses demonstrate that organic chemistry is a powerful tool for mimicking glycoproteins synthesised in nature, there are some drawbacks to this approach. Firstly, extensive carbohydrate protection and deprotection strategies are necessary to retain chiral integrity. Secondly, peptides and proteins with identical amino acid sequences but different carbohydrate residues require their own unique synthesis if post sequence glycosylation is not possible. Thirdly, synthesis of glycosyl amino acid building blocks may require complicated multi–step synthesis. Finally, coupling of the glycosyl amino acid building blocks to peptide sequences can require a large excess of reagents to drive the reaction to completion in SPPS.

Brimble *et al*. synthesised the VNTR region of MUC1 because this GalNAc glycosylated peptide was reported as a ligand for the MGL receptor.[20, 25] To solve the problem of synthesising fully protected glycosyl amino–acid building blocks and then incorporating these into SPPS, the Brimble group synthesised MUC1 neoglycopeptides using click chemistry.[103, 104] This approach avoided the problems discussed in the previous paragraph. Firstly, non–protected carbohydrates could be

installed post synthesis. Secondly, the use of protecting group strategies allowed synthesis of one peptide sequence which could be derivatised post–synthesis with different carbohydrate residues. Thirdly, the approach of synthesising click chemistry compatible amino acid building blocks is also more straightforward than using glycosyl amino acid building blocks. Finally, due to the convergent nature of the syntheses, fewer of the individual carbohydrate and amino acid building blocks are needed to complete a new glycopeptide synthesis.

Brimble *et al.* synthesised carbohydrate building blocks which included an azide handle, installed via the CuAAC reaction onto peptides which contained amino acids functionalised with alkyne groups.[103] A library of these MUC1 sequences with different glycosylated positions were synthesised (Figure 1.22).[104]

These compounds were intended to bind to MGL and go through the process of cross presentation which would result in a CD8+ T–cell response. Unfortunately cell binding studies with these compounds conducted in the Dunbar group showed that these MUC1 sequences did not successfully bind to MGL and elicit a CD8+ T–cell response (unpublished work). Building on the foundations of the previous study, a new approach was necessary to synthesise MGL targeting compounds.

HGVTSAPDTRPAGSTAPPA

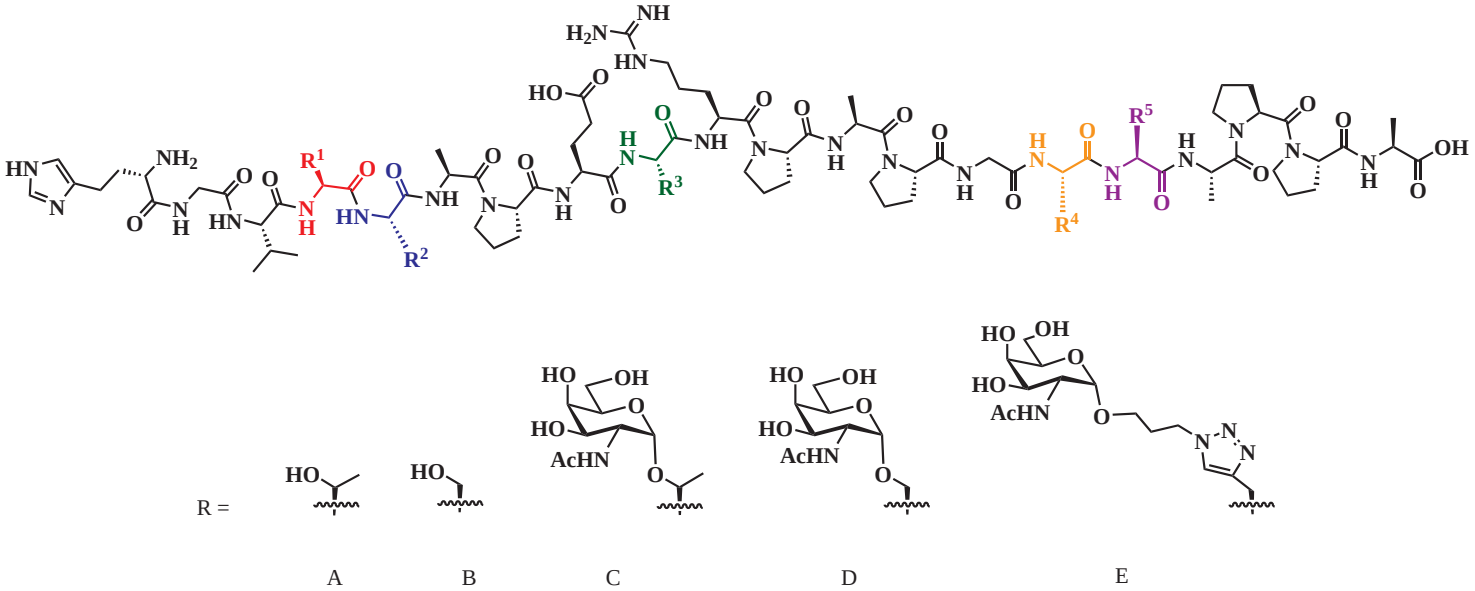

Peptide 1, R^1= A, R^2= B, R^3= A, R^4= B, R^5= A
Peptide 2, R^1= C, R^2= D, R^3 = A, R^4= D, R^5= C
Peptide 3, R^1= E, R^2= B, R^3 = A, R^4= B, R^5= A
Peptide 4, R^1= E, R^2= E, R^3= A, R^4= B, R^5= A
Peptide 5, R^1= E, R^2= B, R^3= A, R^4= B, R^5= E
Peptide 6, R^1= E, R^2= B, R^3= E, R^4= B, R^5= E
Peptide 7, R^1= E, R^2= E, R^3= A, R^4= E, R^5= E
Peptide 8, R^1= E, R^2= E, R^3= E, R^4= E, R^5= E

The repeating 20 amino acid sequence has five possible glycosylation sites at Thr and Ser residues, which have been highlighted.

Figure 1.22: The structures of the VNTR region of MUC1 synthesised by Brimble *et al.*[103, 104]

1.8 Aim

In previous sections the MGL receptor has been highlighted as a key target for developing a delivery system to DCs, which are important APCs for the stimulation of CD8+ T–cells. Examples of compounds which could carry GalNAc residues and have been used sucessfully in other biological studies have also been described. Tam's polylysine dendrimers have been shown to be suitable scaffolds for biological delivery due to their non–immunogenic nature and ability to present multiple antigens.[45, 43] Previous work by Danishefsky, Djedaïni–Pilard or Brimble *et al.* have all shown that the triazole linker is a suitable replacement for the native *O*–glycoside bond in the installation of carbohydrate moieties.[52, 76, 103, 104] Finally, compounds such as Leclerc's MAGs have been used to demonstrate that branched T_N–antigen–containing dendrimers can deliver epitopes to the immune system.[94]

The aim of the current work is to design a glycopeptide which selectively targets the MGL receptor expressed by DC (Scheme 1.8). The glycopeptide will contain GalNAc as the carbohydrate to specifically target the carbohydrate recognition domain of MGL. We plan to use the CuAAC reaction to install the GalNAc moiety in an efficient manner, which does not require unnecessary protection and deprotection of the carbohydrate. A dendrimer scaffold will provide a more suitable way to present carbohydrate ligands than the previous unsuccessful linear MUC1 sequences.

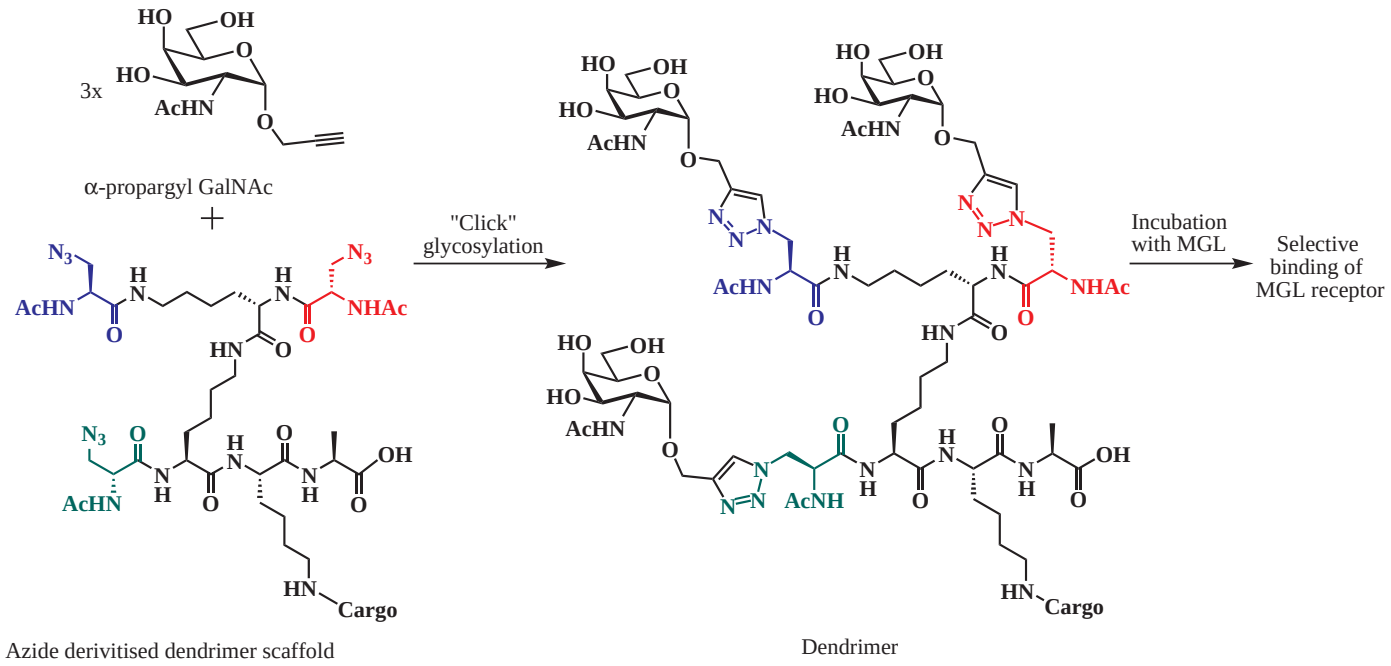

Scheme 1.8: Synthesis of a glycopeptide which selectively targets the MGL receptor for use in therapeutic vaccines to stimulate CD8+ T–cells.

The glycopeptide will then be evaluated for strength, selectivity and quantity of binding to the MGL CRD. The most successful candidates will have the potential to be conjugated to peptide epitopes which can stimulate CD8+ T–cell immune responses.

A therapeutic vaccine based on a glycopeptide which can stimulate CD8+ T–cell immune responses could be used in conjunction with immune checkpoint blockade drugs, such as Ipilimumab.[4] This combination should lead to increased efficacy of the immune system, allowing the body to overcome cancer immunosupression.[5]

Chapter 2

Initial synthesis of generation I and II dendrimers for targeting MGL

N-Acetylgalactosamine (GalNAc) is an immunologically significant carbohydrate due to its selectivity for MGL which has a role in immune responses.[29] GalNAc is found in glycoproteins such as MUC1 which is a protein overexpressed in adenocarcinomas.[30, 25, 32] GalNAc is also found in the well–known T_N–antigen, in which serine or threonine residues are glycosylated with GalNAc (Figure 2.1).[29] Macrophage galactose binding lectin (MGL) is a trimeric cluster protein and the carbohydrate recognition domain (CRD) of MGL specifically binds GalNAc and glycoproteins which express the T_N–antigen such as MUC1.[29, 30, 31]

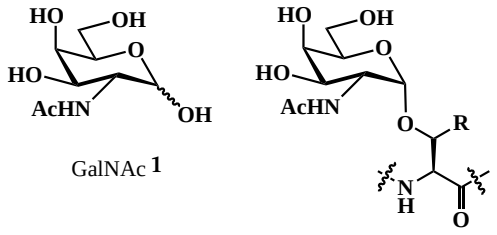

Figure 2.1: GalNAc and the T_N-antigen.

The synthetic tractability of the T_N antigen and its ease of incorporation into glycopeptides renders the MGL an obvious target for introducing antigens to the immune cascade. By designing a compound which links GalNAc residues to peptide epitope antigens, an immune response may be induced when the hybrid molecule is presented to dendritic cells (DCs) expressing MGL.[29, 105, 106] A single carbohydrate has a small binding affinity to a receptor, but a dramatic increase is observed when multiple sugar residues are present, presumably due to multivalent binding to the receptor, either by a clustering effect or simultaneous binding to constituent CRD sites of the receptor.[107, 108]

2.1 The design of a dendrimer

The distance between the three CRD domains of MGL is unknown. Therefore, we envisaged designing a series of mini-dendrimeric structures with three branchs containing GalNAc moieties in order to achieve optimal binding to MGL. A dendrimer is a branched macromolecule with precise shape and size that extends out from a central core, and is commonly used as a multi–dentate ligand.[109, 82] The general design of the dendrimer is depicted in Figure 2.2.

The dendrimer used in the present research will consist of a common core which then branches into X, Y and Z chains. The core is made up of lysine residues due to its branched structure and its ease of assembly via solid phase peptide synthesis (SPPS). SPPS is also used for the synthesis of the X, Y and Z chains.[i] These chains include spacer units to control the length of the chains and a triazole linker was chosen to attach the GalNAc residues to the end of each chain for binding to the CRDs of MGL. An antigen cargo can be attached to the core and this cargo would be transferred across the membrane when MGL internalises the dendrimer. A fluorophore can also be installed instead of the antigen cargo at the same site in order to facilitate biological studies.

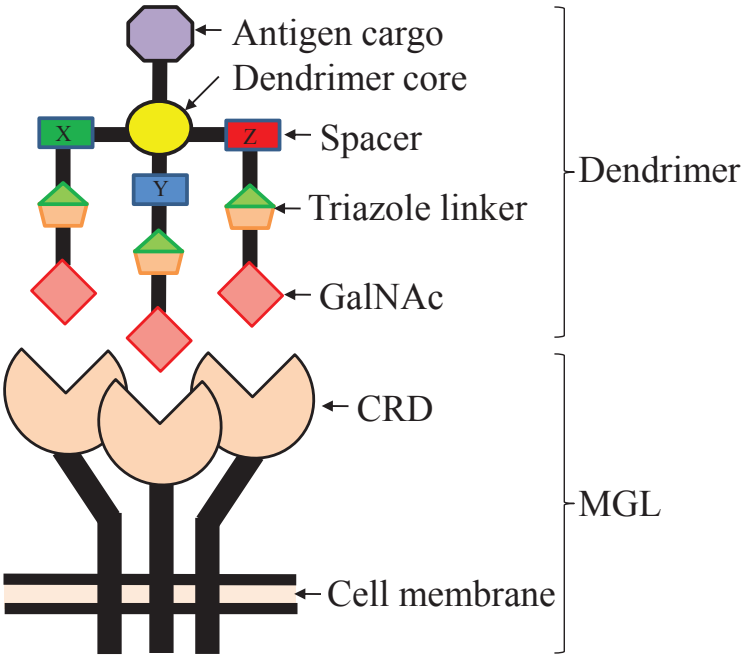

Figure 2.2: A schematic diagram of a dendrimer binding to the carbohydrate recognition domains (CRD) of MGL.

The spacer unit chosen for the dendrimers was mini-PEG (8-amino-3,6-dioxaoctanoic acid), a popular solubilising linker that can be incorporated in peptide synthesis (structure shown later in Scheme 2.2)[85]. Mini–PEG has a defined length, is water soluble and has an adaptable

[i]For easy distinction in the schemes or figures, the X-chain will be in green, the Y-chain will be in blue and the Z-chain will be in red.

structure.[84] Mini–PEG can be used in multiple units in sequence, in order to adjust the desired chain length. The flexibility was essential to allow the freedom of movement of each chain and to increase the chance of the dendrimer to orientate itself correctly for binding to MGL.

2.2 Retrosynthesis of the dendrimer-glycan

The retrosynthesis of the dendrimers **2** and **3** is shown in Scheme 2.1. The first step of the retrosynthesis is the disconnection of α–propargyl GalNAc **4** from the dendrimer to give azido dendrimer scaffold **5**. This late stage glycosylation with α–propargyl GalNAc **4** would avoid the compromising the chiral integrity of the GalNAc, which is important for selective binding. Cu(I)–catalysed Huisgen azide–alkyne cycloaddition (CuAAC or simply referred as a "click" reaction),[56, 57] is specific, mild, high yielding and the resulting triazole linker is stable towards enzymatic degradation, oxidation and reducing conditions.[59] The CuAAC is an ideal reaction for conjugating the GalNAc residues to the dendrimer scaffolds.[57] α-Propargyl GalNAc **4** can be synthesised in four steps from commercially available galactosamine hydrochloride **6**.[110]

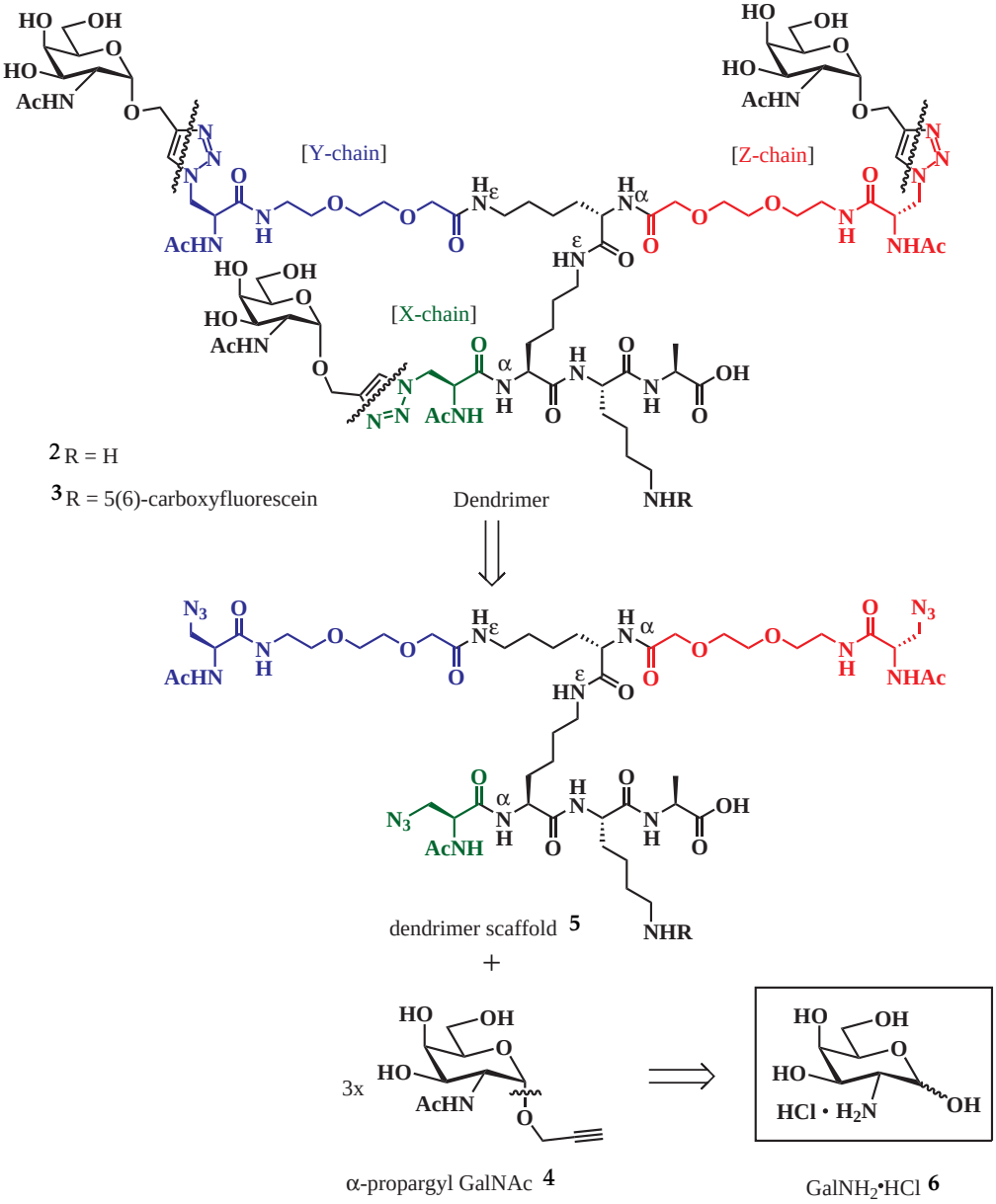

Scheme 2.1: Retrosynthesis of dendrimer **2** and **3** to dendrimer scaffold **5** and the carbohydrate.

As mentioned in section 2.1, the dendrimer scaffold consists of three chains which branch out from a common poly-lysine core and will be synthesised by SPPS (Scheme 2.2). In order to adjust the spatial arrangement of the GalNAc residues, flexible mini–PEG spacers are positioned at intervals to vary the chain length and thus vary the distance between the terminal GalNAc residues and bridge the gap between the CRDs.[111, 84, 112] The three chains of the dendrimers are referred to as the X chain, the Y chain and the Z chain. The X chain is the first chain to be synthesised and is connected to the N^{α} group of the middle lysine in the poly–lysine core. The Y and Z chains are connected to the same lysine residue, with the Y chain connected to the N^{ϵ} group and the Z chain connected to the N^{α} group of the lysine. The final branch of the dendrimer to be derivatised is the lysine closest to the C terminus, the R group will either contain an unprotected amine or the fluorophore

5(6)–carboxyfluorescein depending on the assay in which it will be tested.

The retrosynthesis of azido dendrimer scaffold **5** hinges on disconnection of the mini-PEG spacer and Fmoc–azidoalanine to reveal the poly–lysine core **7**. The poly–lysine core **7** in turn is synthesised from three lysine units and the core is connected to the polystyrene resin via an alanine and HMPP linker **8**.

Fmoc–azidoalanine **9** provides the azide handles required for the CuAAc reaction and is synthesised from commercially available N^{α}–Fmoc–diaminopropionic acid **10** via a diazo–transfer reaction.

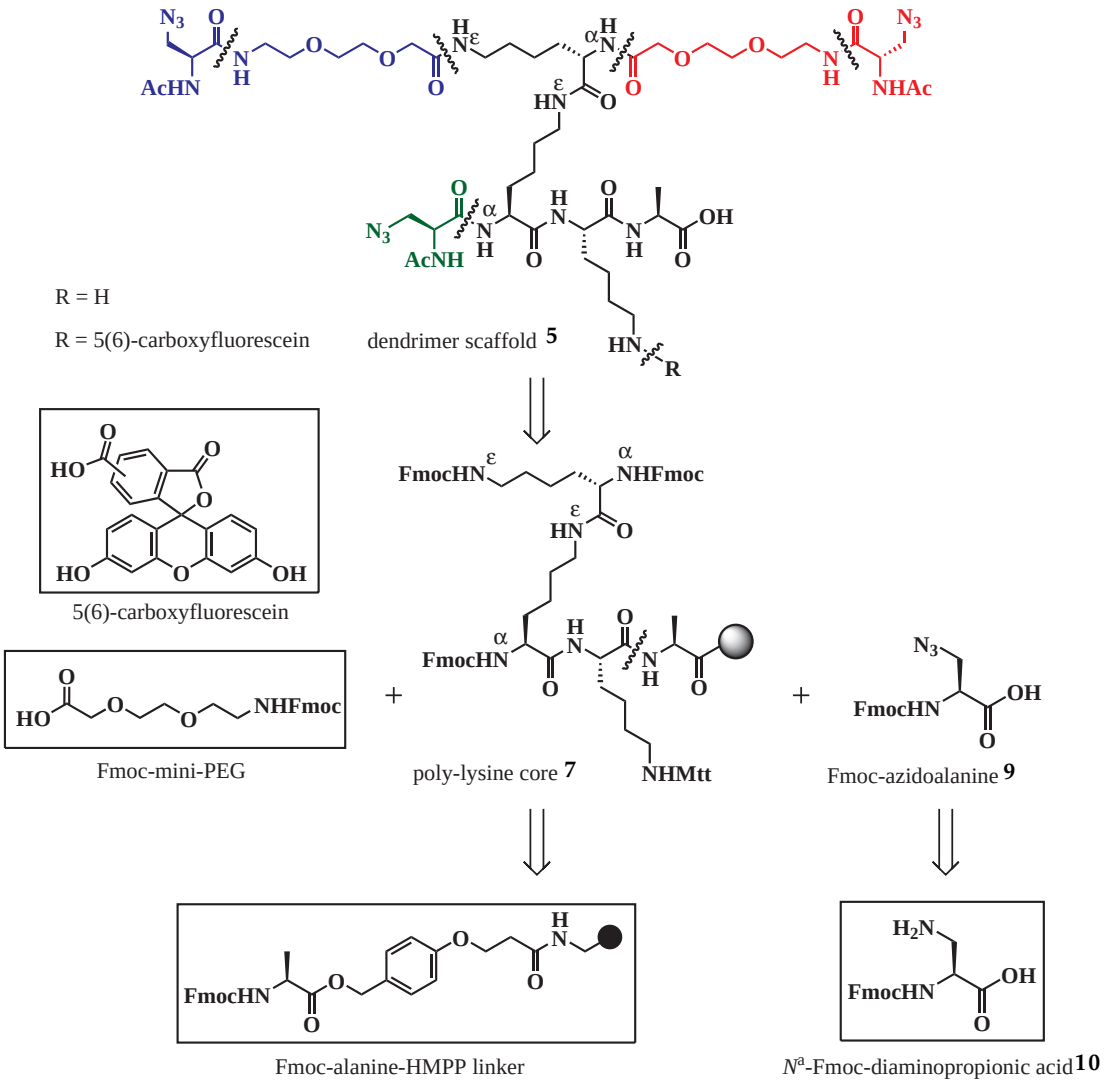

Scheme 2.2: Retrosynthesis of dendrimer scaffold **5** to commercially available starting materials.

2.3 Synthesis of building blocks: Fmoc–azidoalanine and α–propargyl GalNAc(Ac)$_3$

2.3.1 Synthesis of Fmoc–azidoalanine

Fmoc–azidoalanine **9** was synthesised from commercially available N^{α} Fmoc–diaminopropionic acid and diazo–transfer reagent based on the previous work carried out in the Brimble group.[110] Azidoalanine **9** was seen as a safer alternative than propylglycine, as the latter amino acid has been shown to effect the cardiac muscle and be responsible for Yunnan Sudden Unexplained Death.[113]

The diazo–transfer reaction retains the original stereochemistry of the starting material while installing the azide functional group at the amine position.[114] Most azide–containing reagents are inherently explosive. For example, trifluoromethanesulfonyl azide is a highly explosive reagent which is also prepared from highly toxic starting materials (sodium azide and trifluoromethanesulfonic anhydride). Other similar diazo–transfer reagents include azidotrimethylsilane, tosylazide and imidazole–1–sulfonyl azide.[115]

Stick *et al*. reported a shelf stable diazo–transfer reagent[ii] imidazole–1–sulfonyl azide hydrochloride **11** which was suitable for the conversions of amines to azides under mild conditions.[118] Stick's diazo–transfer reagent was originally reported to be more stable and less explosive than neat trifluoromethanesulfonyl azide and it is also a crystalline solid which renders it easy to handle. The synthesis of imidazole-1-sulfonyl azide hydrochloride began with the reaction of sodium azide with sulfuryl chloride to afford azide **12** (Scheme 2.3), which was then reacted with imidazole to form the active diazo–transfer reagent **13**. The reagent was converted to its shelf stable salt form upon reaction with hydrochloric acid generated *in situ*.

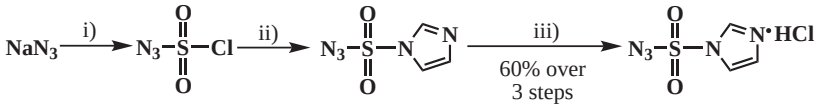

12 **13** **11**

Reagents and conditions: (i) SO_2Cl_2, MeCN; (ii) imidazole, MeCN; (iii) AcCl, EtOH.

Scheme 2.3: The synthesis of the diazo–transfer reagent imidazole-1-sulfonyl azide hydrochloride **11**.[118]

[ii] It was reported that Stick's diazo–transfer reagent may not be stable and may be explosive if heated above 112 °C or after a strong impact.[116, 117] However, our observations to date have suggested that this reagent is "shelf stable" (2010-2014) when kept below 4 °C.

Fmoc–azidoalanine **9** was synthesised in one step in over 90% yield by reacting N^{α} Fmoc–diaminopropionic acid with diazo–transfer reagent **11** (Scheme 2.4).[110, 119, 118] Initially, the yields obtained for this diazo–transfer reaction were only 70%. The yield was increased substantially by the addition of EDTA to the work–up mixtures in order to form a complex with the copper species, thereby reducing degradation of the desired Fmoc–azidoalanine **9**.

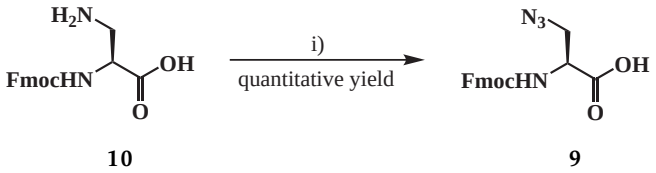

10 **9**

Reagents and conditions: (i) imidazole-1-sulfonyl azide hydrochloride, $CuSO_4$, K_2CO_3, MeOH, H_2O.

Scheme 2.4: Diazo–transfer reaction to give Fmoc–azidoalanine **9**.[110]

2.3.2 Synthesis of α–propargyl GalNAc(Ac)$_3$

The building block α–propargyl GalNAc(Ac)$_3$ **14** is a key intermediate required to effect the glycosylation of the dendrimer scaffolds. The Cu(I)-catalysed Huisgen azide–alkyne cycloaddition (CuAAC) was used to effect the glycosylation of the dendrimers with α–propargyl GalNAc(Ac)$_3$ **14a**. Synthesis of α–propargyl GalNAc(Ac)$_3$ **14a** has been reported twice in the literature. The original synthesis was reported by Brimble *et al.* (Scheme 2.5)[110] and the second synthesis was reported by Sewald *et al.* (Scheme 2.6).[120]

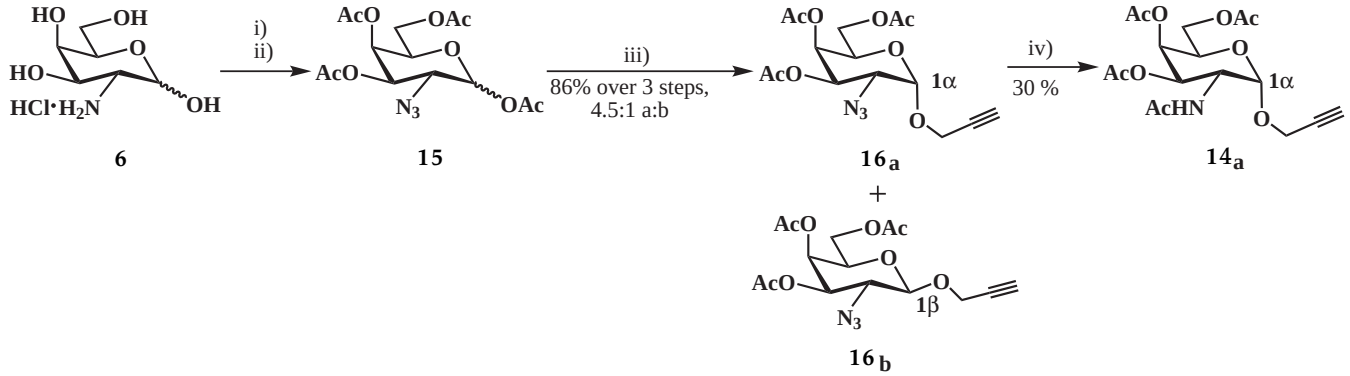

6 **15** **16$_a$** **14$_a$** **16$_b$**

Reagents and conditions: (i) imidazole-1-sulfonyl azide hydrochloride, $CuSO_4$, K_2CO_3, MeOH, H_2O, 3 h; (ii) pyridine, Ac_2O, <40 ºC, 18 h; (iii) propargyl alcohol, $BF_3{\cdot}Et_2O$, CH_2Cl_2, 35 ºC, 7 h; (iv) a. Zn, AcOH; b. pyridine, Ac_2O.

Scheme 2.5: Synthesis of α–propargyl GalNAc(Ac)$_3$ **14a** by Brimble *et al.*[110]

The synthesis of α–propargyl GalNAc(Ac)$_3$ **14a** reported by Brimble *et al.* (Scheme 2.5) started with commercially available galactosamine hydrochloride **6** which was subjected to a diazo–transfer reaction followed by acetylation to afford the inseperable glycosyl acetates **15**.[118] Propargyl alcohol was then glycosylated with glycosyl acetate **15** to afford azido glycosides **16a** and **16b**. Reductive acetylation of α–anomer **16a** using zinc in acetic acid of followed by acetylation afforded α–propargyl GalNAc(Ac)$_3$ **14a** in 21% yield over three steps. The low yielding reductive acetylation of azido glycosides **16a** is the major drawback of this synthetic route.

The synthesis of α–propargyl GalNAc(Ac)$_3$ **14a** reported by Sewald *et al.*[120] employed glycosyl chloride **17** as the glycosyl donor to effect the glycosylation of propargyl alcohol catalysed by silver (Scheme 2.6). α–Azido glycoside **16a** was the major product with an α:β ratio of 5:1. The major α–azido glycoside **16a** then underwent reductive acetylation using thioacetic acid and pyridine to produce α–propargyl GalNAc(Ac)$_3$ **14a** in 17.5% over two steps. Sewald's route proceeded with better anomeric selectivity than the synthesis reported by Brimble *et al.* although the overall of azido glycoside **16a** and **16b** yield was lower.

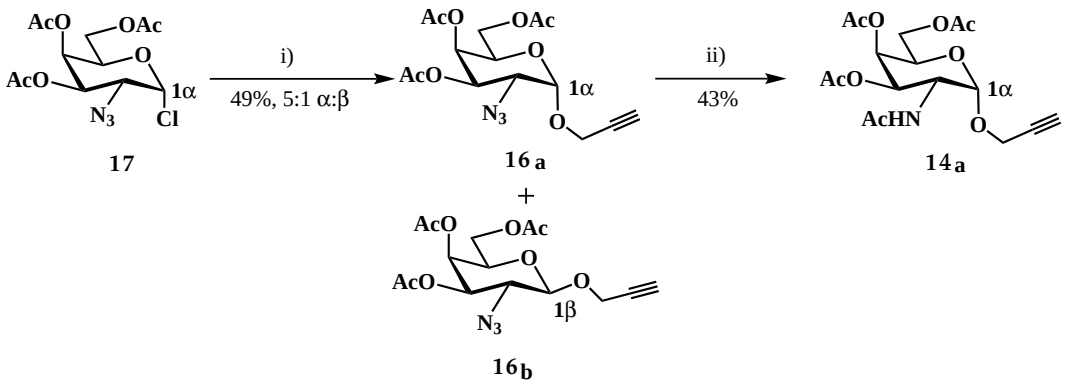

Reagents and conditions: (i) propargyl alcohol, Ag_2CO_3, $AgClO_4$, CH_2Cl_2/toluene (1:1), 40 h; (ii) AcSH/pyridine (2:1), toluene, 50 ºC, 30 min.

Scheme 2.6: Synthesis of α–propargyl GalNAc(Ac)$_3$ **14a** by Sewald *et al.*[120]

Aiming to obtain a higher yield of α-propargyl GalNAc(Ac)$_3$ in the current work, a modified version of the Brimble synthesis was investigated using a more efficient reductive acetylation (Scheme 2.9).

The original synthesis of glycosyl acetate **15** described by Yan *et al.*[114] used TfN_3 to install the azide at the C2 position, followed by acetylation to give an overall yield of 94%. Subsequently Stick *et al.* synthesised the same glycosyl acetate **15** using the "safer" diazo–transfer reagent imidazole-1-sulfonyl azide hydrochloride **11** and achieved a comparable yield of 87%.[118] Unfortunately when Stick's synthesis was repeated in the present work, only 40-50% yield of glycosyl acetate **15** was obtained. It was postulated that the excess copper in the reaction mixture degraded the glycosyl

azide product during work–up resulting in a lower yield. This theory was supported when EDTA was added to the work–up mixture to sequester any copper ions resulting in an improved 81% yield (Scheme 2.7).

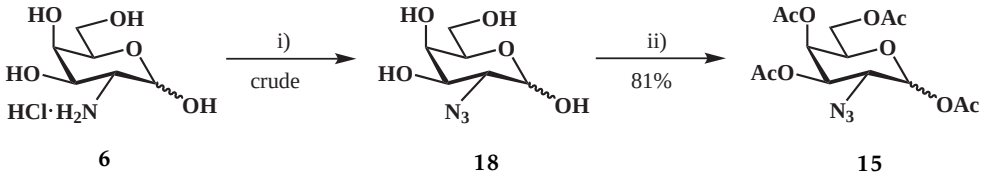

6 **18** **15**

Reagents and conditions: (i) a. imidazole-1-sulfonyl azide hydrochloride, Na_2CO_3, $CuSO_4$, H_2O, MeOH, b. 3 h then EDTA·4Na; (ii) pyridine, Ac_2O, < 40 ºC, overnight.

Scheme 2.7: Diazo-transfer reaction performed on galactosamine hydrochloride **6** followed by acetylation.[118]

The crude azido sugar **18** was subsequently acetylated following the procedure reported by Stick *et al*.[118] affording a relatively poor recovery of glycosyl acetate **15**. Because the addition of acetic anhydride to pyridine was exothermic, it was proposed that the elevated temperature caused degradation of the product. By carefully controlling the reaction temperature during the addition of acetic anhydride to below 40 °C, an improved yield of 81% of glycosyl acetate **15** was afforded even when the reaction was performed on a large scale (>20 g) (Scheme 2.7).

The key step in the synthesis of α–propargyl GalNAc$(Ac)_3$ is the glycosylation of propargyl alcohol. Since only the α anomer **16a** is required, it is important to consider the influence of the neighbouring group at C2 on the resulting stereochemistry at C1. The *N*-acetyl group in **19** affects the approach of the incoming nucleophile by the formation of intermediate **20** during the glycosylation step (Scheme 2.8).[121, 122, 123] Use of a non-participating protecting group such as an azide makes it possible to synthesise predominately azido glycoside **16a**, under the direction of anomeric effect. The diastereomeric mixture of anomers of azido glycoside **16** can then be separated by flash chromatography.

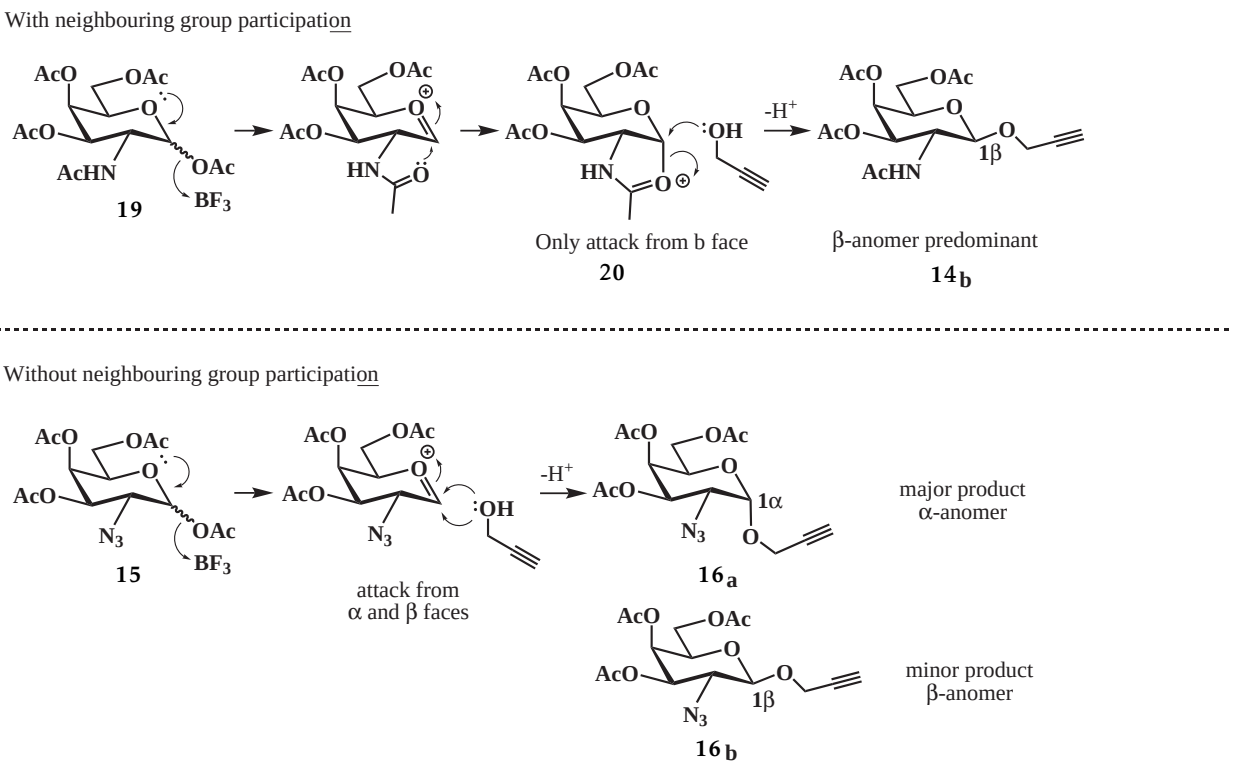

Scheme 2.8: An illustration of how functional groups at the C2 position affect the stereochemistry of azido glycosides **16a** and **16b** and α–propargyl GalNAc(Ac)$_3$ **14b**.

Using an alternative reductive acetylation to that previously reported by Brimble *et al.*[124], the mixture of azides was treated with zinc, water, acetic acid, acetic anhydride and THF with catalytic copper sulphate resulting in dramatic increase in the yield of propargyl GalNAc(Ac)$_3$ **14a** and **14b** obtained (96%, 1.6:1 α:β) (Scheme 2.9).[120] While the anomeric selectivity for the glycosylation of propargyl alcohol was lower than the synthesis reported by Sewald *et al*,[120] an increased yield at each step established for this route afforded a higher yielding synthesis overall. The final yield of α–propargyl GalNAc(Ac)$_3$ **14a** was increased to 43% over three steps from starting material **6**. The selectivity and overall yield of glycosylation the three routes to α–propargyl GalNAc(Ac)$_3$ **14a** are summarised in Table 2.1.

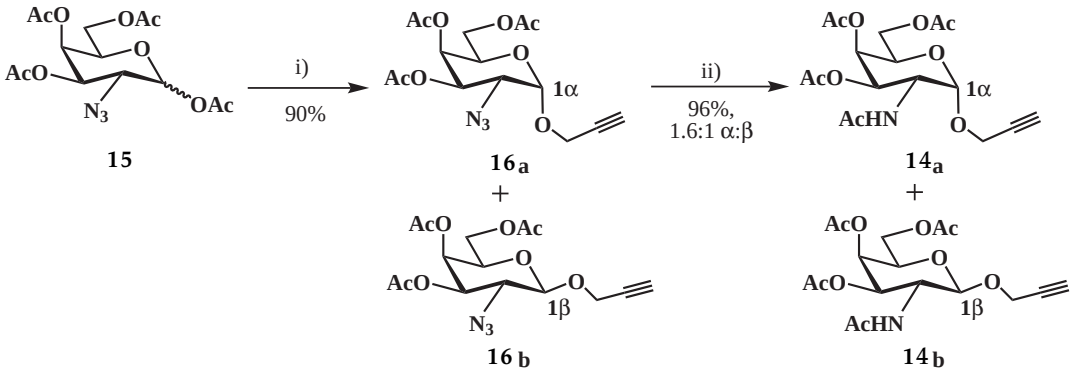

Reagents and conditions: (i) propargyl alcohol, $BF_3{\cdot}Et_2O$, CH_2Cl_2, 35 °C, 18 h; (ii) Zn, $CuSO_4$, H_2O, THF, AcOH, Ac_2O, 1 h.

Scheme 2.9: The current improved synthesis of α–propargyl GalNAc$(Ac)_3$ anomers **14a** and **b**.

Table 2.1: Comparison of synthetic routes to α–propargyl GalNAc$(Ac)_3$

Route	# of Steps	Anomeric selectivity	Yield of anomeric step	Overall yield
Brimble *et al.*[110] original synthesis	4	4.5:1	86% (α 70%)	21%
Sewald *et al.*[120] original synthesis	2	5:1	49% (α 41%)	17.5%
Brimble *et al.* improved synthesis	4	1.6:1	90% (α 55%)	43%

2.4 Synthesis of the generation I dendrimers

The aim of the current research was to generate dendrimers with different chain lengths assembled from a poly–lysine core to specifically target the MGL receptor. The distance between binding sites was predicted by Dr Chris Squire to be between 50 and 60 angstroms, dendrimers were designed on the assumption that they would bind to one MGL homotrimer and would bridge the CRD Figure 2.3. The structural elements used are depicted in Figure 2.4 and the combination of structural elements for the generation I dendrimers are shown in Table 2.2. The dendrimers included a poly–lysine core (coloured black in Figure 2.4) from which three chains branched out (depicted in Figure 2.4 with X chain in green, Y chain in blue and Z chain in red). Each structure was generated as a set of two compounds with R = H for the thermal melt assay and R = 5(6)-carboxyfluorescein for the cell binding assay. The generation I dendrimers were designed to find the optimum chain length between the GalNAc residues. In order to vary the length between the GalNAc residues, the spacer unit mini-PEG was incorporated.

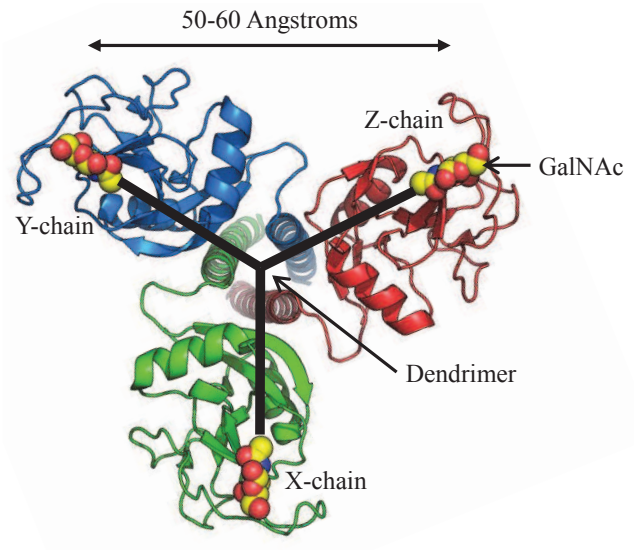

Figure 2.3: A schematic diagram of a dendrimer binding to the model of the carbohydrate recognition domains (CRD) of the 1fih homotrimer which has a similar structure to the MGL homotrimer.

The 'reach' of the dendrimer is dictated by the number of mini–PEG spacer units which are grafted on to the poly–lysine core residues. Four dendrimers were created with increasing distances between the GalNAc residues. This generation I dendrimers incorporated up to six mini–PEG spacer units in total per dendrimer. No individual chain had more than two mini–PEG spacers. The distribution of mini–PEG spacers are designed to have a range of distances which don't overlap between the GalNAc residues at the terminus of each of the X, Y and Z chains.

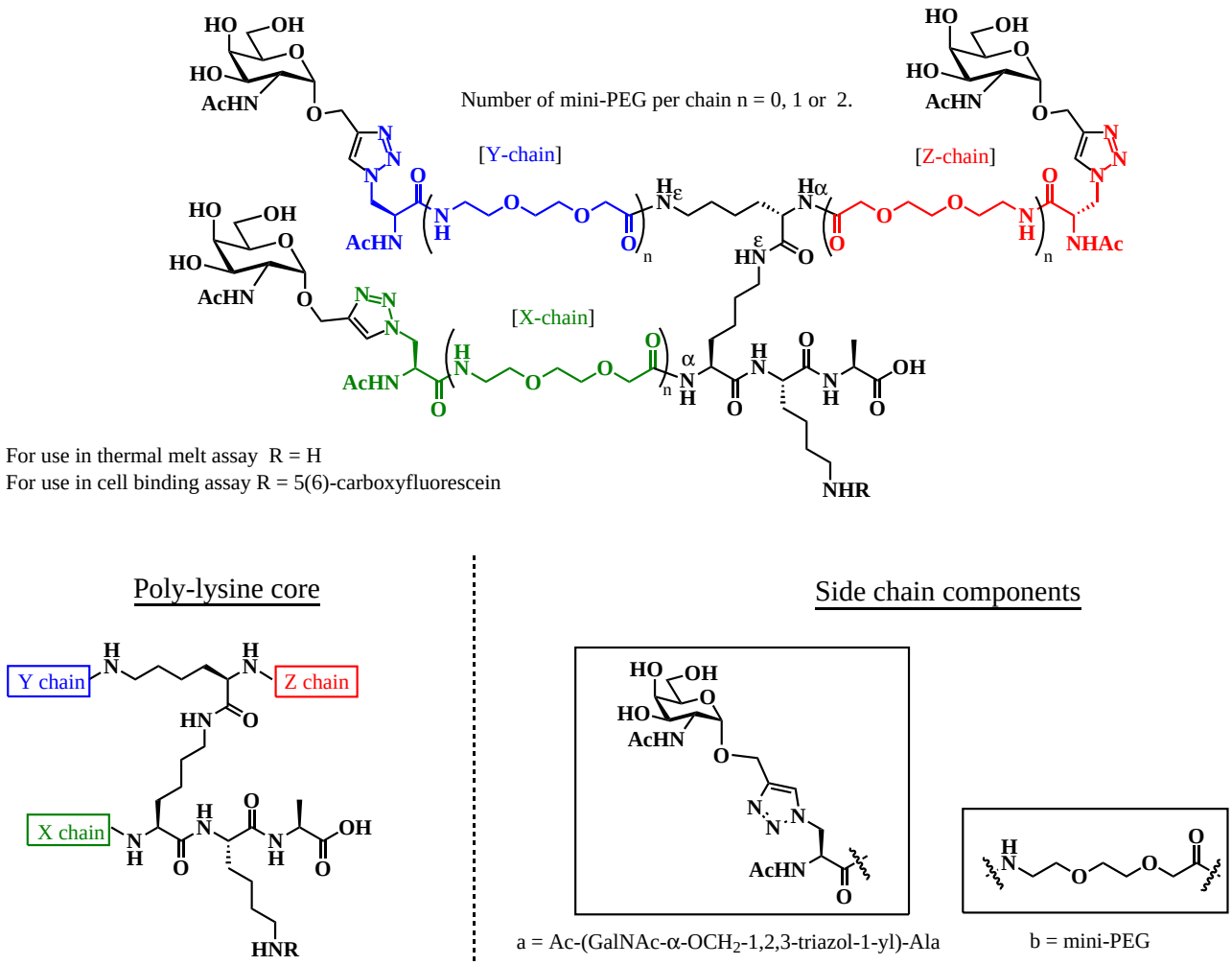

Figure 2.4: Basic structure of the generation I dendrimers.

Table 2.2: The combination of structural elements used for the generation I dendrimers.

Entry	R = H	R = 5(6)-Carboxyfluorescein	X	Y	Z
1	Dendrimer **21**	Dendrimer 22	a-	a-	a-
2	Dendrimer 2	Dendrimer **3**	a-	a-b-	a-b-
3	Dendrimer **23**	Dendrimer **24**	a-b-	a-b-b-	a-b-
4	Dendrimer **25**	Dendrimer **26**	a-b-b-	a-b-b-	a-b-b-

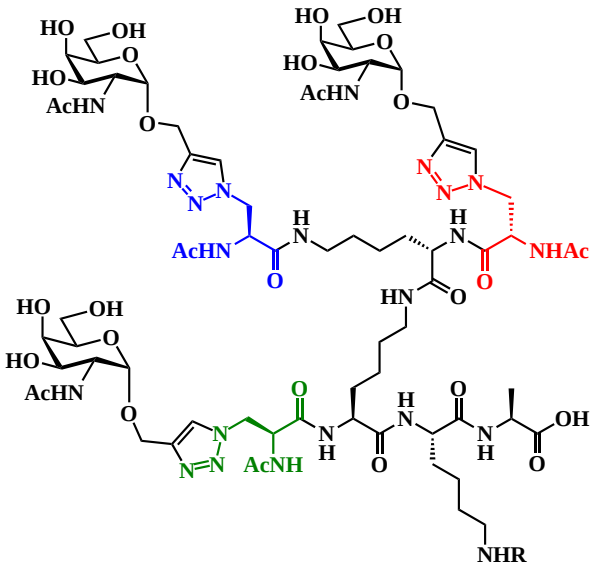

21 R = H

22 R = 5(6)-carboxyfluorescein

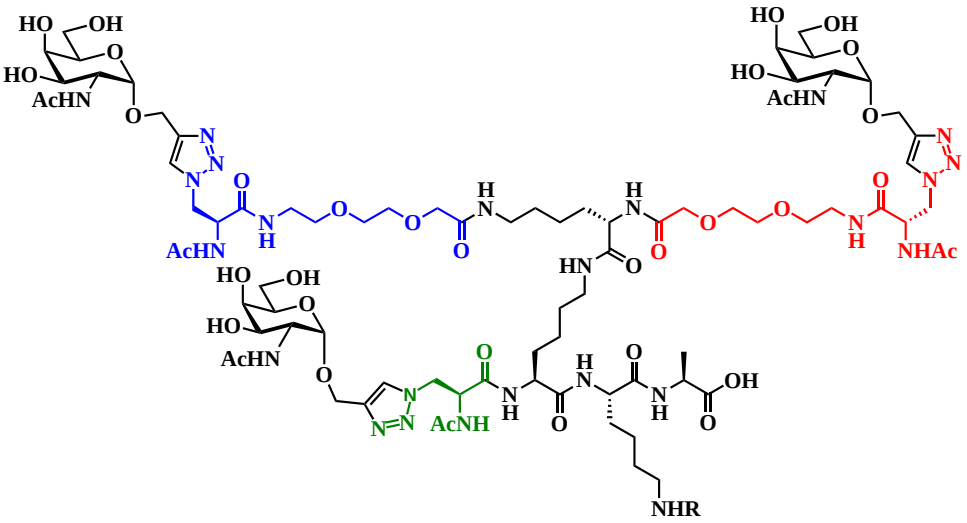

2 R = H

3 R = 5(6)-carboxyfluorescein

Figure 2.5: The structures of dendrimers **2**, **3**, **21** and **22**.

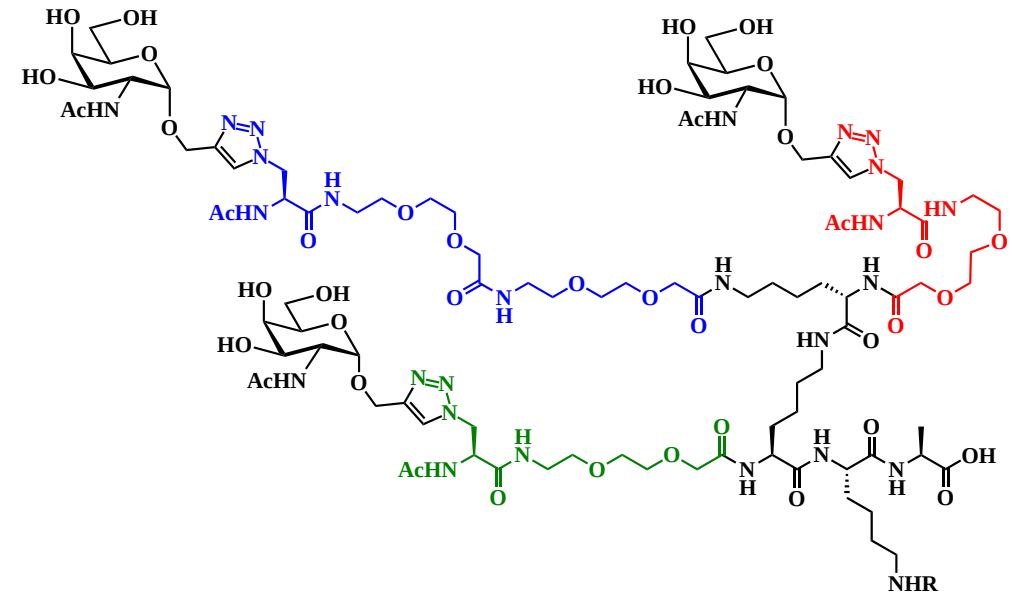

23 R = H

24 R = 5(6)-carboxyfluorescein

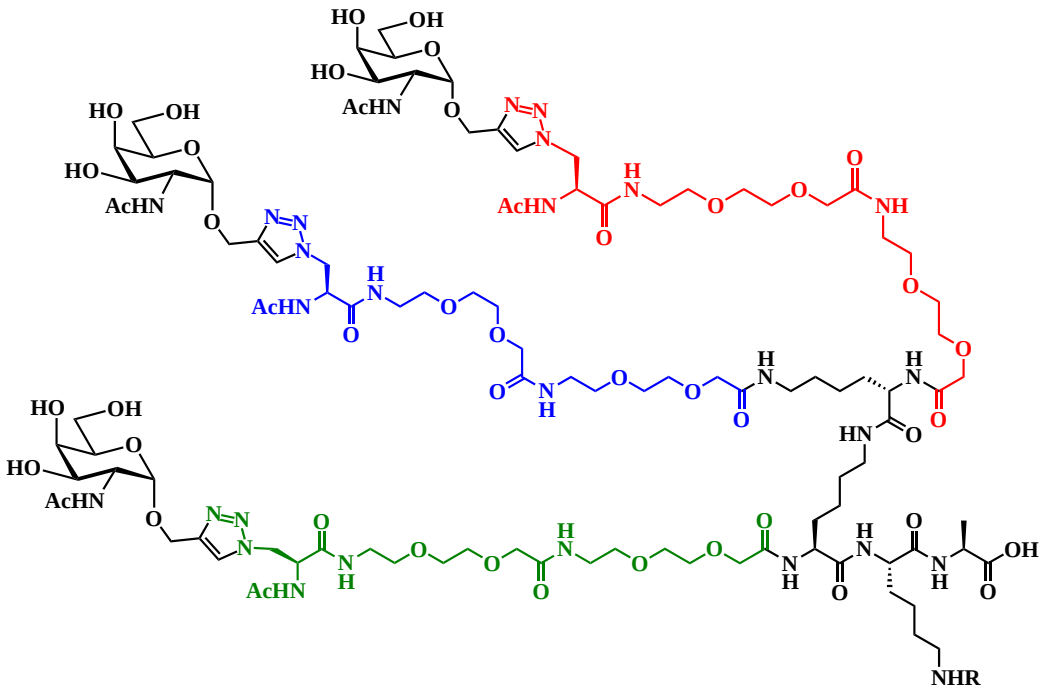

25 R = H

26 R = 5(6)-carboxyfluorescein

Figure 2.6: The structures of dendrimers **23**, **24**, **25** and **26**.

With the target dendrimer structures chosen, a detailed synthetic route was designed. The synthesis of dendrimers **21** and **22** is depicted in Scheme 2.14. The following sections will initially focus on the synthesis of the dendrimer scaffold.

The retrosynthesis of dendrimers **2** and **3** was previously discussed in detail (Scheme 2.1 Section 2.2). The retrosynthesis of dendrimers **21** and **22** is shown in Scheme 2.10. The retrosynthesis started with the disconnection of α–propargyl GalNAc **4** from the dendrimer to give azido dendrimer scaffold **27**. The CuAAC reaction was used to conjugate α–propargyl GalNAc **4** to azidoalanines located at the terminus of the X, Y and Z chains.

Disconnection of azido dendrimer scaffold **27** generates the common poly–lysine core **28** which is used to synthesise all the dendrimers in the current study. The Y and Z chains are connected to the third lysine residue of the core, with the Y chain connected to the N^{ϵ} group and the Z chain connected to the N^{α} group. The final branch of the dendrimer to be derivatised is the first lysine residue, in that the R group will either contain an unprotected amine or the fluorophore 5(6)-carboxyfluorescein depending on the nature of the lectin binding assay to be conducted. The C–terminal carboxylic acid group of the dendrimer will be generated when the dendrimer scaffold is cleaved from the resin.

Poly-lysine core **28** is an important scaffold common to all of the dendrimers, in that it provides the structure necessary for branching. Disconnection of Fmoc–Lys(Fmoc) reveals the initial linear peptide **7** which contains the X chain. Further disconection of the X chain peptide **7** gives the aminomethyl polystyrene resin loaded with commercially available hydroxymethylphenoxypropionic acid (HMPP) linker bearing the first amino acid Fmoc–alanine **8**.

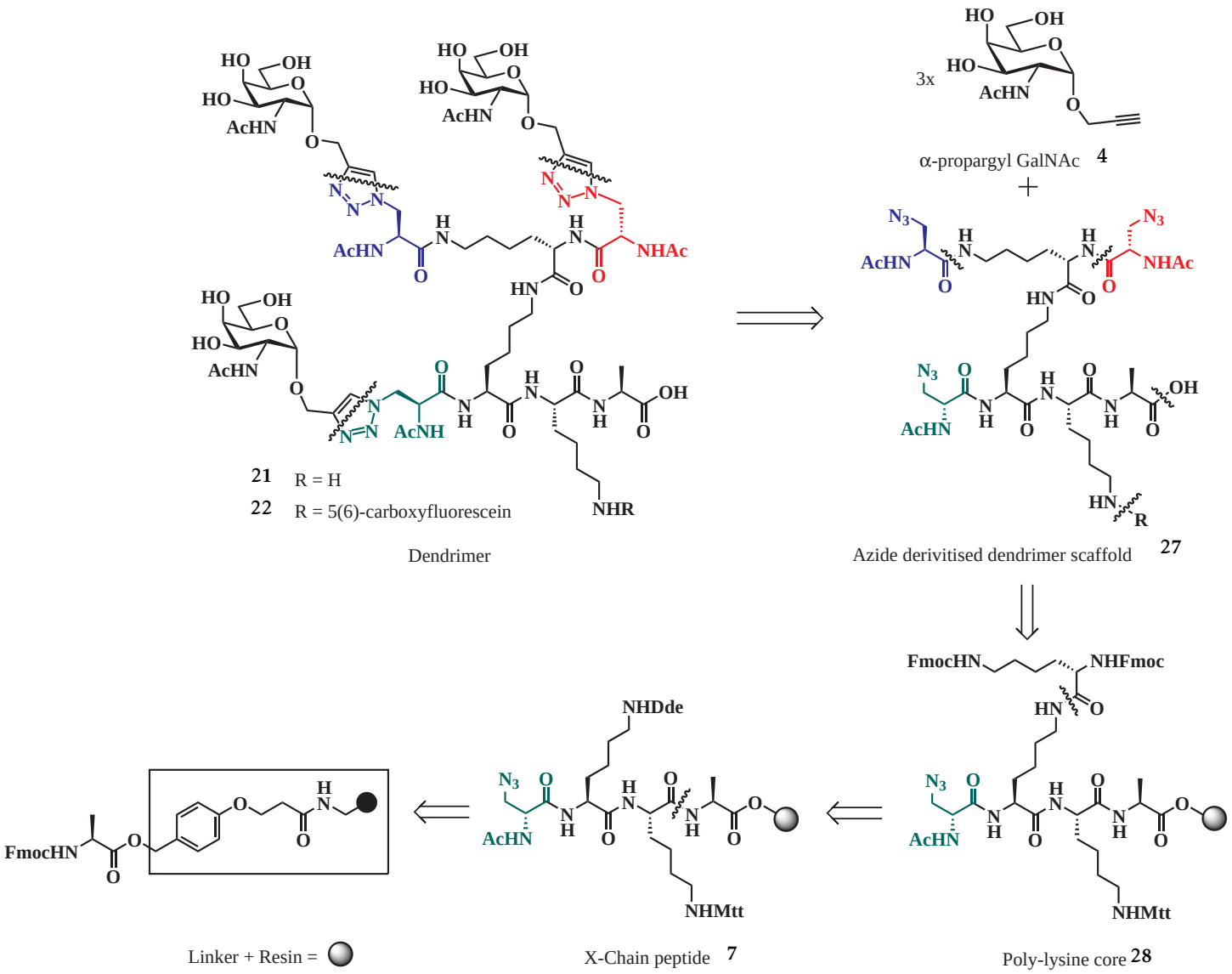

Scheme 2.10: Retrosynthesis of the generation I dendrimers **21** and 22.

2.4.1 Nature of the resin and linker

Solid phase peptide synthesis (SPPS) was used to execute the synthesis of the dendrimer and polystyrene (PS) was chosen as the solid phase due to its inertness to the solvents and chemicals used for the Fmoc peptide synthesis. Commercially available PS resin was prepared via free radical polymerisation between styrene and divinylbenzene as shown in Scheme 1.13.[125] The PS resin was then functionalised with an aminomethyl group by direct aminomethylation.[126] The polymeric chains of the resin have good solvation and swelling properties in DMF and dichloromethane, and they enabled efficient diffusion of reagents to the attached peptide chains. Aggregation of peptides was reduced by the divinylbenzene crosslinks of the polystyrene resin, allowing more efficient solvation of peptides resulting in higher yields after each coupling reaction.[127] With the resin ready for SPPS, the next stage was to couple a cleavable linker on to the resin.

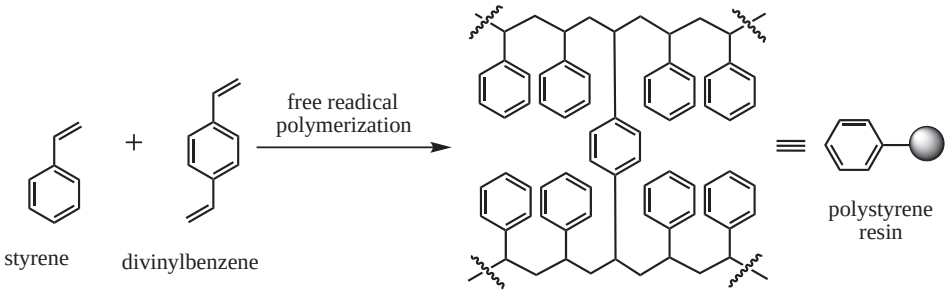

Scheme 2.11: The polystyrene resin.

Commercially available hydroxymethylphenoxypropionic acid (HMPP) linker bearing the first amino acid Fmoc–Ala, was coupled to the PS resin using DIC in dichloromethane to give **8** (Scheme 1.14). The HMPP linker was used due to its stability towards basic and nucleophilic conditions that are commonly used throughout the course of the dendrimer synthesis. The HMPP linker can be cleaved from the PS resin using a strong acid affording a peptide with a *C*–terminal acid.

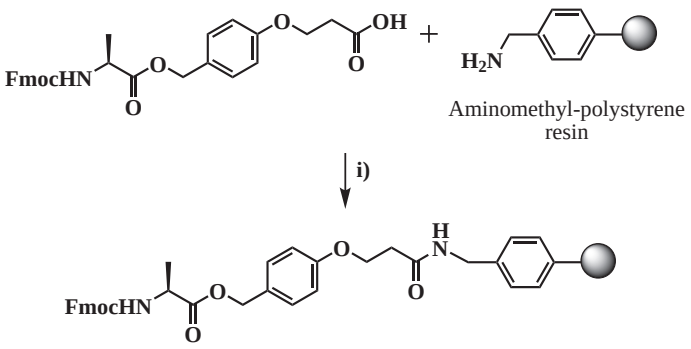

Reagents and conditions: (i) DIC, CH_2Cl_2, 2 h.

Scheme 2.12: Attachment of the HMPP linker bearing the first amino acid Fmoc–Ala to the aminomethyl polystyrene resin.

2.4.2 Coupling reagents

The coupling reagents used throughout the synthesis of the dendrimers are shown in Figure 2.7. Initially, the uronium coupling reagent HBTU was used for coupling reactions, but the reactions did not go to completion as indicated by the Kaiser test.[128] Multiple cycles of coupling reactions were required for complete conversion to the desired product using HBTU. The coupling reactions went to completion more consistently when HCTU was used. The more active coupling agent HATU was also used when less equivalents of valuable amino acids were used.

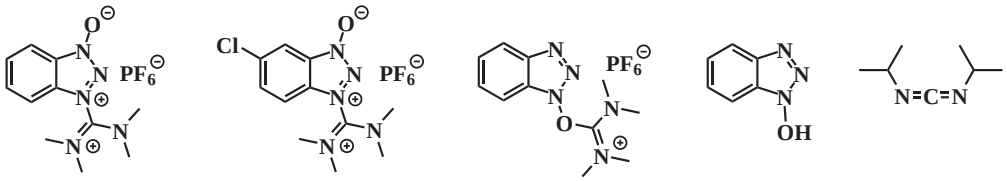

HBTU HCTU HATU HOBt DIC

Figure 2.7: The coupling reagents used throughout the synthesis of the dendrimers.

The fluorophore 5(6)–carboxyfluorescein was difficult to couple in a single reaction using the uronium salts HBTU or HCTU. Such coupling reactions readily form ester polymers while leaving some free amine groups as indicated by the Kaiser test.[128] Formation of the polymers was inevitable, and these are easily removed using 20% piperidine in DMF (Scheme 2.13). After many experiments, the best yield was achieved using excess 5(6)-carboxyfluorescein, DIC and HOBt. Under these conditions, the reaction consistently went to completion after one coupling when the reaction was monitored by the Kaiser test.[128]

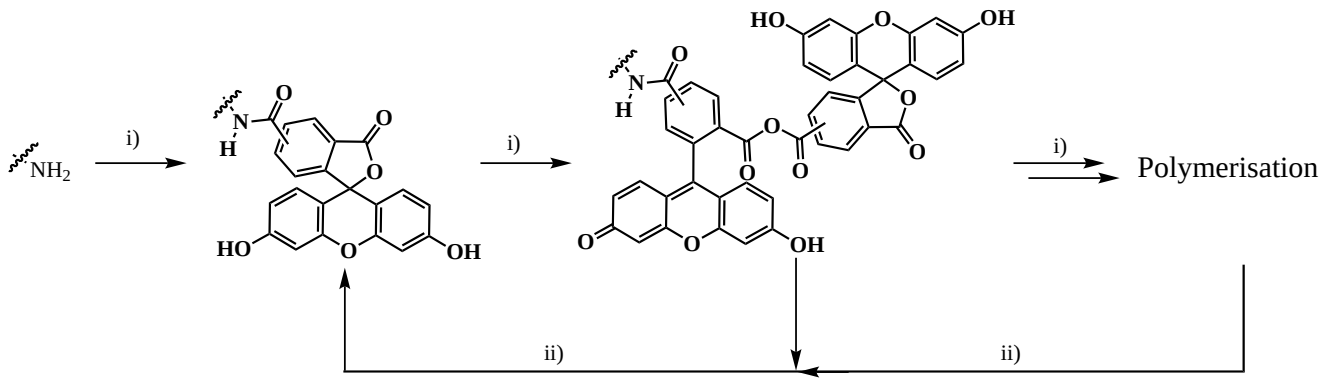

Reagents and conditions: (i) 5(6)–carboxyfluorescein, DIC, HoBT, DMF; (ii) piperidine, DMF.

Scheme 2.13: Coupling reaction of amine with excess 5(6)–carboxyfluorescein resulting the reaction going to completion, but also formation of carboxyfluorescein polymers. Destruction of polymers to produce monomeric 5(6)–carboxyfluorescein achieved by treating with piperidine in DMF.

2.4.3 Synthesis of the X chain

The synthesis of dendrimers **21** and **22** started with the coupling of HMPP linker bearing the first amino acid alanine to the resin to give **8** (Scheme 2.14). After Fmoc deprotection of the alanine, Fmoc–Lys(Mtt) was coupled to the chain to give peptide **29**, which contained the first lysine of the poly–lysine core and the potential site for fluorophore attachment. Fmoc–Lys(Dde) was then coupled to **29** to generate tripeptide **30**, which has the important side chain for branching. Fmoc–azidoalanine **9** was coupled to peptide **30** and subsequent acetylation capped the X chain to furnish peptide **7**.

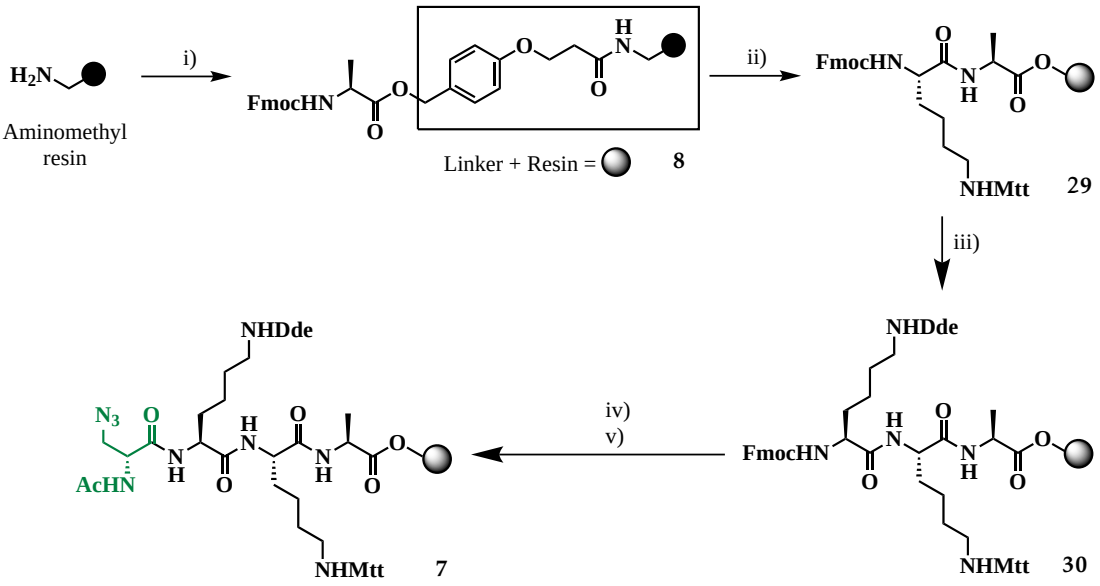

Reagents and conditions: (i) Fmoc–Ala–HMPP, DIC, CH_2Cl_2; (ii) a. 20% piperidine/DMF; b. Fmoc–Lys(Mtt)-OH, DIPEA, HCTU, DMF: (iii) a. 20% piperidine/DMF; b. Fmoc–Lys(Dde)-OH, HATU, DIPEA, DMF; (iv) a. 20% piperidine/DMF; b. Fmoc–Ala(N_3)-OH, HATU, DIPEA, DMF; (v) a. 20% piperidine/DMF; b. Ac_2O, DIPEA, DMF;

Scheme 2.14: Synthesis of X chain to afford intermediate peptide **7** in the synthesis of dendrimer **21** and **22**.

2.4.4 Protecting groups

The synthesis of the common poly–lysine core was designed to allow for independent chain growth and attachment of the fluorophore. In order to prevent uncontrolled side branch growth, selective protection of the side chain of poly–lysine core is essential. Specific protecting groups belonging to different classes were chosen so that they can be removed independently in any order, while not interfering with other functional groups. Two protecting groups, Mtt and Dde which can be cleaved in an orthogonal[iii] fashion to the Fmoc group were chosen for the synthesis of the dendrimer scaffolds (Figure 2.8).

The Mtt protecting group can be removed using acidic washes of 1% TFA in dichloromethane.[iv] The Mtt group was used to protect the lysine closest to the PS resin. For the batch destined for the thermal melt assay, the Mtt group of the lysine was removed at the same time as the peptide was cleaved from the resin which resulted in a free amine in the final product.

The Dde protecting group is orthogonal to both Fmoc and Mtt removal and it is cleaved under nucleophilic conditions.[130] The deprotection of Dde was carried out by the addition of 2% hydrazine in DMF for 5 min, and resulted in the formation of a free amino group on the peptide and 3,6,6-trimethyl-4-oxo-4,5,6,7-tetrahydro-1*H*-indazole.[131, 129] As Dde would not be removed by TFA, it was chosen as a suitable protecting group to control the chain growth during the synthesis of the X, Y and Z chains. All Dde groups must therefore be removed before the dendrimer scaffold is cleaved from the resin by TFA.

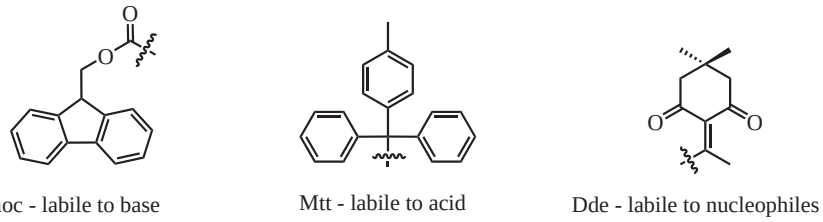

Figure 2.8: The three protecting groups Fmoc, Mtt and Dde used in the current synthesis.

[iii] Orthogonality, is the idea that two or more protecting groups belong to independent classes and are removed by distinct mechanisms.[129]

[iv] The Mtt cation was bright yellow when dissolved in dichloromethane, after repeated washes, a colourless solution indicated that the deprotection was complete.

2.4.5 Development of symmetrical Y and Z chains

With the X chain completed, the Dde protecting group of the side chain of **7** was removed and coupled to Fmoc–Lys(Fmoc) to give **28**, and both Y and Z chains were ready to be developed (Scheme 2.15). The Fmoc groups were simultaneously removed from peptide **28**, allowing the Y and Z chains to be grown in parallel with the coupling of Fmoc–azidoalanine **9**. Subsequent Fmoc deprotection and acetylation yielded azido dendrimer scaffold **27**.

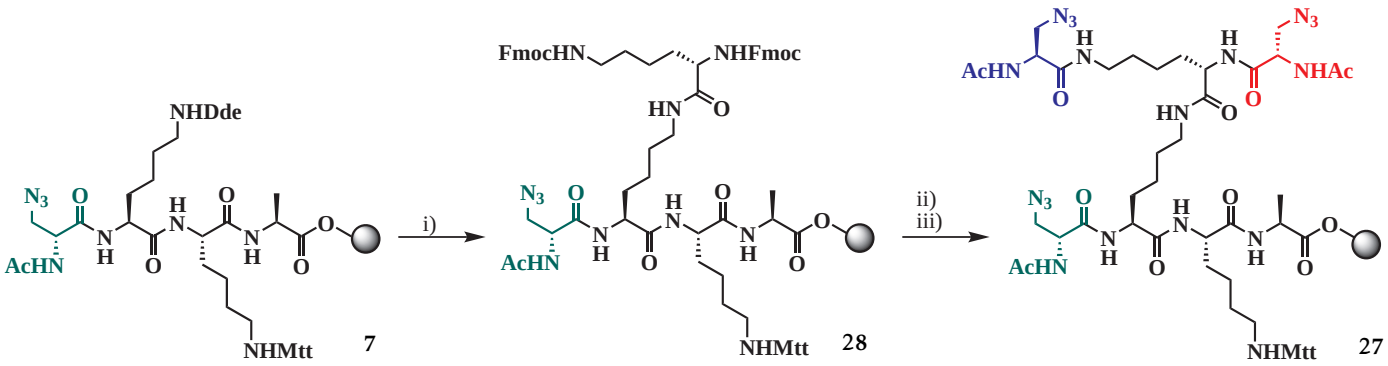

Reagents and conditions: (i) a. 2% N_2H_2/DMF; b. Fmoc–Lys(Fmoc)-OH, HCTU, DIPEA, DMF; (vi) a. 2% N_2H_2/DMF; b. Fmoc–Lys(Fmoc)-OH, HCTU, DIPEA, DMF; (ii) a. 20% piperidine/DMF; b. Fmoc–Ala(N_3)-OH, DIPEA, HATU, DMF; (iii) a. 20% piperidine/DMF; b. Ac_2O, DIPEA, DMF.

Scheme 2.15: Synthesis of the azido dendrimer scaffold **27**.

2.4.6 Dendrimers with unsymmetrical chains

Dendrimers **23** and **24** have unsymmetrical chains, and therefore a slightly different synthetic route was to the other generation I dendrimers was required to prepare them. The synthesis of these dendrimers requires a slightly modified route to the dendrimers mentioned previously in 2.4.5. As depicted in Scheme 2.16, the Dde protecting group was important to shape these scaffolds.

Elaborating from scaffold **30** that already been synthesised, the X chain of **30** was extended by coupling to Fmoc–mini-PEG. After subsequent coupling to Fmoc–azidoalanine **9** the X chain was capped with acetate to prevent further chain growth successfully affording **31**. The Dde group was removed with hydrazine allowing the Y and Z chains to be installed.

Fmoc–Lys(Dde) was installed on the N^{ϵ} group of the deprotected lysine to form branched core structure **32**. The two orthogonal protecting groups, Dde and Fmoc, allow the Y and Z chains to be grown independently. The Z chain was extended after removal of the Fmoc group and coupling to the mini-PEG spacer. The Fmoc group of mini-PEG was removed and Fmoc–azidoalanine **9** was coupled to the growing peptide chain. After the removal of the Fmoc group, the Z chain was capped with acetate to form **33**.

Having completed the construction of the Z chain, the Dde group was then removed and the Y chain was next installed. Two Fmoc-mini-PEG units were coupled sequentially to the Y chain. The final mini-PEG was deprotected followed by coupling of Fmoc–azidoalanine **9**. The Y chain was capped using acetic anhydride to give dendrimer scaffold **34**. From this point onwards the synthesis followed the same route as the synthesis of the dendrimers with symmetrical Y and Z chains.

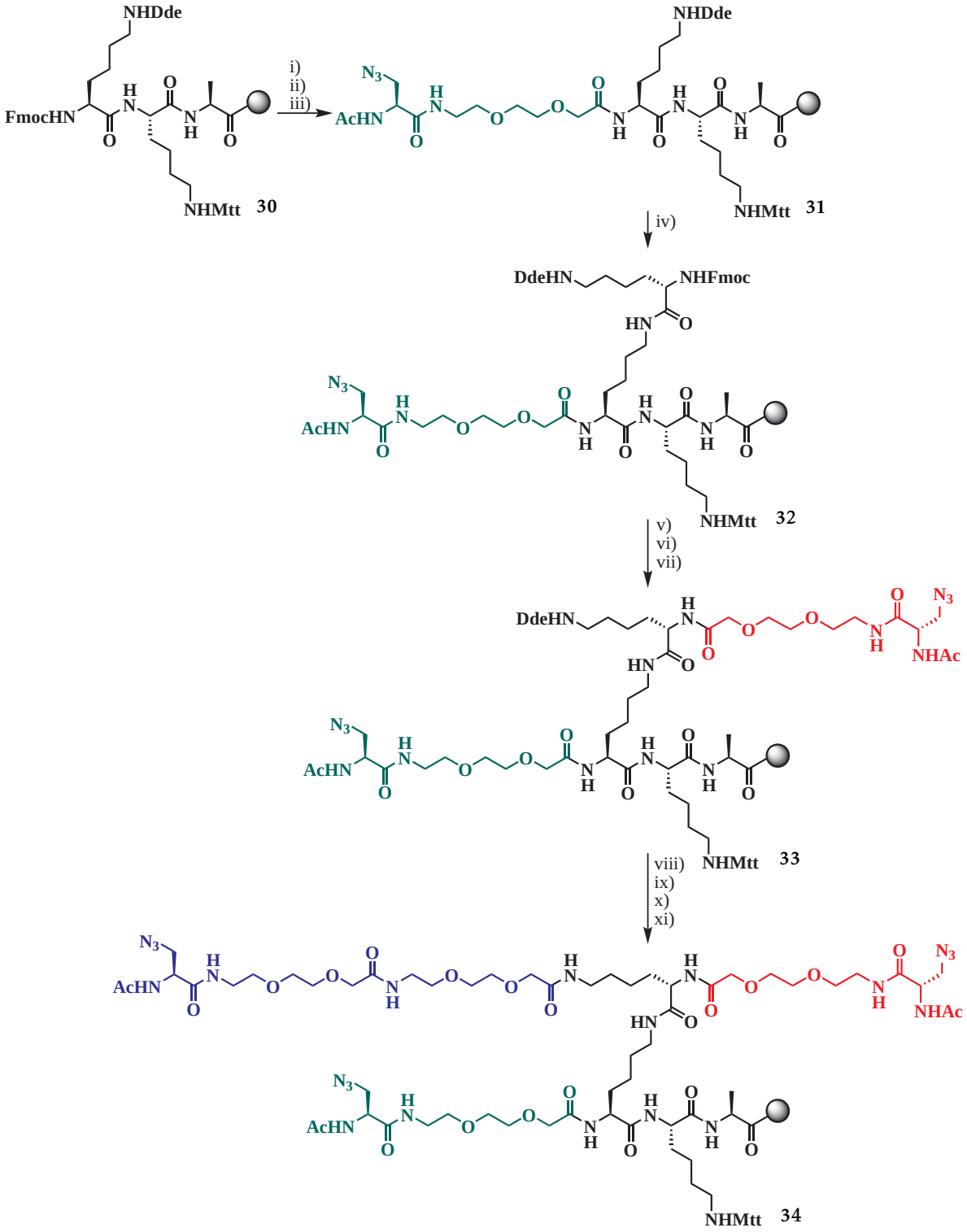

Reagents and conditions: (i) a. 20% piperidine/DMF; b. Fmoc–mini-PEG, HATU, DIPEA, DMF; (ii) a. 20% piperidine/DMF; b. Fmoc–Ala(N_3)-OH, HATU, DIPEA, DMF; (iii). a. 20% piperidine/DMF; b. Ac_2O, DIPEA, DMF; (iv) a. 2% N_2H_2/DMF; b. Fmoc–Lys(Dde)-OH, HATU, DIPEA, DMF; (v) a. 20% piperidine/DMF; b. Fmoc–mini-PEG, HATU, DIPEA, DMF; (vi) a. 20% piperidine/DMF; b. Fmoc–Ala(N_3)-OH, HATU, DIPEA, DMF; (vii) a. 20% piperidine/DMF; b. Ac_2O, DMF, DIPEA; (viii) 2% N_2H_2/DMF; b. Fmoc–mini-PEG, HATU, DIPEA, DMF; (ix) a. 20% piperidine/DMF; b. Fmoc–mini-PEG, HATU, DIPEA, DMF; (x) a. 20% piperidine/DMF; b. Fmoc–Ala(N_3)-OH, HATU, DIPEA, DMF; (xi) a. 20% piperidine/DMF; b. Ac_2O, DIPEA, DMF.

Scheme 2.16: Using Dde to control the growth of dendrimer scaffold **34** with unsymmetrical Y and Z chains.

2.4.7 Derivatising dendrimer scaffolds for biological assays and cleavage from the resin

With the X, Y and Z chains completed, the resin was split in half. For the batch of dendrimers destined for the thermal melt assay, azido dendrimer scaffold **27** was cleaved from the resin using TFA in water and the Mtt group was removed simultaneously to generate **35** (Scheme 2.17). For the batch of dendrimers destined for the cell binding assay, the Mtt group was removed with 1% TFA in dichloromethane and fluorophore 5(6)-carboxyfluorescein was coupled to yield peptide **36**. The fluorescent dendrimer scaffold was then cleaved from the resin using TFA / water (49:1) to generate peptide **37**.

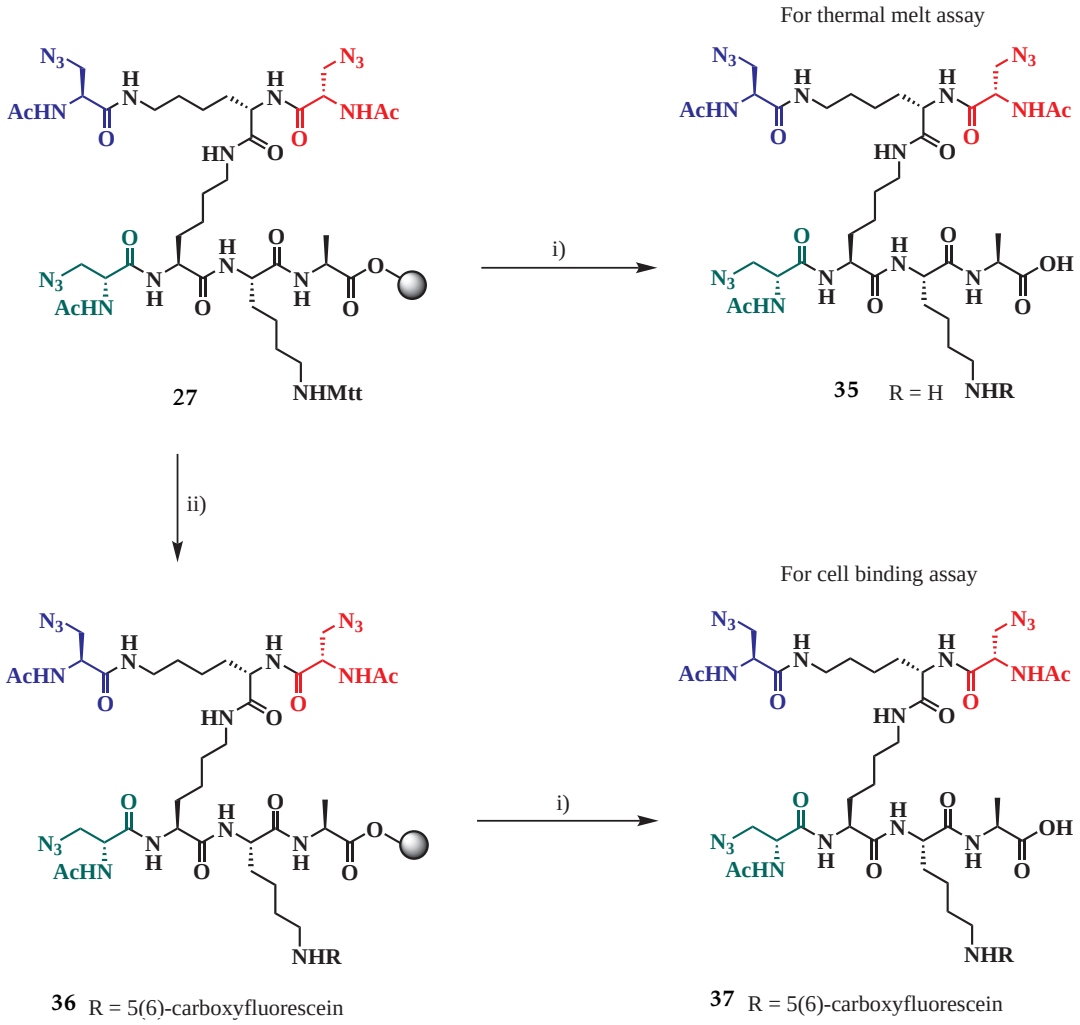

Reagents and conditions: (i) 98% TFA/H_2O; (ii) a. 1% TFA/CH_2Cl_2; b. 5(6)-carboxyfluorescein, HoBT, DIC, DMF; c. 20% piperidine/DMF.

Scheme 2.17: Derivatisation of the resin–bound scaffold **27** to generate the dendrimer scaffolds **35** and **37**.

During the cleavage of the peptide scaffolds from the resin, analysis showed that the azide functional groups were reduced. This was surprising as all mini-cleavages carried out up to this point showed that the dendrimer scaffolds had their azides intact as indicated by the negative Kaiser test. Hence, it was suggested that the scavengers used in the cleavage cocktail were the problem (Scheme 2.18). Originally triisopropylsilane (TIPS) was used but amine by–products were formed (such as **36**). 3,6-Dioxa-1,8-octanedithiol (DODT) was then trialled but the undesired amine by–products persisted. Finally, the cleavage was conducted with no scavengers. Gratifyingly, the formation of amine by-products were not detected, allowing scaffolds bearing azide handles such as **38** to be formed.

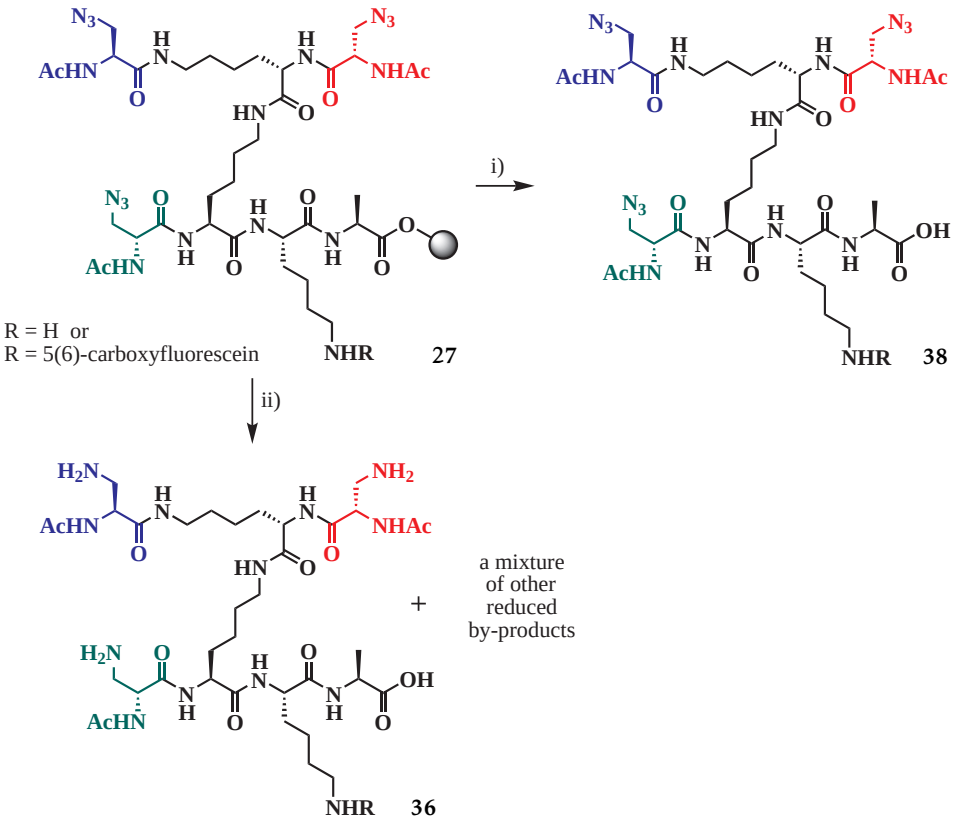

Reagents and conditions: (i) 98% TFA/H_2O, 2 h; (ii) 90% TFA, 5% H_2O, 5% DODT or 5% TIPS, 2 h.

Scheme 2.18: The cleavage conditions used for the dendrimer scaffolds.

2.4.8 GalNAc glycosylation of dendrimers using "click" chemistry

The glycosylation using the copper (I)–catalysed Huisgen azide-alkyne cycloaddition (CuAAC) or "click" reaction will be covered in greater detail in section 2.5, but a brief account of the final step for the dendrimer synthesis is covered here.

With the azide handles and the dendrimer scaffold in place, the dendrimers were ready for the key glycosylation reaction with α–propargyl GalNAc **4** using the CuAAC reaction (Scheme 2.19). The dendrimer scaffolds **35** and **37** were reacted with α–propargyl GalNAc **4** in the presence of sodium ascorbate and copper sulfate, in dimethyl sulfoxide and water. The resulting tri–clicked products were dendrimer **21** for the thermal melt assay and dendrimer **22** for the cell binding assay respectively.

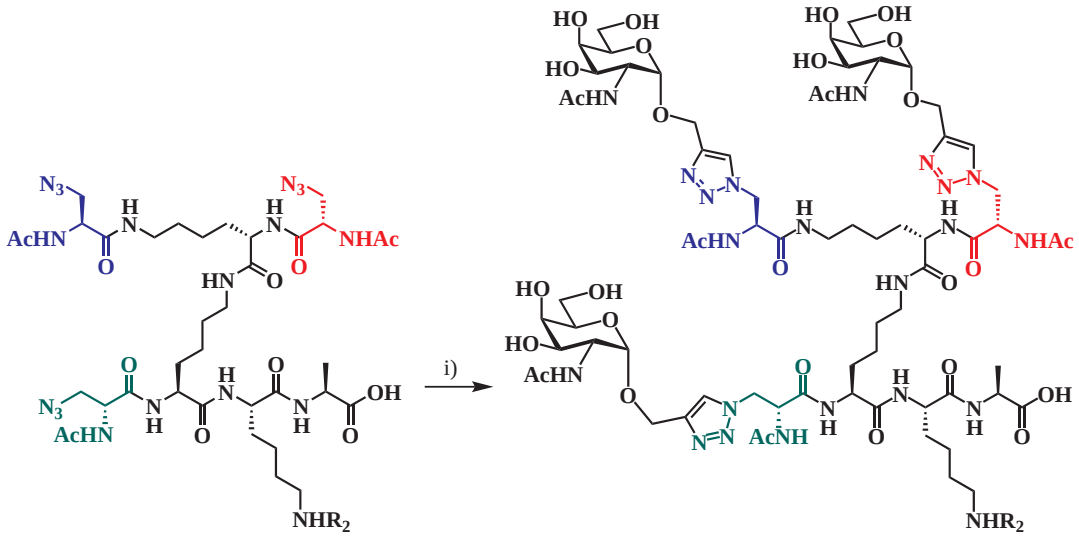

Reagents and conditions: (i) 5 eq. α-propargyl GalNAc, 5 eq. sodium ascorbate, 10 eq. $CuSO_4$, 1:2 H_2O/DMSO.

Scheme 2.19: Glycosylation of dendrimer scaffolds **35** to generate dendrimer **21** for the thermal melt assay, and dendrimer scaffolds **37** to generate dendrimer **21** for the cell binding assays.

2.5 The CuAAC reaction

The final GalNAc glycosylation step for the dendrimers was briefly outlined in section 2.4.8. The following section will discuss in detail the optimisation process which resulted in the final conditions used.

2.5.1 The CuAAC reaction with α–propargyl GalNAc(Ac)$_3$

With both α–propargyl GalNAc(Ac)$_3$ **14** and Fmoc–azidoalanine **9** in hand, the attention was shifted to the click reaction. It is known that optimisation of the copper (I)–catalysed Huisgen azide-alkyne cycloaddition (CuAAC) is required as every system is different.[59] Therefore a trial CuAAC reaction was performed between Fmoc–azidoalanine **9** and α–propargyl GalNAc(Ac)$_3$ **14** as shown in Scheme 2.20.

This trial reaction would provide a useful system for glycosylating azide derivatised peptide dendrimer scaffolds,[110] and the reaction would also generate building block **39** that could be used in SPPS directly.

The initial synthesis utilised 0.04 eq of the copper (I) catalyst relative to the azide in a water/^{t}BuOH/CH_2Cl_2 solvent system. The catalyst was generated by mixing aqueous copper sulphate with sodium ascorbate and this mixture was then added to the azide and alkyne starting materials. This procedure afforded building block **39** in 95% yield in 1 hour.

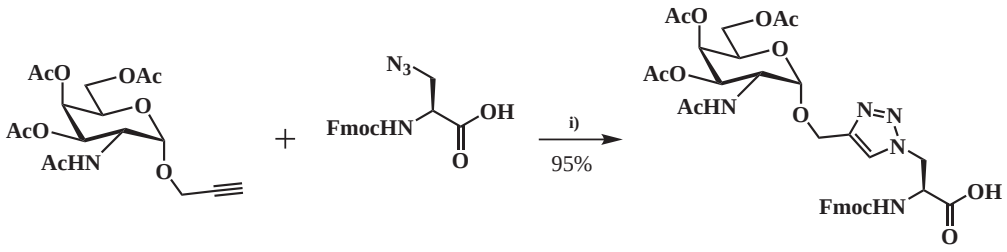

14 **9** **39**

Reagents and conditions: (i) $CuSO_4$, Na ascorbate, ^{t}BuOH, CH_2Cl_2, H_2O, microwave 80 ^{o}C 1 h.

Scheme 2.20: The trial CuAAC reaction between the acetate protected propargyl GalNAc **14** and Fmoc–azidoalanine **9** to form building block **39**.

The next step was to extend these CuAAC conditions to the reaction of α–propargyl GalNAc(Ac)$_3$ **14** and dendrimer scaffold **5** as shown in Scheme 2.21. Table 2.3 summarises the conditions investigated.

The CuAAC conditions used to initially generate click product **39** were tried on dendrimer scaffold **5** with α–propargyl GalNAc$(Ac)_3$ **14** at 80 °C in a microwave reactor under N_2 (Table 2.3 entry 1). Disappointingly, the dendrimer wasn't stable to the elevated temperature and degraded to several fragments and the azides were reduced to amines, as confirmed by LCMS analysis.

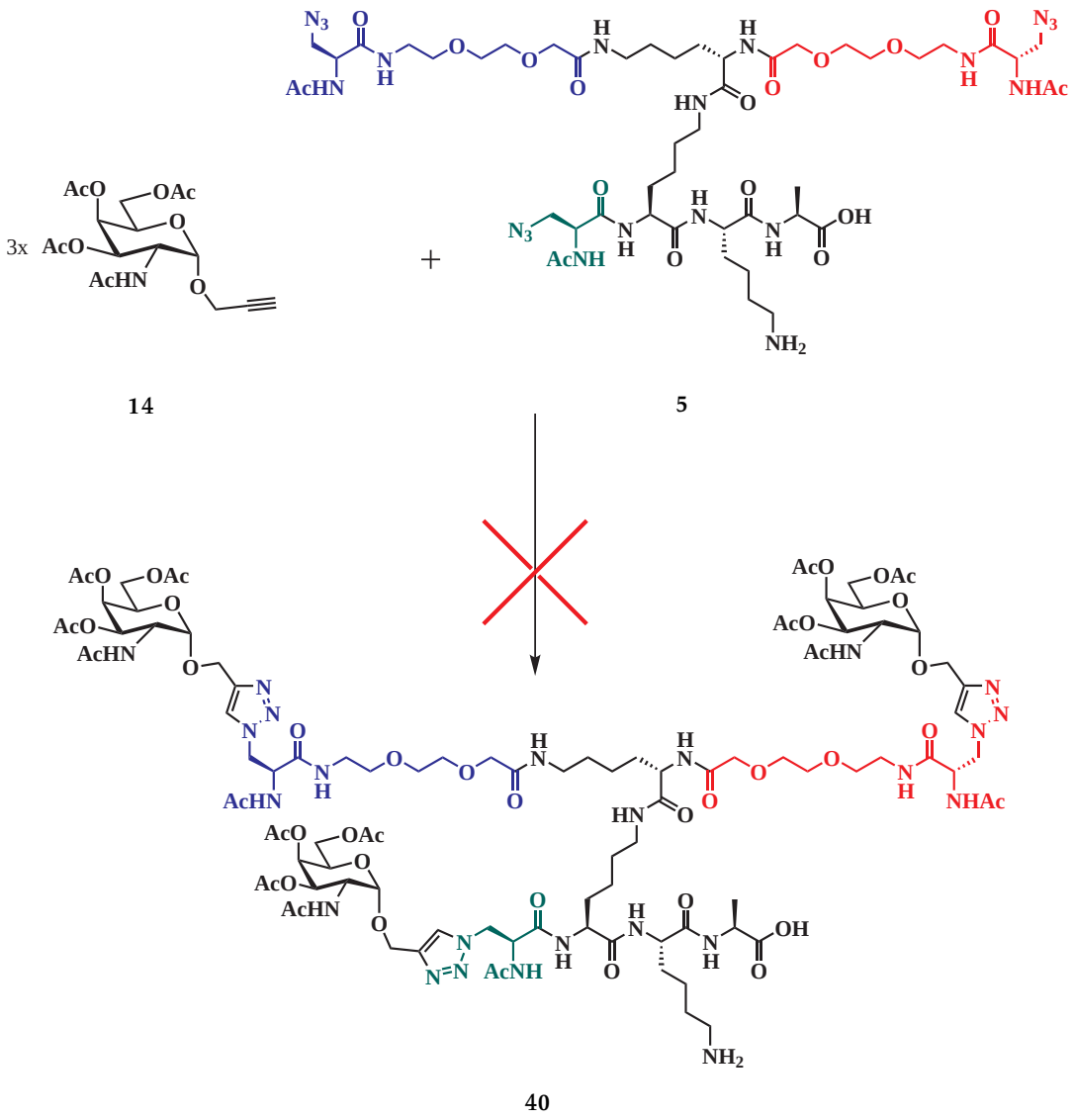

Reagents and conditions: see Table 2.3.

Scheme 2.21: CuAAC reaction between acetate protected α–propargyl GalNAc **14** and dendrimer scaffold **5**. Conditions attempted are summarised in Table 2.3.

The CuAAC reaction was then repeated with the same reagents but at room temperature (Table 2.3 entry 2), but no reaction was observed. Elevating the temperature (Table 2.3 entry 3) to 40 °C still failed to induce the formation of the desired click products with no visible signs of degradation. The CuAAC reaction was tried with an increased amount of copper (I) catalyst, first at

room temperature (Table 2.3 entry 4) and then was heating at 40 °C (Table 2.3 entry 5). The reaction was also performed using *in situ* generation of copper (I), but this also resulted in the reduction of the azides to undesired amines (Table 2.3 entry 6).

It was noticed that while α–propargyl GalNAc(Ac)$_3$ **14** and Fmoc–azidoalanine **9** both dissolved readily in the ^{t}BuOH/CH_2Cl_2/H_2O solvent mixture, dendrimer scaffold **5** did not dissolve. It was suspected that this lack of solubility was a key reason for the reaction failure. Thus a suitable solvent system needed to be investigated.

The click reaction conditions used by Brimble *et al.* for the synthesis of click MUC1 neoglycopeptides was next attempted.[103] The catalytic copper (I) was generated using TCEP and copper sulphate while an aqueous GuHCl and Na_2HPO_4 buffer mixture was used for the solvent. The reaction was performed first at RT (Table 2.3 entry 7) and then at 40 °C (Table 2.3 entry 8) but no reaction took place over a 24 h period when monitoring the reaction by LCMS.

Table 2.3: Reaction conditions and yield for the CuAAC reaction of dendrimer scaffold **5** with α–propargyl GalNAc(Ac)$_3$ **14**. Cu (I) values given with respect to the molar amount of dendrimer.

	Solvent system	Co-oxidant	Cu (I)	Temp.	Time	Results
1	^{t}BuOH/CH_2Cl_2/H_2O	Sodium ascorbate	0.04 eq	80 °C	30 min	degradation
2	^{t}BuOH/CH_2Cl_2/H_2O	Sodium ascorbate	0.04 eq	RT	24 h	no reaction
3	^{t}BuOH/CH_2Cl_2/H_2O	Sodium ascorbate	0.04 eq	40 °C	24 h	no reaction
4	^{t}BuOH/CH_2Cl_2/H_2O	Sodium ascorbate	0.4 eq	RT	24 h	no reaction
5	^{t}BuOH/CH_2Cl_2/H_2O	Sodium ascorbate	0.4 eq	40 °C	24 h	no reaction
6	^{t}BuOH/CH_2Cl_2/H_2O	Sodium ascorbate	0.4 eq	40 °C	1 h	degradation
7	GuHCl/Na_2HPO_4/H_2O	TCEP	0.4 eq	RT	24 h	no reaction
8	GuHCl/Na_2HPO_4/H_2O	TCEP	0.4 eq	40 °C	24 h	no reaction

2.6 The CuAAC reaction with non–protected α–propargyl GalNAc

α–Propargyl GalNAc(Ac)$_3$ **14** had poor solubility in aqueous solvent systems but readily dissolved in organic solvents, whereas the dendrimer readily dissolved in aqueous systems but was much less soluble in organic solvents. To better match the solubility of the two key components it was decided to deprotect α–propargyl GalNAc(Ac)$_3$ **14** at the C3, C4 and C6 positions to afford α–propargyl GalNAc **4** rendering it more water soluble (Scheme 2.22). α–Propargyl GalNAc(Ac)$_3$ **14** was treated with NaOMe in MeOH to remove the acetate groups, generating the deprotected α–propargyl GalNAc **4** in a 98% yield.

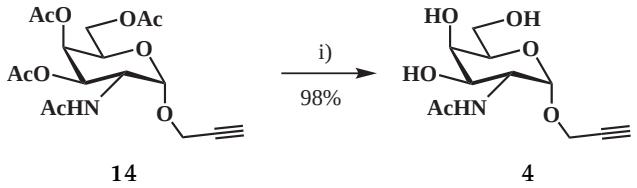

14 **4**

Reagents and conditions: (i) NaOMe, MeOH, 2 h.

Scheme 2.22: The removal of acetates by NaOMe to give α–propargyl GalNAc **4**.

With α–propargyl GalNAc **4** in hand, a trial CuAAC reaction was performed using Fmoc–azidoalanine **9** as shown in Scheme 2.23. The purpose of this model study was to optimise conditions for the CuAAC on these abundant building blocks before using the more scarce dendrimer scaffolds.

Using conditions 1-4 (Table 2.4) α–propargyl GalNAc **4** was reacted with Fmoc–azidoalanine **9** in a mixture of ^{t}BuOH/CH_2Cl_2/H_2O with the copper (I) catalyst generated by treating copper sulfate with sodium ascorbate as described previously. For entry 1 the reaction was performed at RT with 0.04 eq of copper (I) catalyst but since this reaction didn't proceed, the amount of copper (I) catalyst was increased to 0.4 eq (Table 2.4 entry 2) but to no avail. The reaction was heated to 40 °C with 0.4 eq of copper (I) catalyst (entry 3). This procedure generated the triazole **42** in a low yield. In an attempt to increase the yield, TBTA was added (Table 2.4 entry 4).[70] TBTA is a ligand known to complex the copper (I) catalyst thereby helping to maintain its oxidation state during the CuAAC reaction.[59] However, no improvement was observed using this modification.

The solvent system for the CuAAC reaction conditions in entries 5-8 used either a mixture of DMSO/H_2O or a mixture of MeCN/H_2O (Table 2.4 entry 9). The water is a necessary component as it solvates the copper (I) catalyst which wouldn't dissolve in DMSO or MeCN alone. The CuAAC reaction was attempted using 0.04 eq of copper (I) catalyst (entry 5) at RT but no product was formed, and increasing the temperature of the reaction to 40 °C (entry 6) also didn't give the desired product. The best results (Table 2.4 entry 7) were achieved with 10 equivalents of copper (I) catalyst in a mixture of DMSO/H_2O at 40 °C, these conditions yielded the triazole **42** in 70% yield. Addition of TBTA (entry 8) to the reaction also resulted in a similar albeit slightly lower 67% yield. The use of MeCN as the reaction solvent (entry 9) reduced the yield to 56%.

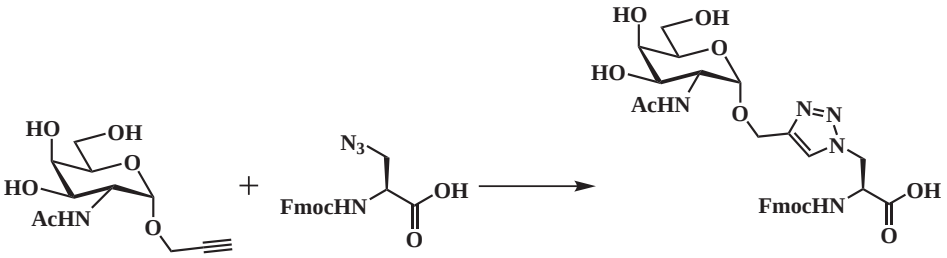

Reagents and conditions: see Table 2.4.

Scheme 2.23: The model CuAAC reaction between α–propargyl GalNAc **4** and Fmoc–azido alanine **9** to form the triazole **42**. The conditions used are listed in Table 2.4.

Table 2.4: Reaction conditions and yield for the CuAAC reaction of Fmoc–azidoalanine **9** with α–propargyl GalNAc **4** using sodium ascorbate as the co–oxidant to form the triazole **42**. Cu (I) values given with respect to the molar amount of dendrimer.

	Solvent system	Co-oxidant	Cu (I)	Temp.	Time	Additive	Result
1	^{t}BuOH/CH_2Cl_2/H_2O	Sodium ascorbate	0.04 eq	RT	24 h	none	no reaction
2	^{t}BuOH/CH_2Cl_2/H_2O	Sodium ascorbate	4 eq	RT	24 h	none	no reaction
3	^{t}BuOH/CH_2Cl_2/H_2O	Sodium ascorbate	4 eq	40 °C	24 h	none	20%
4	^{t}BuOH/CH_2Cl_2/H_2O	Sodium ascorbate	4 eq	40 °C	24 h	TBTA (4 eq)	19%
5	DMSO/H_2O	Sodium ascorbate	0.04 eq	RT	24 h	none	no reaction
6	DMSO/H_2O	Sodium ascorbate	0.04 eq	40 °C	24 h	none	no reaction
7	DMSO/H_2O	Sodium ascorbate	10 eq	40 °C	2 h	none	70%
8	DMSO/H_2O	Sodium ascorbate	10 eq	40 °C	2 h	TBTA (10 eq)	67%
9	MeCN/H_2O	Sodium ascorbate	10 eq	40 °C	2 h	none	56%

The two synthetic approaches to prepare triazole **42** from Fmoc–azidoalanine **9** are summarised in Scheme 2.24. Both approaches afforded the triazole **42** in similar overall yields but the click conditions described for reaction of Fmoc–azidoalanine **9** with α–propargyl GalNAc **4** though ostensibly lower yielding, offer the most relevant conditions for reaction of α–propargyl GalNAc **4** with a dendrimer.

It is also worth noting that a building block such as **39** or **42** can be used directly in SPPS. However, the direct use of such building blocks in SPPS is intrinsically more wasteful than clicking the sugar onto dendrimer scaffolds as a significant excess of the building block is required.

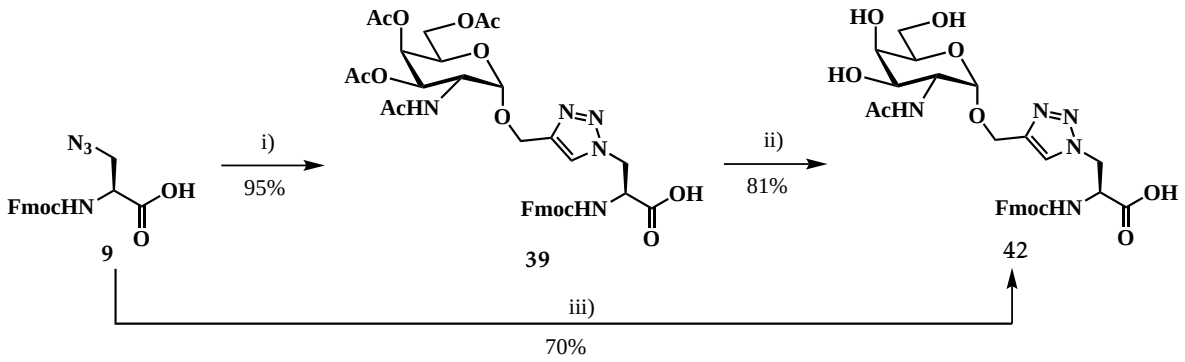

Reagents and conditions: (i) α-propargyl $GalNAc(Ac)_3$, $CuSO_4$, sodium ascorbate, $^tBuOH/CH_2Cl_2/H_2O$, microwave 80 ºC, 1 h ; (ii) NaOMe, MeOH, 2 h; (iii) α-propargyl $GalNAc_3$, $CuSO_4$, sodium ascorbate, DMSO, H_2O, 40 ºC.

Scheme 2.24: The two synthetic routes to triazole **42** from Fmoc–azidoalanine **9**.

2.6.1 Trial CuAAC reaction between propargyl GalNAc and a dendrimer scaffold

Dendrimer scaffold **5** was used for establishing conditions for the CuAAC reaction as shown in Scheme 2.25 and Table 2.5. The aim was to use the CuAAC reaction to install three GalNAc residues, each clicked onto the individual terminal azide groups in each chain in a single step.

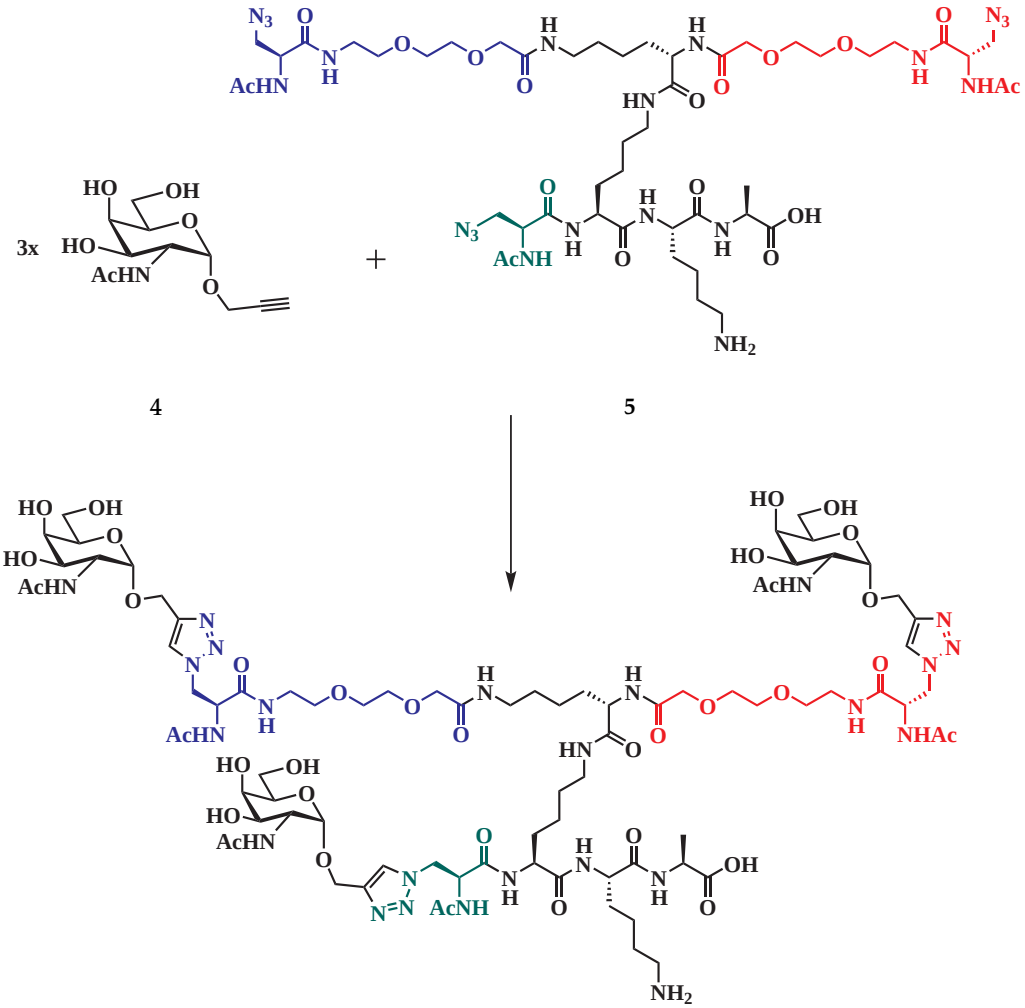

Reagents and conditions: see Table 1.5.

Scheme 2.25: CuAAC reaction between the α–propargyl GalNAc **4** and dendrimer scaffold **5** to form dendrimer **2**.

The initial conditions (Table 2.5, entry 1) used catalytic amounts of copper (I) catalyst and the reaction was monitored at 1 h, 2 h, 6 h and 24 h at room temperature . No progress or degradation was observed, therefore the next reaction was heated to 40 °C and fresh copper (I) catalyst was added at intervals with the aim to drive the reaction to completion (Table 2.5, entry 2). At this point the CuAAC reaction started to proceed. Initially the mono– and di– "clicked" products were observed after 1 eq of copper (I) catalyst was added, but no tri–"clicked" products were formed. The reactions were left for a further 24 h but no progress occurred. There was no sign of degradation so more equivalents of copper (I) catalyst were added (Table 2.5, entry 2).

The reaction was repeated with dendrimer scaffold **5** and α–propargyl GalNAc **4** at 40 °C with 4.5 eq of copper (I) catalyst (Table 2.5, entry 3). Curiously the reaction did not go to completion. This is probably due to a combination of factors such as the "freshness" of copper (I) catalyst. Dissolved oxygen may remove copper (I) catalyst too rapidly or the dendrimer and sugar may sequester the copper (I) catalyst so it is unavailable for the click reaction, therefore an excess is needed especially while working on a small scale. The reaction also proceeded slowly, and stopped at a mixture of mono–, di– and tri–clicked products after 24 h. The reaction did proceed to completion upon being given fresh copper (I) catalyst with a final concentration of copper (I) catalyst being 10 eq.

When the reaction was repeated with TBTA (Table 2.5, entry 4), a similar outcome was observed, with the TBTA making no visible improvement. The reaction was then repeated using 10 eq of copper (I) catalyst from the start (Table 2.5, entry 5) and proceeded to completion smoothly in 2 hours.

The conditions from entry 5 were repeated but with the addition of TBTA (Table 2.5, entry 6) and the outcome was the same. Since the progress of the CuAAC reaction was similar to the reaction without TBTA, it was therefore concluded that adding the TBTA ligand didn't have any beneficial effect on this CuAAc reaction.

Table 2.5: Reaction conditions and results for the CuAAC reaction of dendrimer scaffold **5** with α–propargyl GalNAc **4** using sodium ascorbate as the co–oxidant to form the dendrimer **2**. Cu (I) values given with respect to the molar amount of dendrimer.

	Solvents	Cu(I)	Temp.	Time	Additive	Result
1	DMSO/H_2O	0.04 eq	RT	24 h	-	no reaction
2	DMSO/H_2O	0.04-4.5 eq*	40 °C	26 h	-	tri-clicked products
3	DMSO/H_2O	4.5 eq	40 °C	24 h	-	mixture of clicked products
4	DMSO/H_2O	4.5 eq	40 °C	24 h	TBTA (4.5 eq)	mixture of clicked products
5	DMSO/H_2O	10 eq	40 °C	2 h	-	tri-clicked products
6	DMSO/H_2O	10 eq	40 °C	2 h	TBTA (10 eq)	tri-clicked products

*Fresh copper (I) catalyst was added at multiple time points during the reaction.

The LCMS traces for entry 5 are displayed in Figure 2.9. The starting material (peak a) was observed to be consumed as the reaction progresses. After 1 hour, a mixture of unreacted starting material (peak a), mono–clicked dendrimers (peak b), di–clicked dendrimers (peak c) and tri–clicked dendrimers for (peak d) were visible. After 2 hours all of the starting material was consumed and only a trace of the di–clicked dendrimers was observed (peak c), with the major peak (peak d) consisting of the desired tri-clicked product dendrimer **2**. This set of conditions used made it apparent that the reaction needed large excesses of copper (I) catalyst rather than the catalytic equivalents used in the literature.

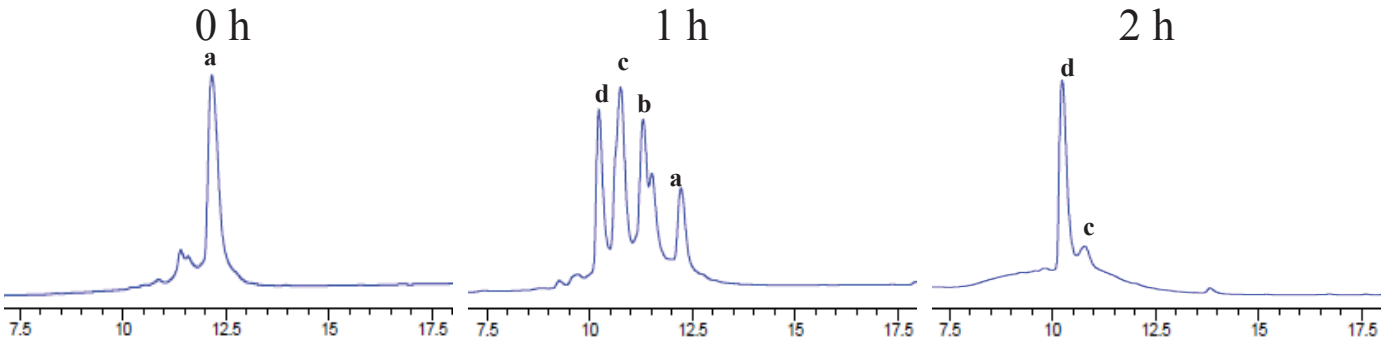

Figure 2.9: Progress of the CuAAc reaction for dendrimer **2** (Table 2.3 entry 5) by HPLC using MeCN/H_2O with 0.1% v/v formic acid solvent system initially and increased with a linear gradient going from 0-60% over 30 min. Peak a starting material, peak b mono–clicked dendrimers, peak c di–clicked dendrimers and peak d is the tri–clicked product dendrimer **2**.

The optimised conditions were used in a generic context and were applied to the derivatisation of all the remaining scaffolds. At this stage, the focus was to obtain sufficient material rather than optimise the yield of the click reactions.

In the course of the project it was found that performing the 'click' reaction on crude material proceeded with satisfactory yields. Although monitoring the completion of the 'click' reaction was more difficult when crude material was used, a higher overall yield was generally obtained.

2.7 Generation II dendrimers

The original dendrimers synthesised up to this point were supposed to bind selectively to MGL because they contained GalNAc residues which act as specific ligands to the binding domains. But what if the sugar wasn't the reason for binding? Without a crystal structure of the dendrimer's GalNAcs docking to the binding domain it is uncertain that the dendrimers are binding as we predict. Due to flexibility of MGL and its position as a transmembrane receptor, getting a X–ray structure wasn't possible.

While it is uncertain that the dendrimers would bind to MGL, it is possible to find out which parts of the dendrimer are responsible for binding. By synthesising dendrimers with similar structures but with no GalNAc moiety, it was possible to elucidate what is important for dendrimer binding to MGL. These generation II dendrimers from here on shall be referred to as negative controls.

For the negative controls, azidoalanines for the click reaction were replaced with alanines, thus leading to structures of dendrimers without the triazole sugar component. A list of the possible results is shown in Table 2.6. The structures of the negative controls synthesised are depicted in Figure 6.2. The results learnt from these compounds will be discussed in Chapters 4, 6, 7 and 8.

Table 2.6: Possible results from negative controls.

Possible results	What these results would mean
Only compounds with GalNAc bind to MGL.	We have created compounds which bind selectively to MGL, and that GalNAc is the important feature for binding.
All compounds bind to MGL (with or without GalNAc).	Non selective binding is occurring, the dendrimer scaffold is involved in binding.
Only compounds with no GalNAc bind to MGL (negative controls).	The GalNAc residues are detrimental for binding and the scaffold is binding to MGL.
Nothing binds to MGL.	Neither the GalNAc nor the scaffold are conducive to binding.

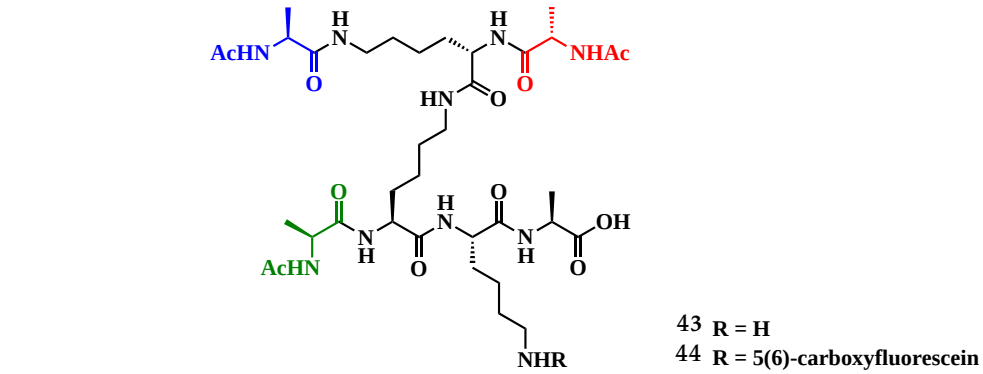

43 R = H
44 R = 5(6)-carboxyfluorescein

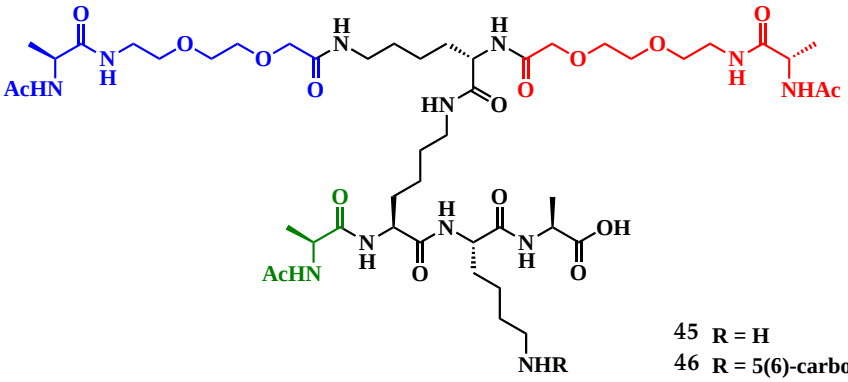

45 R = H
46 R = 5(6)-carboxyfluorescein

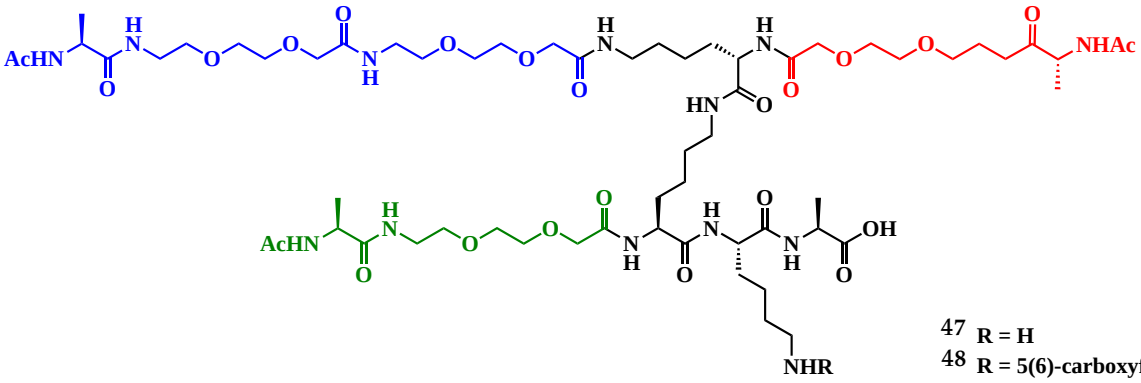

47 R = H
48 R = 5(6)-carboxyfluorescein

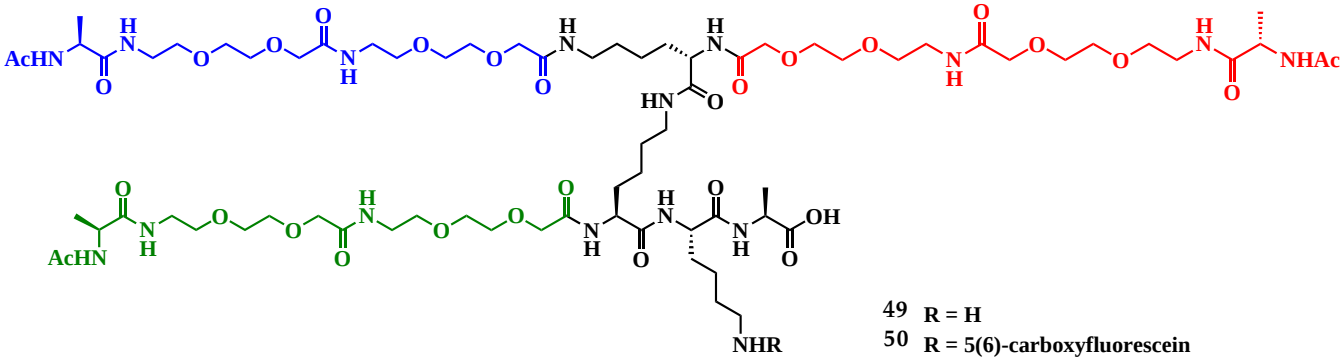

49 R = H
50 R = 5(6)-carboxyfluorescein

Figure 2.10: Structures of generation II negative control dendrimers **43**, **44**, **45**, **46**, **47**, **48**, **49** and **50**.

The eight generation II negative control dendrimers are matched with their equivalent generation I dendrimers in Table 2.7

Table 2.7: Pairs of generation I and II dendrimers.

Generation I dendrimer	Deneration II dendrimer
Dendrimer **21**	Dendrimer **43**
Dendrimer **22**	Dendrimer **44**
Dendrimer **2**	Dendrimer **45**
Dendrimer **3**	Dendrimer **46**
Dendrimer **23**	Dendrimer **47**
Dendrimer **24**	Dendrimer **48**
Dendrimer **25**	Dendrimer **49**
Dendrimer **26**	Dendrimer **50**

Chapter 3

Initial work on the thermal melt assay

This chapter will examine the initial work performed using the thermal melt assay. This was the first biological assay to be performed using the generation I dendrimers which were synthesised in chapter 2. The generation I dendrimers used in experiments mentioned in this chapter are shown in Figure 3.1.

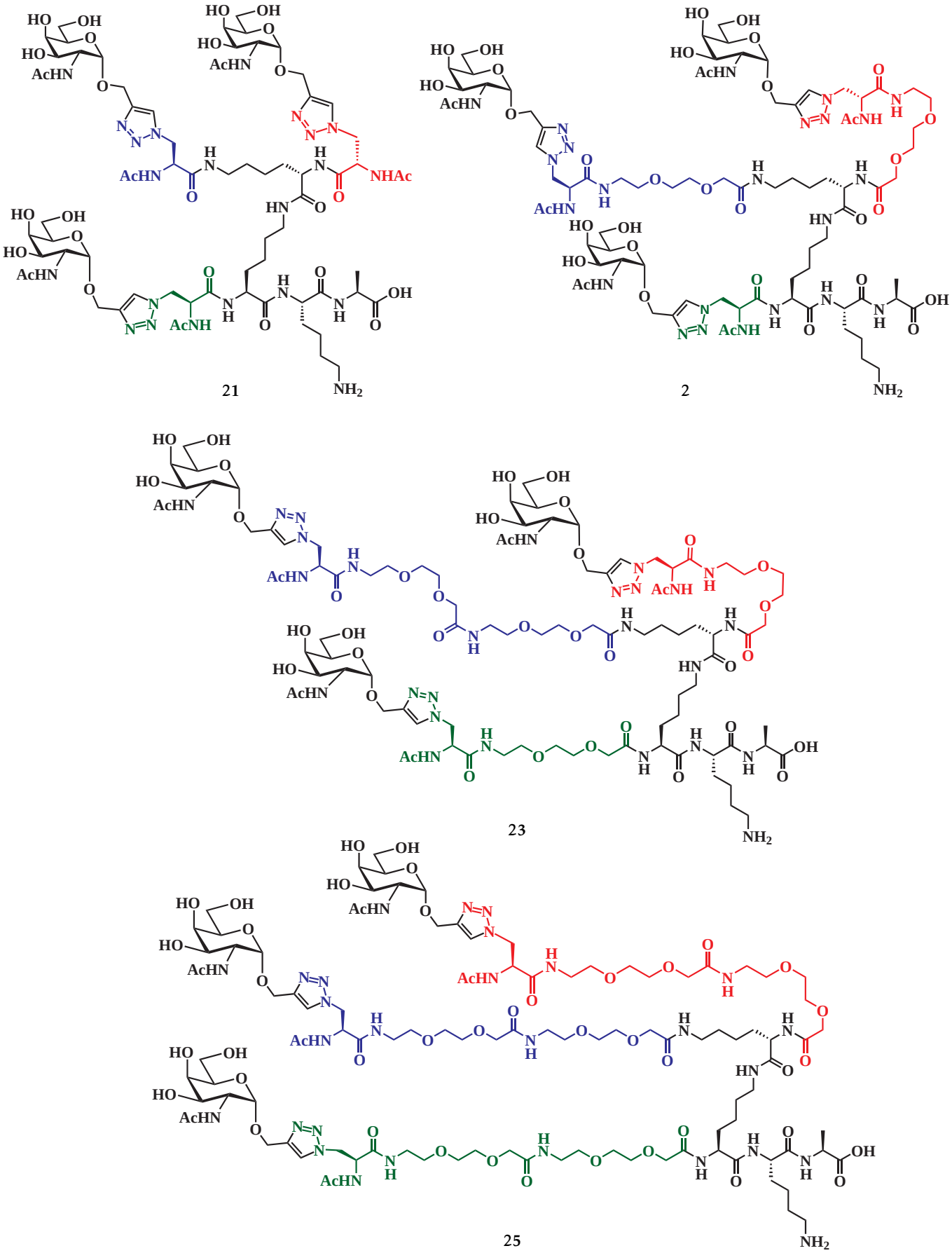

Figure 3.1: Structures of the generation I dendrimers **21**, **2**, **23** and **25**.

3.1 Introduction to differential scanning fluorimetry

The cell binding assay described in Chapter 4 has some inherent difficulties. These cell assays require healthy donated blood, from which the peripheral blood mononucleated cells (PBMC) need to be separated. PBMC are cultured for four days to develop into monocyte dendritic cells (MoDC) which express macrophage galactose binding lectin (MGL). MoDC have a limited lifetime and do not produce accurate results after being frozen and thawed. A fresh batch of PBMC needs to be cultured for every experiment, making it a costly and time consuming procedure. An alternative method for studying MGL binding during the optimisation of dendrimer design would be preferable.

An alternative to culturing PBMC to generate MGL expressing MoDC, would be to clone the DNA sequence for MGL and then to express the MGL protein in bacteria such as *E. coli*. This removes the need for human blood, and the MGL expressing bacteria can be generated from a stock whenever needed. Since the MGL from protein expression behaves the same before and after being frozen and thawed, a stockpile of MGL truncations could be created and then defrosted when needed, as opposed to waiting for four days to perform a cell binding experiment.

MGL has previously been cloned and expressed independently by Suzuki *et al.* and Valladeau *et al.*[12] In 1996 Suzuki *et al.* first cloned the cDNA from a library derived from 1l–2 treated peripheral blood monocytes and then expressed the MGL recombinantly in COS-1 cells.[132] From the lysate of the cells, Suzuki *et al.* were able to separate out a protein of 38 kDa which was MGL, and then they went on to show that it bound to the T_N antigen. In 2001, Valladeau *et al.* cloned a MGL splice variant which they named DC-asialoglycoprotein receptor.[133] The protein differs from MGL due to an insertion of 27 amino acids and a deletion of 3 amino acids in the neck domain.

In 2010 Drickamer expressed truncated MGL using an analogous T7 promoter system. With this system it was demonstrated that the presence of extended binding sites within a single carbohydrate recognition domain (CRD) can enhance binding interaction with branched glycans.[134] Drickamer went on to show that the presentation of branched glycans which contain GalNAc on a glycoprotein surface increases binding affinity by 15–to 20–fold, possibly due to low-specificity interactions with the surface of the protein or restriction in the conformation of the glycans. Recently in 2013 Drickamer *et al.* cloned and expressed portions of the α–helical neck region and the globular CRD regions of MGL.[14] These fragments were used to confirm that MGL was a trimeric cluster due to its similarities in sequence with serum mannose-binding protein.

Truncations of MGL can be expressed by bacteria. It was hoped that truncations of MGL could be used in a thermal melt assay as a pre–screening tool to select ligands before submitting them for the cell binding assay. When this project started it was unknown whether this approach would be an accurate tool for predicting dendrimer binding to MGL, as it was unknown whether the MGL

truncations would behave in a similar fashion to the presumably trimeric MGL found on MoDCs.

The thermal melt assay uses Differential Scanning Fluorimetry (DSF) to show the strength of binding of the compounds to MGL in a semi–quantitative manner. The better a ligand binds to the protein, the more stable the protein becomes, and therefore more thermal energy is needed to denature the protein. A compound which binds strongly will stabilise the protein and therefore will need a higher temperature to break up the tertiary structure compared to the protein on its own. The DSF experiment requires a fluorescent dye (SYPRO orange dye) which binds to hydrophobic amino acids of denatured proteins. As the temperature rises, the protein unfolds and hydrophobic amino acids which normally reside in the protein's interior are exposed. The dye binds to these amino acids, and this results in a fluorescent signal. The DSF experiment produces plots in which the fluorescence intensity of the SYPRO Orange dye interacting with the peptide is plotted against temperature. The point of inflection on this graph indicates the temperature at which the protein denatures or "melts" (Figure 3.2).

As the point of inflection is often hard to see on the plots, the derivative curve (rate of change of fluorescence intensity against temperature) is normally used, since the point of inflection has become a minimum (Figure 3.2). The appendix of this thesis includes all of the DSF curves and derivative plots that were measured for this project. The melting points were obtained from the minima of the derivative graphs. The bar charts in this chapter were derived from the derivative graphs found in the appendix.

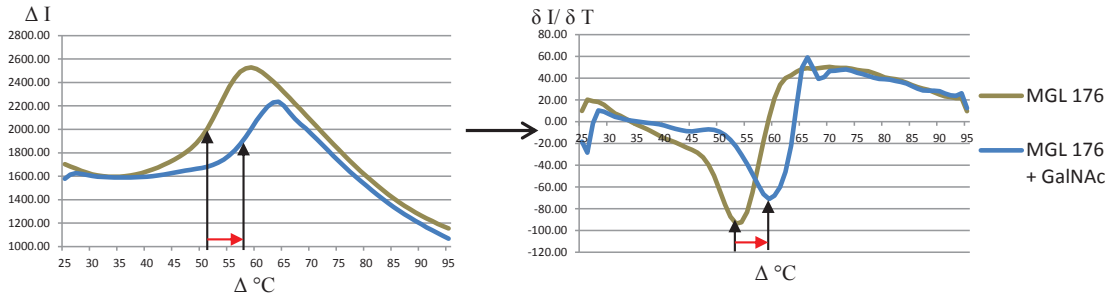

Figure 3.2: (Left) DSF plot which shows the melting point as the point of inflection. (Right) DSF derivative plot which shows the melting point as a minima.

MGL is known to bind to GalNAc,[29, 30, 31] therefore GalNAc was used as a positive control for the thermal melt assay while the protein–only samples were used as a negative control. A compound will be considered a strong binder if the melting point is greater than that with GalNAc. Compounds which induce a lesser positive shift in the melting point than that of the GalNAc–MGL binding pair will be considered weaker binders. Compounds with zero or negative shift in melting point will be considered not to bind in a positive fashion (they may be destabilising the MGL or not interacting at all).

When preparing to run the thermal melt assay, the MGL sample was kept on ice to reduce the chances of the protein denaturing or aggregating before the experiment. The stock solution of protein in buffer was made and then pipetted between each sample to maintain a consistent concentration of MGL. To each sample of MGL, the dendrimers were added and then the solution was diluted to the desired concentration with buffer solution. Five minutes before the experiment was run the fluorescent dye was added to each sample to reduce the chance of non-specific dye binding to the protein before the DSF. A sample of each additive (the dendrimers/peptides/GalNAc monomer) was run with only the buffer, as well as with the buffer and the dye, to monitor for unwanted fluorescent signalling which may bias the test. Fortunately none of these compounds interacted with the dye or the buffer to produce a fluorescent signal.

3.1.1 The four MGL proteins

To perform the thermal melt assay, the MGL truncations were expressed recombinantly. Figure 3.3 [135] shows the complete MGL amino acid sequence and the four MGL truncation sequences which were expressed for this project. The MGL truncation sequences are: MGL 144 (amino acid 144 to 316, 21 kDa), MGL 155 (155 to 316, 20 kDa), MGL 166 (166 to 316, 19 kDa), and MGL 176 (176 to 316, 18 kDa). We chose to express the truncated sequences in bacteria rather than produce them by chemical synthesis for the following reasons:

- The long protein sequence would require substantial time to optimise the synthesis and folding of MGL if it was made using solid phase peptide synthesis.
- Expression using bacteria is cheaper and faster than solid phase synthesis, and also produces proteins in larger quantities.
- The MGL truncations have been expressed before by researchers in the Squire group at the University of Auckland. The extraction and the folding have already been optimised to give correctly folded protein.

The biggest MGL truncation is MGL 144 which includes the largest portion of the coiled coil domain. The length of the coiled coil domain decreases with each subsequent truncation to the point that MGL 176 does not include any of the coiled coil domain. We postulate that the longer the coiled coil domain in the truncation, the more likely the MGL truncation forms trimeric MGL sequences that we hypothesise to be the most biologically relevant. Using this logic, we expect MGL 176 to be a monomer, while the larger sequences such as MGL 144 and MGL 155 is expected to form trimers.

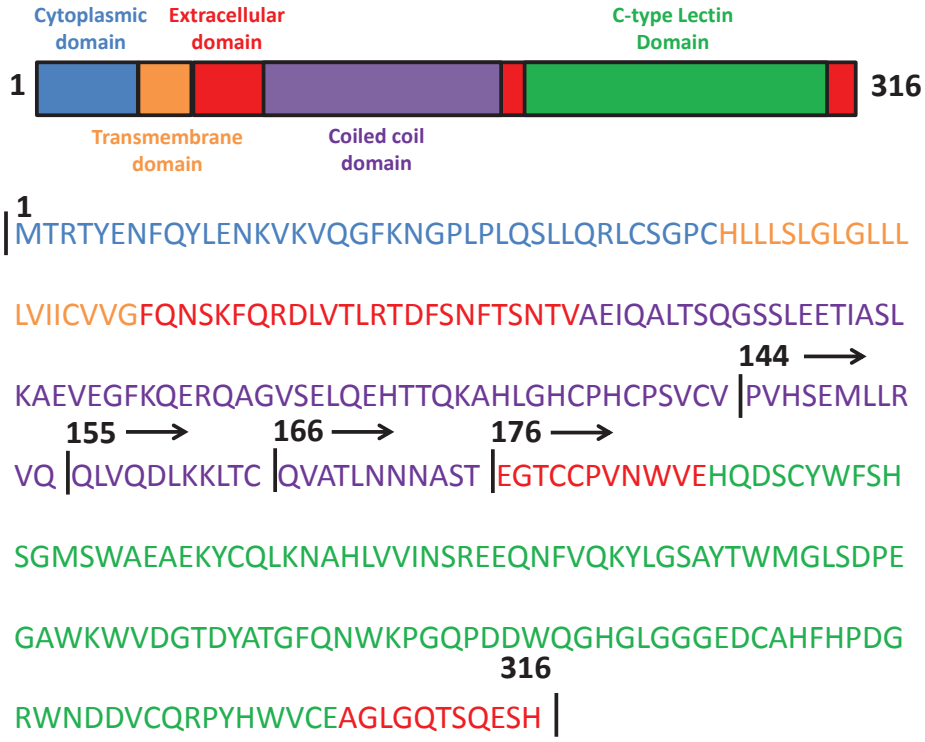

Figure 3.3: The full amino acid sequence of Macrophage Galactose binding Lectin (MGL).

3.1.2 Expression of the four MGL constructs

The four MGL truncation domain constructs were provided by Dr. Christopher Squire (SBS, UoA). These four sequences had already been inserted into the pDEST17 Gateway vector (Invitrogen) and transformed into *E. coli* BL21(DE3). The transformed bacteria were grown on agar plates supplemented with 56 nM ampicillin at 37 °C and left to incubate for 18 hours. pDEST17 confers ampicillin resistance and has the protein encoding sequence under a T7 promoter. This should reduce the amount of *E. coli* produced which do not express the MGL sequences. A single colony was taken from the agar plate after the incubation and was then transferred into liquid media to continue to be expressed.

Initially we used the isopropyl β–D–1–thiogalactopyranoside (IPTG) to trigger the transcription of the *lac* operon and induce protein expression. IPTG induction was very low yielding, and therefore we switched to using Terrific Broth un-induced expression which expressed more protein. After expression, the supernatant was separated from the *E. coli* solids by centrifugation, and the resulting pellet was re-suspended in a tris buffer solution. The suspension was put through a constant cell disruption system instrument to lyse the cells.

After the cell lysis, the mixture underwent centrifugation and the supernatant was separated from the pellet. The sodium dodecyl sulfate (SDS) polyacrylamide gel electrophoresis (PAGE) of the four MGL sequences (Figure 9.22, appendix), showed that the MGL is located in the pellet rather than the supernatent as expected from previous expression experiments. The pellet was re–suspended in a buffer containing guanidinium, calcium chloride and β–mercaptoethanol (β–ME) to solubilise the inclusion bodies which contain the MGL. The solution was agitated overnight at 4 °C. The solubilised MGL was then separated from the rest of the cell debris by centrifugation. Unfortunately SDS–PAGE analysis can not be performed at this stage, as the guanidinium disrupts the shape of the gel. The concentration of the MGL in solution was normally measured using a Nano–drop fluorospectrometer. Unfortunately again due to the guandinium, the Nanodrop fluorospectrometer does not give accurate results for the concentration measurement.

The MGL at this stage was in an unfolded state, and the protein must be allowed to refold into its functional 3D shape. The MGL solution was added very slowly to a large excess of refolding buffer at 4 °C and left to stir overnight. The rapid dilution of protein should dilute the β–ME and guanidinium enough to allow the protein to refold to its native conformation. A fraction of the protein deposits out overnight and the solution goes slightly cloudy.

The refolding buffer with MGL was then filtered and concentrated from 500 mL down to 200 μL. The filter allows proteins smaller than 10 kDa to pass through but stops the larger proteins (which include each of our MGL truncations) from passing through. The more concentrated the solution, the more protein precipitates. When the solution was 200 μL in volume, a Nanodrop fluorospectrometer measurement was performed, which revealed the concentration of the MGL. The supernatant before size exclusion chromatography produced an SDS–PAGE trace which was a lot cleaner than the initial expression. An example of SDS–PAGE for MGL 144 truncation before size exclusion chromatography is included in Figure 3.4.

3.1.3 Size exclusion chromatography

The concentrated supernatant contains a mixture of proteins which remain after the rapid dilution and filtering. To separate the desired MGL truncation, size exclusion chromatography was performed. Initially we tried to purify the samples on a Superdex 75 10/300 column with just the refolding buffer. Unfortunately the column blocked repeatedly due to the MGL truncations precipitating. This problem could be solved by adding a small amount of BME (β-mercaptoethanol) to the refolding buffer. The profile of the MGL traces is shown in the appendix (Figure 9.24 to Figure 9.26).

While all of the smaller truncations gave a similar trace, MGL 144 eluted in the void volume when we attempted to purify using the Superdex 75 10/300 column (Figure 3.4). To solve this issue, a Superdex 200 10/300 column was used instead (Figure 3.5). The fractions for each run were collected and then tested using SDS–PAGE to identify the fractions with the desired protein. These fractions were concentrated to 200 μL and then their protein concentration was measured using a nanodrop fluorospectrometer.

The protein was then diluted with 20% glycerol and flash–frozen in liquid nitrogen at -80 °C to prevent degradation. The expression of the MGL truncations was good but the final yields were always low because of the insolubility of the protein during the purification process and especially during the refolding steps. Due to time limitations, we did not explore the use of other refolding buffers, the buffer used was known to work from previous unpublished work from the Squire group. If the yield of the expression from MGL truncations were to be improved, the refining of the refolding conditions would be the primary focus.

The Superdex 75 10/300 column is suitable for small proteins, and it is suitable to resolve monomeric MGL truncations which have a molecular weight of around 20 kDa. MGL 144 was the last truncation to be purified using size exclusion chromatography. All of the smaller truncations were purified without issue. Therefore the size exclusion chromatography trace for MGL 144 shown in Figure 3.4 with only one main peak was unexpected.

A calibration experiment was performed using proteins of known mass and the calibration protein of 60 kDa eluted near the void volume, leading us to believe that MGL 144 (monomer of 21 kDa) may form trimeric structures (due to containing the longest portion of the coiled coil domain). The SDS-PAGE shown in Figure 3.4 showed protein with masses between 50 and 70 kDa present, which could correspond to the molecular weight of the 63 kDa MGL 144 trimer. The MGL 144 monomer was also separated during the purification, which suggests that the formation of the quaternary structure did not go to completion with the current refolding conditions producing a monomer/trimer equilibrium.

When MGL 144 was purified using the Superdex 200 10/300 column, a better resolved size exclusion trace was generated (Figure 3.5) when compared to the Superdex 75 10/300 column (Figure 3.4). The MGL 144 trace has a similar profile to the other smaller MGL truncations which were purified on the Superdex 75 10/300 column.

Size exclusion chromatography multi–angle laser light scattering (SEC-MALS) was briefly considered as a way to prove the trimeric structure of the MGL 144 protein. Unfortunately, the refolding buffer which contains a high concentration of glucose made calibration impossible. Due to time constraints, alternative solvent systems weren't explored, and therefore SEC-MALS wasn't performed. Future research could be directed towards the optimisation of solvent systems for: MGL refolding, purification, SEC-MALS and crystallisation as this could reveal the precise quaternary structure.

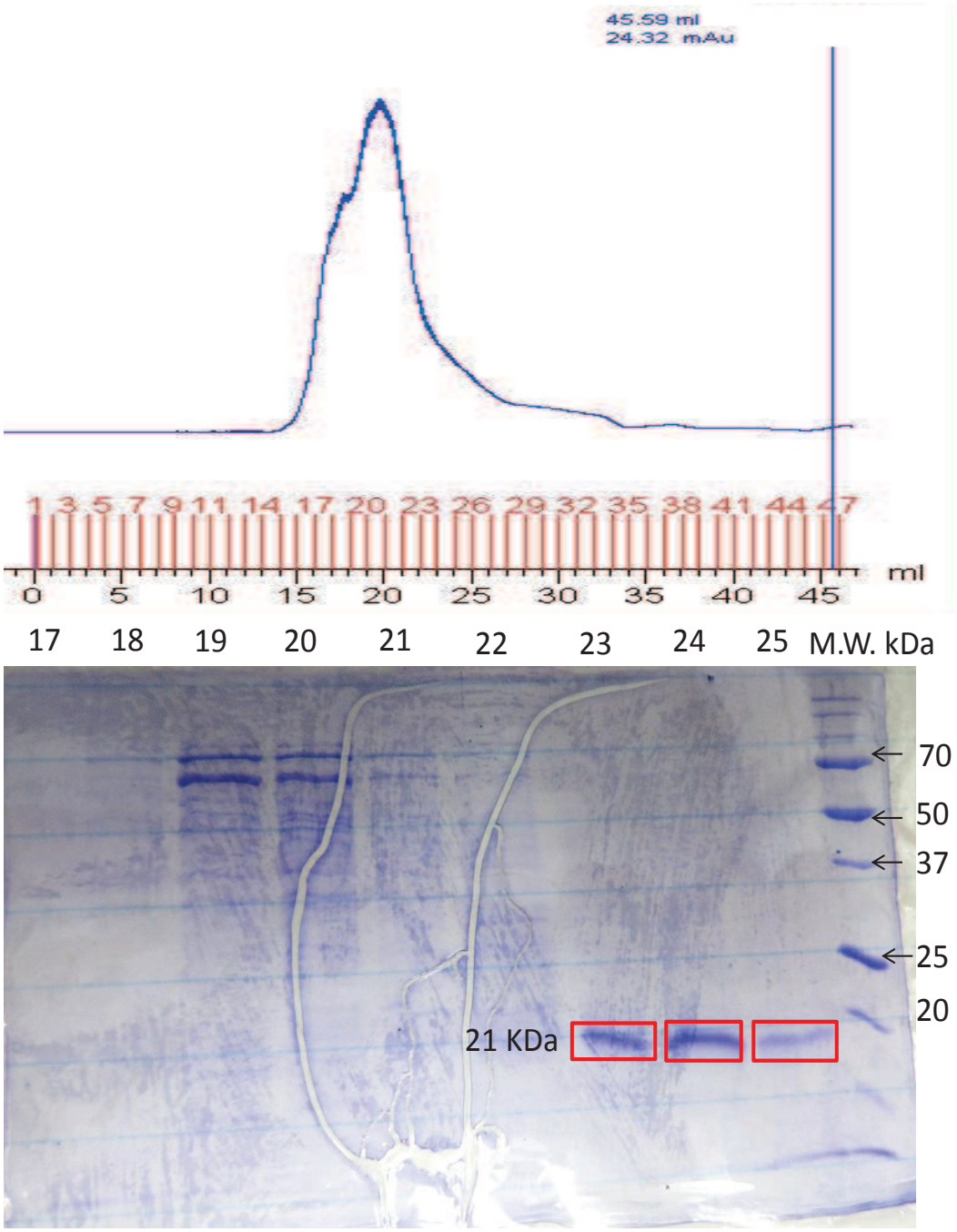

Figure 3.4: (Top) Size exclusion chromatography trace for MGL 144 purified on s75 10/300 column. (Bottom) The SDS-PAGE for the purification.

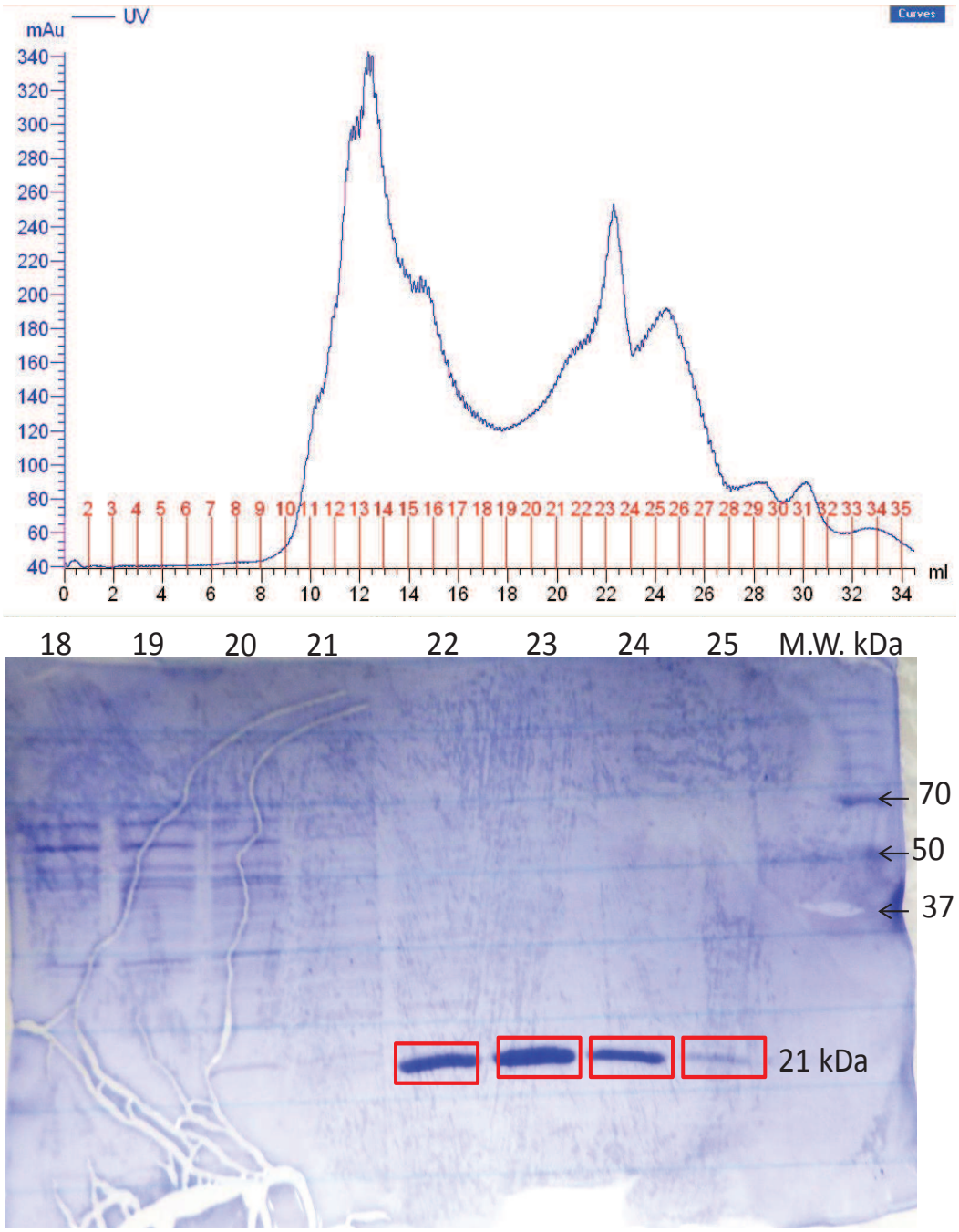

Figure 3.5: (Top) Size exclusion chromatography trace for MGL 144 purified on s200 10/300 column. (Bottom) The SDS-PAGE for the purification.

3.2 The initial thermal melt assay

Dr Julie McIntosh provided the initial samples of MGL 176 protein which were used for the first DSF experiments. MGL 176 is expected to be monomeric as it contains the carbohydrate binding domain of MGL but does not contain the coiled coil domain which induces oligomerisation. The coiled coil domain is thought to be important for the formation of trimeric clusters in MGL. We hoped to use MGL 176 as a model system to compare to the full MGL sequence, as it contained the full carbohydrate binding domain which was where we were expecting the GalNAc dendrimers to bind.

The initial thermal melt assay was a titration experiment using monomeric GalNAc and the generation I dendrimers: **21**, **2**, **23** and **25**. The results are shown in Table 3.1 and Figure 3.6. MGL is known to bind to GalNAc, and was therefore used as a positive control for the experiment.[29, 30, 31] The GalNAc induced an increase in the melting point of MGL (from 2 °C at the lowest concentration to 4 °C at the highest concentration). The dendrimers **21**, **2** and **23** all performed better than GalNAc. The shifts of over +5 °C by the three dendrimers which bound to MGL (compounds **21**, **2** and **23**) were very encouraging. Dendrimer **2** performed particularly well, and was able to induce an 8.5 °C shift in melting point at a 300 μM concentration. Dendrimer **25** performed poorly, and induced either no shift or a negative shift in the melting point.

Table 3.1: DSF titration of MGL 176 with GalNAc and generation I dendrimers **21**, **25** **2** and **23**.

Plot	Additive	Concentration	+/−	Av. shift in M.P. (°C)
1	none			-
2	GalNAc	(600 μM)	+	4.0
3	GalNAc	(300 μM)	+	4.5
4	GalNAc	(30 μM)	+	2.0
5	Dendrimer **21**	(600 μM)	+	6.5
6	Dendrimer **21**	(300 μM)	+	5.0
7	Dendrimer **21**	(30 μM)	+	5.0
8	Dendrimer **2**	(600 μM)	+	6.0
9	Dendrimer **2**	(300 μM)	+	8.5
10	Dendrimer **2**	(30 μM)	+	7.0
11	Dendrimer **23**	(600 μM)	+	7.0
12	Dendrimer **23**	(300 μM)	+	6.0
13	Dendrimer **23**	(30 μM)	+	5.5
14	Dendrimer **25**	(600 μM)	-	-
15	Dendrimer **25**	(300 μM)	-	-
16	Dendrimer **25**	(30 μM)	−	1.5

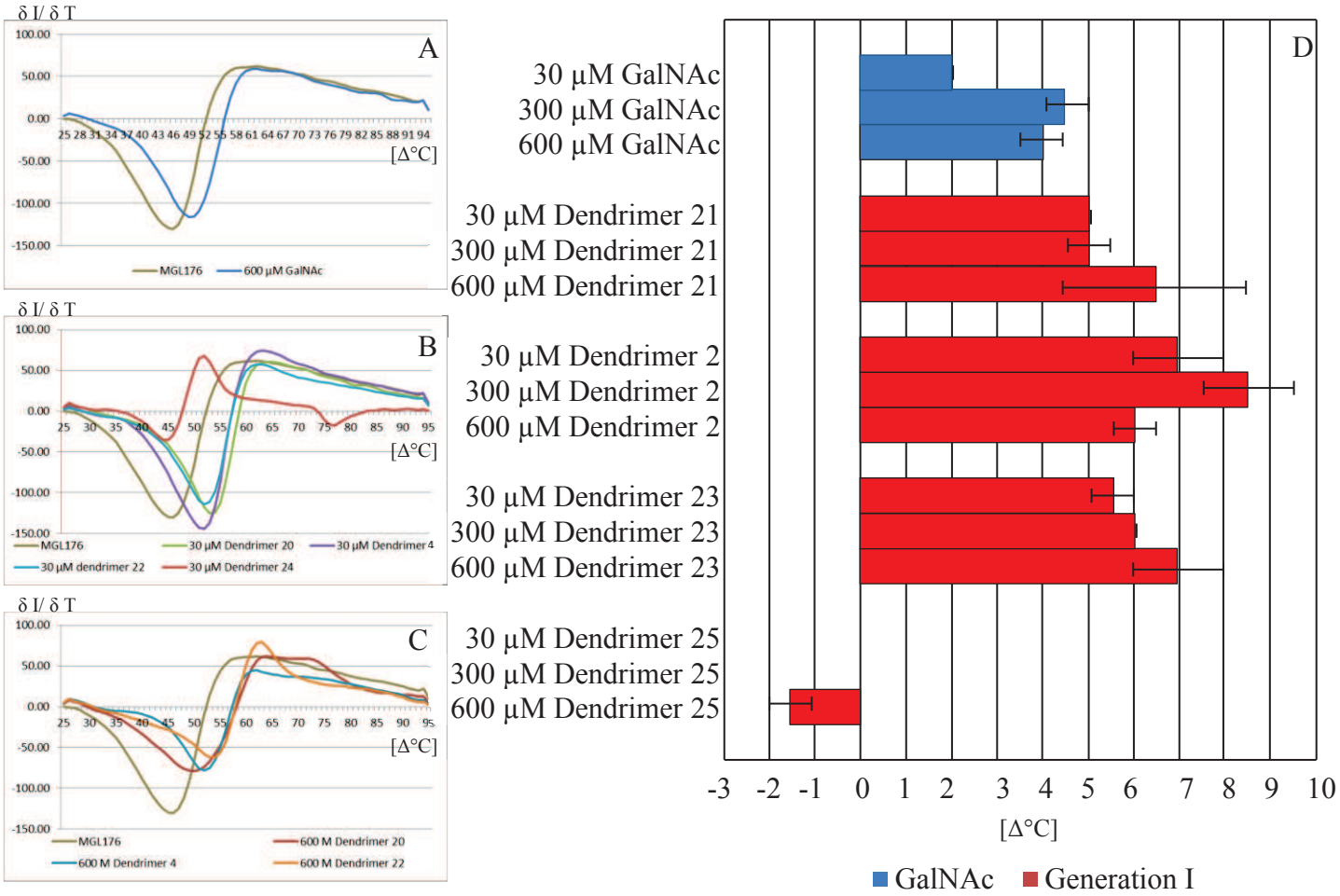

Figure 3.6: The shifts in melting point in °C for different additives with MGL 176. A) Differential DSF plot comparison of untreated MGL 176 and MGL 176 incubated with 600 μM GalNAc. B) Differential DSF plot comparison of untreated MGL 176 and all of the different dendrimers at 30 μM. C) Differential DSF plot comparison of untreated MGL 176 and the different dendrimers at 600 μM. D) The average shifts in melting point in °C for different additives with MGL 176 over different concentrations.

3.3 Thermal melt assay titration

The original DSF experiments followed a procedure developed in the laboratory of Dr Christopher Squire (SBS, UoA); unfortunately this showed a limited range of concentration for additives to interact with MGL. The aim of this work was to improve the experiment to show how the difference in concentration affects the binding to MGL and hence find the optimum concentration of the dendrimers for the thermal melt assay experiments. The concentration range used for the titration DSF was from 1 nM of the additive, which was also the lowest concentration used for additives in the cell binding assay, to 1 mM the maximum concentration that could be used in multiple experiments, without rapidly exhausting all of the dendrimer stocks. GalNAc was once again used as the positive control.[29, 30, 31] Two samples per additive were used in the DSF procedure originally developed by Squire *et al*. This was increased to three samples per additive in order to increase the statistical relevance.

The average melting points for the titration experiment are shown in Table 3.2 and Figure 3.7. The results indicate that when GalNAc binds to MGL in the concentration range of 1 nM to 100 μM, the melting point increases by roughly 2 °C. Incubations at 1 mM of GalNAc result in the melting point of MGL 176 increasing significantly by 6 °C. Dendrimer **21** always had at least a 1 °C larger shift in melting point increase than GalNAc over all concentrations. Dendrimer **21** also showed that the critical concentration for larger shifts in melting point occur was at 1 mM, where it induced much larger shifts in melting point (10 °C) than GalNAc (6 °C). The error bars for the experiment are small as there is a small spread in the data which resulted in the small standard deviation. Since the largest shifts in melting point for the titration experiment consistently occurring at 1 mM it was decided that the subsequent experiments for the thermal melt assay would use this concentration when comparing different additives.

The curve of the titration shown in Figure 3.7 shows that the binding to MGL 176 has not become saturated yet. Saturation would normally be indicated by a plateau forming in the plot, at which increasing the concentration of the additive will not increase in the melting point temperature. For the practical reason of dendrimer conservation, the experiment did not use larger concentrations, as this would deplete the stock too quickly.

The initial thermal melt assays showed that the GalNAc–containing generation I dendrimers would interact in a positive fashion with the carbohydrate recognition domain of monomeric MGL, and that the strength of binding was in proportion to the concentration of the dendrimer incubated with MGL. The next step would be to test the binding of the dendrimers to cells which express MGL.

Table 3.2: Titration of MGL 176 with GalNAc and dendrimer **21**.

Plot	Additive	Average M.P. (°C)	+/−	Av. shift in M.P. (°C)
17	none	50.0		-
18	GalNAc (1 nM)	51.7	+	1.7
19	GalNAc (10 nM)	51.7	+	1.7
20	GalNAc (100 nM)	52.0	+	2.0
21	GalNAc (1 μM)	50.7	+	0.7
22	GalNAc (10 μM)	51.3	+	1.3
23	GalNAc (100 μM)	52.3	+	2.3
24	GalNAc (1 mM)	56.3	+	6.3
25	Dendrimer **21** (1 nM)	53.0	+	3.0
26	Dendrimer **21** (10 nM)	52.3	+	2.3
27	Dendrimer **21** (100 nM)	52.7	+	2.7
28	Dendrimer **21** (1 μM)	52.0	+	2.0
29	Dendrimer **21** (10 μM)	52.0	+	2.0
30	Dendrimer **21** (100 μM)	53.3	+	3.3
31	Dendrimer **21** (1 mM)	60.0	+	10.0

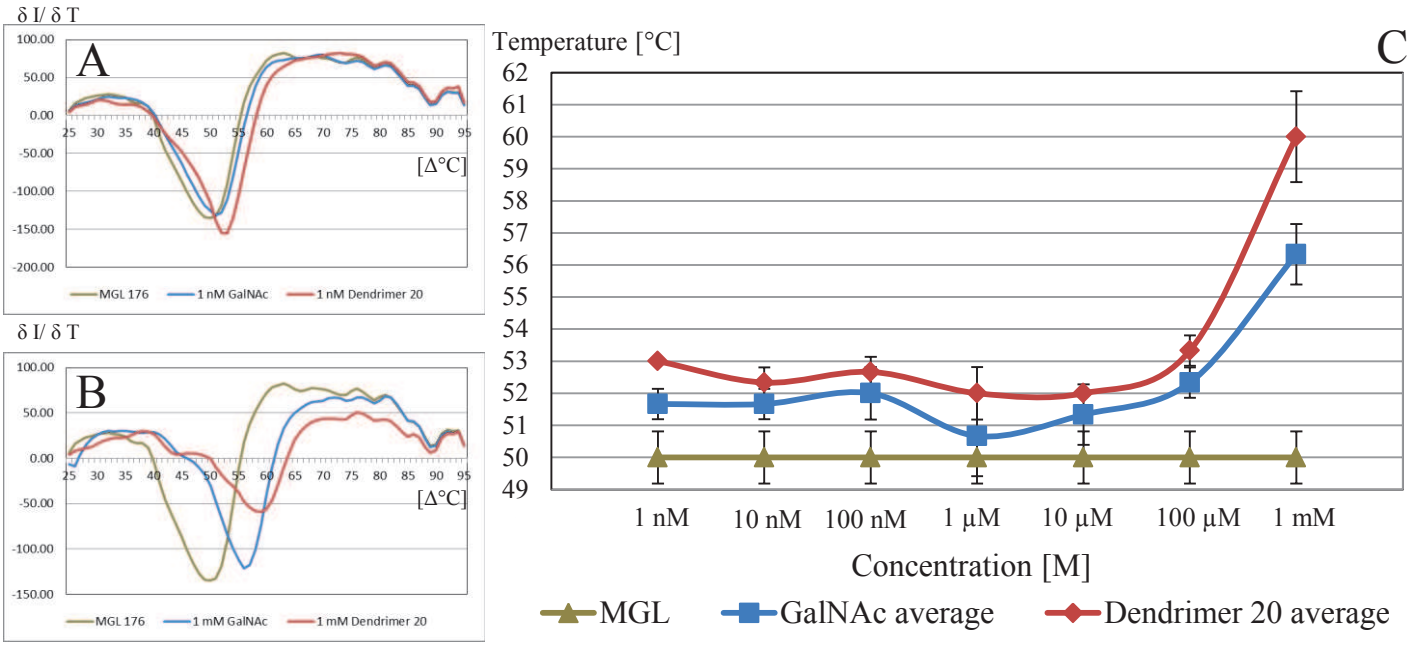

Figure 3.7: Melting point [°C] for MGL 176 with different molar concentrations of GalNAc or dendrimer **21**. A) Differential DSF plot comparison of untreated MGL 176 to MGL176 treated with 1 nM GalNAc and 1 nM dendrimer **21**. B) Differential DSF plot comparison of untreated MGL 176 to MGL 176 treated with 1 mM GalNAc and 1 mM dendrimer **21**. C) Comparison of average melting points for untreated MGL 176 to MGL176 treated with GalNAc and dendrimer **21**.

Chapter 4

Ability of GalNAc compounds to bind MGL–expressing human cells at 0 °C

This chapter will examine the initial work performed using the MGL cell binding assay. This was the first biological assay to be performed using both the generation I and II dendrimers which were synthesised in Chapter 2. The generation I dendrimers (which each contain three GalNAc moieties) used in these experiments are shown in Figure 4.1, and the generation II dendrimers (which aren't glycosylated) are shown in Figure 4.2.

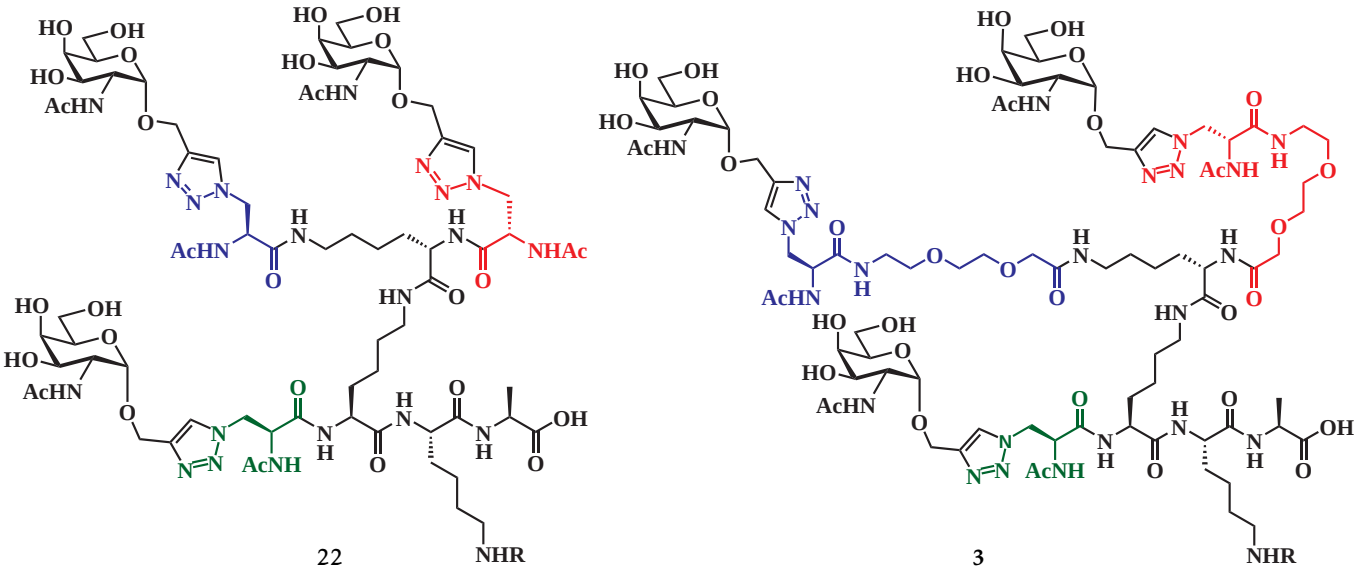

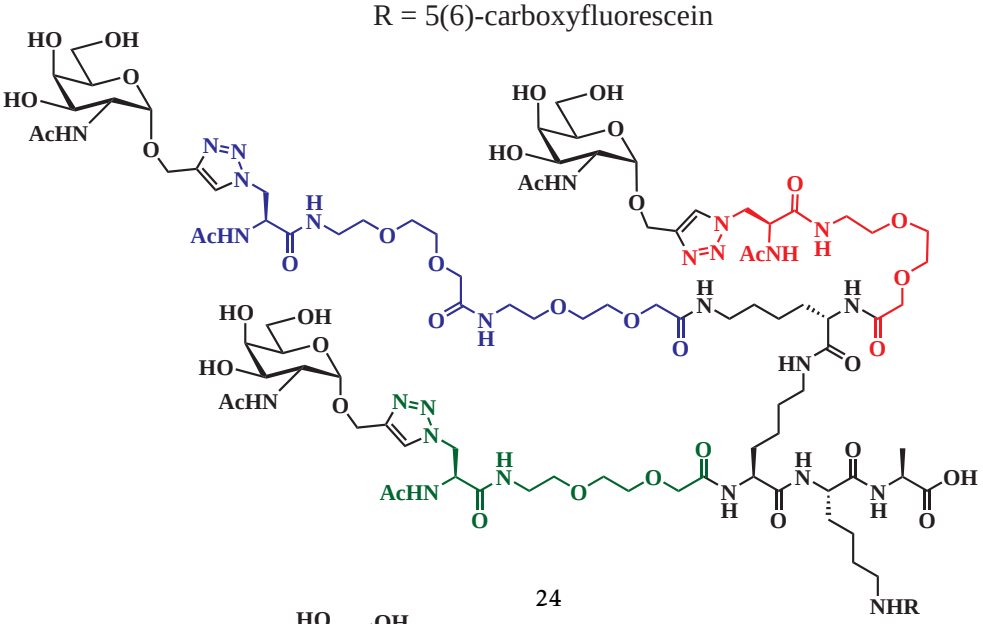

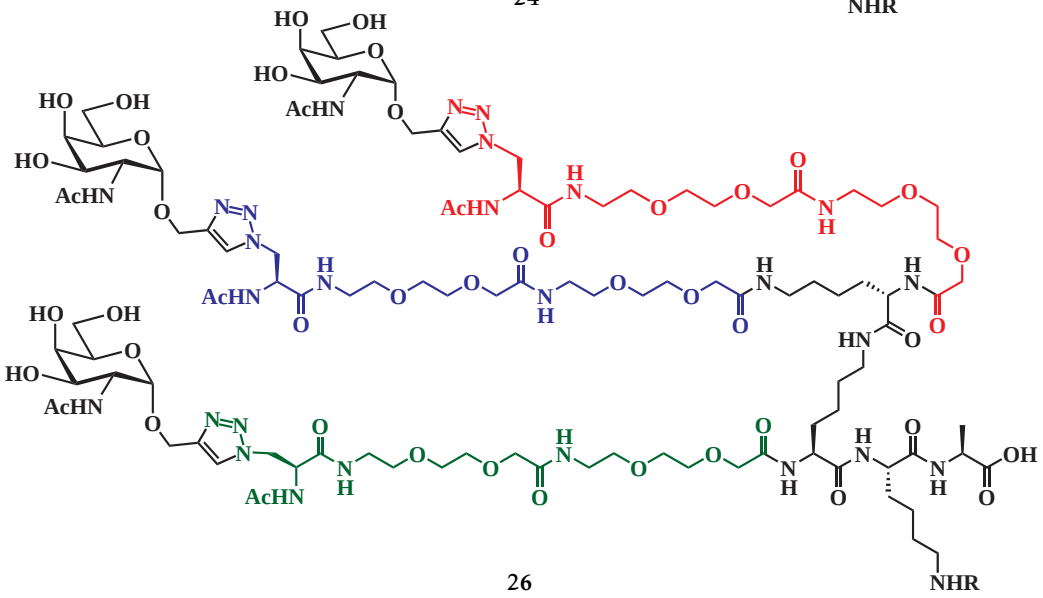

Figure 4.1: Structures of the generation I dendrimers **22**, **3**, **24** and **26**.

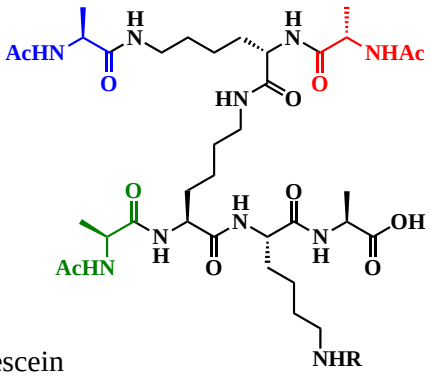

R = 5(6)-carboxyfluorescein 44

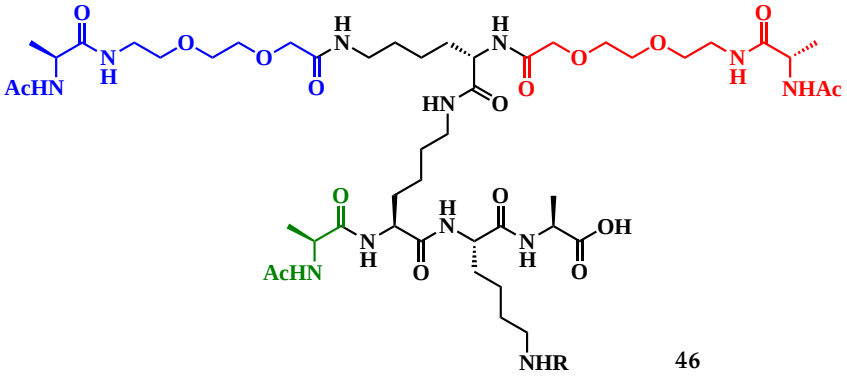

46

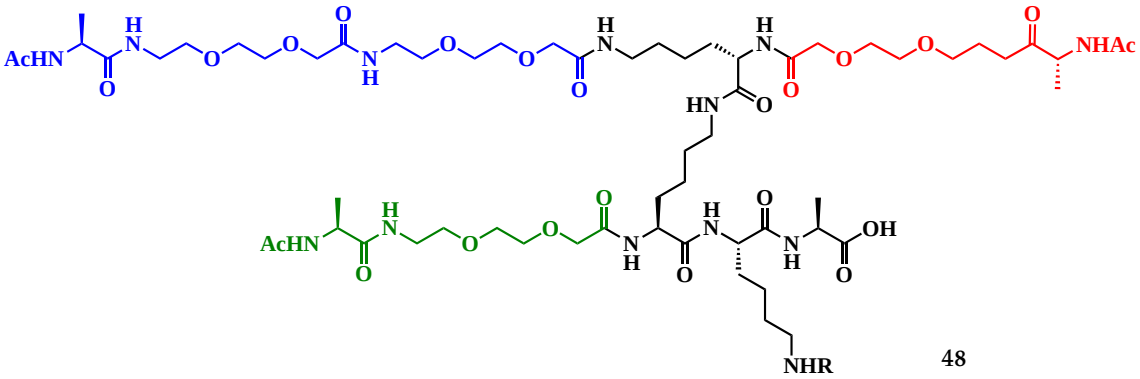

48

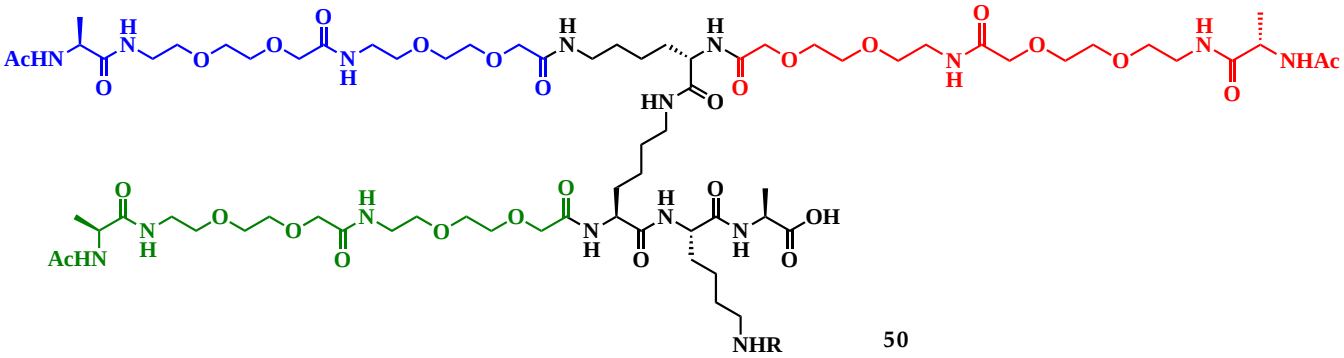

50

Figure 4.2: Structures of the negative control generation II dendrimers **44**, **46**, **48** and **50**.

4.1 Introduction

In Chapter 3 the results from the initial thermal melt study demonstrated that the GalNAc–containing generation II dendrimers bound to the carbohydrate recognition domain of the monomeric MGL 176 truncation. The focus of this chapter will be on the binding interactions of cells which express MGL with the generation I and II dendrimers at 0 °C.

4.1.1 Previous binding studies of MGL

The migration of mature monocyte derived dendritic cells (MoDCs) and the role played by MGL receptor has been studied.[136] An assay which looked at the expression of MGL in lymph nodes and the thymus was performed. The cells from these organs were incubated with anti–MGL antibodies which confirmed the presence of MGL on the surface. The lymph nodes and the thymus cells were also incubated with antibodies which would bind GalNAc (specifically α–GalNAc–specific snail lectin *Helix pomatia* agglutinin (HPA)) to identify the presence of ligands which would bind MGL. MGL protein and its ligands are two entities which are expressed in close proximity at similar anatomical locations in lymph nodes or the thymus. MGL specifically interacts with endothelial cells in an α–GalNAc–dependent manner. Immature MoDCs which expressed MGL, bound to sinusoidal and lymphatic endothelium cells which expressed GalNAc–containing ligands. Mature MoDCs which don't express MGL did not bind to these sinusoidal and lymphatic endothelium cells, and are therefore able to migrate. MGL does not facilitate migration, but it does restrict the ability of the MoDCs to migrate away from GalNAc–containing ligands found on certain types of cells.

An example of a common GalNAc–glycosylated ligands for MGL are the mucin sequences. Interactions of MUC1 glycosylated with GalNAc and immature monocyte derived dendritic cells (MoDCs) which express MGL have been studied.[20] Binding of MGL varies with glycan changes on MUC1 in colon carcinoma.[25] When MoDCs mature the MGL receptor is down modulated, which coincides with loss of MUC1 binding. As anti MGL antibodies were proven to compete with MUC1 binding it was concluded that all C–type lectin receptor binding for MUC1 to MoDCs was mediated by MGL. It was also shown that MUC1 proteins from primary colon carcinoma bind to MGL–expressing immature MoDCs. MGL is highly expressed on immature tolerigenic antigen presenting cells where there could be interactions between the MUC1 sequence which lead to immunosuppressive effects. Incubation of peptides based on the MUC1 sequence with MoDCs was evaluated for binding. MGL was observed to bind MUC1 and GalNAc carrying immunogen underwent internalization. For MUC1 presentation the number of carbohydrate structures was important in determining the strength of binding between an antibody and an antigen.[20]

The effect of incubating the T_N antigen containing MUC1 sequence or a MGL antibody effected MoDCs.[137] MGL oligomerises to form homodimers or homotrimers after incubation with either the MUC1 sequence or the MGL antibody. The additives interactions with MGL lead to phosphorylation of extracellular signal-regulated kinase 1,2 (ERK1,2) and nuclear factor–KB (NF–KB) activation; this eventually leads to DC maturation which results in initiation of a strong $CD8^+$ T-cell immune response. The results from these experiments led to the conclusion that MGL would be an optimal candidate for targeting with a vaccine for immunotherapy.

Other ligands for MGL include the GalNAc–glycosylated fluke *Schistosoma mansoni* soluble egg antigens (SEA). Research on how the blood fluke SEA are internalized by human MoDCs has been undertaken.[27] Three C-type lectin receptors (CLR)s were important for binding of the SEA to MoDCs: DC-SIGN, mannose receptor and MGL. Cell adhesion of MGL–expressing cells to the two antigens of SEA; kappa-5 and IPSE/α1 demonstrate the influence of GalNAcs on MGL binding.[138] The kappa–5 antigen which contains terminal GalNAc residues in its major glycan structure bound strongly to MGL. IPSE/α1 does not contain terminal GalNAc residues, and therefore was a weaker binder to the MGL receptor. The binding was shown to be calcium dependent which is typical for binding to to a CLR. The binding of kappa-5 antigens to MGL was abolished when the terminal GalNAc residues were removed.

In 2010 Leclerc *et al*. performed a series of assays designed to target dermal MoDCs with fully synthetic multiple antigen glycopeptides (MAG) in an attempt to stimulate antibody responses.[139] The MAG used were polylysine dendrimers with four arms which were connected to a peptide backbone. The dendrimer contained a $CD4^+$ epitope from the polio virus (PV) and were either trimeric or hexameric T_N residues at the N terminus of the peptide as shown in Figure 4.3, the binding was compared to MUC6:T_N glycoprotein sequences. The binding of MUC6 recombinant proteins to MGL^+ MoDCs was dependent on the carbohydrate content of the protein. MUC6 sequence glycosylated with GalNAc efficiently bound to MGL^+ MoDCs, whereas the non–glycosylated sequence failed to show conclusive evidence of binding.[139] The MAGs also showed strong binding to MGL^+ MoDCs. Leclerc *et al*. showed that through targeting MoDCs with T_N Glycopeptides, a $CD4^+$ Th2 response can be stimulated. Leclerc's MAG interaction with MGL induced high levels of antibodies specific for the tumor–associated T_N antigen.[139]

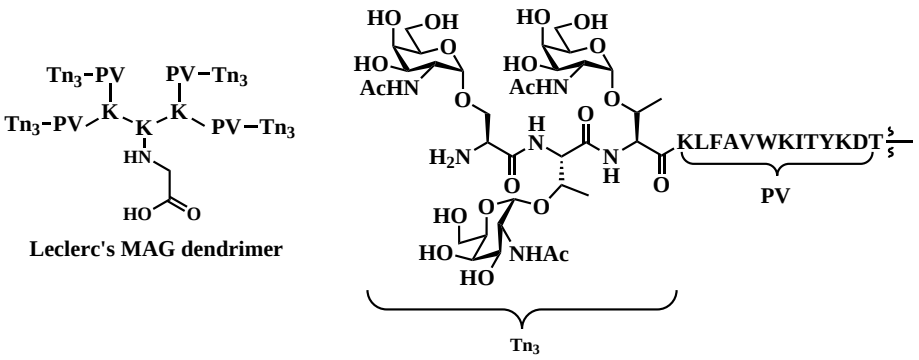

Figure 4.3: The multiple antigen glycopeptide (MAG) which contains a polylysine core connected to a $CD4^+$ epitope from the polio virus (PV) with N-terminal T_N antigens synthesised by Leclerc *et al.*[139]

Given the high affinity and specificity of MGL for the GalNAc moiety, it has been proposed that targeting the MoDC with synthetic vaccines and pathogens could create a desired immune response. Future studies on the interactions of glycoproteins with MGL would be beneficial for vaccine design and modulation of immune response.[25, 20, 138]

While many of the binding studies presented here involved proteins and cells which are of natural origin,[136, 27] the synthetic branched MAGs which contain the GalNAc residues also bound to MGL expressing cells.[139] Interestingly, even though the density of T_N antigens in the native sequences is higher than the synthetic dendrimers (such as Leclerc's MAG) the relative binding of the two types of compounds was comparable. The relatively good binding of the dendrimers with a lower density of GalNAc residues may be due to the nature of the polydentate binding and the clustering effect. We postulated that the glycodendrimers which were designed in Chapter 2 could achieve selective binding to MGL even though they have a lower density of GalNAc residues compared to the ligands previously mentioned, by taking advantage of polydentate binding and clustering effects.

4.2 Gating strategy for flow cytometry experiments.

From the data acquired from the flow cytometer, it is possible to identify the cells that are conjugated to fluorescent molecules due to their shape and the fluorescence of the antibodies against phenotypic markers. In the program FlowJo the data from the cells can be used to work out how the cells fluoresce, and hence identify which cells have the dendrimers bound to them. An example of the gating strategy is shown Figure 4.4.

The two cell populations, MoDC and LG2 cells, were identified using similar gating strategies. The first plot shows the cells initial forward and side scatter. The second plot gates the cells which express the identifying cell marker. MoDC express CD1a, therefore we identify MoDC by a CD1a antibody which has the fluorophore Alexa Fluor 647 attached to it. The cells which have a high fluorescence of Alexa Fluor 647 express CD1a and are therefore MoDC. LG2 cells express CD20 therefore we identify LG2 by a CD20 antibody which has the PE fluorophore conjugated to it. The cells which have a high fluorescence of PE are therefore LG2 cells. The third plot gates on the forward and side scatter of the main population of these cell types. The MoDC have one major population, whereas the LG2 cells have two populations. The fourth plots gates the cells against the fluorescence of 7AAD, which binds to dead cells. The cells with a high fluorescence of 7AAD are dead and are therefore removed. The fifth plot shows the fluorescence of the gated cells in the fluorescence of 5(6)–carboxyfluorescein, which is the fluorescent marker attached to the dendrimers. Cells with high fluorescence in this channel will have dendrimers bound to them. The mean fluorescence intensity (MFI) of the channel 5(6)–carboxyfluorescein is measured and gives a numerical value which can be used to compare different samples for the same cell type and the same experiment.

Cells have a natural autofluorescence which occurs even in the absence of fluorescent dendrimers or antibodies. The strength of binding can be judged by the difference in MFI of the cell population incubated with additives compared to the autofluorescence of the untreated cells. When the fluorescence of the sample is less than or equal to the autofluorescence of the cells the MFI will be equal or smaller, indicating there has been no binding. When there is a positive shift in the fluorescence of the sample incubated with a fluorescent additive, binding is occurring. The larger the difference in MFI the stronger the binding. The greater the shift of the MFI the more important the binding is. The graphs for the cell binding assays performed are plotted using the change in MFI which was worked out using following equation (MFI of the treated sample) - (MFI of the autofluorescence) = (The change in MFI). Any values less than 0 were treated as 0.

The FACS plots for each experiment are shown in the appendix. Due to the large number of FACS plots generated for each experiment, the data has been compiled into bar graphs which plot the average change in MFI for each sample to provide a way for clear comparisons between samples. These graphs are also plotted on a logarithmic scale in a similar fashion to the data the presented on

the FACS plots.

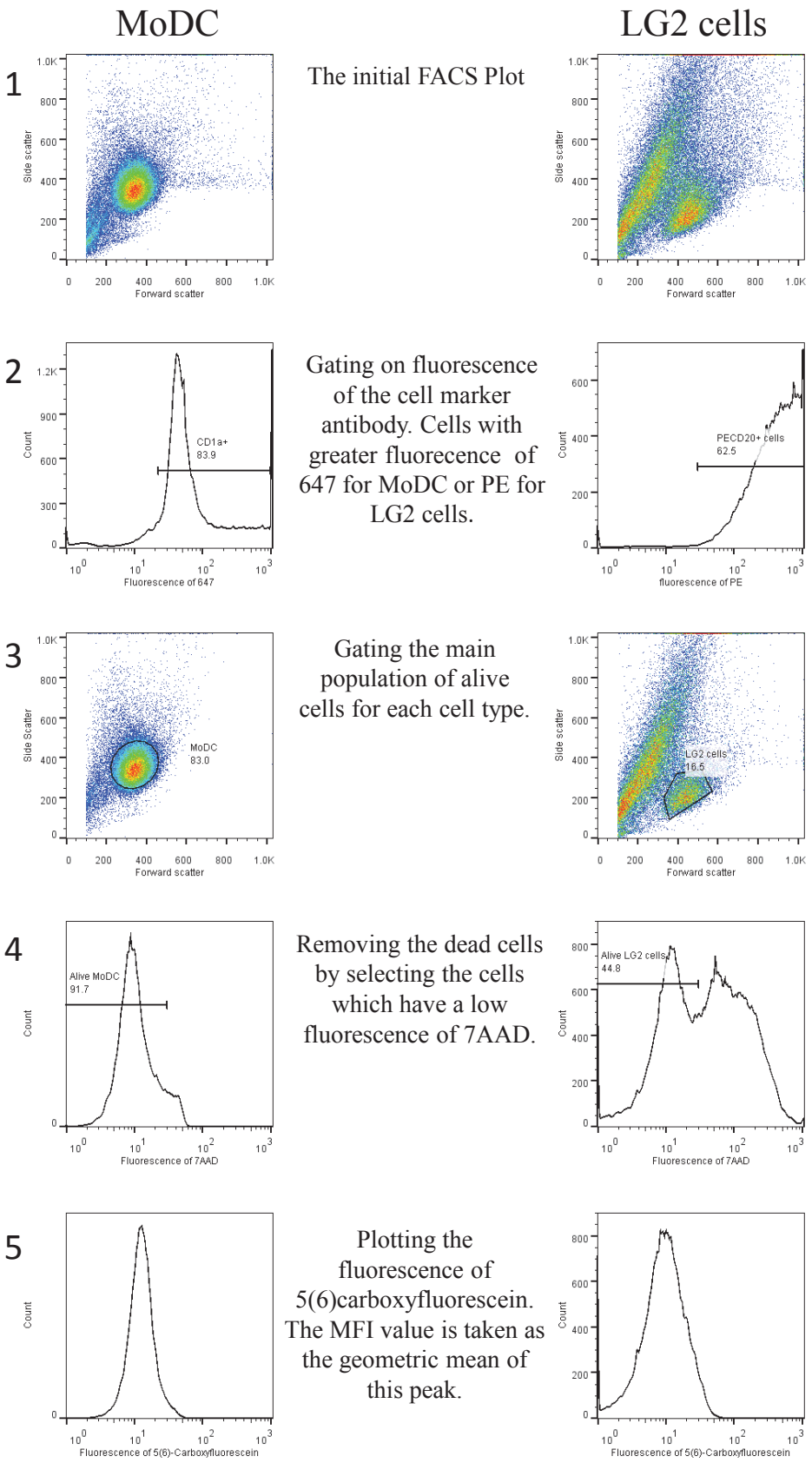

Figure 4.4: Gating strategy for selection of MoDC and LG2 and determining MFI of cells in relation to the 5(6)–carboxyfluorescein channel.

4.3 MGL–expression and selection of the MGL negative LG2 cells for the cell binding assay

The ability of the glycosylated constructs produced in Chapter 3 to bind to MGL expressed on the cell surface, was tested using immature MoDC. These cells were shown to express high levels of MGL on the cell surface (Figure 4.5) as previously described.[29, 105, 106] To test the requirement of the presence of cell surface–MGL for binding a cell that lacked expression of surface MGL was required. To this end, the Epstein–Barr transformed B cell line LG2 was tested MGL expression, since the LG2 cells does not express MGL it was a suitable negative control cell type. Any binding which occurs to the LG2 cells will be non–specific binding.

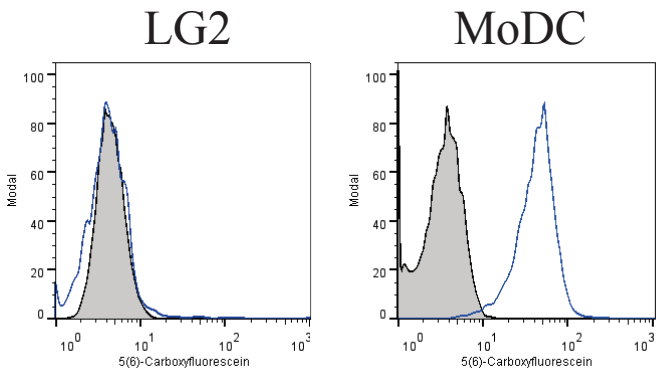

Figure 4.5: MGL expression on different cell types have been tested using an antibody conjugated with fluorescein. LG2 cells do not express MGL, whereas MoDC express MGL and therefore binds the antibody resulting in an increase in MFI.

4.4 Optimisation at 0 °C

Initially the conditions of the binding assay were optimised to ensure whether the dendrimers bound to MGL–expressing cells selectively. A series of experiments were performed in order to work out the parameters for the final experiment in which all the dendrimers and peptides would be tested for binding to MGL–expressing MoDC. The following parameters were examined:

- Concentration of additives.
- Length of incubation of additives.
- Temperature of incubation.
- Reaction solvent.

The initial experiments were performed at 0 °C using the TSM buffer used by Van Kooyk *et al.*[25] It had been postulated that at this temperature the cells are unlikely to take up the dendrimer. Therefore by performing an assay at at 0 °C, the binding between additives will be down to interactions with the receptors present on the surface of the cells.

The generation I dendrimers all have GalNAc residues, while the generation II denrimers have the similar branched scaffolds without GalNAc residues. Each generation I dendrimer has an equivalent generation II dendrimer. The pairs of dendrimers are: **22** and **44**, **3** and **46**, **24** and **48**, **26** and **50**. Each dendrimer was compared to its non–GalNAc control pair and to the other compounds from its generation.

As the generation I dendrimers contain T_N antigen mimics these dendrimers are expected to bind stronger to MGL expressing cells such as the MGL–expressing MoDC used in the assays than the non-glycosylated generation II dendrimers.

4.4.1 Time course experiments to define optimum length of time for binding

The initial focus was to see how the incubation period affected binding of the additives to the MoDC and LG2 cells. A time course experiment was performed over a period of 2 hours at 0 °C to see how binding varied with different incubation time periods. Nuti *et al*.[137] and Van Kooyk *et al*.[136] both performed binding studies with incubation periods which ranged between 30 minutes and 1 hour, whereas Leclerc *et al*.[139] Die *et al*.[27] and Hooke *et al*.[138] all used time periods of an hour. Based on these previous studies, the times chosen were 30 minutes, 1 hour and 2 hours.

The averaged results for the time course are shown in plot C in Figure 4.6. Dendrimer **44** shows no binding to MoDC in this experiment. The shift in MFI shows an increase in binding for the GalNAc–glycosylated dendrimer **22** over the time period, with the largest shift in FACS plot A in Figure 4.6. There is very little binding at 30 minutes, with a great increase after 1 hour of incubation. The change in MFI for dendrimer **22** is small in comparison from 1 hour to 2 hours.

Neither dendrimer **22** nor **44** shows any binding to the LG2 cells over these incubation periods. An example of the FACS plots are shown in FACS plot B in Figure 4.6. The population of dead cells seemed to increase with longer incubation periods at 0 °C for both cell types and both dendrimers, but especially for LG2 cells.

While there is an increase in binding by the glycosylated dendrimer **22** towards MoDC at 2 hours, there was also an increase in dead cells which was monitored by the 7AAD+ dye (data not shown). As an increase in cell death is seen with 2 hours of incubation, 1 hour was chosen as the length of time to incubate.

This experiment showed that GalNAc–containing glycodendrimers selectively bound to MoDC over the LG2 cells. It cannot be definitively stated that the binding is occurring at the MGL proteins expressed on the surface of MGL. The dendrimer could be binding to any lectin on the surface of the MoDC. To prove the site of binding a crystal structure of the protein with the dendrimer docking would be required, which is outside the scope of this project.

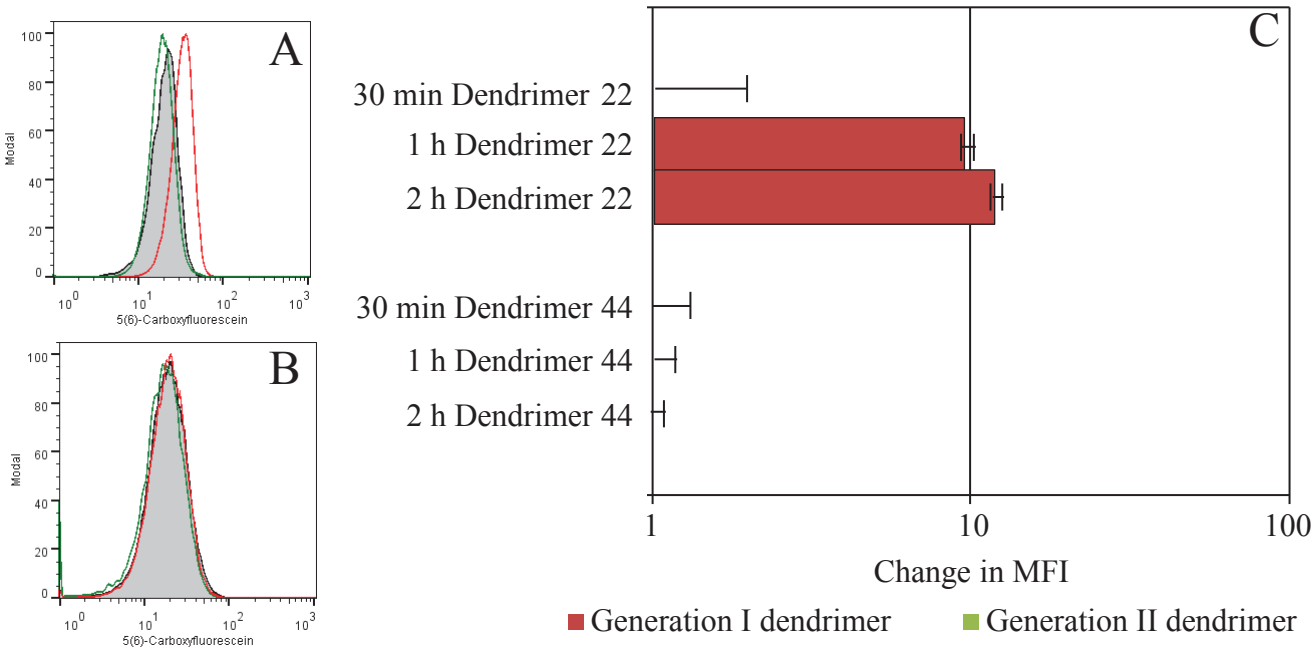

Figure 4.6: Time course experiment for binding to MoDC and LG2 cells at 0 °C using dendrimers **22** and **44** at 1 μM concentrations. A) FACS histogram plot indicating binding of 1 μM of the dendrimer **22** (red) and **44** (green) to MoDC with a 2 h incubation. B) FACS histogram plot indicating binding of 1 μM of the dendrimer **22** (red) and **44** (green) to LG2 with a 2 h incubation. C) Change in MFI is given as the average for triplicate samples for each dendrimer incubation.

4.4.2 Titration experiments to define binding limits

Low concentration titration

A series of titration experiments were performed to determine the concentrations at which binding of the glycodendrimers could be observed. These experiments initially focused on lower concentrations of additives and then moved onto experiments with higher concentrations.

The first titration experiment to use both MoDC and LG2 in the same sample explored the interactions of dendrimers at lower concentration. The titration was performed at 0 °C for 1 hour with LG2 cells and MoDC using dendrimer **26** and the equivalent negative control dendrimer **50**, with the concentrations 1 μM, 100 nM and 1 nM.

The generation I dendrimer **26** selectively bound to the MGL–expressing MoDC compared to the LG2 cells. FACS plot A in Figure 4.7 shows the GalNAc–glycosylated dendrimer **26** and the non–glycosylated generation II dendrimer **50** fluorescence curve when incubated with MoDC. The increase in MFI for dendrimer **26** shows binding whereas dendrimer **50** produces curves which overlap the autofluorescence of MoDC indicating that it does not bind.

The bar graph C in Figure 4.7 demonstrates that binding to MoDC for dendrimer **26** was dose dependent. The binding by dendrimer **26** to MGL–expressing MoDC was visible at 100nM and the strength of binding increases with concentration.

There was no binding to the LG2 cells observed by any of the dendrimers at any concentration. The FACS plot B in Figure 4.7 is a typical representation of the LG2 fluorescence curves for all additives at concentrations between 1 nM and 1 μM.

One of the aims of the experiment was to show that even with other cells present the GalNac hybridised dendrimer would selectively bind the MGL–expressing MoDC over the negative control LG2 cells. The titration experiments demonstrated that the dendrimers would selectively bind MoDC in the presence of LG2 cells.

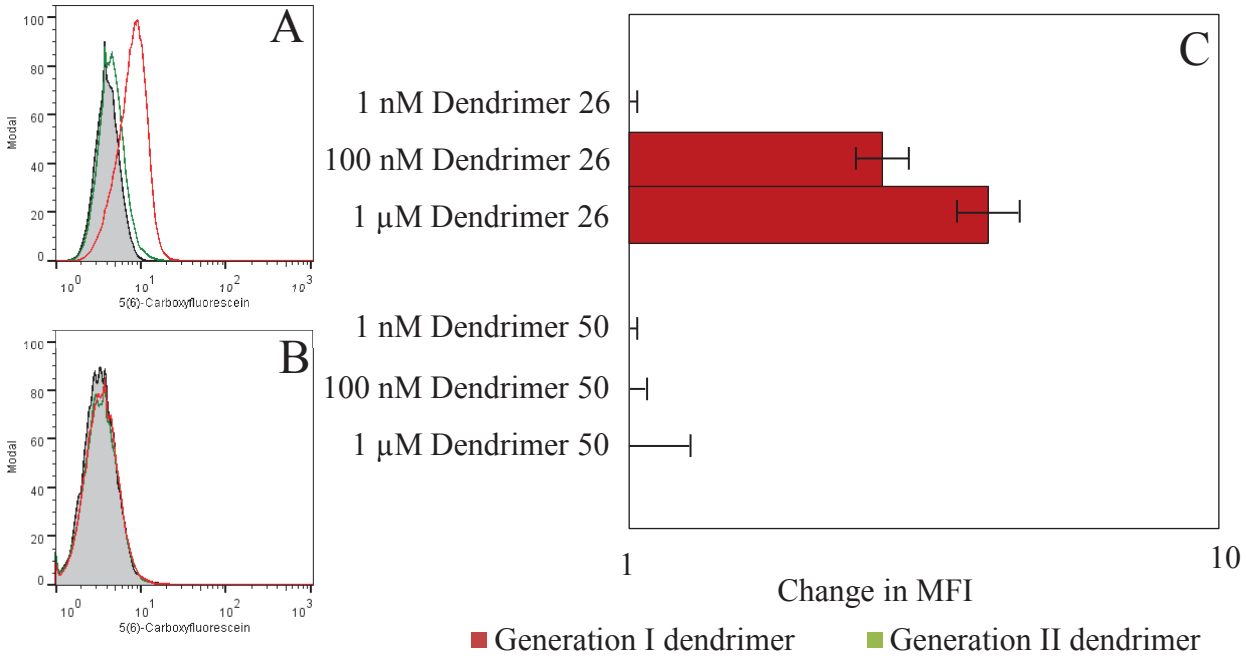

Figure 4.7: Titration of dendrimers **26** and **50** at 0 °C for 1 hour with 1 μM, 100 nM and 1 nM concentrations. A) FACS histogram plot indicating binding of 1 μM of the dendrimer **26** (red) and **50** (green) to MoDC.
B) FACS histogram plot indicating binding of 1 μM of the dendrimer **26** (red) and **50** (green) to LG2.
C) Change in MFI is given as the average for duplicate samples for each dendrimer incubation.

A similar titration was next performed which omitted the lowest concentration (due to the lack of binding previously observed) and used all of the generation I and II dendrimers. The conditions used were an incubation at 0 °C for 1 hour with 1 μM and 100 nM concentration of additives.

The FACS plot A in Figure 4.8 shows a comparison of the change in MFI for dendrimer **26** and **50**, which is representative of all the FACS plots for the dendrimer pairs. The shift in the fluorescence curve is small for the MoDC incubated with generation I dendrimers (in this case **26**) but was consistent, whereas the cells incubated with generation II dendrimer (in this case **50**) will have a fluorescence curve that overlaps the autofluorescence.

The bar graph C in Figure 4.8 shows a clear binding pattern for the titration experiment. The shifts in MFI for MoDC incubated with first generation dendrimers of the 100 nM concentration ranged from 2.4 for dendrimer **26** to 1.2 for dendrimer **3**. The shifts in MFI for MoDC incubated with generation I dendrimers of the 1 μM concentration ranged from 3.4 for dendrimer **26** to 1.7 for dendrimer **3**. The MoDC appear to show a preference for binding to the generation I dendrimers compared to the generation II dendrimers, as every generation I dendrimer induces a larger shift in MFI than the largest shift of the generation II dendrimers. This is expected as the generation I dendrimers contain T_N antigen mimics whereas the generation II dendrimers do not. This shift is so apparent that even the 100 nM concentration generation I dendrimers induce larger shift than the generation II dendrimers with a concentration of 1 μM.

FACS plot B in Figure 4.8 shows a representative example of the lack of binding by dendrimers to the LG2 cells. No observable non–specific binding was occurring to the LG2 cells.

The shift in MFI for is concentration dependent for the generation I dendrimers binding to MODC, with the same pattern of MFI shifts being shown for each concentration (with lower MFI shifts for 100 nM). To rank the four generation I dendrimers in this experiment based on shift in MFI: 1st **26**, 2nd **24**, 3rd **22** and 4th **3**.

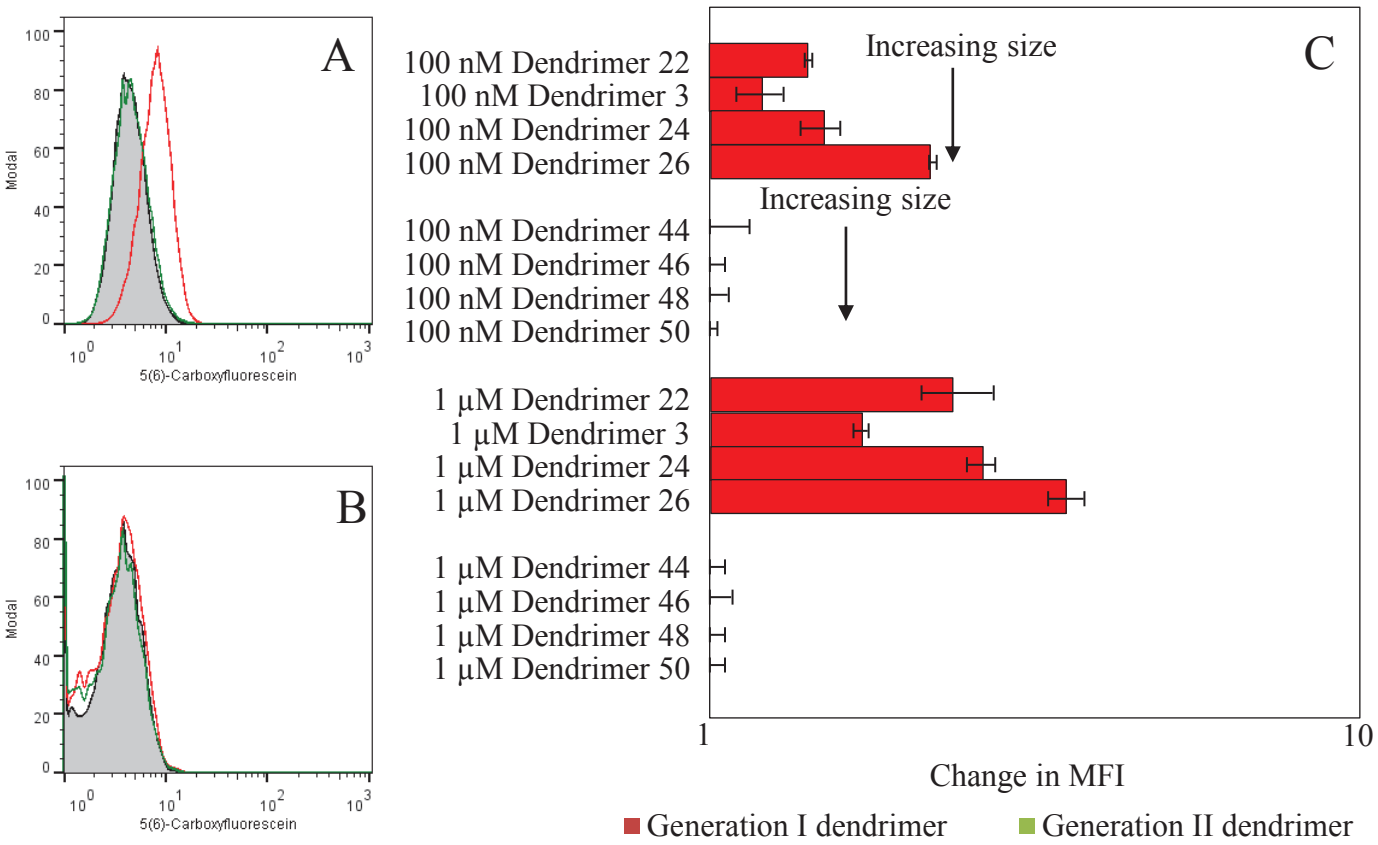

Figure 4.8: The cell binding assay performed with the generation I and II dendrimers 1 μM, 100 nM concentrations. A) FACS histogram plot indicating binding of 1 μM of the dendrimer **26** (red) and **50** (green) to MoDC. B)FACS histogram plot indicating binding of 1 μM of the dendrimer **26** (red) and **50** (green) to LG2.
C)Change in MFI is given as the average for duplicate samples for each dendrimer incubation.

High concentration titration

The titrations previously had only focused on the lower concentrations, a titration which used higher concentrations of additives was also performed. The shifts in MFI of MoDC and LG2 cells incubated with additives at 50 μM, 10 μM, 5 μM and 1 μM concentrations were examined. The dendrimers used were the largest pair of dendrimers **26** and **50**, as well as the smallest pair of dendrimers **22** and **44**.

The largest shift in MFI for MoDC was dendrimer **22** which induced the largest shift with dendrimer **26** producing the second largest shift in MFI every time. FACS plot A in Figure 4.9 shows the comparison of the generation I and II pair dendrimer **22** and dendrimer **44** at 50 μM. While the shift in the fluorescence curve is much larger for dendrimer **22** compared to the lower concentration results, the shift in the fluorescence curve for dendrimer **44** has become visible.

FACS plot B in Figure 4.9 compares the generation I and II pair dendrimer **22** and dendrimer **44** at 1 μM. At this concentration dendrimer **22** shows signs of binding (although weaker than at 50 μM), whereas dendrimer **44** no longer shows any sign of binding.

The generation II dendrimers showed no sign of binding to MoDC at lower concentrations in the previous experiments, but when the concentration was increased past 1 μM binding was observed. The generation II dendrimers **44** and **50** had similar shifts in MFI at each concentration which were both smaller than the equivalent generation I dendrimer.

Bar Graph C in Figure 4.9 shows the average results for the high concentration titration experiment. The general trend was for the MFI to increase with higher concentrations of additives.

FACS histogram plot indicating binding of 1 μM of the dendrimer **22** (red) and **44** (green) to MoDC.

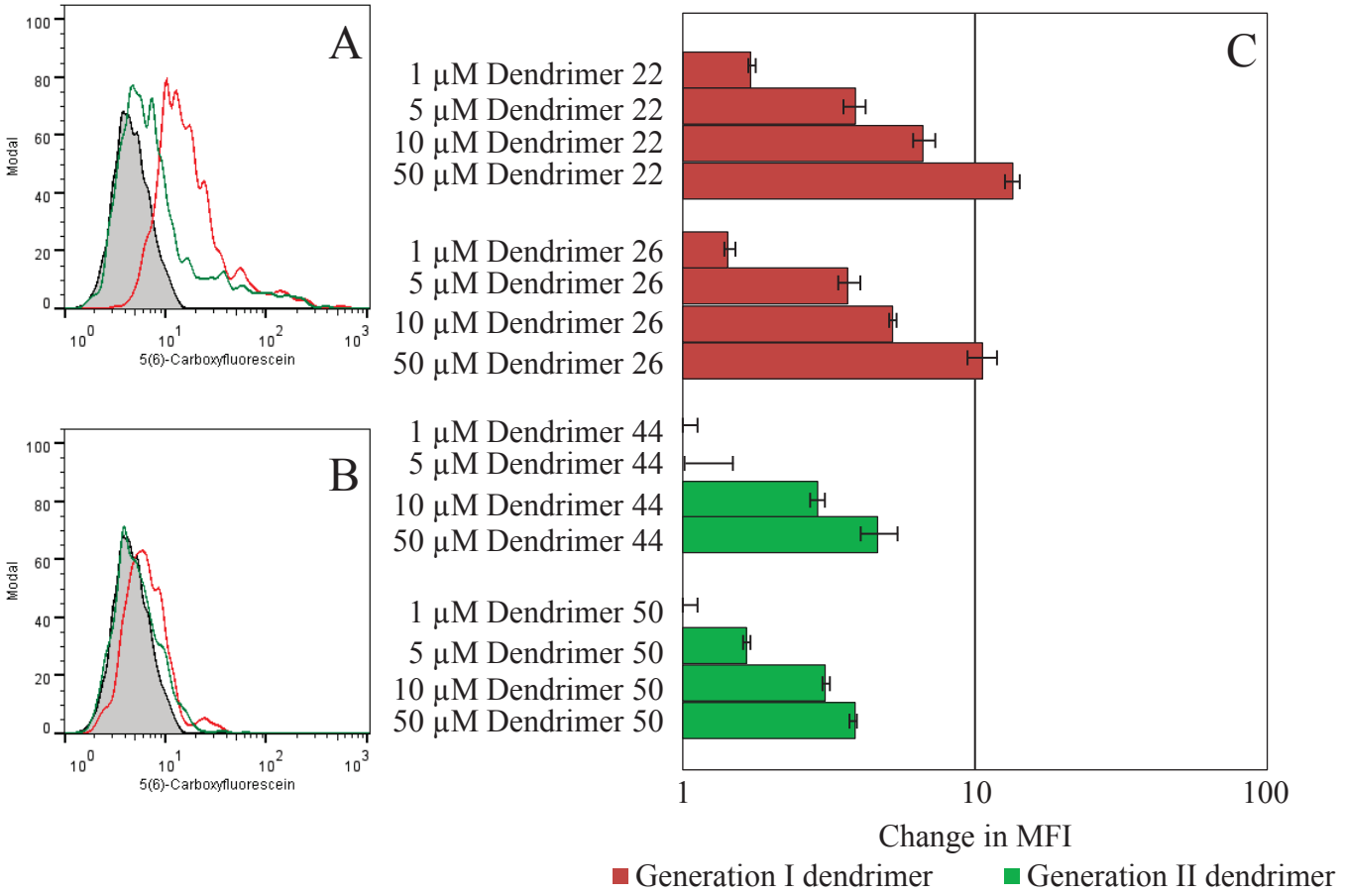

Figure 4.9: A titration experiment at 0 °C for 1 h with concentrations of 50 μM, 10 μM, 5 μM and 1 μM. A) FACS histogram plot indicating binding of 50 μM of the dendrimer **22** (red) and **44** (green) to MoDC. B) FACS histogram plot indicating binding of 1 μM of the dendrimer **22** (red) and **44** (green) to MoDC.
C)Change in MFI is given as the average for duplicate samples for each dendrimer incubation.

The binding of LG2 cells to the generation I and II dendrimers was analysed next, the results are shown in Figure 4.10. This experiment demonstrates that increasing the concentration above 1 μM leads to a greater amount of non specific binding. FACS plot A from Figure 4.10 shows a comparison of dendrimer **22** and dendrimer **44** at 50 μM concentration, with dendrimer **22** having the greater increase in MFI for LG2 cells. FACS plot B in Figure 4.10 is a representative example of the 1 μM fluorescence curve for both generation I and II dendrimers with LG2 cells.

Bar graph C from Figure 4.10 shows the average MFI shifts for the high concentration experiment for LG2 cells incubated with the different additives. The shift in MFI for LG2 cells was dependent on the concentration of the dendrimer. All of the dendrimers showed no sign of binding to LG2 cells at a concentration of 1 μM. When the concentration was increased to 5 μM the shift in MFI increased to around 1. The shift in MFI is more variable between compound at 10 μM, with MFI shifts of between 0.4 for dendrimer **26** and 2.3 for dendrimer **22**. The shift in MFI for additives incubated at a 50 μM concentration is around 3 for all of the dendrimers except **22** which has a MFI of around 6.

The results of the titration experiments led to the decision that a concentration of 1 μM would be used for future experiments. These conditions gave shifts in MFI where the generation I dendrimers had a visible shift in MFI, while shifts in MFI for the negative control generation II dendrimers were still small and not indicative of binding. There was also no sign of significant binding to LG2 cells by either dendrimer. 1 μM concentration gives a balance between shifts in MFI which are large enough to be relevant while not producing non specific binding by the LG2 cells and dendrimers with no GalNAc residues.

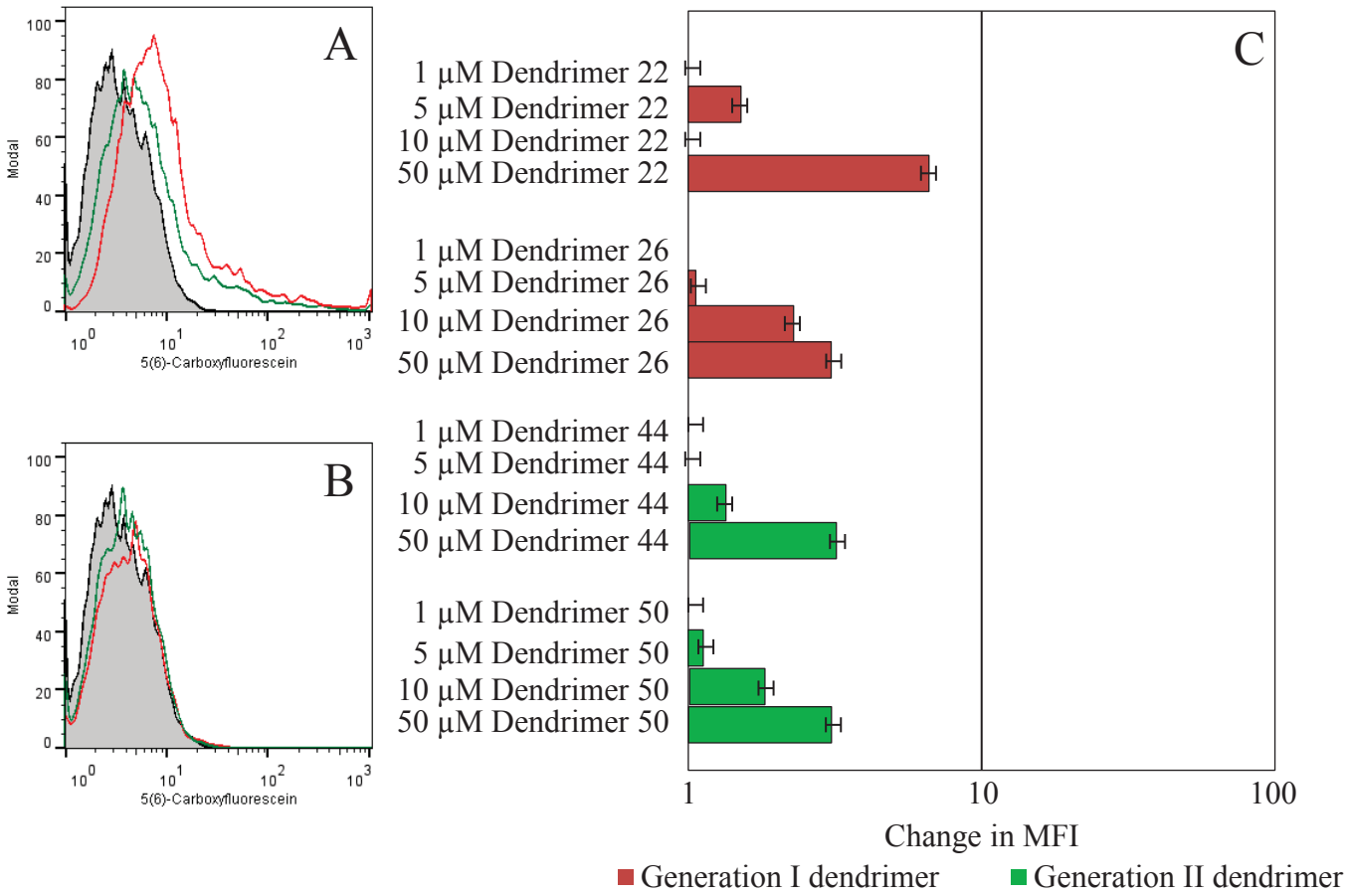

Figure 4.10: A titration experiment at 0 °C and 1 hour incubation time for additives at 50 μM, 10 μM, 5 μM and 1 μM concentrations with LG2 cells. A) FACS histogram plot indicating binding of 50 μM of the dendrimer **22** (red) and **44** (green) to LG2. B) FACS histogram plot indicating binding of 1 μM of the dendrimer **22** (red) and **44** (green) to LG2. C) Change in MFI is given as the average for duplicate samples for each dendrimer incubation.

4.5 Optimised 0 °C conditions

With both time period and concentration of additives optimised, an experiment was performed with the generation I and II dendrimers. This experiment would decide which direction should be taken in the future when designing the future generations of compounds.

The generation I dendrimers (**22**, **3**, **24** and **26**) along with the generation II dendrimers (the negative controls (**44**, **46**, **48** and **50**) were incubated with MoDC and LG2 with the optimised conditions chosen previously, the results are shown in Figure 4.11.

The FACS plot A in Figure 4.11 shows a representative comparison of a glycosylated generation I dendrimer and a generation II dendrimer fluorescence curve with MGL expressing MoDC. The generation I dendrimers always showed a small shift in fluorescence which equates to weak binding. The generation II dendrimers which were incubated with the MoDC all have very small average shifts in MFI of below 0.5 and had overlapping fluorescence curves with the autofluorescence of MoDC. This indicates that no binding is occurring.

The average change in MFI for MoDCs incubated with each dendrimer was plotted in graph C in Figure 4.11. The MoDCs which were incubated with the generation I dendrimers all have average shifts in the MFI of over 1.3, with dendrimer **26** inducing the largest average MFI shift of 1.7. The generation I dendrimers used in this experiment are ranked based on shift in MFI: 1) dendrimer **26**; 2) dendrimer **24**; 3) dendrimer **22**, 4) dendrimer **3**.

None of the dendrimers had an average shift in MFI above 0.5 when incubated with the LG2 cells, the FACS plots show complete overlap for the fluorescence curves with additives and without (FACS plot B from Figure 4.11 is a typical representation of the LG2 FACS plots). This indicates that no dendrimers were binding to the LG2 cells.

After the initial experiments dendrimer **26** was marginally better than the other dendrimers and was therefore chosen as the lead compound from which future generations of dendrimers would be designed.

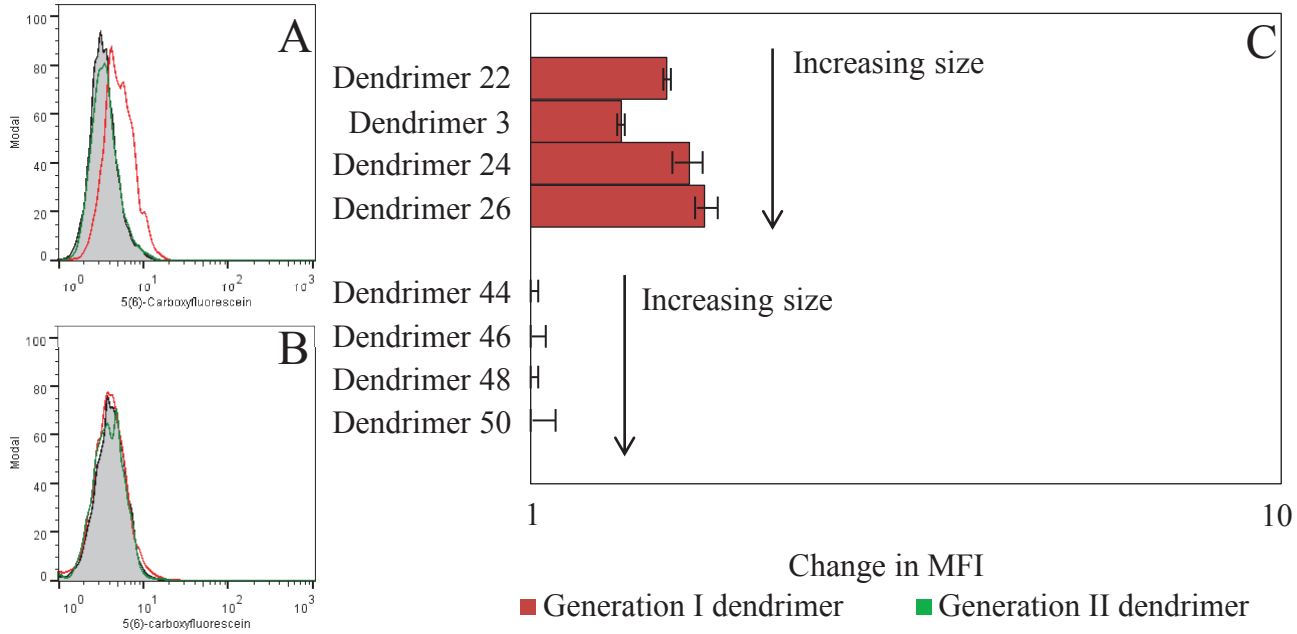

Figure 4.11: The cell binding assay performed with the generation I and II dendrimers using 1 μM concentration with 1 hour incubation at 0 °C. A) FACS histogram plot indicating binding of 1 μM of the dendrimer **26** (red) and **50** (green) to MoDC. B) FACS histogram plot indicating binding of 1 μM of the dendrimer **26** (red) and **50** (green) to LG2. C) Change in MFI is given as the average for duplicate samples for each dendrimer incubation.

Chapter 5

Synthesis of generation III, IV and V MGL targeting compounds

5.1 The importance of the X, Y and Z chain to binding.

Initial cell binding assay results at 0 °C showed that dendrimer **26** (Figure 5.1) was the strongest binding compound. Therefore it was decided to construct six analogues based on dendrimer **26**. The purpose of these dendrimers was to investigate which of the X,Y and Z chains were the most important for binding.

For the generation III dendrimers each dendrimer pair have two GalNAc glycosylated chains while one chain which is underivatised (Figure 6.3). For the generation IV dendrimers, each dendrimer pair have one GalNAc glycosylated chain and two chains are underivatised (Figure 6.4).

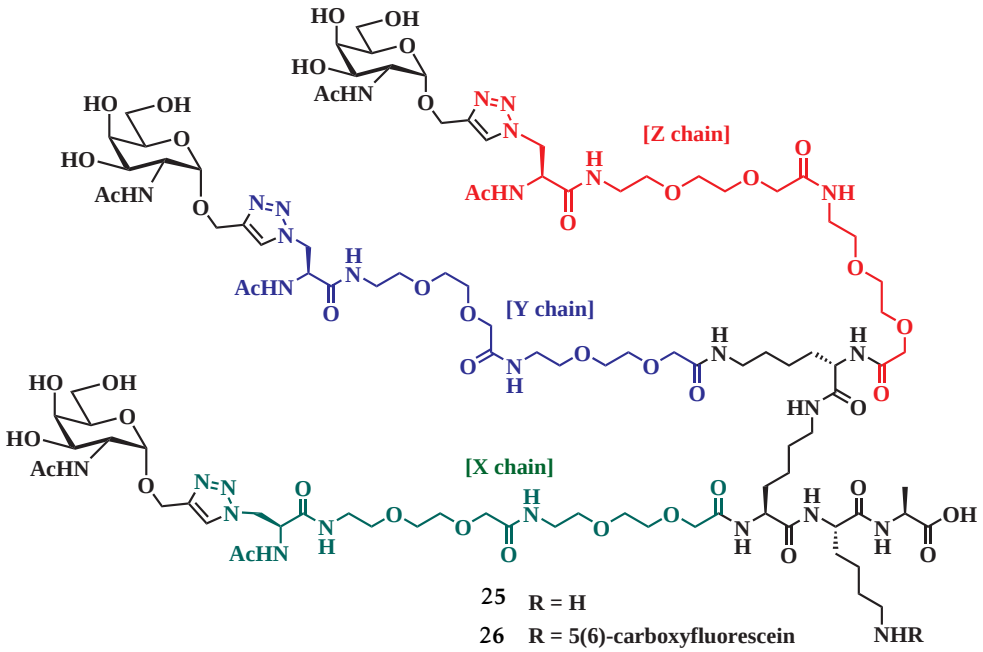

Figure 5.1: Structure of the strongest binder of the cell binding assay dendrimer **26** and its equivalent from the thermal melt assay dendrimer **25**.

5.1.1 Generation III dendrimers, two out of three chains GalNAc–glycosylated

The three followings sets of dendrimer pairs with two GalNAc derivatised chain (Figure 6.3):

- **51** and **52**, X and Y chains are GalNAc–glycosylated.
- **53** and **54**, X and Z chains are GalNAc–glycosylated.
- **55** and **56**, Y and Z chains are GalNAc–glycosylated.

Synthesis of dendrimers **55** and **56** was similar to the synthesis of dendrimer **26** which has the Y and Z chains grown in a symmetrical fashion as shown in Scheme 2.15 in Chapter 2. Whereas the unsymmetrical dendrimers **53** and **54**, **51** and **52** were all constructed with the Y and Z chains elongated independently using a route similar to dendrimer **24** (Scheme 2.16 in Chapter 2).

It was expected that the generation III dendrimers with two GalNAc residues would bind in a weaker fashion than the generation I dendrimer **26** which has three GalNAc residues due to the reduced number of carbohydrate binding residues. There was two possible outcomes when comparing the results within the generation III dendrimers. Firstly, one combination of GalNAc–glycosylated chains would prove significantly stronger binder than the others. This would mean that these chains

have the most optimum distance for binding. Secondly depending on the binding strength observed by the generation III dendrimer:

- A decrease in strength of binding compared to dendrimer **26** would suggest that binding strength increases with numbers of GalNAc.
- Equal strength of binding compared to dendrimer **26** would suggest that dendrimer **26** is primarily binding through two chains rather than three.
- An increase in strength of binding compared to dendrimer **26** would suggest that having three chains GalNAc–glycosylated is detrimental for binding of the dendrimer, with the third chain destabilising the binding of the other two.

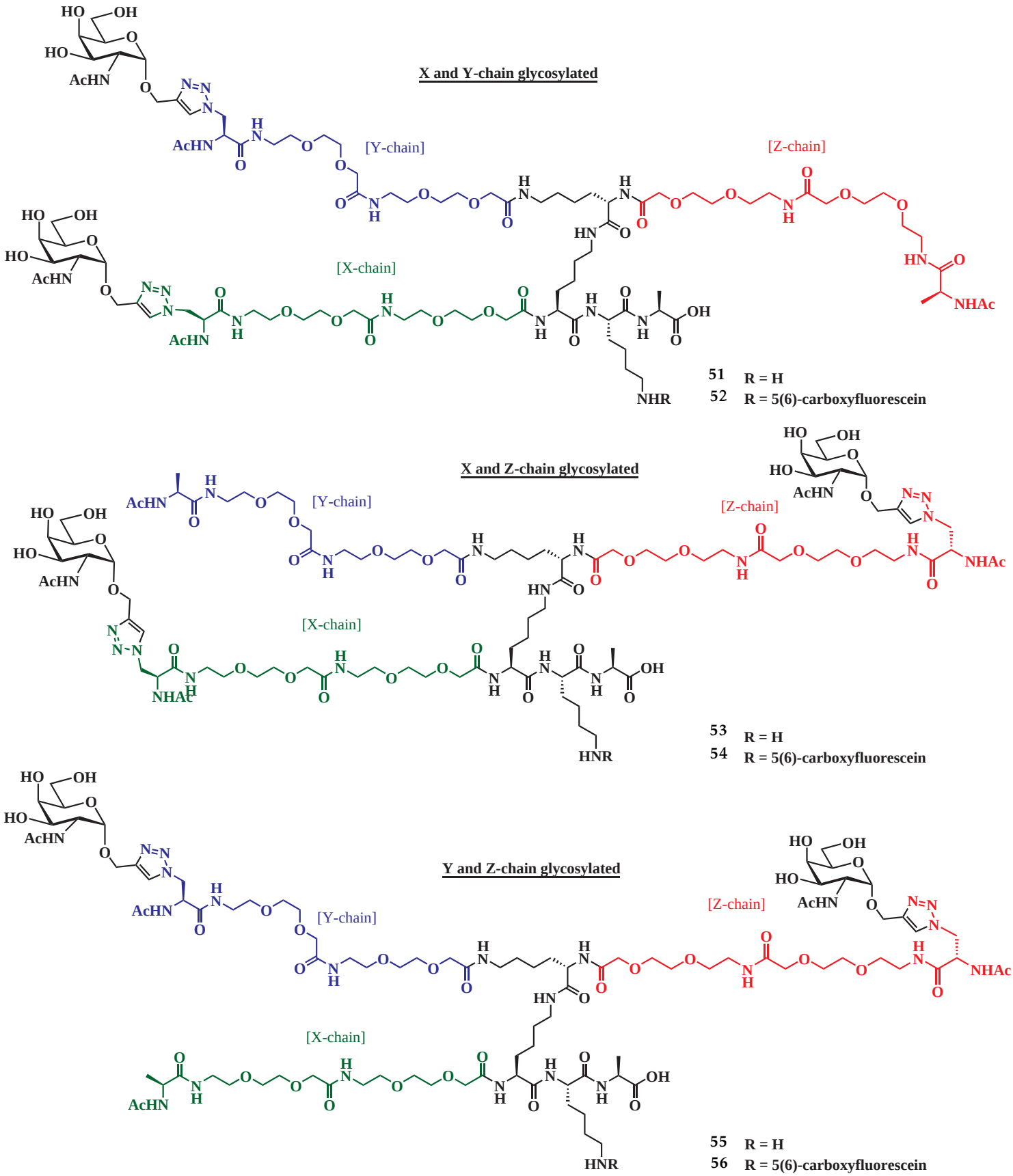

Figure 5.2: The structures of the generation III dendrimers **51**, **52**, **53**, **54**, **55** and **56**.

5.1.2 Generation IV dendrimers, one out of three chains GalNAc–glycosylated

The following shows the three sets of dendrimer pairs with a single GalNAc moiety (Figure 6.4):

- **57** and **58**, X chain is GalNAc–glycosylated.
- **59** and **60**, Y chain is GalNAc–glycosylated.
- **61** and **62**, Z chain is GalNAc–glycosylated.

Dendrimers **57** and **58** have a similar synthesis to that of dendrimer **26** in which the Y and Z chains grown in a symmetrical fashion (Scheme 2.15 in Chapter 2). The unsymmetrical dendrimers **59** and **60**, **61** and **62** were all constructed with the Y and Z chains elongated independently using a route similar to dendrimer **24** (Scheme 2.16 in Chapter 2).

The generation IV dendrimers with one GalNAc residue were expected to bind in a weaker fashion than the generation I dendrimer **26** which has three GalNAc residues and the generation III dendrimers with two GalNAc residues. The generation IV dendrimers with one GalNAc residue were in terms expected to bind in a stronger fashion than the generation II dendrimer **50** which has no carbohydrate residues.

There was two possibles for outcomes when comparing the results within the generation IV dendrimers. Firstly, one GalNAc–glycosylated chain would prove significantly stronger binder than others indicated the chain that is the most important for binding. Secondly, if no binding would occur, this would confirm that multiple sugar residues are needed for a successful binding interaction.

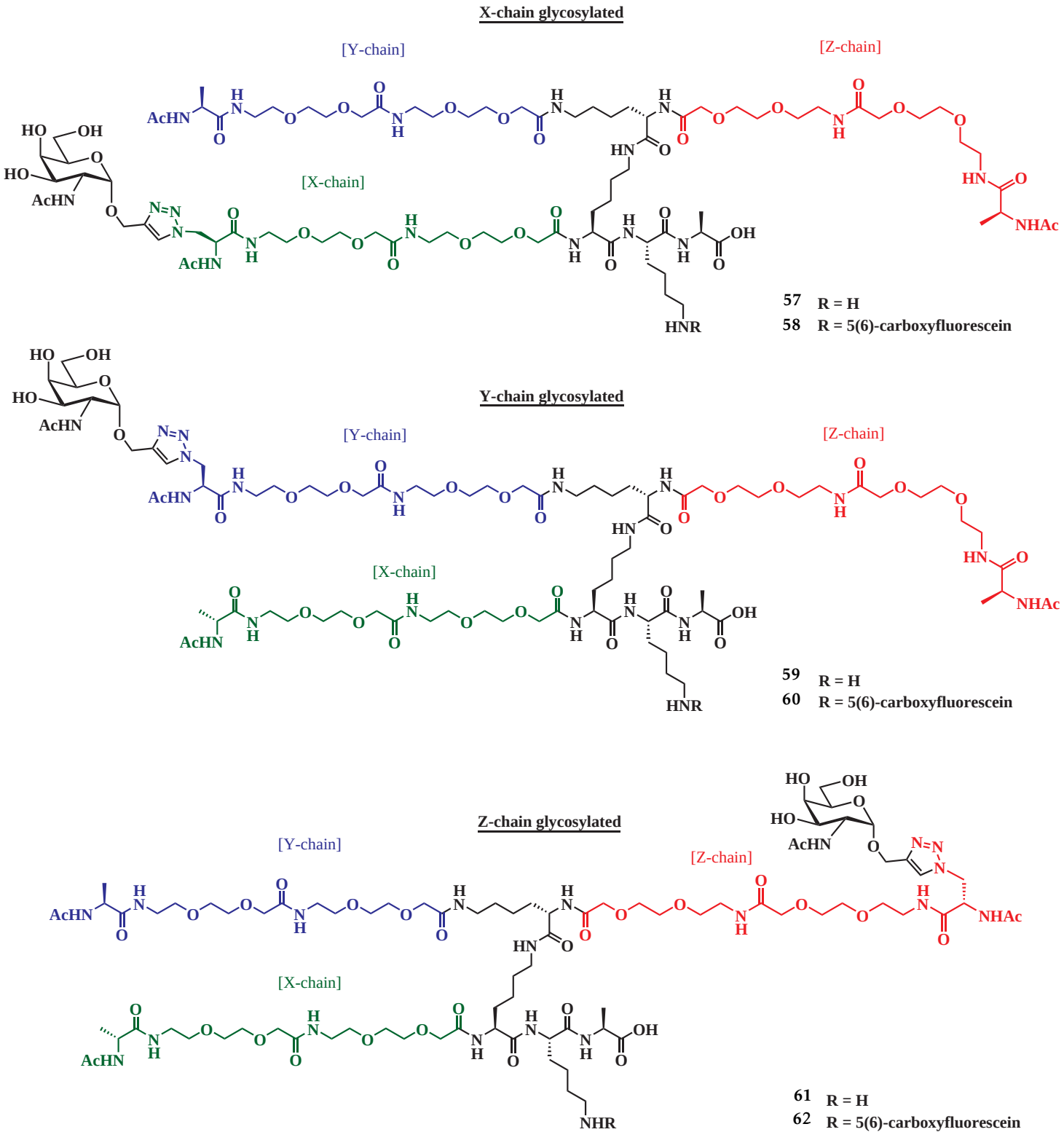

Figure 5.3: The structures of the generation IV dendrimers **57**, **58**, **59**, **60**, **61** and **62**.

5.1.3 Generation V peptides and triazole derivatised negative controls

Before conducting the final experiments for the cell binding assay and the thermal melt assay, two objectives were decided:

1. Synthesis of the smallest compound with 3 "clicked" sugars.
2. Establish that the triazole was not causing the binding in its own right.

To achieve these objectives six compounds were designed as shown in Figure 6.5. The first objective can be investigated by synthesising the straight chain peptides **63** and **64**. The simplicity of the small peptide makes it ideal for scale up, or to be incorporated into SPPS. The peptides **63** and **64** allows the comparison for activity of the linear vs the branched structure.

The negative control peptide **65** was synthesised as an analogue of peptides **64** in which each of the azidoalanines were replaced with alanines. The relationship between peptide **64** and **65** mirrors that of the generation I and II dendrimers.

To establish whether the triazole was responsible for binding peptide **66** and dendrimers **67** and **68** were created for these debdrimers, where the CuAAC reaction was performed with propargyl alcohol instead of α–propargyl GalNAc **4**. If the triazole was causing significant binding in the biological assays, the results from dendrimers **67** and **68** would be similar to dendrimers **21** and 22.

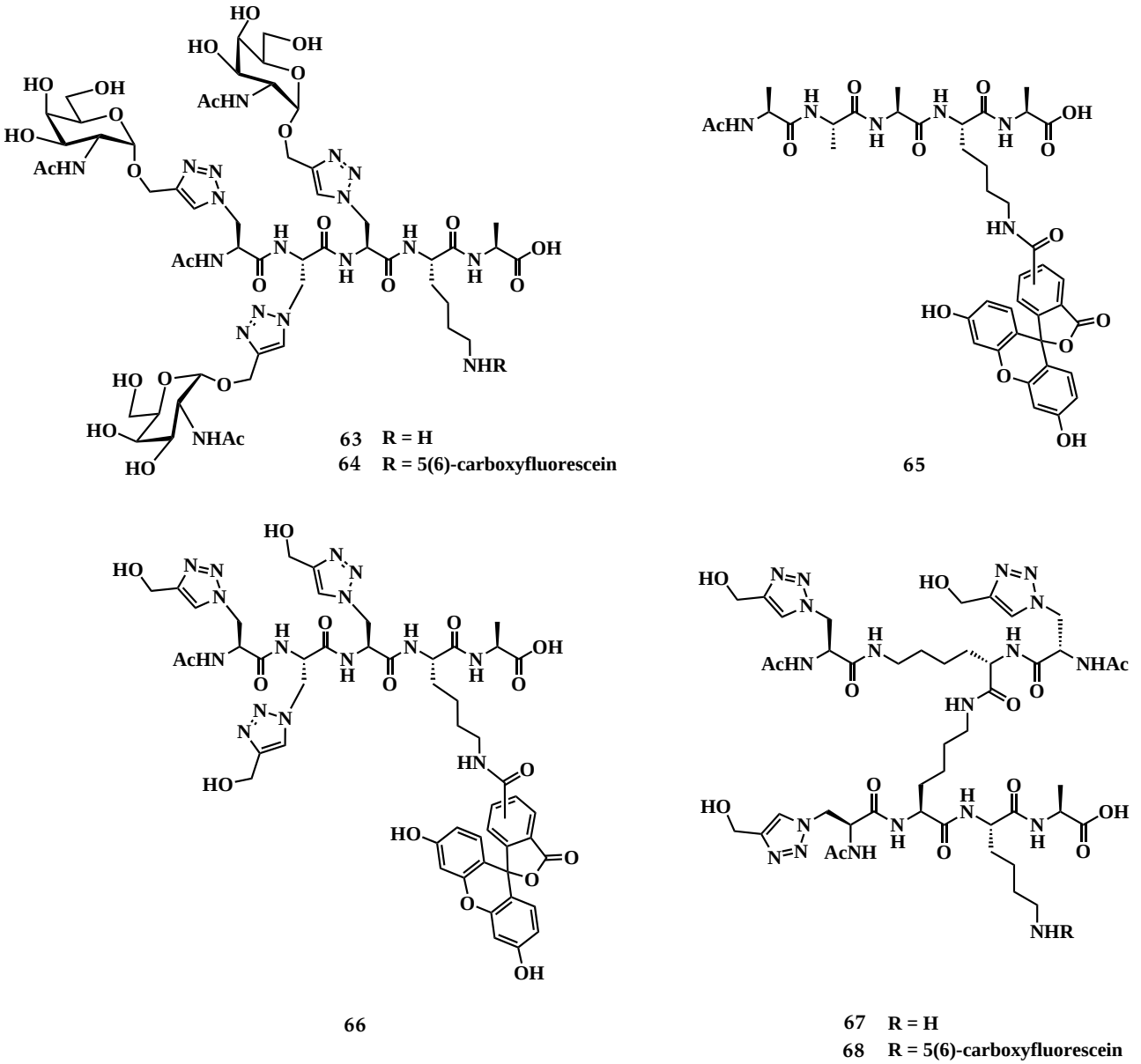

Figure 5.4: The structures of the GalNAc–glycosylated straight chain peptides **63** and **64**, the straight chain peptide negative control **65**, and the triazole analogues straight chain peptide negative control **66** and the dendrimers **67** and **68**.

Synthesis of straight chain peptides 62 and 63

Synthesis of straight chain peptide **63** for the thermal melt assay and peptides **64** for the cell binding assay is shown in Scheme 5.1. Synthesis used HMPP linker bearing the first amino acid alanine to the resin (Chapter 2 Scheme 2.14). After Fmoc deprotection of the alanine, Fmoc–Lys(Mtt) was coupled to the chain to give peptide **29**. Three Fmoc–azidoalanine **9** were coupled sequentially, this was followed by the capping of the chain using acetic anhydride which generated azido peptide scaffold **69**.

For peptide **63** which was destined for the thermal melt assay, peptide scaffold **69** was cleaved from the resin using TFA in water and the Mtt group was removed simultaneously to generate straight chain azido peptide **70** (Scheme 5.1). For the batch of straight chain peptides destined for the cell binding assay, the Mtt group was removed with 1% TFA in dichloromethane and fluorophore 5(6)-carboxyfluorescein was coupled. The fluorescent peptide was then cleaved from the resin using TFA / water (49:1) to generate straight chain azido peptide **37**. The CuAAC reaction was performed on the two azido peptides **69** and **70** using the conditions described in section 2.4.8 to glycosylate the peptides with α–propargyl GalNAc **4**. This generated straight chain peptide **63** for the thermal melt assay and peptides **64** for the cell binding assay.

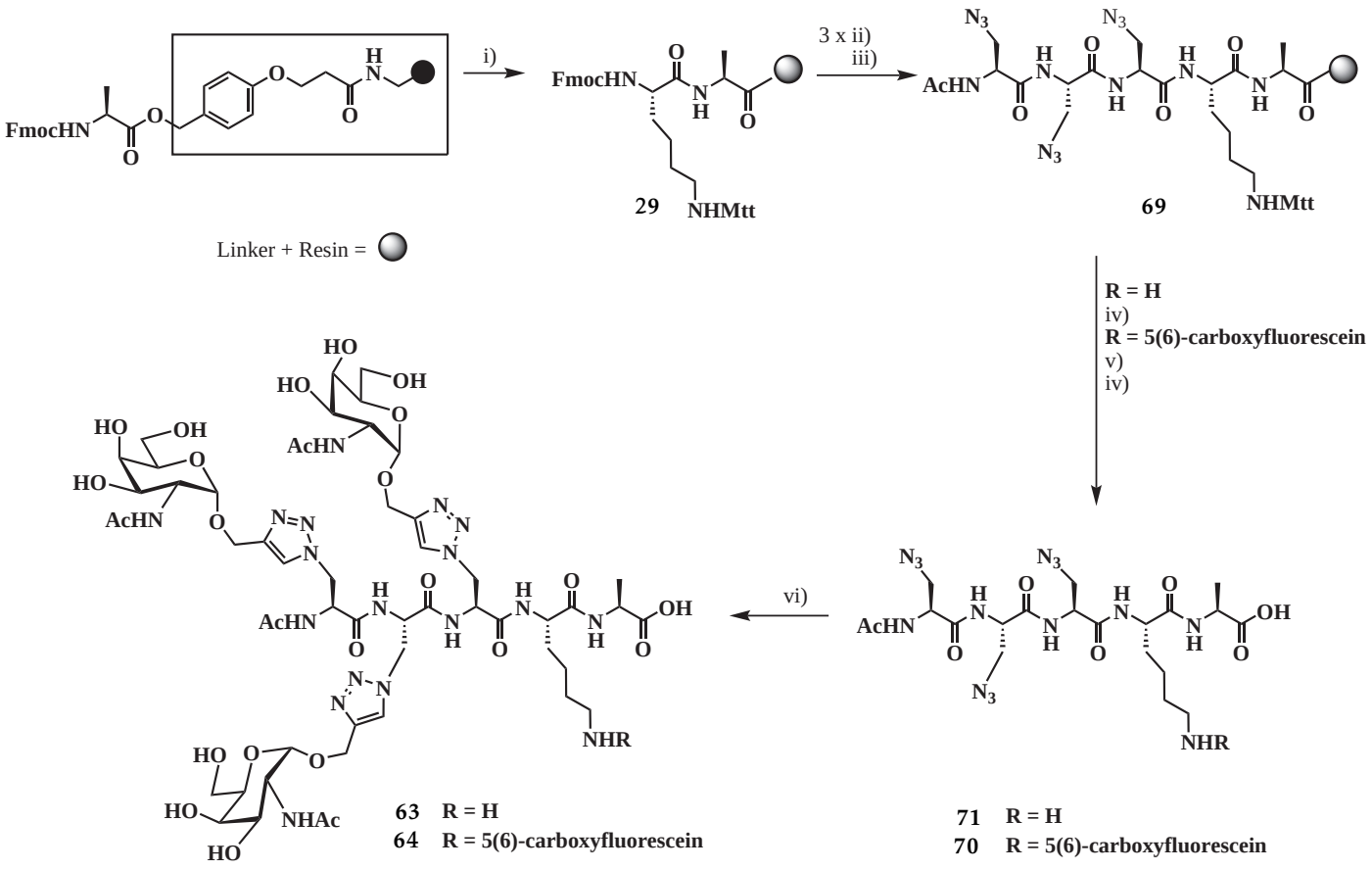

Reagents and conditions: (i) a. 20% piperidine/DMF; b. Fmoc-Lys(Mtt)-OH, DIPEA, HCTU, DMF:
(ii) a. 20% piperidine/DMF; b. Fmoc-Ala(N_3)-OH, HATU, DIPEA, DMF; (iii) a. 20% piperidine/DMF; b. Ac_2O, DIPEA, DMF;
(iv) a. 1% TFA/CH_2Cl_2; b. 5(6)-carboxyfluorescein, HoBT, DIC, DMF; c. 20% piperidine/DMF; (v) 98% TFA/H_2O;
(vi) 5 eq. α-propargyl GalNAc, 5 eq. sodium ascorbate, 10 eq. $CuSO_4$, 1:2 H_2O/DMSO.

Scheme 5.1: Synthesis of Synthesis of straight chain peptide **63** for the thermal melt assay and peptide **64** for the cell binding assay.

Synthesis of triazole dendrimer and peptide analogues using the click reaction

Formation of the triazole analogue straight chain negative control peptide **66** and the triazole analogue dendrimers **67** and **68** via the click reaction with propargyl alcohol is shown in Scheme 5.2. Synthesis of the dendrimer scaffold **35** and **37** were covered in section 2.4.8. Dendrimer scaffold **35** and **37** were reacted with propargyl alcohol in the presence of sodium ascorbate and copper sulfate, in dimethyl sulfoxide and water. The resulting tri–clicked products were dendrimer **72** for the thermal melt assay and dendrimer **68** for the cell binding assay respectively. A similar reaction was performed using straight chain azido peptide **70** to produce straight chain negative control peptide **66**.

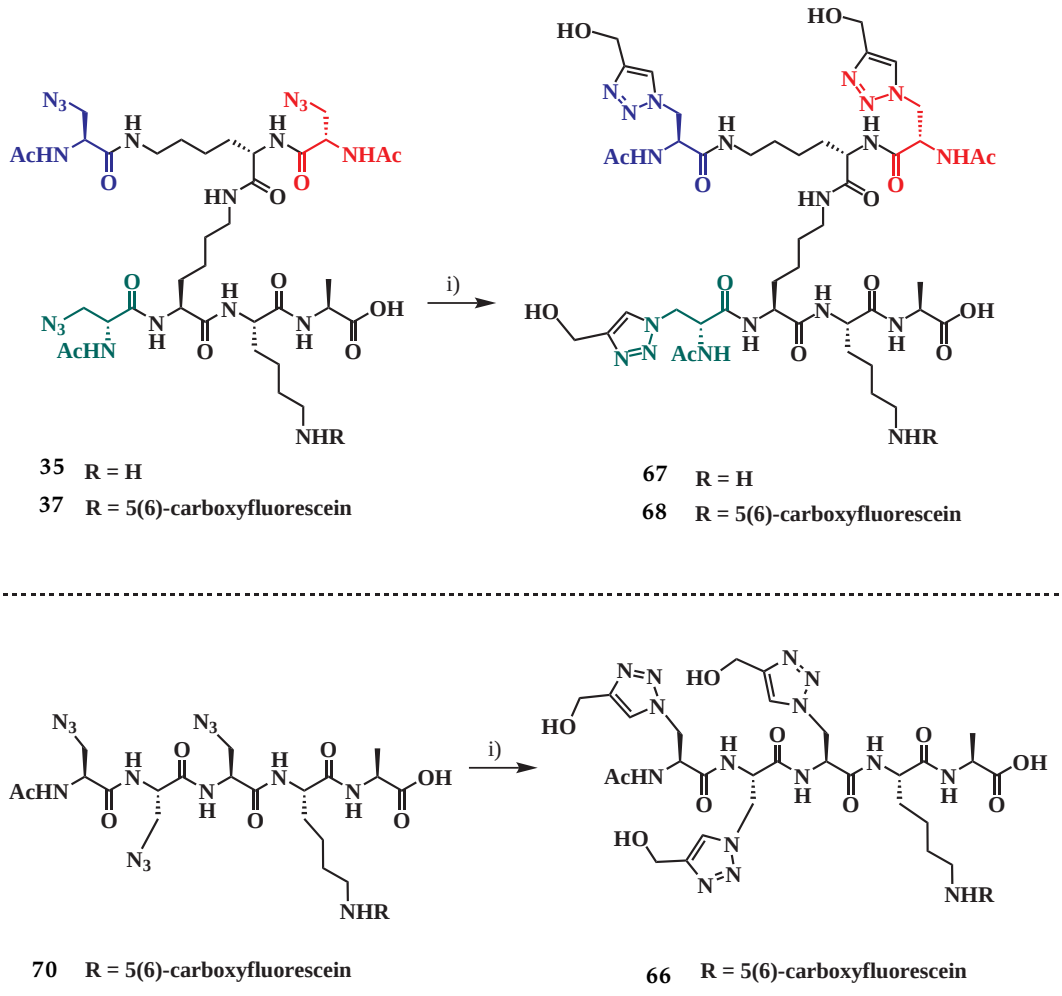

35 R = H
37 R = 5(6)-carboxyfluorescein

67 R = H
68 R = 5(6)-carboxyfluorescein

70 R = 5(6)-carboxyfluorescein

66 R = 5(6)-carboxyfluorescein

Reagents and conditions: (i) 5 eq. propargyl alcohol, 5 eq. sodium ascorbate, 10 eq. $CuSO_4$, 1:2 H_2O/DMSO

Scheme 5.2: Synthesis of triazole analogue straight chain negative control peptide **66** and the triazole analogue dendrimers **67** and **68**.

Chapter 6

Thermal melt studies on the four MGL truncations

Dendrimers used in the experiments described in this chapter are depicted in the following figures:

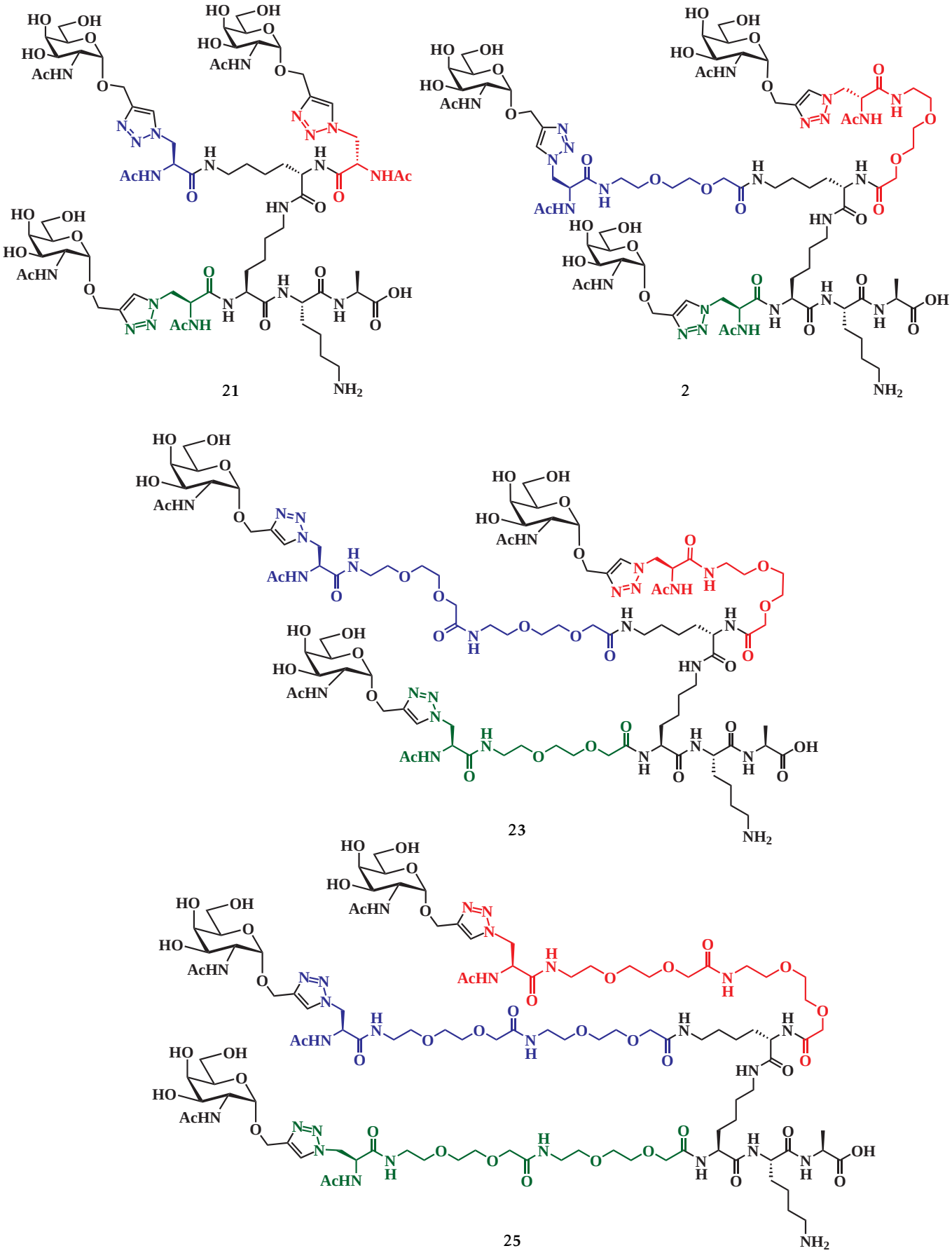

Figure 6.1: Structures of generation I dendrimers **21**, **2**, **23** and **25**.

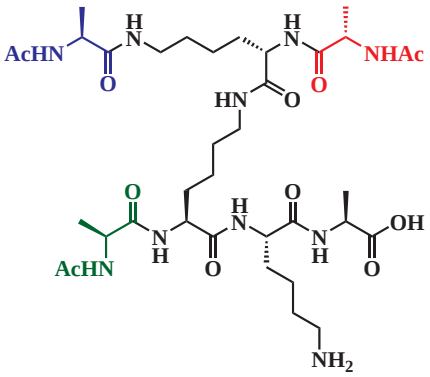

43

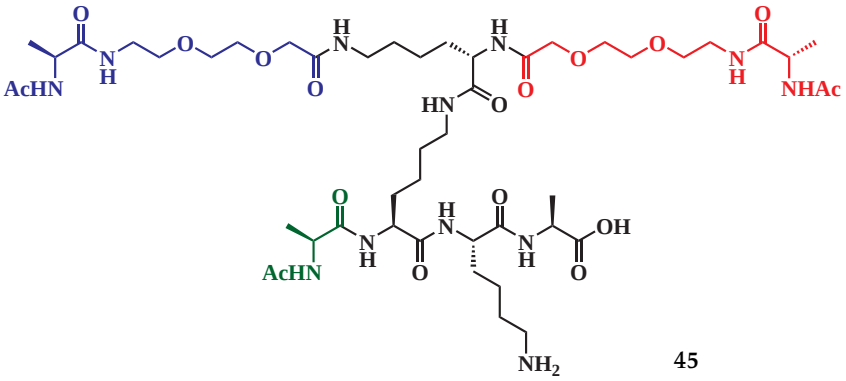

45

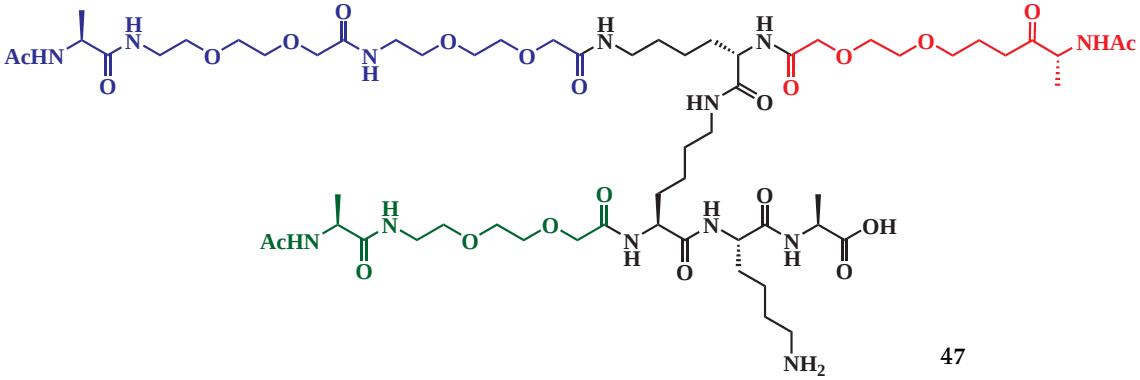

47

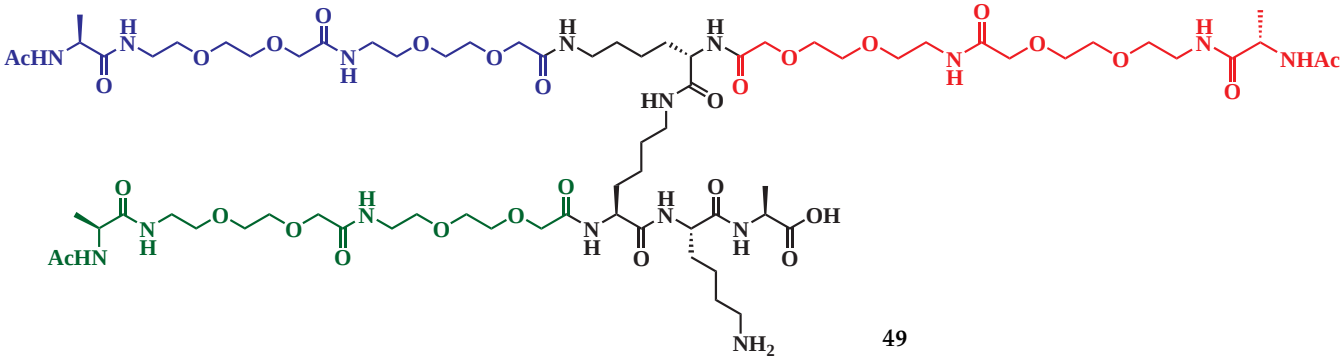

49

Figure 6.2: Structures of the negative control generation II dendrimers **43**, **45**, **47** and **49**.

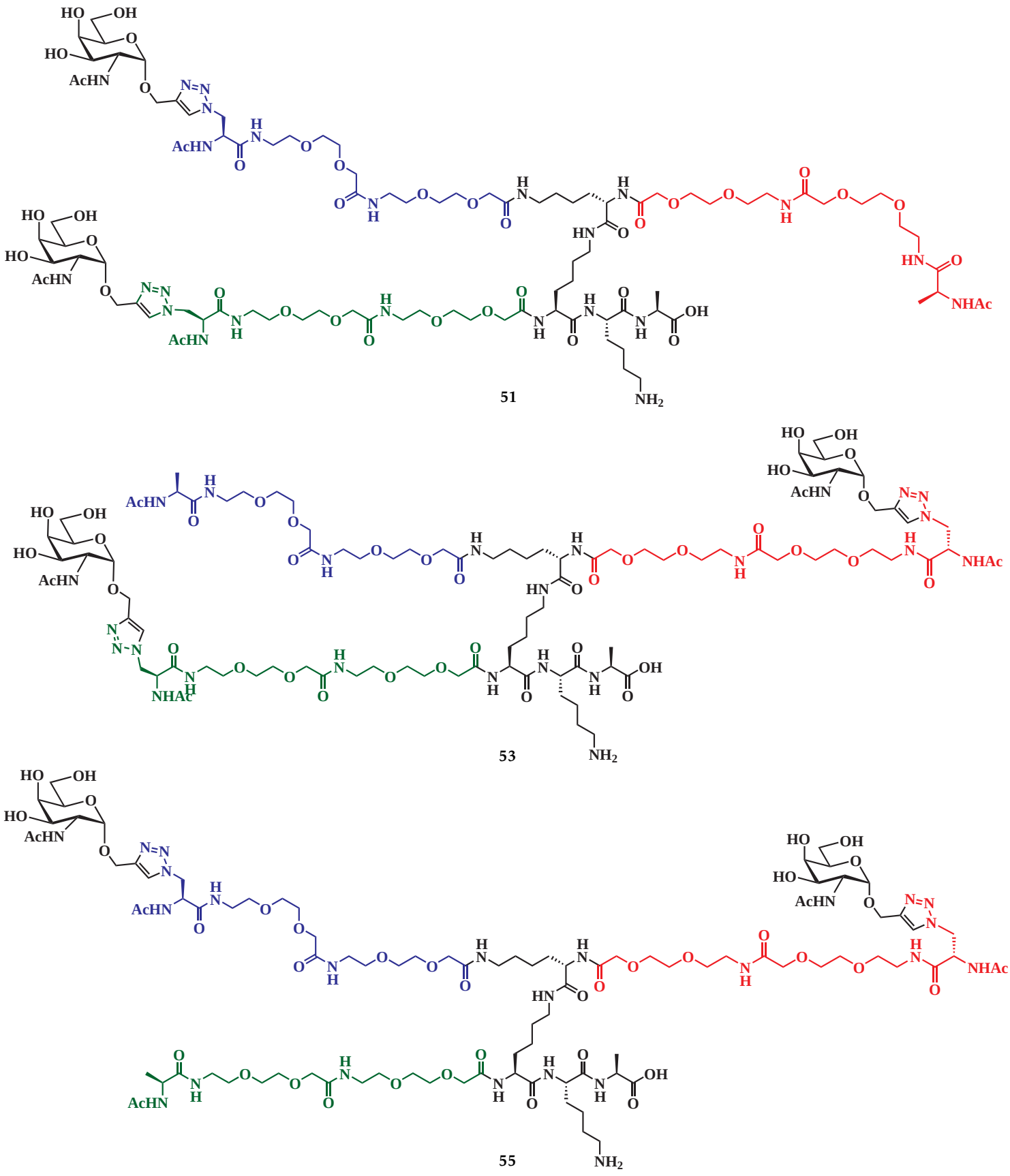

Figure 6.3: The structures of the generation III dendrimers **51**, **53** and **55**.

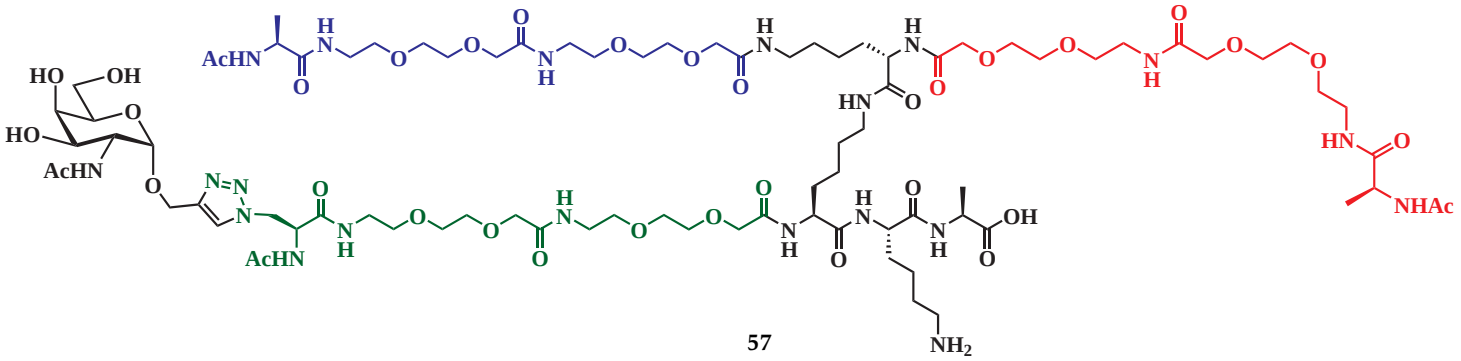

57

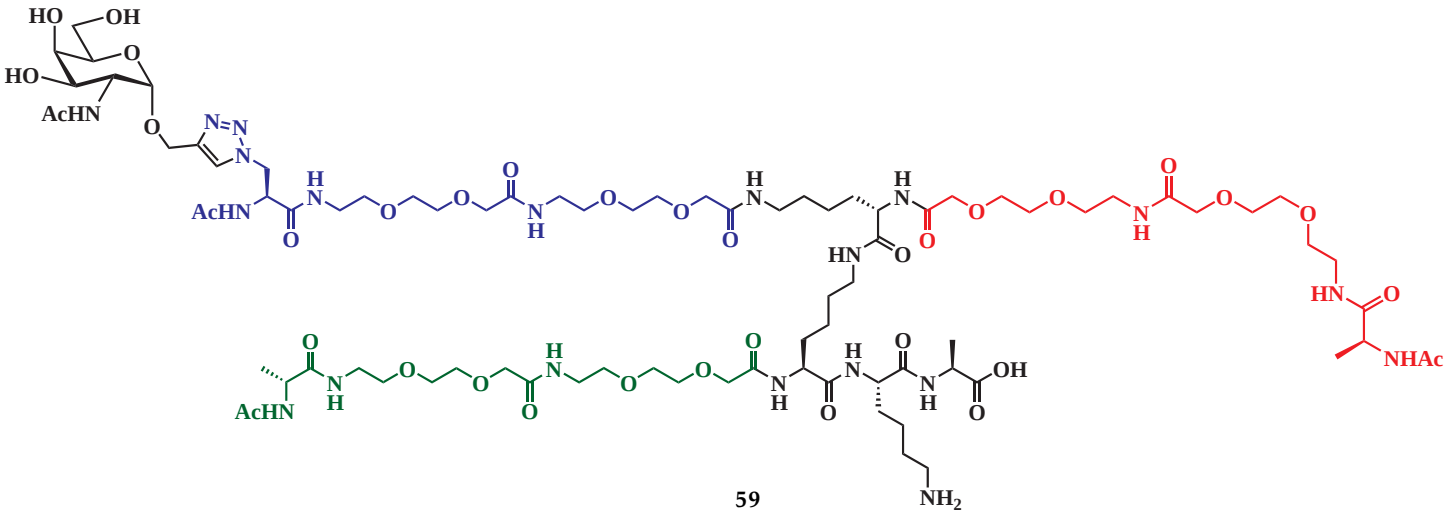

59

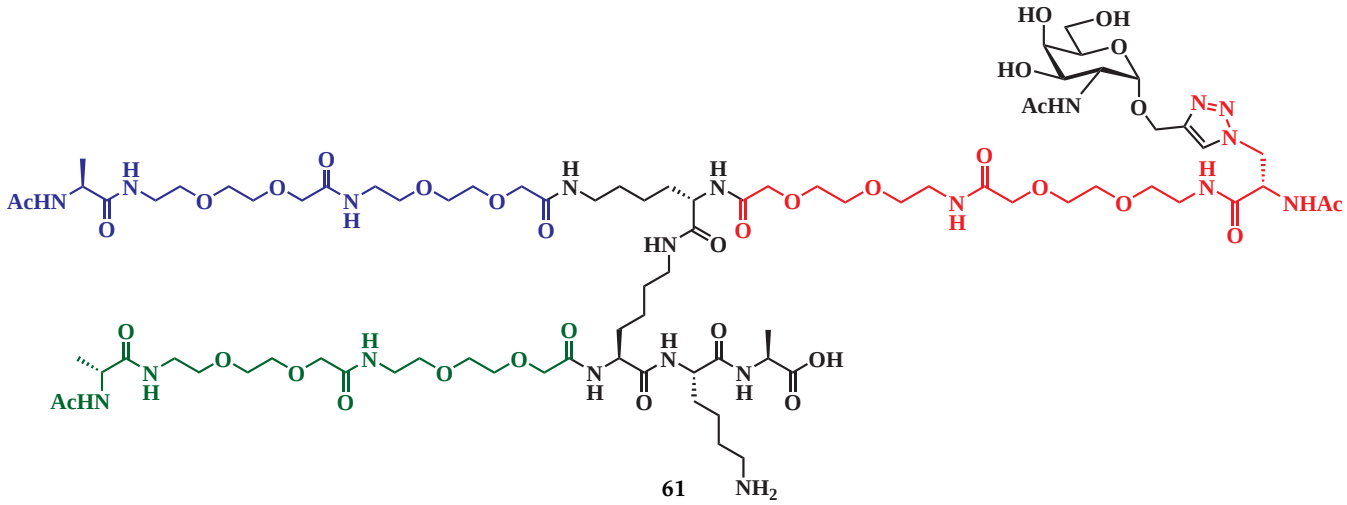

61

Figure 6.4: The structures of the generation IV dendrimers **57**, **59** and **61**.

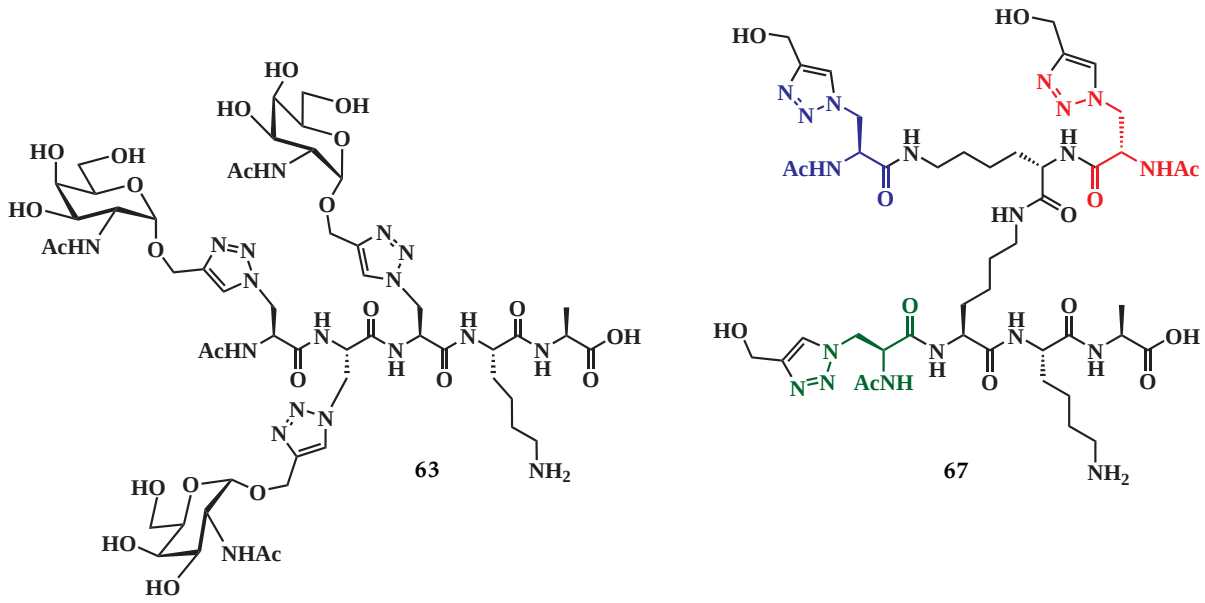

Figure 6.5: The structures of the GalNAc–glycosylated straight chain peptides **63** and the triazole analogue dendrimer **67**.

6.1 Thermal melt assay for the four truncations of MGL using the library of dendrimers

With all four truncations of MGL available (see Chapter 3), the thermal melt assay was performed using the full library of dendrimers. The following section will first look at how the MGL truncations behaved with each peptide additive, followed by a comparison of the different truncation results.

6.1.1 Thermal melt assay using MGL 176 protein

The results from the thermal melt assay using the smallest protein truncation MGL 176 are shown in Table 6.1, and Figure 6.6. A positive shift in the melting point of around 6 °C was observed when MGL was incubated with GalNAc. The MGL 176 truncation was less selective at binding to the additives than anticipated, as all the additives except three compounds (dendrimers **25**, **45** and **59**) increased the melting point. Three of the four generation II dendrimers (**43**, **47** and **49**) also bound to MGL 176 truncation. Dendrimer **23** with three GalNAc bound significantly better than its equivalent dendrimer **45** with no GalNAc while dendrimer **25** bound significantly worse than its negative control dendrimer **49**.

Four differential scanning fluorimetry (DSF) derivative plots are shown in Figure 6.6. Plot A shows the melting point for the MGL 176 protein and how the melting point increased with the addition of GalNAc. Plot B shows that the increase was the most pronounced for peptide **63** which induced the largest shift in melting point. Plot C compares the melting points of dendrimer **25** and its analogues when incubated with MGL 176 protein. It was unexpected that the generation I dendrimer **25** destabilised MGL 176 while all of the analogues increased the melting point. Plot D shows the comparison on the melting point of MGL 176 with dendrimer **21** and its two analogues, dendrimer **43** and **67**. Dendrimer **21** induced the greatest positive shift on the melting point within the series, while triazole analogue **67** induced the smallest increase in melting point.

The average changes in the observed melting points are shown in graph E in Figure 6.6. The compound which induced the largest shift in melting point (+14 °C) was the generation V peptide **63** which carried three GalNAc residues. The generation III dendrimers (**51**, **53** and **55**) performed the next best with shifts in melting point of 8.5–10.5 °C. The generation IV dendrimers (**57**, **59** and **61**) were the third best group to stabilise MGL 176, inducing shifts of 7–9 °C. The generation I dendrimers (**21**, **2** and **23**) with three GalNAc residues induced shifts of 3–8 °C while dendrimer **25** lowered the melting point by 3 °C. The generation II dendrimers (**43**, **47** and **49**) with no GalNAc residues bound to MGL in a positive fashion but only induced increases in the melting point of 2–6 °C. Seven compounds bound better than the GalNAc monomer (dendrimers **21**, **51**, **53**, **55**, **57**,

61 and peptide **63**), and all of these structures had at least one GalNAc residue attached using click chemistry.

Table 6.1: Thermal melt assay of MGL 176 with dendrimers **21** - **67**. The original rfu plots and differential graphs are shown in the Appendix (Figures 9.35–9.38).

Generation	Additive (1 mM)	Appendix plot	Av. shift in M.P. (°C)
-	none	32	-
	GalNAc	33	+6.3
I (dendrimers with 3 GalNAc)	Dendrimer **21**	34	+7.7
	Dendrimer **2**	37	+3.0
	Dendrimer **23**	39	+5.7
	Dendrimer **25**	41	−3.0
II (dendrimers with 0 GalNAc)	Dendrimer **43**	36	+6.0
	Dendrimer **45**	38	−4.0
	Dendrimer **47**	40	+5.7
	Dendrimer **49**	42	+5.3
III (dendrimers with 2 GalNAc)	Dendrimer **51**	43	+10.3
	Dendrimer **53**	44	+9.3
	Dendrimer **55**	45	+8.7
IV (dendrimers with 1 GalNAc)	Dendrimer **57**	46	+7.0
	Dendrimer **59**	47	−4.3
	Dendrimer **61**	48	+9.0
V (peptide with 3 GalNAc)	Peptide **63**	49	+14.0
Triazole analogue	Dendrimer **67**	35	+2.3

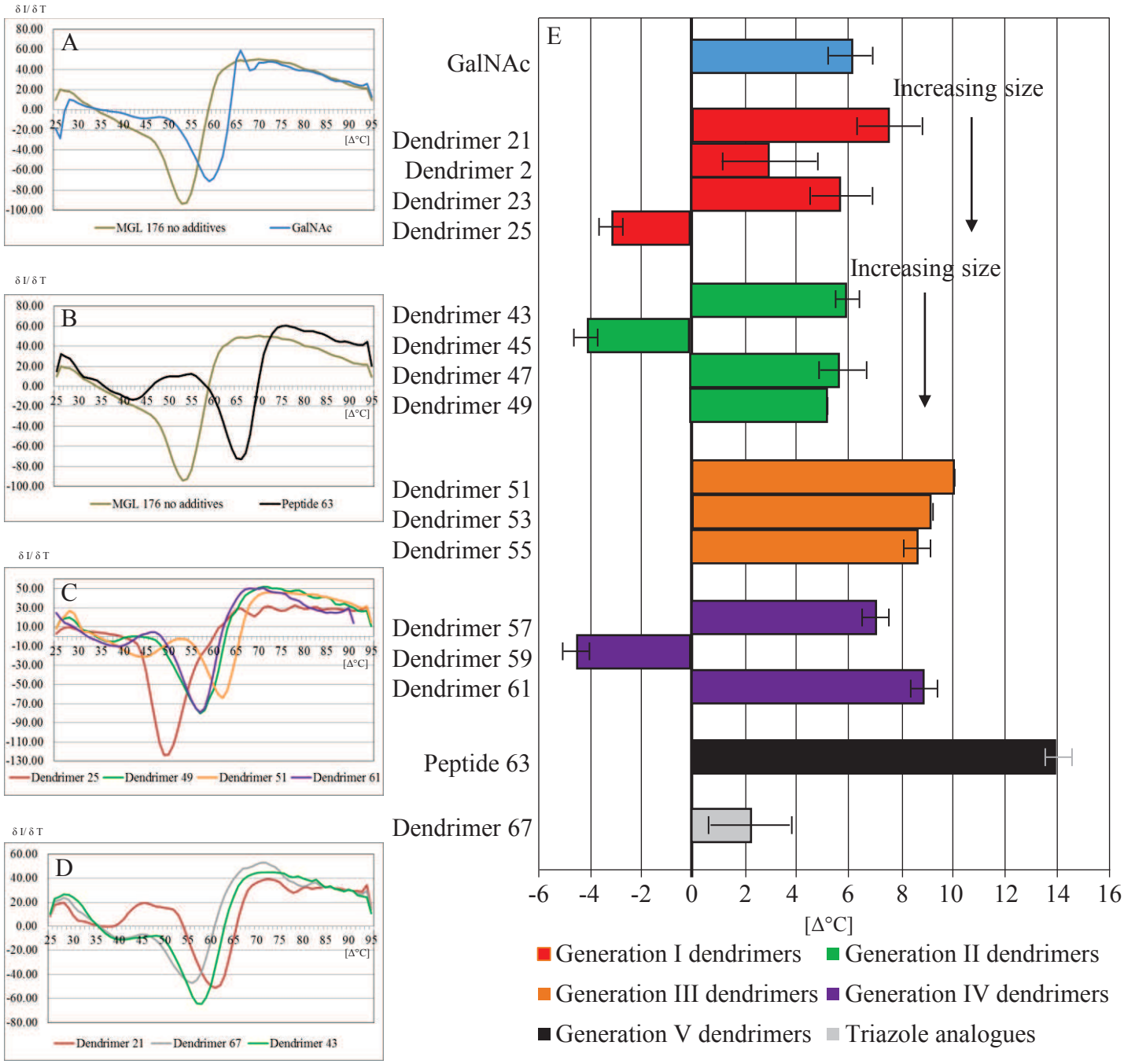

Figure 6.6: The change in melting point [°C] with the peptide additives at 1 mM concentration for MGL 176 compared to MGL 176 with no additives. A) DSF derivative plot of MGL 176 alone and with GalNAc. B) DSF derivative plot of MGL 144 alone and with peptide **63**. C) DSF derivative plot of MGL 176 incubated with dendrimers **25**, **49**, **51** and **61**. D) DSF derivative plot of MGL 176 incubated with dendrimers **21**, **43** and **67**. E) Average change of melting point of MGL 176 when incubated with different additives.

6.1.2 Thermal melt assay using MGL 166 protein

The results for the second smallest protein truncation MGL 166 are shown in Table 6.2, and Figure 6.7. A positive increase in the melting point of around 3 °C was observed when MGL was incubated with GalNAc. Four additives (dendrimers **25**, **45**, **59** and **67**) destabilised the MGL 166 protein and decreased the melting point. All of the negative control dendrimers (no GalNAc) showed either very modest increases (<1 °C) or destabilised the MGL by lowering the melting point. Overall the generation II dendrimers with no GalNAc residues induce less shift in the melting point than the equivalent dendrimer (**25**) with three GalNAc residues .

The four DSF derivative plots shown in Figure 6.7 for MGL 166 show a similar pattern to what was observed for MGL 176 in Figure 6.6. The main difference between thermal melts using the various protein truncations was that the shifts in melting point are smaller for MGL 166 which may be due to the increased size of the protein relative to MGL 176.

The compound which induced the maximum shift in melting point was the generation V peptide **63**, which stabilised MGL 166 by an additional 10 °C. The generation III dendrimers (**51**, **53** and **55**) with two GalNAc residues performed the next best with shifts in melting point of 3–6 °C. The generation I dendrimers (**21**, **2** and **23**) with three GalNAc residues were the third best series to increase the melting point of MGL 166 inducing shifts of 3–5 °C. The generation IV dendrimers (**57** and **61**) with only one GalNAc moiety were the least effective compounds for stabilising MGL 166 by inducing shifts of 1.5–4.0 °C. Five compounds (dendrimers **21**, **51**, **53**, **61** and peptide **63**) bound better than the GalNAc monomer. All of these structures had at least one GalNAc residue attached using click chemistry.

Table 6.2: Thermal melt assay of MGL 166 with dendrimers **21** - **67**. The original rfu plots and differential graphs are shown in the Appendix (Figures 9.39–9.42).

Generation	Additive (1 mM)	Appendix plot	Av. shift in M.P. (°C)
-	none	50	-
	GalNAc	51	+3.3
I (dendrimers with 3 GalNAc)	Dendrimer **21**	52	+4.7
	Dendrimer **2**	55	+3.3
	Dendrimer **23**	57	+3.0
	Dendrimer **25**	59	−1.3
II (dendrimers with 0 GalNAc)	Dendrimer **43**	54	0.0
	Dendrimer **45**	56	−3.0
	Dendrimer **47**	58	+0.7
	Dendrimer **49**	60	+0.3
III (dendrimers with 2 GalNAc)	Dendrimer **51**	61	+5.3
	Dendrimer **53**	62	+4.3
	Dendrimer **55**	63	+3.3
IV (dendrimers with 1 GalNAc)	Dendrimer **57**	64	+1.7
	Dendrimer **59**	65	−2.3
	Dendrimer **61**	66	+3.7
V (peptide with 3 GalNAc)	Peptide **63**	67	+9.7
Triazole analogue	Dendrimer **67**	53	−0.3

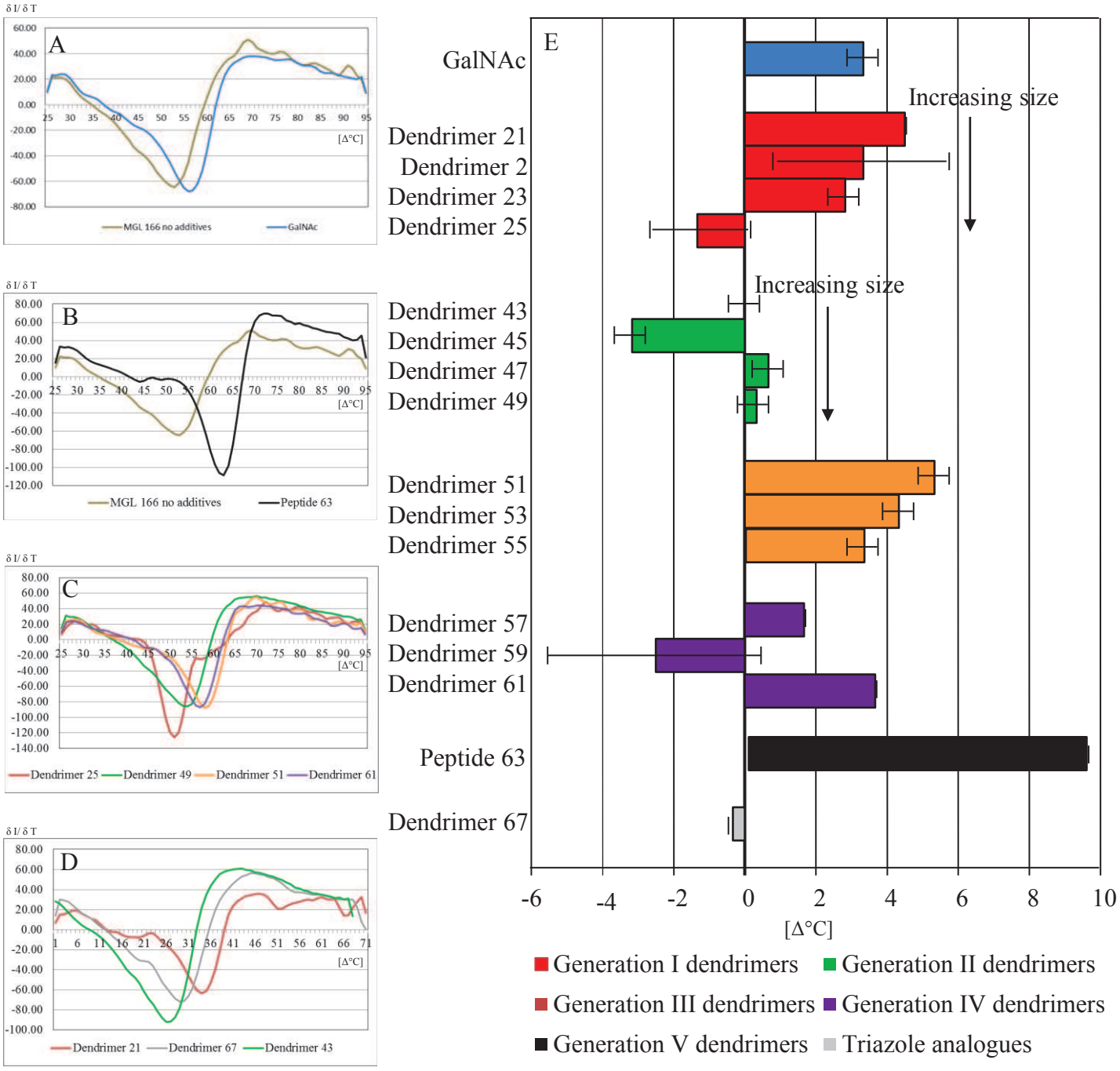

Figure 6.7: The change in melting point [°C] with the additives at 1 mM concentration for MGL 166 compared to MGL 166 with no additives. A) DSF derivative plot of MGL 166 alone and with GalNAc. B) DSF derivative plot of MGL 144 alone and with peptide **63**. C) DSF derivative plot of MGL 166 incubated with dendrimers **25**, **49**, **51** and **61**. D) DSF derivative plot of MGL 166 incubated with dendrimers **21**, **43** and **67**. E) Average change of melting point of MGL 166 when incubated with different additives.

6.1.3 Thermal melt assay using MGL 155 protein

The results for the second largest protein truncation MGL 155 are shown in Table 6.3, and Figure 6.8. A positive shift in the melting point of 4 °C was observed when MGL was incubated with GalNAc (Figure 6.8 plot A). Four additives (dendrimers **25**, **45**, **59** and **67**) destabilised MGL 155 and lowered the melting point. Almost all of the negative control dendrimers were significantly worse than the equivalent dendrimer with GalNAc residues. Only dendrimer **43** had a positive affect on the melting point (<1 °C). The remaining negative control either did not affect the melting point or destabilised the MGL and lowered the melting point.

The compound which was best at stabilising the melting point of MGL 155 was also peptide **63** with three glycosylated moieties and inducing a +10 °C shift in melting point (Figure 6.8 plot B). The series of di–glycosylated generation III dendrimers (**51**, **53** and **55**) performed the next best with increased melting points of 1.5–6.5 °C. The DSF derivative curve for dendrimer **51** exhibited the largest increase in melting point of the group (Figure 6.8 plot C). The triple GalNAc glycosylated generation I dendrimers (**21**, **2** and **23**) bound in a positive fashion, and induced shifts of 1–5 °C which was the largest range of shift observed for any of the series of compounds. The largest increase in melting point for MGL 155 incubated with a generation I dendrimer is shown in Figure 6.8 plot D. The mono GalNAc glycosylated generation IV dendrimers (**57** and **61**) induced a smaller range of shift of 2.0–4.5 °C. Five compounds (dendrimers **21**, **51**, **53**, **61** and peptide **63**) bound better than the GalNAc monomer. All of these structures had at least one GalNAc residue attached using click chemistry.

Table 6.3: Thermal melt assay of MGL 155 with dendrimers **21** - **67**. The original rfu plots and differential plots are shown in the Appendix (Figures 9.43–9.46).

Generation	Additive (1 mM)	Appendix plot	Av. shift in M.P. (°C)
-	none	68	-
	GalNAc	69	+4.0
I (dendrimers with 3 GalNAc)	Dendrimer **21**	70	+4.7
	Dendrimer **2**	73	+1.3
	Dendrimer **23**	75	+2.7
	Dendrimer **25**	77	−0.3
II (dendrimers with 0 GalNAc)	Dendrimer **43**	72	+0.3
	Dendrimer **45**	74	−4.3
	Dendrimer **47**	76	0.0
	Dendrimer **49**	78	0.0
III (dendrimers with 2 GalNAc)	Dendrimer **51**	79	+6.3
	Dendrimer **53**	80	+4.3
	Dendrimer **55**	81	+1.7
IV (dendrimers with 1 GalNAc)	Dendrimer **57**	82	+2.3
	Dendrimer **59**	83	−4.7
	Dendrimer **61**	84	+4.3
V (peptide with 3 GalNAc)	Peptide **63**	85	+10.3
Triazole analogue	Dendrimer **67**	71	−3.3

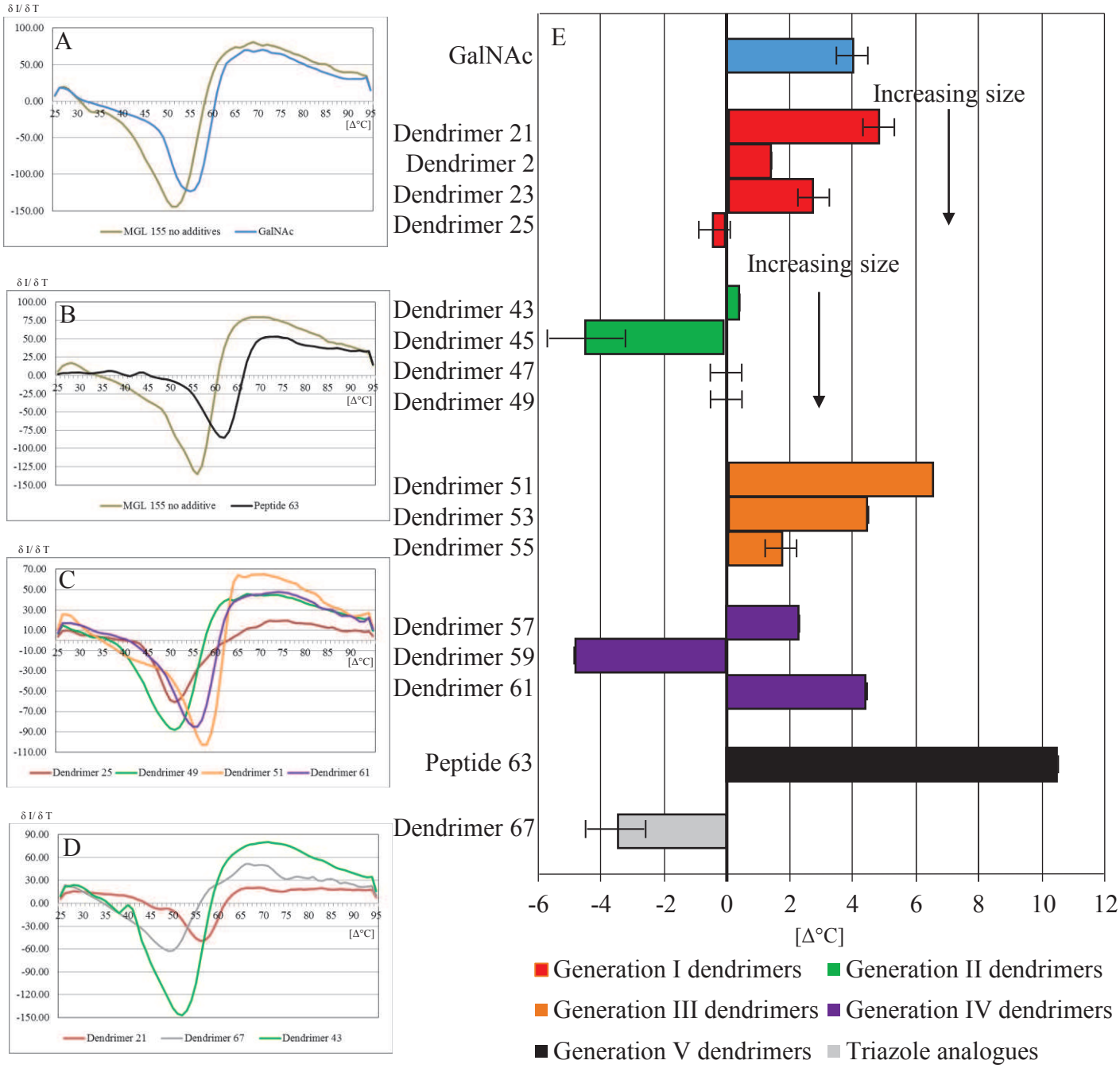

Figure 6.8: The change in melting point [°C] with the additives at 1 mM concentration for MGL 155 compared to MGL 155 with no additives. A) DSF derivative plot of MGL 144 alone and with GalNAc. B) DSF derivative plot of MGL 155 alone and with peptide **63**. C) DSF derivative plot of MGL 155 incubated with dendrimers **25**, **49**, **51** and **61**. D) DSF derivative plot of MGL 155 incubated with dendrimers **21**, **43** and **67**. E) Average change of melting point of MGL 155 when incubated with different additives.

6.1.4 Thermal melt assay using MGL 144 protein

The thermal melt assay results for the largest protein truncation MGL 144 are shown in Table 6.4 and Figure 6.9. A positive shift in the melting point of 4 °C was observed when MGL was incubated with GalNAc as shown in plot A. Only dendrimer **45** was found to lower the melting point of MGL 144 (Figure 6.9 plot B). None of the other generation II dendrimers had any effect on the melting point.

The compound which induced the largest shift in melting point was dendrimer **51** (plot C of Figure 6.9) which stabilised the MGL 144 by an additional 7 °C. The generation III dendrimers (**51**, **53** and **55**) with two GalNAc residues performed the best with shifts in melting point of 4.5–7 °C. The generation I dendrimers (**21**, **2**, **23** and **25**) with three GalNAc residues all bound in a positive fashion and induced shifts of 3.0–6.5 °C. Plot D of Figure 6.9 shows the largest increase in melting point within the generation I (dendrimer **21**). The generation IV dendrimers (**57** and **61**) with one sugar exhibited a smaller range inducing shifts of 3.5–5.5 °C. Five compounds (dendrimers **21**, **51**, **53**, **55** and **61**) bound better than the GalNAc monomer. All of these structures had at least one GalNAc residue attached using click chemistry.

The melting point for MGL 144 incubated with peptide **63** was undefined because the point of inflection on the rfu plot was unclear. Examination of the derivative plot for peptide **63** suggests a sharp rise of fluorescence that may indicate significant stabilisation perhaps greater than 7 °C. The plots for peptide **63** can be viewed in the Appendix (Figure 9.50). Due to lack of time and proteins, the experiment wasn't repeated and an accurate melting point for peptide **63** was not determined.

Table 6.4: Thermal melt assay of MGL 144 with dendrimers **21** - **67**. The original rfu plots and differential graphs are shown in the Appendix (Figures 9.47–9.50).

Generation	Additive (1 mM)	Appendix plot	Av. shift in M.P. (°C)
-	none	86	-
	GalNAc	87	+4.3
I (dendrimers with 3 GalNAc)	Dendrimer **21**	88	+6.3
	Dendrimer **2**	91	+3.7
	Dendrimer **23**	93	+3.0
	Dendrimer **25**	95	+3.3
II (dendrimers with 0 GalNAc)	Dendrimer **43**	90	0.0
	Dendrimer **45**	92	−0.3
	Dendrimer **47**	94	0.0
	Dendrimer **49**	96	0.0
III (dendrimers with 2 GalNAc)	Dendrimer **51**	97	+6.7
	Dendrimer **53**	98	+5.0
	Dendrimer **55**	99	+4.7
IV (dendrimers with 1 GalNAc)	Dendrimer **57**	100	+3.7
	Dendrimer **59**	101	0.0
	Dendrimer **61**	102	+5.3
V (peptide with 3 GalNAc)	Peptide **63**	103	undefined
Triazole analogue	Dendrimer **67**	89	0.0

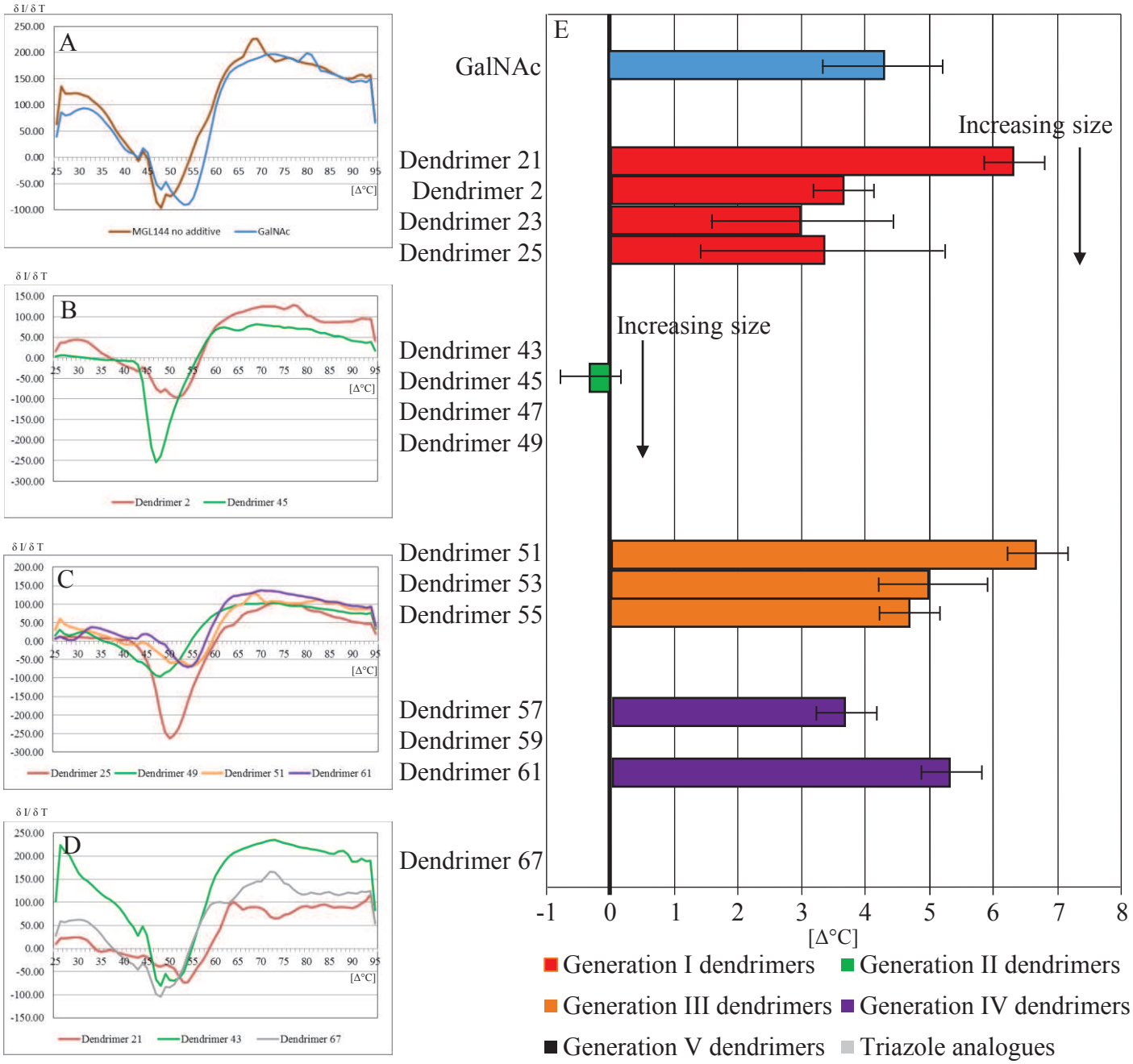

Figure 6.9: Change in melting point [°C] with the additives at 1 mM concentration for MGL 144 compared to MGL 144 with no additives. A) DSF derivative plot of MGL 144 alone and with GalNAc. B) DSF derivative plot of MGL 144 incubated with dendrimers **2** and **45**. C) DSF derivative plot of MGL 144 incubated with dendrimers **25**, **49**, **51** and **61**. D) DSF derivative plot of MGL 144 incubated with dendrimers **21**, **43** and **67**. E) Average change in melting point of MGL 144 when incubated with different additives.

6.1.5 Comparison of the four MGL truncation thermal melt assays

The results showed that the larger the MGL protein, the more selective the MGL truncation protein bound to the peptides. The smallest protein MGL 176 bound to almost every compound, whereas the largest protein MGL 144 only bound the additives containing GalNAc. This result is not surprising given that the known biological ligands for MGL are GalNAc–containing moieties. The most effective additives for stabilising the MGL truncations are shown in Figure 6.10.

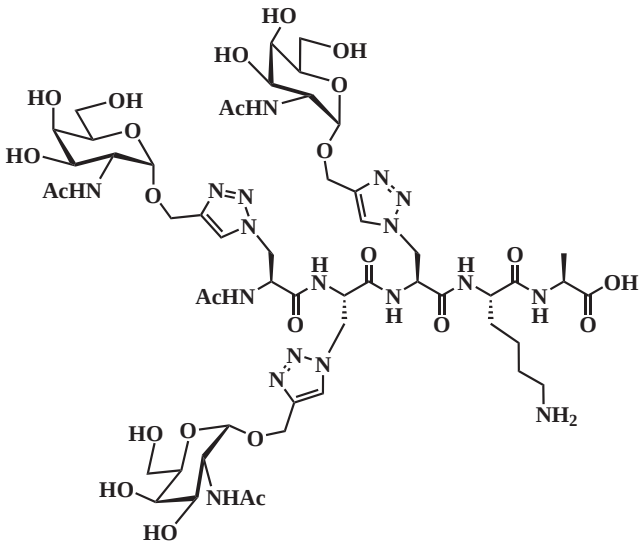

63

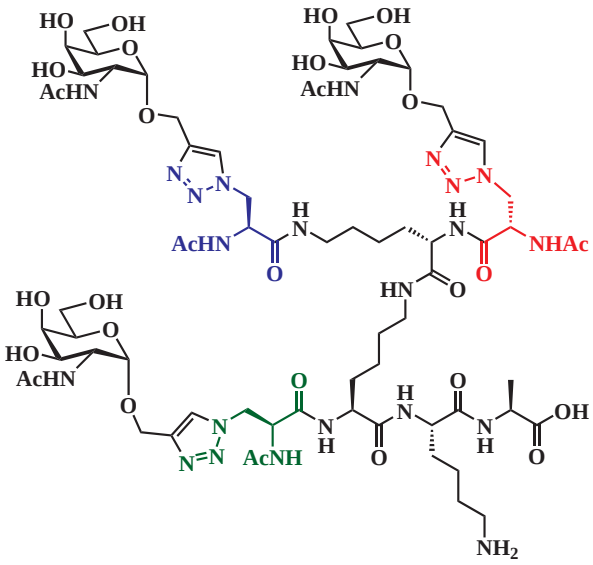

21

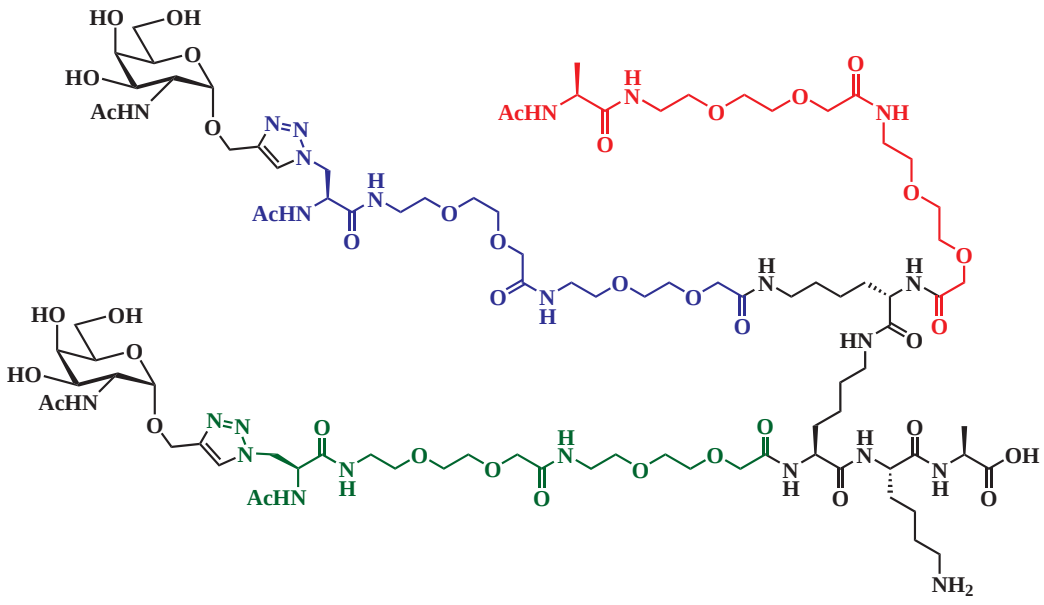

51

Figure 6.10: The three compounds which induce the greatest shifts in melting point for the MGL truncations: peptide **63**, dendrimer **51** and dendrimer **21**.

In three out of four MGL truncation thermal melt assays, peptide **63** (three GalNAc residues) bound significantly better than the rest of the compounds tested and induced a positive shift in the melting point. Dendrimer **51** (two GalNAc residues) induced the second largest shifts for three out of four of the thermal melt assays, and induced the largest shift in melting point for MGL 144. Dendrimer **21** (three GalNAc residues) was the best performing of the dendrimers containing three GalNAc residues for all four truncations of MGL. Dendrimer **61** induced the largest shift in the observed melting point for all four truncations of all the compounds that contained one GalNAc residue.

No correlation between the size of dendrimer or the number of sugars and the change in melting point for the MGL truncations was observed. It is also clear that the dendrimers containing GalNAc proteins bound better than the equivalent structure without. This result was also expected as the known biological selectivity of the MGL CRD is towards the GalNAc containing compounds.[29, 30, 31] The results of the thermal melt assay would also indicate the availability of GalNAc on the additives to the MGL CRD. The compounds which failed to increase the melting points of truncated MGL were likely to either not contain GalNAc or be positioned in such a way that the sugar isn't available for binding in solution and hence unable to stabilise the protein with increasing temperatures.

Chapter 7

The MGL–expressing MoDC binding assay at 37 °C

This chapter will develop the initial work done with the cell binding assay in Chapter 4, using the dendrimers from chapter 2 (Figure 7.1 and Figure 7.2) as well as using the compounds described in Chapter 5 (Figure 7.3–7.5) for the first time in a biological assay. Along with these compounds, MUC1 sequences synthesised by Dr Lee (Figure 7.6) were also tested.

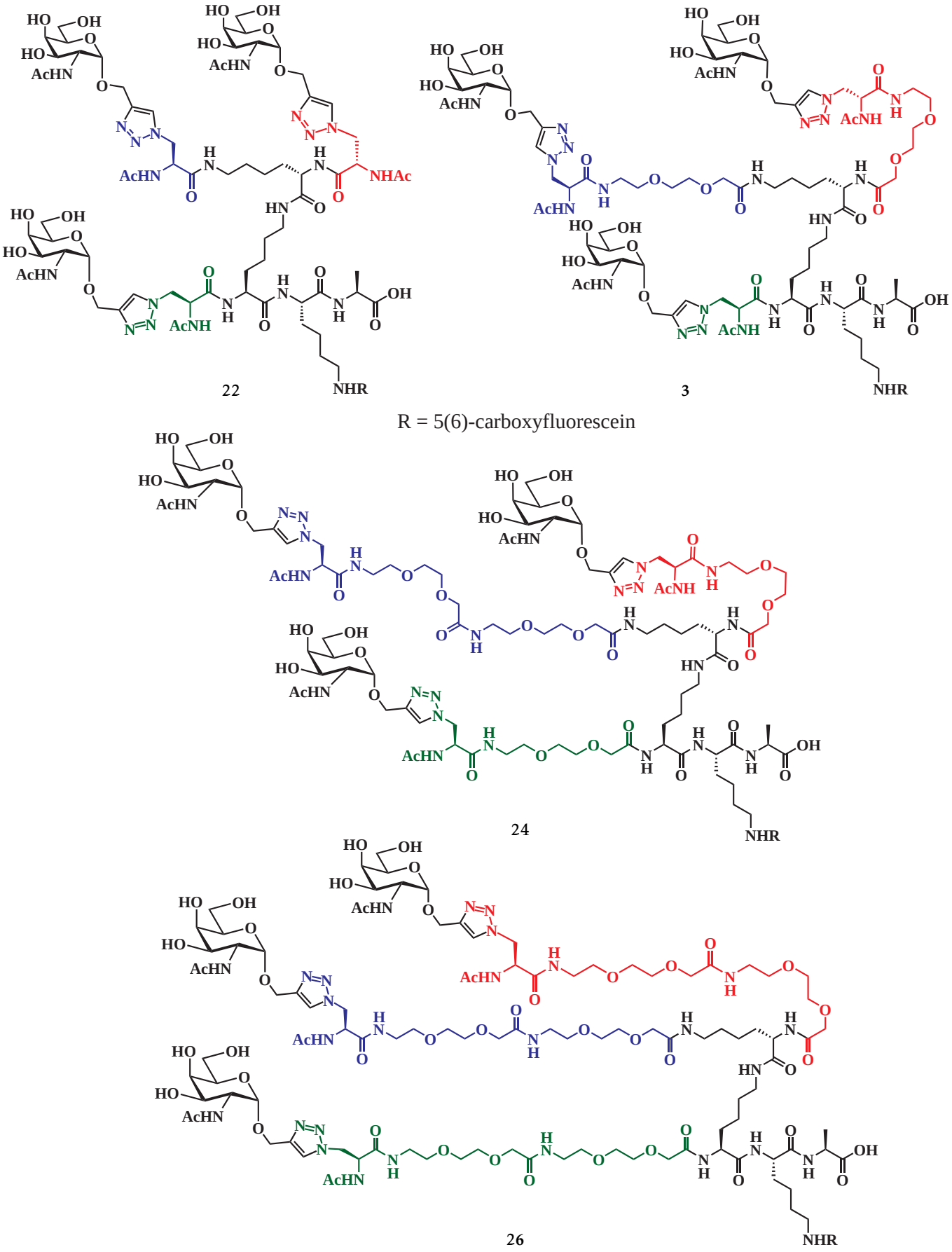

Figure 7.1: Structures of the generation I dendrimers **22**, **3**, **24** and **26**.

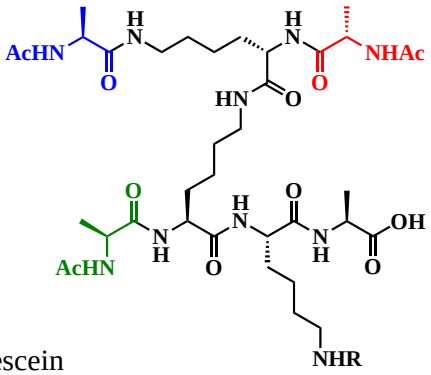

R = 5(6)-carboxyfluorescein **44**

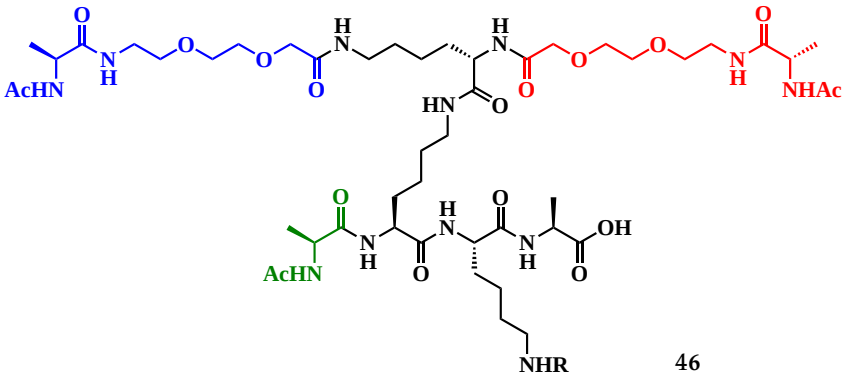

46

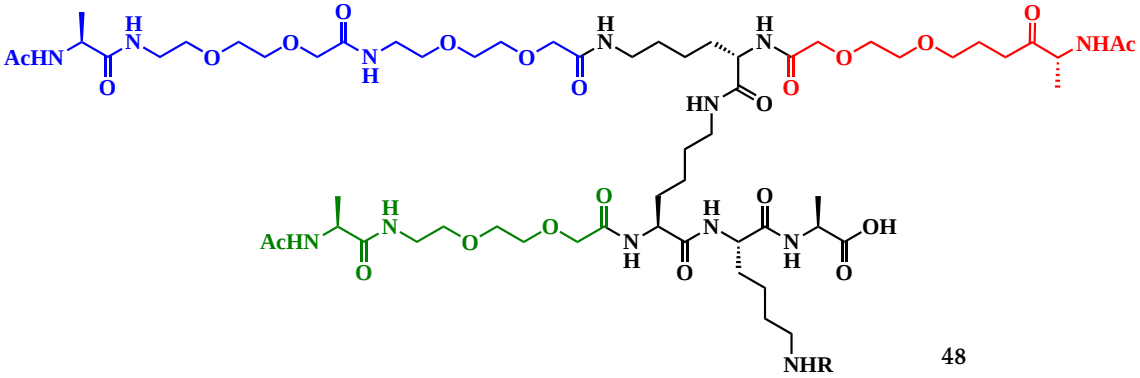

48

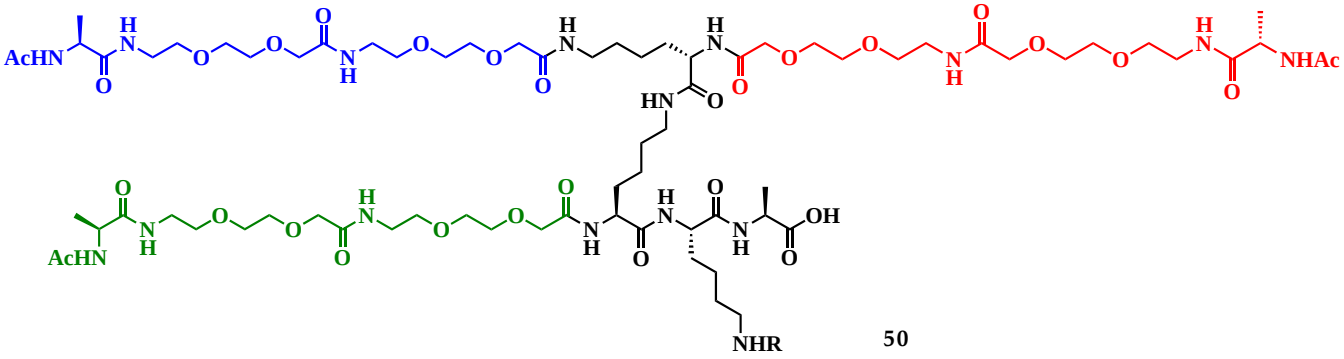

50

Figure 7.2: Structures of the negative control generation II dendrimers **44**, **46**, **48** and **50**.

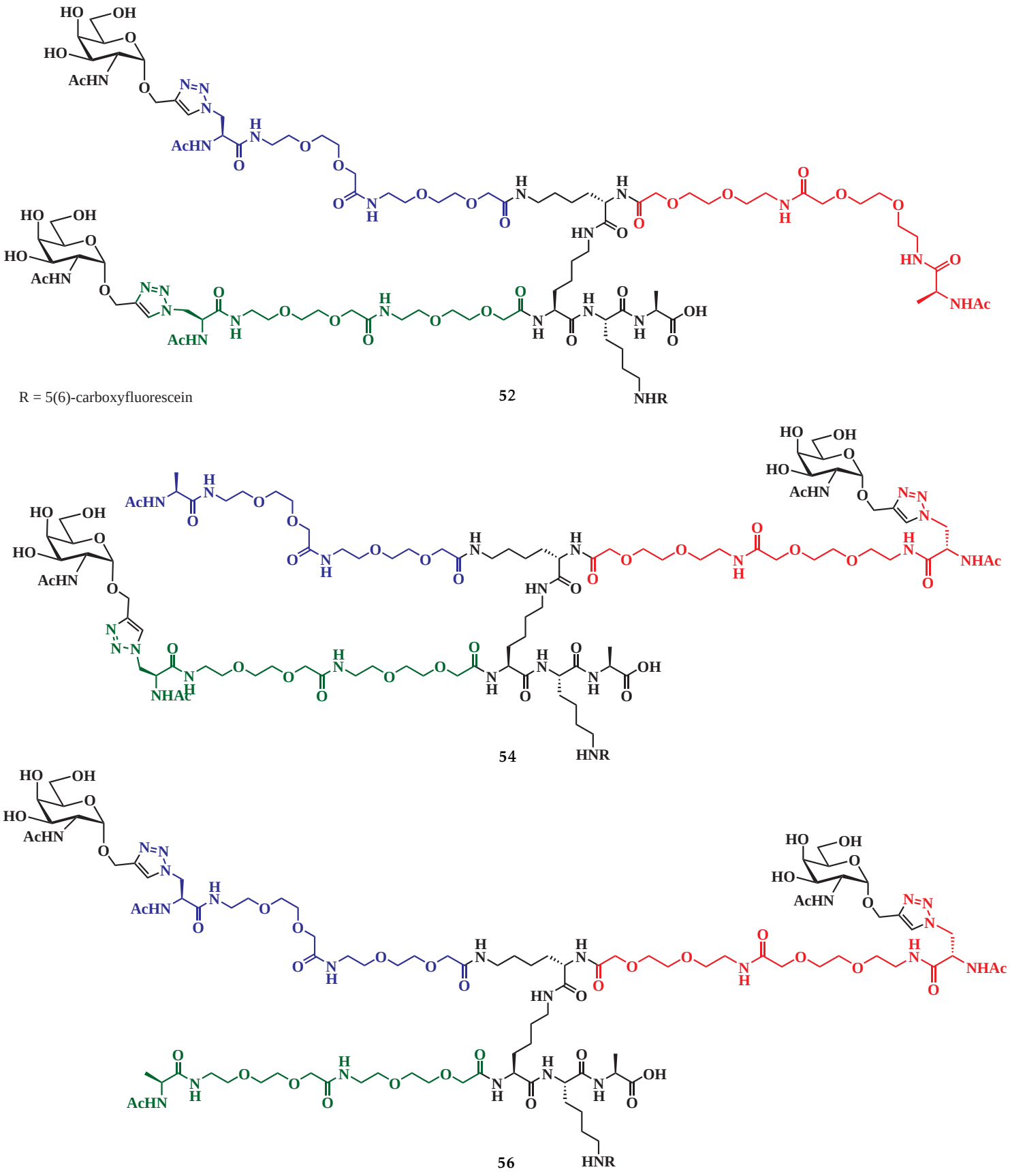

Figure 7.3: Structures of the generation III dendrimers **52**, **54** and **56**.

R = 5(6)-carboxyfluorescein

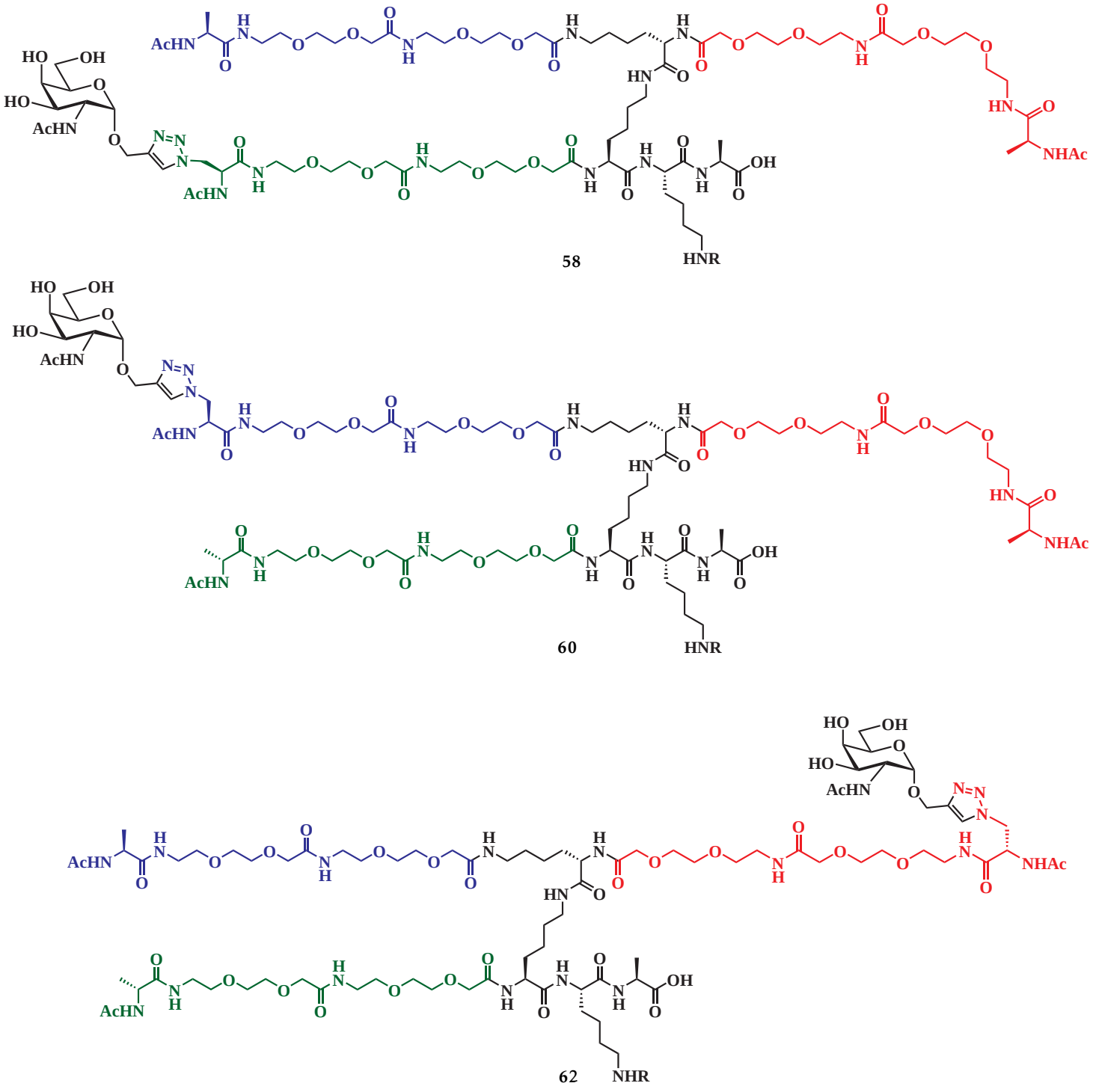

Figure 7.4: Structures of the generation IV dendrimers **58**, **60** and **62**.

R = 5(6)-carboxyfluorescein

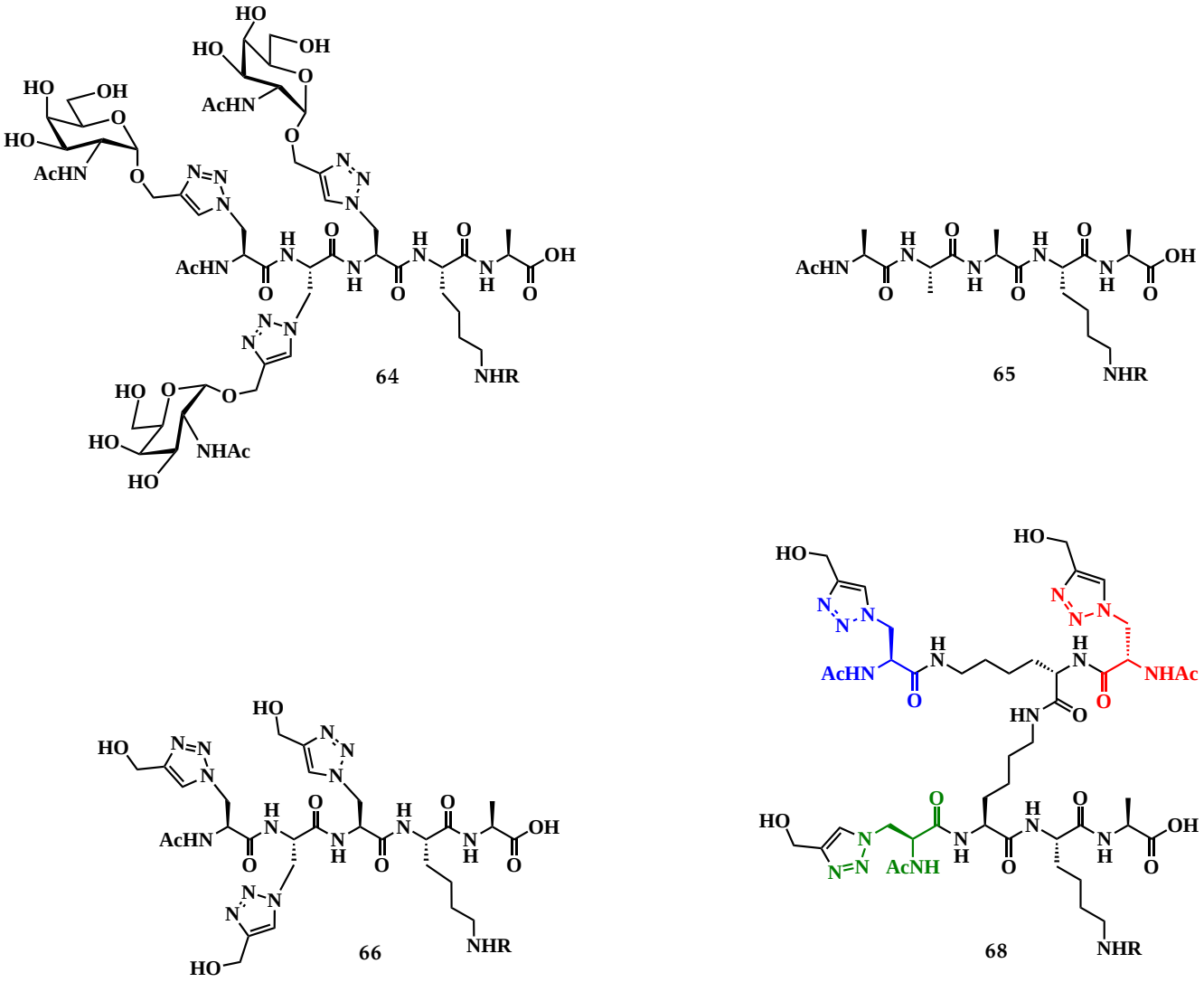

Figure 7.5: Structures of the generation V compounds: GalNAc–glycosylated straight chain peptide **64**, the straight chain peptide negative control **65**, triazole analogues straight chain peptide negative control **66** and the triazole dendrimers **68**.

7.1 MUC1 sequences synthesised by Dr Lee

Previous work by Dr Lee produced three MUC1 sequences shown in Figure 7.6.[103, 140, 104] These compounds were synthesised to act as immunological probes for studying MGL before this project was started. As these peptides were available and the MUC1 sequence has been shown to bind to MGL,[20] they were included in the cell binding studies for a comparison of quantity of binding. The first peptide was MUC1 J, which contains serine and threonines that have been glycosylated with GalNAc.[103] The second sequence referred to as MUC1 K, is a neo-glycopeptide which attached GalNAc residues through the triazole linker to the MUC1 sequence.[140] The final sequence does not contain any sugars and is called MUC1 L.[103] The MUC1 sequences were made as 10 mM stock solutions by Dr Lee and kept in a freezer at -80 °C for three years prior to the experiment being performed. The solutions were checked by mass spectrometry and contained the MUC1 sequences without degradation.

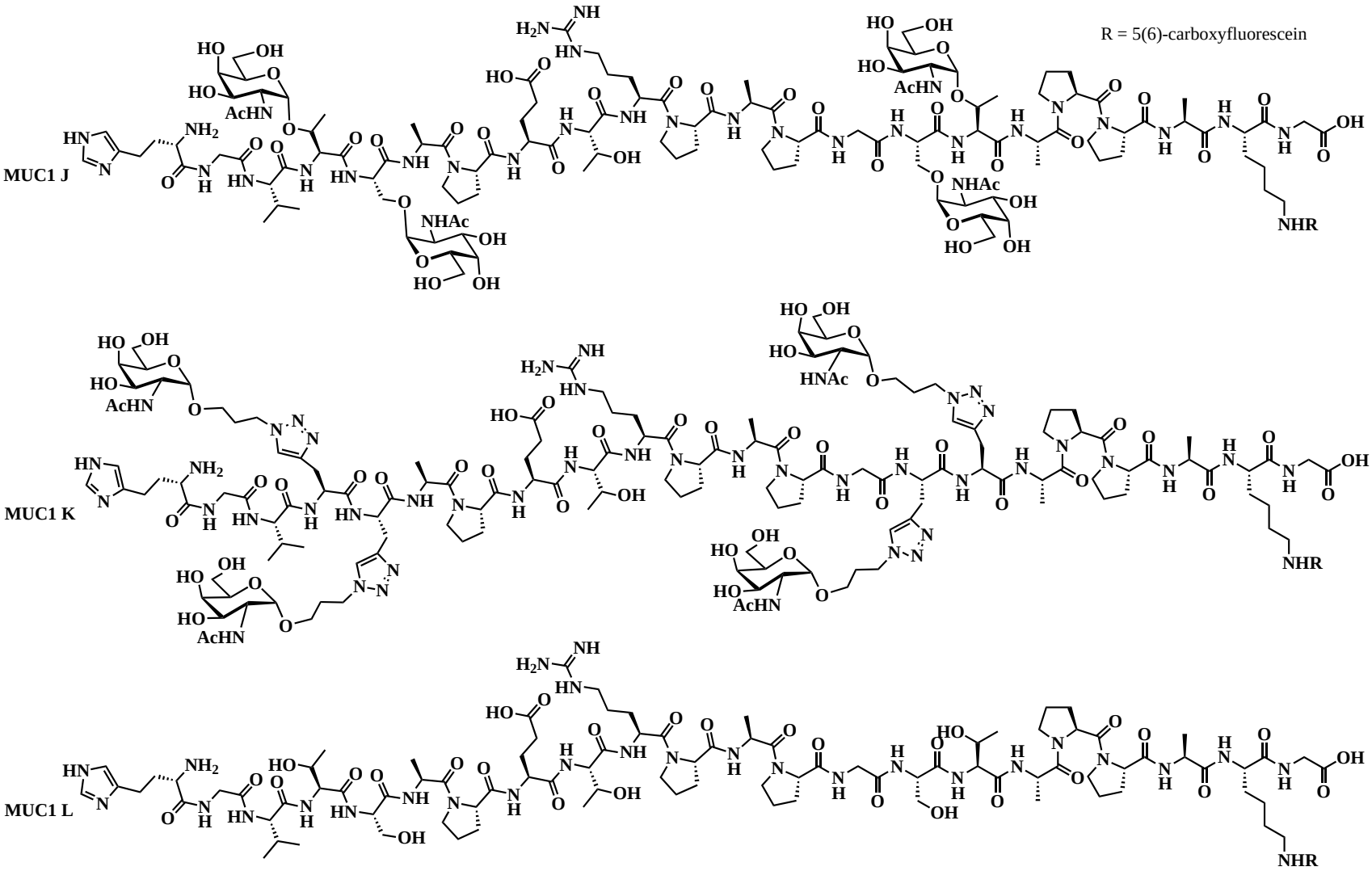

Figure 7.6: The structures of the three truncated MUC1 sequences synthesised by Dr Lee: the O–GalNAc glycosylated MUC1 J, the neo–glycopeptide MUC1 K and the non–glycosylated sequence MUC1 L

7.2 Optimisation at 37 °C

The loading of the dendrimers to MoDC was low at 0 °C, therefore in order to increase the magnitude of this binding the temperature was increased to 37 °C. This would result in greater differences between the MFI for binding dendrimers and non binding dendrimers to MoDC.

7.2.1 Media system optimisation

Initial experiments were performed at 37 °C using the TSM buffer, however it was observed that a lower proportion of cell recovery was occurring when cells were incubated for an extended period of time (Figure 7.7). Therefore a comparison of three different media at 0 and 37 °C was performed. The three media used were TSM, RF10[i] and AIMV[ii]. The incubation period was 1 h, the concentration of dendrimer additive was 1 μM and the dendrimers used were **22** and **44**. Both LG2 and MGL–expressing MoDC cells were used for this experiment. All sample conditions were performed in triplicate. The results are presented in Figure 7.8.

Cell recovery was calculated by the following equation:

% Cell recovery = 100×(number of alive cells)/(total number of cells)

The average cell recovery for MoDC was much lower for the TSM buffer than the other media with average recovery of around 50% whereas the RF10 and AIMV both have a 70% average cell recovery (Figure 7.7). RF10 had a similar level of cell recovery, with slightly more cells recovered than AIMV. The cell recovery for LG2 cells was lower than MoDC, but this was because there was a higher proportion of dead cells. There was no major difference between the two dendrimers when the cell recovery was compared for each media. The general trend was an average cell recovery of around 30% for TSM and the RF10 and AIMV both have a 70% cell recovery. The cell recovery was lower for LG2 cells, this may be due to the fact that these cells are more susceptible to cell death when incubated with the additives at 37 °C. Another possibility would be that the LG2 cells were due to be passaged after this experiment took place (this happens on a 4 day cycle) and therefore had a higher % of dead cells than normal. If the experiment had been performed after the new sub culture had been set up the % of dead cells would be much lower in comparison to the number of alive cells.

[i] the medium the MoDC are cultured in, which contains fetal bovine serum and nutrients to sustain cells.
[ii] a medium which contains similar nutrients to sustain cells like RF10 but does not contain bovine serum, and instead contains a defined protein component.

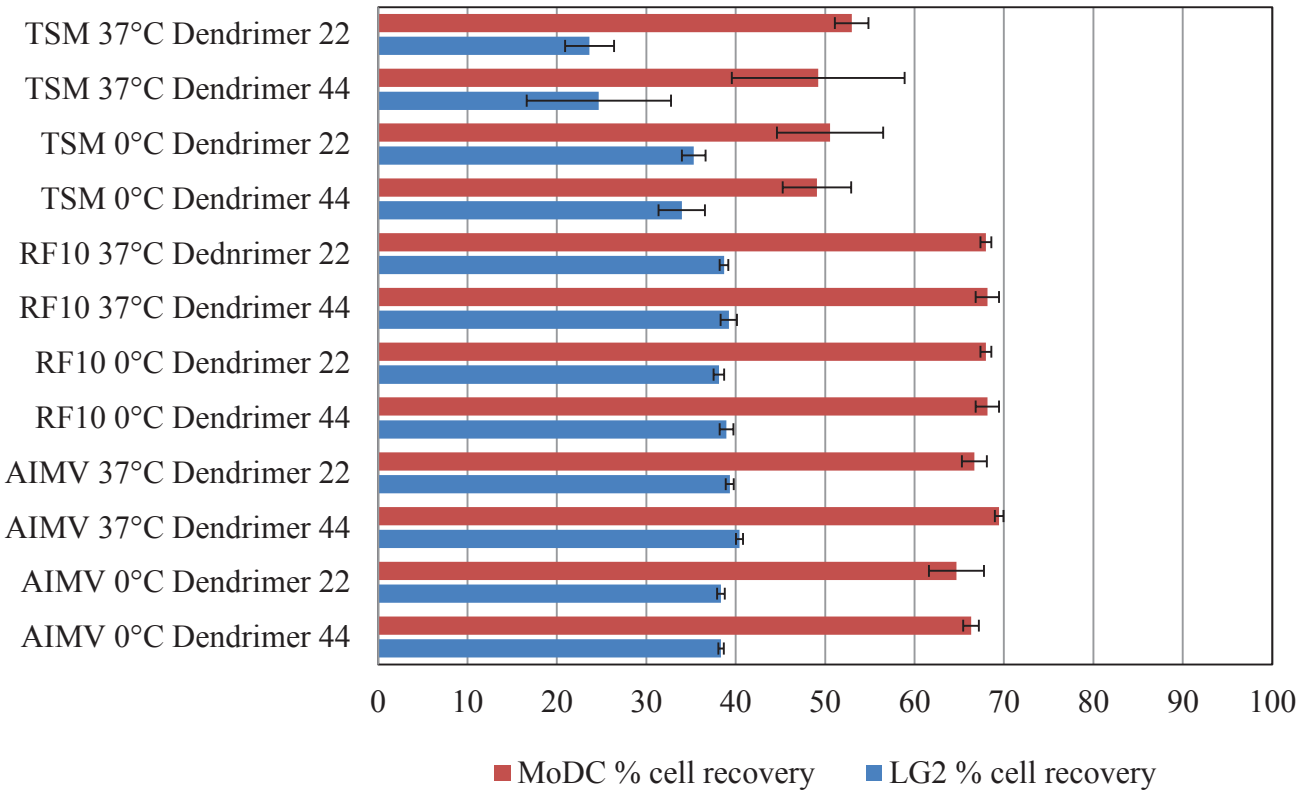

Figure 7.7: Average cell recovery for triplicate samples for dendrimer **22** and **44** incubation using 1 μM concentrations at 0 °C and 37 °C for 1 hour with the media TSM, RF10 and AIMV.

FACS plot A in Figure 7.8 shows a comparison of generation I dendrimer **22** which exhibited the highest levels of loading, and the generation II dendrimer **44** which did not bind when incubated at 37 °C in RF10. The shifts in fluorescence are much larger at the elevated temperature.

Bar graph C in Figure 7.8 shows the average results for each dendrimer incubated at each temperature for each media system. For all three media, the negative control dendrimer **44** did not bind at any temperature to either cell type. This was encouraging as the dendrimer had not bound at 0 °C in previous work (see Chapter 4), and it shows that the media do not induce non–specific binding.

In general there was no binding or very low binding of the dendrimers to the LG2 cells under any experimental condition tested. FACS Plot B in Figure 7.8 is representative of the results of all the LG2 cells plots. This was expected, as in general the LG2 cells have not shown specific binding at a concentration of 1 μM.

For all of the media at 37 °C, dendrimer **22** showed increased binding towards MoDC compared to the binding observed at 0 °C. Of the three media, binding assays conducted in RF10 gave the highest loading, with AIMV also binding well. The dendrimer **22** in TSM buffer showed binding, but it was much less than that observed in the other two media. This suggests that the nature of the medium may be important in determining the ability to bind to the cells, potentially by affecting

the availability of the GalNAc moieties on the dendrimer for binding to MGL. The medium will also have a role in the health of the cells, which may be important for expression of MGL for MoDC. RF10 was selected as the buffer to use for the rest of the experiments because it gave the high average cell recovery and also large MFI differences between dendrimers with GalNAc and dendrimers without GalNAc.

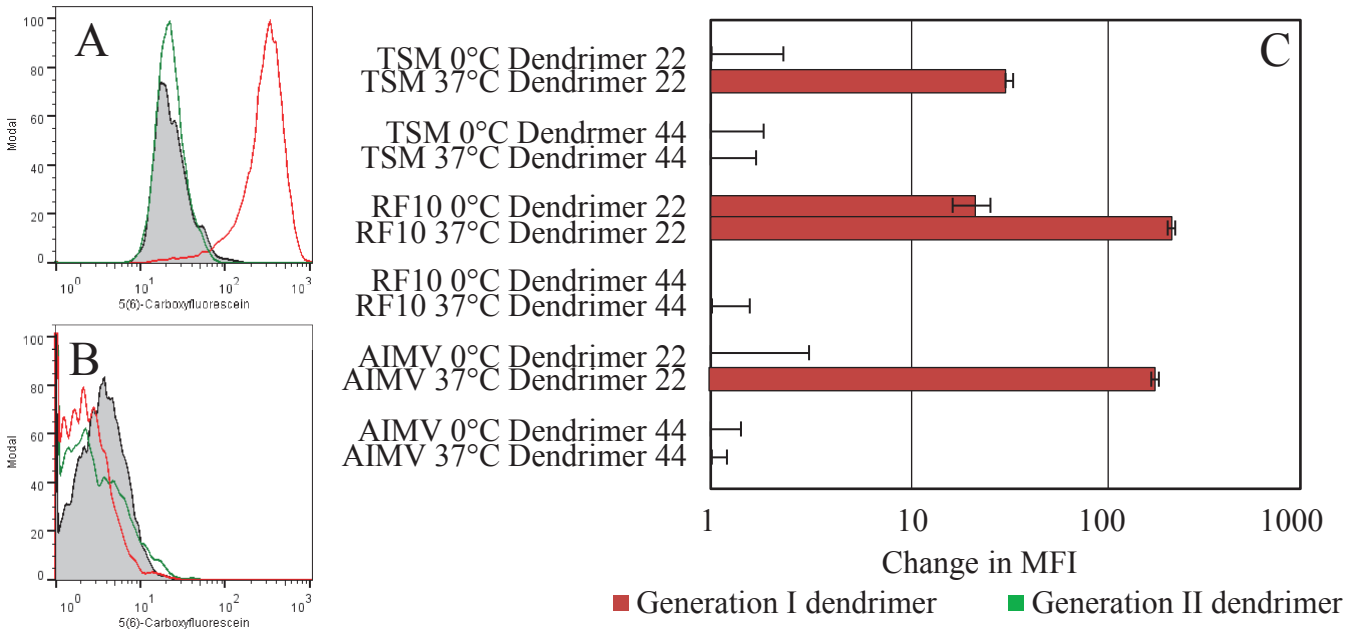

Figure 7.8: Change in MFI for MoDC incubated with different peptide media with 1 μM concentrations at 0 °C and 37 °C for 1 hour. A) FACS histogram plot indicating binding of 1 μM of the dendrimer **22** (red) and **44** (green) to MoDC in RF10 buffer at 37 °C. B) FACS histogram plot indicating binding of 1 μM of the dendrimer **22** (red) and **44** (green) to LG2 in RF10 buffer at 37 °C. C) Change in MFI is given as the average for triplicate samples for each dendrimer incubation.

7.2.2 Time course experiment at 37 °C

A time course experiment was performed at 37 °C with MoDC and LG2 cells with dendrimers **22** and **44** at 1 μM. The timepoints analysed were 30 minutes, 1 hour and 2 hours to allow direct comparison with the results in Chapter 4 (Figure 4.6). The results are shown in Figure 7.9.

FACS plot A in Figure 7.9 shows a comparison of dendrimers **22** and **44** after a 2 hour incubation with MoDC. While both dendrimers bound to MoDC, the increase MFI was much larger for dendrimer **22** which was expected due to it being glycosylated with GalNAc. The other time points followed a similar pattern with these two dendrimers. The MFI for dendrimers increases with longer incubation periods, more binding by dendrimers to MGL–expressing MoDC is observed with longer incubations.

Bar graph C in Figure 7.9 shows the average change in MFI for each dendrimer incubated with MoDC during the time course. Dendrimer **22** showed increases in binding dependent on the length of incubation to MGL–expressing MoDC. The change in MFI increased from 30 minutes to 1 hour and again with 2 hour incubations.

Dendrimer **44** showed no signs of binding to MGL–expressing MoDC at 30 minutes, very low binding at 1 hour and slightly more binding (but still low) at 2 hours. This shows that the longer dendrimer **44** is incubated, the more likely it is to non–selectively bind or be internalized by MoDC. This is not surprising as the function of MoDC is to take up antigens from its surroundings, mature then migrate to the lymph node.

There was no binding of either of the dendrimers to the LG2 cells at any timepoint. FACS plot B in Figure 7.9 is representative of the binding observed for these compounds to LG2 cells for all of the FACS plots in this experiment.

The results at 37 °C showed the same general trend that was observed at 0 °C, however the increase in MFI was more pronounced for each increase in incubation period at the higher temperature. The other difference was that the non–specific binding of dendrimer **44** to MoDC was not visible at lower temperatures.

The results of this experiment indicated that an incubation period of 1 hour was sufficient to detect binding of the compound and that longer incubation periods may result in non–specific binding and internalisation.

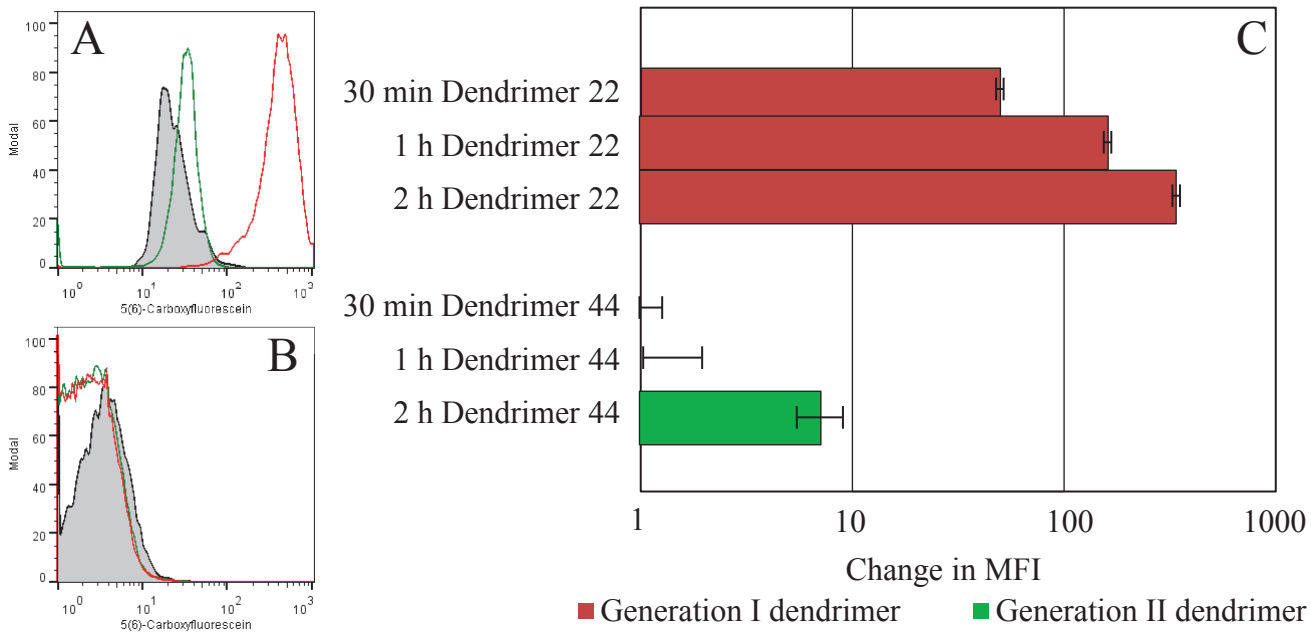

Figure 7.9: Change in MFI for MoDC incubated with indicated dendrimer at 1 μM at 37 °C for 1 hour. A) FACS histogram plot indicating binding of dendrimer **22** (red) and **44** (green) to MoDC with a 2 hour incubation. B) FACS histogram plot indicating binding of dendrimer **22** (red) and **44** (green) to LG2 with a 2 hour incubation. C) Change in MFI is given as the average for triplicate samples for each dendrimer incubation with standard deviations in the form of error bars included.

7.2.3 Titration at 37 °C

A titration was performed at 37 °C with MoDC and LG2 cells with dendrimers **22** and **44** with a 1 hour incubation period. The concentrations used were 1 nM, 10 nM, 100 nM, 1 μM and 10 μM. Concentrations below 1 nM were not used as previous experiments at 0 °C had been unable to detect binding at such low concentrations. Concentrations above 10 μM were not used as non-specific binding had been observed above this concentration.

FACS plot A in Figure 7.10 shows the fluorescence curves for dendrimer **22** and **44** at 10 μM. This is the only concentration where dendrimer **44** binds to MoDC. These conditions also resulted in the largest increase in MFI for dendrimer **22**, and hence the more binding to MGL–expressing MoDC.

FACS plot B in Figure 7.10 shows the fluorescence curves for dendrimer **22** and **44** at 1 nM. The change in MFI is low for both dendrimers **22** and **44**, which indicates that dendrimer binding is not detectable at this low concentration to MoDC.

Graph C in Figure 7.10 shows the average change in MFI for each compound following incubations with MoDC at different concentrations. The binding of the GalNAc glycosylated dendrimer **22** to MGL–expressing MoDC increases steadily as the concentration increases. For every factor of 10 the concentration of dendrimer **22** increases, the MFI doubles (~50 at 10 nM, ~100 at 100 nM, ~200 at 1 μM and ~400 at 10 μM.). Therefore the observed binding of dendrimer **22** was dose–dependent across the range of concentrations tested.

The shifts in MFI are much higher at 37 °C compared to those observed at 0 °C in Section 4.4.2, although these 0 °C experiments were performed in TSM buffer as opposed to the RF10 buffer. The general trend for greater dendrimer binding with increased concentration remains the same for both temperatures. The increase in binding between 0 °C and 37 °C will be due to the increased temperature which supplies more energy to the molecules which increases the chance of a successful binding interaction.

There was no binding observed by either dendrimer to the LG2 cells at the concentrations tested. From this experiment it was decided that 1 μM would be used to test the binding efficiency across all the compounds produced in Chapter 2 and 5. At this concentration, binding of the GalNAc–containing compound to MGL–expressing MoDC was observed with little non–specific binding/internalisation of the generation II dendrimers. The large difference in MFI would allow a dynamic range of responses to be observed allowing quantitative evaluation of dendrimer binding.

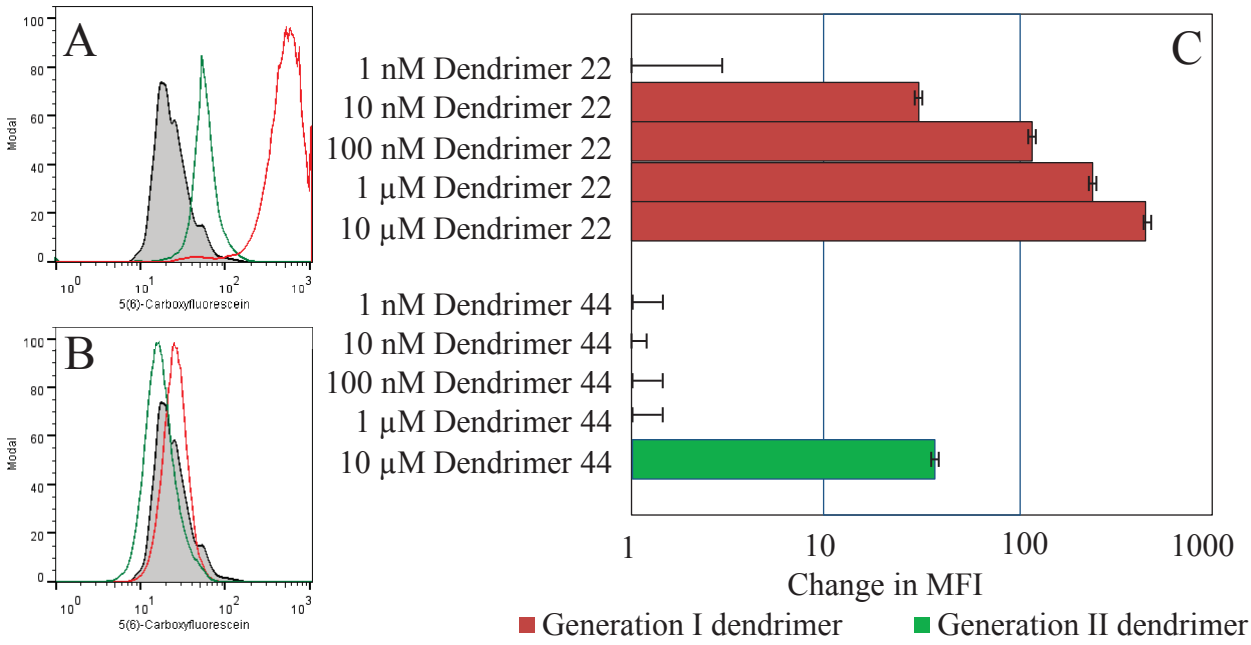

Figure 7.10: Change in MFI for MoDC incubated the indicated dendrimers at concentrations between 1 nM and 10 μM at 37 °C for 1 hour. A) FACS histogram plot indicating binding of 10 μM of the dendrimer **22** (red) and **44** (green) to MoDC. B) FACS histogram plot indicating binding of 1 nM of the dendrimer **22** (red) and **44** (green) to MoDC. C) Change in MFI is given as the average for triplicate samples for each dendrimer incubation with standard deviations in the form of error bars included.

7.3 Results from optimised conditions

The library of dendrimers and peptides generated in Chapter 2 and 5 was tested for binding to MoDC using the conditions obtained from the optimisation experiments. The standard conditions employed used RF10 as the medium, the temperature was 37 °C, the concentration would be 1 μM for each additive and the incubation time was 1 h.

7.3.1 Binding assay for comparison of synthetic glycodendrimers and glycopeptides and their non-glycosylated analogues to MGL$^+$ MoDC

The compounds for this experiment can be split into 7 groups:

- Generation 1 dendrimers (3 GalNAc)
- Generation 2 negative control dendrimers (0 GalNAc)
- Generation 3 dendrimers (2 GalNAc)
- Generation 4 dendrimers (1 GalNAc)
- Generation 5 peptides
- Triazole analogues
- MUC1 sequences

The results of the MoDC binding are shown in Graph D in Figure 7.11, with the structure of the highest loading compound from each group in Figure 7.12. The following sections provide a more detailed analysis of the results observed in the binding assay.

Generation I dendrimers (3 GalNAc)

The generation I dendrimers all have three GalNAc moieties. Dendrimer **24** gave the largest shifts in MFI from the experiment and hence exhibited the highest level of binding of the compounds tested. There is no obvious correlation when it comes to structure size or arrangement of GalNAc in relation to amount of binding, as the dendrimer with the second highest level of binding was dendrimer **22** which is the smallest dendrimer. The 'least' binding of the generation I compounds was observed with dendrimer **3** which is the second smallest dendrimer of the set, and yet it still

had greater loading to MoDC than the majority of other additives tested. Dendrimer **3** exhibited lower levels of loading than the generation III dendrimer **54** with two sugars.

Generation II negative control dendrimers (0 GalNAc)

The generation II dendrimers are structurally similar to the generation I dendrimers but contain no GalNAc residues. These dendrimers all had lesser changes in MFI than the equivalent structures from the generation I and III dendrimers. The negative control dendrimers do not follow the same trend in lowest to highest MFI shift as the generation I dendrimers. These non–glycosylated generation II dendrimers in general showed the smallest MFI of all of the dendrimers tested. This was expected as these dendrimers contain no GalNAc residues which are important for binding to MGL. If any MoDC binding interactions occurs to these dendrimers, is is not through GalNAc interactions. Generation II dendrimers are likely to interact with MoDC through either non–specific interactions or low levels of internalisation of the dendrimer over the period of incubation.

FACS plot A in Figure 7.11 shows the comparison of the fluorescence curves for GalNAc–glycosylated generation I dendrimer **24** which exhibited the highest levels of loading from the experiment and the equivalent generation II dendrimer **48**. The difference in MFI is large between the two dendrimers, showing the importance of the GalNAc residues for binding. The fluorescence curve for dendrimer **24** is similar in position and shape to all of the other generation I dendrimers. The presence of GalNAc moieties in the dendrimer structure improves the targeting of a dendrimer towards the MGL receptor. MoDC are likely to internalise/non–selectively bind compounds as it is part of their function which is why some uptake of compounds incubated with MoDC is always expected. Targeting of the MGL receptor through GalNAc–mediated binding dramatically increases the amount of binding which is important for vaccine delivery of compounds directly to MoDC. This is the main reason why the GalNAc–glycosylated dendrimer **24** should always exhibit greater binding than the non–glycosylated dendrimer **48**.

Generation III dendrimers (2 GalNAc)

The generation III dendrimers exhibited the second highest level of binding to MoDC, with all of the dendrimers binding more than the mono–glycosylated equivalent in the series of generation IV dendrimers. All of these compounds were based on dendrimer **26**, with different combinations of glycosylated X, Y and Z chains. Dendrimer **54** bound with a very similar MFI to dendrimer **26** while the other two dendrimers bound less to MGL expressing MoDC. Dendrimer **52** was a better binder than **56**.

Generation IV dendrimers (1 GalNAc)

All of these compounds were based on dendrimer **26**, with only one of the X, Y and Z chains glycosylated with GalNAc. The generation IV dendrimers showed the lowest level of binding for dendrimers which contained GalNAc, which may be expected as every other generation contains more GalNAc residues which increase the amount of binding to MGL–expressing MoDC. Polyvalency of the ligand with multiple GalNAc residues would increase the loading of the MGL CRD. Increasing the loading for MGL would therefore result in increased amounts of ligand binding to MoDC. Dendrimer **60** was the highest loading for the generation IV series, with dendrimer **62** exhibiting the second highest levels of loading of the generation and dendrimer **58** being the least binding dendrimer.

FACS Plot C in Figure 7.11 shows a comparison of dendrimer **26** and all of the highest loading compounds from each generation. The fluorescence curve for dendrimer **26** and the generation III dendrimer **54** overlap, while the generation IV dendrimer **60** fluorescence curve is between the autofluorescence of MoDC and dendrimer **26**. Dendrimer **50** was a lower binder than dendrimer **60**, which is expected as it has no GalNAc residues.

The generation IV dendrimers results highlight how important polyvalent binding to observe increased binding. As none of these compounds with only a single GalNAc residue are able to employ a clustering effect when binding to MGL–expressing MoDC the amount of binding is reduced. Generation I and III dendrimers have mulitple GalNAc residues available and are able to employ this clustering effect, the multi–dentate binding which occurs results in greater quantities of dendrimers binding with each GalNAc added.

Generation V straight chain peptides

Straight chain peptide **64** contains three GalNAc residues clicked to alanines in sequence, whereas the straight chain peptide **65** has three non–glycosylated alanines in sequence. The linear GalNAc–glycosylated straight chain peptide **64** showed greater levels of binding to MoDC than peptide **65**. It was observed that straight chain peptide **64** bound more abundantly than all of the generation IV dendrimers and the generation III dendrimer **56**, but bound comparatively less than the other generation III dendrimers. This was surprising as it was expected that the straight chain peptide **64** would bind in a similar fashion to the generation I dendrimers as both have three GalNAc residues. This result shows that the distance between the GalNAc residues may be a better determinant of the ability of the compound to bind rather than the number of carbohydrate moieties present.

It was surprising that the non–glycosylated straight chain peptide **65** bound more than the mono–glycosylated generation IV dendrimer **58**. Neither of these compounds were impressive binders, as they both have similar MFI values to the generation II dendrimers. This may indicate that non–specific binding or internalisation by MoDC was taking place.

Triazole negative control compounds

Two compounds were synthesised where simple triazole moieties were attached to a peptide backbone instead of "clicked" sugars. These compounds were prepared to show the effect of the triazole moieties on binding to MoDC. Straight chain peptide **66** was similar in structure to peptide **64**. The triazole peptide **66** was a slightly better binder than the GalNAc glycosylated peptide **64**.

The other compound with triazoles was dendrimer **68** which is similar in structure to generation I dendrimer **22** and generation II dendrimer **44**. All three fluorescence curves for the dendrimers are shown in FACS plot B of Figure 7.11. Dendrimer **68** bound more than dendrimer **44**, but less than dendrimer **22**. Dendrimer **68** has a similar MFI to the mono–glycosylated generation IV dendrimers.

The triazoles for the glycosylated dendrimers are situated between the sugar and the amino acids of the dendrimer scaffold. Due to the shielding by the sugar and the dendrimer there is likely to be limited access for receptors like MGL to interact with the triazole. Straight chain peptide **66** and dendrimer **68** do not have the GalNAc residue to shield the triazole. While these two compounds showed greater binding than the equivalent molecules with alanine, the binding observed was not superior than that observed for GalNAc containing molecules. GalNAc binds to MGL through the hydroxyl groups on the carbohydrate. It is possible that straight chain peptide **66** and dendrimer **68** are not binding through the triazole moiety. Instead the hydroxymethyl group on the triazoles in straight chain peptide **66** and dendrimer **68** may be positioned in such a way that hydrogen bonding can occur in a similar fashion to the interaction between GalNAc and MGL.

MUC1 sequences

The MUC1 sequences originally synthesised by Dr Lee were compared to the compounds produced in this current study. MUC1 J contains T_N antigens, whereas MUC1 K is a neo–glycopeptide sequence with triazoles linking the GalNAc residues, finally the MUC1 L sequence is non–glycosylated. The triazole containing sequence MUC1 K had the highest loading of the three sequences, overall was a low binder. MUC1 J showed a very small shift in MFI, and MUC1 L did not bind.

Both MUC1 J and K sequences have four GalNAc residues in the same positions along the chain. If the number of GalNAc present dictated which compound exhibited greater levels of loading then these two compounds would have been the two highest loading, however this is not the case. The MUC1 compounds show lower binding compared to any of the dendrimers.

Overview of MoDC results

In general there is a clear correlation between the number of GalNAc residues present on the dendrimer structures and the strength of the binding to MoDC with polydentate constructs binding stronger than monodentate constructs. This result indicates a cluster effect occurrs with the poly–GalNAc dendrimers such as those found in the generation I and III. The dendrimers in the generation I and III series both have less GalNAc residues than the MUC1 sequences J and K, but all of these dendrimers bind more than the straight chain peptides. This suggests that the positioning of GalNAc in these branched dendrimers allows more binding to MGL compared to the straight chain MUC1 sequences. The results of the MoDC binding is shown in Figure 7.11, with the structure of the highest loading compound from each group in Figure 7.12.

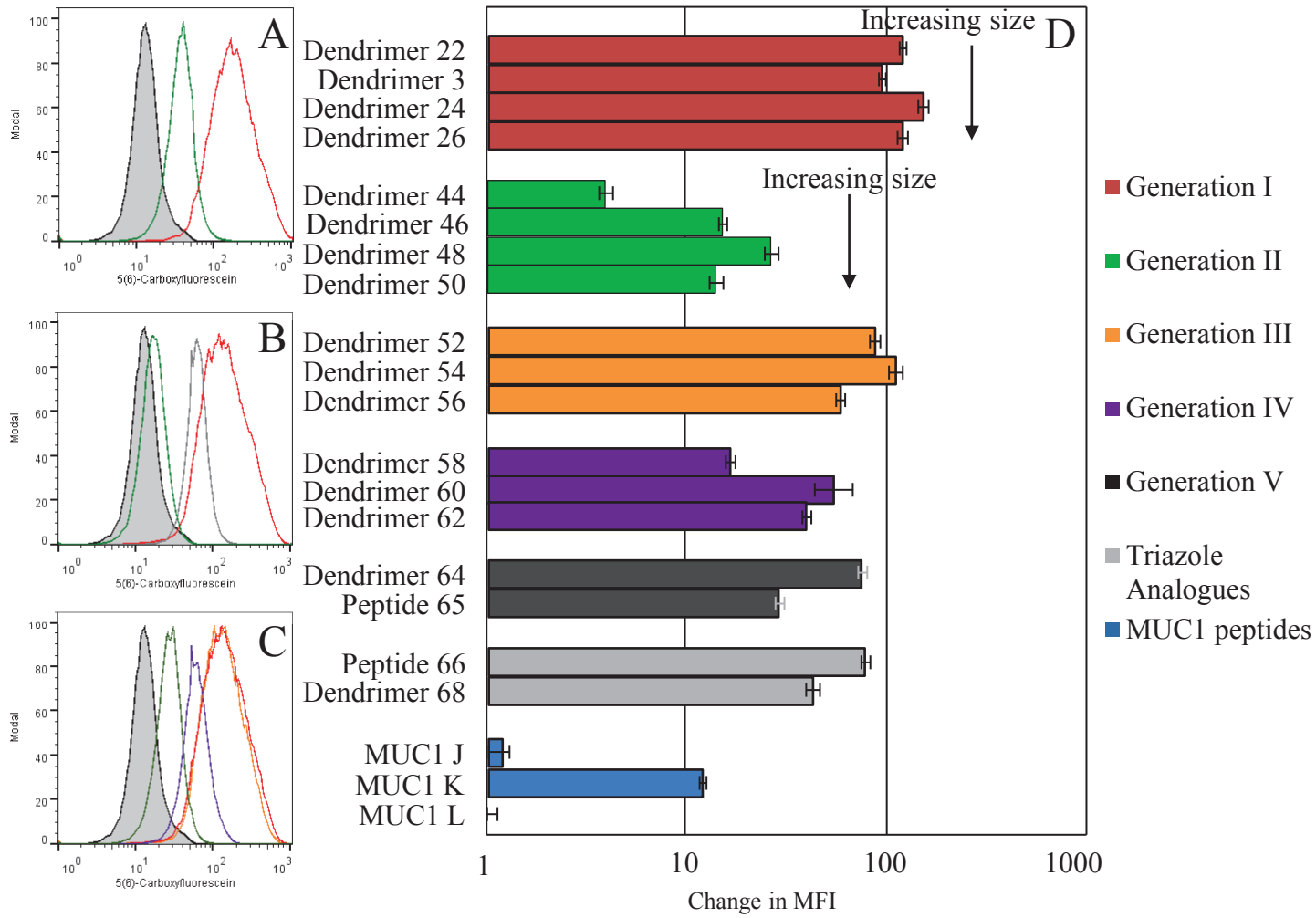

Figure 7.11: Change in MFI for MoDC incubated with different peptide additives with 1 μM concentrations at 37 °C for 1 hour. A) FACS histogram plot indicating binding of 1 μM of the dendrimer **24** (red) and **48** (green) to MoDC. B) FACS histogram plot indicating binding of 1 μM of the dendrimer **22** (red), **68** (grey) and **44** (green) to MoDC. C) FACS histogram plot indicating binding of 1 μM of the dendrimer **26** (red), **54** (orange), **60** (purple) and **50** (green) to MoDC. D) Change in MFI is given as the average for triplicate samples for each dendrimer incubation with standard deviations in the from of error bars included.

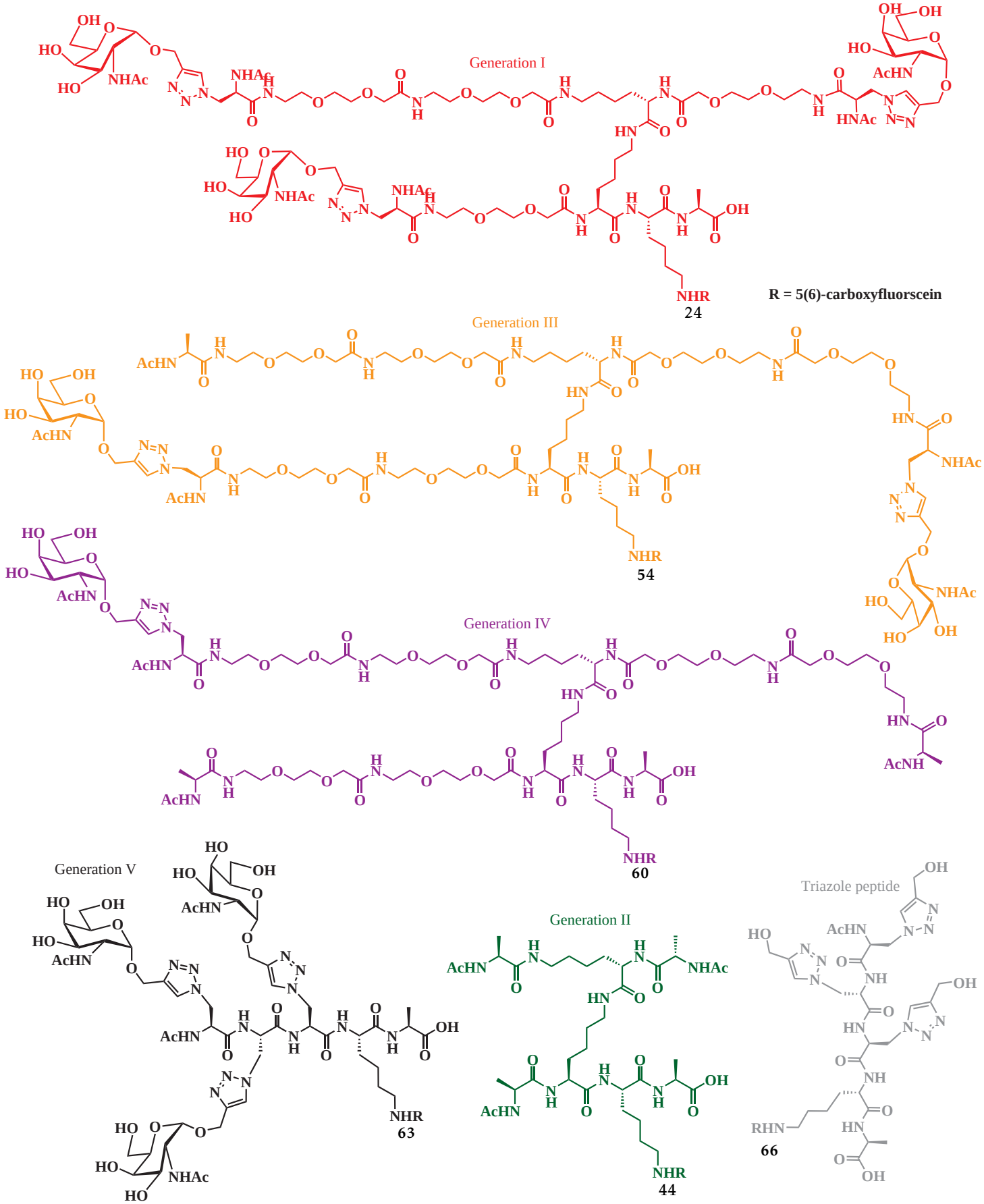

Figure 7.12: Structures of highest loading additives to MoDC for each generation with 1 μM concentrations at 37 °C for 1 hour.

7.3.2 Binding assay for comparison of synthetic glycodendrimers and glycopeptides and their non-glycosylated analogues to MGL$^-$ LG2 cells

The negative control LG2 cells do not express MGL therefore any binding of the dendrimers to the LG2 cells is not specific to GalNAc interactions with MGL. The levels of additive loading for the LG2 cells was much lower which resulted in a smaller change in MFI than for the MGL–expressing MoDC cells. The binding of the different dendrimers and peptides are all similar to the LG2 cells, this suggests that very low levels of non–specific binding is occurring and dominates the interactions between LG2 cells and these constructs. All of these cells have much lower MFI with an additive than their equivalent result for MoDC. This suggest that the quantity of constructs bound to LG2 cells is far lower than the amount of binding observed for MoDC. The averaged results for this assay are shown in Figure 7.13.

FACS plot A in Figure 7.13 shows that dendrimer **24** and **48** have similar MFI and the curves overlap. These results would indicate that the binding of these dendrimers to the LG2 cells is not mediated by GalNAc. FACS plot B in Figure 7.13 shows the fluorescence curves for dendrimers **22**, **68** and **44**. Both dendrimer **68** and triazole peptide **66** have larger shifts in MFI than their anologues. This shows non–specific binding occurs with triazole analogues to LG2 cells. At 0 °C the dendrimers did not show binding to LG2 cells, however at 37 °C binding is observed to LG2 cells. The binding level of dendrimers to LG2 cells is still low in comparison to the binding observed to MoDC. This result provides further evidence that the binding interaction is GalNAc–mediated and targeting of the MGL receptor is responsible for the large increases in MFI observed when both GalNAc and MGL is present.

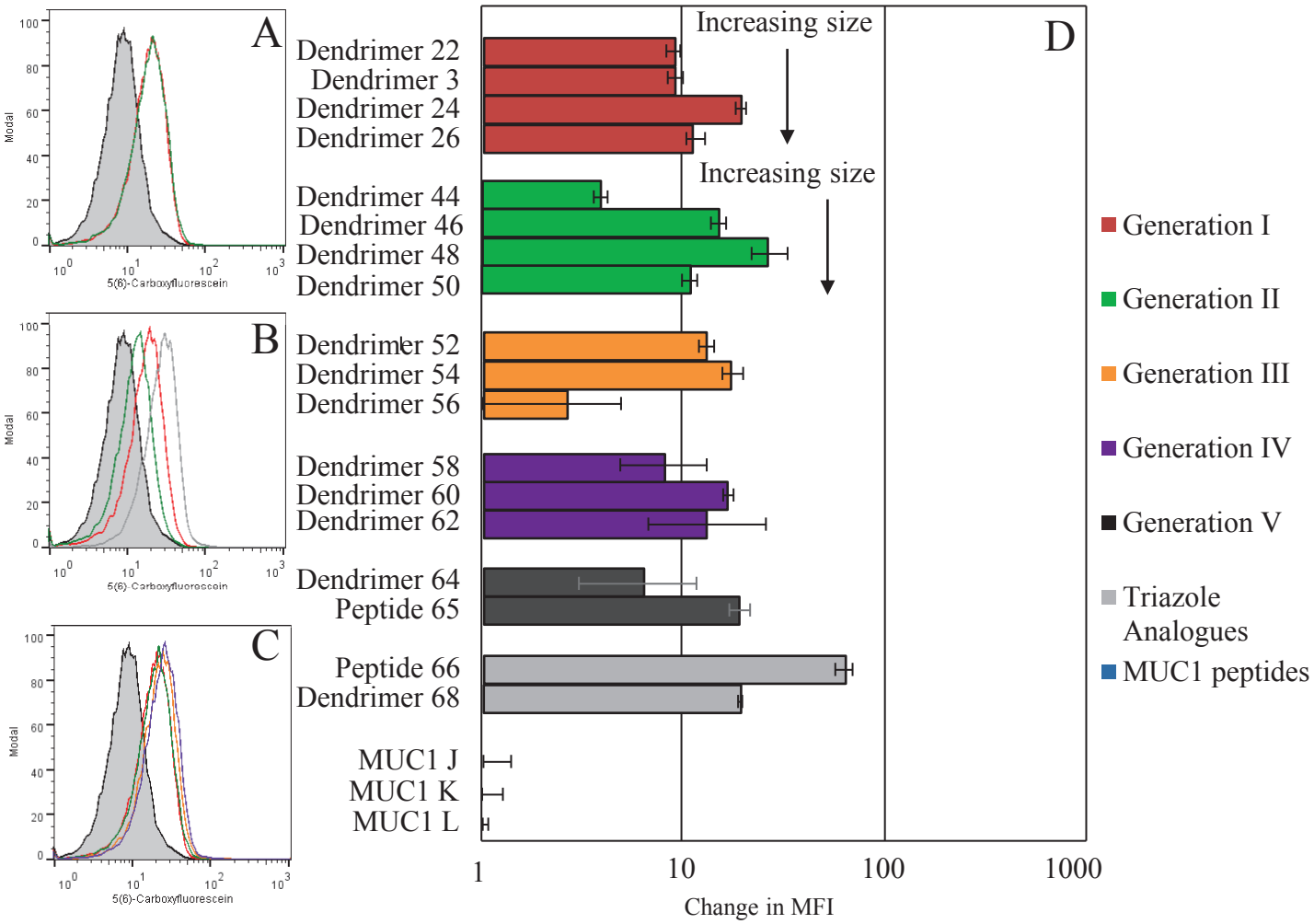

Figure 7.13: Change in MFI for LG2 incubated with different peptide additives with 1 μM concentrations at 37 °C for 1 hour. A) FACS histogram plot indicating binding of 1 μM of the dendrimer **24** (red) and **48** (green) to LG2. B) FACS histogram plot indicating binding of 1 μM of the dendrimer **22** (red), **68** (grey and **44** (green) to LG2. C) FACS histogram plot indicating binding of 1 μM of the dendrimer **26** (red), **54** (orange), **60** (purple) and **50** (green) to LG2. D) Change in MFI is given as the average for triplicate samples for each dendrimer incubation with standard deviations in the from of error bars included.

7.4 Discussion

7.4.1 Trends in the data

Contribution of GalNAc residues

The results presented in this chapter indicate that the size or molecular weight of a dendrimer/peptide is not the most important factor for binding to MGL–expressing MoDC. The experimental results have shown that compounds with high molecular weight or large branched structures can bind with weaker or similar strength than a smaller or lower molecular weight molecule. For example dendrimer **22** is one of the smallest compounds with one of the lowest molecular weights yet it binds with greater loading than dendrimers **26** and **50** which are far larger and heavier. The most important factor which determines whether the additives in the experiments performed binds is the presence or absence of GalNAc residues.

The ordering of the binding for dendrimers to MoDC was dependent on the number of GalNAc residues attached to the scaffold, with the more glycosylated dendrimers inducing greater binding affinities. The order of loading for binding to MoDC for dendrimers was observed as follows:

1. Generation I dendrimers (3 GalNAc)
2. Generation III dendrimers (2 GalNAc)
3. Generation IV dendrimers (1 GalNAc)
4. Generation II dendrimers (0 GalNAc)

A schematic representation of the different strengths of binding is shown in Figure 7.14. The schematic shows a simplified version of what could be happening when dendrimers bind to the trimeric cluster of MGL. In reality the X, Y and Z chain could bind to multiple or an individual CRD of the trimeric cluster of MGL on MoDC.

Compounds with three GalNAc residues typically bind better than the equivalent structures with fewer GalNAc residues. This could be due to the MGL cluster having three carbohydrate recognition domains and the dendrimers with three GalNAc residues are more likely to have 1 or more chains binding to these sites. There is also a chance that the GalNAc residues are binding to another receptor which isn't MGL on these MoDC cells which aren't expressed on the LG2 cells. Future work on this project would involve acquiring a crystal structure of the molecule binding to the MGL

receptor, or performing a cell binding assay which blocks the MGL receptor with an antibody to inhibit dendrimer binding to prove MGL binding.

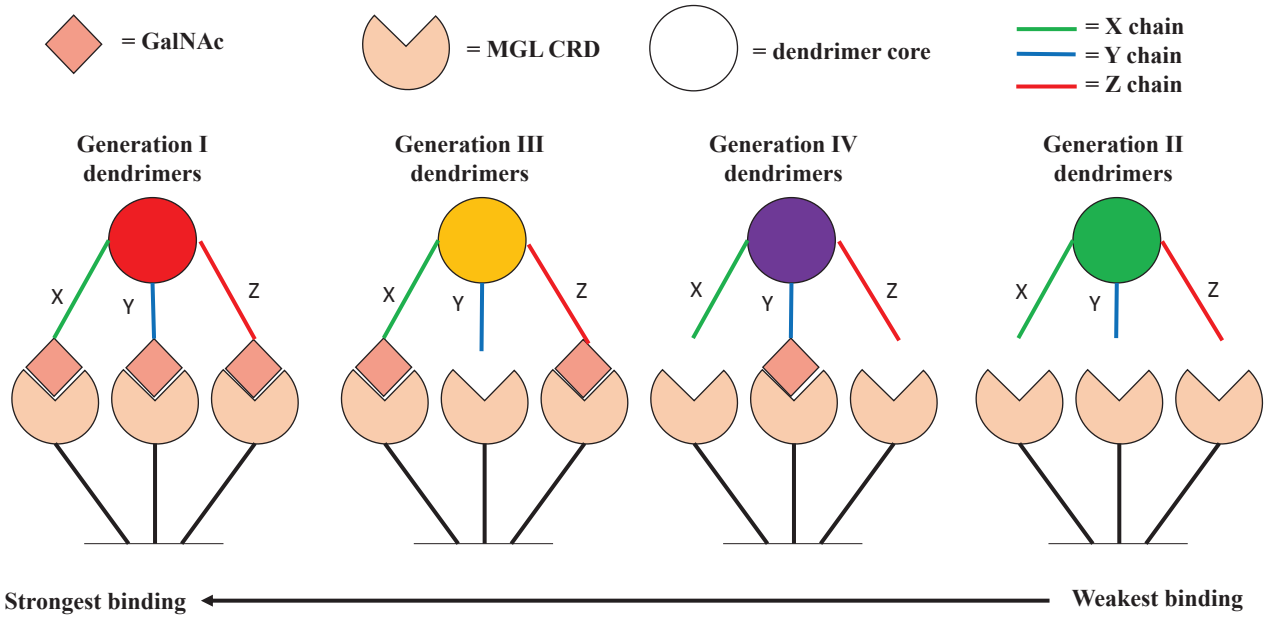

Figure 7.14: Comparison of strength of binding between the generation I, II, III and IV dendrimers.

Orientation and distance between GalNAc is more important for MoDC binding than density of GalNAc residues

The generation I dendrimers and straight chain peptide **64** all have three GalNAc residues but there is a clear distinction between the highest loading (dendrimers **24** and **22**) and the lowest loading (straight chain peptide **64** and dendrimer **3**).

It appears that the orientation/distance between the GalNAc moieties is one of the more important factors for binding to MoDC which express MGL. Straight chain peptide **64** and MUC1 J and K are the three compounds with the highest density of GalNAc in the smallest volume. Even with the greater densities of GalNAc these compounds are weaker binders than other compounds with a similar number of GalNAc moieties. It is proposed that this result is due to a combination of the orientation of the GalNAc moiety and distance between the GalNAc residues.

Straight chain peptide **64** has three amino acids glycosylated in a row, whereas the MUC1 sequences J and K have pairs of amino acids next to each other which are glycosylated. It is possible that the MUC1 sequences are folded in such a way that the GalNAc residues do not interact with the MGL receptor. The proximity between the GalNAc residues in the straight chain may promote polydentate binding to an individual CRD of an MGL cluster, but it is unlikely that one peptide **64** will bind to multiple different CRD of the trimeric MGL. The most effective generation IV den-

drimers which only have one GalNAc residue bind with a similar MFI to straight chain peptide **64**. The generation IV dendrimers are likely to bind primarily through one CRD as they only have one GalNAc, so therefore it seems logical that straight chain peptide **64** would have a similar MFI.

The importance of the spacing of the GalNAc is further evidenced by comparison of dendrimer **26** which has three GalNAc moieties and the generation III dendrimers which have two GalNAc residues. Dendrimer **26** and **54** produce an almost identical change in MFI when incubated with MoDC. This suggests that binding is primarily happening through the GalNAc found on the terminus of the X and Z chains for dendrimer **26**, with chain Y having a minimal positive influence on binding.

Dendrimer **55** has the least effective binding for generation III, this would suggest that the distance of the GalNAc glycosylated Y and Z chain is the least optimum for binding to MoDC which express MGL for a dendrimer of similar structure to dendrimer **26**.

Dendrimer **52** has GalNAc glycosylated onto the termini of the X and Y chain. As the X and Z chain combination gives the highest loading and the Y and Z chain gives the least effective binding, the conclusion from this is that the X chain is most important chain for multidentate binding, and the Y chain is the least important for multidentate binding.

The mono–glycosylated generation IV dendrimers are unable to participate in polydentate binding through GalNAc residues, therefore the data from these results can only indicate how great the affinity of an individual chain is to bind to MGL–expressing MoDC as determined by how well the chain can orientate for binding. Surprisingly, the X chain GalNAc glycosylated dendrimer **58** was the least effective binder of the three dendrimers to MoDC. The Z chain glycosylated dendrimer **62** established the highest loading of the generation IV dendrimers. A schematic representation of the different strengths of binding for the generation IV dendrimers compared to dendrimer **50** with no GalNAc residues is shown in Figure 7.15.

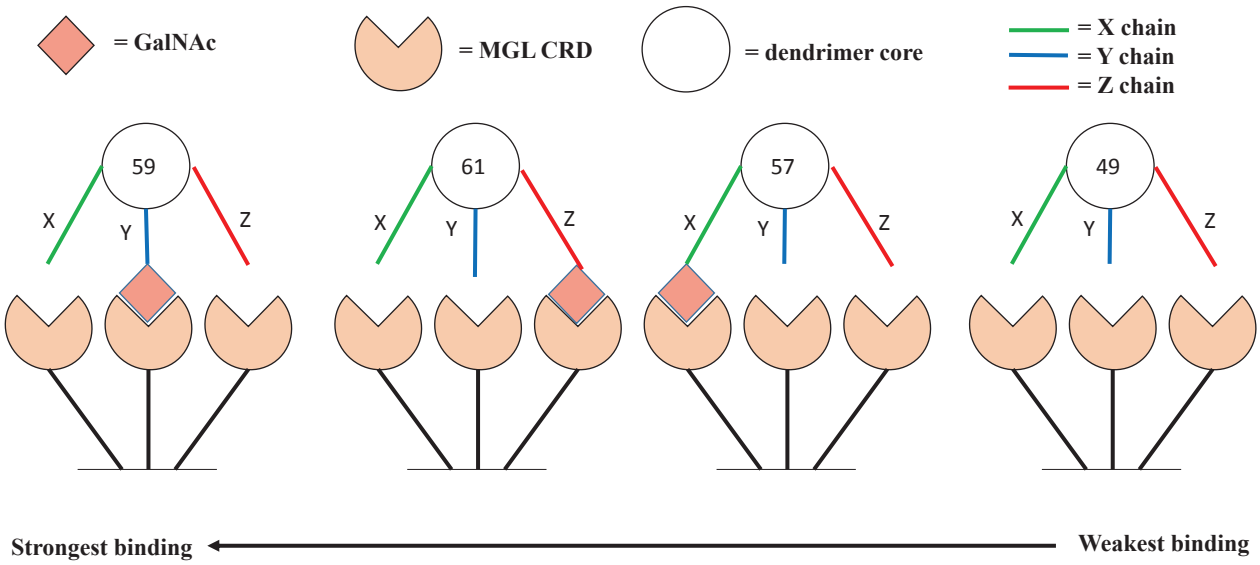

Figure 7.15: Comparison of binding between generation II dendrimer **50** with no GalNAc residues and generation IV dendrimers **62**, **60**, and **58** which have one GalNAc residue.

The results from the generation IV dendrimers may help to explain why dendrimer **54** from the generation III series has the highest loading from its generation. The results from the generation IV series revealed that both the Y and the Z chain are high loading individual binders. The X chain on the other hand is a lot weaker binder (as proven by the performance of dendrimer **58**). We postulate the reason that dendrimers **26** and **54** having similar strength binding could be due to the orientation of the molecule. For these dendrimers the Z chain may be bound with greater loading to MoDC, the dendrimer then orientates the X chain in such a way that it binds to MGL while not destabilising the bond between the Z chains GalNAc ligand. The Y chain on dendrimers **26** and **54** has less influence for binding. A similar situation could happen with the Y and X chain for dendrimer **52**, but the X chain may slightly destabilise the binding of the Y chain which would result in weaker binding than observed for dendrimers **26** and **54**. Dendrimer **55** was the weakest binder of the generation III dendrimers. This may be because as the Y and Z chains compete to bind the MGL receptor in a high loading fashion which leads to neither chain binding to its full potential that resulting in each chain destabilising the other with weaker overall binding being observed. A schematic representation of the different strengths of binding for the generation III dendrimers compared to the generation I dendrimer **26** is shown in Figure 7.16.

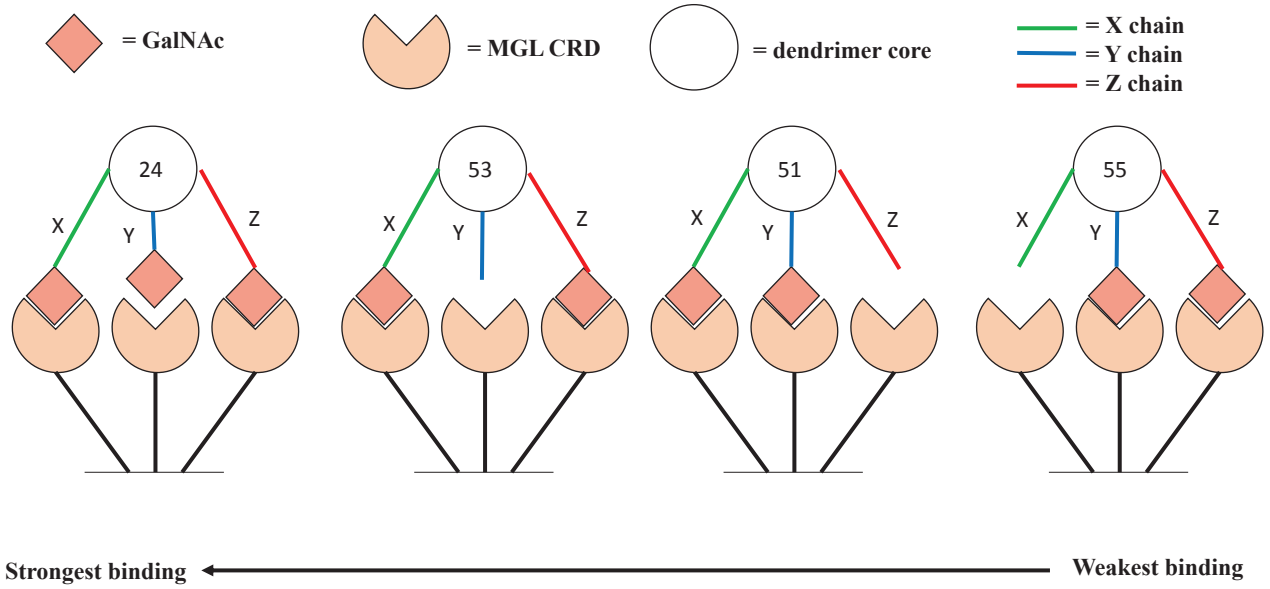

Figure 7.16: Comparison of binding between generation I dendrimer **26** with 3 GalNAc residues and generation III dendrimers **54**, **52**, and **55** which have 2 GalNAc residue.

The distance between GalNAc residues may not be the sole reason for one dendrimer binding better than another. If the distance between GalNAc residues was the most important factor, it would be predicted that dendrimer **3** should be performing better than dendrimer **22** as it has chain lengths which are longer and of similar size to dendrimer **24** which was the highest loading dendrimer. However, this was not the observed result. Similarly orientation of the GalNAc residues alone does not appear to be the sole reason for a greater ability of one dendrimer binding to MGL–positive cells better than another. If this was the case dendrimer **26** which contains the most mini–PEG residues should be the most flexible and able to position its chains in such a way that multiple GalNAc residues would bind to the carbohydrate recognition domain(s).

Dendrimer **24** binds with the greatest loading because it has 3 GalNAc residues and the balance of the right distance between carbohydrate residues while being able to orientate its chains so that the highest loading can happen without destabilising the interaction between GalNAc and the carbohydrate recognition domains of MGL.

Contribution of triazoles

The importance of the triazole group on the ability of the compound to bind to MGL was analysed by the synthesis of two constructs that contained triazole moieties instead of GalNAc residues. If the triazole was the most important factor for binding, it would be expected that dendrimer **68** and straight chain peptide **66** would be two of the highest loading compounds. This is not the case, however these two compounds bind with greater loading than the generation II dendrimers which

have no GalNAc residues and have no triazole functional groups.

MGL binds to GalNAc due to the way that the hydroxyl groups on the sugar (specifically at the three and four carbon positions) are presented to the carbohydrate recognition domain. Binding may be occurring for dendrimer **68** and straight chain peptide **66** due to the way they present the hydroxyl group on each triazole. Another option is that the triazole can be orientated in such a way that an interaction is happening between it and another non–MGL receptor on the MoDC. This interaction is not as specific, nor has as high a loading as the GalNAc interaction, as these compounds in general bind in a weaker or similar fashion to the equivalent GalNAc–glycosylated compound.

MUC1 K has higher loading than MUC1 J. The two peptides have the same number of GalNAc residues in the same positions along the chain. The difference is that GalNAc residues on MUC1 K are bound through triazole linkers and have the potential to be further away from the peptide, whereas MUC1 J is bound through O–glycosidic bonds and has the GalNAc closer to the peptide. The GalNAc residues are able to extend further away from the MUC1 peptide when bound through the triazole linker compared to the O–glycosidic bonds. This may make them more accesible for binding to the CRD, and hence increase the likelihood of binding. Another option is that the triazoles themselves are involved in the binding causing a polydentate effect which makes MUC1 K bind stronger than the MUC1 J sequence which can only bind through interactions with the GalNAc.

The triazoles may be involved with binding to the CRD of MGL, though positioning/orientation of the sugars or the sheer distance created between the peptide chain and the sugar. The interaction may not be strong, but it might have a positive effect on the ability of the dendrimers to bind to the CRD of MGL.

7.5 Conclusion

The conditions for optimum binding were similar at 37 °C and 0 °C, although the TSM buffer system originally used at 0 °C was changed due to increased cell death being observed when the temperature was increased.

At 0 °C all four of the generation I dendrimers bound to MGL–expressing MoDC with an MFI between 1 and 10. Dendrimer **26** was the most abundant binder, with dendrimer **24** as the second most abundant and dendrimer **22** closely behind in third place, while dendrimer **3** bound the least of the generation. None of the generation II dendrimers bound.

At 37 °C the outcome is different, and the MFI values are all close to 100 for the first generation I dendrimers. Dendrimer **24** is now the most abundant binder, with dendrimer **22** the second most abundant binder and dendrimer **26** close behind, while dendrimer **3** still remains the lowest binding of the generation. The generation II dendrimers now have an MFI of around 10. By increasing the temperature from 0 °C to 37 °C the amount of binding increased with the MFI increasing by around a factor of 10 on a log scale.

7.6 Does the thermal melt assay predict the results of the cell binding assay?

Table 7.1 shows a comparison of the relative performances of each dendrimer in the thermal melt assay and the cell binding assay. The compounds are grouped as either high loading/strong binding compounds (+++++), medium loading/mediocre binding compounds (+++) or low loading/weak binding compounds (+) depending on how they had performed overall in each experiment.

For nine of the compounds, the results of the thermal melt assay are predictive; the relative performance of the compound in the thermal melt was similar to the cell binding assay. There were four exceptions where the compounds that bound to MGL–expressing MoDC exhibited lesser affinity for the recombinant MGL in the thermal melt assay. Dendrimer **25** performed averagely in the thermal melt assay, but its equivalent in the cell binding assay dendrimer **26** was one of the higher loaders to MGL. Dendrimer **23** which performed well in the thermal melt assay, while dendrimer **24** was the strongest binder in the cell binding assay. The negative control dendrimer **67** showed almost no activity in the thermal melt assay, whereas the equivalent negative control dendrimer **68** showed some binding in the cell binding assay.

The thermal melt assay predicted three scaffolds to perform better in the cell binding assay than they did in reality. The generation IV dendrimer **51** and **61** were consistently two of the highest loading constructs in the thermal melt assay, but the equivalent generation IV dendrimers **52** and **62** were not high loading for the cell binding assay. The strongest binding construct in the thermal melt assay straight chain peptide **63** was average at loading the MGL–expressing MoDC in the cell binding assay and was outperformed by the generation I and III dendrimers.

Dendrimer **57** was weak binding, which suggests that it was unable to efficiently present GalNAc to the monomeric GalNAc in the thermal melt assay. The other mono–glycosylated dendrimers were far better at presenting GalNAc and were therefore able to have much stronger binding. Dendrimer **58** was the fluorescent analogue of dendrimer **57**. Dendrimer **58** was a low loading compound in the cell binding assay, this suggests that this scaffold is unable to present GalNAc to MGL in an efficient manner. If the thermal melt assay was to screen compounds GalNAc presentation to MGL, dendrimer **58** would not be considered for testing using the cell binding assay.

Table 7.1: Comparison of the relative dendrimer and peptide performances in the thermal melt assay to the 6 hour cell binding assay.

Generation	Thermal melt assay compound	Performance	Cell binding assay compound	Performance
I (dendrimer 3 GalNAc)	Dendrimer **21**	+++++	Dendrimer **22**	+++++
	Dendrimer **2**	+++	Dendrimer **3**	+++++
	Dendrimer **23**	+++	Dendrimer **24**	+++++
	Dendrimer **25**	+++	Dendrimer **26**	+++++
II (dendrimer 0 GalNAc)	Dendrimer **43**	+	Dendrimer **44**	+
	Dendrimer **45**	+	Dendrimer **46**	+
	Dendrimer **47**	+	Dendrimer **48**	+
	Dendrimer **49**	+	Dendrimer **50**	+
III (dendrimer 2 GalNAc)	Dendrimer **51**	+++++	Dendrimer **52**	+++
	Dendrimer **53**	+++	Dendrimer **54**	+++++
	Dendrimer **55**	+++	Dendrimer **56**	+++
IV (dendrimer 1 GalNAc)	Dendrimer **57**	+	Dendrimer **58**	+
	Dendrimer **59**	+++++	Dendrimer **60**	+++
	Dendrimer **61**	+++++	Dendrimer **62**	+++
V (peptide 3 GalNAc)	Peptide **63**	+++++	Peptide **64**	+++
Triazole analogues	Dendrimer **67**	+	Dendrimer **68**	+++

Individual MGL truncations were better at predicting the cell binding assay results. Table 7.2 compares the accuracy of each MGL truncation for predicting the loading effectiveness of an additive in the cell binding assay. We use the cell binding assay as a more definitive experiment as this sample contains native MGL and is a biologically relevant environment rather than truncations of MGL. The reason the thermal melt assay was employed was to screen the ability of the compounds to bind to MGL in a cost effective, quick but robust experiment.

The MGL 176 truncation, the smallest protein, is also the least accurate for predicting the cell binding assay as 4 of the compounds gave different results (predicting dendrimer **60** and **26** should be weak binders and predicting peptide **73** and dendrimer **50** should be strong binders when in fact the reverse is true).

The MGL 166 truncation is more accurate for prediction than MGL 176, this construct only mispredicts three dendrimers (MGL 166 wrongly predicts dendrimers **26** and **60** and the triazole dendrimer analogue **67** should be weak binders).

MGL 155 predicts three dendrimers wrongly (incorrectly predicting dendrimers **26** and **60** and triazole dendrimer analogue **67** would be weak binders).

The largest protein MGL 144 only mispredicts two compounds (incorrectly predicting dendrimer **60** and the triazole dendrimer analogue **67** should be weak binders). It is therefore the most accurate for predicting whether a compound will bind MGL–expressing cells.

Table 7.2: A comparison of the number of positive binders vs negative binders for the different thermal melts assays vs the average cell binding results.

Assay	strong binders	weak binders	% Correct
Cell binding assay average (the standard)	11	5	100
MGL 176 thermal melt assay	13	3	75
MGL 166 thermal melt assay	9	7	81
MGL 155 thermal melt assay	10	6	81
MGL 144 thermal melt assay	9	6	87

7.6.1 Conclusion on thermal melt assay screening for lead compounds

The results shown in Table 7.1 show the overall thermal melt assay predictions, with nine out of sixteen (56%) predicted correctly by thermal melt assay as binding (compared to the cell binding assay). While this is a reasonable predictive rate if this approach was being used as a pre–screen for the highest loading compounds to carry through to cell based assays, it may be too inaccurate as a quantitative tool.

If the thermal melt assay was used purely to predict whether a compound would bind to MGL–expressing cells by being able to present GalNAc as shown Table 7.2, then the assay is an accurate tool. The largest truncation, MGL 144 predicted 13 out of 15 compounds correctly (87%).

The current issue with the thermal melt assay is that the purification of the MGL is laborious, inefficient and results in low yields of protein. Should the refolding and purification process be optimised for yielding higher concentration of MGL, the thermal melt assay would be viable for an initial screen of a library of compounds to identify which compounds are able to present GalNAc efficiently to the CRD of MGL.

7.7 Targeting MGL–expressing cells in peripheral blood mononucleated cells

A cell binding assay using peripheral blood mononucleated cells (PBMC) purified from human blood was used to compare the selectivity of the highest affinity binder from the thermal melt assay (peptide **64**)[iii] and the highest loading binder from the MoDC addhesion assay performed at 37 °C (dendrimer **24**). The non–glycosylated analogues of each compound were also tested to demonstrate the importance of the GalNAc residue compared to the dendrimer or peptide scaffold.

The PBMC binding assay was performed in a similar manner to the 37 °C experiment. The experiment used 1 μM concentration additives incubated for 1 h at 37 °C. The experiment was performed and analysed by Dr Anna Brooks as the experiment required a multicolour panel to analyze each cell subset, which required a dedicated flow cytometrist.

The results from the thermal melt assay indicated which compound bound with the highest affinity to an individual MGL protein, whereas the MoDC binding assay results show the quantity of binding to cells expressing MGL trimers. In the previous section the question was posed whether the thermal melt assay could predict the results of the MoDC binding assay.

[iii] Peptide **64** has the equivalent structure with a fluorescent label to peptide **63** which was used in the thermal melt assay

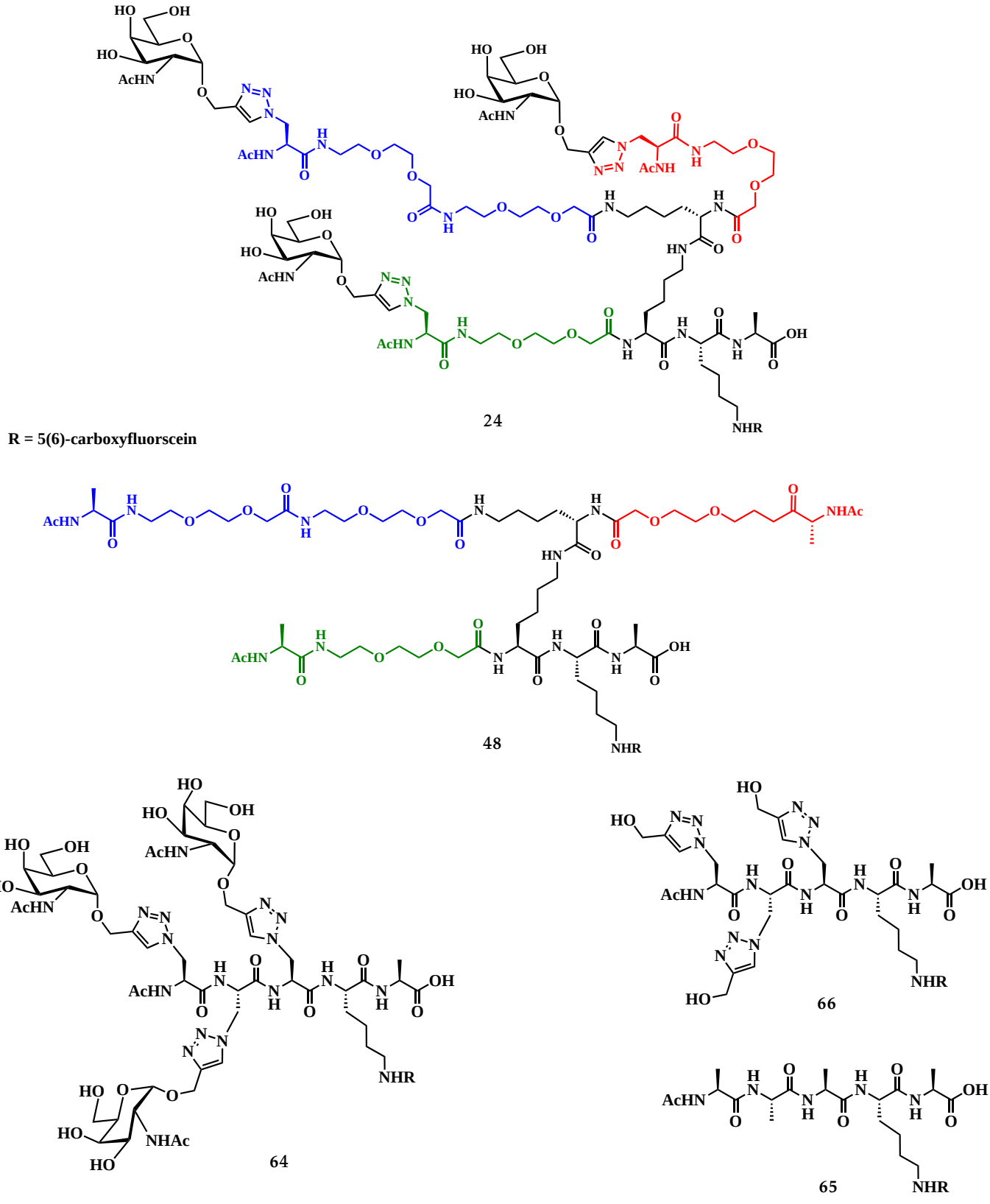

Figure 7.17: Dendrimers and peptides used in the PBMC binding assay. GalNAc–glycosylated dendrimer **24** and its non–glycosylated dendrimer **48**. GalNAc–glycosylated peptide **64**, the triazole derivatised peptide **66** and the non–glycosylated peptide **65**.

7.8 Results of binding of dendrimers to white blood cells in human blood

The peripheral blood mononucleated cells (PBMC) binding assay experiment looked at four subsets of cells:

- Dendritic cells: defined by the markers CD1c, CLEC9a and pDC
- Monocytes: the major monocyte population defined by the markers $CD14^+$ and the minor monocytes populations $CD14^+CD16^+$ and $CD16^+$.
- T–cells
- B–cells

The MGL–expression of each of these subsets are shown in Figure 9.68 and the Appendix in 9.5.3. The CD1c population of cells expressed the highest levels of MGL. The CLEC9a, pDC, $CD14^+CD16^+$, $CD16^+$ and $CD14^+$ subsets had some expression of MGL while the pDCs had a slight shift in MFI indicating low levels of expression of MGL. B–cells and T–cells showed little expression of MGL.

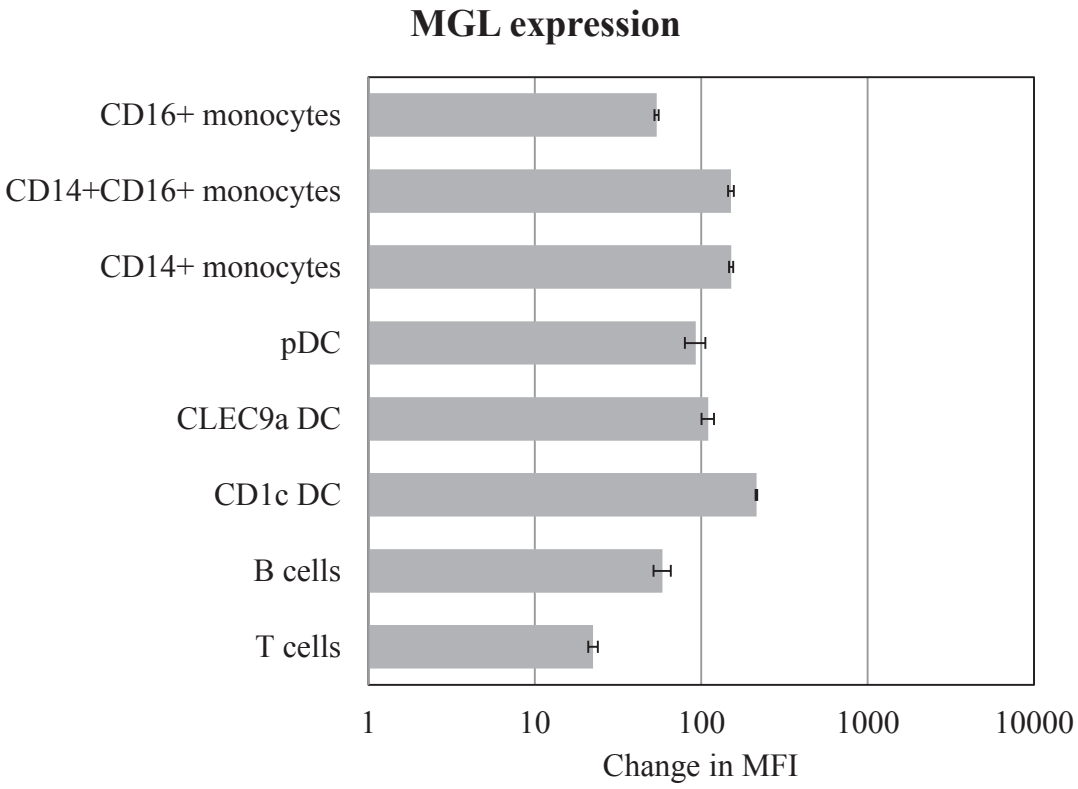

Figure 7.18: Change in MFI is given as the average for duplicate samples for each additive incubation for expression of MGL on cells with standard deviations in the form of error bars included.

The results of the binding of constructs for each population are shown in (Figure 7.19 and Figure 7.20). The experiment was repeated with two different donors and gave consistent results each time.

The two GalNAc–glycosylated compounds (dendrimer **24** and peptide **64**) followed a similar pattern for binding with each of the cell types, which correlated with MGL expression. Typically incubation with dendrimer **24** gave greater changes in MFI indicating that more of this dendrimer was targeted to the cell. CD1c DCs were the cell population which expressed the most MGL, the two GalNAc–glycosylated compounds showed the most binding to this cell type. This is the only cell type where the binding is likely to be predominantly mediated by MGL.

Due to the similarities in the shifts in MFI between the glycosylated compounds (dendrimer **24** and peptide **64**) and their non–glycosylated alanine equivalents (dendrimer **48** and peptide **65**) it is unlikely that the binding observed to the monocytes, or the CLEC9a dendritic cells is mediated by MGL. These shifts appear to be non–specific binding, although the slightly increased binding visible by GalNAc–glycosylated compounds compared to non–glycosylated compounds to $CD14^{+}CD16^{+}$ cells could be due to MGL–expression or also because of low levels of internalisation. No selective binding was visible for any of the compounds tested to B–cells and T–cells (Figure 7.20). Dendrimers **24** and **48** and peptides **64** and **65** did not bind to pDC dendritic cells.

Triazole derivatised peptide **66** acted very differently to the other compounds tested. Peptide **66** bound indiscriminately to all of the monocytes and dendritic cell subsets. The binding was of a greater magnitude than the other peptides in almost all cases. The exception was the high MGL–expressing CD1c dendritic cells, the triazole derivatised peptide **66** bound more than the non–glycosylated peptide **65** but less than the GalNAc–glycosylated peptides **64**. This data suggests that the binding of triazole derivatised peptide **66** is not dependent on MGL.

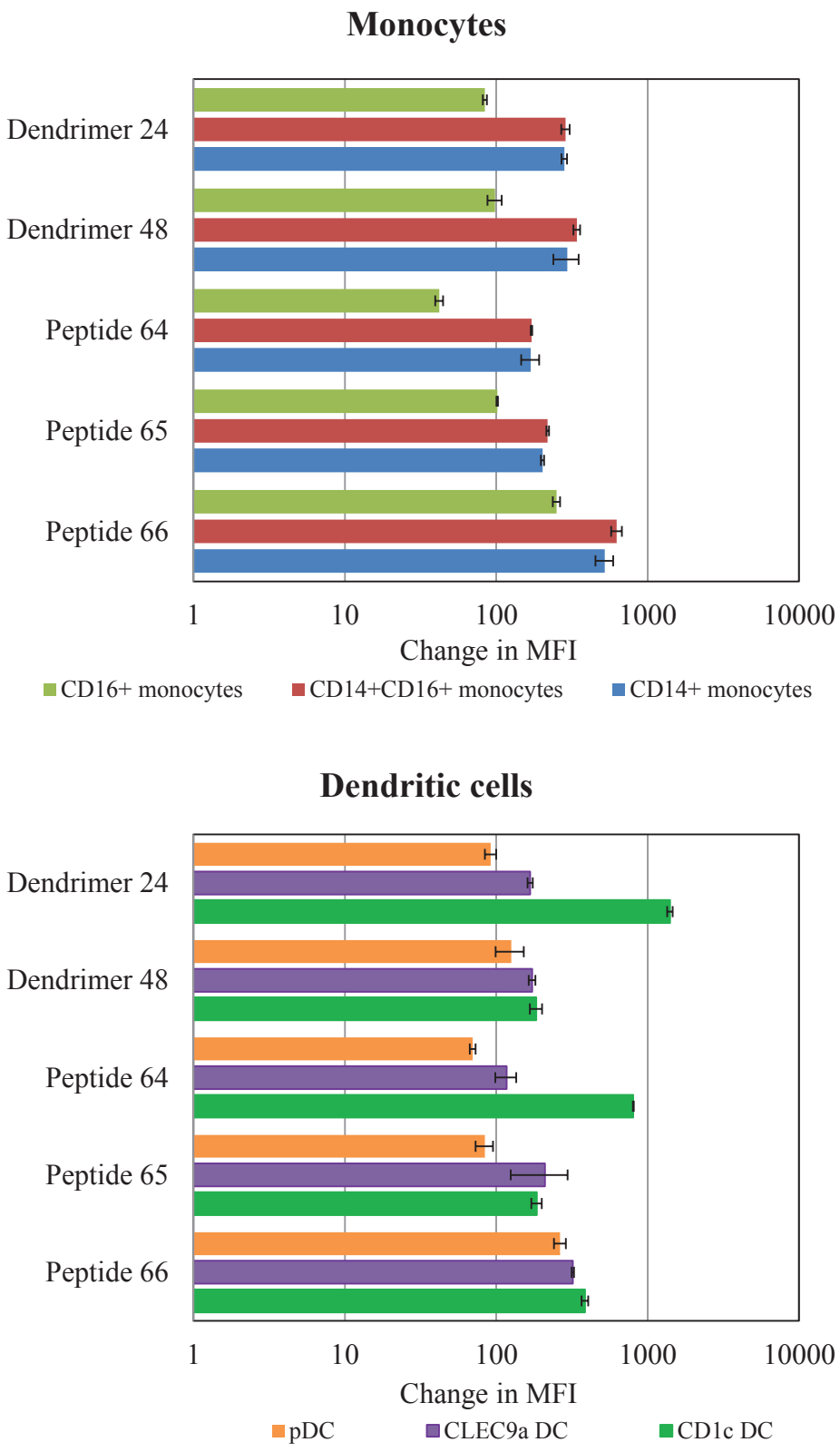

Figure 7.19: Change in MFI is given as the average for duplicate samples for each additive incubation for monocytes and dendritic cells with standard deviations in the form of error bars included.

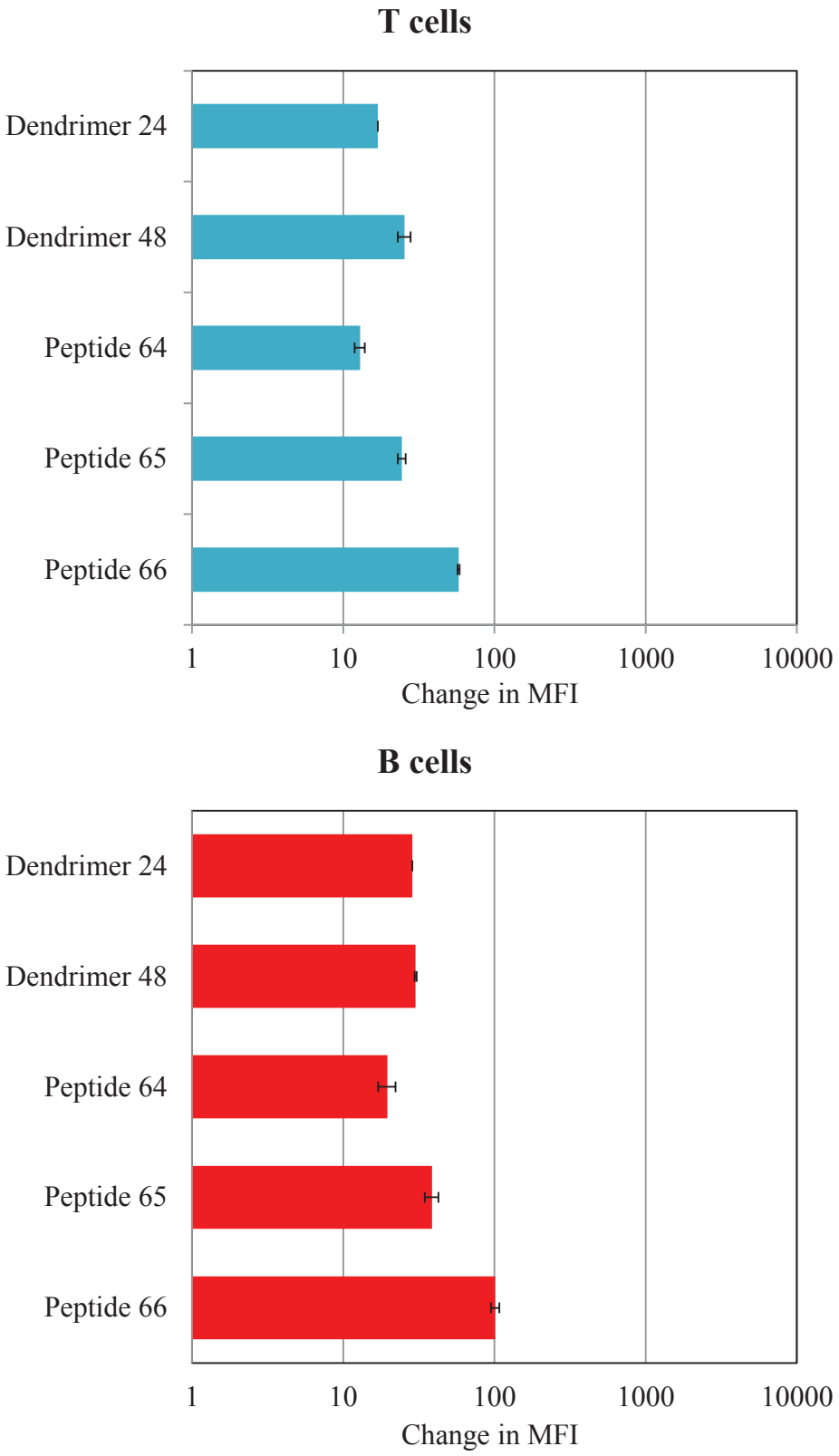

Figure 7.20: Change in MFI is given as the average for duplicate samples for each additive incubation for T–cells and B–cells with standard deviations in the form of error bars included.

7.9 Discussion of binding of dendrimers to white blood cells in human blood

7.9.1 Comparison of dendrimers to peptides

The GalNAc–glycosylated dendrimer **24** bound more than the GalNAc–glycosylated peptide **64**. Dendrimer **24** is a far superior binder than peptide **64**. This agrees with the data of the cell binding assay which showed dendrimer **24** to be a better binder than peptide **64** to MoDC which express MGL. The thermal melt assay showed that both of the equivalent dendrimers and peptides to dendrimer **24** and peptide **64** were able to successfully present GalNAc to the CRD of MGL. The thermal melt assay performed on monomeric MGL protein is therefore suitable model for initial screening of compounds for binding to MGL, as equivalent structures are able to present GalNAc and selectively bind to MGL expressing cells.

7.9.2 Triazole binding

The results from the triazole analogue peptide **66** were quite surprising. Due to the indiscriminate binding of the triazole containing peptide **66**, it can not be conclusively proven that the binding is occurring to the MGL receptor. The MoDC binding assay showed that peptide **66** bound more strongly to MGL–expressing MoDC than the negative control peptide **65** and less strongly than the GalNAc–glycosylated peptide **64**. The CD1c cells which were the population of cells which expressed the most MGL gave results similar to what was observed in the MoDC binding assay. The other populations of cells which express less MGL all preferentially bound to the triazole analogue peptide **66**.

The results for triazole analogue peptide **66** are very similar in MFI value to the results for the glycosylated dendrimer **24**, except when it comes to binding the CD1c cells which express MGL where it is far inferior. This suggests that the binding of the cells (excluding the CD1c) to these molecules is not based on size and weight, but may in fact be down to the ability to orientate the triazoles present in the molecule into position. Peptide **64** is less flexible than dendrimer **24**, therefore it is harder for peptide **64** to align its triazoles so that the GalNAc don't interfere with binding to these other cell types. As triazole analogue peptide **66** does not have GalNAc to get in the way, it may be able to bind through these groups to receptors on the surface of cells in a similar fashion to the flexible dendrimer **24**. This affect isn't seen by either of the alanine based negative control compounds dendrimer **48** or peptide **65** as while they have the similar structures they do not contain the triazole moiety which facilitates binding.

7.10 Summary of the thesis

A library of peptide–based dendrimers were synthesised with an aim to selectively bind the MGL receptor commonly expressed by dendritic cells and macrophages. A brief overview of the synthetic route is shown in Scheme 7.1.

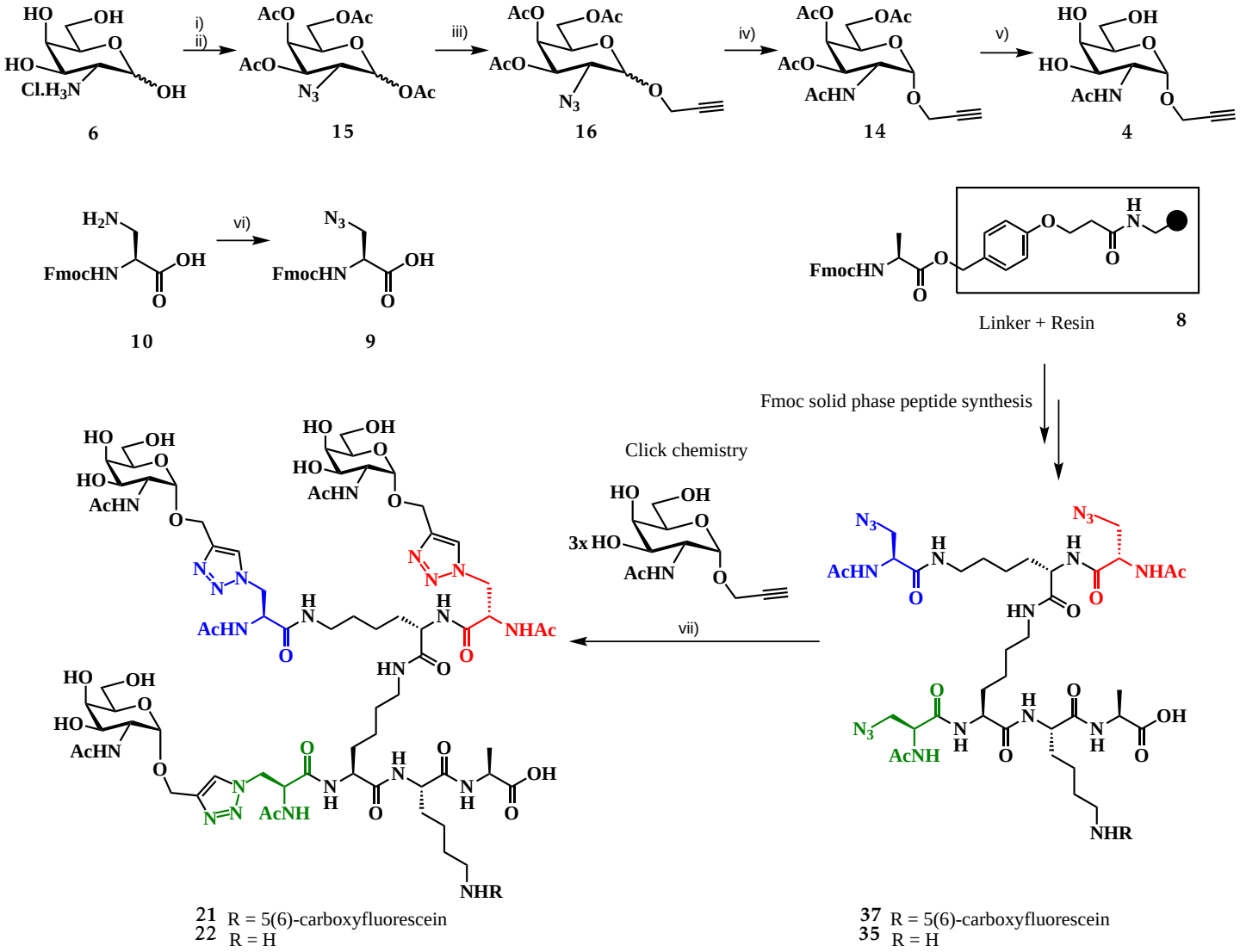

Reagents and conditions: (i) a. imidazole-1-sulfonyl azide hydrochloride, Na_2CO_3, $CuSO_4$, H_2O, MeOH, b. 3 h then EDTA· 4Na; (ii) pyridine, Ac_2O, < 40 ºC, overnight; (iii) propargyl alcohol, BF_3 Et_2O, CH_2Cl_2, 35 ºC, 18 h; (iv) Zn, $CuSO_4$, H_2O, THF, AcOH, Ac_2O, 1 h; (v) NaOMe, MeOH, 2 h; (vi) imidazole-1-sulfonyl azide hydrochloride, $CuSO_4$, K_2CO_3, MeOH, H_2O; (vii) 5 eq. α-propargyl GalNAc, 5 eq. sodium ascorbate, 10 eq. $CuSO_4$, H_2O/DMSO 1:2.

Scheme 7.1: Summary of the synthesis of dendrimers **22** and **21**, which is the general chemistry for this thesis.

Initially the synthesis of α–propargyl GalNAc **4** from the starting material galactosamine hydrochloride **6** over five steps was refined. Fmoc–azidoalanine **9** was synthesised and incorporated via solid phase peptide synthesis into various dendrimer scaffolds. These compounds were designed to test the effect of different chain lengths and numbers of GalNAc residues for binding to MGL protein. Using an orthogonal protecting group strategy the polylysine core was synthesised, and the controlled growth of individual chains was possible. The dendrimer scaffold was synthesised on resin and then cleaved, where upon the α–propargyl GalNAc **4** was appended using the CuAAC reaction to complete the dendrimer. For every GalNAc–glycosylated compound an equivalent structure was made with no carbohydrate residues. A library of eighteen compounds with a fluorescent tag for the cell binding assay, and sixteen compounds without the tag were synthesised for the thermal melt assay.

Three biological assays were performed on the library of dendrimers. A thermal melt assay assessed the strength of binding between the non–fluorescent compounds and different truncations of recombinant monomeric MGL. Four different truncations of MGL were expressed recombinantly and then refolded and purified. While this process successfully produced four different MGL truncations, it suffered from poor recovery yields after refolding due to the insoluble nature of the protein. Non–fluorescent dendrimers were incubated with the four different MGL truncations and their ability to stabilise the proteins with increasing temperatures was assessed. This initial study established that the GalNAc–glycosylated compounds bound to the protein stronger than monomeric GalNAc and established which dendrimers were able to successfully present GalNAc residues to the MGL truncations. With larger truncations of MGL, the protein was more selective as to which type of compounds bound. In particular, the largest truncation MGL 144 preferentially bound GalNAc–glycosylated compounds compared to non–glycosylated compounds. The most densely glycosylated compound, peptide **63** was found to be the strongest binder to truncated MGL protein, outperforming every other compound on three out of four truncations.

MGL is found as a homotrimer on certain types of cells, thus the next step was to perform binding studies on trimeric MGL. The cell binding assay incubated the fluorescently labelled dendrimers with MoDC which express MGL and LG2 cells which do not express MGL. The MoDC were grown over four days in cell cultures from monocytes purified from human blood. The ability of the dendrimers to bind to MGL expressing MoDC was assessed at 0 °C and 37 °C at a variety of concentrations and incubation lengths. The GalNAc–glycosylated dendrimers preferentially bound to MGL–expressing MoDCs in the presence of LG2 cells in a dose dependent manner. Compounds with no GalNAc residues did not bind to MoDC or LG2 cells unless the concentration was increased to the point where non–specific binding occurred. Likewise, compounds would not bind to LG2 cells unless the concentration was raised to levels where non–specific binding would occur. The amount of binding was dependent on the temperature, with greater quantities of GalNAc–glycosylated dendrimers bound at higher temperatures. Performing the different assays allowed for comparison of

binding to MGL between the early iterations of dendrimers, which affected the design of subsequent dendrimers and peptides. Dendrimers with more GalNAc residues bound better than those with less. The GalNAc–glycosylated dendrimers were compared to straight chain peptides and MUC1 sequences for binding and were found to be superior to both. The lead compound, dendrimer **24**, was the best performing compound from this assay.

After demonstrating the successful binding of GalNAc–glycosylated dendrimers to homotrimeric MGL, the next step was to show the quantity and selectivity of binding to MGL expressing cells in PBMC *ex vivo*. Dr Anna Brooks performed the final cell binding assay which incubated PBMCs with the most successful structures from the previous two assays. Dendrimer **24** and its non–glycosylated partner dendrimer **48** were compared to the peptide **64** (the fluorescent equivalent of peptide **63**) and its non–glycosylated partners; peptides **66** and **65**. All compounds showed very little binding to cells which lacked expression of MGL. The glycosylated compounds, dendrimer **24** and peptide **64** both bound in greater quantities than the non–glycosylated compounds to MGL–expressing cells. The branched dendrimer **24** bound more than the linear peptide **64**, which may be due to the greater distance between GalNAc residues, affording better opportunities for polydentate binding to one or more of the MGL proteins in the homotrimer.

Each assay was necessary to assess the viability of GalNAc–glycosylated "click" peptide dendrimers to act as delivery agents for targeting MGL–expressing cells. These experiments have shown that strong selective binding of MGL can be achieved even in the presence of non–MGL expressing cells. Further work would need to be performed to advance these glycodendrimers along the path to become delivery agents of immunogenic cargoes in therapeutic vaccines for the treatment of cancer.

7.11 Future work

7.11.1 Future modifications to the dendrimer

There are many different modifications to the dendrimers which could be made in an attempt to improve binding to MGL. The evidence so far has shown that the more carbohydrates presented, the greater the binding of the dendrimer to MGL. By increasing the number of branches of the dendrimer, the number of GalNAcs presented to MGL should increase. A library of dendrimers with increasing number of branches could be synthesised to find the optimum number of GalNAc residues to bind to an MGL expressing cell.

Future studies could also determine whether changes in the linking of the sugar could have an effect on the efficacy or strength of binding to MGL. There are many different click reactions

which could be used to install GalNAc residues, such as free radical hydrothiolation,[141] or the olefin metathesis (Scheme 7.2). Another option would be to synthesise dendrimers with T_N antigens instead of triazole linkers using Danishefsky's cassette,[49, 79, 78] which could then be deprotected to give the T_N antigens at the end of the synthesis. A study of the effect of the linker structure on MGL binding could then be undertaken.

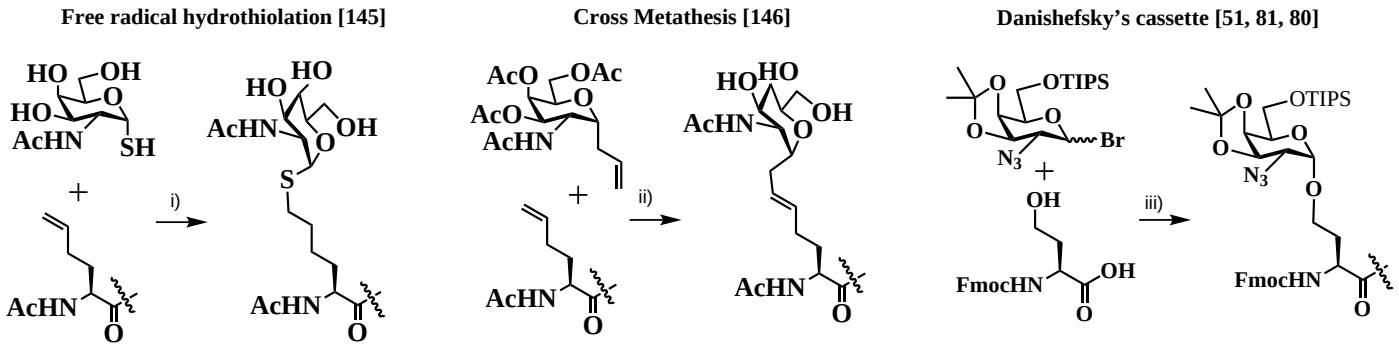

Reagents and conditions: (i) AIBI, NaOAc (pH 4) buffer, H_2O, UV light; (ii) a. Grubbs II catalyst 50 mol%, CH_2Cl_2; b. NaOMe, MeOH, 2 h; (iii) TMSOTf, THF, -78 ºC.

Scheme 7.2: Alternative glycosylation reactions to the CuAAC reaction: free radical hydrothiolation[141], olefin metathesis[142] and Danishefsky's cassette.[49, 79, 78]

A further point of investigation is whether the nature of the dendrimer scaffold or the distance between GalNAc residues is more important. There is a defined length between the X and Y, Y and Z, X and Z chains. Since dendrimer **24** performed the best in the PBMC cell binding assay, it seems plausible that it could have the optimum length between carbohydrate residues. To investigate whether the distance between residues is more critical than using dendrimer **24** as the scaffold, the straight chain peptides in Figure 7.21 could be investigated. These structures mimic different chain length combinations from dendrimer **24**. A cell binding assay could be performed on any of these straight chain peptides and the binding compared to dendrimer **24**. If the binding is similar or greater for a straight chain peptide compared to dendrimer **24** it would be unnecessary to make dendrimers, and the distance between GalNAc residues was more important than the dendrimer structure.

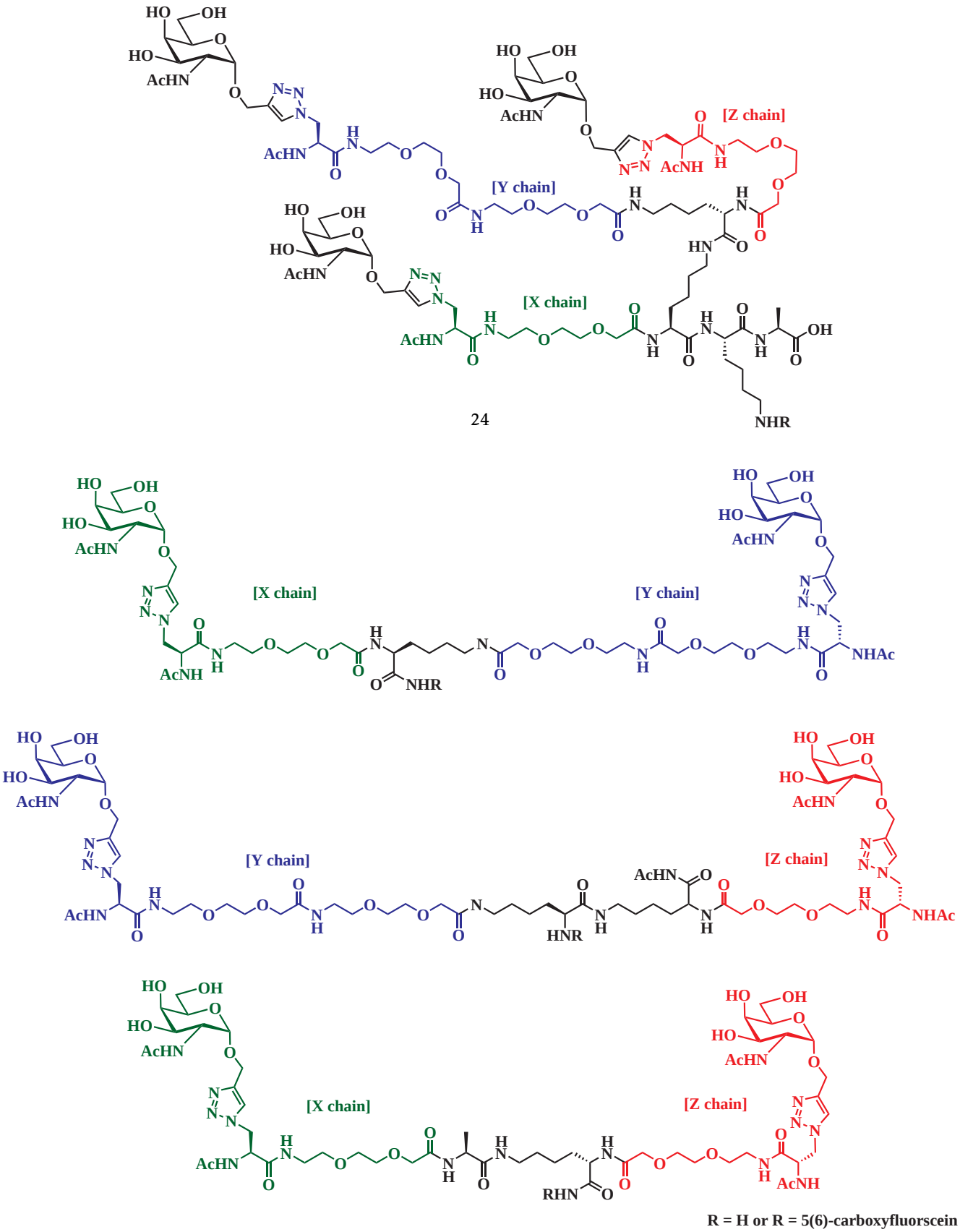

Figure 7.21: Straight chain peptides which mimic the distances between terminal GalNAc residues for dendrimer **24**.

The results of the cell binding assay suggest that the dendrimer **24** scaffold facilitates the best presentation due to optimal orientation/positioning of GalNAc residues to MGL–expressing cells compared to other structures tested, such as linear peptides. Assuming that little improvement in binding to MGL can be gained by modification of the dendrimer core, the next logical modification would be to vary the number of GalNAc residues presented by the dendrimer. Figure 7.22 shows possible options for a dendrimer library where the number of GalNAc residues is varied. Increasing the number of GalNAc residues may result in a dendrimer which binds more effectively to the MGL proteins expressed on cells as this trend has been witnessed throughout the cell binding assays in this research. Peptide **63** was the strongest binder to the CRD of truncated MGL. It contained a cluster of three sequential GalNAc residues attached via triazole linkers to alanine residues at the end of the peptide chain. A dendrimer with a GalNAc cluster at the end of each chain may be far more effective at binding than dendrimers with just one terminal triazole bound GalNAc. In support of this theory, it may be noted that Leclerc's MAG and Danifshesky's T_N antigen–clustered conjugates both had three GalNAc residues at the end of each chain and both of these were able to effectively deliver an immunogenic cargo to generate T–cell responses.[94, 79, 78]

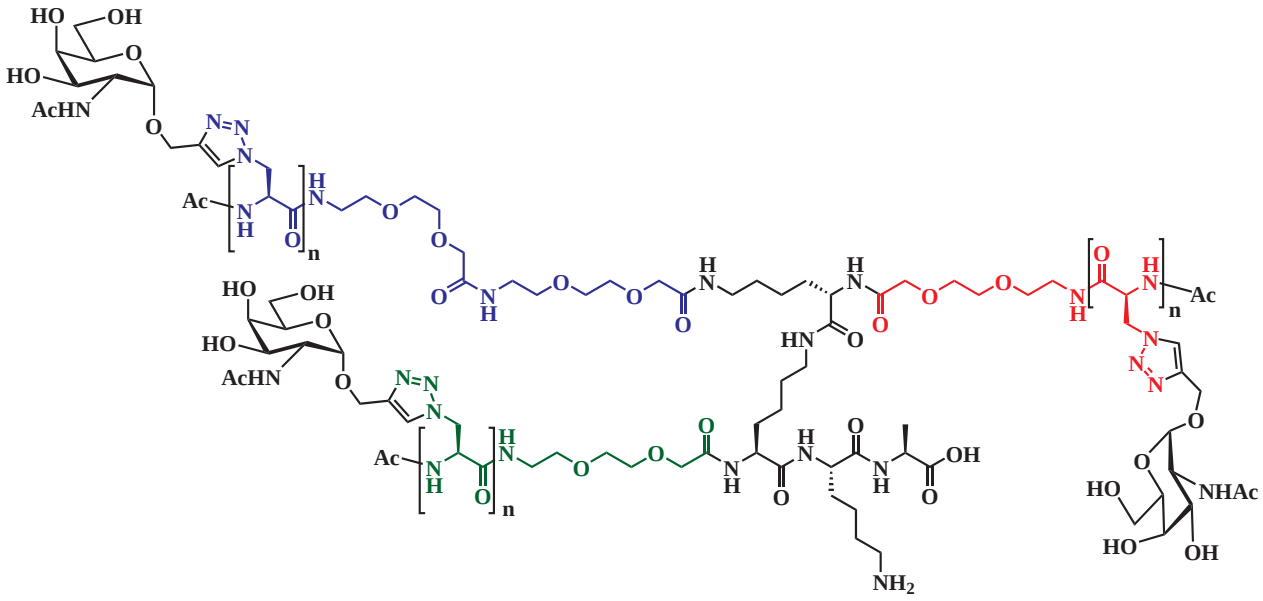

Figure 7.22: Analogues of dendrimer **24** with different numbers of GalNAc residues at the end of each chain.

The aim of the project was to produce a delivery system for cargoes to target MGL, so that ultimately this might be used as a mechanism for producing a CD8+ T-cell response. The results from the cell binding assay and the PBMC binding assay have shown that dendrimer **24** is the best construct for targeting MGL expressing cells, therefore the next step could be the attachment of various different cargoes onto the amino acids in box A and B in Figure 7.23. The cargoes could ideally trigger a CD8+ T–cell response after cross presentation.

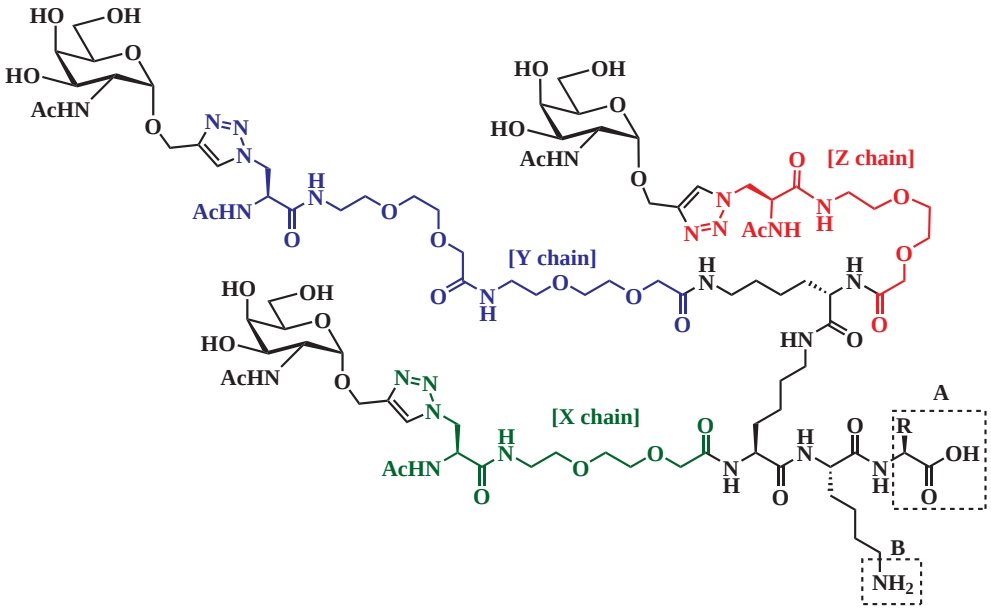

Figure 7.23: Positions for conjugation of cargoes on dendrimer **24**.

The method of attachment for the cargo is dependent on the tolerance for the CuAAC reaction with the peptide. The simplest option would be to include the azide–bearing scaffold in the SPPS synthesis. Either the dendrimer could be included at the beginning of the synthesis, and the peptide cargo included at the lysine in box B, or at the end of the synthesis and coupled to the amino acid at point A. While the synthesis of the dendrimer–cargo peptide may be simpler, larger peptides are more prone to sequestering copper which would make the CuAAC reaction harder to force to completion. Also the availability of the azide sites may change when the peptide folds, which may restrict the glycosylation via the CuAAC reaction. The dendrimer **24** could be synthesised first and then coupled to the peptide cargo through native chemical ligation at site A.[127] Another option for conjugation of the peptide would be the incorporation of an unnatural amino acid at site A which could undergo a click reaction (such as a free radical hydrothiolation[141], olefin metathesis[142] or another CuAAC reaction.[77]).

After the delivery system is bound to the MGL receptor it is hoped that the molecule will be internalised into the APC and processed so it can be presented by MHC I protein. For a successful therapeutic vaccine, the CD8+ T–cells must be activated by an antigen presented via MHC I, and also CD4+ T–cells must be activated by MHC II, which can amplify the response of CD8+ T–cells and B–cells.[2] The cytomegalovirus (CMV) expresses the pp65 protein which has a number of well characterised, highly immunogenic epitopes that can stimulate both CD4+ and CD8+ T–cells, and could therefore be used as a model antigen to be coupled to the dendrimer.

7.11.2 Future research on the truncated MGL protein

Once the optimised dendrimer and cargo have been chosen, attention could turn to a study of the interaction of MGL with additives. Ideally, solving the crystal structure of MGL binding to a dendrimer would provide insight into the binding mechanism, and this could help refinement of the dendrimer structure. If crystallisation is not possible, another option for studying the binding would be to create resin–bound dendrimers in a similar fashion to Ježek et al. and to perform confocal laser microscopy and NMR spectroscopy.[83]

The purification and refolding solvent system of the four MGL truncations was found to be very inefficient. The quaternary protein structure of the four truncations of MGL expressed recombinantly was never solved because there was not an appropriate solvent system to perform SEC–MALS (Size Exclusion Chromatography coupled with Multi–Angle Light Scattering, to give absolute molecular weights) which would reveal the hydrodynamic properties allowing determination of the oligimerisation. Screening a variety of buffer systems may solve both of these problems and provide a higher yielding source of MGL. Once significant quantities of MGL have been purified, the protein can be stored for future testing. The thermal melt assay may be an effective pre–screening tool for evaluating the availability of the GalNAc dendrimers binding.

7.11.3 Future studies on MGL expressing cells

The experiments discussed in this thesis have shown that the dendrimers bind to MGL–expressing cells, but little else is known. The ability of the compounds to induce DC maturation has not been determined. Mature DCs migrate to the lymph nodes and activate T–cells, therefore it is important that the DCs are able to mature and migrate after binding of the dendrimer has occurred. An assay could investigate if the MoDC and DC mature after incubation with the dendrimer and then migrate to present the antigens to T–cells. Dendrimer **24** contains a fluorescent tag, so it would be interesting to try to visualise the distribution of the dendrimer on the cell at different time points over the course of the assay. By following the accumulation of fluorescence on different parts of the cell at different time points, it may be possible to see the intracellular route dendrimers follow when internalised by MGL. Different locations within the cell can be identified by biological markers, and therefore it would be possible to determine the intracellular trafficking route taken by the internalised denrimer. If the dendrimers can not be internalised, it is very unlikely that they will be able to be processed by MHC I proteins and presented to CD8+ T–cells.

An assay could be performed to monitor the immune response after MoDC and DC are incubated with dendrimer **24**. Another assay could specifically look to see if any T–cells are generated. Due to the non–immunogenic nature of the polylysine scaffold,[44] it is unlikely that dendrimer **24** would

generate a response. However, once an appropriate immunogenic cargo has been attached to the dendrimer, it is more likely to generate a T–cell response. The cytokine expression and upregulation of activation markers on T–cells can be measured by FACS, which will reveal the effect of the cargo and delivery system on the APC.

7.11.4 Evidence that MGL may be involved in tolerance by the immune system

Cancer vaccines need to generate CD8+ T–cell responses which increase the immune system's reaction. The following section provides evidence that MGL may be involved in tolerising the immune system.

Role of MGL in infectious diseases

Takada *et al.* studied the interactions of MGL with filoviruses responsible for infectious diseases such as Ebola or Marburg virus.[26] This research showed that the heavily glycosylated filoviruses use C–type lectins such as MGL to gain cellular entry and then promote viral replication.

Gonorrhea is one of the most prevalent sexually transmitted diseases in the world with a global incidence of 62 million infected annually.[143, 144] Van Kooyk *et al.* studied how the Gram negative bacteria *Neisseria gonorrhoeae* (which is responsible for the STI Gonorrhea) interacts with MGL.[144] The F62 phenotype *C Neisseria gonorrhoeae* has terminal GalNAc–containing lipooligosaccharides and is processed by MGL–expressing DCs, resulting in suppression of T–cells which would fight the disease.

Role of MGL in autoimmune diseases since 1996

Many studies have been completed on the mechanism of autoimmune diseases with MGL. Irimura *et al.* identified that MGL was involved in the immune response against organ transplants and malignant tumours in rodents.[132] Macrophages expressing MGL were shown to accumulate at the site of chronic rejection of heart transplants in rats. Both Irimura *et al.* and Oo-puthinan *et al.* have studied MGL–deficient mice and shown that the protein is important for clearance of apoptotic cells in developing embryos.[16, 145] Irimura also proposed that MGL plays a crucial role in the prevention of stress–related embryonic death.

Schistosomiasis is a disease caused by helminths (a type of parasitic worm) which can infect the urinary tract and the intestines.[27] In the short term the disease causes diarrhoea and blood in the stool and urine, while in the long term it can cause liver damage and kidney failure. The eggs

of the helminths *Schistosoma mansoni* produce soluble egg antigens (SEA) which contain a mixture of glycoproteins and glycolipids, some of which bind to MGL expressed by DCs. In 2006 Van Die *et al*. studied the binding of the SEA to different C–type lectins.[27] The research showed that internalisation of SEA by multiple C–type lectins, such as MGL and DC–SIGN, could suppress the maturation of immature DCs followed by reduced cytokine production. This process is involved in reduced T–helper cell responses.

Building on this helminth research, Van Die *et al*. have applied their knowledge to the treatment of Crohn's disease and multiple sclerosis.[28] These two inflammatory diseases are caused by an overactive immune response to harmless components or self molecules. These two diseases are being experimentally treated using the helminth *Trichuris suis*, a pig whipworm which suppresses the host's immune system. Modern sanitation conditions and vaccination have caused humans to have reduced exposure to parasites such as pig whipworm, which may have lead to autoimmune diseases becoming more prevelant.[28] DCs help determine the effector T–cell response by recognition and sampling of antigens. Activated DCs produce pro–inflamatory cytokines which are involved in Crohn's disease and multiple sclerosis. *Trichuris suis* soluble proteins interact with C–type lectin receptors on DCs such as MGL and DC–SIGN, dampening pro–inflammatory responses for inflammatory diseases. The mechanisms of action are not completely understood, but being able to target DCs through MGL may result in new treatments for these inflammatory diseases.

MGL binds the GalNAc glycosylated proteins such as MUC1 or SEA.[19, 27] The APC which is expressing the MGL binding the protein will process these proteins and present their antigens either via MHC I or II proteins to T–cell. The T–cell response will depend on the MHC protein which presented the antigens. Currently there is evidence that MGL is involved in both stimulation and suppression of the immune system. Any molecule which selectively targets MGL will have potential to be used as a drug for either immune stimulation or suppression.

If there is evidence that the dendrimers interacting with MGL are responsible for tolerizing the immune system it would no longer be a suitable therapeutic vaccine to treat cancer. However, the application of the dendrimer could be changed to treating autoimmune diseases, where tolerizing the immune system is a desired trait. Whatever direction the research takes, this project has achieved its aim of successfully designing a delivery system to target antigens for delivery to APC via the MGL receptor.

Chapter 8

Experimental

8.1 Experimental conditions and analytical parameters

Procedures that resulted in the recovery or decomposition of starting material are not included in this chapter. All reactions were continuously stirred using a magnetic stirrer bar and a stirrer hot plate. Commercially available reagents were purchased as reagent grade and used as received without further purification.

Anhydrous dichloromethane was obtained by distillation over calcium hydride. Water as a solvent or co-solvent refers to Milli-Q ultrapure de-ionised water. Removal of low boiling point solvents (<100 °C) *in vacuo* was achieved using, a b*ü*chi rotary evaporator (30-40 °C) followed by a high vacuum line at room temperature. For solvents with higher boiling points (>100 °C), a combination of b*ü*chi rotary evaporator (water bath tempeeratures of 30-60 °C), high vacuum and lyophilisation was used to dry the product. Solvents for HPLC were purchased as HPLC grade and used without further purification.

Thin layer chromatography (TLC) was performed using aluminium-backed 0.2 mm plates of Kieselgel F_{254} (Merck) and visualised by UV fluorescence at 254 nm, then stained with vanillin solution (unless otherwise stated) followed by heating. Column chromatography was carried out using Kieselgel F_{254} 63-100 μm (Ridel-de Ha*ë*n) silica gel with indicated solvents.

Melting points were determined on an Kofler hot-stage melting point apparatus and are uncorrected.

^{1}H and ^{13}C NMR spectra were recorded on the Bruker AVANCE DRX400 spectrometer (^{1}H, 400 MHz and ^{13}C, 100 MHz) at ambient temperature and in the solvent indicated, using standard pulse techniques. Chemical shifts (δ) are reported in parts per million (ppm) relative to the residual solvent peak or $SiMe_4$. Coupling constants (J) are reported to the nearest 0.1 Hz. Multiplicities are abbreviated as follows: s (singlet), d (doublet), t (triplet), q (quartet), quin (quintet), and m (multiplet). Assignments of signals were made using COSY, DEPT, HMQC, HSQC and HMBC experiments.

Electrospray ionisation mass spectra (ESI-MS) were recorded either on an Agilent Technologies 1120 Compact LC connected to a HP Series 1100 MSD spectrometer or a Bruker microTOF-Q II spectrometer. Samples were introduced using direct flow injection at 0.1-0.2 mL/min into an ESI source in positive mode. Major and significant fragments are quoted in the form × (mass to charge ratio). Only molecular ions (M^+), fragments from the molecular ions and other major peaks are reported. High resolution mass spectra were recorded on a VG-70SE mass spectrometer at a nominal accelerating voltage of 70 eV and are accurate to ±5 ppm.

Infrared spectra were recorded on a Perkin Elmer Spectrum One fourier transformed infrared spectrometer on a film ATR sampling accessory. Absorption maxima (v_{max}) are reported in wavenumbers (cm^{-1}) with the following abbreviations: s (strong), m (medium), w (weak) and br (broad). The structure for peak values were assigned with the help of the book "Structure Determination of Organic Compounds. Tables of Spectral Data" by E. Pretsch P. Buhlmann and C. Affolter.[146]

Microwave irradiation was carried out using a CEM Discover 1 microwave reactor using 10 mL reaction vials with snap-on caps.

Optical rotations were determined using the sodium D line (589 nm) at 20 °C on a Rudolph Research Autopol IV polarimeter with the concentration of the sample measured in grams per 100 mL. Optical rotations are given in units of 10^{-1}deg cm^2g^{-1}.

8.2 Synthesis of unnatural amino acids and carbohydrate building blocks

8.2.1 Imidazole-sulfonyl azide hydrochloride

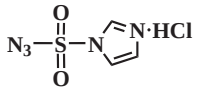

11

SO_2Cl_2 (15.0 mL, 185 mmol) was added slowly to NaN_3 (12.0 g, 185 mmol) at 0 °C. The yellow reaction mixture with white precipitate was stirred at room temperature, becoming clear overnight. Imidazole (25.0 g, 370 mmol) was added at 0 °C and the mixture was stirred for 2 h then filtered, diluted with EtOAc (50 mL) and EtOH (20.0 mL), and washed with H_2O (2 × 10 mL) and saturated $NaHCO_3$ (aq) (10.0 mL). The organic phase was dried using $MgSO_4$ and filtered, AcCl (19.8 mL, 278 mmol) was added and stirred for 1 h at 0 °C. The resulting precipitate was filtered and dried in a desiccator. The *title compound* **11** was recovered as a white solid (23.0 g, 59%). The spectral data was in agreement with the literature.[118]

8.2.2 Fmoc–azido alanine

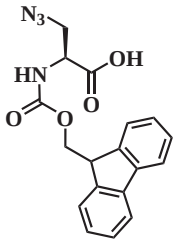

9

N-α–Fmoc–diaminopropionic acid (1.0 g, 3.07 mmol) was dissolved in 1:1 H_2O/MeOH (80 mL). $CuSO_4$ (10 mg, 0.03 mmol), K_2CO_3 (590 mg, 4.29 mmol) and compound **11** (900 mg, 4.29 mmol) were added and the reaction stirred overnight. The resulting blue solution promptly changed to yellow upon addition of tetrasodium ethylenediaminetetraacetic acid (28 mg, 0.06 mmol), and after 1 h of stirring the solution was acidified to pH 2 with conc HCl then extracted with CH_2Cl_2 (3 × 30 mL). The organic phase was dried using $MgSO_4$ and concentrated *in vacuo*. The resulting oil was then purified by flash chromatography with 0.1 % (v/v) acetic acid in a mixture of 45:1 CH_2Cl_2/MeOH. The resulting oil was co–eluted with toluene *in vacuo* and then lyophilised to give the *title compound* **9** as a light brown solid (1.08 g, quantitative yield). mp 105 °C; $[\alpha]_D^{20}$ = 31.2 (c 1.00, MeOH); **IR** (neat)/cm^{-1} ν_{max} 3310 (OH, s) 2981 (CH, w) 2108 (N_3, s), 1688 (COOH, s), 1536 (NH, s), 1253 (CO, s); **^{1}H NMR (400 MHz, $CDCl_3$)** δ7.76 (d, *J* = 7.5 Hz, 2H, Fmoc), 7.59 (d, *J* = 7.1 Hz, 2H, Fmoc), 7.38 (t, *J* = 7.1 Hz, 2H, Fmoc), 7.31 (t, *J* = 7.5 Hz, 2H, Fmoc), 5.63 (d, *J* = 8.4, 1H, NH), 4.58 (t, *J* = 4.2, 1H, NCH), 4.43 (d, *J* = 2.4 Hz, 2H CH_2, Fmoc), 4.23 (t, *J* = 7.2 Hz, 1H, Fmoc), 3.81 (dd, *J* = 12.7, 4.2 Hz, 2H, CH_2); **^{13}C NMR (100 MHz, $CDCl_3$)** δ156.0 (C), 143.5 (C), 141.3 (C), 127.8 (CH, Fmoc), 127.1 (CH, Fmoc), 125.1 (CH, Fmoc), 120.1 (CH, Fmoc), 67.5 (CH_2, Fmoc), 54.0 (CH, NCH), 51.2 (CH_2), 47.1 (CH, Fmoc); ***m/z*** MS(ESI) 353.1238 ($[M + H]^+$ requires 352.1244). The spectral data in the literature was done in DMSO-d_6, these assignments are consistent with those reported.[119]

8.2.3 1,3,4,6-Tetra-*O*-acetyl-2-azido-2-deoxy-D-galactopyranose

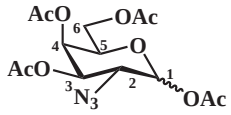

15

Galactosamine hydrochloride (19.9 g, 92.3 mmol) was dissolved in 2:1 H_2O/MeOH (120 mL). Na_2CO_3 (11.7 g, 110.7 mmol) and $CuSO_4{\cdot}5H_2O$ (190 mg, 1.2 mmol) were added slowly over 15 min. The free base of **11** was obtained by disolving **11** in H_2O (20 mL) and extracting into EtOAc (3 × 10 mL). The aqueous layer was discarded and the resulting EtoAc solution of imidazole-sulfonyl azide was mixed with 1:1 H_2O/MeOH (80 mL) and added to the sugar solution. After 3 h, the colour changed from green to a dark cloudy grey whereupon tetrasodium ethylenediaminetetraacetic acid (77 mg, 1.84 mmol) was added, inducing a dark brown colour. The solution was concentrated under vacuum to give a brown solid. A mixture of pyridine (200 mL) and Ac_2O (120 mL) was added slowly over 1 h to the solid, ensuring that the temperature did not rise above 40 °C. This solution was stirred overnight at room temperature, after which the starting material was no longer present and only product visible by TLC analysis. The pyridine was removed under reduced pressure (28 mbar and 45 °C) to give a viscous brown oil which was dissolved in EtOAc (300 mL) and washed with 5 M HCl (3 × 300 mL), H_2O (2 × 300 mL) and brine (300 mL). The organic extracts were dried using $MgSO_4$, concentrated and the residue was purified by flash chromatography using 7:3 hexane/EtOAc . The *title compound* **15** was obtained as a light brown solid (27.2 g, 81%); mp 95 °C; **IR** (neat)/cm^{-1} ν_{max} 2945 (CH, w), 2115 (N_3, s), 1750 (COAc, s), 1365 (CN, m), 1209 (COAc, s), 1064 (COC, s), 1035 (COC, s); **^{1}H NMR (400 MHz, $CDCl_3$)** δ5.57 (d, *J* = 8.5 Hz, 1H, H5), 5.38 (dd, *J* = 3.5, 1 Hz, 1H, H4), 4.90 (dd, *J* = 11.0, 3.5 Hz, 1H, H3), 4.13 (ddd, *J* = 10.9, 6.9, 0.3 Hz, 2H, H6), 4.03 (dt, *J* = 7.0, 1.0 Hz, 1H, H5), 3.84 (dd, *J* = 11.0, 8.5 Hz, 1H, H2), 2.22 (s, 3H, Ac), 2.17 (s, 3H, Ac), 2.07 (s, 3H, Ac), 2.05 (s, 3H, Ac); **^{13}C NMR (100 MHz, $CDCl_3$)** δ 169.9 (CO, Ac), 169.6 (CO, Ac), 169.0 (CO, Ac), 168.5 (CO, Ac), 92.8 (CH, C1), 71.6 (CH, C5), 71.2 (CH, C3), 66.1 (CH, C4), 60.9 (CH_2, C6), 59.6 (CH, C2), 20.8 (CH_3, Ac), 20.6 (CH_3, Ac), 20.5 (CH_3, Ac), 20.5 (CH_3, Ac); ***m/z*** MS(ESI) 390.1013 ($[M + Na]^+$ requires 390.1000). The spectral data was in agreement with the literature.[147]

8.2.4 (Prop-2-yn-1-yl)-(3,4,6-triacetyl-2-azido-2-deoxy-D-galactopyranoside

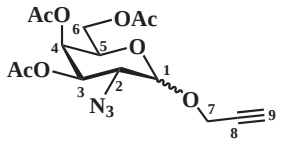

16

In anhydrous conditions under N_2, **15** (2.04 g, 5.47 mmol) was dissolved in dry CH_2Cl_2 (54 mL) at 35 °C. Propargyl alcohol (760 μL, 13.7 mmol) was added, followed by $BF_3{\cdot}Et_2O$ (7 mL, 54.7 mmol) and stirred overnight. The mixture was washed with saturated aqueous $NaHCO_3$ (3 × 30 mL) and the combined aqueous layer was extracted with CH_2Cl_2 (3 × 10 mL). The organic extracts were dried over Na_2SO_4, filtered and concentrated *in vacuo*. The resulting oil was purified by flash chromatography using 4:1 toluene/EtOAc. The solution was concentrated *in vacuo* to give the *title compound* **16** as a colorless oil (1.82 g, 90%) (as a 2:1 mixture of α and β anomers). **IR** (neat)/cm^{-1} ν_{max} 2112 (N_3, s), 1743 (COAc, s), 1370 (CN, m), 1214 (COAc, s), 1040 (COC, s); ***m/z*** MS(ESI) 370.1252 ($[M + H]^+$ requires 370.1245).

Alpha-anomer
$[\alpha]_D^{20}$ = 72.82° (c 1.00, EtOAc); **^{1}H NMR (400 MHz, $CDCl_3$)** δ5.46 (dd, *J* = 3.4, 1.1 Hz, 1H, H4), 5.36 (dd, *J* = 11.0, 3.5 Hz, 1H, H3), 5.23 (d, *J* = 3.5 Hz, 1H, H1), 4.33 (d, *J* = 2.5 Hz, 2H, H7), 4.26 (dt, *J* = 6.7, 1.1 Hz, 1H, H5), 4.11 (t, *J* = 7.1 Hz, 2H, H6), 3.75 (dd, *J* = 11.2, 3.4 Hz, 1H, H2), 2.53 (t, *J* = 2.5 Hz, 1H, H9), 2.05 (s, 3H, Ac), 2.05 (s, 3H, Ac), 2.15 (s, 3H, Ac); **^{13}C NMR (100 MHz, $CDCl_3$)** δ170.3 (CO, Ac), 169.9 (CO, Ac), 169.7 (CO, Ac), 96.6 (CH, C1), 77.9 (C, C8), 75.6 (CH, C9), 68.3 (CH, C3), 67.5 (CH, C4), 67.1 (CH, C5), 61.4 (CH_2, C6), 57.2 (CH, C2), 55.3 (CH_2, C7), 20.67 (CH_3, Ac), 20.63 (CH_3, Ac), 20.60 (CH_3, Ac). The spectral data was in agreement with the literature.[120]

Beta-anomer
^{1}H NMR (400 MHz, $CDCl_3$) δ4.83 (dd, *J* = 11.0, 3.5 Hz, 1H, H3), 4.64 (d, *J* = 7.6 Hz, 1H, H1), 4.46 (t, *J* = 2.5 Hz, 2H, H7), 4.16 (dt, *J* = 11.3, 6.4 Hz, 2H, H6), 4.10 (d, *J* = 1.6 Hz, 1H, H4), 3.90 (dt, *J* = 6.5, 1.0 Hz, 1H, H5), 3.71 (dd, *J* = 11.0, 8.1 Hz, 1H, H2), 2.54 (t, *J* = 2.3 Hz 1H, H9); **^{13}C NMR (100 MHz, $CDCl_3$)** δ170.3 (CO, Ac), 170.0 (C, C8), 169.9 (CO, Ac), 169.7 (CO, Ac), 99.6 (CH, C1), 75.9 (CH, C9), 71.1 (CH, C3), 70.8 (CH, C5), 66.3 (CH, C4), 61.1 (CH_2, C6), 60.5 (CH, C2), 56.1 (CH_2, C7), 20.67 (CH_3, Ac), 20.63 (CH_3, Ac), 20.60 (CH_3, Ac).

8.2.5 (Prop-2-yn-1-yl)-(2-acetamido-3,4,6-triacetyl-2-deoxy-α-D-galactopyranoside

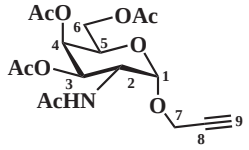

14

The mixture of anomers **16** (7.08 g, 19.0 mmol) was dissolved in a mixture of THF (150 mL), Ac_2O (100 mL) and glacial AcOH (50 mL). Zinc powder (8.10 g, 123.9 mmol) and saturated aqueous $CuSO_4$ (15 mL) were added. The resulting mixture was stirred for 1 h, filtered and the filtrate was azeotroped with toluene *in vacuo*. The resulting oil was purified by flash chromatography using 1:1 EtOAc/hexane. The two separated anomers were concentrated *in vacuo* to give two solids. The *title compound* **14** was isolated as a white solid (4.57 g, 65%) and the β anomer as a white solid (2.51 g, 31%); mp 95 °C; **IR** (neat)/cm^{-1} v_{max} 3246 (CH, w), 1747 (COAc, s), 1659 (NHAc, m), 1539 (NHAc, m), 1367 (CN, m), 1221 (COAc, s), 1028 (COC, s); ***m/z*** MS(ESI) 386.1456 ($[M + H]^+$ requires 386.1446); **Alpha-anomer** $[\alpha]_D^{20}$ = 112.15° (c 1.00, EtOAc); **^{1}H NMR (400 MHz, $CDCl_3$)** δ5.70 (d, *J* = 9.5 Hz, 1H, NH), 5.39 (dd, *J* = 3.7, 1.5 Hz, 1H, H4), 5.17 (dd, *J* = 11.4, 3.2 Hz, 1H, H3), 5.08 (d, *J* = 4.0 Hz, 1H, H1), 4.63 (ddd, *J* = 13.1, 9.9, 3.7 Hz, 1H, H2), 4.27 (ddd, *J* = 21.3, 16.0, 2.5 Hz, 2H, H7), 4.21 (dt, *J* = 6.4 1.3 Hz, 1H, H5), 4.12 (m, 2H, H6), 2.50 (t, *J* = 2.5 Hz, 1H, H9), 2.17 (s, 3H, Ac), 2.05 (s, 3H, Ac), 2.00 (s, 3H, Ac), 1.98 (s, 3H, NAc); **^{13}C NMR (100 MHz, $CDCl_3$)** δ170.9 (CO, NHAc), 170.4 (CO, Ac), 170.3 (CO, Ac), 170.2 (CO, Ac), 96.6 (CH, C1), 78.3 (C, C8), 75.4 (CH, C9), 68.2 (CH, C3), 67.3 (CH, C5 and C4), 61.7 (CH, C6), 55.3 (CH_2, C7), 47.5 (CH, C2), 23.3 (CH_3, HNAc), 21.0 (CH_3, Ac), 20.7 (CH_3, Ac), 20.68 (CH_3, Ac). The spectral data was in agreement with the literature.[120]

8.2.6 Propargyl 2-*O*-α-D-Acetylgalactosamine

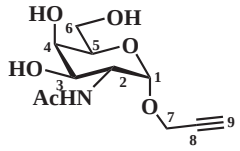

4

Solid sodium pieces (230 mg, 10 mmol) were dissolved in MeOH (10 mL) at 0 °C to make NaOMe solution (1 M). The resulting NaOMe solution (5 mL) was added to **14** (200 mg, 515 μmol) and stirred for 2 h. Dowex resin (100 mg) was added and the mixture was stirred for 1 h before acidification to pH 2 using conc HCl. Solvent was removed under reduced pressure and the resulting solution lyophilised. Purification by flash chromatography using 19:1 CH_2Cl_2/MeOH afforded the *title compound* **4** as white crystals (132 mg, 98%). **IR** (neat)/cm^{-1} v_{max} 3246 (OH, b), 1653 (NHAc, s), 1547 (NHAc, m), 1404 (CN, s), 1026 (COC, s); $[\alpha]_D^{20}$ = 222.06° (c 1.00, MeOH); **^{1}H NMR (400 MHz, CD_3OD)** δ5.04 (d, *J* = 4.2 Hz, 1H, H1), 4.33 (ddd, *J* = 11.2, 7.0, 3.8 Hz, 1H, H2), 4.29 (t, *J* = 2.7 Hz, 2H, H7), 3.92 (dd, *J* = 3.4, 1.4 Hz, 1H, H4), 3.83 (t, *J* = 6.6 Hz, 1H, H5), 3.79 (dd, *J* = 11.1, 3.1 Hz, 1H, H3), 3.73 (dt, *J* = 11.3, 5.3 Hz, 1H, H6), 2.87 (t, *J* = 2.5 Hz, 1H, H9), 2.01 (s, 3H, NAc); **^{13}C NMR (100 MHz, CD_3OD)** δ173.95 (C, NAc), 97.4 (CH, C1), 80.1 (C, C8), 76.0 (CH, C9) 73.0 (CH, C5), 70.4 (CH, C4), 69.6 (CH, C3), 62.8 (CH_2, C6), 55.4 (CH_2, C7), 51.3 (CH, C2), 22.6 (CH_3, NHAc); ***m/z*** MS(ESI) 282.0929 ($[M + H]^+$ requires 282.0948). The spectral data was in agreement with the literature.[120]

8.2.7 (2*S*)-2-[(9*H*-Fluoren-9-ylmethoxy)carbonyl]amino-3-(4-[(2,3,4,6-tetra-*O*-acetyl-α-D-galactopyranoyl)oxy]-1*H*-1,2,3-triazol-1-yl)propanoic acid

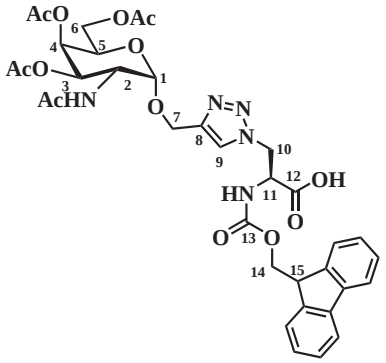

39

Protected sugar **14** (58.0 mg, 150 μmol) and synthetic Fmoc–azido alanine (**9**) (35.0 mg, 100 μmol) were dissolved in 900 μL of a 1:1:1 mixture of H_2O, TBA and CH_2Cl_2. A stock solution of $CuSO_4$ (16 mg, 100 μmol) and sodium ascorbate (50 mg, 250 μmol) in H_2O (500μL) was prepared and 10 μL of this stock solution was added to the reaction mixture. The reaction mixture was heated at 80 °C in a sealed reaction vessel using the microwave reactor (120 W max). After 30 mins, the mixture was diluted with H_2O (1 mL), acidified with citric acid (100 μL), and extracted with CH_2Cl_2 (5 × 5 mL). The combined organic extracts were dried and concentrated *in vacuo*. Purification by flash chromatography 0.1 % (v/v) acetic acid in a mixture of 98:2 CH_2Cl_2/MeOH afforded the *title compound* **39** as a colourless oil (88.0 mg, 95%); mp 145 °C; $[\alpha]_D^{20}$ = 78.5° (c 1.00, $CHCl_3$); **IR** (neat)/cm^{-1} ν_{max} 1740 (COAc, s), 1537 (NHAc, m), 1218 (COAc, s), 1042 (COC, s); **^{1}H NMR (400 MHz, CDCl3)** δ7.76 (d, *J* = 7.5 Hz, 2H, Fmoc), 7.60 (d, *J* = 7.5 Hz, 2H, Fmoc), 7.52 (s, 1H, H9), 7.40 (t, *J* = 7.2 Hz, 2H, Fmoc), 7.31 (t, *J* = 7.5 Hz, 2H, Fmoc), 6.53 (d, *J* = 9.2 Hz, 1H, NHAc), 6.16 (d, *J* = 6.9 Hz, 1H, NHFmoc), 5.37 (d, *J* = 2.34 Hz, 1H, H4), 5.16 (dd, *J* = 11.4, 3.0 Hz, 1H, H3), 4.89 (m, 2H, H14), 4.91 (s ,1H, H1), 4.82 (m, 2H, H11, H10), 4.64 (d, *J* = 13.2 Hz, 1H, H10), 4.46 (m, C7, 3H, H2), 4.25 (m, 2H, C5, H15), 4.10 (d, *J* = 5.4 Hz, 2H, H6), 2.12 (s, 3H, Ac), 2.04 (s, 3H, Ac), 1.97 (s, 3H, Ac), 1.88 (s, 3H, NAc); **^{13}C NMR (100 MHz, $CDCl_3$)** δ176.7 (C), 174.8 (C), 172.3 (CO, NAc) 171.0 (CO, Ac), 170.8 (CO, Ac), 170.4 (CO, Ac) , 156.0 (C), 143.7 (C), 141.4 (C), 127.8 (CH, Fmoc), 127.2 (CH, Fmoc), 125.1 (CH, Fmoc and C9), 120.5 (CH, Fmoc), 95.8 (CH, C1), 67.9 (CH, C3), 67.3 (CH, C4), 67.1 (CH, C5), 67.1 (CH_2, C7), 61.9 (CH_2, C6), 59.7 (CH_2, C10), 54.0 (CH, C11), 51.2 (CH_2, C14), 48.0 (CH, C2), 47.1 (CH, C15), 22.7 (CH_3, NAc), 20.7 (CH_3, Ac); ***m/z*** MS(ESI) 738.2168 ($[M + H]^+$ requires 738.2617).

8.2.8 (2*S*)-2-(((9*H*-fluoren-9-yl)methoxy)carbonylamino)-3-(1-deoxy-2-acet -amido-α-D-galactopyranosyl)-oxymethyl)-1*H*-1,2,3-triazol-1-yl)propanoic acid

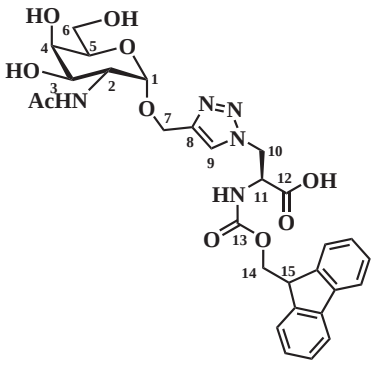

42

Solid sodium pieces (230 mg, 10 mmol) were dissolved in MeOH (10 mL) at 0 °C to make NaOMe solution (1 M). The resulting NaOMe solution (5 mL) was added to **39** (32.0 mg, 36.0 μmol) and stirred for 2 h. Dowex resin (100 mg) was added and the mixture was stirred, for 1 h before acidification to pH 2. The solution was filtered, and the resin was washed with MeOH (3 × 5 mL). The combined washings were concentrated *in vacuo* and the resulting mixture was lyophilised. Purification by flash chromatography using 19:1 CH_2Cl_2/MeOH afforded the *title compound* **42** as white crystals (22.0 mg, 81%); mp 127 °C; $[\alpha]_D^{20}$ = 80.2° (c 1.00, MeOH); **IR** (neat)/cm^{-1} v_{max} 3319 (OH, b) 2520 (OH, b), 2160 (N triazole, s), 2028 (N triazole, s), 1707 (C=O, w), 1523 (C=C, w), 1129 (COC, s), 1043 (COC, s); **^{1}H NMR (400 MHz, CD_3OD)** δ7.94 (s, 1H, C9), 7.81 (d, *J* = 7.3 Hz, 2H, Fmoc), 7.64 (d, *J* = 7.3 Hz, 2H, Fmoc), 7.41 (t, *J* = 9.1 Hz, 2H, Fmoc), 7.32 (t, *J* = 9.1 Hz, 2H, Fmoc), 4.94 (m, 1H, C10a), 4.9 (d, *J* = 4.0 Hz, 1H, C1), 4.78 (m, 1H, C10b), 4.75 (m, 1H, C7a), 4.72 (m, 1H, C11), 4.60 (d, *J* = 8.0 Hz, 1H, C7b), 4.33 (m, 1H, C4), 4.30 (m, 2H, C6), 4.22 (t, textitJ = 7.2 Hz, 1H, C15), 3.87 (d, *J* = 3.0 Hz, 1H, C3), 3.81 (dd, *J* = 10.8, 7.2 Hz, C5), 3.75 (m, 3H, C2 and C14), 1.96 (s, 3H, NAc); **^{13}C NMR (100 MHz, CD_3OD)** δ174.1 (C, NAc), 171.9 (C, COOH), 158.3 (C, NCO_2), 145.2 (C, triazole), 142.6 (C, Fmoc), 128.8 (CH, triazole), 128.2 (CH, Fmoc), 126.3 (CH, Fmoc), 126.0 (CH, Fmoc), 121.0 (CH, Fmoc), 98.4 (CH, C1), 72.9 (CH, C5), 70.4 (CH, C3), 69.8 (CH_2, C14), 68.2 (CH, C4), 62.9 (CH, C2), 61.2 (CH, C7), 55.48 (CH, C11), 51.6 (CH_2, C6), 51.4 (CH_2, C14), 48.3 (CH, C15) 22.7(CH_3, Ac); ***m/z*** 612.22 MS(ESI) ($[M + H]^+$ requires 612.22).

8.3 General methods for the synthesis of dendrimer and peptide scaffolds

8.3.1 Attachment of Fmoc–Ala–HMPP linker to resin

A fritted glass reaction vessel was used for the manual synthesis of the dendrimer and peptide scaffolds. Aminomethyl polystyrene resin derivatised with Fmoc–Ala–HMPP was employed for all dendrimers and peptide sequences. Fmoc–Ala–HMPP–OH linker (100 mg, 200 μmol) and DIC (20 μL, 200 μmol) were dissolved in CH_2Cl_2 (3 mL) and reacted with the resin (100 mg of 1 mmol/g, 100 μmol) for 2 h. The mixture was drained, the resin washed with DMF (3 × 3 mL) and CH_2Cl_2 (3 × 3 mL) and the resin was then dried *in vacuo*. A small sample of the resulting resin was subjected to a Kaiser test and the coupling was repeated if a positive test was observed.[128]

8.3.2 Fmoc removal

Fmoc protecting groups were removed from 50 μmol of resin using 20% piperidine solution in DMF (5 mL for 10 min, 2 cycles). The resin was washed with DMF (3 × 3 mL), CH_2Cl_2 (3 × 3 mL) and dried. A Kaiser test was performed on a small quantity of resin to confirm the deprotection has been taken place.

8.3.3 Dde removal

A solution of 2% hydrazine in DMF was prepared by diluting hydrazine hydrate (500 μL) with DMF (4 mL). Removal of the Dde protecting group from the N^{ϵ} group of the lysine residue on the resin (50 μmol) was performed using this solution (2 mL for 3 min, 2 cycles).

8.3.4 Mtt removal

Removal of the Mtt protecting group from the N^{ϵ} group of the lysine residue was accomplished by agitating the resin (50 μmol) with 2% v/v TFA in CH_2Cl_2 (3 mL, 5 min). The resulting mixture was filtered and the procedure was repeated (approximately 10 repetitions) until the filtrate changed colour from dark yellow to colourless.

8.3.5 Mini–cleavage

A mixture of TFA (460 μL) and H_2O (40 μL) was added to resin (approx 1 mg) and the mixture was shaken for 2 h. The supernatant was decanted and diluted with a cold mixture of hexane/Et_2O (1:1, 0.5 mL) to precipitate the peptide. The suspension was centrifuged at 4000 rpm to form a pellet and the supernatant discarded. The pellet was dissolved with 100 μL of 1:1 MeCN/H_2O, then analysed using flow injection mass spectrometry.

8.3.6 Chromatographic purification of peptides and dendrimer scafolds

Purification of dendrimer scaffolds, dendrimers and peptides was performed on a Phenomenex Gemini C_{18} column (5 μ, 110 Å, 10 mm × 250 mm), using a linear gradient of 0 to 100% MeCN in water (with 0.1% v/v TFA) over 100 min, with a flow rate of 5 mL min^{-1}. Analysis of the purified compound was performed using a Phenomenex Gemini C_{18} column, (5 μ, 110 Å, 2.00 mm × 10.00 mm) using a linear gradient of 0 to 60% MeCN in water (with 0.1% v/v formic acid) over 30 min, with a flow rate of 0.3 mL min^{-1}. Hydrophilic compounds (**63** and **67**) were analysed using an Agilent Zorbax C_3 column (5 μ, 110 Å, 3.00 mm × 150.00 mm) using a linear gradient of 0 to 30% MeCN in water (with 0.1% v/v formic acid) over 30 min with a flow rate of 0.3 mL min^{-1}.

8.4 General amino acid coupling methods

Eight different methods for amino–acid coupling were used. Coupling of Fmoc-amino acids was performed using one of the methods 1 - 4. Coupling of the synthetic amino acid: Fmoc–azidoalanine **9** used either method 5 or 6. Capping of the chains was performed using method 7 or 8 and coupling of 5(6)–carboxyfluorescein was performed using method 9.

8.4.1 Method 1: coupling using HCTU

Protected amino acid (5 eq, 250 μmol) and HCTU (101 mg, 245 μmol) were dissolved in DMF (3 mL). To this mixture was added DIPEA (175 μL, 500 μmol). The mixture was then transferred to the reaction vessel and was agitated with the resin (0.05 mmol) for 30 min. The reaction mixture was filtered and the resin washed with DMF (3 × 3 mL) and CH_2Cl_2 (3 × 3 mL).

8.4.2 Method 2: coupling using HATU

Protected amino acid (3 eq, 150 μmol) was dissolved in DMF (3 mL). HATU (55.1 mg, 145 μmol) was added and the mixture was shaken until dissolved. To this mixture was added DIPEA (90 μL, 0.5 mmol), the mixture was then transferred to the reaction vessel and agitated with the resin for 30 min. The reaction mixture was filtered and the resin washed with DMF (3 × 3 mL) and CH_2Cl_2 (3 × 3 mL).

8.4.3 Method 3: coupling using HATU

Protected amino acid (6 eq, 300 μmol) was dissolved in DMF (3 mL). HATU (112 mg, 295 μmol) was added and the mixture was shaken until dissolved. To this mixture was added DIPEA (180 μL, 1.0 mmol). The mixture was then transferred to the reaction vessel and agitated with the resin (50 μmol) for 30 min. The reaction mixture was filtered and the resin washed with DMF (3 × 3 mL) and CH_2Cl_2 (3 × 3 mL).

8.4.4 Method 4: coupling using HCTU

Protected amino acid (10 eq, 500 μmol) was dissolved in DMF (3 mL). HCTU (202 mg, 490 μmol) was added and the mixture was shaken until dissolved. To this mixture, was added DIPEA (180 μL 1.0 mmol), the mixture was then transferred to the reaction vessel and agitated with the resin (50 μmol) for 30 min. The reaction mixture was filtered and the resin washed with DMF (3 × 3 mL) and CH_2Cl_2 (3 × 3 mL).

8.4.5 Method 5: coupling of Fmoc–azidoalanine using HATU

Fmoc–azidoalanine **9** (52 mg, 150 μmol) was dissolved in DMF (3 mL). HATU (55 mg, 145 μmol) was added and the mixture was shaken until dissolved. To this mixture was added DIPEA (175 μL, 500 μmol). The mixture was then transferred to the reaction vessel and agitated with the resin for 1 h. The reaction mixture was filtered and the resin washed with DMF (3 × 3 mL) and CH_2Cl_2 (3 × 3 mL).

8.4.6 Method 6: coupling of Fmoc–azidoalanine using HATU

Fmoc–azidoalanine **9** (104 mg, 300 μmol) was dissolved in DMF (3 mL). HATU (112 mg, 295 μmol) was added and the mixture was shaken until dissolved. To this mixture was added DIPEA (180 μL, 1.0 mmol), the mixture was then transferred to the reaction vessel and agitated with the resin (50 μmol) for 1 h. The reaction mixture was filtered and the resin washed with DMF (3 × 3 mL) and CH_2Cl_2 (3 × 3 mL).

8.4.7 Method 7: capping using acetic anhydride

Excess DIPEA (200 μL) and Ac_2O (200 μL) were dissolved in DMF (3 mL) and shaken with the resin (0.05 mmol) for 30 min. The resin was filtered and washed with DMF (3 × 3 mL) and CH_2Cl_2 (3 × 3 mL).

8.4.8 Method 8: coupling of 5(6)–carboxyfluorescein using HOBt and DIC

5(6)-Carboxyfluorescein (188 mg, 500 μmol) and HOBt (76 mg, 500 μmol) were dissolved in DMF (3 mL). DIC (45 μL, 450 μmol) was added and the mixture was transferred to the resin (50 μmol) and agitated for 1 h. The reaction vessel was drained and the resin washed with DMF (3 × 3 mL). The resin was shaken with 20% piperidine mixture in DMF (3 mL for 10 min, 5 cycles until the filtrate became clear) to remove the 5(6)–carboxyfluorescein oligomers. The resin was washed with DMF (3 × 3 mL) and CH_2Cl_2 (3 × 3 mL).

8.5 Cleavage methods

Four methods were used to effect cleavage of the peptides from the resin depending on the presence or absence of fluorophores and azide groups.

8.5.1 Method 9: cleavage using TFA for peptides containing azides and fluorophores

TFA (2.7 mL) and H_2O (300 μL) were added to the resin (50 μmol) in the reaction vessel and the mixture was shaken for 2 h. The mixture was filtered and the resin washed with TFA (1 mL). The

peptide was precipitated using a cold mixture of hexane/Et_2O (1:1, 10 mL). The mixture was centrifuged to form a pellet using a Kubota 2420 centrifuge at 4000 rpm, and the supernatant was decanted. The pellet was dissolved in MeCN/H_2O (1:1, 10 mL) and lyophilised.

8.5.2 Method 10: cleavage using TFA for peptides containing azides with no fluorophores

TFA (2.7 mL) and H_2O (300 μL) were added to the resin (50 μmol) in the reaction vessel was shaken for 2 h. The mixture was filtered and the resin washed with TFA (1 mL). The filtrate was diluted in MeCN/H_2O (1:1, 10 mL) and lyophilised.

8.5.3 Method 11: cleavage using TFA for peptides containing fluorophores with no azides

TFA (2.7 mL), H_2O (100 μL), triisopropylsilane (100 μL) and 3,6-dioxa-1,8-octanedithiol (100 μL) were added to the resin (50 μmol) in a reaction vessel and the mixture was shaken for 2 h. The mixture was filtered and the resin washed with TFA (1 mL). The peptide was precipitated using a cold mixture of hexane/Et_2O (1:1, 10 mL). The mixture was centrifuged to form a pellet using a Kubota 2420 centrifuge at 4000 rpm, and the supernatant was decanted. The pellet was dissolved in MeCN/H_2O (1:1, 10 mL) and lyophilised.

8.5.4 Method 12: cleavage using TFA for peptides containing no azides or fluorphores

TFA (2.7 mL), H_2O (100 μL), triisopropylsilane (100 μL) and 3,6-dioxa-1,8-octanedithiol (100 μL) were added to the resin (50 μmol) in a reaction vessel and the mixture was shaken for 2 h. The mixture was filtered and the resin washed with TFA (1 mL). The mixture was diluted in MeCN/H_2O (1:1, 10 mL) and lyophilised.

8.6 Synthesis of dendrimer and peptide ligands

8.6.1 Dendrimers and peptides for the cell binding assay

The following dendrimer and peptide ligands were synthesised for the cell binding assay.

8.6.2 Generation I dendrimers

Dendrimer 22

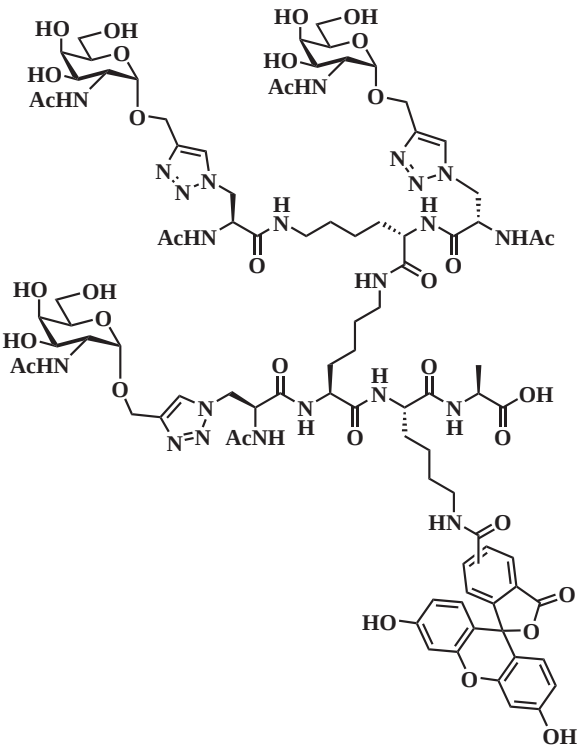

22

Resin **8** (50 μmol) was prepared as described (*Section 8.3.1*). Deprotection of the Fmoc group was carried out as described (*Section 8.3.2*). Fmoc–Lys(Mtt) was coupled to the resulting resin (*8.4.1 method 1: using HCTU*) to afford **29**. After cleaving the Fmoc group, Fmoc–Lys(Dde) was coupled (*Section 8.4.2 method 2: using HATU*) to give **30**. Removal of the Fmoc group was carried out using 20% pyridine in DMF, followed by coupling of the synthesised Fmoc–azidoalanine **9** (*Section 8.4.5 method 5: using HATU*). Fmoc group was removed and the peptide chain was capped (*Section 8.4.7 method 7: using Ac_2O*) to prevent further growth and afford **7**. Dde group was cleaved (*Section 8.3.3*) and Fmoc–Lys(Fmoc) was installed (*Section 8.4.1 method 1: using HCTU*) to afford **28**. The two Fmoc groups on the scaffold were removed and the two exposed chains were grown in parallel by coupling

one Fmoc–azidoalanine **9** to the end of each chain (*Section 8.4.6 method 6: using HATU*). Fmoc groups were cleaved and the two exposed chains capped (*Section 8.4.7 method 7: using Ac_2O*) to afford **27**. The Mtt group was removed (*Section 8.3.4*) and 5(6)–carboxyfluorescein was coupled (*Section 8.4.8 method 8: using HOBt and DIC*). The dendrimer scaffold was cleaved from resin (*Section 8.5.1 method 9: using TFA*) and was then lyophilised and purified by HPLC to yield dendrimer **37** (7.0 mg).

Propargyl GalNAc (**4**) (15.0 mg, 59.2 μmol) and dendrimer **37** (7.0 mg) were dissolved in DMSO (1.2 mL) and the mixture was heated to 50 °C. A solution of sodium ascorbate (4.2 mg, 24.3 μmol) and $CuSO_4$ (13 mg, 54 μmol) in H_2O (585 μL) was heated to 50 °C for 10 min then added to the above DMSO mixture and the reaction was shaken for 2 h at 50 °C. The mixture was cooled to room temperature, diluted with H_2O (45 mL) and purified by HPLC. The desired fractions were lyophilised to give the *title compound* **22** as an orange solid (5.6 mg, 6% isolated yield, 90% purity); R_t 13.5 min; ***m/z*** MS(ESI) 1036.4 ($[M + 2H]^{2+}$ requires 1036.4).

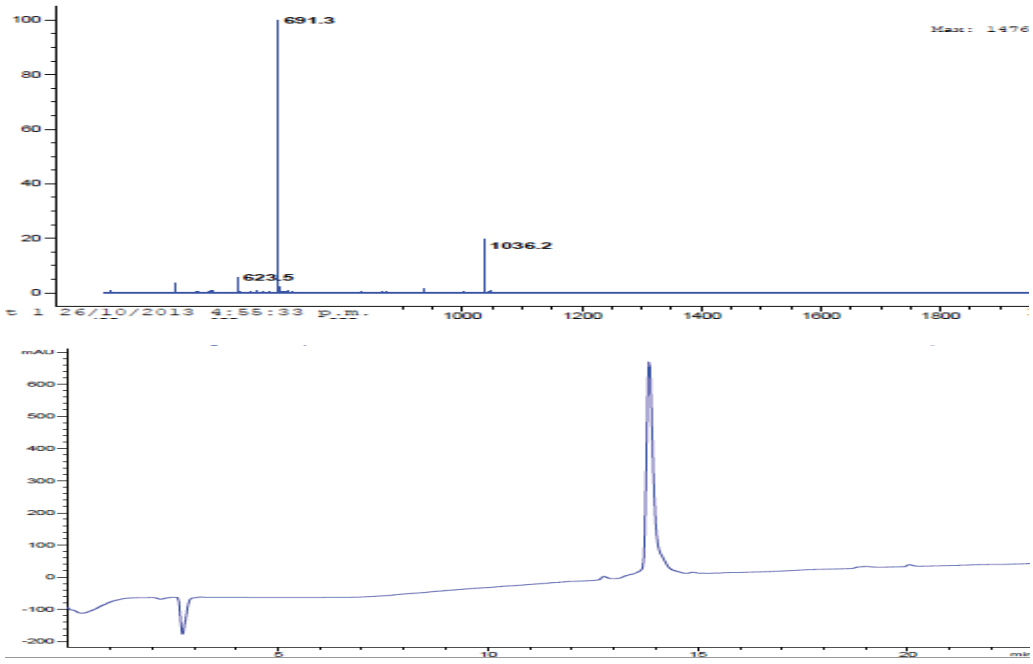

Figure 8.1: HPLC spectrum following purification for dendrimer **22**. R_t 13.5 min; ***m/z*** MS(ESI) 1036.4 ($[M + 2H]^{2+}$ requires 1036.4).

Dendrimer 3

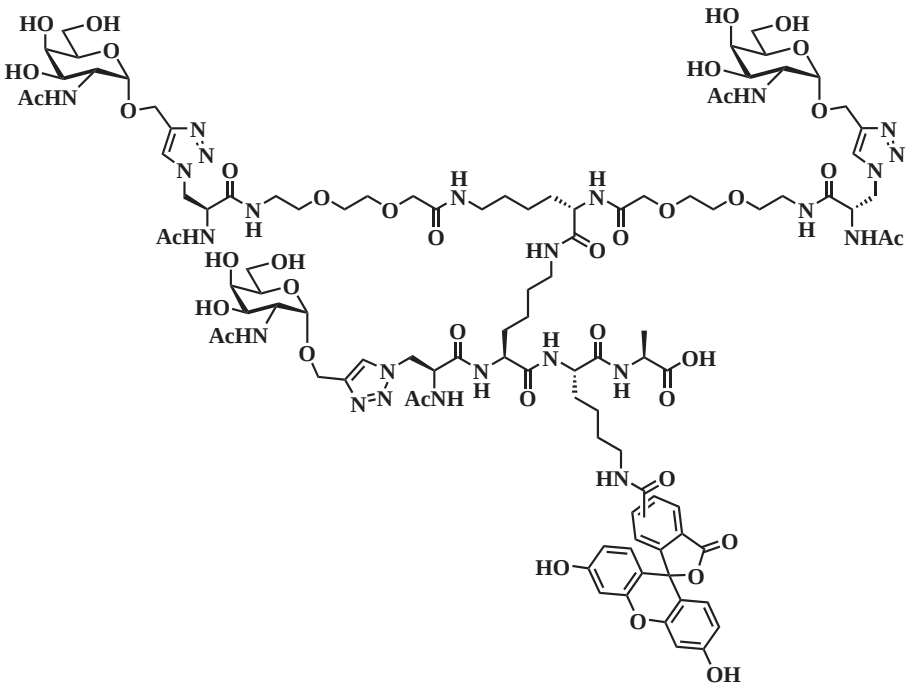

3

Resin **8** (50 μmol) was prepared as described (*Section 8.3.1*). Deprotection of the Fmoc group was carried out as described (*Section 8.3.2*). Fmoc–Lys(Mtt) was coupled (*8.4.1 method 1: using HCTU*) to afford **29**. After removal of the Fmoc group, Fmoc–Lys(Dde) was coupled (*Section 8.4.2 method 2: using HATU*) to give **30**. Fmoc group was removed and Fmoc–azidoalanine **9** was installed (*Section 8.4.5 method 5: using HATU*). Fmoc group of the $AlaN_3$ was removed, followed by capping of the chain (*Section 8.4.7 method 7: using Ac_2O*) to prevent further growth and afford **7**. Dde group was cleaved (*Section 8.3.3*) and Fmoc–Lys(Fmoc) was installed (*8.4.1 method 1: using HCTU*). After double Fmoc group removal, the two exposed chains were grown in parallel by coupling Fmoc–mini–PEG (*Section 8.4.3 method 3: using HATU*). The mini–PEGs were deprotected and Fmoc–azidoalanine **9** was coupled to the end of each chain (*Section 8.4.6 method 6: using HATU*). Fmoc groups were cleaved and the two exposed chains were capped (*Section 8.4.7 method 7: using Ac_2O*). Mtt group was removed (*Section 8.3.4*) and 5(6)–carboxyfluorescein was coupled (*Section 8.4.8 method 8: using HOBt and DIC*). The dendrimer scaffold was cleaved from the resin (*Section 8.5.1 method 9: using TFA*), lyophilised, then purified by HPLC (28 mg).

Propargyl GalNAc (**4**) (15 mg, 59.2 μmol) and dendrimer scaffold (4 mg, 3.264 μmol) were dissolved in DMSO (712 μL) and the mixture was heated to 50 °C. A solution of sodium ascorbate (4.2 mg, 24.3 μmol) and $CuSO_4$ (8 mg, 32.6 μmol) in H_2O (352 μL) was heated to 50 °C for 10 min then added to the above DMSO mixture. The click reaction mixture was heated for 2 h at 50 °C. The mixture was diluted with water (45 mL) and purified by HPLC. The desired fractions were lyophilised to give the *title compound* **3** as an orange solid (1 mg, 1% isolated yield, 95% purity);

R_t 14.0 min; ***m/z*** MS(ESI) 1181.7 ($[M + 2H]^{2+}$ requires 1181.5).

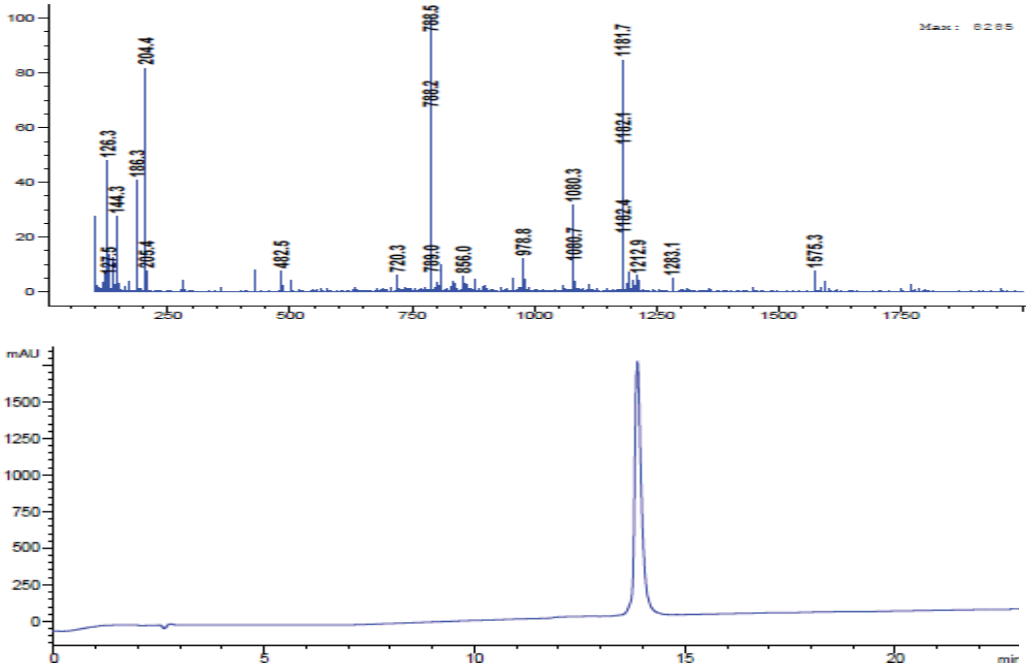

Figure 8.2: HPLC spectrum following purification for dendrimer **3**. R_t 14.0 min; ***m/z*** MS(ESI) 1181.7 ($[M + 2H]^{2+}$ requires 1181.5).

Dendrimer 24

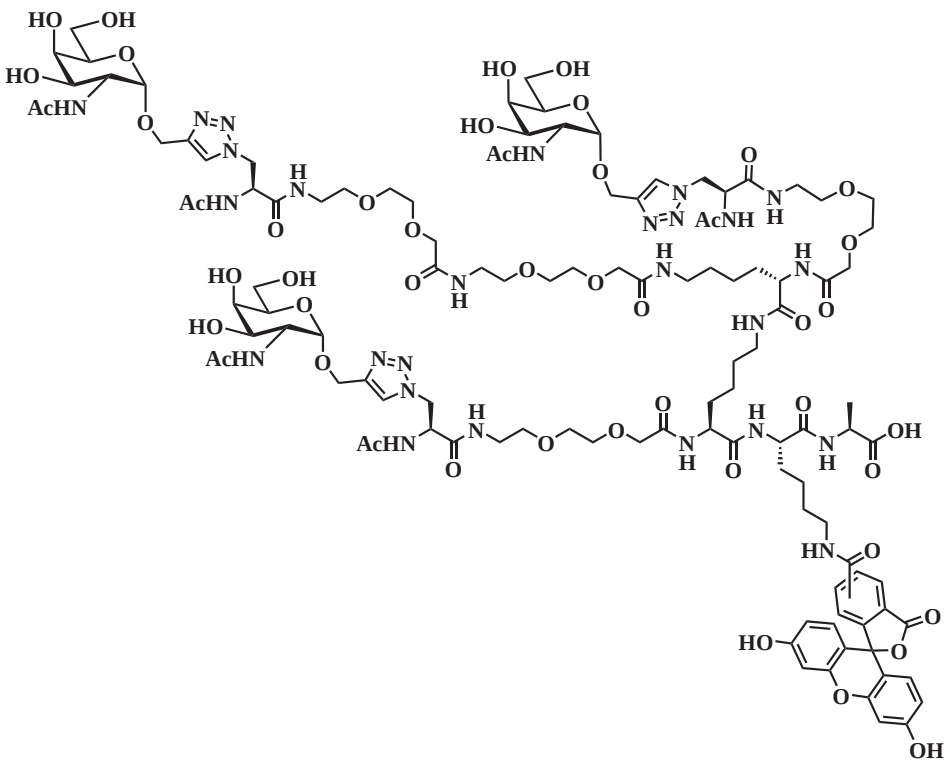

24

Resin **8** (50 μmol) was prepared as described (*Section 8.3.1*). Deprotection of the Fmoc group was carried out as described (*Section 8.3.2*). Fmoc–Lys(Mtt) was coupled (*8.4.1 method 1: using HCTU*) to afford **29**. After removal of the Fmoc group, Fmoc–Lys(Dde) was coupled (*Section 8.4.2 method 2: using HATU*) to give **30**. Fmoc group was removed, followed by coupling of Fmoc–mini–PEG (*Section 8.4.2 method 2: using HATU*). Removal of the Fmoc group was carried out using 20% pyridine in DMF, followed by coupling of the synthesised Fmoc–azidoalanine **9** (*Section 8.4.5 method 5: using HATU*). Fmoc group was removed and the peptide chain was capped (*Section 8.4.7 method 7: using Ac_2O*) to prevent further growth. Dde group was cleaved (*Section 8.3.3*) and Fmoc–Lys(Dde) was coupled (*Section 8.4.2 method 2: using HATU*). Fmoc group was removed, followed by coupling of Fmoc–mini–PEG (*Section 8.4.2 method 2: using HATU*). Removal of the Fmoc group was carried out using 20% pyridine in DMF, followed by coupling of the synthesised Fmoc–azidoalanine **9** (*Section 8.4.5 method 5: using HATU*). Fmoc group was removed and the peptide chain was capped (*Section 8.4.7 method 7: using Ac_2O*) to prevent further growth. Dde group was cleaved (*Section 8.3.3*) and was followed by coupling of Fmoc–mini–PEG (*Section 8.4.2 method 2: using HATU*). The mini–PEG group was deprotected and the second Fmoc–mini–PEG was installed (*Section 8.4.2 method 2: using HATU*). Removal of the Fmoc group was carried out using 20% pyridine in DMF, followed by coupling of the synthesised Fmoc–azidoalanine **9** (*Section 8.4.5 method 5: using HATU*). Fmoc group was removed and the peptide chain was capped (*Section 8.4.7 method 7: using Ac_2O*) to prevent fur-

ther growth. The Mtt group was removed (*Section 8.3.4*) and 5(6)–carboxyfluorescein was coupled (*Section 8.4.8 method 8: using HOBt and DIC*). The dendrimer scaffold was cleaved from the resin (*Section 8.5.1 method 9: using TFA*), lyophilised, then purified by HPLC (9 mg).

Propargyl GalNAc (**4**) (11 mg, 43.2 μmol) was dissolved in DMSO (1 mL) with dendrimer scaffold (9 mg) and was heated to 50 °C. A solution of sodium ascorbate (12.7 mg, 72 μmol) with $CuSO_4$ (39 mg, 158 μmol) in H_2O (500 μL) was heated to 50 °C for 10 min and then added to the DMSO solution. The click reaction was agitated for 2 h at 50 °C. The solution was diluted with water and then purified by HPLC. The desired fractions were lyophilised to give the *title compound* **24** as an orange solid (3.6 mg, 3% isolated yield, 96% purity); R_t 14.3 min; ***m/z*** MS(ESI) 1326.6 ($[M + 2H]^{2+}$ requires 1326.9).

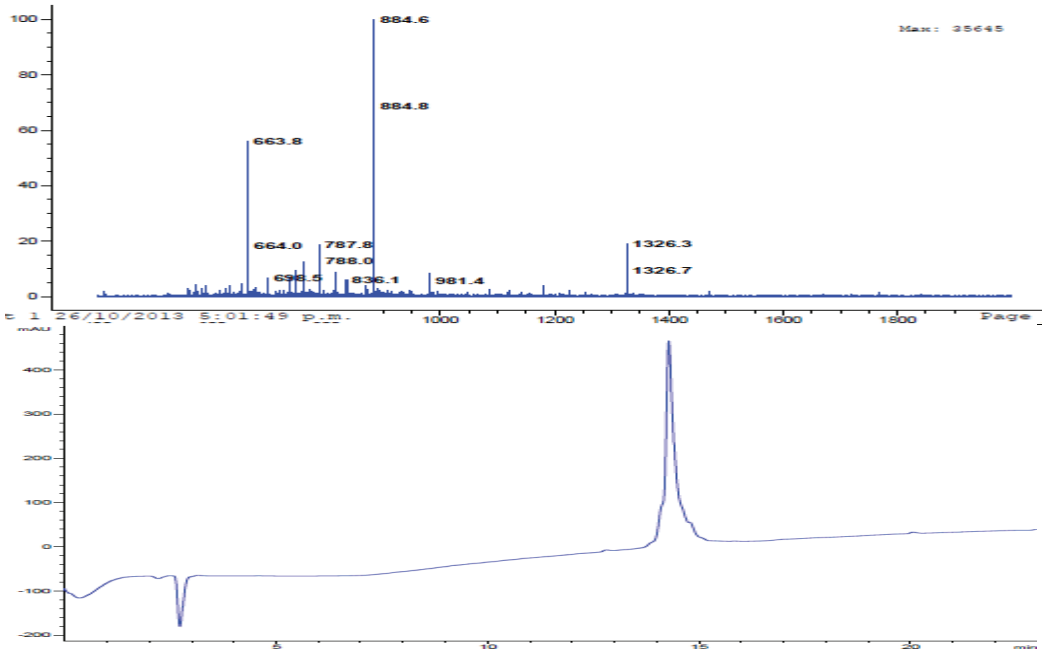

Figure 8.3: HPLC spectrum following purification for dendrimer **24**. R_t 14.3 min; ***m/z*** MS(ESI) 1326.6 ($[M + 2H]^{2+}$ requires 1326.9).

Dendrimer 26

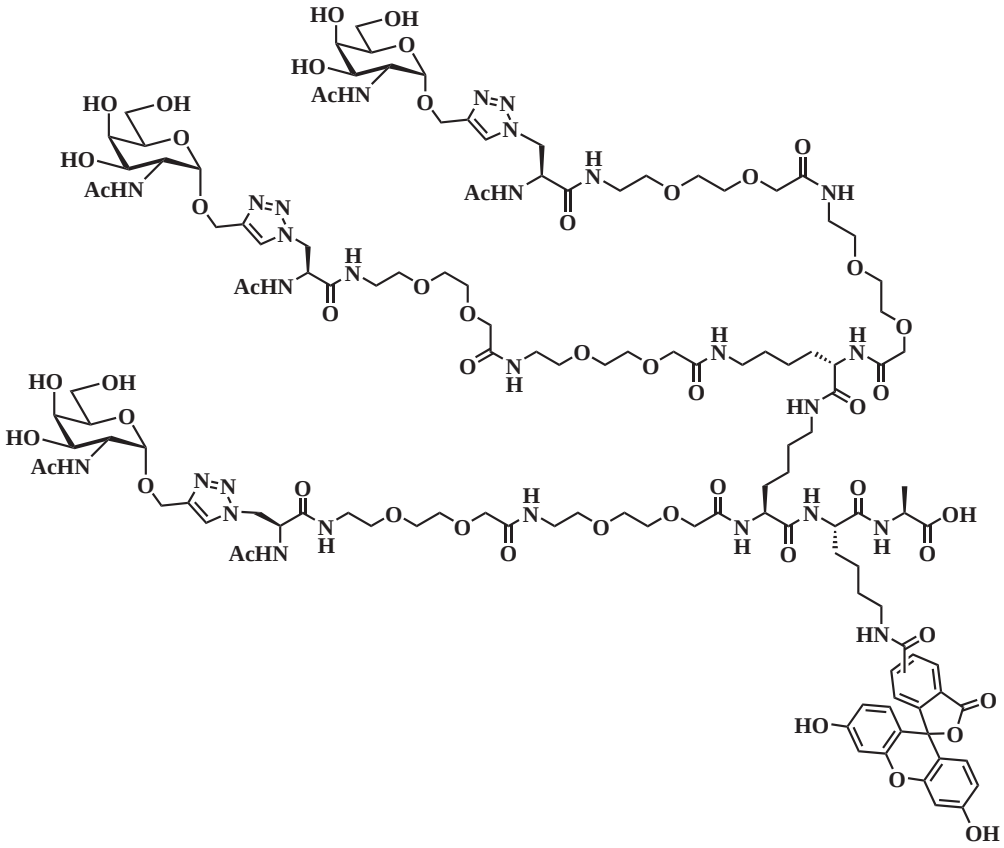

26

Resin **8** (50 μmol) was prepared as described (*Section 8.3.1*). Deprotection of the Fmoc group was carried out as described (*Section 8.3.2*). Fmoc–Lys(Mtt) was coupled (*8.4.1 method 1: using HCTU*) to afford **29**. After removal of the Fmoc group, Fmoc–Lys(Dde) was coupled (*Section 8.4.2 method 2: using HATU*) to give **30**. Fmoc group was removed, followed by coupling of Fmoc–mini–PEG (*Section 8.4.2 method 2: using HATU*). Fmoc group was removed, followed by coupling of Fmoc–mini–PEG (*Section 8.4.2 method 2: using HATU*). Removal of the Fmoc group was carried out using 20% pyridine in DMF, followed by coupling of the synthesised Fmoc–azidoalanine **9** (*Section 8.4.5 method 5: using HATU*). Fmoc group was removed and the peptide chain was capped (*Section 8.4.7 method 7: using Ac_2O*) to prevent further growth. Dde group was cleaved (*Section 8.3.3*) and Fmoc–Lys(Fmoc) was installed (*8.4.1 method 1: using HCTU*). After double Fmoc group removal, the two exposed chains were grown in parallel by coupling Fmoc–mini–PEG (*Section 8.4.3 method 3: using HATU*). The two new chains were deprotected and the second Fmoc–mini–PEG spacer on each chain was installed (*Section 8.4.3 method 3: using HATU*). Fmoc groups were cleaved, Fmoc–azidoalanine **9** was coupled to each of these chains (*8.4.6 method 6: using HATU*). Fmoc group was removed and the peptide chain was capped (*Section 8.4.7 method 7: using Ac_2O*) to prevent further growth. The Mtt group was removed (*Section 8.3.4*) and 5(6)–carboxyfluorescein was coupled (*Section 8.4.8 method 8:*

using HOBt and DIC). The dendrimer scaffold was cleaved from resin (*Section 8.5.1 method 9: using TFA*), lyophilised, then purified by HPLC (8.8 mg).

Propargyl GalNAc (**4**) (9.4 mg, 36.6 μmol) was dissolved in DMSO (854 μL) with dendrimer scaffold (8.8 mg) and was heated to 50 °C. A solution of sodium ascorbate (3.2 mg, 18.3 μmol) with $CuSO_4$ (10 mg, 40.7 μmol) in H_2O (427 μL) was heated to 50 °C for 10 min and then added to the DMSO solution. This mixture was reacted for 2 h at 50 °C. The solution was diluted with water and then purified by HPLC. The desired fractions were lyophilised to give the *title compound* **26** as an orange solid (2.4 mg, 2% isolated yield, 91% purity); R_t 14.5 min; ***m/z*** MS(ESI) 1471.6 ($[M + 2H]^{2+}$ requires 1471.6).

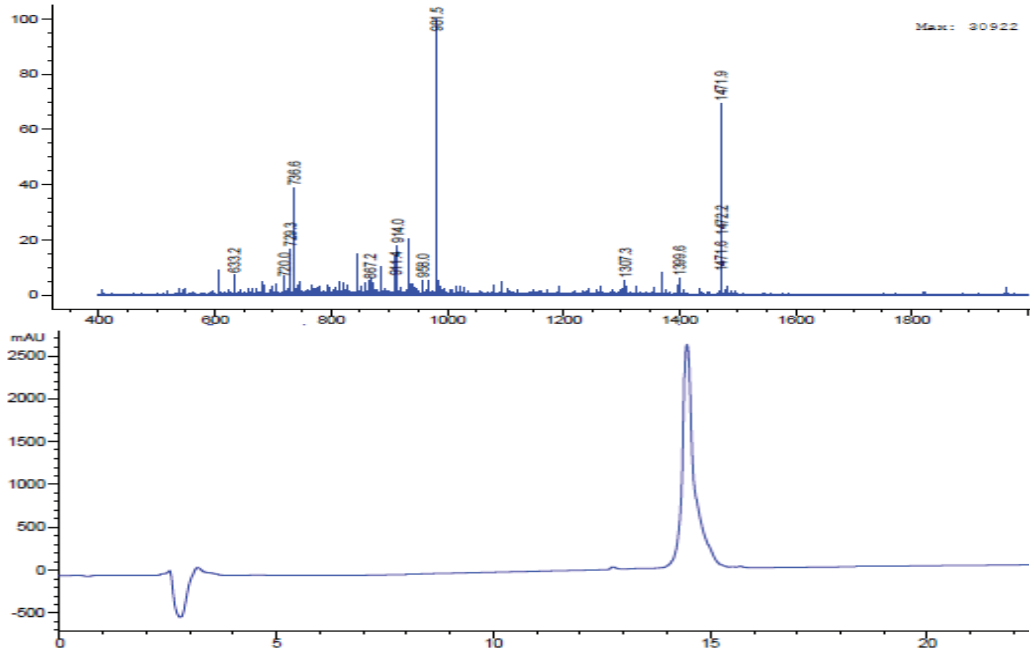

Figure 8.4: HPLC spectrum following purification for dendrimer **26**. R_t 14.5 min; ***m/z*** MS(ESI) 1471.6 ($[M + 2H]^{2+}$ requires 1471.6).

8.6.3 Generation II dendrimers

Dendrimer 44

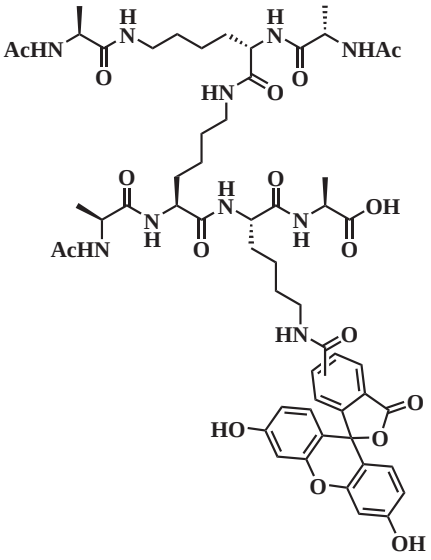

44

Resin **8** (50 μmol) was prepared as described (*Section 8.3.1*). Deprotection of the Fmoc group was carried out as described (*Section 8.3.2*). Fmoc–Lys(Mtt) was coupled (*8.4.1 method 1: using HCTU*) to afford **29**. After removal of the Fmoc group, Fmoc–Lys(Dde) was coupled (*Section 8.4.2 method 2: using HATU*) to give **30**. Fmoc group was removed and followed by coupling of Fmoc–Ala (*8.4.1 method 1: using HCTU*). Fmoc group was removed and the peptide chain was capped (*Section 8.4.7 method 7: using Ac_2O*) to prevent further growth. Dde group was cleaved (*Section 8.3.3*) and Fmoc–Lys(Fmoc) was installed (*8.4.1 method 1: using HCTU*). The two Fmoc groups were removed and the two exposed chains were grown in parallel by coupling Fmoc–Ala (*8.4.4 method 4: using HCTU*). The two terminal Fmoc groups were removed and the peptide chain was capped (*Section 8.4.7 method 7: using Ac_2O*) to prevent further growth. The Mtt group was removed (*Section 8.3.4*) and 5(6)–carboxyfluorescein was coupled (*Section 8.4.8 method 8: using HOBt and DIC*). The dendrimer scaffold was cleaved from resin (*Section 8.5.3 method 11: using TFA*), lyophilised, then purified by HPLC to give the *title compound* **44** as an orange solid (16.6 mg, 28% isolated yield, 93% purity); R_t 15.5 min; ***m/z*** MS(ESI) 1171.3 ($[M + H]^+$ requires 1171.5).

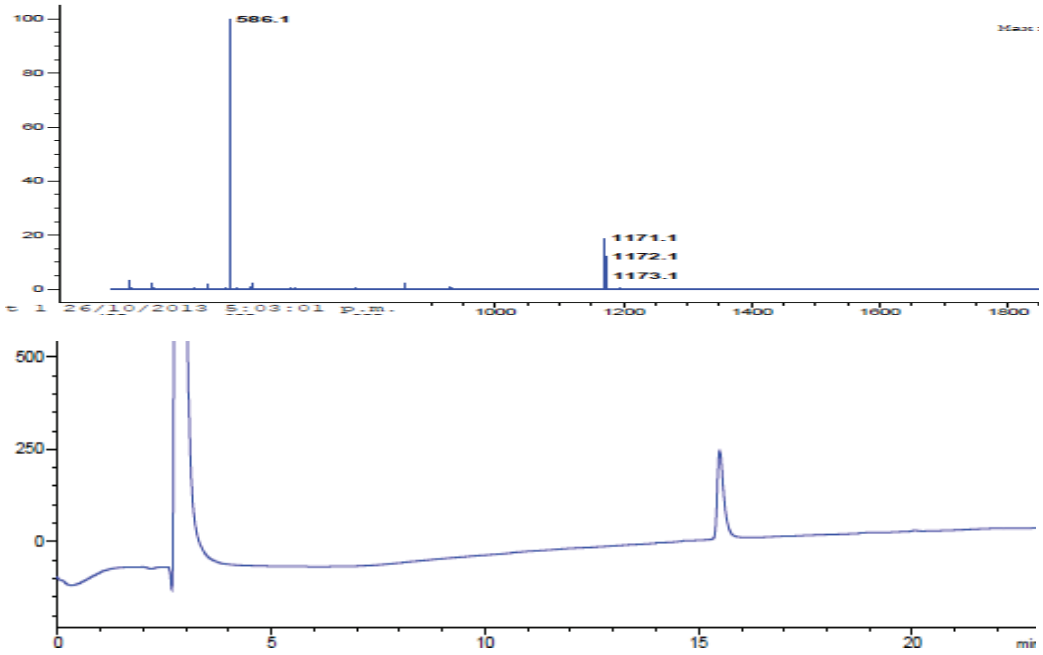

Figure 8.5: HPLC spectrum following purification for dendrimer **44**. R_t 15.5 min; ***m/z*** MS(ESI) 1171.3 ($[M + H]^+$ requires 1171.5).

Dendrimer 46

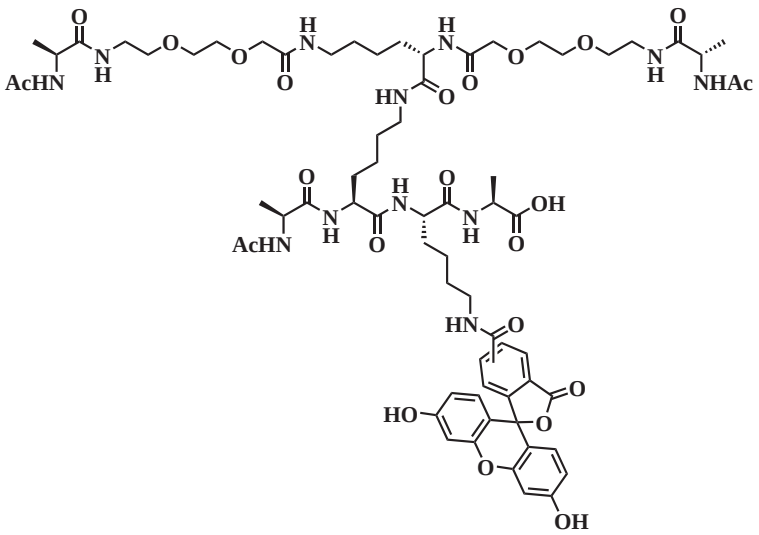

46

Resin **8** (50 μmol) was prepared as described (*Section 8.3.1*). Deprotection of the Fmoc group was carried out as described (*Section 8.3.2*). Fmoc–Lys(Mtt) was coupled (*8.4.1 method 1: using HCTU*) to afford **29**. After removal of the Fmoc group, Fmoc–Lys(Dde) was coupled (*Section 8.4.2 method 2: using HATU*) to give **30**. Fmoc group was removed, followed by coupling of Fmoc–Ala (*8.4.1 method 1: using HCTU*). Fmoc group was removed and the peptide chain was capped (*Section 8.4.7 method 7: using Ac_2O*) to prevent further growth. Dde group was cleaved (*Section 8.3.3*) and Fmoc–Lys(Fmoc) was installed (*8.4.1 method 1: using HCTU*). After double Fmoc group removal, the two exposed chains were grown in parallel by coupling Fmoc–mini–PEG (*Section 8.4.3 method 3: using HATU*). Fmoc groups were cleaved and Fmoc–Ala were coupled (*8.4.4 method 4: using HCTU*). Fmoc groups were removed and the peptide chain was capped (*Section 8.4.7 method 7: using Ac_2O*) to prevent further growth. The Mtt group was removed (*Section 8.3.4*) and 5(6)–carboxyfluorescein was coupled (*Section 8.4.8 method 8: using HOBt and DIC*). The dendrimer scaffold was cleaved from resin (*Section 8.5.3 method 11: using TFA*), lyophilised, then purified by HPLC to give the *title compound* **46** as an orange solid (36 mg, 49% isolated yield, 95% purity); R_t 15.5 min; ***m/z*** MS(ESI) 731.3 ($[M + 2H]^{2+}$ requires 731.3).

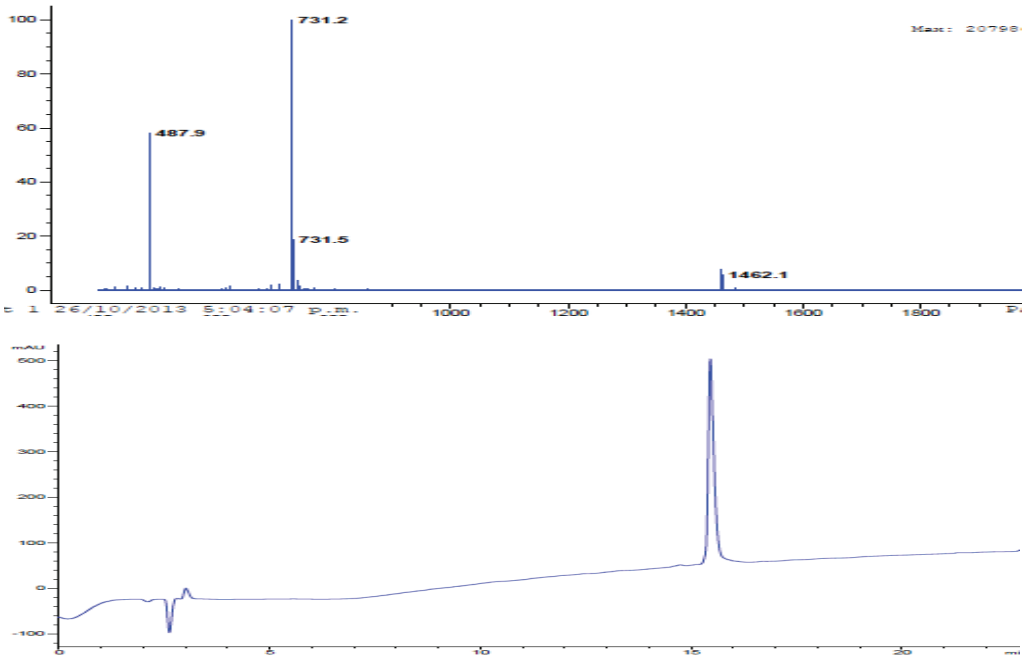

Figure 8.6: HPLC spectrum following purification for dendrimer **46**. R_t 15.5 min; ***m/z*** MS(ESI) 731.3 ($[M + 2H]^{2+}$ requires 731.3).

Dendrimer 48

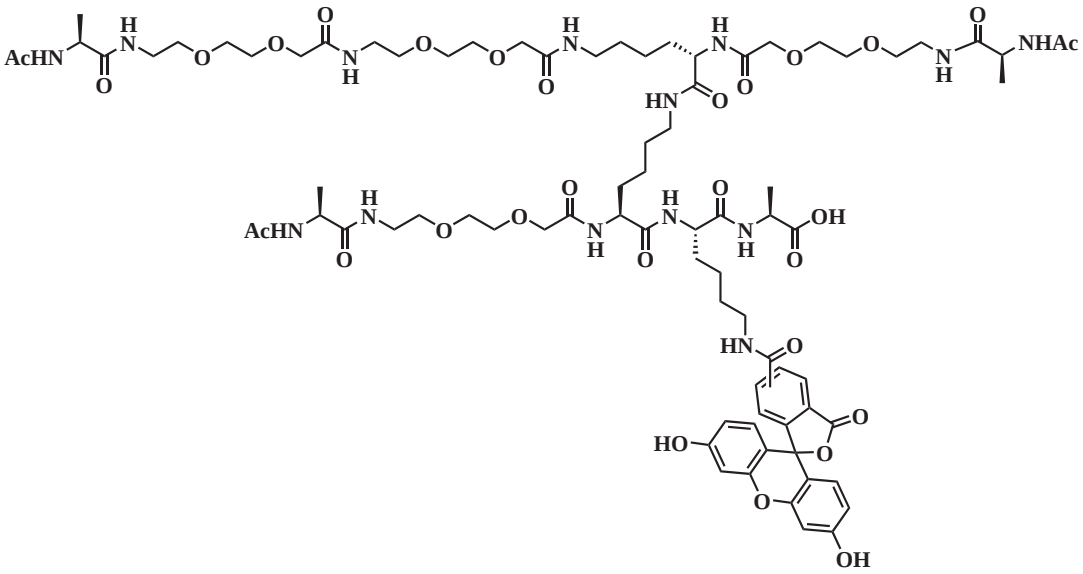

48

Resin **8** (50 μmol) was prepared as described (*Section 8.3.1*). Deprotection of the Fmoc group was carried out as described (*Section 8.3.2*). Fmoc–Lys(Mtt) was coupled (*8.4.1 method 1: using HCTU*) to afford **29**. After removal of the Fmoc group, Fmoc–Lys(Dde) was coupled (*Section 8.4.2 method 2: using HATU*) to give **30**. Fmoc group was removed, followed by coupling of Fmoc–mini–PEG (*Section 8.4.2 method 2: using HATU*). The mini–PEG was deprotected and Fmoc–Ala was coupled was installed (*8.4.1 method 1: using HCTU*). Fmoc group was removed and the peptide chain was capped (*Section 8.4.7 method 7: using Ac_2O*) to prevent further growth. Dde group was cleaved (*Section 8.3.3*) and Fmoc–Lys(Dde) was coupled (*Section 8.4.2 method 2: using HATU*). Fmoc group was removed, followed by coupling of Fmoc–mini–PEG (*Section 8.4.2 method 2: using HATU*). Fmoc group was removed and Fmoc–Ala was installed (*8.4.1 method 1: using HCTU*). Fmoc group was removed and the peptide chain was capped (*Section 8.4.7 method 7: using Ac_2O*) to prevent further growth. Dde group was cleaved (*Section 8.3.3*) and Fmoc group was removed, followed by coupling of Fmoc–mini–PEG (*Section 8.4.2 method 2: using HATU*). Fmoc group was removed and the next Fmoc–mini–PEG was installed on the chain (*Section 8.4.2 method 2: using HATU*). The mini–PEG was deprotected and the final Fmoc–Ala was installed (*8.4.1 method 1: using HCTU*). Fmoc group was removed and the peptide chain was capped (*Section 8.4.7 method 7: using Ac_2O*) to prevent further growth. The Mtt group was removed (*Section 8.3.4*) and 5(6)–carboxyfluorescein was coupled (*Section 8.4.8 method 8: using HOBt and DIC*). The dendrimer scaffold was cleaved from the resin (*Section 8.5.3 method 11: using TFA*), lyophilised, then purified by HPLC to give the *title compound* **48** as an orange solid (43 mg, 50% isolated yield, 94% purity); R_t 15.5 min; ***m/z*** MS(ESI) 876.5 ($[M + 2H]^{2+}$ requires 876.4).

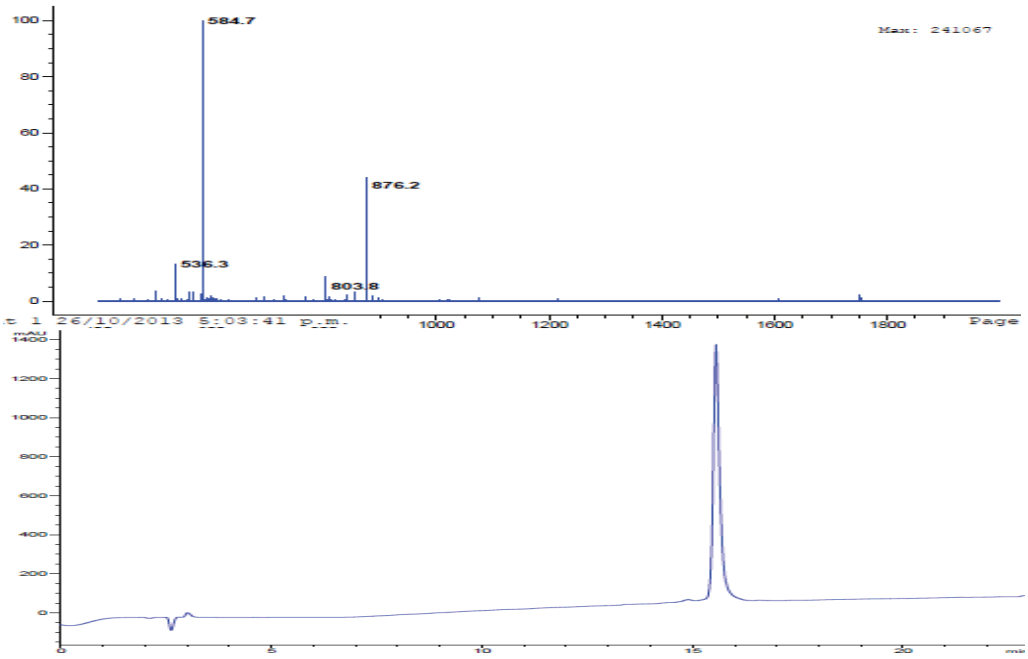

Figure 8.7: HPLC spectrum following purification for dendrimer **48**. R_t 15.5 min; ***m/z*** MS(ESI) 876.5 ($[M + 2H]^{2+}$ requires 876.4).

Dendrimer 50

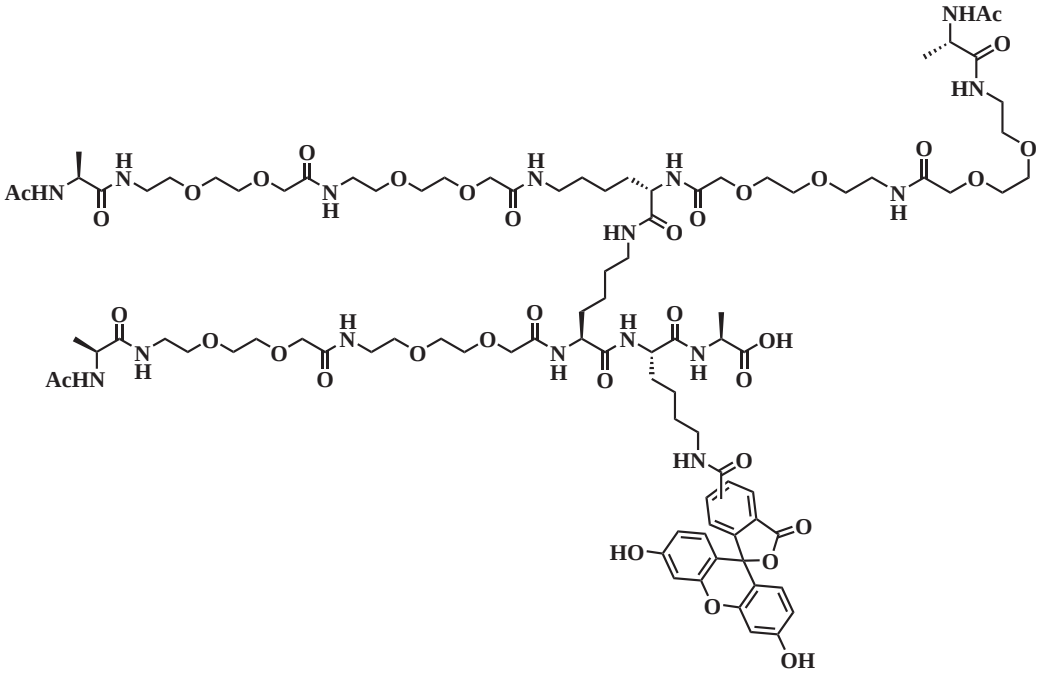

50

Resin **8** (50 μmol) was prepared as described (*Section 8.3.1*). Deprotection of the Fmoc group was carried out as described (*Section 8.3.2*). Fmoc–Lys(Mtt) was coupled (*8.4.1 method 1: using HCTU*) to afford **29**. After removal of the Fmoc group, Fmoc–Lys(Dde) was coupled (*Section 8.4.2 method 2: using HATU*) to give **30**. Fmoc group was removed, followed by coupling of Fmoc–mini–PEG (*Section 8.4.2 method 2: using HATU*). Fmoc group was removed, followed by coupling of Fmoc–mini–PEG (*Section 8.4.2 method 2: using HATU*). The mini–PEG was deprotected and Fmoc–Ala was installed (*8.4.1 method 1: using HCTU*). Fmoc group was removed and the peptide chain was capped (*Section 8.4.7 method 7: using Ac_2O*) to prevent further growth. Dde group was cleaved (*Section 8.3.3*) and Fmoc–Lys(Fmoc) was installed (*8.4.1 method 1: using HCTU*). After double Fmoc group removal, the two exposed chains were grown in parallel by coupling Fmoc–mini–PEG (*Section 8.4.3 method 3: using HATU*). The two chains were deprotected and the second Fmoc–mini–PEG spacer on each chain was installed (*Section 8.4.3 method 3: using HATU*). Fmoc groups were cleaved and Fmoc–Ala were coupled (*8.4.4 method 4: using HCTU*). Fmoc groups were removed and the peptide chains was capped (*Section 8.4.7 method 7: using Ac_2O*) to prevent further growth. The Mtt group was removed (*Section 8.3.4*) and 5(6)–carboxyfluorescein was coupled (*Section 8.4.8 method 8: using HOBt and DIC*). The dendrimer scaffold was cleaved from resin (*Section 8.5.3 method 11: using TFA*), lyophilised, then purified by HPLC to give the *title compound* **50** as an orange solid (39 mg, 38% isolated yield, 92% purity); R_t 15.5 min; ***m/z*** MS(ESI) 1021.7 ($[M + 2H]^{2+}$ requires 1021.5).

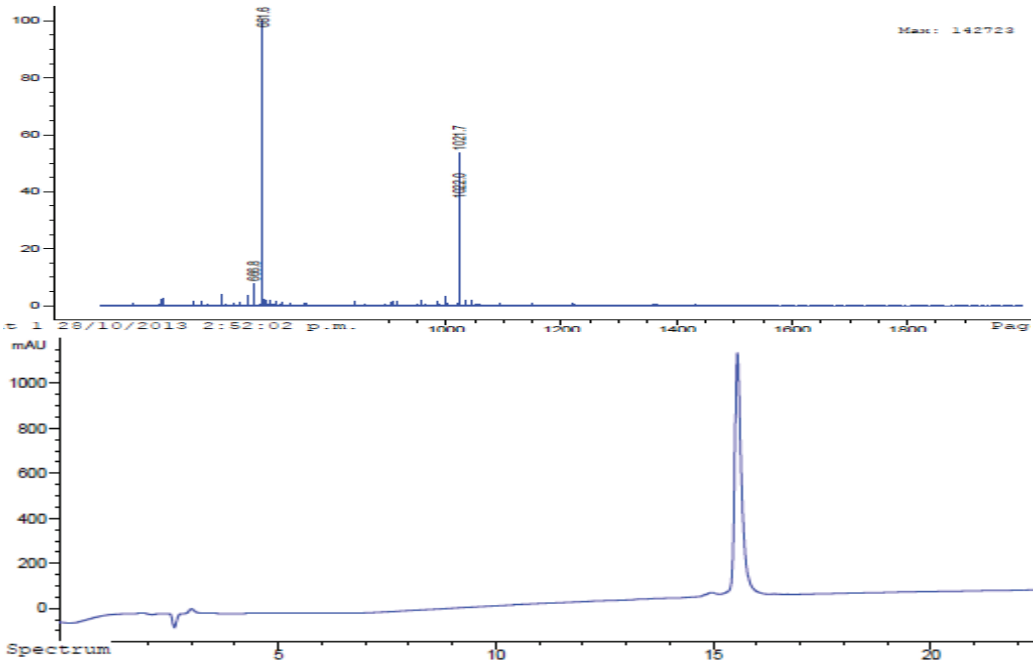

Figure 8.8: HPLC spectrum following purification for dendrimer **50**. R_t 15.5 min; ***m/z*** MS(ESI) 1021.7 ($[M + 2H]^{2+}$ requires 1021.5).

8.6.4 Generation III dendrimers

Dendrimer 52

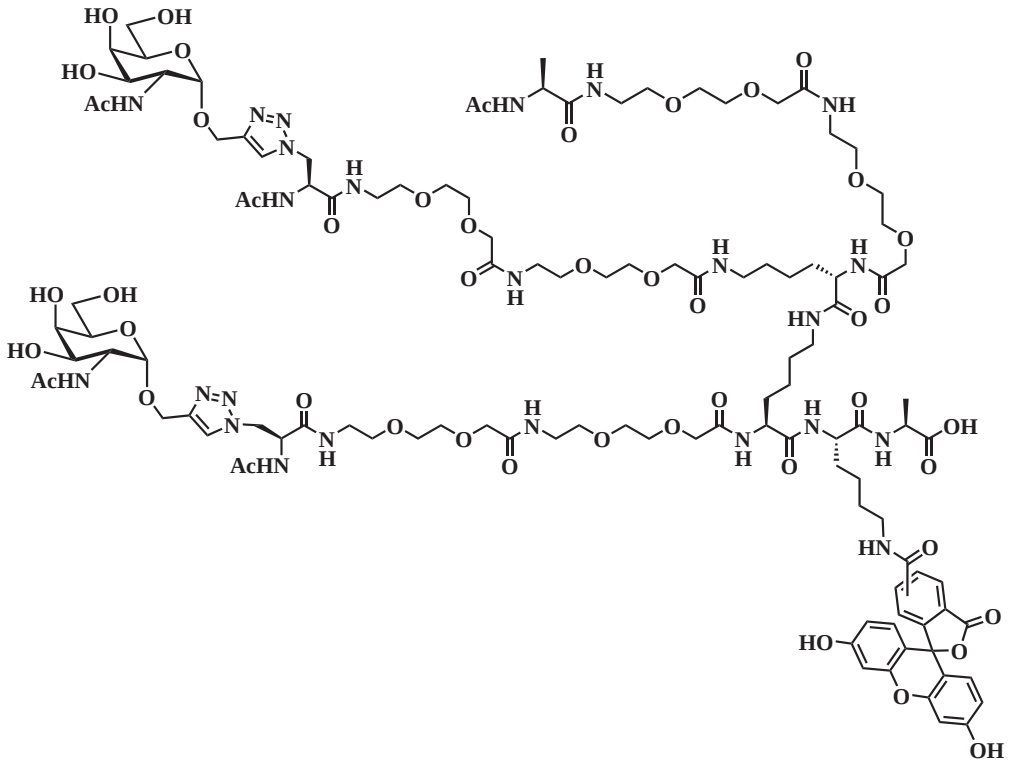

52

Resin **8** (50 μmol) was prepared as described (*Section 8.3.1*). Deprotection of the Fmoc group was carried out as described (*Section 8.3.2*). Fmoc–Lys(Mtt) was coupled (*8.4.1 method 1: using HCTU*) to afford **29**. After removal of the Fmoc group, Fmoc–Lys(Dde) was coupled (*Section 8.4.2 method 2: using HATU*) to give **30**. Fmoc group was removed, followed by coupling of Fmoc–mini–PEG (*Section 8.4.2 method 2: using HATU*). The mini–PEG was deprotected and was followed by coupling of Fmoc–mini–PEG (*Section 8.4.2 method 2: using HATU*). Removal of the Fmoc group was carried out using 20% pyridine in DMF, followed by coupling of the synthesised Fmoc–azidoalanine **9** (*Section 8.4.5 method 5: using HATU*). Fmoc group was removed and the peptide chain was capped (*Section 8.4.7 method 7: using Ac_2O*) to prevent further growth. Dde group was cleaved (*Section 8.3.3*) and Fmoc–Lys(Dde) was coupled (*Section 8.4.2 method 2: using HATU*). Fmoc group was removed, followed by coupling of Fmoc–mini–PEG (*Section 8.4.2 method 2: using HATU*). Fmoc group was removed, followed by coupling of Fmoc–mini–PEG (*Section 8.4.2 method 2: using HATU*). The mini–PEG was deprotected and Fmoc–Ala was installed (*8.4.1 method 1: using HCTU*). Fmoc group was removed and the peptide chain was capped (*Section 8.4.7 method 7: using Ac_2O*) to prevent further growth. Dde group was cleaved (*Section 8.3.3*) and Fmoc group was removed, followed by coupling of Fmoc–mini–PEG (*Section 8.4.2 method 2: using HATU*). Fmoc group was removed, followed by coupling of Fmoc–mini–PEG (*Section 8.4.2 method 2: using HATU*). Removal of the Fmoc group was

carried out using 20% pyridine in DMF, followed by coupling of the synthesised Fmoc–azidoalanine **9** (*Section 8.4.5 method 5: using HATU*). Fmoc group was removed and the peptide chain was capped (*Section 8.4.7 method 7: using Ac_2O*) to prevent further growth. The Mtt group was removed (*Section 8.3.4*) and 5(6)–carboxyfluorescein was coupled (*Section 8.4.8 method 8: using HOBt and DIC*). The dendrimer scaffold was cleaved from resin (*Section 8.5.1 method 9: using TFA*), and the crude scaffold was lyophilised (132 mg).

Propargyl GalNAc (**4**) (52 mg, 200 μmol) was dissolved in DMSO (11.27 mL) with dendrimer scaffold (132 mg) and was heated to 50 °C. A solution of sodium ascorbate (40 mg, 225 μmol) with $CuSO_4$ (125 mg, 500 μmol) in H_2O (5.63 mL) was heated to 50 °C for 10 min and then added to the DMSO solution. The click reaction was agitated for 2 h at 50 °C. The solution was diluted with H_2O and then purified by HPLC. The desired fractions were lyophilised to give the *title compound* **52** as an orange solid (3 mg, 2% isolated yield, 94% purity); R_t 14.0 min; ***m/z*** MS(ESI) 1321.6 ($[M + 2H]^2+$ requires 1321.6).

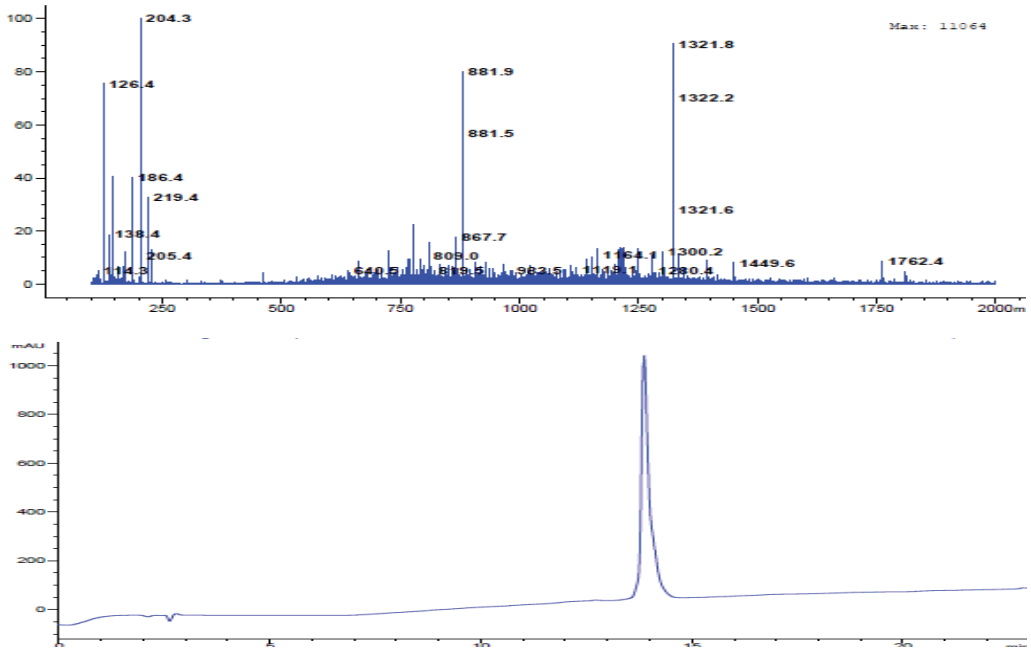

Figure 8.9: HPLC spectrum following purification for dendrimer **52**. R_t 14.0 min; ***m/z*** MS(ESI) 1321.6 ($[M + 2H]^2+$ requires 1321.6).

Dendrimer 54

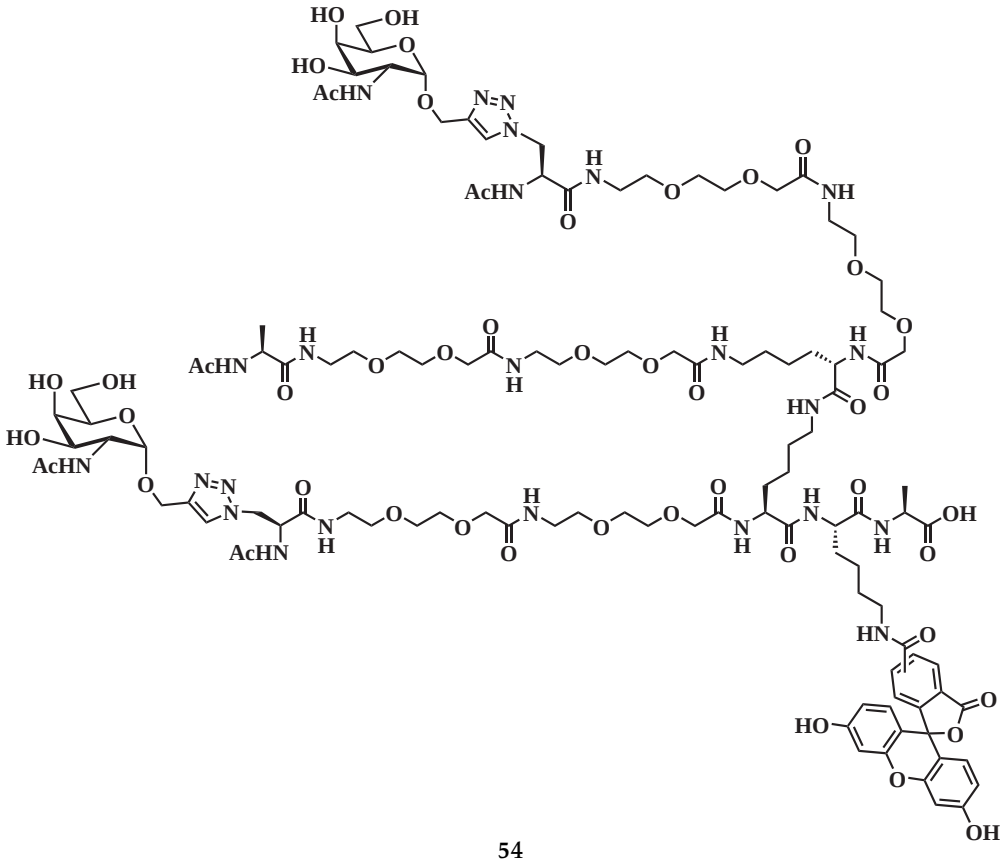

54

Resin **8** (50 μmol) was prepared as described (*Section 8.3.1*). Deprotection of the Fmoc group was carried out as described (*Section 8.3.2*). Fmoc–Lys(Mtt) was coupled (*8.4.1 method 1: using HCTU*) to afford **29**. After removal of the Fmoc group, Fmoc–Lys(Dde) was coupled (*Section 8.4.2 method 2: using HATU*) to give **30**. Fmoc group was removed, followed by coupling of Fmoc–mini–PEG (*Section 8.4.2 method 2: using HATU*). The mini–PEG was deprotected and the second Fmoc–mini–PEG group was coupled (*Section 8.4.2 method 2: using HATU*). Removal of the Fmoc group was carried out using 20% pyridine in DMF, followed by coupling of the synthesised Fmoc–azidoalanine **9** (*Section 8.4.5 method 5: using HATU*). Fmoc group was removed and the peptide chain was capped (*Section 8.4.7 method 7: using Ac_2O*) to prevent further growth. Dde group was cleaved (*Section 8.3.3*) and the FmocLys(Dde) was installed (*Section 8.4.2 method 2: using HATU*). Fmoc group was removed, followed by coupling of Fmoc–mini–PEG (*Section 8.4.2 method 2: using HATU*). Fmoc group was removed, followed by coupling of Fmoc–mini–PEG (*Section 8.4.2 method 2: using HATU*). Removal of the Fmoc group was carried out using 20% pyridine in DMF, followed by coupling of the synthesised Fmoc–azidoalanine **9** (*Section 8.4.5 method 5: using HATU*). Fmoc group was removed and the peptide chain was capped (*Section 8.4.7 method 7: using Ac_2O*) to prevent further growth. Dde group was cleaved (*Section 8.3.3*) and Fmoc–Lys(Dde) was coupled (*Section 8.4.2 method 2: using HATU*). Fmoc group was removed, followed by coupling of Fmoc–mini–PEG (*Section 8.4.2 method 2: using*

HATU). Fmoc group was removed, followed by coupling of Fmoc–mini–PEG (*Section 8.4.2 method 2: using HATU*). The mini–PEG group was deprotected and Fmoc–Ala was installed (*8.4.1 method 1: using HCTU*). Fmoc group was removed and the peptide chain was capped (*Section 8.4.7 method 7: using Ac_2O*) to prevent further growth. The Mtt group was removed (*Section 8.3.4*) and 5(6)–carboxyfluorescein was coupled (*Section 8.4.8 method 8: using HOBt and DIC*). The dendrimer scaffold was cleaved from resin (*Section 8.5.1 method 9: using TFA*) and the crude scaffold was lyophilised (154 mg).

Propargyl GalNAc (**4**) (52 mg, 200 μmol) was dissolved in DMSO (11.27 mL) with dendrimer scaffold (154 mg) and was heated to 50 °C. A solution of sodium ascorbate (40 mg, 225 μmol) with $CuSO_4$ (125 mg, 500 μmol) in H_2O (5.63 mL) was heated to 50 °C for 10 min and then added to the DMSO solution. The click reaction was heated for 2 h at 50 °C. The solution was diluted with H_2O and then purified by HPLC. The desired fractions were lyophilised to give the *title compound* **54** as an orange solid (8 mg, 6% isolated yield, 91% purity); R_t 15.5 min; ***m/z*** MS(ESI) 1321.6 ($[M + 2H]^{2+}$ requires 1321.6).

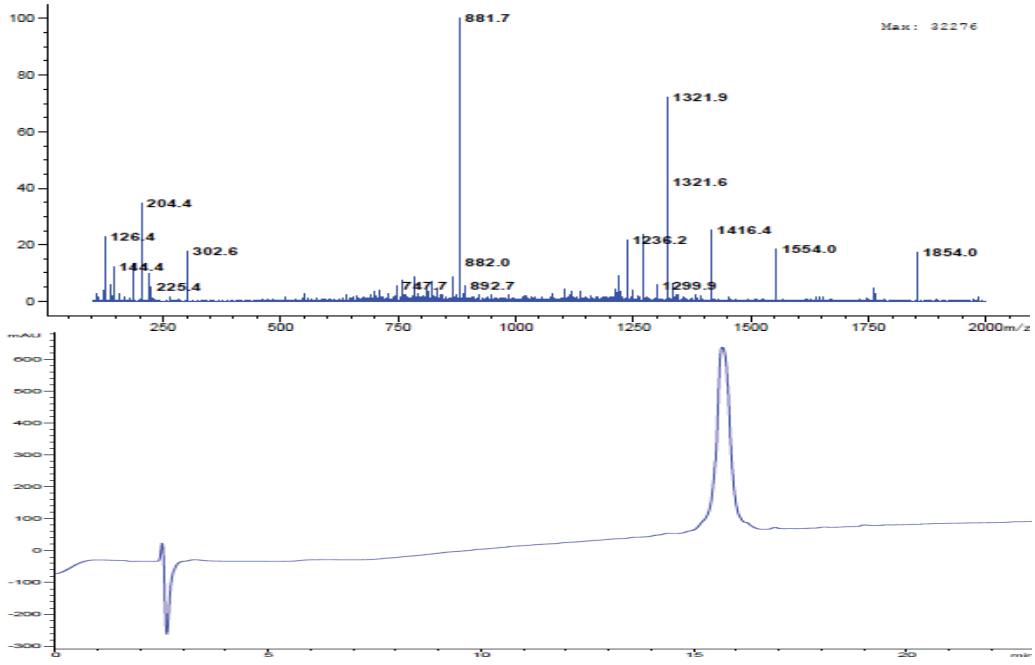

Figure 8.10: HPLC spectrum following purification for dendrimer **54**. R_t 15.5 min; ***m/z*** MS(ESI) 1321.6 ($[M + 2H]^{2+}$ requires 1321.6).

Dendrimer 56

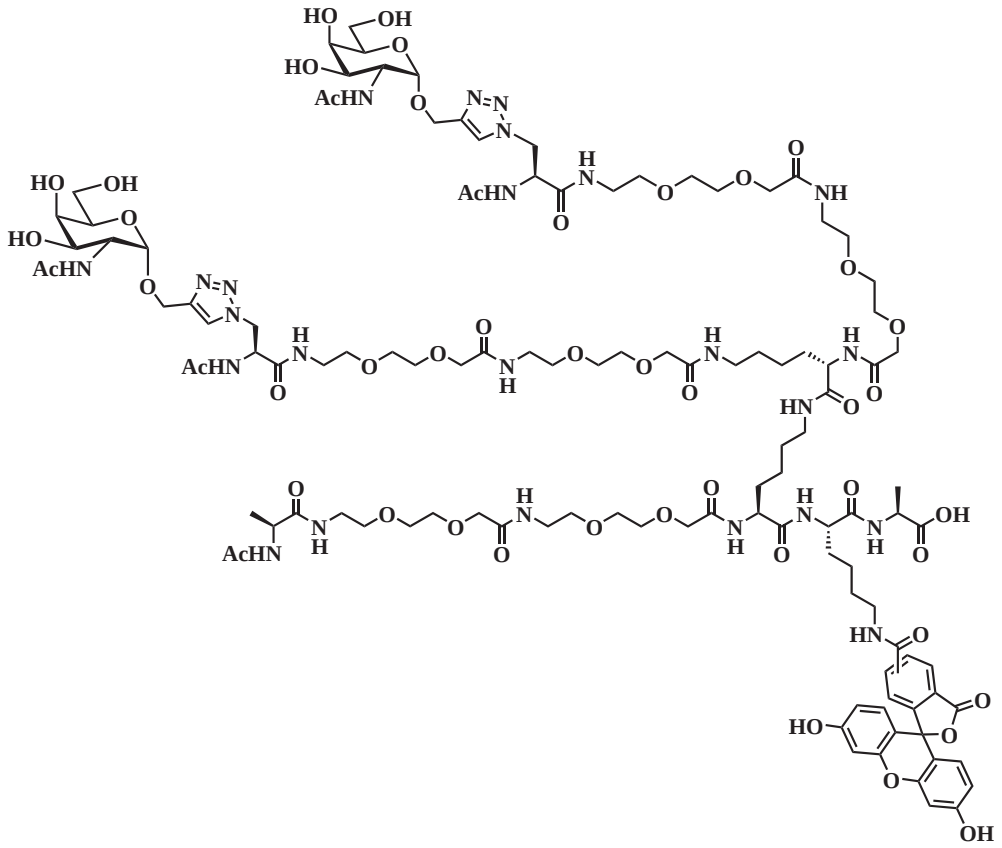

56

Resin **8** (50 μmol) was prepared as described (*Section 8.3.1*). Deprotection of the Fmoc group was carried out as described (*Section 8.3.2*). Fmoc–Lys(Mtt) was coupled (*8.4.1 method 1: using HCTU*) to afford **29**. After removal of the Fmoc group, Fmoc–Lys(Dde) was coupled (*Section 8.4.2 method 2: using HATU*) to give **30**. Fmoc group was removed, followed by coupling of Fmoc–mini–PEG (*Section 8.4.2 method 2: using HATU*). Fmoc group was removed, followed by coupling of Fmoc–mini–PEG (*Section 8.4.2 method 2: using HATU*). Fmoc was cleaved and Fmoc–Ala was installed (*8.4.1 method 1: using HCTU*). Fmoc group was removed and the peptide chain was capped (*Section 8.4.7 method 7: using Ac_2O*) to prevent further growth. Dde group was cleaved (*Section 8.3.3*) and Fmoc–Lys(Fmoc) was installed (*8.4.1 method 1: using HCTU*). After double Fmoc group removal, the two exposed chains were grown in parallel by coupling Fmoc–mini–PEG (*Section 8.4.3 method 3: using HATU*). The two chains were deprotected and the second Fmoc–mini–PEG spacer on each chain was installed (*Section 8.4.3 method 3: using HATU*). The mini–PEG were deprotected and Fmoc–azidoalanine **9** was coupled to the end of each chain (*8.4.6 method 6: using HATU*). Fmoc groups were removed and the peptide chains were capped (*Section 8.4.7 method 7: using Ac_2O*) to prevent further growth. The Mtt group was removed (*Section 8.3.4*) and 5(6)–carboxyfluorescein was coupled (*Section 8.4.8 method 8: using HOBt and DIC*). The dendrimer scaffold was cleaved from

resin (*Section 8.5.1 method 9: using TFA*) and the crude scaffold was lyophilised (21 mg).

Propargyl GalNAc (**4**) (10 mg, 39.5 μmol) was dissolved in DMSO (2.2 mL) with dendrimer scaffold (21 mg) and was heated to 50 °C. A solution of sodium ascorbate (7.8 mg, 44.5 μmol) with $CuSO_4$ (24.7 mg, 98.9 μmol) in H_2O (1.1 mL) was heated to 50 °C for 10 min and then added to the DMSO solution. The click reaction was agitated for 2 h at 50 °C. The solution was then diluted with H_2O and purified by HPLC. The desired fractions were lyophilised to give the *title compound* **56** as an orange solid (4 mg, 3% isolated yield, 93% purity); R_t 15.9 min; ***m/z*** MS(ESI) 1322.4 ($[M + 2H]^{2+}$ requires 1321.6).

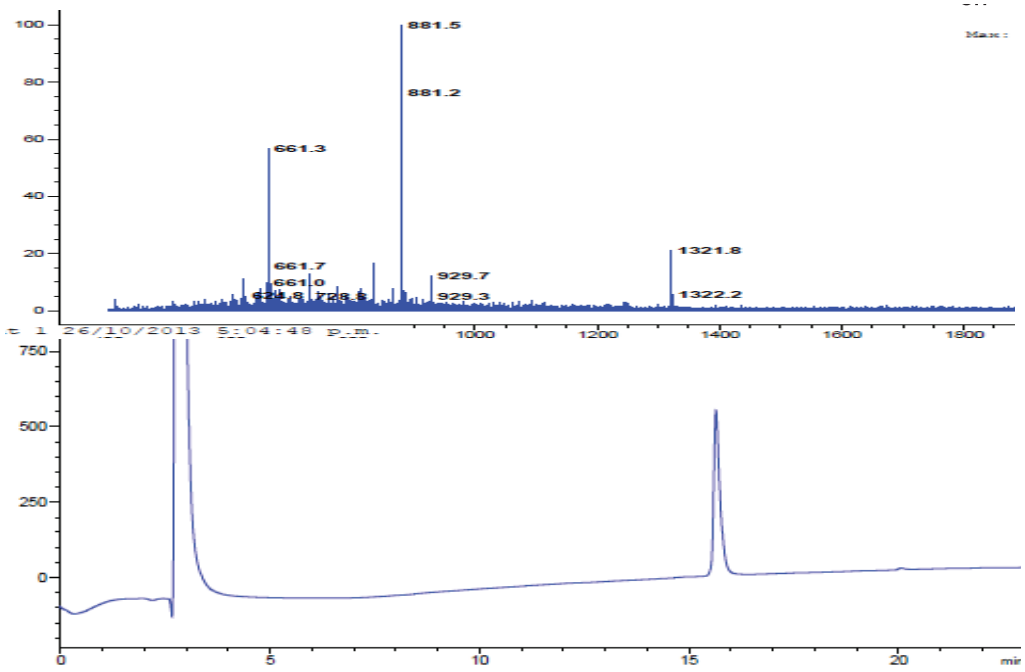

Figure 8.11: HPLC spectrum following purification for dendrimer **56**. R_t 15.9 min; ***m/z*** MS(ESI) 1322.4 ($[M + 2H]^{2+}$ requires 1321.6).

8.6.5 Generation IV dendrimers

Dendrimer 58

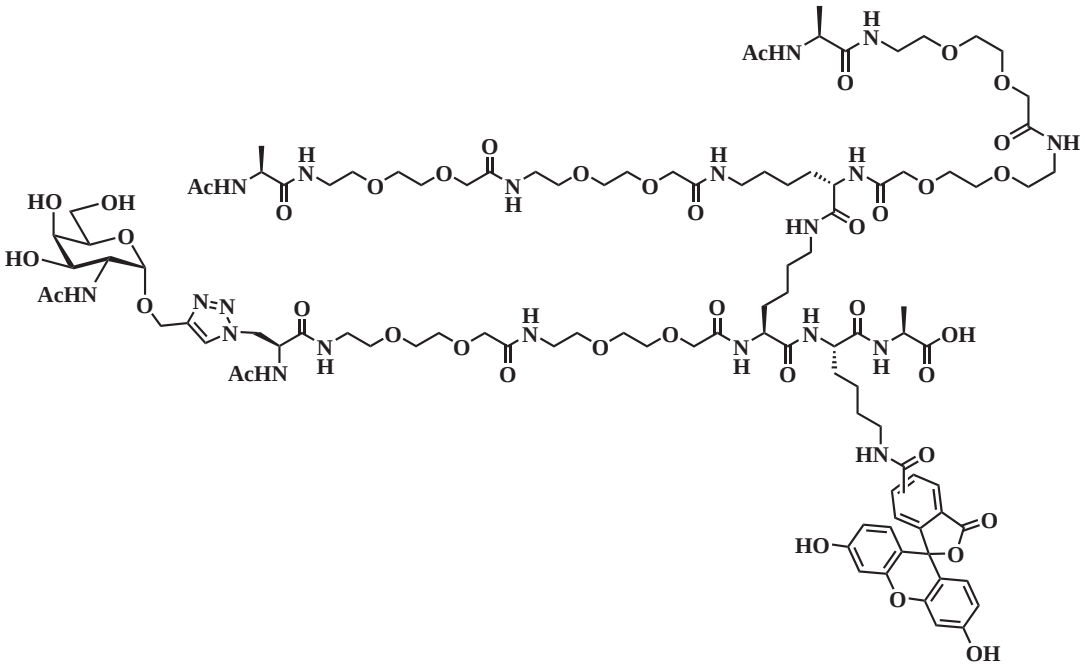

58

Resin **8** (50 μmol) was prepared as described (*Section 8.3.1*). Deprotection of the Fmoc group was carried out as described (*Section 8.3.2*). Fmoc–Lys(Mtt) was coupled (*8.4.1 method 1: using HCTU*) to afford **29**. After removal of the Fmoc group, Fmoc–Lys(Dde) was coupled (*Section 8.4.2 method 2: using HATU*) to give **30**. Fmoc group was removed, followed by coupling of Fmoc–mini–PEG (*Section 8.4.2 method 2: using HATU*). Fmoc group was removed, followed by coupling of Fmoc–mini–PEG (*Section 8.4.2 method 2: using HATU*). Removal of the Fmoc group was carried out using 20% pyridine in DMF, followed by coupling of the synthesised Fmoc–azidoalanine **9** (*Section 8.4.5 method 5: using HATU*). Fmoc group was removed and the peptide chain was capped (*Section 8.4.7 method 7: using Ac_2O*) to prevent further growth. Dde group was cleaved (*Section 8.3.3*) and Fmoc–Lys(Fmoc) was installed (*8.4.1 method 1: using HCTU*). After double Fmoc group removal, the two exposed chains were grown in parallel by coupling Fmoc–mini–PEG (*Section 8.4.3 method 3: using HATU*). The two chains were deprotected and the second Fmoc–mini–PEG spacer on each chain was installed (*Section 8.4.3 method 3: using HATU*). Fmoc groups were removed and Fmoc–Ala were coupled to each chain (*8.4.4 method 4: using HCTU*). Fmoc groups were removed and the peptide chains were capped (*Section 8.4.7 method 7: using Ac_2O*) to prevent further growth. The Mtt group was removed (*Section 8.3.4*) and 5(6)–carboxyfluorescein was coupled (*Section 8.4.8 method 8: using HOBt and DIC*). The dendrimer scaffold was cleaved from resin (*Section 8.5.1 method 9: using TFA*) and the crude scaffold was lyophilised (98 mg).

Propargyl GalNAc (**4**) (13 mg, 49.93 μmol) was dissolved in DMSO (5.54 mL) with dendrimer scaffold (98 mg) and was heated to 50 °C. A solution of sodium ascorbate (20 mg, 112 μmol) with $CuSO_4$ (62 mg, 240 μmol) in H_2O (2.77 mL) was heated to 50 °C for 10 min and then added to the DMSO solution. The click reaction was heated for 2 h at 50 °C. The solution was then diluted with H_2O and purified by HPLC. The desired fractions were lyophilised to give the *title compound* **58** as an orange solid (4 mg, 3% isolated yield, 91% purity); R_t 16.7 min; ***m/z*** MS(ESI) 1171.8 ($[M + 2H]^{2+}$ requires 1171.5).

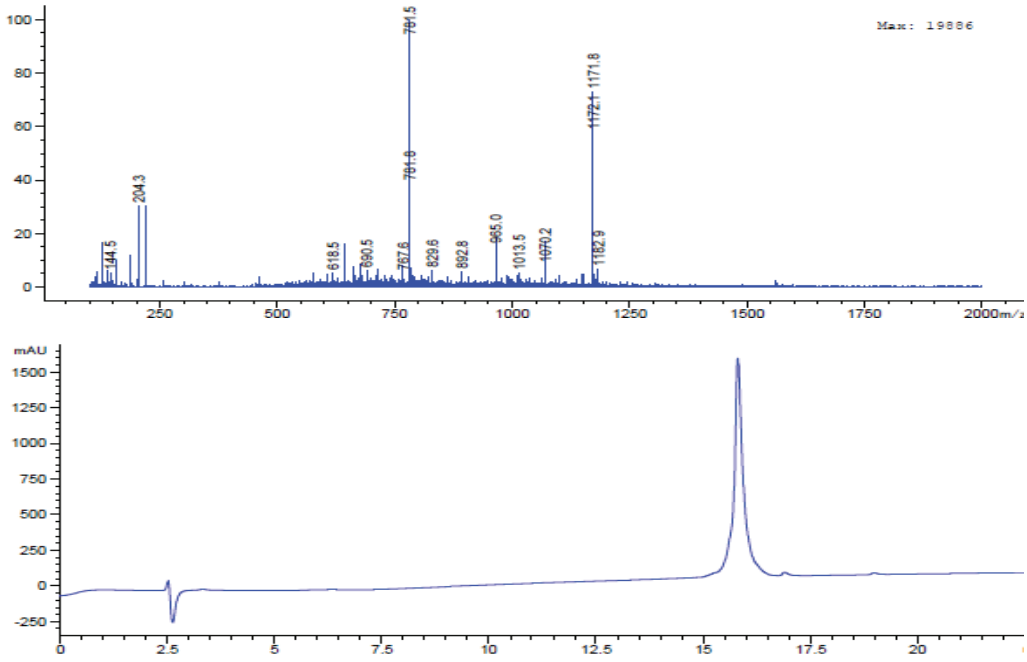

Figure 8.12: HPLC spectrum following purification for dendrimer **58**. R_t 16.7 min; ***m/z*** MS(ESI) 1171.8 ($[M + 2H]^{2+}$ requires 1171.5).

Dendrimer 60

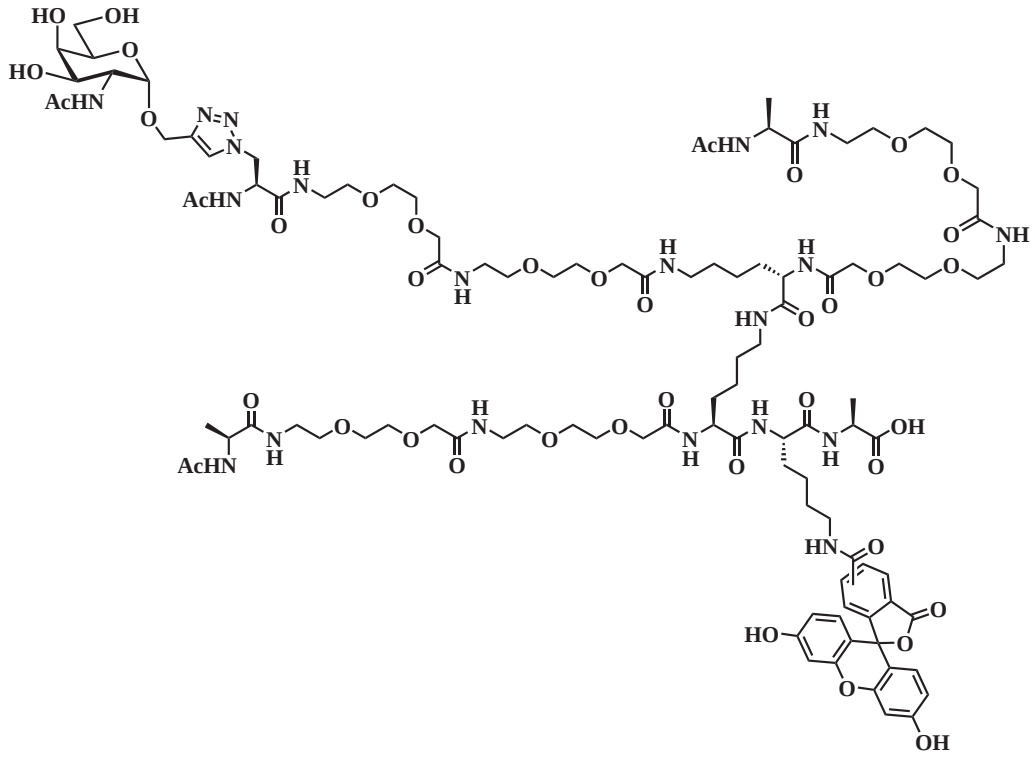

60

Resin **8** (50 μmol) was prepared as described (*Section 8.3.1*). Deprotection of the Fmoc group was carried out as described (*Section 8.3.2*). Fmoc–Lys(Mtt) was coupled (*8.4.1 method 1: using HCTU*) to afford **29**. After removal of the Fmoc group, Fmoc–Lys(Dde) was coupled (*Section 8.4.2 method 2: using HATU*) to give **30**. Fmoc group was removed, followed by coupling of Fmoc–mini–PEG (*Section 8.4.2 method 2: using HATU*). Fmoc group was removed, followed by coupling of Fmoc–mini–PEG (*Section 8.4.2 method 2: using HATU*). The mini–PEG was deprotected and Fmoc–Ala was installed (*8.4.1 method 1: using HCTU*). Fmoc group was removed and the peptide chain was capped (*Section 8.4.7 method 7: using Ac_2O*) to prevent further growth. Dde group was cleaved (*Section 8.3.3*) and Fmoc–Lys(Dde) was coupled (*Section 8.4.2 method 2: using HATU*). Fmoc group was removed, followed by coupling of Fmoc–mini–PEG (*Section 8.4.2 method 2: using HATU*). Fmoc group was removed, followed by coupling of Fmoc–mini–PEG (*Section 8.4.2 method 2: using HATU*). Fmoc group was removed and Fmoc–Ala was installed (*8.4.1 method 1: using HCTU*). Fmoc group was removed and the peptide chain was capped (*Section 8.4.7 method 7: using Ac_2O*) to prevent further growth. Dde group was cleaved (*Section 8.3.3*) and Fmoc group was removed, followed by coupling of Fmoc–mini–PEG (*Section 8.4.2 method 2: using HATU*). Fmoc group was removed, followed by coupling of Fmoc–mini–PEG (*Section 8.4.2 method 2: using HATU*). Removal of the Fmoc group was carried out using 20% pyridine in DMF, followed by coupling of the synthesised Fmoc–azidoalanine **9** (*Section 8.4.5 method 5: using HATU*). Fmoc group was removed and the peptide chain was capped

(*Section 8.4.7 method 7: using Ac_2O*) to prevent further growth. The Mtt group was removed (*Section 8.3.4*) and 5(6)–carboxyfluorescein was coupled (*Section 8.4.8 method 8: using HOBt and DIC*). The dendrimer scaffold was cleaved from resin (*Section 8.5.1 method 9: using TFA*) and the crude scaffold was lyophilised (117 mg).

Propargyl GalNAc (**4**) (25 mg, 98.9 μmol) was dissolved in DMSO (11.27 mL) with dendrimer scaffold (117 mg) and was heated to 50 °C. A solution of sodium ascorbate (40 mg, 225 μmol) with $CuSO_4$ (125 mg, 500 μmol) in H_2O (5.63 mL) was heated to 50 °C for 10 min and then added to the DMSO solution. The click reaction was heated for 2 h at 50 °C. The solution was diluted with H_2O and then purified by HPLC. The desired fractions were lyophilised to give the *title compound* **60** as an orange solid (10 mg, 9% isolated yield, 90% purity); R_t 15.3 min; ***m/z*** MS(ESI) 1171.6 ($[M + 2H]^{2+}$ requires 1171.6).

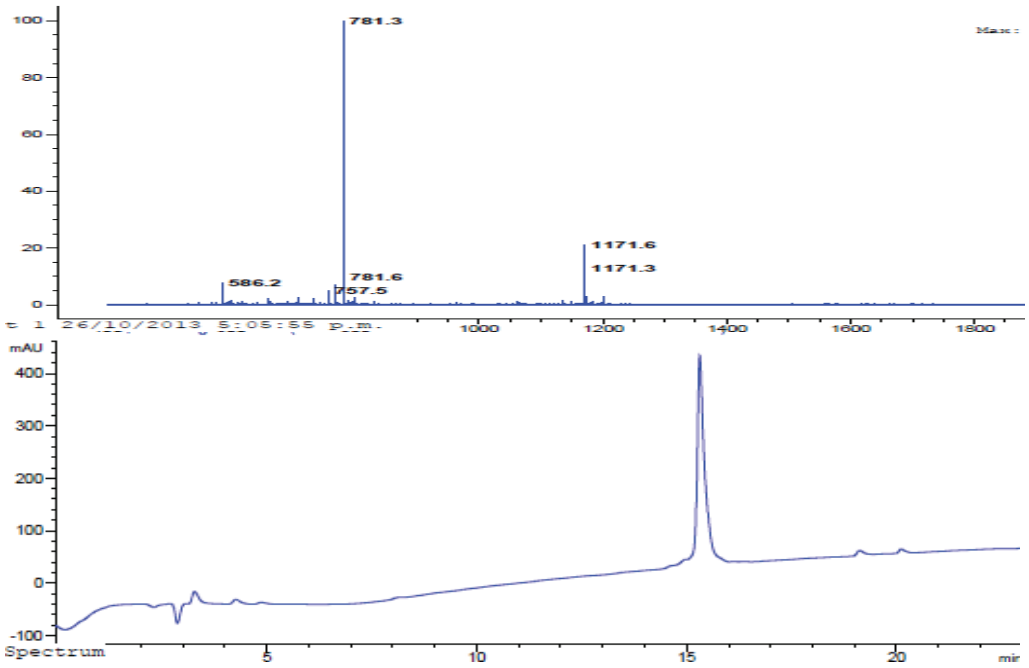

Figure 8.13: HPLC spectrum following purification for dendrimer **60**. R_t 15.3 min; ***m/z*** MS(ESI) 1171.6 ($[M + 2H]^{2+}$ requires 1171.6).

Dendrimer 62

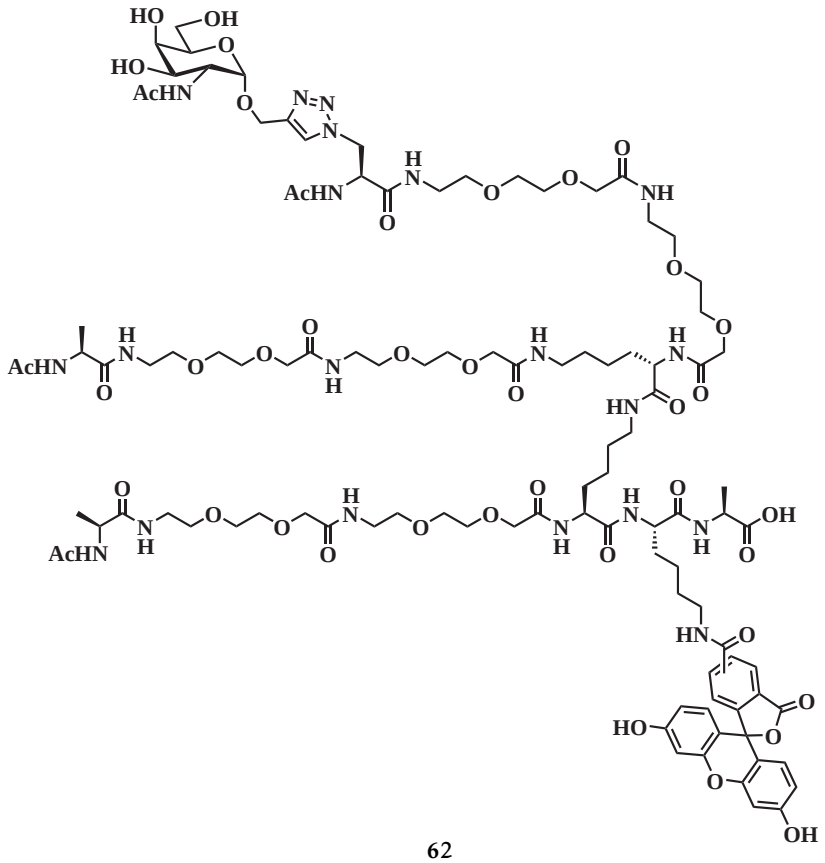

62

Resin **8** (50 μmol) was prepared as described (*Section 8.3.1*). Deprotection of the Fmoc group was carried out as described (*Section 8.3.2*). Fmoc–Lys(Mtt) was coupled (*8.4.1 method 1: using HCTU*) to afford **29**. After removal of the Fmoc group, Fmoc–Lys(Dde) was coupled (*Section 8.4.2 method 2: using HATU*) to give **30**. Fmoc group was removed, followed by coupling of Fmoc–mini–PEG (*Section 8.4.2 method 2: using HATU*). Fmoc group was removed, followed by coupling of Fmoc–mini–PEG (*Section 8.4.2 method 2: using HATU*). The mini–PEGs were deprotected and Fmoc–Ala was installed (*8.4.1 method 1: using HCTU*). Fmoc group was removed and the peptide chain was capped (*Section 8.4.7 method 7: using Ac_2O*) to prevent further growth. Dde group was cleaved (*Section 8.3.3*) and Fmoc–Lys(Dde) was coupled (*Section 8.4.2 method 2: using HATU*). Fmoc group was removed, followed by coupling of Fmoc–mini–PEG (*Section 8.4.2 method 2: using HATU*). The mini–PEG were deprotected and the second Fmoc–mini–PEG was installed (*8.4.2 method 2: using HATU*). Removal of the Fmoc group was carried out using 20% pyridine in DMF, followed by coupling of the synthesised Fmoc–azidoalanine **9** (*Section 8.4.5 method 5: using HATU*). Fmoc group was removed and the peptide chain was capped (*Section 8.4.7 method 7: using Ac_2O*) to prevent further growth. Dde group was cleaved (*Section 8.3.3*) and Fmoc–Lys(Dde) was coupled (*Section 8.4.2 method 2: using HATU*). Fmoc group was removed, followed by coupling of Fmoc–mini–PEG (*Section 8.4.2 method 2: using HATU*). Fmoc group was removed, followed by coupling of Fmoc–mini–PEG

(*Section 8.4.2 method 2: using HATU*). The mini–PEG group was deprotected and Fmoc–Ala was installed (*8.4.1 method 1: using HCTU*). Fmoc group was removed and the peptide chain was capped (*Section 8.4.7 method 7: using Ac_2O*) to prevent further growth. The Mtt group was removed (*Section 8.3.4*) and 5(6)–carboxyfluorescein was coupled (*Section 8.4.8 method 8: using HOBt and DIC*). The dendrimer scaffold was cleaved from resin (*Section 8.5.1 method 9: using TFA*) and the crude scaffold was lyophilised (103 mg).

Propargyl GalNAc (**4**) (25 mg, 98.9 μmol) was dissolved in DMSO (11.27 mL) with dendrimer scaffold (103 mg) and was heated to 50 °C. A solution of sodium ascorbate (40 mg, 225 μmol) with $CuSO_4$ (125 mg, 500 μmol) in H_2O (5.63 mL) was heated to 50 °C for 10 min and then added to the DMSO solution. The click reaction was agitated for 2 h at 50 °C. The solution was diluted with water and then purified by HPLC. The desired fractions were lyophilised to give the *title compound* **62** as an orange solid (10 mg, 9% isolated yield, 95% purity); R_t 13.0 min; ***m/z*** MS(ESI) 1171.6 ($[M + 2H]^{2+}$ requires 1171.5).

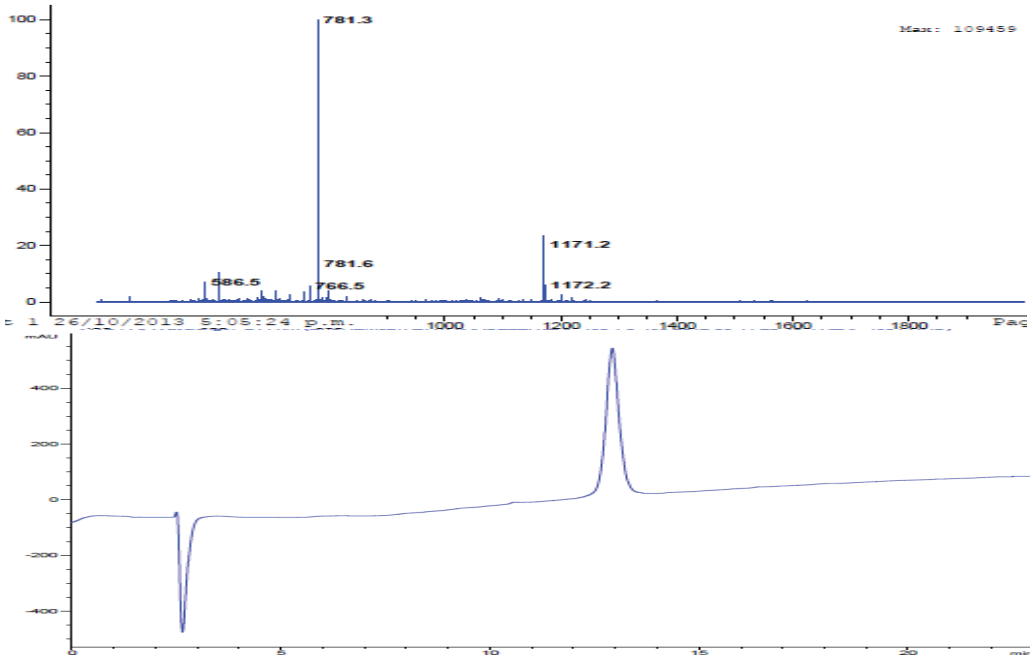

Figure 8.14: HPLC spectrum following purification for dendrimer **62**. R_t 13.0 min; ***m/z*** MS(ESI) 1171.6 ($[M + 2H]^{2+}$ requires 1171.5).

8.6.6 Generation V peptides

Peptide 64

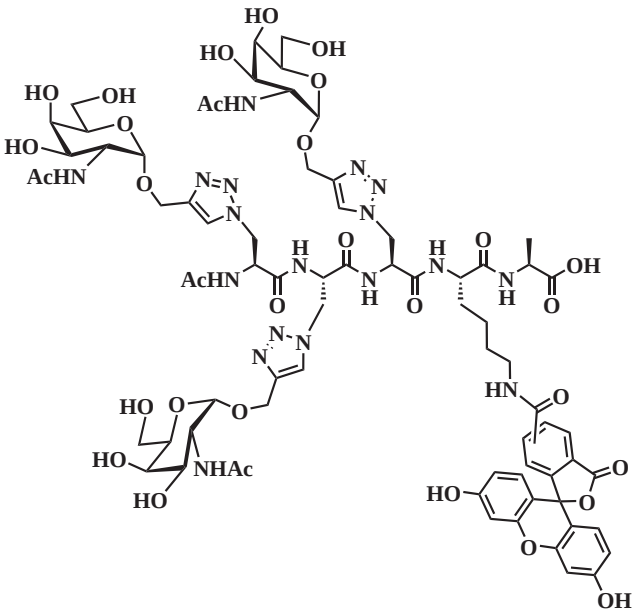

64

Resin **8** (50 μmol) was prepared as described (*Section 8.3.1*), to this Fmoc–Lys(Mtt) was coupled using (*8.4.1 method 1: using HCTU*). Fmoc group was cleaved and Fmoc–azidoalanine **9** was coupled using was coupled (*8.4.2 method 2: using HATU*). The terminal Fmoc group was removed and the second Fmoc–azidoalanine **9** was coupled (*8.4.2 method 2: using HATU*). Fmoc group was removed and the final Fmoc–azidoalanine **9** was installed (*8.4.2 method 2: using HATU*). Fmoc group was removed and the peptide chain was capped (*Section 8.4.7 method 7: using Ac_2O*) to prevent further growth. The Mtt group was removed (*Section 8.3.4*) and 5(6)–carboxyfluorescein was coupled (*Section 8.4.8 method 8: using HOBt and DIC*). The peptide scaffold was cleaved from resin (*Section 8.5.1 method 9: using TFA*) and the crude scaffold was lyophilised, then purified by HPLC (8.0 mg).

Propargyl GalNAc (**4**) (1 mg, 4.20 μmol) was dissolved in DMSO (220 μL) with the peptide scaffold (1 mg) and was heated to 50 °C. A solution of sodium ascorbate (1 mg, 4.9 μmol) with $CuSO_4$ (2.6 mg, 10 μmol) in H_2O (110 μL) was heated to 50 °C for 10 min and then added to the DMSO solution. The click reaction was heated for 2 h at 50 °C. The solution was diluted with H_2O and then purified by HPLC. The desired fractions were lyophilised to give the *title compound* **64** as an orange solid (0.5 mg, 28% isolated yield, 92% purity); R_t 12.5 min; ***m/z*** MS(ESI)) 866.2 ($[M + 2H]^{2+}$ requires 866.3).

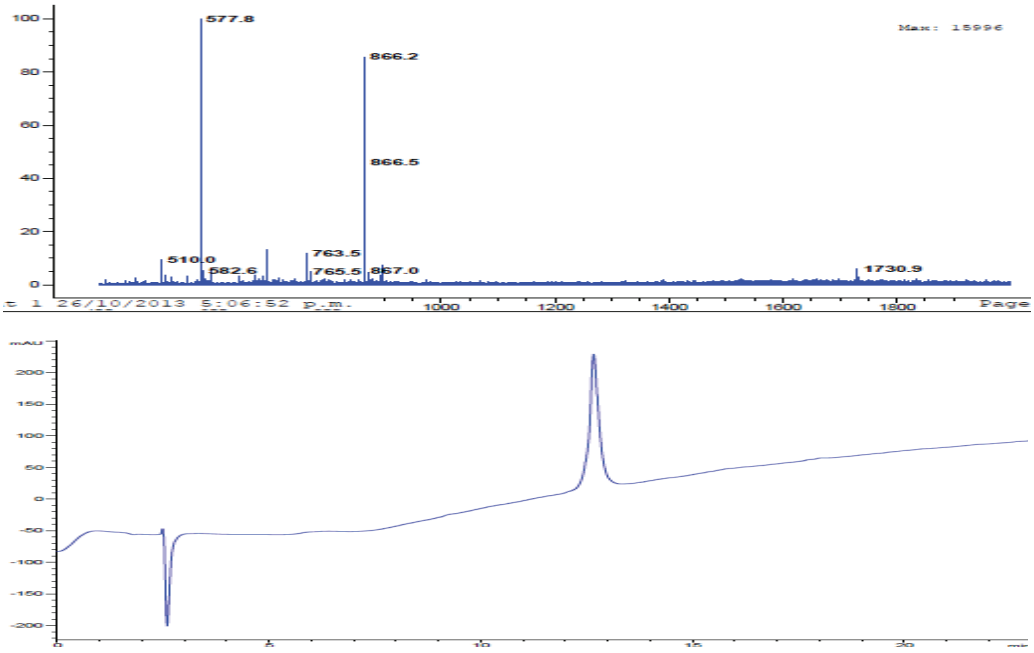

Figure 8.15: HPLC spectrum following purification for peptide **64**. R_t 12.5 min; ***m/z*** MS(ESI)) 866.2 ($[M + 2H]^{2+}$ requires 866.3).

Peptide 65

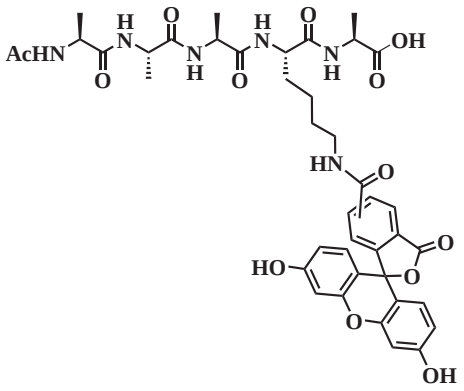

65

Resin **8** (50 μmol) was prepared as described (*Section 8.3.1*), to this Fmoc–Lys(Dde) was coupled (*8.4.2 method 2: using HATU*). Fmoc group was removed and Fmoc–Ala was installed (*8.4.1 method 1: using HCTU*). Fmoc group was removed and the second Fmoc–Ala was coupled (*8.4.1 method 1: using HCTU*). Fmoc group was cleaved and the final Fmoc–Ala was installed (*8.4.1 method 1: using HCTU*). Fmoc group was removed and the peptide chain was capped (*Section 8.4.7 method 7: using Ac_2O*) to prevent further growth. Dde group was cleaved (*Section 8.3.3*) and 5(6)–carboxyfluorescein was coupled (*Section 8.4.8 method 8: using HOBt and DIC*). The peptide scaffold was cleaved from the resin (*Section 8.5.3 method 11: using TFA*), lyophilised, then purified by HPLC to give the *title compound* **65** as an orange solid (13 mg, 31% isolated yield, 92% purity); R_t 17.5 min; ***m/z*** MS(ESI) 831.6 ($[M + H]^+$ requires 831.3).

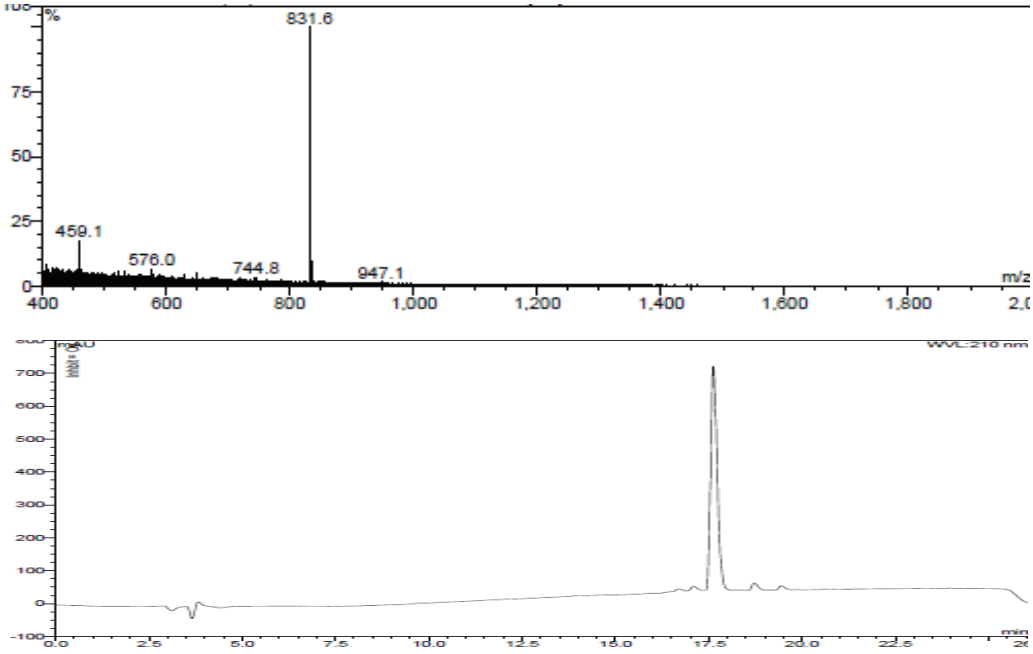

Figure 8.16: HPLC spectrum following purification for peptide **65**. R_t 17.5 min; ***m/z*** MS(ESI) 831.6 ($[M + H]^+$ requires 831.3).

8.6.7 Triazole negative control analogues

Peptide 66

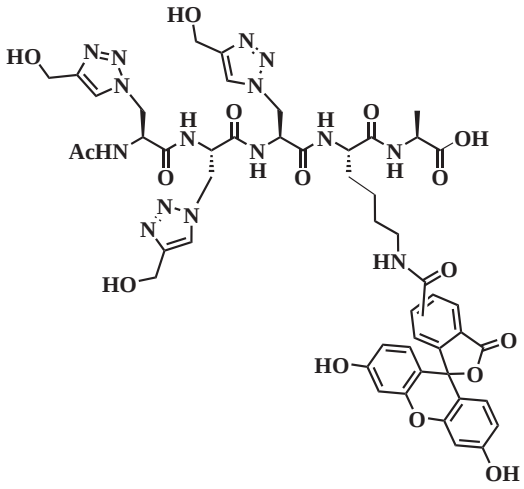

66

Resin **8** (50 μmol) was prepared as described (*Section 8.3.1*). to this Fmoc–Lys(Dde) was coupled (*8.4.2 method 2: using HATU*) to give **30**. Fmoc group was cleaved and Fmoc–azidoalanine **9** was coupled (*8.4.2 method 2: using HATU*). The terminal Fmoc group was removed and the second Fmoc–azidoalanine **9** was coupled (*8.4.2 method 2: using HATU*). Fmoc group was removed and the final Fmoc–azidoalanine **9** was coupled (*8.4.2 method 2: using HATU*). Fmoc group was removed and the peptide chain was capped (*Section 8.4.7 method 7: using Ac_2O*) to prevent further growth. Dde group was cleaved (*Section 8.3.3*) and 5(6)–carboxyfluorescein was coupled (*Section 8.4.8 method 8: using HOBt and DIC*). The peptide scaffold was cleaved from resin (*Section 8.5.1 method 9: using TFA*) and the crude scaffold was lyophilised to give the crude peptide (95 mg).

Propargyl alcohol (17 μL, 310 μmol) and dendrimer scaffold (75 mg) were dissolved in DMSO (16 mL) and was heated to 50 °C. A solution of sodium ascorbate (126 mg, 708 μmol) with $CuSO_4$ (392 mg, 4.5 mmol) in H_2O (8 mL) was heated to 50 °C for 10 min and then added to the DMSO solution. The click reaction was heated for 2 h at 50 °C. The solution was diluted with H_2O and then purified by HPLC. The desired fractions were lyophilised to give the *title compound* **66** as an orange solid (5 mg, 9% isolated yield, 95% purity); R_t 15.3 min; ***m/z*** MS(ESI) 1121.9 ($[M + H]^+$ requires 1122.4).

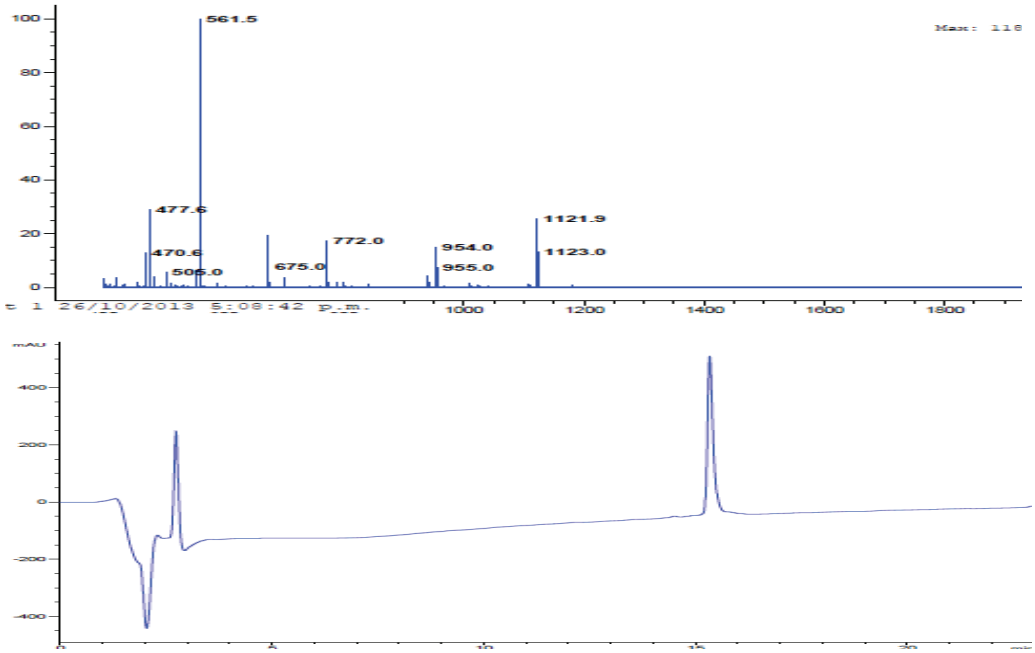

Figure 8.17: HPLC spectrum following purification for peptide **66**. R_t 15.3 min; ***m/z*** MS(ESI) 1121.9 ($[M + H]^+$ requires 1122.4).

Dendrimer 68

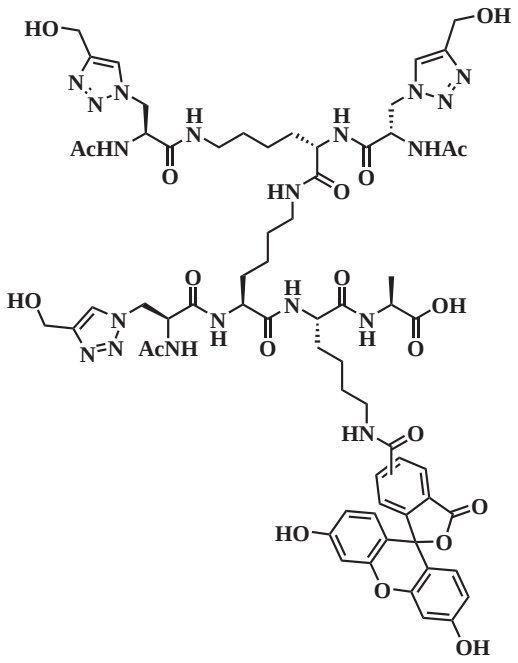

68

Resin **8** (50 μmol) was prepared as described (*Section 8.3.1*). Deprotection of the Fmoc group was carried out as described (*Section 8.3.2*). Fmoc–Lys(Mtt) was coupled (*8.4.1 method 1: using HCTU*) to afford **29**. After removal of the Fmoc group, Fmoc–Lys(Dde) was coupled (*Section 8.4.2 method 2: using HATU*) to give **30**. Removal of the Fmoc group was carried out using 20% pyridine in DMF, followed by coupling of the synthesised Fmoc–azidoalanine **9** (*Section 8.4.5 method 5: using HATU*). Fmoc group was removed and the peptide chain was capped (*Section 8.4.7 method 7: using Ac_2O*) to prevent further growth. Dde group was cleaved (*Section 8.3.3*) and Fmoc–Lys(Fmoc) was installed (*8.4.1 method 1: using HCTU*). The two Fmoc groups on the scaffold were removed and the two exposed chains were grown in parallel by coupling one Fmoc–azidoalanine **9** to the end of each chain (*8.4.6 method 6: using HATU*). Fmoc groups were removed and the peptide chains were capped (*Section 8.4.7 method 7: using Ac_2O*) to prevent further growth. The Mtt group was removed (*Section 8.3.4*) and 5(6)–carboxyfluorescein was coupled (*Section 8.4.8 method 8: using HOBt and DIC*). The dendrimer scaffold was cleaved from resin (*Section 8.5.1 method 9: using TFA*), lyophilised, then purified by HPLC (19.0 mg).

Propargyl alcohol (1 μL, 28 μmol) and dendrimer scaffold (9 mg) were dissolved in DMSO (1.62 mL) and the mixture was heated to 50 °C. A solution of sodium ascorbate (11 mg, 63 μmol) with $CuSO_4$ (34 mg, 139 μmol) in H_2O (810 μL) was heated to 50 °C for 10 min and then added to the DMSO solution. The click reaction was heated for 2 h at 50 °C. The solution was diluted with H_2O and then purified by HPLC. The desired fractions were lyophilised to give the *title compound* **68**

as an orange solid (1 mg, 9.8% isolated yield, 90% purity); R_t 13.8 min; ***m/z*** MS(ESI) 731.9 ($[M + H]^+$ requires 731.8).

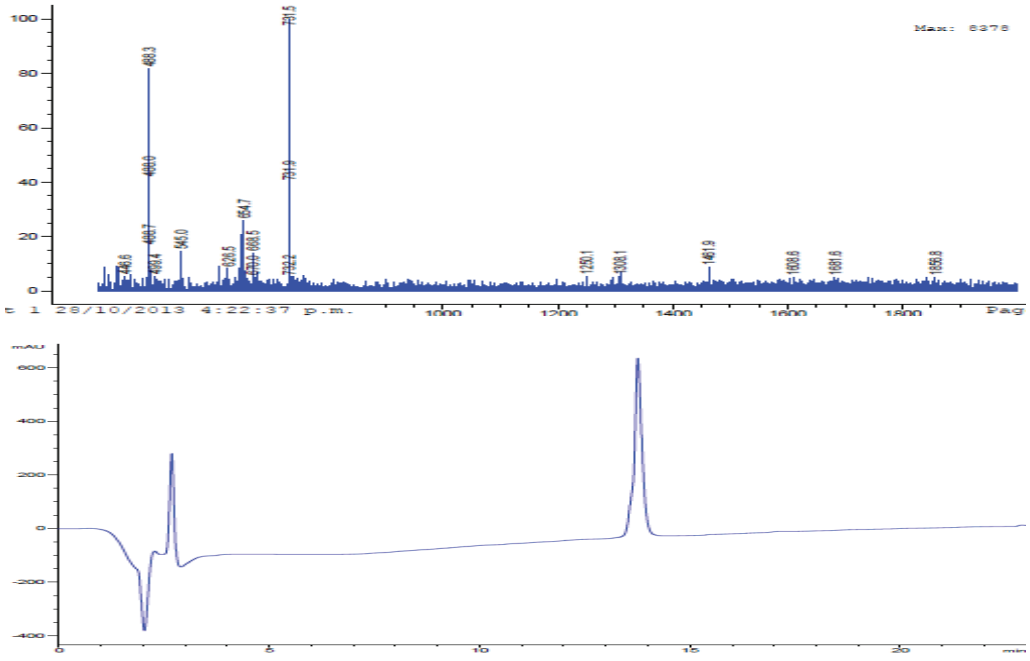

Figure 8.18: HPLC spectrum following purification for dendrimer **68**. R_t 13.8 min; ***m/z*** MS(ESI) 731.9 ($[M + H]^+$ requires 731.8).

8.6.8 Dendrimers and peptides for the thermal melt assay

All of the following compounds were made in parallel with the equivalent dendrimer for the cell binding assay. The difference between the ligands in this section was that they do not contain a fluorophore, as it was not necessary for the thermal melt assay.

8.6.9 Generation I dendrimer

Dendrimer 21

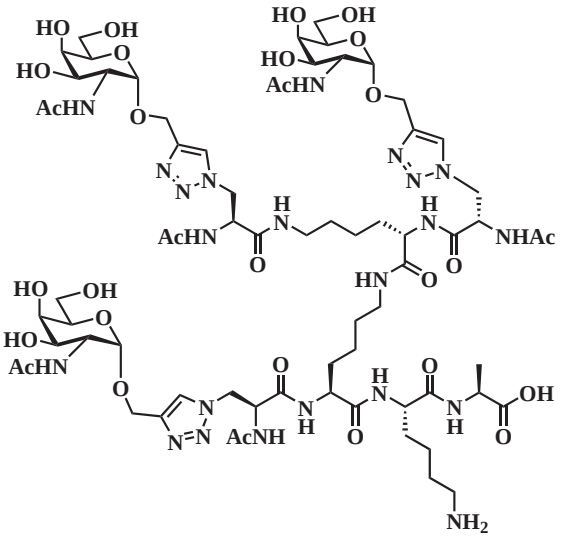

21

Resin **8** (50 μmol) was prepared as described (*Section 8.3.1*). Deprotection of the Fmoc group was carried out as described (*Section 8.3.2*). Fmoc–Lys(Mtt) was coupled (*8.4.1 method 1: using HCTU*) to afford **29**. After removal of the Fmoc group, Fmoc–Lys(Dde) was coupled (*Section 8.4.2 method 2: using HATU*) to give **30**. Removal of the Fmoc group was carried out using 20% pyridine in DMF, followed by coupling of the synthesised Fmoc–azidoalanine **9** (*Section 8.4.5 method 5: using HATU*). Fmoc group was removed and the peptide chain was capped (*Section 8.4.7 method 7: using Ac_2O*) to prevent further growth and afford **7**. Dde group was cleaved (*Section 8.3.3*) and Fmoc–Lys(Fmoc) was installed (*8.4.1 method 1: using HCTU*). The two Fmoc groups were removed and the two exposed chains were grown in parallel by coupling one Fmoc–azidoalanine **9** to the end of each chain (*8.4.6 method 6: using HATU*). Fmoc group was removed and the peptide chain was capped (*Section 8.4.7 method 7: using Ac_2O*) to prevent further growth. The dendrimer scaffold was cleaved from the resin (*Section 8.5.2 method 10: using TFA*), lyophilised, then purified by HPLC (5.5 mg).

Propargyl GalNAc (**4**) (15 mg, 59.2 μmol) was dissolved in DMSO (1.17 mL) with dendrimer scaffold (5.5 mg) and was heated to 50 °C. A solution of sodium ascorbate (4.2 mg, 24.3 μmol) with $CuSO_4$ (13 mg, 54 μmol) in H_2O (585 μL) was heated to 50 °C for 10 min and then added to the DMSO solution. The click reaction was heated for 2 h at 50 °C. The solution was diluted with H_2O and then purified by HPLC. The desired fractions were lyophilised to give the *title compound* **21** as a white solid (5.3 mg, 6% isolated yield, 95% purity); R_t 13.9 min; ***m/z*** MS(ESI) 857.4 ($[M + 2H]^{2+}$ requires 857.4).

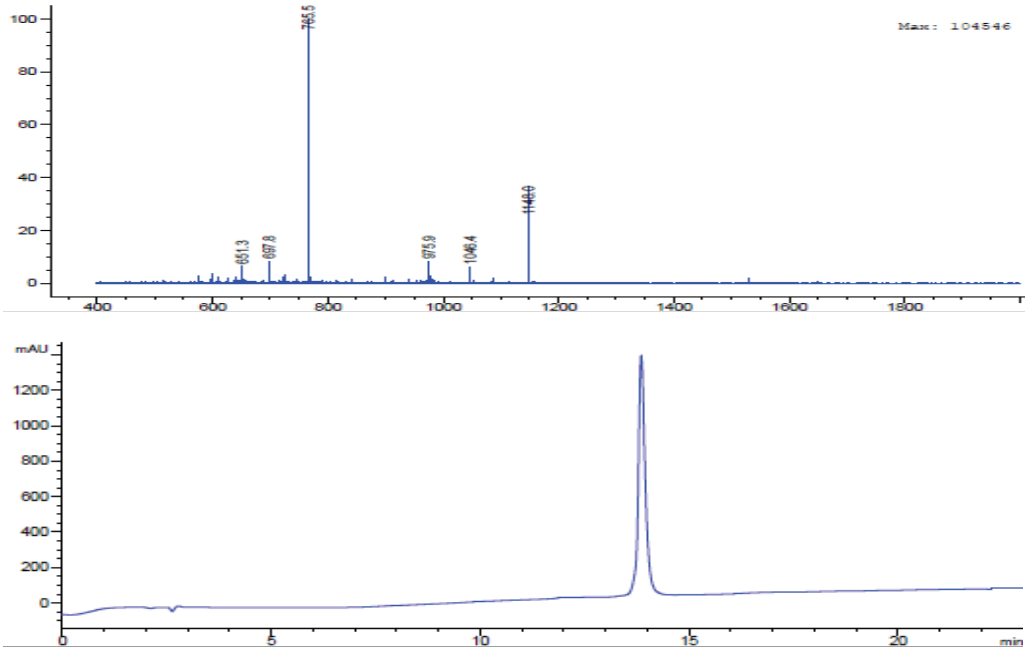

Figure 8.19: HPLC spectrum following purification for dendrimer **21**. R_t 13.9 min; ***m/z*** MS(ESI) 857.4 ($[M + 2H]^{2+}$ requires 857.4).

Dendrimer 2

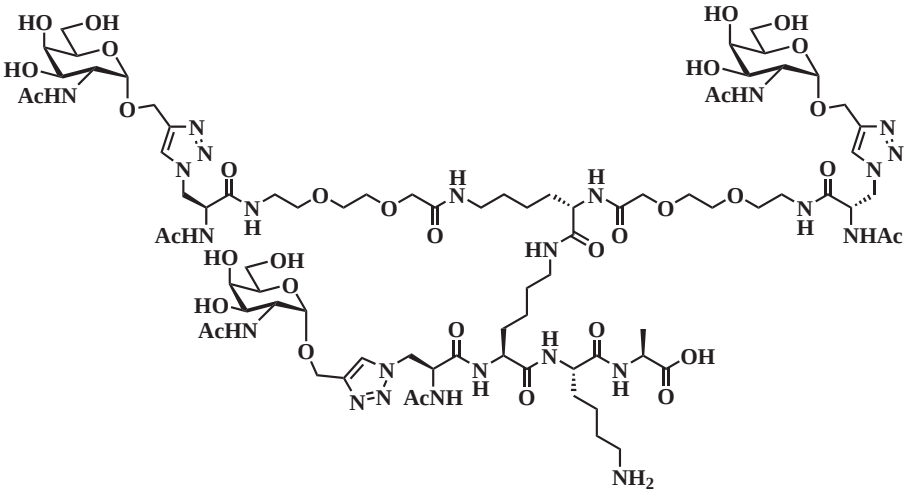

2

Resin **8** (50 μmol) was prepared as described (*Section 8.3.1*). Deprotection of the Fmoc group was carried out as described (*Section 8.3.2*). Fmoc–Lys(Mtt) was coupled (*8.4.1 method 1: using HCTU*) to afford **29**. After removal of the Fmoc group, Fmoc–Lys(Dde) was coupled (*Section 8.4.2 method 2: using HATU*) to give **30**. Fmoc group was removed, followed by coupling of the synthesised Fmoc–azidoalanine **9** (*8.4.4 method 4: using HCTU*). Fmoc group was removed and the peptide chain was capped (*Section 8.4.7 method 7: using Ac_2O*) to prevent further growth. Dde group was cleaved (*Section 8.3.3*) and Fmoc–Lys(Fmoc) was installed (*8.4.1 method 1: using HCTU*). After double Fmoc group removal, the two exposed chains were grown in parallel by coupling Fmoc–mini–PEG (*Section 8.4.3 method 3: using HATU*). The mini–PEGs were deprotected and one Fmoc–azidoalanine **9** was coupled to the end of each chain (*8.4.6 method 6: using HATU*). Fmoc groups were removed and the peptide chains were capped (*Section 8.4.7 method 7: using Ac_2O*) to prevent further growth. The dendrimer scaffold was cleaved from the resin (*Section 8.5.2 method 10: using TFA*), lyophilised, then purified by HPLC (12 mg).

Propargyl GalNAc (**4**) (15 mg, 59.2 μmol) was dissolved in DMSO (712 μL), with dendrimer scaffold (4 mg, 3.264 μmol) and was heated to 50 °C. A solution of sodium ascorbate (4.2 mg, 24.3 μmol) with $CuSO_4$ (8 mg, 32.6 μmol) in H_2O (352 μL) was heated to 50 °C for 10 min and then added to the DMSO solution. The click reaction was agitated for 2 h at 50 °C. The solution was diluted with H_2O and then purified by HPLC. The desired fractions were lyophilised to give the *title compound* **2** as a white solid (1 mg, 1% isolated yield, 95% purity); R_t 14.0 min; ***m/z*** MS(ESI) 1002.6 ($[M + 2H]^{2+}$ requires 1001.5).

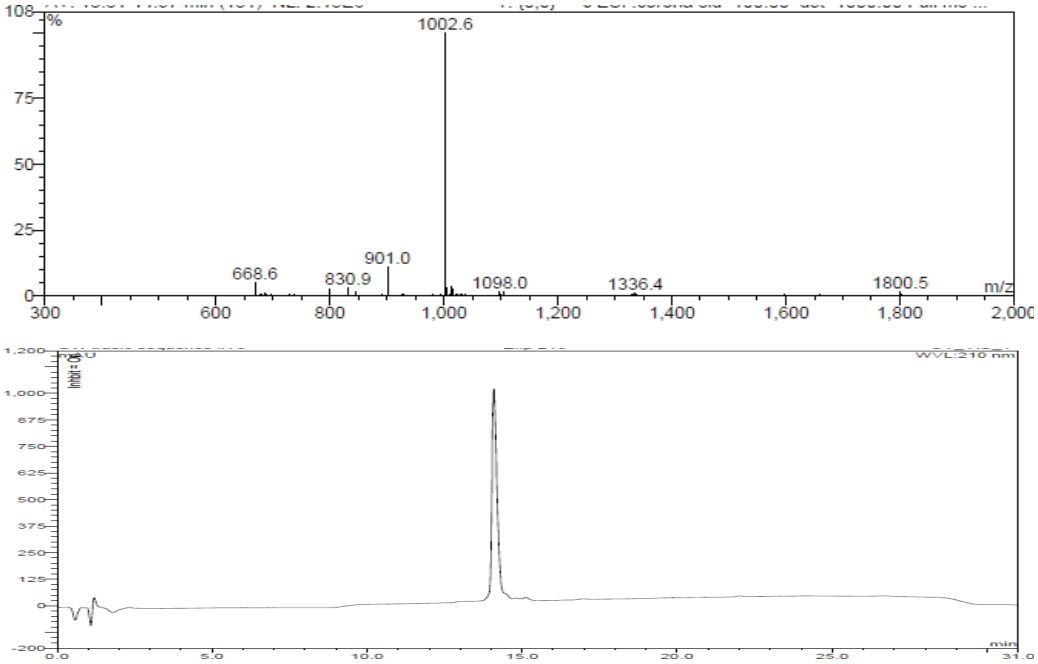

Figure 8.20: HPLC spectrum following purification for dendrimer **2**. R_t 14.0 min; ***m/z*** MS(ESI) 1002.6 ($[M + 2H]^{2+}$ requires 1001.5).

Dendrimer 23

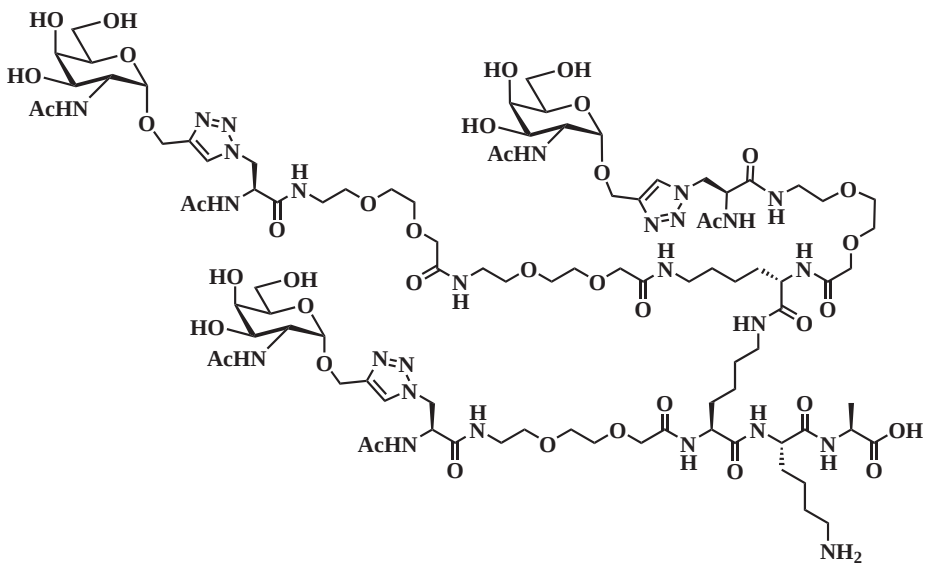

23

Resin **8** (50 μmol) was prepared as described (*Section 8.3.1*). Deprotection of the Fmoc group was carried out as described (*Section 8.3.2*). Fmoc–Lys(Mtt) was coupled (*8.4.1 method 1: using HCTU*) to afford **29**. After removal of the Fmoc group, Fmoc–Lys(Dde) was coupled (*Section 8.4.2 method 2: using HATU*) to give **30**. Fmoc group was removed, followed by coupling of Fmoc–mini–PEG using was coupled (*8.4.2 method 2: using HATU*). Removal of the Fmoc group was carried out using 20% pyridine in DMF, followed by coupling of the synthesised Fmoc–azidoalanine **9** (*Section 8.4.5 method 5: using HATU*). Fmoc group was removed and the peptide chain was capped (*Section 8.4.7 method 7: using Ac_2O*) to prevent further growth. Dde group was cleaved (*Section 8.3.3*) and Fmoc–Lys(Dde) was coupled (*Section 8.4.2 method 2: using HATU*). Fmoc group was removed, followed by coupling of Fmoc–mini–PEG (*Section 8.4.2 method 2: using HATU*). Removal of the Fmoc group was carried out using 20% pyridine in DMF, followed by coupling of the synthesised Fmoc–azidoalanine **9** (*Section 8.4.5 method 5: using HATU*). Fmoc group was removed and the peptide chain was capped (*Section 8.4.7 method 7: using Ac_2O*) to prevent further growth. Dde group was cleaved (*Section 8.3.3*) and was followed by coupling of Fmoc–mini–PEG (*Section 8.4.2 method 2: using HATU*). Fmoc group was removed and the final Fmoc–mini–PEG was installed on the chain (*Section 8.4.2 method 2: using HATU*). Removal of the Fmoc group was carried out using 20% pyridine in DMF, followed by coupling of the synthesised Fmoc–azidoalanine **9** (*Section 8.4.5 method 5: using HATU*). Fmoc group was removed and the peptide chain was capped (*Section 8.4.7 method 7: using Ac_2O*) to prevent further growth. The dendrimer scaffold was cleaved from the resin (*Section 8.5.2 method 10: using TFA*), lyophilised, then purified by HPLC (5.1 mg).

Propargyl GalNAc (**4**) (7.9 mg, 30.3 μmol) was dissolved in DMSO (707 μL) with dendrimer scaffold (5.1 mg) and was heated to 50 °C. A solution of sodium ascorbate (2.6 mg, 15.2 μmol) with $CuSO_4$ (8.7 mg, 33.7 μmol) in H_2O (353 μL) was heated to 50 °C for 10 min and then added to the DMSO solution. The click reaction was heated for 2 h at 50 °C. The solution was diluted with H_2O and then purified by HPLC. The desired fractions were lyophilised to give the *title compound* **23** as a white solid (1.1 mg, 1% isolated yield, 91% purity); R_t 11.4 min; ***m/z*** MS(ESI) 1147.8 ($[M + 2H]^{2+}$ requires 1147.6).

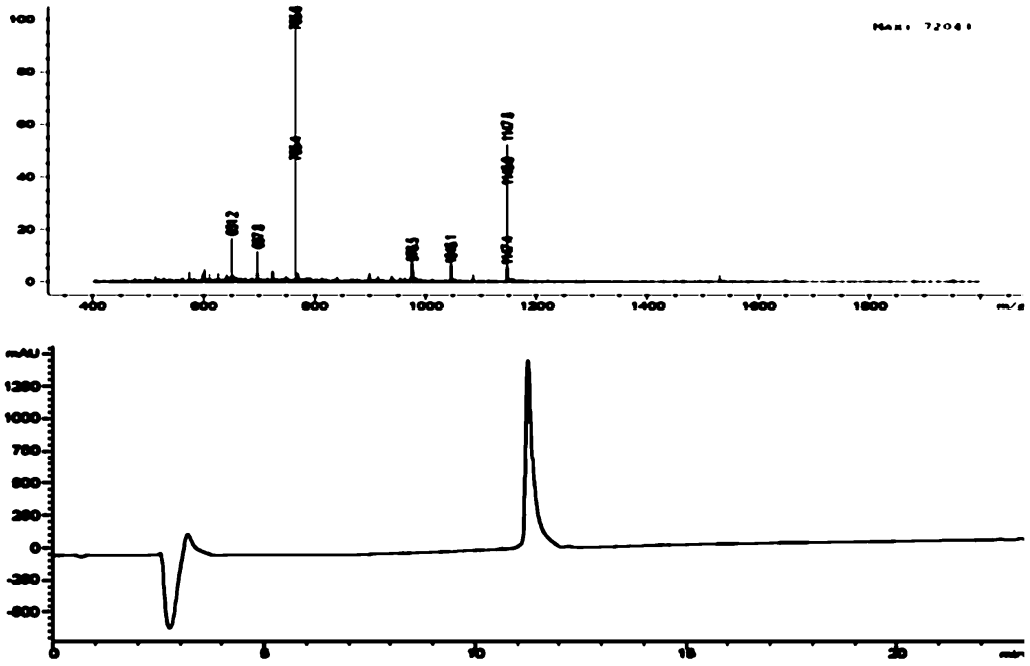

Figure 8.21: HPLC spectrum following purification for dendrimer **23**. R_t 11.4 min; ***m/z*** MS(ESI) 1147.8 ($[M + 2H]^{2+}$ requires 1147.6).

Dendrimer 25

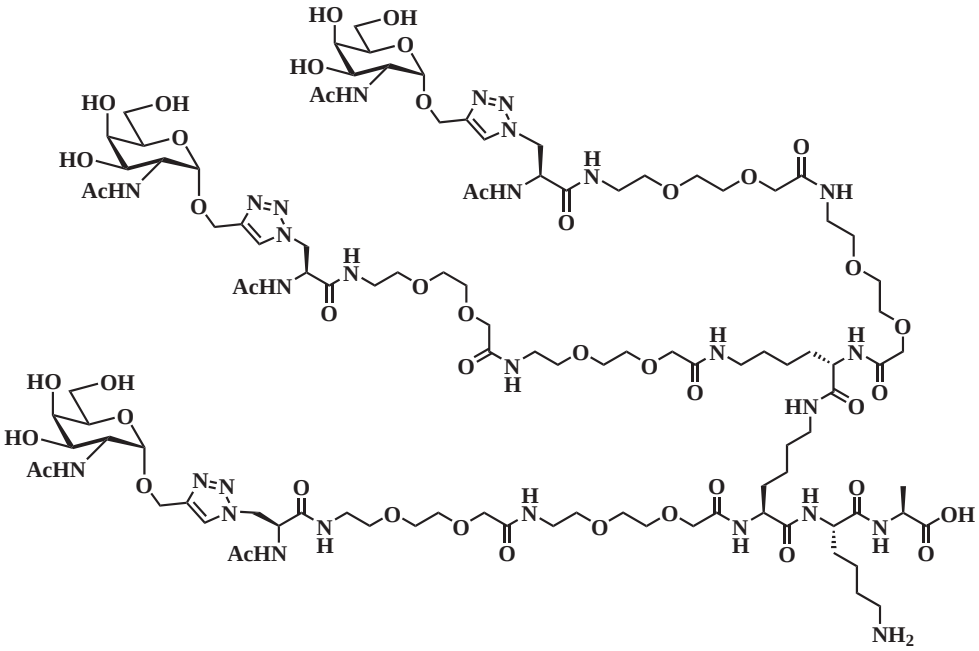

25

Resin **8** (50 μmol) was prepared as described (*Section 8.3.1*). Deprotection of the Fmoc group was carried out as described (*Section 8.3.2*). Fmoc–Lys(Mtt) was coupled (*8.4.1 method 1: using HCTU*) to afford **29**. After removal of the Fmoc group, Fmoc–Lys(Dde) was coupled (*Section 8.4.2 method 2: using HATU*) to give **30**. Fmoc group was removed, followed by coupling of Fmoc–mini–PEG (*Section 8.4.2 method 2: using HATU*). Fmoc group was removed, followed by coupling of Fmoc–mini–PEG (*Section 8.4.2 method 2: using HATU*). Removal of the Fmoc group was carried out using 20% pyridine in DMF, followed by coupling of the synthesised Fmoc–azidoalanine **9** (*Section 8.4.5 method 5: using HATU*). Fmoc group was removed and the peptide chain was capped (*Section 8.4.7 method 7: using Ac_2O*) to prevent further growth. Dde group was cleaved (*Section 8.3.3*) and Fmoc–Lys(Fmoc) was installed (*8.4.1 method 1: using HCTU*). After double Fmoc group removal, the two exposed chains were grown in parallel by coupling Fmoc–mini–PEG (*Section 8.4.3 method 3: using HATU*). The two chains were deprotected and the second Fmoc–mini–PEG spacer on each chain was installed (*Section 8.4.3 method 3: using HATU*). Fmoc groups were cleaved and the synthesised Fmoc–azidoalanine **9** were coupled at the end of each chain (*8.4.6 method 6: using HATU*). Fmoc groups were removed and the peptide chains were capped (*Section 8.4.7 method 7: using Ac_2O*) to prevent further growth. The dendrimer scaffold was cleaved from the resin (*Section 8.5.2 method 10: using TFA*), lyophilised, then purified by HPLC (15.2 mg).

Propargyl GalNAc (**4**) (19.7 mg, 75.9 μmol) was dissolved in DMSO (1.766 mL) with dendrimer scaffold (15.2 mg) and was heated to 50 °C. A solution of sodium ascorbate (6.7 mg, 37.9 μmol) with H_2O (21 mg, 84.3 μmol) in H_2O (883 mL) was heated to 50 °C for 10 min and then added to the

DMSO solution. The click reaction was agitated for 2 h at 50 °C. The solution was diluted with H_2O and then purified by HPLC. The desired fractions were lyophilised to give the *title compound* **25** as a white solid (11 mg, 9% isolated yield, 92% purity); R_t 13.7 min; ***m/z*** MS(ESI) 1292.9 ($[M + 2H]^{2+}$ requires 1292.6).

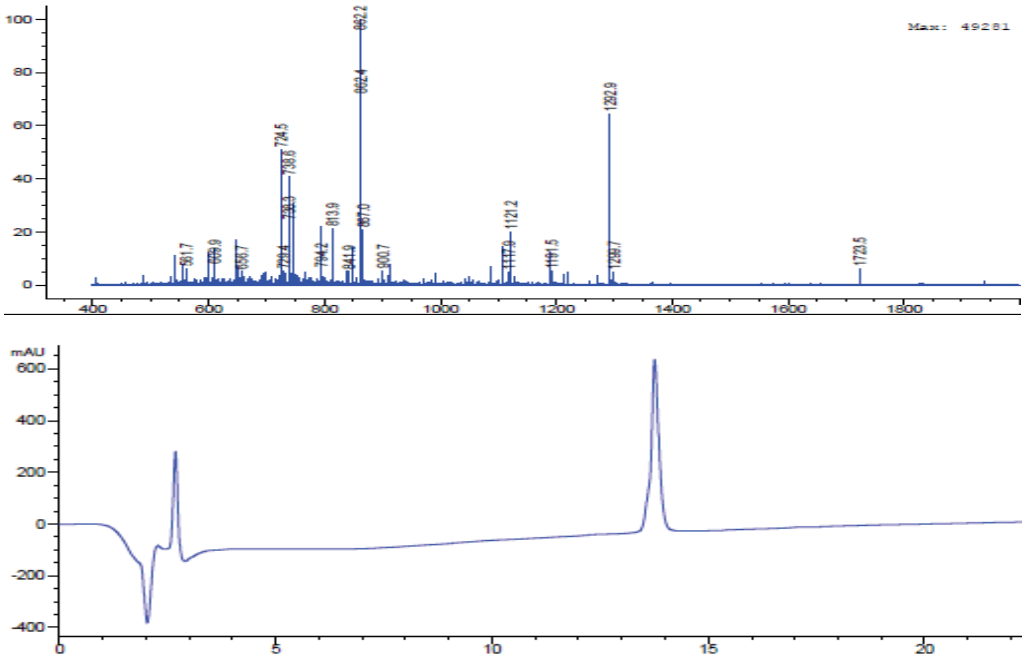

Figure 8.22: HPLC spectrum following purification for dendrimer **25**. R_t 13.7 min; ***m/z*** MS(ESI) 1292.9 ($[M + 2H]^{2+}$ requires 1292.6).

8.6.10 Generation II dendrimers

Dendrimer 43

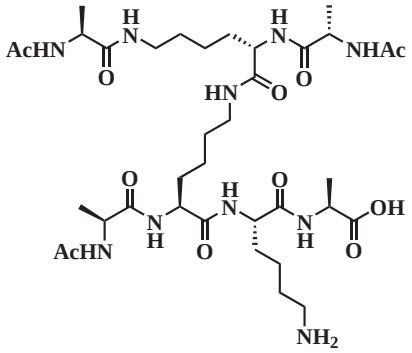

43

Resin **8** (50 μmol) was prepared as described (*Section 8.3.1*). Deprotection of the Fmoc group was carried out as described (*Section 8.3.2*). Fmoc–Lys(Mtt) was coupled (*8.4.1 method 1: using HCTU*) to afford **29**. After removal of the Fmoc group, Fmoc–Lys(Dde) was coupled (*Section 8.4.2 method 2: using HATU*) to give **30**. Fmoc group was removed, followed by coupling of Fmoc–Ala (*8.4.1 method 1: using HCTU*). Fmoc group was removed and the peptide chain was capped (*Section 8.4.7 method 7: using Ac_2O*) to prevent further growth. Dde group was cleaved (*Section 8.3.3*) and Fmoc–Lys(Fmoc) was installed (*8.4.1 method 1: using HCTU*). The two Fmoc groups were cleaved and the two exposed chains were grown in parallel by coupling Fmoc–Ala (*8.4.4 method 4: using HCTU*). Fmoc groups were removed and the peptide chain was capped (*Section 8.4.7 method 7: using Ac_2O*) to prevent further growth. The dendrimer scaffold was cleaved from the resin (*Section 8.5.4 method 12: using TFA*), and the crude scaffold was lyophilised, then purified by HPLC give the *title compound* **43** as a white solid (16.3 mg, 40% isolated yield, 94% purity); R_t 12.8 min; ***m/z*** MS(ESI) 407.4 ($[M + 2H]^{2+}$ requires 407.2).

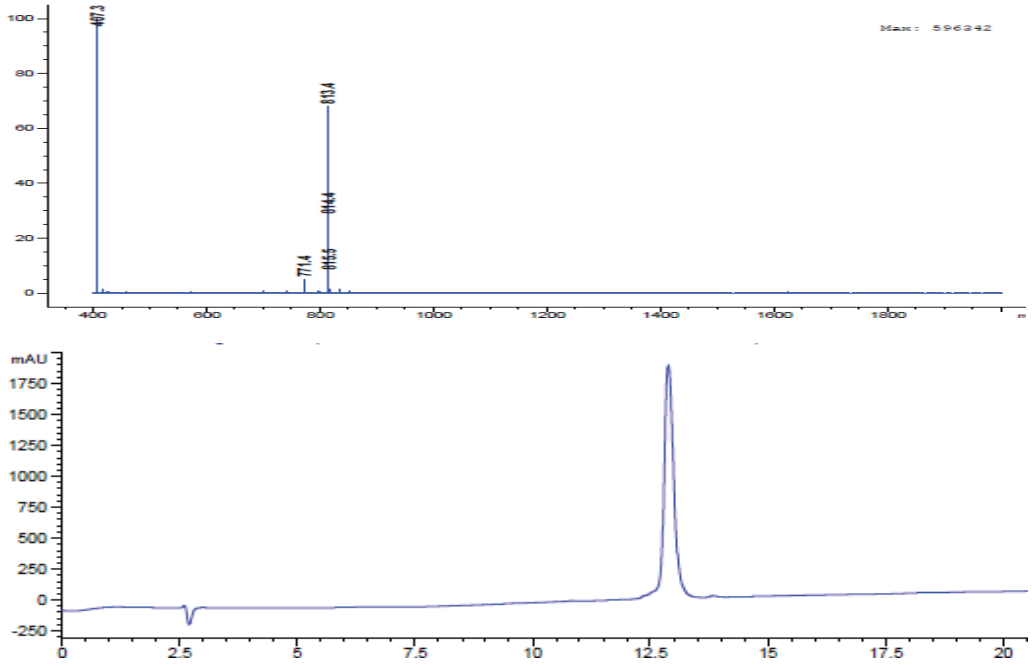

Figure 8.23: HPLC spectrum following purification for dendrimer **43**. R_t 12.8 min; ***m/z*** MS(ESI) 407.4 ($[M + 2H]^{2+}$ requires 407.2).

Dendrimer 45

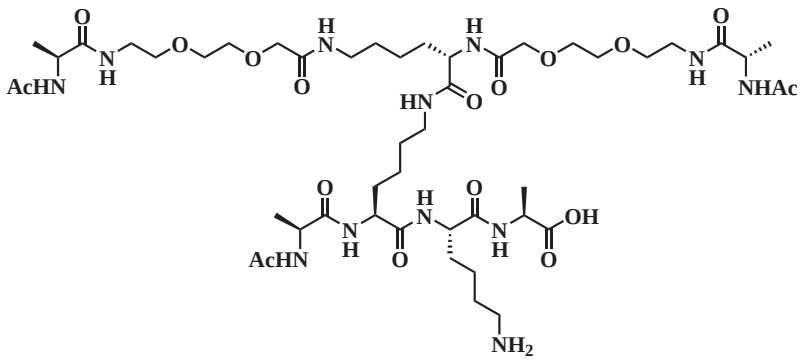

45

Resin **8** (50 μmol) was prepared as described (*Section 8.3.1*). Deprotection of the Fmoc group was carried out as described (*Section 8.3.2*). Fmoc–Lys(Mtt) was coupled (*8.4.1 method 1: using HCTU*) to afford **29**. After removal of the Fmoc group, Fmoc–Lys(Dde) was coupled (*Section 8.4.2 method 2: using HATU*) to give **30**. Fmoc group was removed, followed by coupling of Fmoc–Ala (*8.4.1 method 1: using HCTU*). Fmoc group was removed and the peptide chain was capped (*Section 8.4.7 method 7: using Ac_2O*) to prevent further growth. Dde group was cleaved (*Section 8.3.3*) and Fmoc–Lys(Fmoc) was installed (*8.4.1 method 1: using HCTU*). After double Fmoc group removal, the two exposed chains were grown in parallel by coupling Fmoc–mini–PEG (*Section 8.4.3 method 3: using HATU*). Fmoc groups were both removed and Fmoc–Ala were coupled onto the end of each chain (*8.4.4 method 4: using HCTU*). Fmoc groups were removed and the peptide chains were capped (*Section 8.4.7 method 7: using Ac_2O*) to prevent further growth. The dendrimer scaffold was cleaved from the resin (*Section 8.5.4 method 12: using TFA*), lyophilised, then purified by HPLC give the *title compound* **45** as a white solid (2 mg, 4% isolated yield, 90% purity); R_t 11.0 min; ***m/z*** MS(ESI) 1103.6 ($[M + H]^+$ requires 1103.6).

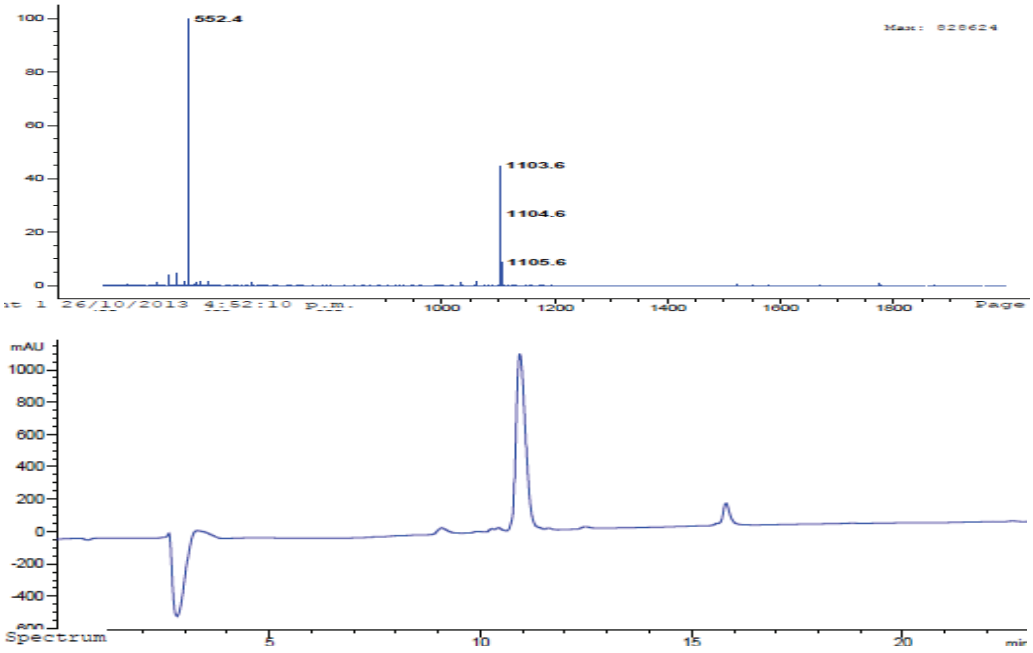

Figure 8.24: HPLC spectrum following purification for dendrimer **45**. R_t 11.0 min; ***m/z*** MS(ESI) 1103.6 ($[M + H]^+$ requires 1103.6).

Dendrimer 47

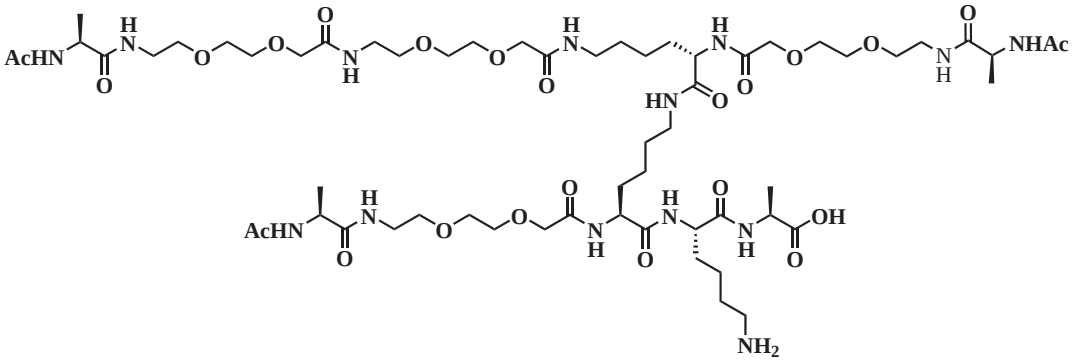

47

Resin **8** (50 μmol) was prepared as described (*Section 8.3.1*). Deprotection of the Fmoc group was carried out as described (*Section 8.3.2*). Fmoc–Lys(Mtt) was coupled (*8.4.1 method 1: using HCTU*) to afford **29**. After removal of the Fmoc group, Fmoc–Lys(Dde) was coupled (*Section 8.4.2 method 2: using HATU*) to give **30**. Fmoc group was removed, followed by coupling of Fmoc–mini–PEG (*Section 8.4.2 method 2: using HATU*). The mini–PEGs Fmoc protecting group was removed and Fmoc–Ala was installed (*8.4.1 method 1: using HCTU*). Fmoc group was removed and the peptide chain was capped (*Section 8.4.7 method 7: using Ac_2O*) to prevent further growth. Dde group was cleaved (*Section 8.3.3*) and Fmoc–Lys(Dde) was coupled (*Section 8.4.2 method 2: using HATU*). Fmoc group was removed and Fmoc–mini–PEG was coupled (*8.4.2 method 2: using HATU*). The mini–PEG was deprotected and Fmoc–Ala was installed (*8.4.1 method 1: using HCTU*). Fmoc group was removed and the peptide chain was capped (*Section 8.4.7 method 7: using Ac_2O*) to prevent further growth. Dde group was cleaved (*Section 8.3.3*) and was followed by coupling of Fmoc–mini–PEG (*Section 8.4.2 method 2: using HATU*). Fmoc group was removed, followed by coupling of Fmoc–mini–PEG (*Section 8.4.2 method 2: using HATU*). The mini–PEGs amine group was deprotected and the final Fmoc–Ala was installed (*8.4.1 method 1: using HCTU*). Fmoc group was removed and the peptide chain was capped (*Section 8.4.7 method 7: using Ac_2O*) to prevent further growth. The dendrimer scaffold was cleaved from the resin (*Section 8.5.4 method 12: using TFA*), lyophilised, then purified by HPLC give the *title compound* **47** as a white solid (24.9 mg, 36% isolated yield, 90% purity); R_t 11.8 min; ***m/z*** MS(ESI) 697.4 ($[M + 2H]^{2+}$ requires 697.4).

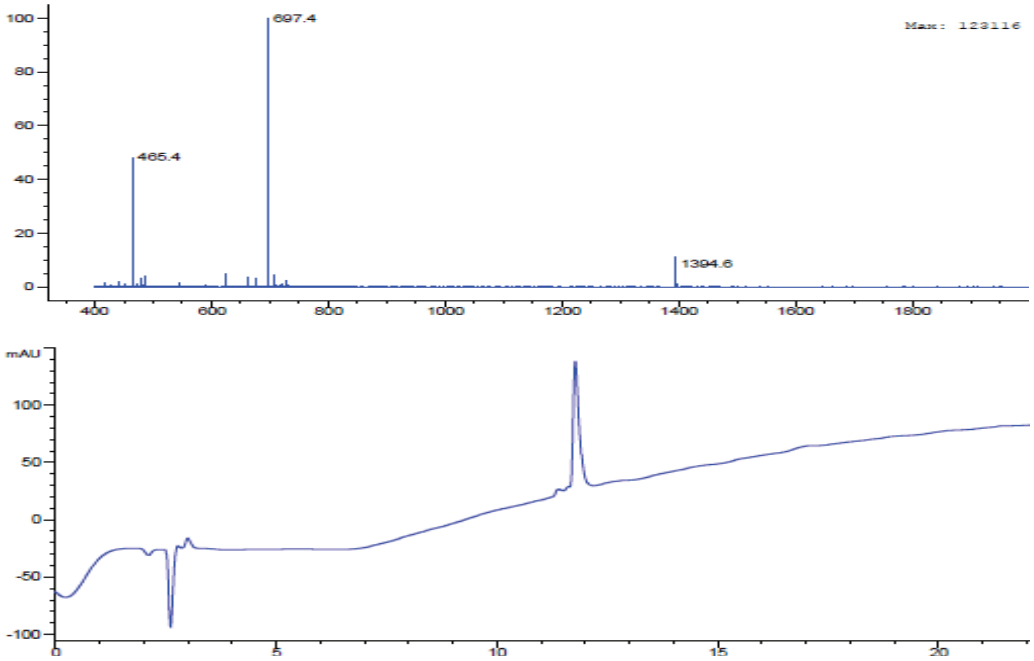

Figure 8.25: HPLC spectrum following purification for dendrimer **47**. R_t 11.8 min; ***m/z*** MS(ESI) 697.4 ($[M + 2H]^{2+}$ requires 697.4).

Dendrimer 49

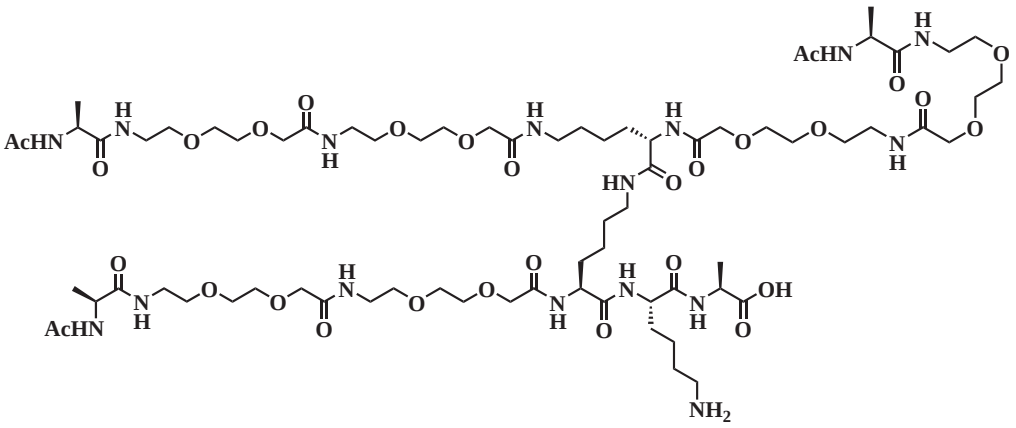

49

Resin **8** (50 μmol) was prepared as described (*Section 8.3.1*). Deprotection of the Fmoc group was carried out as described (*Section 8.3.2*). Fmoc–Lys(Mtt) was coupled (*8.4.1 method 1: using HCTU*) to afford **29**. After removal of the Fmoc group, Fmoc–Lys(Dde) was coupled (*Section 8.4.2 method 2: using HATU*) to give **30**. Fmoc group was removed, followed by coupling of Fmoc–mini–PEG (*Section 8.4.2 method 2: using HATU*). Fmoc group was removed, followed by coupling of Fmoc–mini–PEG (*Section 8.4.2 method 2: using HATU*). The mini–PEGs Fmoc protecting group was cleaved and Fmoc–Ala was installed (*8.4.1 method 1: using HCTU*). Fmoc group was removed and the peptide chain was capped (*Section 8.4.7 method 7: using Ac_2O*) to prevent further growth. Dde group was cleaved (*Section 8.3.3*) and Fmoc–Lys(Fmoc) was installed (*8.4.1 method 1: using HCTU*). After double Fmoc group removal, the two exposed chains were grown in parallel by coupling Fmoc–mini–PEG (*Section 8.4.3 method 3: using HATU*). The two chains were deprotected and the second Fmoc–mini–PEG spacer on each chain was installed (*Section 8.4.3 method 3: using HATU*). The two Fmoc groups were removed and an Fmoc–Ala was coupled onto the end of each chain (*8.4.4 method 4: using HCTU*). Fmoc group was removed and the peptide chain was capped (*Section 8.4.7 method 7: using Ac_2O*) to prevent further growth. The dendrimer scaffold was cleaved from the resin (*Section 8.5.4 method 12: using TFA*), lyophilised, then purified by HPLC give the *title compound* **49** as a white solid (44.8 mg, 53% isolated yield, 92% purity); R_t 12.3 min; ***m/z*** MS(ESI) 842.5 ($[M + 2H]^{2+}$ requires 842.5).

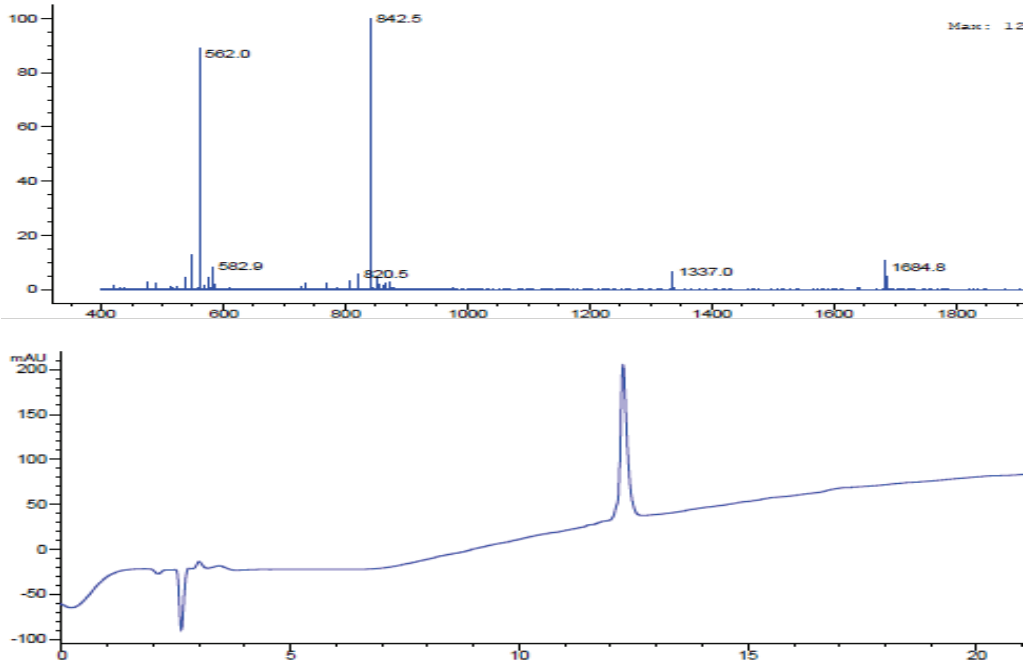

Figure 8.26: HPLC spectrum following purification for dendrimer **49**. R_t 12.3 min; ***m/z*** MS(ESI) 842.5 ($[M + 2H]^{2+}$ requires 842.5).

8.6.11 Generation III dendrimers

Dendrimer 51

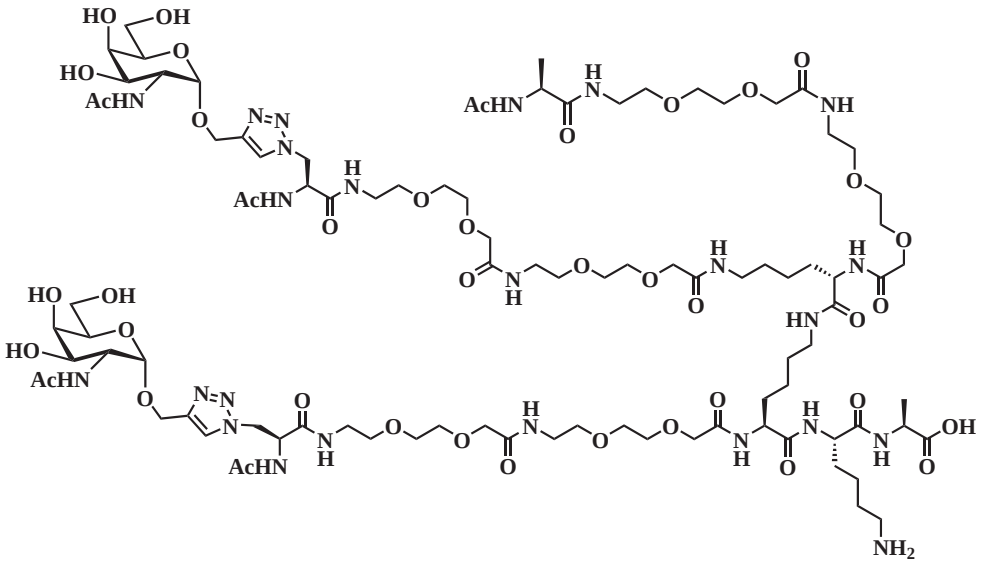

51

Resin **8** (50 μmol) was prepared as described (*Section 8.3.1*). Deprotection of the Fmoc group was carried out as described (*Section 8.3.2*). Fmoc–Lys(Mtt) was coupled (*8.4.1 method 1: using HCTU*) to afford **29**. After removal of the Fmoc group, Fmoc–Lys(Dde) was coupled (*Section 8.4.2 method 2: using HATU*) to give **30**. Fmoc group was removed, followed by coupling of Fmoc–mini–PEG (*Section 8.4.2 method 2: using HATU*). Fmoc group was removed, followed by coupling of Fmoc–mini–PEG (*Section 8.4.2 method 2: using HATU*). Removal of the Fmoc group was carried out using 20% pyridine in DMF, followed by coupling of the synthesised Fmoc–azidoalanine **9** (*Section 8.4.5 method 5: using HATU*). Fmoc group was removed and the peptide chain was capped (*Section 8.4.7 method 7: using Ac_2O*) to prevent further growth. Dde group was cleaved (*Section 8.3.3*) and Fmoc–Lys(Dde) was coupled (*Section 8.4.2 method 2: using HATU*). Fmoc group was removed, followed by coupling of Fmoc–mini–PEG (*Section 8.4.2 method 2: using HATU*). Fmoc group was removed, followed by coupling of Fmoc–mini–PEG (*Section 8.4.2 method 2: using HATU*). Fmoc group was cleaved and Fmoc–Ala was installed (*8.4.1 method 1: using HCTU*). Fmoc group was removed and the peptide chain was capped (*Section 8.4.7 method 7: using Ac_2O*) to prevent further growth. Dde group was cleaved (*Section 8.3.3*) and was followed by coupling of Fmoc–mini–PEG (*Section 8.4.2 method 2: using HATU*). Fmoc group was removed, followed by coupling of Fmoc–mini–PEG (*Section 8.4.2 method 2: using HATU*). Removal of the Fmoc group was carried out using 20% pyridine in DMF, followed by coupling of the synthesised Fmoc–azidoalanine **9** (*Section 8.4.5 method 5: using HATU*). Fmoc group was removed and the peptide chain was capped (*Section 8.4.7 method 7: using Ac_2O*) to prevent further growth. The dendrimer scaffold was cleaved from the resin (*Section 8.5.2*

method 10: using TFA), and the crude scaffold was lyophilised (114 mg).

Propargyl GalNAc (**4**) (52 mg, 200 μmol) was dissolved in DMSO (11.27 mL), with dendrimer scaffold (114 mg) and was heated to 50 °C. A solution of sodium ascorbate (40 mg, 225 μmol) with $CuSO_4$ (125 mg, 500 μmol) in H_2O (5.63 mL) was heated to 50 °C for 10 min and then added to the DMSO solution. The click reaction was agitated for 2 h at 50 °C. The solution was diluted with H_2O and then purified by HPLC. The desired fractions were lyophilised to give the *title compound* **51** as a white solid (11 mg, 8% isolated yield, 97% purity); R_t 14 min; ***m/z*** MS(ESI) 1142.6 ($[M + 2H]^{2+}$ requires 1142.6).

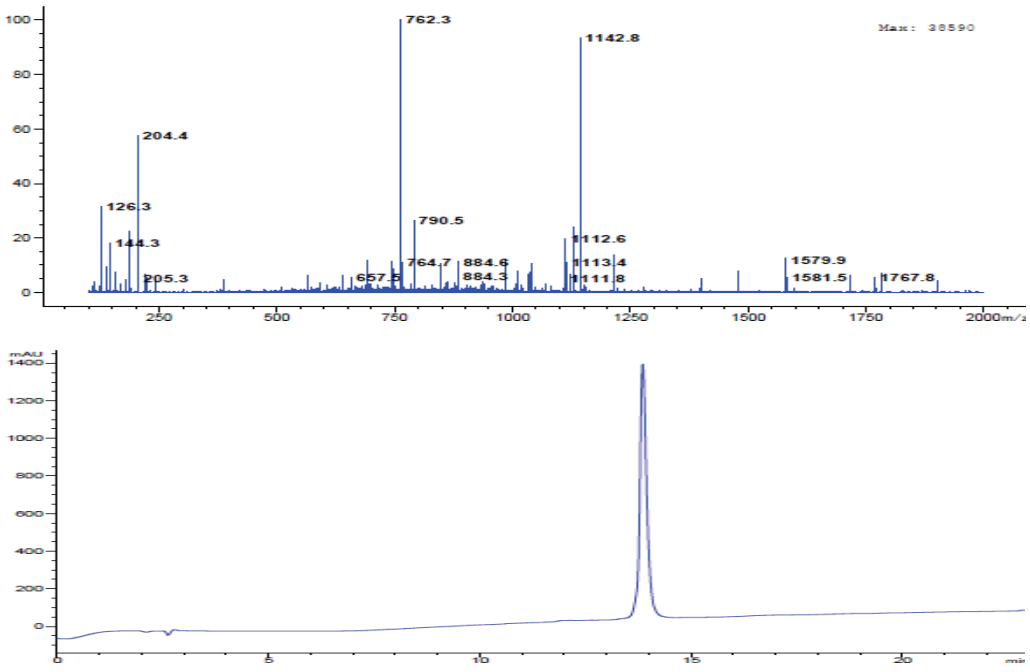

Figure 8.27: HPLC spectrum following purification for dendrimer **51**. R_t 14 min; ***m/z*** MS(ESI) 1142.6 ($[M + 2H]^{2+}$ requires 1142.6).

Dendrimer 53

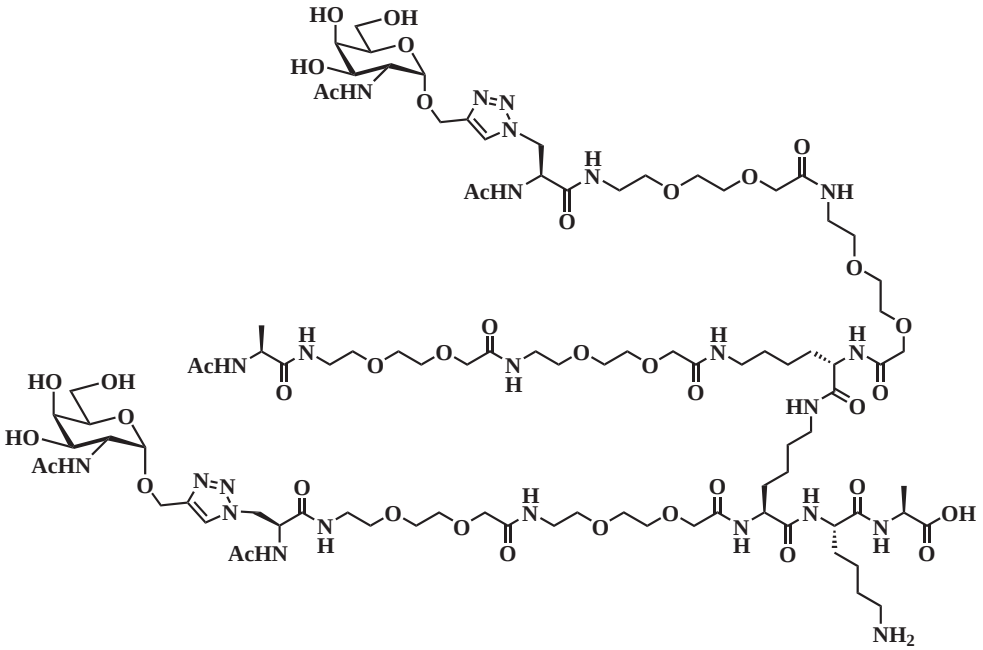

53

Resin **8** (50 μmol) was prepared as described (*Section 8.3.1*). Deprotection of the Fmoc group was carried out as described (*Section 8.3.2*). Fmoc–Lys(Mtt) was coupled (*8.4.1 method 1: using HCTU*) to afford **29**. After removal of the Fmoc group, Fmoc–Lys(Dde) was coupled (*Section 8.4.2 method 2: using HATU*) to give **30**. Fmoc group was removed, followed by coupling of Fmoc–mini–PEG was coupled (*8.4.2 method 2: using HATU*). Fmoc group was cleaved and the second Fmoc–mini–PEG group was coupled was coupled (*8.4.2 method 2: using HATU*). Removal of the Fmoc group was carried out using 20% pyridine in DMF, followed by coupling of the synthesised Fmoc–azidoalanine **9** (*Section 8.4.5 method 5: using HATU*). Fmoc group was removed and the peptide chain was capped (*Section 8.4.7 method 7: using Ac_2O*) to prevent further growth. Dde group was cleaved (*Section 8.3.3*) and Fmoc–Lys(Dde) was coupled (*Section 8.4.2 method 2: using HATU*). Fmoc group was removed, followed by coupling of Fmoc–mini–PEG (*Section 8.4.2 method 2: using HATU*). Fmoc group was removed, followed by coupling of Fmoc–mini–PEG (*Section 8.4.2 method 2: using HATU*). Removal of the Fmoc group was carried out using 20% pyridine in DMF, followed by coupling of the synthesised Fmoc–azidoalanine **9** (*Section 8.4.5 method 5: using HATU*). Fmoc group was removed and the peptide chain was capped (*Section 8.4.7 method 7: using Ac_2O*) to prevent further growth. Dde group was cleaved (*Section 8.3.3*) and was removed, followed by coupling of Fmoc–mini–PEG (*Section 8.4.2 method 2: using HATU*). Fmoc group was removed, followed by coupling of Fmoc–mini–PEG (*Section 8.4.2 method 2: using HATU*). The subsequent deprotection to remove the Fmoc group was followed by the coupling of Fmoc–Ala (*8.4.1 method 1: using HCTU*). Fmoc group was removed and the peptide chain was capped (*Section 8.4.7 method 7: using Ac_2O*) to prevent further

growth. The dendrimer scaffold was cleaved from the resin (*Section 8.5.2 method 10: using TFA*), and the crude scaffold was lyophilised (120 mg).

Propargyl GalNAc (**4**) (52 mg, 200 μmol) was dissolved in DMSO (11.27 mL), with dendrimer scaffold (120 mg) and was heated to 50 °C. A solution of sodium ascorbate (40 mg, 225 μmol) with $CuSO_4$ (125 mg, 500 μmol) in H_2O (5.63 mL) was heated to 50 °C for 10 min and then added to the DMSO solution. The click reaction was heated for 2 h at 50 °C. The solution was diluted with H_2O and then purified by HPLC. The desired fractions were lyophilised to give the *title compound* **53** as a white solid (16 mg, 14% isolated yield, 95% purity); R_t 12.5 min; ***m/z*** MS(ESI) 1142.6 ($[M + 2H]^{2+}$ requires 1142.6).

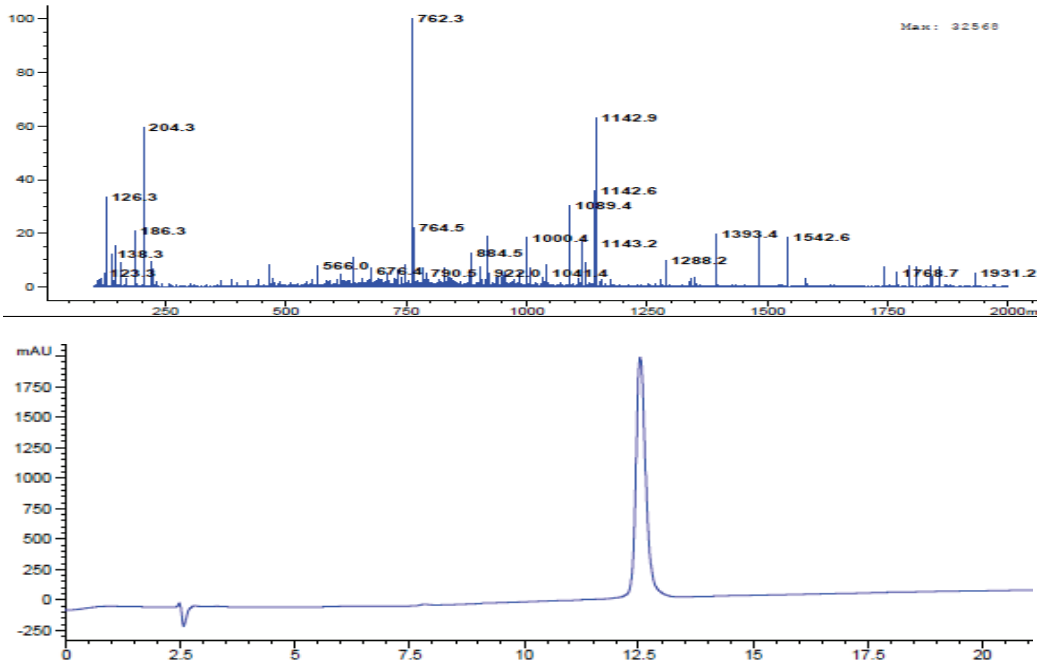

Figure 8.28: HPLC spectrum following purification for dendrimer **53**. R_t 12.5 min; ***m/z*** MS(ESI) 1142.6 ($[M + 2H]^{2+}$ requires 1142.6).

Dendrimer 55

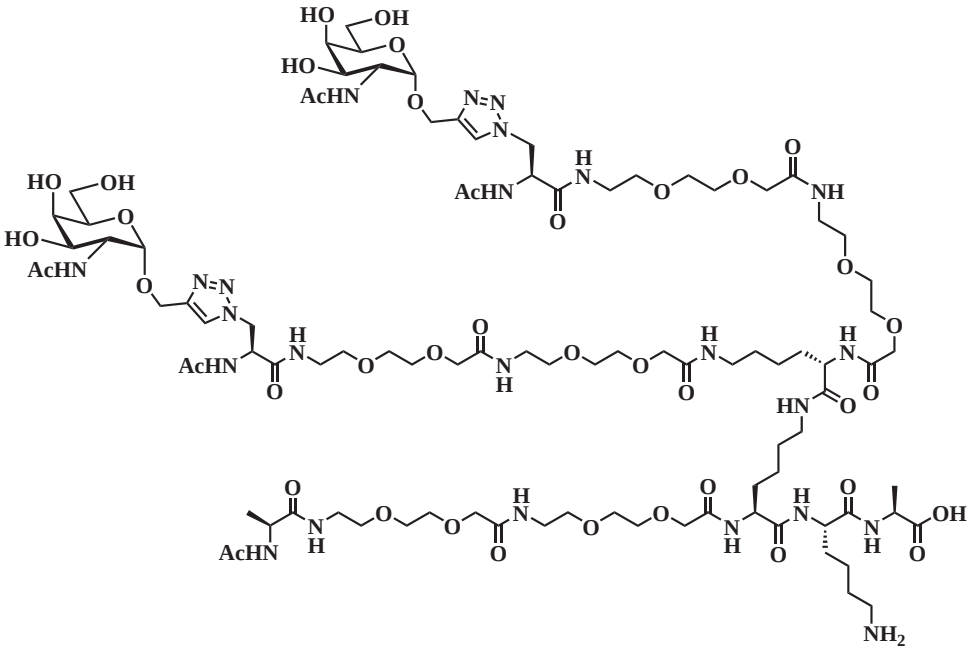

55

Resin **8** (50 μmol) was prepared as described (*Section 8.3.1*). Deprotection of the Fmoc group was carried out as described (*Section 8.3.2*). Fmoc–Lys(Mtt) was coupled (*8.4.1 method 1: using HCTU*) to afford **29**. After removal of the Fmoc group, Fmoc–Lys(Dde) was coupled (*Section 8.4.2 method 2: using HATU*) to give **30**. Fmoc group was removed, followed by coupling of Fmoc–mini–PEG (*Section 8.4.2 method 2: using HATU*). Fmoc group was removed, followed by coupling of Fmoc–mini–PEG (*Section 8.4.2 method 2: using HATU*). Removal of the Fmoc group was carried out using 20% pyridine in DMF, followed by coupling of the synthesised Fmoc–azidoalanine **9** (*Section 8.4.5 method 5: using HATU*). Fmoc group was removed and the peptide chain was capped (*Section 8.4.7 method 7: using Ac_2O*) to prevent further growth. Dde group was cleaved (*Section 8.3.3*) and Fmoc–Lys(Fmoc) was installed (*8.4.1 method 1: using HCTU*). After double Fmoc group removal, the two exposed chains were grown in parallel by coupling Fmoc–mini–PEG (*Section 8.4.3 method 3: using HATU*). The two chains were deprotected and the second Fmoc–mini–PEG spacer on each chain was installed (*Section 8.4.3 method 3: using HATU*). The mini–PEG groups were deprotected and the synthesised Fmoc–azidoalanine **9** were coupled to each chain (*8.4.6 method 6: using HATU*). Fmoc groups were removed and the peptide chains were capped (*Section 8.4.7 method 7: using Ac_2O*) to prevent further growth. The dendrimer scaffold was cleaved from the resin (*Section 8.5.2 method 10: using TFA*), and the crude scaffold was lyophilised (47 mg).

Propargyl GalNAc (**4**) (27 mg, 75.9 μmol) was dissolved in DMSO (6 mL), with dendrimer scaffold (47 mg) and was heated to 50 °C. A solution of sodium ascorbate (21 mg, 120 μmol) with $CuSO_4$ (66 mg, 266 μmol) in H_2O (3 mL) was heated to 50 °C for 10 min and then added to the DMSO solu-

tion. The click reaction was agitated for 2 h at 50 °C. The solution was diluted with H_2O and then purified by HPLC. The desired fractions were lyophilised to give the *title compound* **55** as a white solid (1 mg, 1% isolated yield, 92% purity); R_t 12.8 min; ***m/z*** MS(ESI) 1142.6 ($[M + 2H]^{2+}$ requires 1142.6).

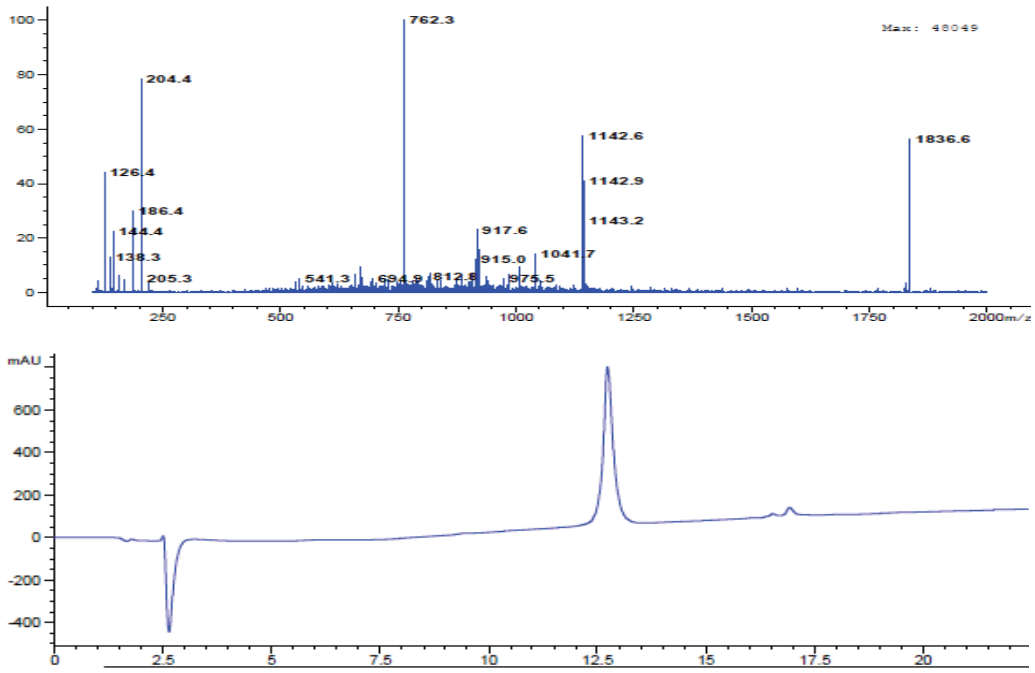

Figure 8.29: HPLC spectrum following purification for dendrimer **55**. R_t 12.8 min ***m/z*** MS(ESI) 1142.6 ($[M + 2H]^{2+}$ requires 1142.6).

8.6.12 Generation IV dendrimers

Dendrimer 57

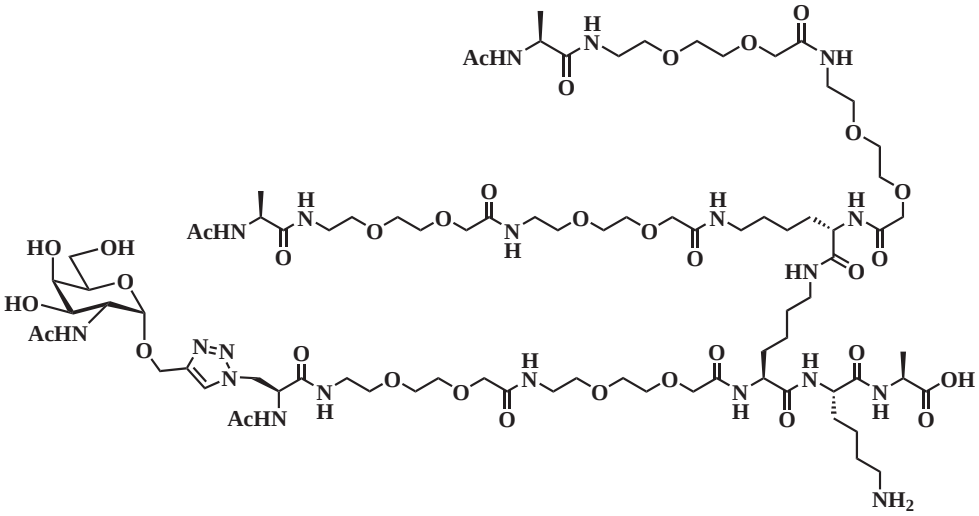

57

Resin **8** (50 μmol) was prepared as described (*Section 8.3.1*). Deprotection of the Fmoc group was carried out as described (*Section 8.3.2*). Fmoc–Lys(Mtt) was coupled (*8.4.1 method 1: using HCTU*) to afford **29**. After removal of the Fmoc group, Fmoc–Lys(Dde) was coupled (*Section 8.4.2 method 2: using HATU*) to give **30**. Fmoc group was removed, followed by coupling of Fmoc–mini–PEG (*Section 8.4.2 method 2: using HATU*). Fmoc group was removed, followed by coupling of Fmoc–mini–PEG (*Section 8.4.2 method 2: using HATU*). Removal of the Fmoc group was carried out using 20% pyridine in DMF, followed by coupling of the synthesised Fmoc–azidoalanine **9** (*Section 8.4.5 method 5: using HATU*). Fmoc group was removed and the peptide chain was capped (*Section 8.4.7 method 7: using Ac_2O*) to prevent further growth. Dde group was cleaved (*Section 8.3.3*) and Fmoc–Lys(Fmoc) was installed (*8.4.1 method 1: using HCTU*). After double Fmoc group removal, the two exposed chains were grown in parallel by coupling Fmoc–mini–PEG (*Section 8.4.3 method 3: using HATU*). The two chains were deprotected and the second Fmoc–mini–PEG spacer on each chain was installed (*Section 8.4.3 method 3: using HATU*). Fmoc groups were removed and Fmoc–Ala were coupled (*8.4.4 method 4: using HCTU*). Fmoc groups were removed and the peptide chains were capped (*Section 8.4.7 method 7: using Ac_2O*) to prevent further growth. The dendrimer scaffold was cleaved from the resin (*Section 8.5.2 method 10: using TFA*), and the crude scaffold was lyophilised (98 mg).

Propargyl GalNAc (**4**) (29 mg, 113.7 μmol) was dissolved in DMSO (12.6 mL), with dendrimer scaffold (98 mg) and was heated to 50 °C. A solution of sodium ascorbate (45 mg, 256 μmol) with $CuSO_4$ (142 mg, 568 μmol) in H_2O (6.3 mL) was heated to 50 °C for 10 min and then added to the

DMSO solution. The click reaction was heated for 2 h at 50 °C. The solution was diluted with H_2O and then purified by HPLC. The desired fractions were lyophilised to give the *title compound* **57** as a white solid (9 mg, 9% isolated yield, 95% purity); R_t 12.8 min; ***m/z*** MS(ESI) 992.9 ($[M + 2H]^{2+}$ requires 992.5).

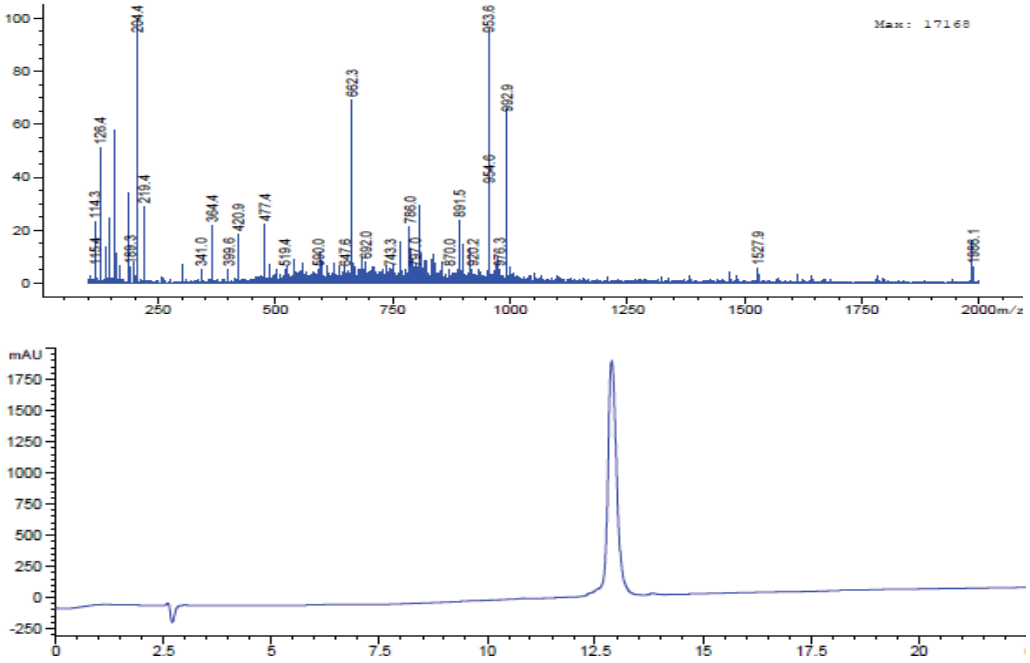

Figure 8.30: HPLC spectrum following purification for dendrimer **57**. R_t 12.8 min; ***m/z*** MS(ESI) 992.9 ($[M + 2H]^{2+}$ requires 992.5).

Dendrimer 59

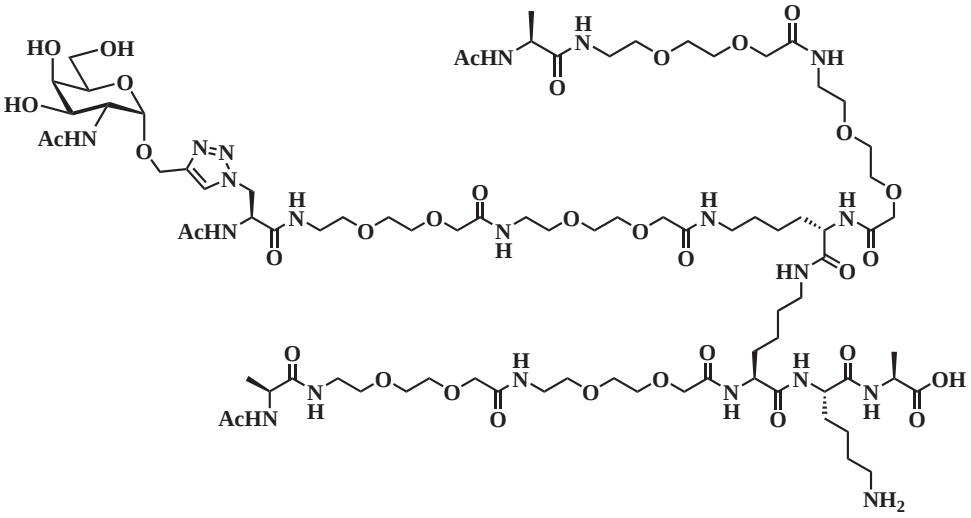

59

Resin **8** (50 μmol) was prepared as described (*Section 8.3.1*). Deprotection of the Fmoc group was carried out as described (*Section 8.3.2*). Fmoc–Lys(Mtt) was coupled (*8.4.1 method 1: using HCTU*) to afford **29**. After removal of the Fmoc group, Fmoc–Lys(Dde) was coupled (*Section 8.4.2 method 2: using HATU*) to give **30**. Fmoc group was removed, followed by coupling of Fmoc–mini–PEG (*Section 8.4.2 method 2: using HATU*). Fmoc group was removed, followed by coupling of Fmoc–mini–PEG (*Section 8.4.2 method 2: using HATU*). The mini–PEGs Fmoc protecting group was cleaved and Fmoc–Ala was installed (*8.4.1 method 1: using HCTU*). Fmoc group was removed and the peptide chain was capped (*Section 8.4.7 method 7: using Ac_2O*) to prevent further growth. Dde group was cleaved (*Section 8.3.3*) and Fmoc–Lys(Dde) was coupled (*Section 8.4.2 method 2: using HATU*). Fmoc group was removed, followed by coupling of Fmoc–mini–PEG (*Section 8.4.2 method 2: using HATU*). Fmoc group was removed, followed by coupling of Fmoc–mini–PEG (*Section 8.4.2 method 2: using HATU*). Fmoc group was removed and Fmoc–Ala was installed (*8.4.1 method 1: using HCTU*). Fmoc group was removed and the peptide chain was capped (*Section 8.4.7 method 7: using Ac_2O*) to prevent further growth. Dde group was cleaved (*Section 8.3.3*) and was removed, followed by coupling of Fmoc–mini–PEG (*Section 8.4.2 method 2: using HATU*). Removal of the Fmoc group was carried out using 20% pyridine in DMF, followed by coupling of the synthesised Fmoc–azidoalanine **9** (*Section 8.4.5 method 5: using HATU*). Fmoc group was removed and the peptide chain was capped (*Section 8.4.7 method 7: using Ac_2O*) to prevent further growth. The dendrimer scaffold was cleaved from the resin (*Section 8.5.2 method 10: using TFA*), and the crude scaffold was lyophilised (86 mg).

Propargyl GalNAc (**4**) (25 mg, 98.9 μmol) was dissolved in DMSO (11.27 mL) with dendrimer scaffold (86 mg) and was heated to 50 °C. A solution of sodium ascorbate (40 mg, 225 μmol) with $CuSO_4$ (125 mg, 500 μmol) in H_2O (5.63 mL) was heated to 50 °C for 10 min and then added to the

DMSO solution. The click reaction was agitated for 2 h at 50 °C. The solution was diluted with H_2O and then purified by HPLC. The desired fractions were lyophilised to give the *title compound* **59** as a white solid (17 mg, 17% isolated yield, 94% purity); R_t 12.9 min; ***m/z*** MS(ESI) 992.6 ($[M + 2H]^{2+}$ requires 992.5).

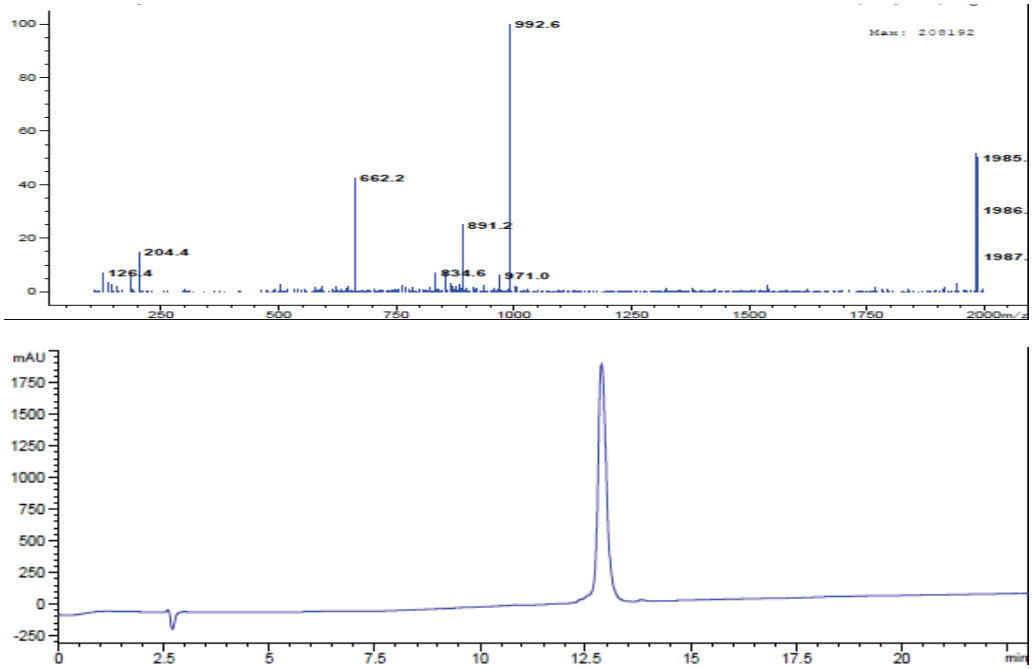

Figure 8.31: HPLC spectrum following purification for dendrimer **59**. R_t 12.9 min; ***m/z*** MS(ESI) 992.6 ($[M + 2H]^{2+}$ requires 992.5).

Dendrimer 61

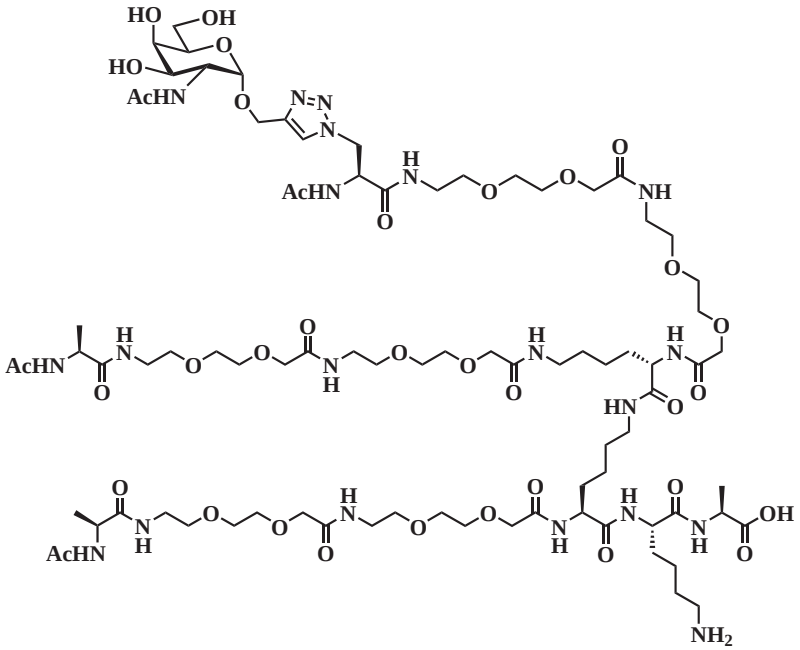

61

Resin **8** (50 μmol) was prepared as described (*Section 8.3.1*). Deprotection of the Fmoc group was carried out as described (*Section 8.3.2*). Fmoc–Lys(Mtt) was coupled (*8.4.1 method 1: using HCTU*) to afford **29**. After removal of the Fmoc group, Fmoc–Lys(Dde) was coupled (*Section 8.4.2 method 2: using HATU*) to give **30**. Fmoc group was removed, followed by coupling of Fmoc–mini–PEG (*Section 8.4.2 method 2: using HATU*). Fmoc group was removed, followed by coupling of Fmoc–mini–PEG (*Section 8.4.2 method 2: using HATU*). Fmoc protecting group was cleaved and Fmoc–Ala was installed (*8.4.1 method 1: using HCTU*). Fmoc group was removed and the peptide chain was capped (*Section 8.4.7 method 7: using Ac_2O*) to prevent further growth. Dde group was cleaved (*Section 8.3.3*) and Fmoc–Lys(Dde) was coupled (*Section 8.4.2 method 2: using HATU*). Fmoc group was removed, followed by coupling of Fmoc–mini–PEG (*Section 8.4.2 method 2: using HATU*). Fmoc group was removed, followed by coupling of Fmoc–mini–PEG (*Section 8.4.2 method 2: using HATU*). Removal of the Fmoc group was carried out using 20% pyridine in DMF, followed by coupling of the synthesised Fmoc–azidoalanine **9** (*Section 8.4.5 method 5: using HATU*). Fmoc group was removed and the peptide chain was capped (*Section 8.4.7 method 7: using Ac_2O*) to prevent further growth. Dde group was cleaved (*Section 8.3.3*) and was removed, followed by coupling of Fmoc–mini–PEG (*Section 8.4.2 method 2: using HATU*). Fmoc group was removed, followed by coupling of Fmoc–mini–PEG (*Section 8.4.2 method 2: using HATU*). The final mini–PEG group was deprotected and Fmoc–Ala was installed (*8.4.1 method 1: using HCTU*). Fmoc group was removed and the peptide chain was capped (*Section 8.4.7 method 7: using Ac_2O*) to prevent further growth. The dendrimer scaffold was cleaved from the resin (*Section 8.5.2 method 10: using TFA*), and the crude scaffold was

lyophilised (103 mg).

Propargyl GalNAc (**4**) (25 mg, 98.9 μmol) was dissolved in DMSO (11.27 mL), with dendrimer scaffold (103 mg) and was heated to 50 °C. A solution of sodium ascorbate (40 mg, 225 μmol) with $CuSO_4$ (125 mg, 500 μmol) in H_2O (5.63 mL) was heated to 50 °C for 10 min and then added to the DMSO solution. The click reaction was agitated for 2 h at 50 °C. The solution was diluted with H_2O and then purified by HPLC. The desired fractions were lyophilised to give the *title compound* **61** as a white solid (10 mg, 10% isolated yield, 91% purity); R_t 12.8 min; ***m/z*** MS(ESI) 992.6 ($[M + 2H]^{2+}$ requires 992.5).

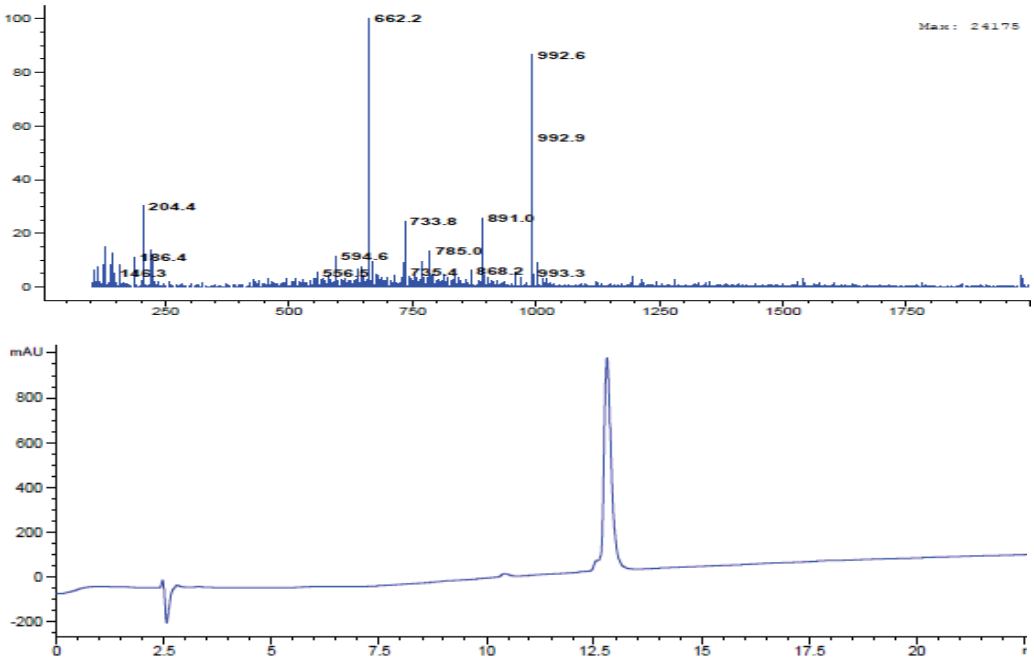

Figure 8.32: HPLC spectrum following purification for dendrimer **61**. R_t 12.8 min; ***m/z*** MS(ESI) 992.6 ($[M + 2H]^{2+}$ requires 992.5).

8.6.13 Generation V peptides

Peptide 63

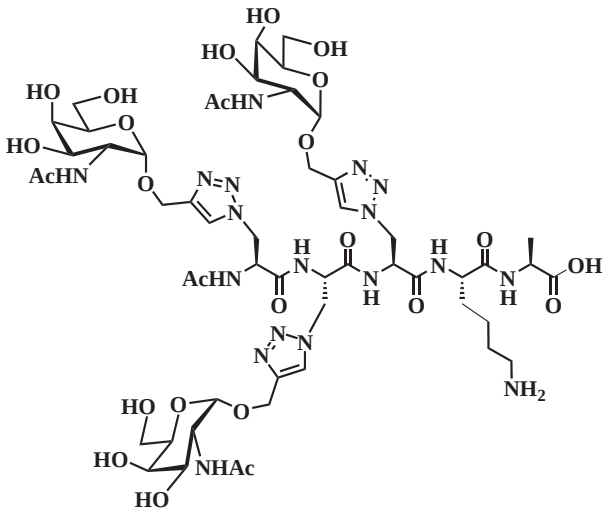

63

Resin **8** (50 μmol) was prepared as described (*Section 8.3.1*). Fmoc–Lys(Mtt) was installed (*8.4.1 method 1: using HCTU*) to afford **29**. Fmoc group was cleaved and Fmoc–azidoalanine **9** was coupled (*8.4.2 method 2: using HATU*). The terminal Fmoc group was removed and the second Fmoc–azidoalanine **9** was coupled (*8.4.2 method 2: using HATU*). Fmoc group was removed and the final Fmoc–azidoalanine **9** was coupled (*8.4.2 method 2: using HATU*). Fmoc group was removed and the peptide chain was capped (*Section 8.4.7 method 7: using Ac_2O*) to prevent further growth. The peptide scaffold was cleaved from the resin (*Section 8.5.2 method 10: using TFA*), then purified by HPLC (14.0 mg).

Propargyl GalNAc (**4**) (16 mg, 61.2 μmol) was dissolved in DMSO (190 μL) with the peptide scaffold (9 mg) and was heated to 50 °C. A solution of sodium ascorbate (27 mg, 138 μmol) with $CuSO_4$ (76 mg, 306 μmol) in H_2O (95 μL) was heated to 50 °C for 10 min and then added to the DMSO solution. The click reaction was heated for 2 h at 50 °C. The solution was diluted with H_2O and then purified by HPLC. The desired fractions were lyophilised to give the *title compound* **63** as a white solid (3 mg, 4.3% isolated yield, 94% purity); R_t 15.7 min; ***m/z*** MS(ESI) 1373.4 ($[M + H]^+$ requires 1373.6).

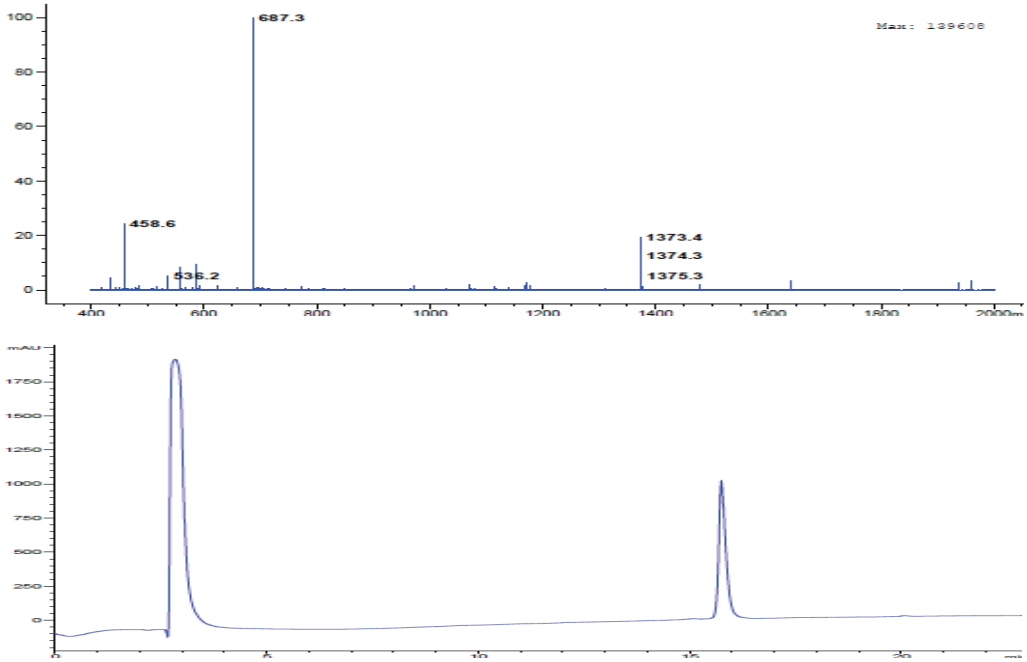

Figure 8.33: HPLC spectrum following purification for peptide **63**. R_t 15.7 min; ***m/z*** MS(ESI) 1373.4 ([M + H]$^+$ requires 1373.6).

8.6.14 Triazole negative control analogues

Dendrimer 67

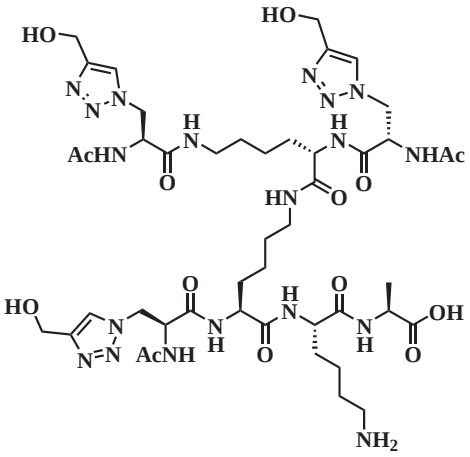

67

Resin **8** (50 μmol) was prepared as described (*Section 8.3.1*). Deprotection of the Fmoc group was carried out as described (*Section 8.3.2*). Fmoc–Lys(Mtt) was coupled (*8.4.1 method 1: using HCTU*) to afford **29**. After removal of the Fmoc group, Fmoc–Lys(Dde) was coupled (*Section 8.4.2 method 2: using HATU*) to give **30**. Removal of the Fmoc group was carried out using 20% pyridine in DMF, followed by coupling of the synthesised Fmoc–azidoalanine **9** (*Section 8.4.5 method 5: using HATU*). Fmoc group was removed and the peptide chain was capped (*Section 8.4.7 method 7: using Ac_2O*) to prevent further growth. Dde group was cleaved (*Section 8.3.3*) and Fmoc–Lys(Fmoc) was installed (*8.4.1 method 1: using HCTU*). The two Fmoc groups on the scaffold were removed and the two exposed chains were grown in parallel by coupling one Fmoc–azidoalanine **9** to the end of each chain (*8.4.6 method 6: using HATU*). Fmoc group was removed and the peptide chain was capped (*Section 8.4.7 method 7: using Ac_2O*) to prevent further growth. The dendrimer scaffold was cleaved from the resin (*Section 8.5.2 method 10: using TFA*), lyophilised, then purified by HPLC (37.0 mg).

Propargyl alcohol (8.3 μL, 154 μmol) and dendrimer scaffold (36 mg) were dissolved in DMSO (8.56 mL) and was heated to 50 °C. A solution of sodium ascorbate (61 mg, 347 μmol) with $CuSO_4$ (191 mg, 770 μmol) in H_2O (4.28 mL) was heated to 50 °C for 10 min and then added to the DMSO solution. The click reaction was heated for 2 h at 50 °C. The solution was diluted with H_2O and then purified by HPLC. The desired fractions were lyophilised to give the *title compound* **67** as a white solid (12 mg, 21% isolated yield, 90% purity); R_t 17.5 min; ***m/z*** MS(ESI) 1104.9 ($[M + H]^+$ requires 1104.6).

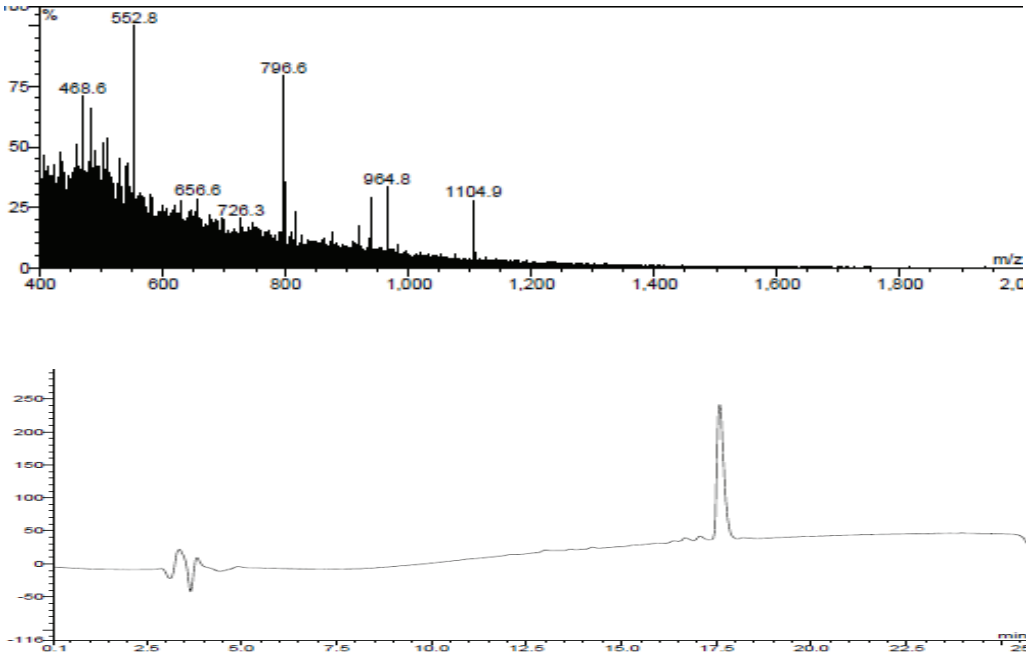

Figure 8.34: HPLC spectrum following purification for dendrimer **67**. R_t 17.5 min; ***m/z*** MS(ESI) 1104.9 ($[M + H]^+$ requires 1104.6).

8.7 Cell binding assay

8.7.1 Materials for Cell Culture

Name	Composition	Source
RPMI	Premade	Invitrogen
Fetal bovine serum		Invitrogen
GlutaMAX^{TM} Supplement	Premade	Invitrogen
Penicillin/ Streptomycin	Premade	Invitrogen
PBS	2.7mM KCl, 1.5mM KH_2PO_4, 140mM NaCl, 1mM Na_2HPO_4, pH 7.4	
RF10	RPMI10% fetal bovine serum, Penicillin Streptomycin and GlutaMAX	
FACS wash	1xPBS, 1%FBS	

8.7.2 Antibodies (conjugated) and viability stains for cell binding assay at 0 °C and 37 °C

Fluorophore	Antigen	Dose	Company	Clone
Alexa647	CD1a	1 μL	Biolegend	
PE	CD20	2 μL	Biolegend	
Fluorescein	2 μL			
7AAD	-	2 μL		

8.7.3 Antibodies (conjugated) and viability stains for PBMC assay

Fluorophore	Antigen	Dose	Company	Clone
Alexa488	CD301 (MGL)	5 μL	Imgenex	125A10.03
PE	CLEC9a	1.25 μL	Biolegend	8F9
PECF594	CD3	1.25 μL	BD	UCHT1
PECF594	CD20	1.25 μL	BD	2H7
PECF594	CD56	1.25 μL	BD	B159
PE-Cy7	CD1c	1.25 μL	Biolegend	L161
PerCpcy5.5	BDCA2	5 μL	Biolegend	201A
APC-Cy7	CD16	1.25 μL	Biolegend	3G8
Alexa700	HLADR	1 μL	Biolegend	L243
BV421	CD11c	1.25 μL	Biolegend	3.9
Qdot655	CD14	1:100 1 μL	Life Tech	TüK4
	DAPI	1 μL		

8.7.4 Peripheral blood mononuclear cells isolation

Blood was taken with informed consent from healthy volunteers. 100 mL of blood was collected from the donor into heparanised tubes. The Blood was diluted 1:1 with RPMI and the PBMCs were purified on a lymphoprep gradient in Leucosept tubes. The samples were centrifuged for 15 min at room temperature with the break off in a Sorvall RT7 with a Sorval RTH-750 swinging bucket rotor. The enriched cell fraction was harvested and combined. The PBMCs were washed twice with RPMI. The pellet would usually contain some visible RBC, therefore 500 μL RBC lysis buffer (BioLegend) with 4.5 mL water was added to the PBMC pellet. The resulting suspension was left for 5 min in the Fridge. The suspension was diluted with 10 mL RPMI and then centrifuged. The supernatent was removed and the pellet suspended in 10 mL RPMI. The cells were counted and resuspended in MACS buffer (see below).

8.7.5 Purification and culture of Monocytes and MODC

Monocytes isolated by positive selection using the MACS Monocyte Isolation Kit II and LS Columns (both Miltenyi Biotec) as per the manufacturer's instructions. All solutions were pre–chilled before use. The PBMCs were suspended in 80 μL of MACS buffer per 10^7 cells. To this solution 20 μL of CD14 MicroBeads were added per 10^7 PBMC cells. The solution was incubated for 15 minutes at 4 °C. The cells were washed with 1 mL of MACS Buffer and pelleted by centrifugation at 400xg for 10 minutes. The supernatant was aspirated completely and the cells resuspended in 500 μL of MACS buffer for every 10^8 cells. An LS Column was placed in the magnetic field of a MACS Separator, and the column rinsed in 3 mL of MACs buffer. The PBMCs suspended in MACS buffer were pipetted onto the top of the column, and allowed to pass through by gravity. The cells with no CD14 magnetic beads attached were washed though with the initial effluent and were collected and set aside. The column was removed from the magnetic field and 5 mL of MACS Buffer was pushed through the column to collect the CD14 positive cells. The cells were counted and then resuspended in 1x10^6 cells/mL in RF10 with 100 ng/mL GM-CSF and 50 ng/mL IL-4. Monocytes were seeded at the equivalent of approximately 4x10^6/well of a 6 well plate. Monocytes were cultured at 37 °C/5% CO_2 for 4 days before use. Every second the plate was centrifuged before removing half of the media and replacing with fresh RF10 with GM-CSF and IL-4.

8.7.6 Culture of LG2 cells

The LG2 cells were cultured with RF10. The culture was split every 3-4 days, and fresh RF10 was added. The LG2 culture was maintained throughout the periods of experimentation.

8.7.7 Cell binding assay at 0 °C and 37 °C

The cell binding assay which was conducted at 0 °C used PBS as the media, the assay conducted at 37 °C used RF10 as the media. The MoDC and LG2 were harvested, the cells were pelleted and then the experiments were resuspended in the appropriate media at $1x10^6$ cells/mL. The experiment used a 96-well plate, with each well used in the experiment containing $1x10^5$ of MoDC (100 μL) and $1x10^5$ of LG2 cells (100 μL). The plate was centrifuged for 10 minutes and the cells pelleted at the bottom of each well. The supernatent was removed and 50 μL of the indicated constructs dissolved in the media of the experiment was added to each well. The plate was then left to incubate for the desired length of time at either 0 °C or 37 °C. For the experiment at 37 °C the plate was placed on ice for 15 min after the incubation. For both experiments each well was washed three times with media (150 μL).

8.7.8 Flow cytometry after cell binding assay

All flow cytometry experiments were completed on the same day the cell binding assay was performed. Cells were kept on ice for the duration after the cell binding assay before being analysed on the FACSCalibre^{TM}. Cells were resuspended in a master mix which contained media and the antibodies PECD20 and CD1a647. The cells were incubated for 30 minutes on ice and then washed with PBS before being transferred to ice cold FACS buffer. 7AAD was added to each sample just prior to analysis. The was data aquired using CellQuest^{TM} software. Further analysis of the data was performed using FlowJo X (Treestar). Live cells were gated based on their forward scatter (FSC) versus the side scatter (SSC).

8.7.9 Cell binding and Flow cytometry of the PBMC assay

I assisted Dr Anna Brooks for this experiment. I helped prepare and stain all of the samples, Dr Anna Brooks ran the Flow cytometry using the FACSCalibre machine.

The PBMC were separated as described in section 8.7.4. The PBMCs were resuspended at a concentration of $1x10^6$/mL and then 100K of cells were put into each well used of a 96 well plate. The cells were centrifuged down at 400xg and the supernatent removed. The cells were resuspended with dendrimers in RF10. The cells were incubated at 37 °C for 1 hour and then put on ice to cool for 15 min. The PBMCs were washed with 100 μL RF10 three times.

Cells were resuspended in a master mix which contained RF10 and the antibodies from table 8.7.3. The cells were incubated for 30 minutes on ice and then washed twice with RF10 before being transferred to ice cold FACS buffer. At this stage Dr Anna Brooks took full control of the experiment. DAPI was added to each sample just before it was run on the machine. All events were collected, and the data analysed using CellQuest^{TM} software. Further manipulation of the data was performed using FlowJo X (Treestar). Live cells were gated based on their forward scatter (FSC) versus the side scatter (SSC). Further gating was dependent on fluorescence.

8.8 Thermal melt assay

8.8.1 Expression

The 4 different Human MGL CRD domains were provided by Dr. Christopher Squire (SBS, UoA). The pDEST17 Gateway vector (Invitrogen). The plasmid was transformed into E.coli BL21(DE3) and grown on agar plates supplemented with 56 nM ampicillin. BL21(DE3) has ampicillin resistance and the protein encoding sequence under a T7 promoter. The protein that was expressed contained a cleavable hexahistidine (His) tag which gave the option for subsequent purification.

8.8.2 Agar plates

A solution containing tryptone (1 g), NaCl (1 g, 17 mmol), yeast extract (0.5 g), Agar (1.5 g) and water (100 mL) was autoclaved. A 200 μL ampicillin solution (10 mg, 28 μmol) was added to the autoclaved agar solution after it had cooled to room temperature. The agar solution was poured into 8 dishes in sterile conditions and allowed to set.

8.8.3 MGL expression

The frozen MGL expressing E. coli were removed from the -80 °C freezer and streaked across the agar plate. The plate was put in a room heated to 37 °C and left to incubate for 18 h. A solution of Terrific Broth (tryptone (6.66 g), yeast (13.33 g), glycerol (2.22 mL) and water (500 mL)) was autoclaved in a bevelled 2.5 L flask, and when the broth had returned to room temperature 500 μL of ampicillin solution (25 mg, 70 μmol) was added. An individual colony from the plate was transferred to the broth, then the solution was incubated for 18 h at 37 °C. The solution was centrifuged at 13000 × g for 30 min, the supernatent was discarded and the pellet kept.

8.8.4 Cell lysis and protein denaturation

The E.coli pellet was resuspended in 1:1 volume with a tris buffer solution (Tris 20 mM, NaCl 150 mM and 10% Glycerol). The solution was put through a constant cell disruption system instrument, then diluted 1:1 with the tris buffer solution and then put through the constant cell disruption system instrument a second time. The mixture containing lysed cells was centrifuged at 13000 × g for 30 min. The pellet was kept and the supernatent discarded. The pellet was resuspended in 5 mL of buffer containing guandinium (6M), and CaCl (0.01%) and BME (30 μL). The protein suspension

was agitated overnight at 4 °C. The suspension was centrifuged at 13000 × g for 30 min and the supernatent was kept and the pellet discarded.

8.8.5 Rapid dilution and concentration

The 5 mL of supernatent containing MGL was spiked with BME (7.5 μL) before being added slowly over the course of an hour to 300 mL of refolding buffer (glucose (500 mM), CHES (pH 9, 50 mM), NDSB 201 (100 mM), $CaCl_2$ (5 mM), KCl (100 mM) and water) with BME (210 μL). The solution was left to stir slowly overnight at 4 °C. The solution was centrifuged at 13000 × g for 30 min and the supernatent was kept and the pellet discarded. The supernatent was passed through a 0.2 μm filter. The solution was concentrated from 300 mL to 10 mL in a gas powered Amicon Stirred Cell Model 8400 concentrator before being transferred to a 10 kDa spin concentrator where the solution was concentrated down to 500 μL using a centrifuge spun at 4500 × g. The solution was filtered one final time before being nanodropped.

8.8.6 Size Exclusion Chromatography

MGL truncations 155-316, 166-316 and 176-316 were purified on a Superdex 75 10/300 column (GE Healthcare) [10 mm diameter x 300 mm length, column volume 24 mL, particle size 13 μm, void volume 7.5 mL]. MGL truncation 144-316 was purified on a Superdex 200 10/300 column. The column was equilibrated with 2 column volumes of the refolding buffer. The UV was monitored at 280 nm, and 1 mL fractions were collected. The size exclusion column was run at 0.3 mL/min. Fractions were characterised using SDS-PAGE and pooled where appropriate. Monomeric MGL was concentrated using 10kDa spin concentrators to 200 μL, diluted with 50 μL of glycerol and flash–frozen in liquid nitrogen to be stored at -80 °C.

8.8.7 Differential scanning fluorimetry (DSF) assay

The experiment was performed in 96-well plate format and assay medium (25 μL) consisted of the additive (1 uM), the MGL truncation (5 μM), SYPRO Orange (1:250 final dilution), glucose (375 mM), CHES (pH 9, 37.5 mM), NDSB 201 (75 mM), $CaCl_2$ (3.75 mM), KCl (75 mM) and water. Fluorescence was taken under the SYBR fluorophore setting (excitation: 494 nm, emission: 521 nm) on the iCycler IQ5 real time-PCR machine (Biorad, Hercules, CA, USA), at 1 °C increments starting at 25 °C. Each temperature change was followed by a 1 min equilibration time prior to measurement. GalNAc was used as a positive control.

Chapter 9

Appendix

9.1 Chemistry appendix

9.1.1 Building blocks

Fmoc–azido alanine

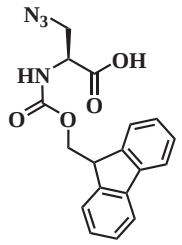

9

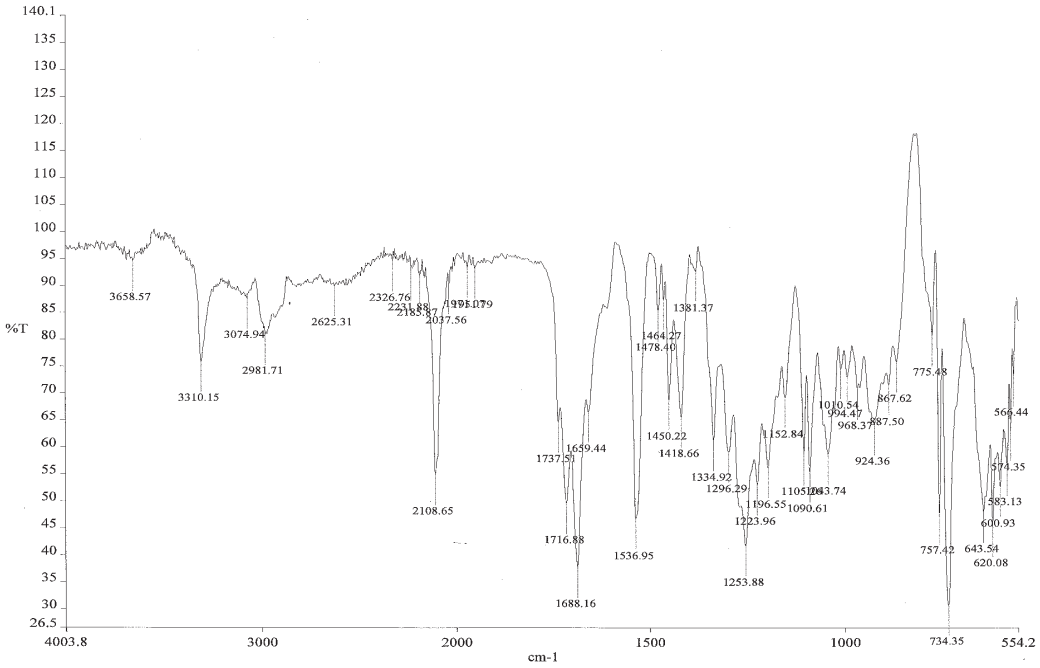

Figure 9.1: IR of Fmoc–azidoalanine

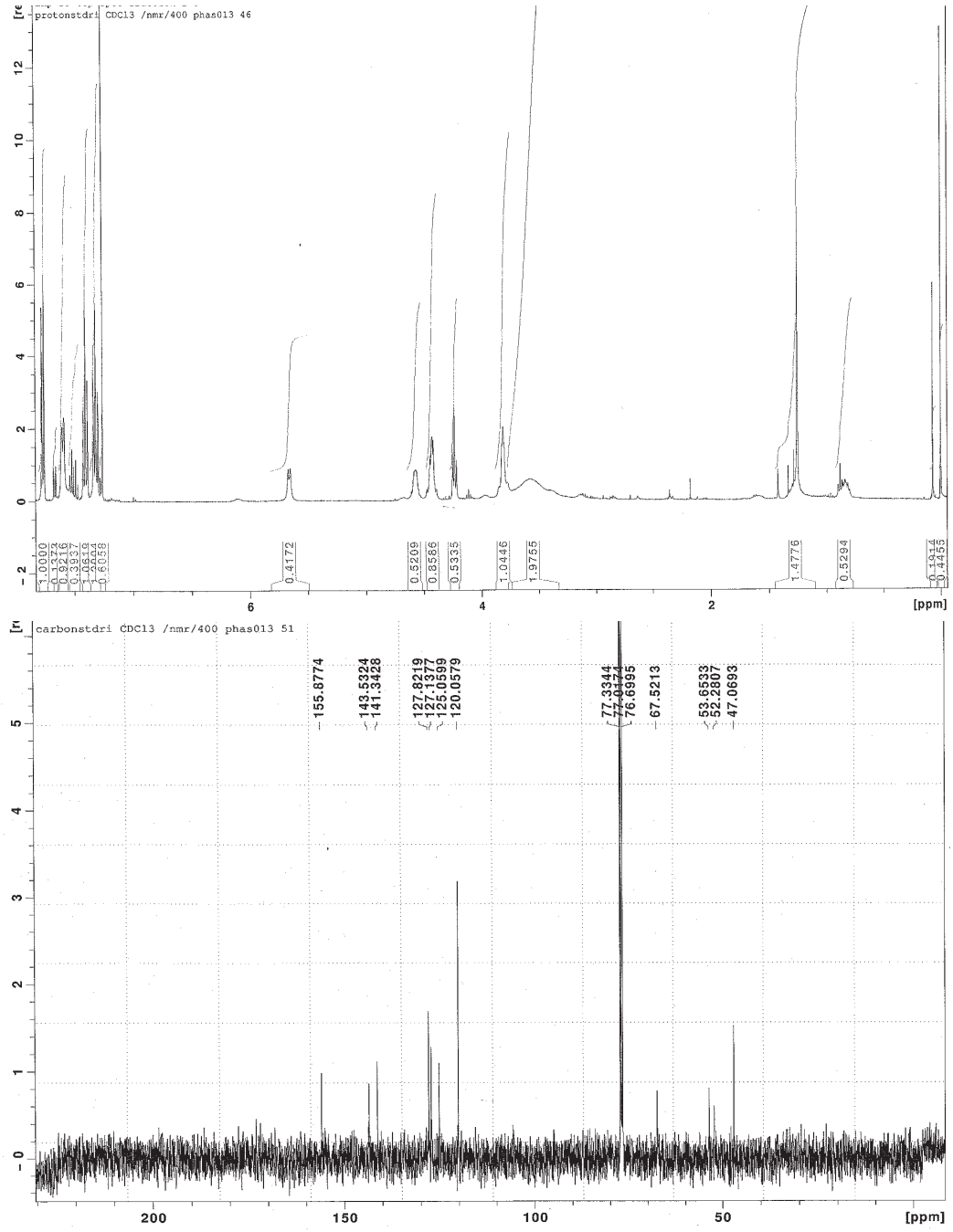

Figure 9.2: (Top) ^{1}H NMR (400 MHz, $CDCl_3$) (Bottom) **^{13}C NMR (100 MHz, $CDCl_3$)** of Fmoc–azidoalanine.

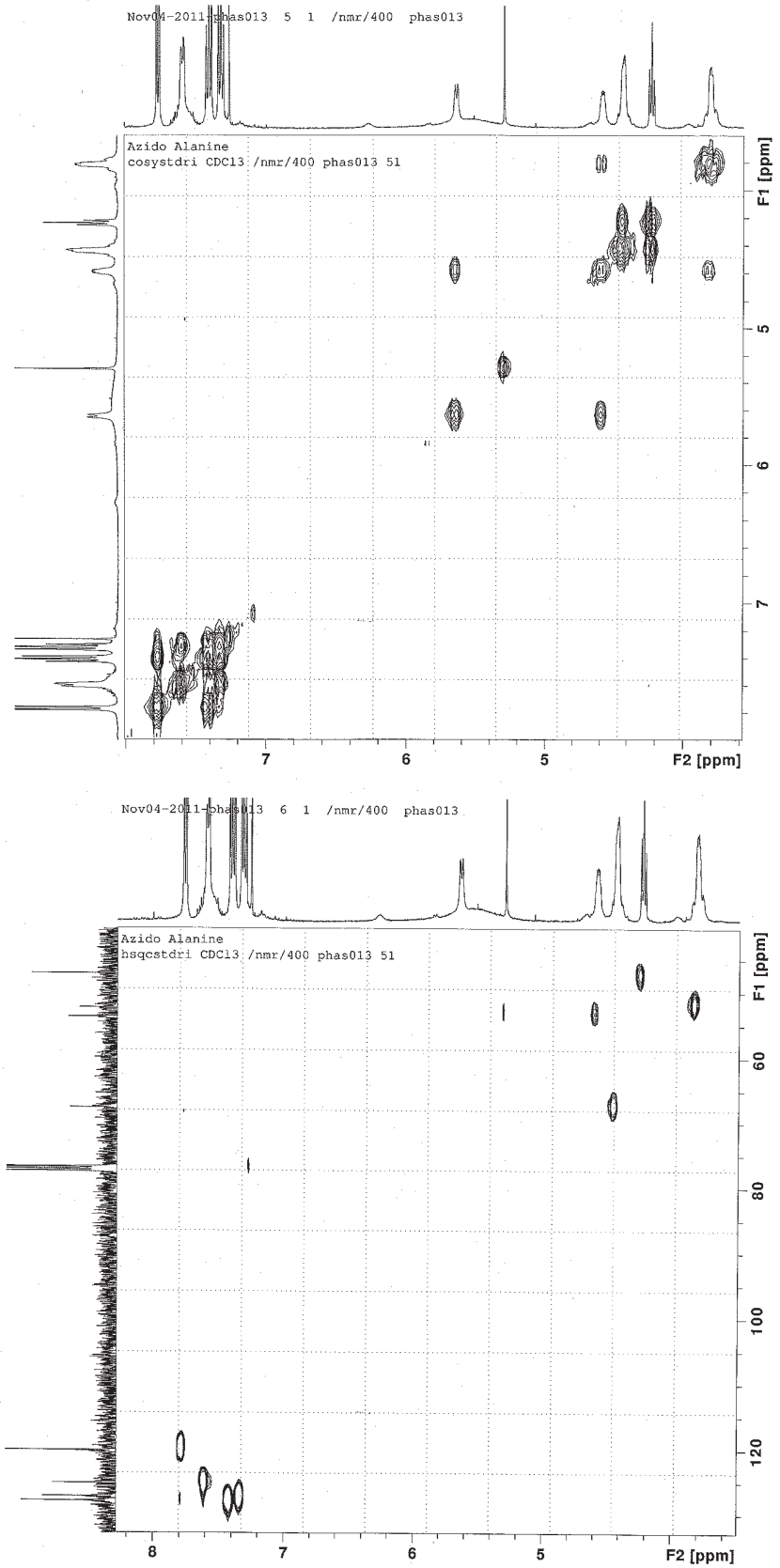

Figure 9.3: (Top) **COSY NMR (400 MHz, $CDCl_3$)** and (Bottom) **HSQC NMR (400 MHz and 100 MHz, $CDCl_3$)** of Fmoc–azidoalanine

1,3,4,6-Tetra-*O*-acetyl-2-azido-2-deoxy-D-galactopyranose

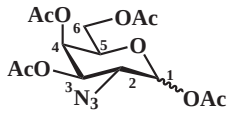

15

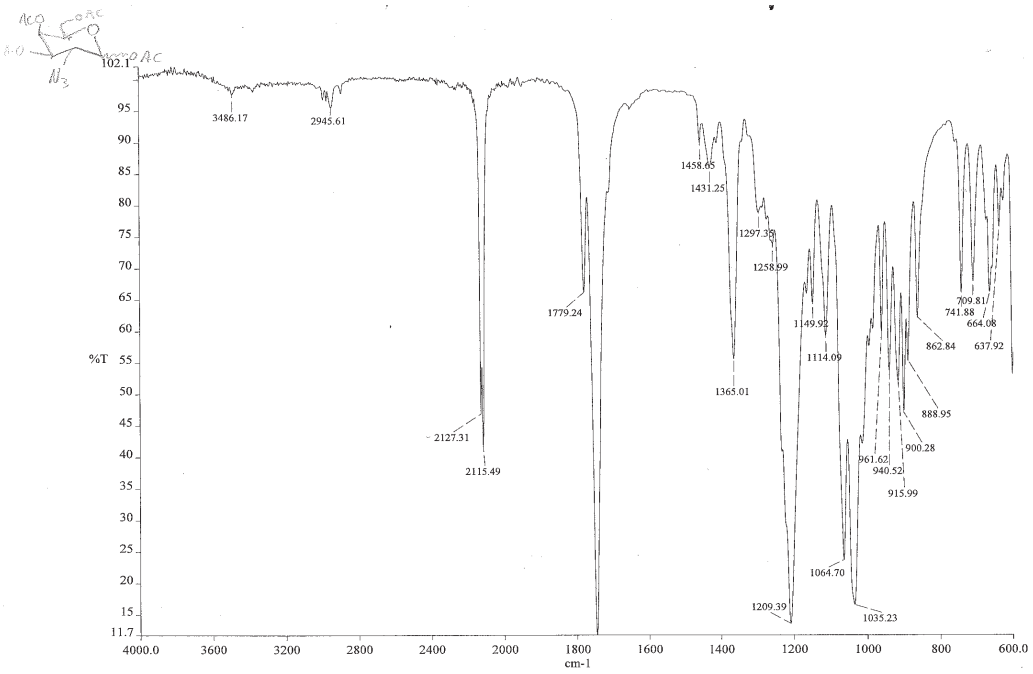

Figure 9.4: IR of glycosyl acetates **15**

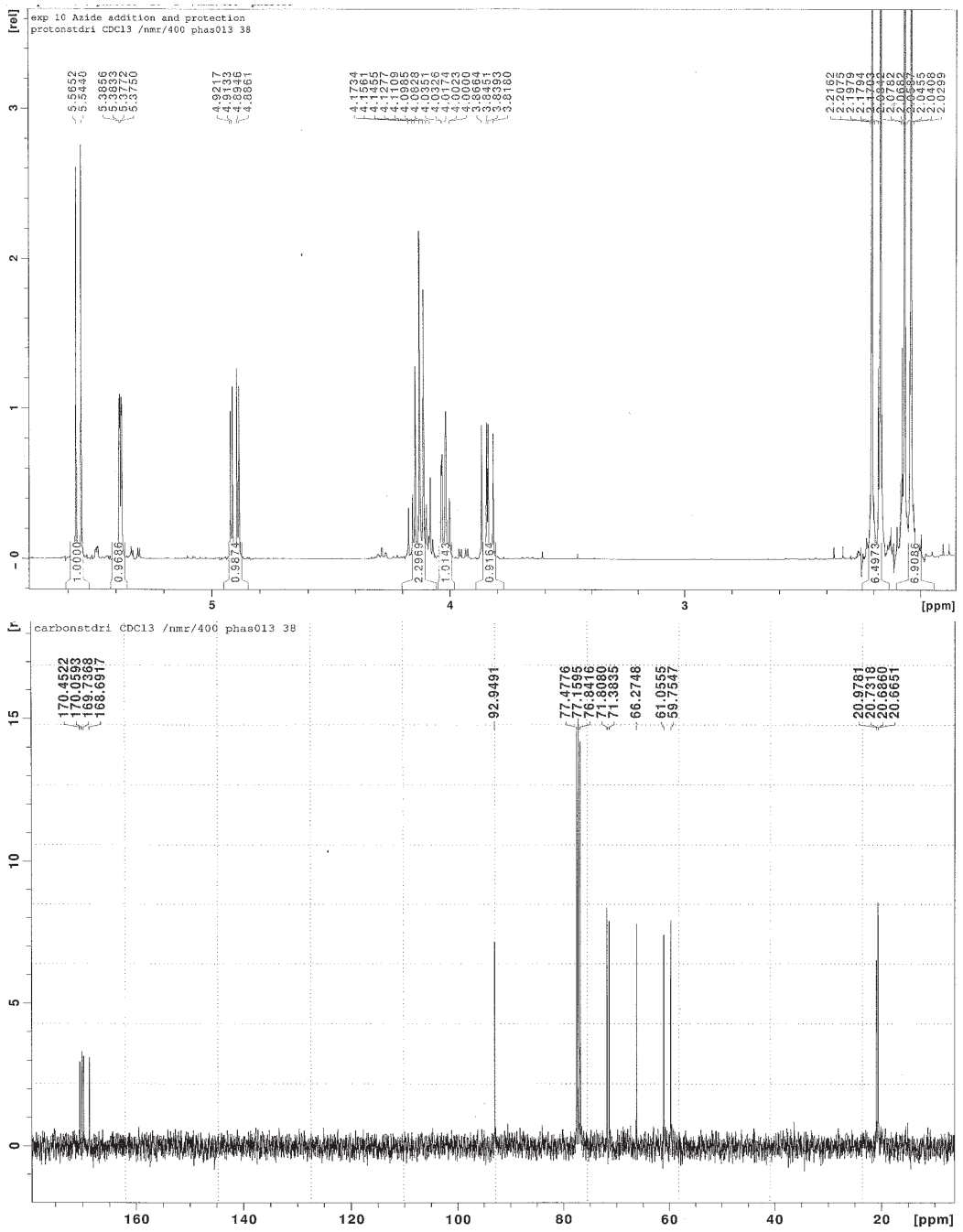

Figure 9.5: (Top)^{1}**H NMR (400 MHz, CDCl$_3$)** and (Bottom) ^{13}**C NMR (100 MHz, CDCl$_3$)** of glycosyl acetates **15**

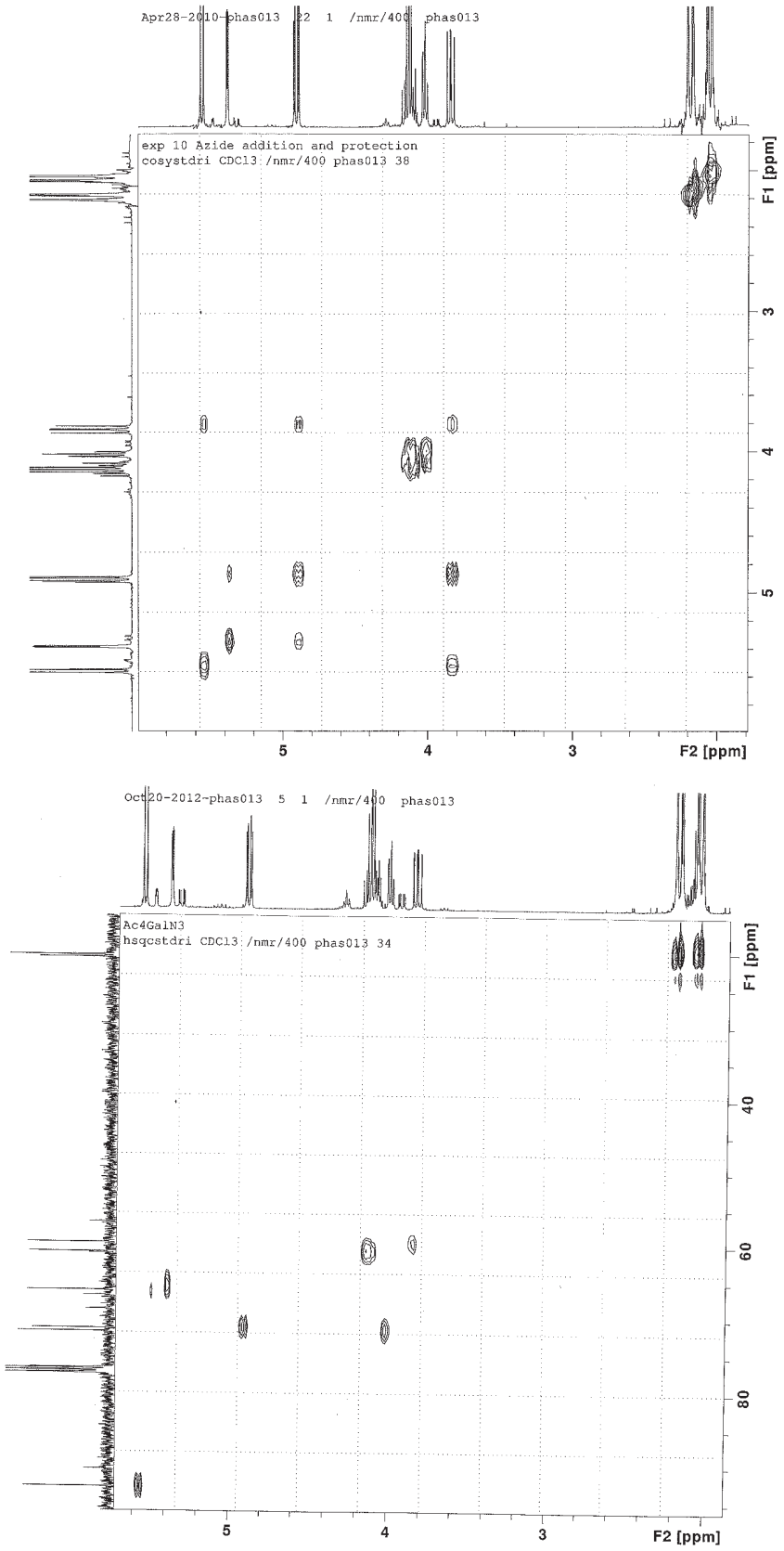

Figure 9.6: (Top) **COSY NMR (400 MHz, $CDCl_3$)** and (Bottom) **HSQC NMR (400 MHz and 100 MHz, $CDCl_3$)** of glycosyl acetates **15**

(Prop-2-yn-1-yl)-(3,4,6-triacetyl-2-azido-2-deoxy-D-galactopyranoside

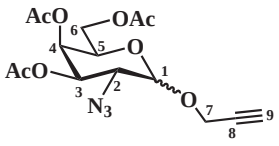

16

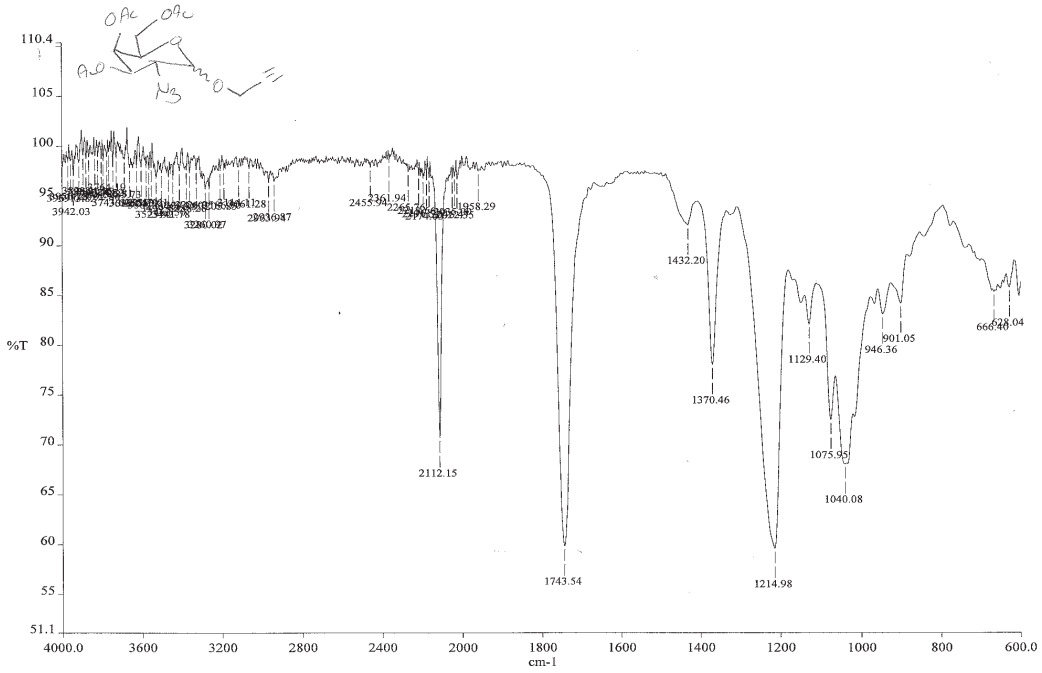

Figure 9.7: IR of α–azido glycosides **16**

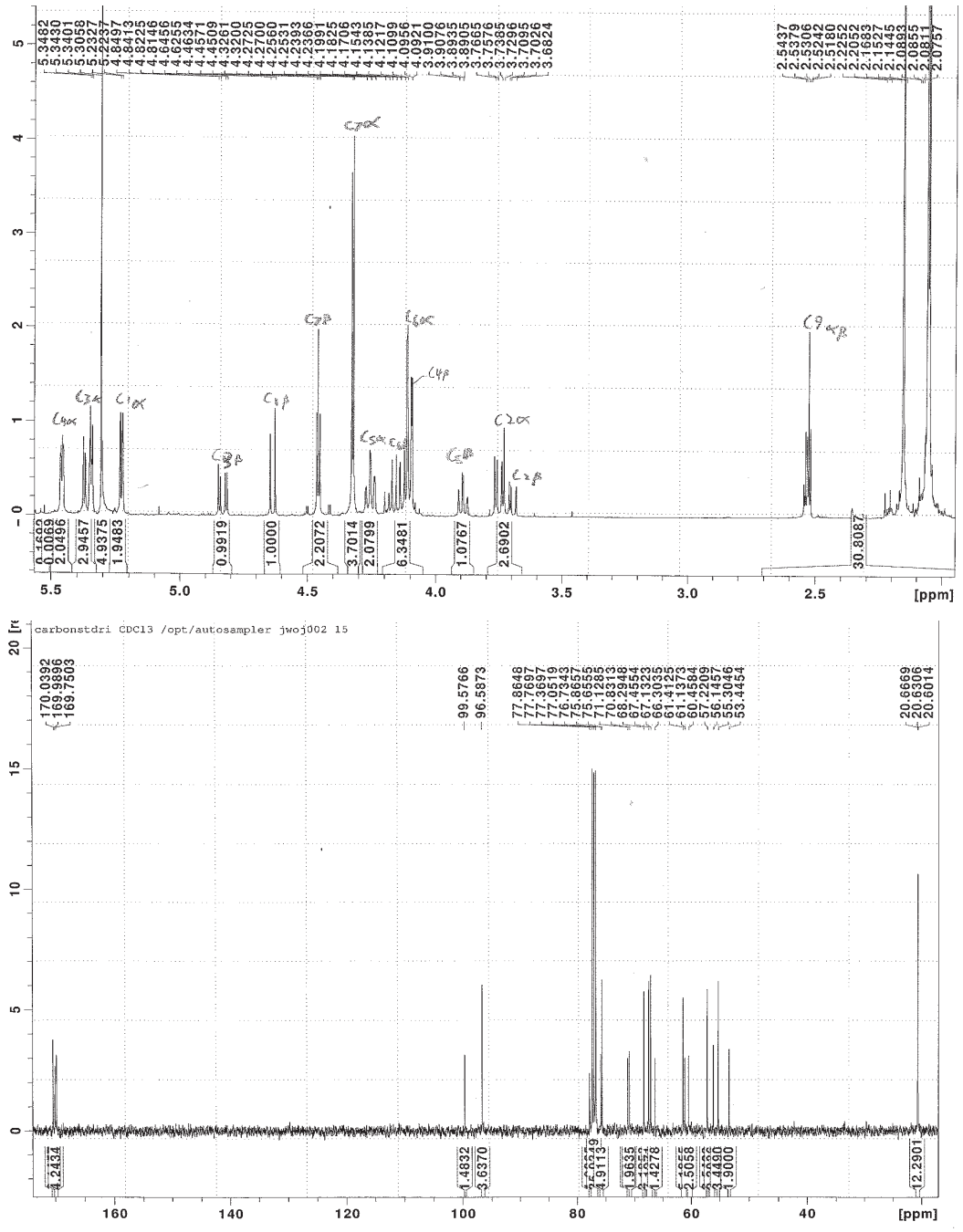

Figure 9.8: (Top) ^{1}**H NMR (400 MHz, CDCl$_3$)** and (Bottom) ^{13}**C NMR (100 MHz, CDCl$_3$)** of α–azido glycosides **16**

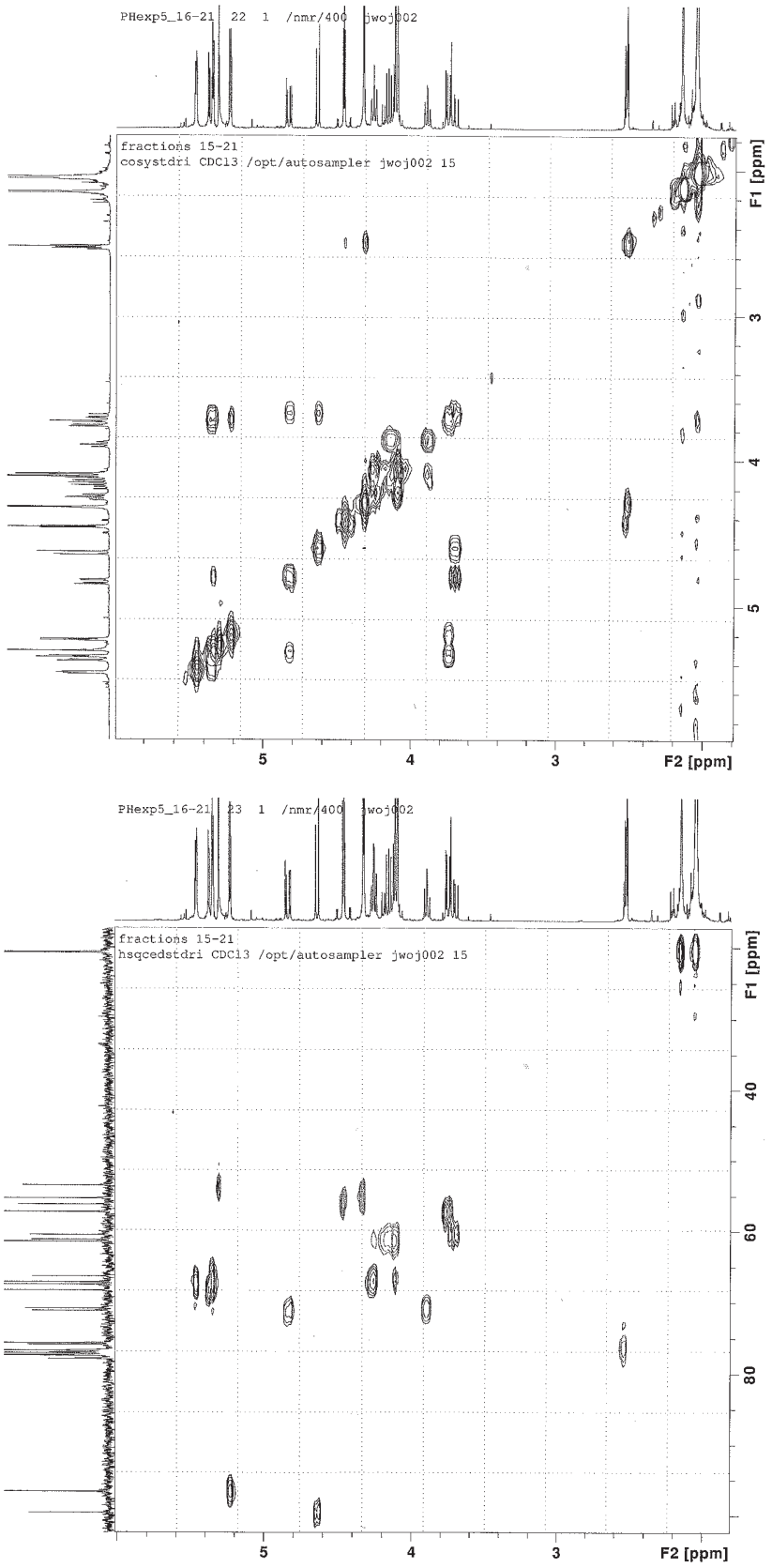

Figure 9.9: (Top) **COSY NMR (400 MHz, $CDCl_3$)** and (Bottom) **HSQC NMR (400 MHz and 100 MHz, $CDCl_3$)** of α–azido glycosides **16**

(Prop-2-yn-1-yl)-(2-acetamido-3,4,6-triacetyl-2-deoxy-α-D-galactopyranoside

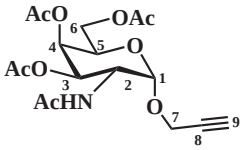

14

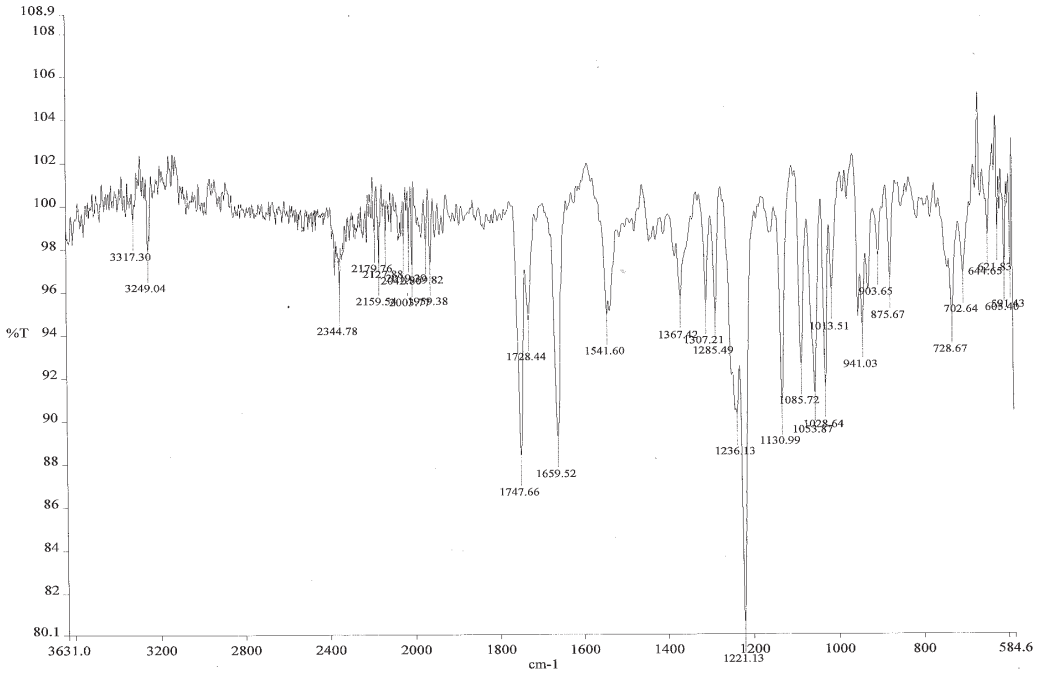

Figure 9.10: IR of α–propargyl GalNAc(Ac)$_3$ **14**

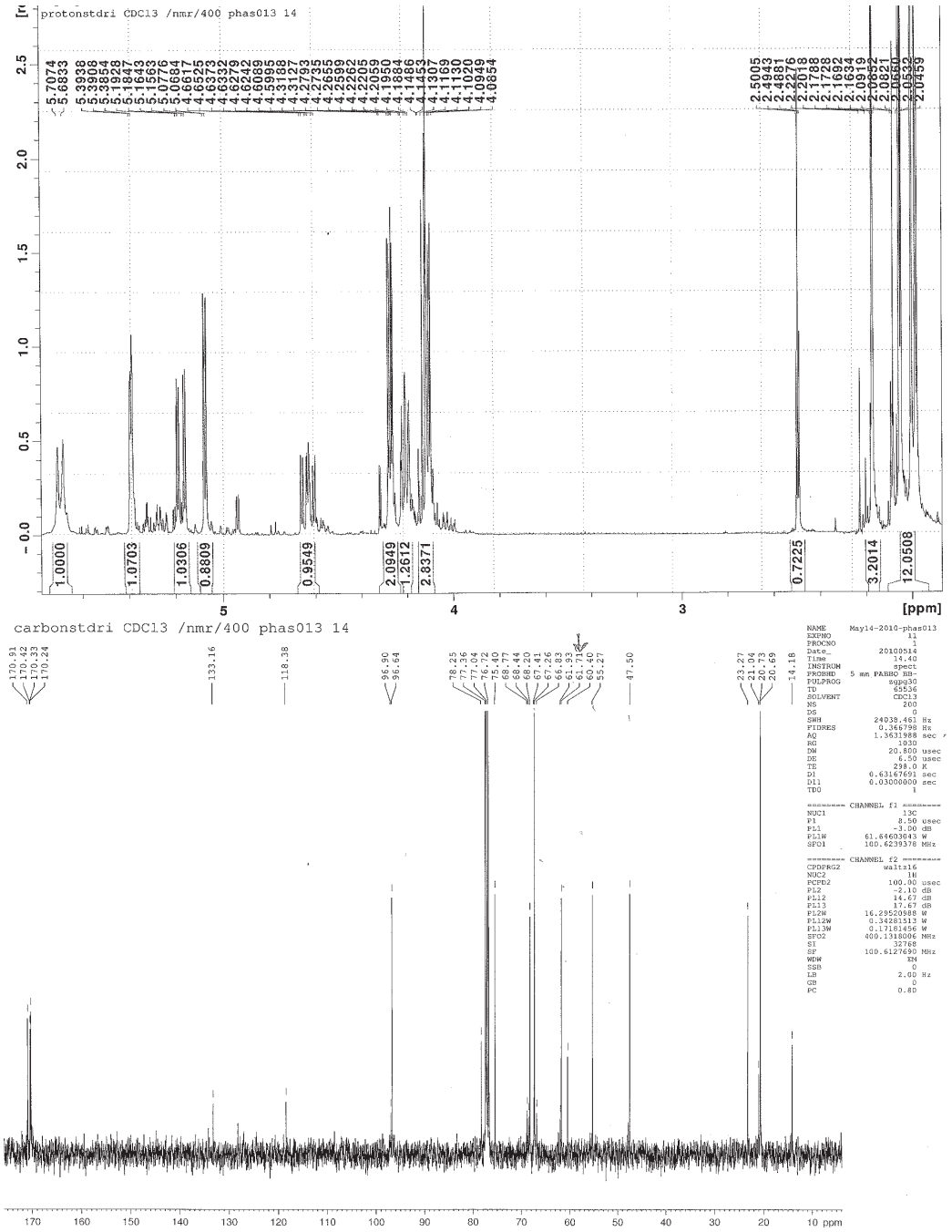

Figure 9.11: (Top) ^{1}**H NMR (400 MHz, CDCl$_3$)** and (Bottom) ^{13}**C NMR (100 MHz, CDCl$_3$)** of α–propargyl GalNAc(Ac)$_3$ **14**

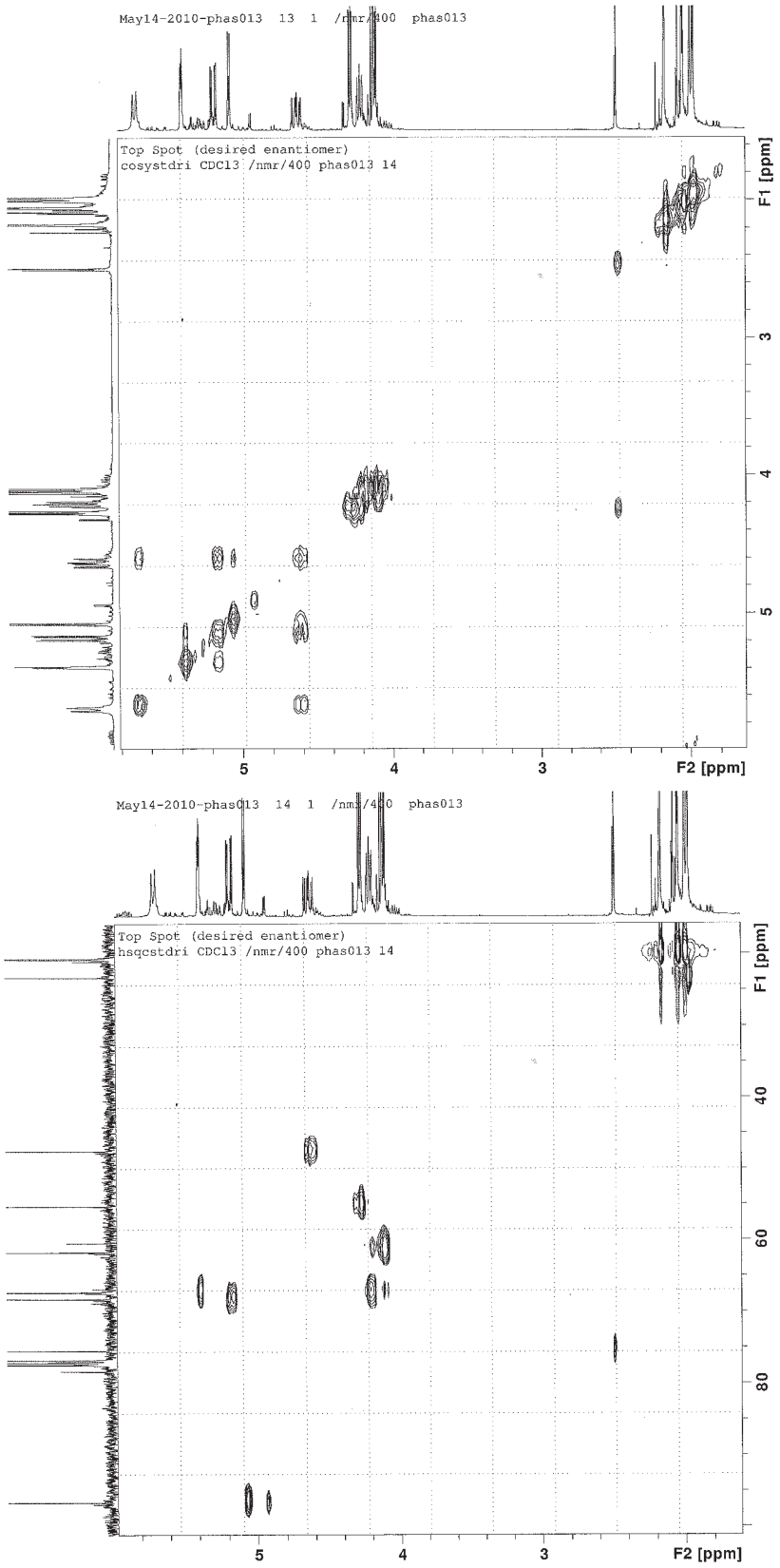

Figure 9.12: (Top) **COSY NMR (400 MHz, $CDCl_3$)** and (Bottom) **HSQC NMR (400 MHz and 100 MHz, $CDCl_3$)** of α–propargyl GalNAc(Ac)$_3$ **14**

**(2*S*)-2-[(9*H*-Fluoren-9-ylmethoxy)carbonyl]amino-3-(4-[(2,3,4,6-tetra-*O*-acetyl-α-D-galactopyranoyl)oxy
1*H*-1,2,3-triazol-1-yl)propanoic acid**

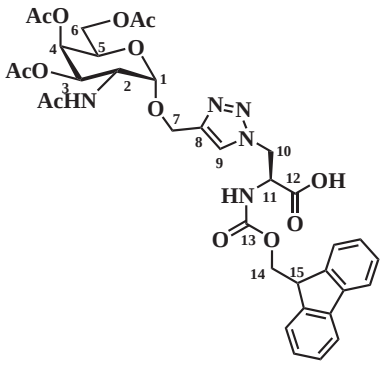

39

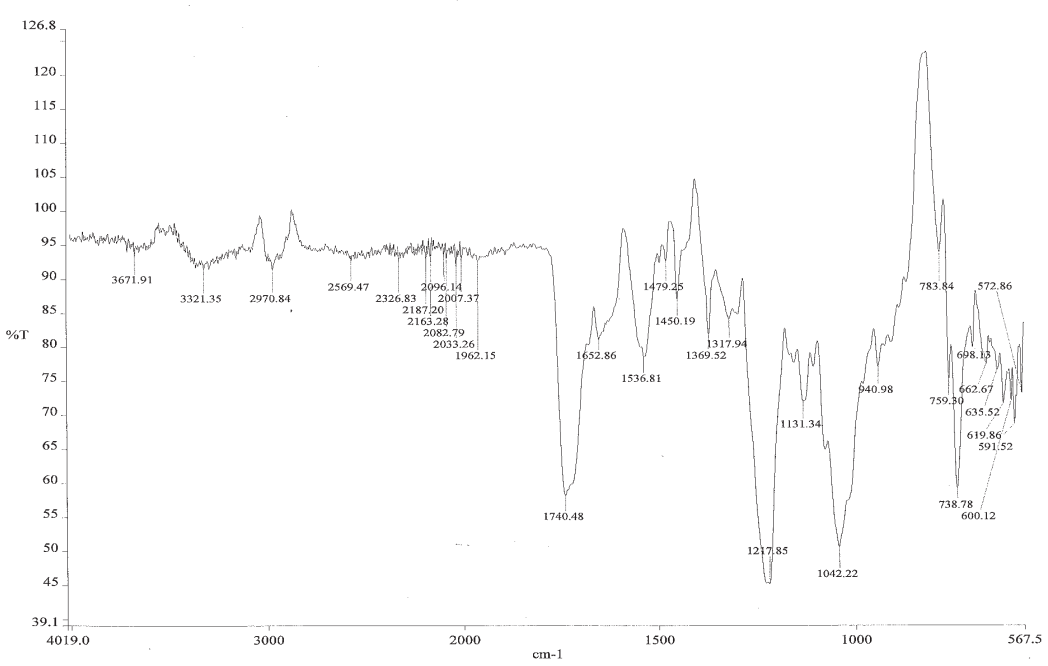

Figure 9.13: IR of acetate protected building block **39**

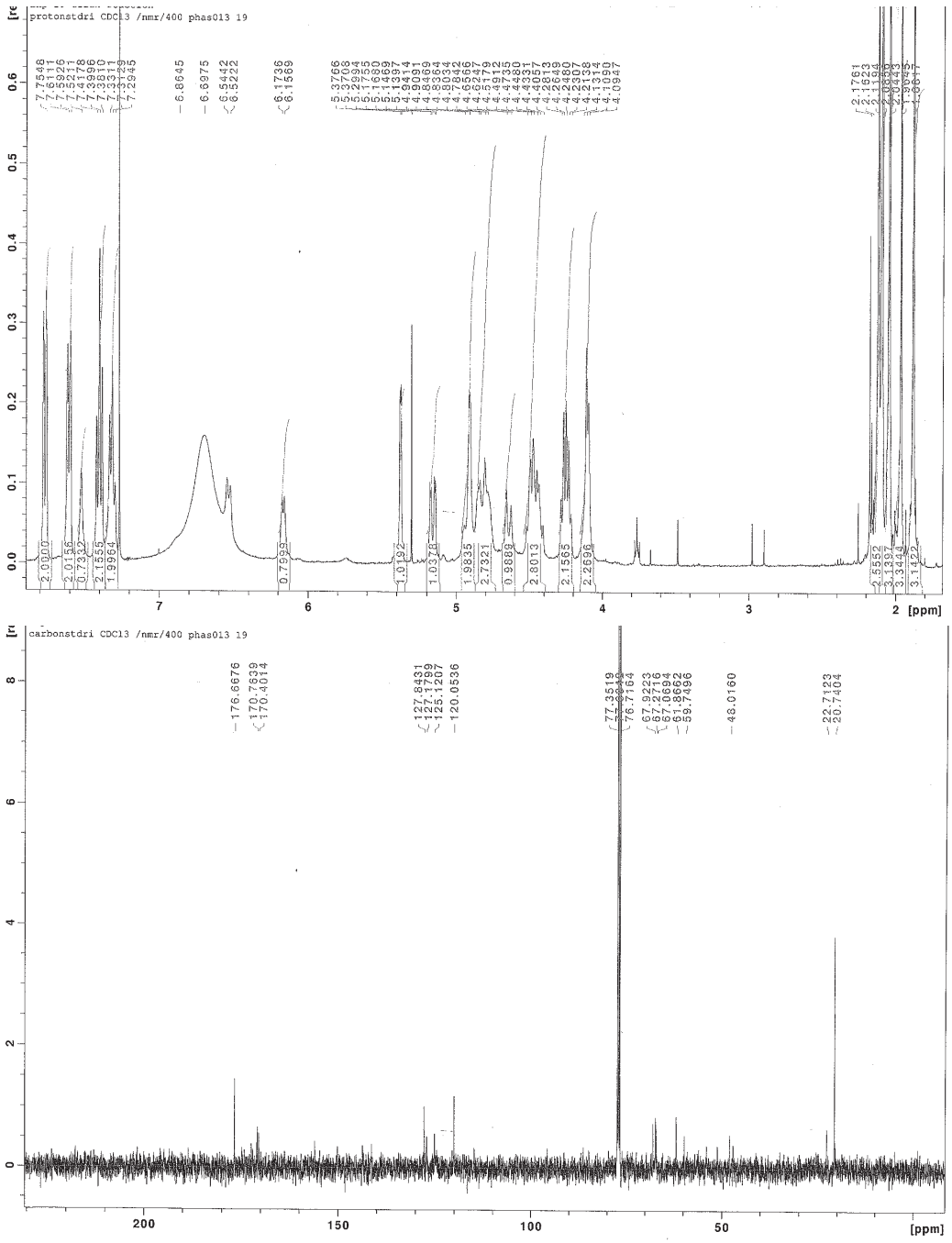

Figure 9.14: ^{1}H NMR (400 MHz, $CDCl_3$) and ^{13}C NMR (100 MHz, $CDCl_3$) of acetate protected building block **39**

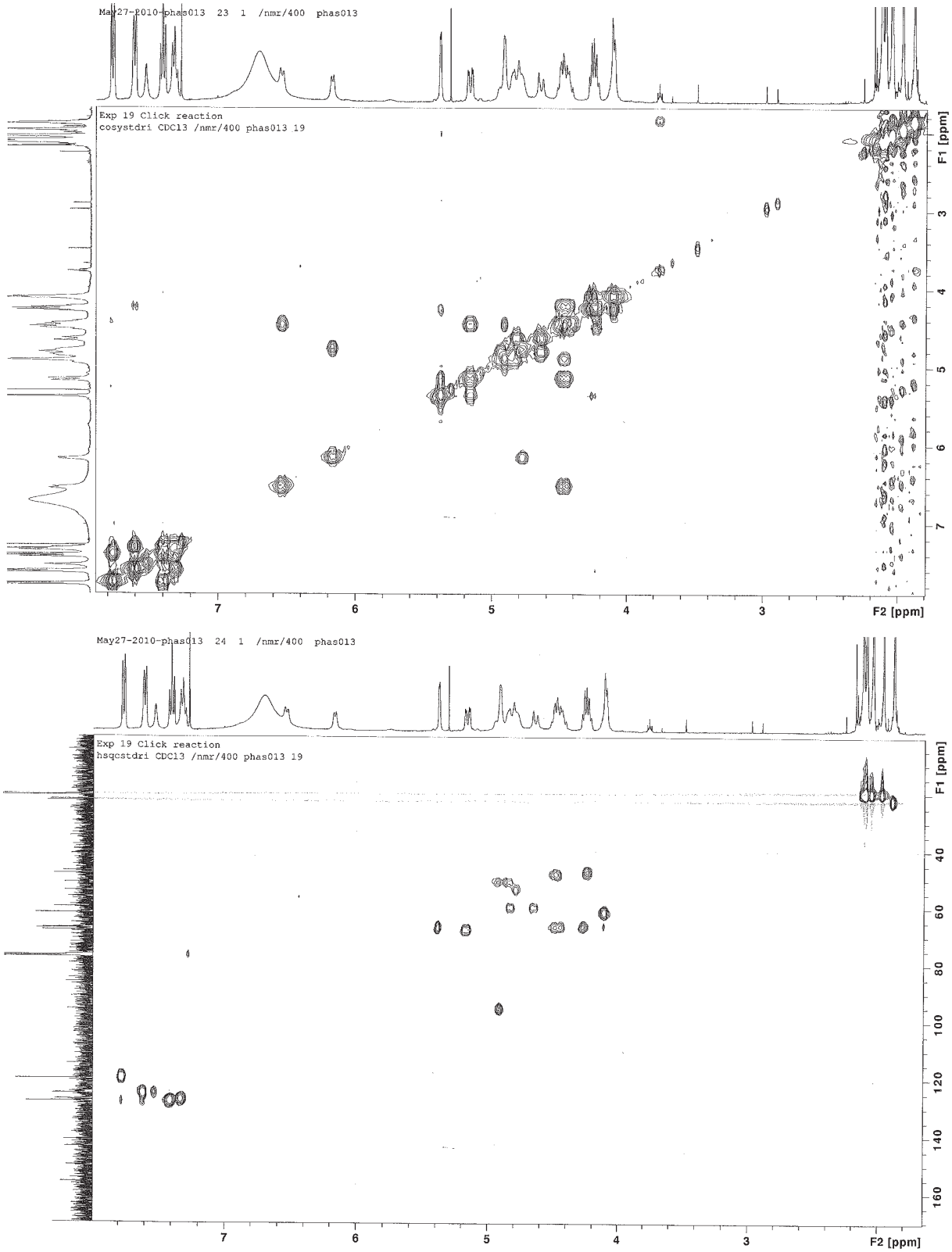

Figure 9.15: (Top) **COSY NMR (400 MHz, $CDCl_3$)** and (Bottom) **HSQC NMR (400 MHz and 100 MHz, $CDCl_3$)** of acetate protected building block **39**

Propargyl 2-*O*-α-D-Acetylgalactosamine

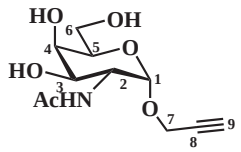

4

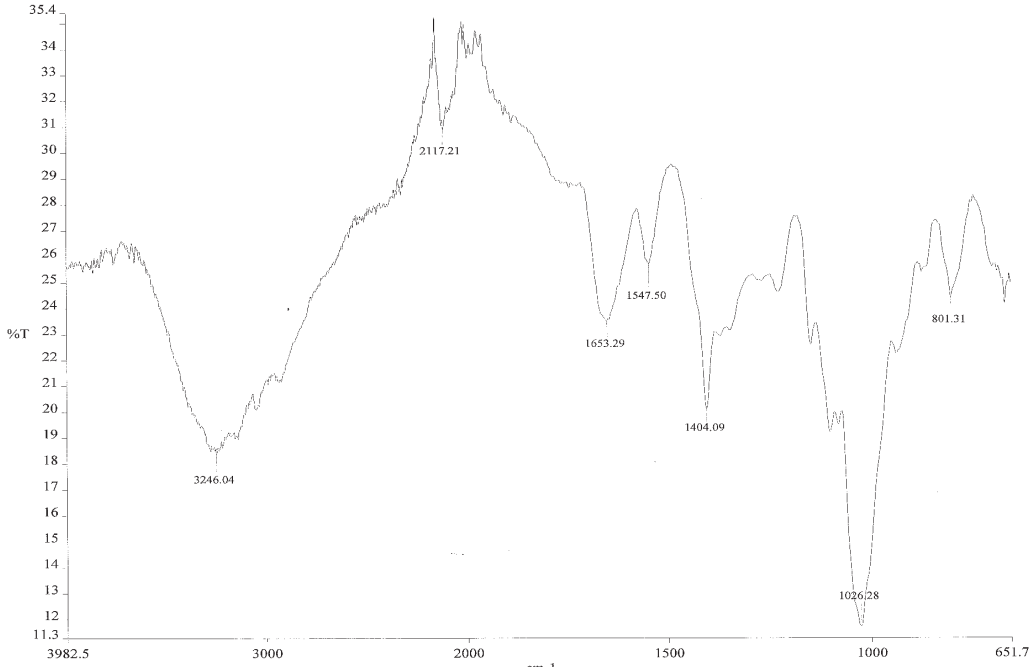

Figure 9.16: IR of α–propargyl GalNAc **4**

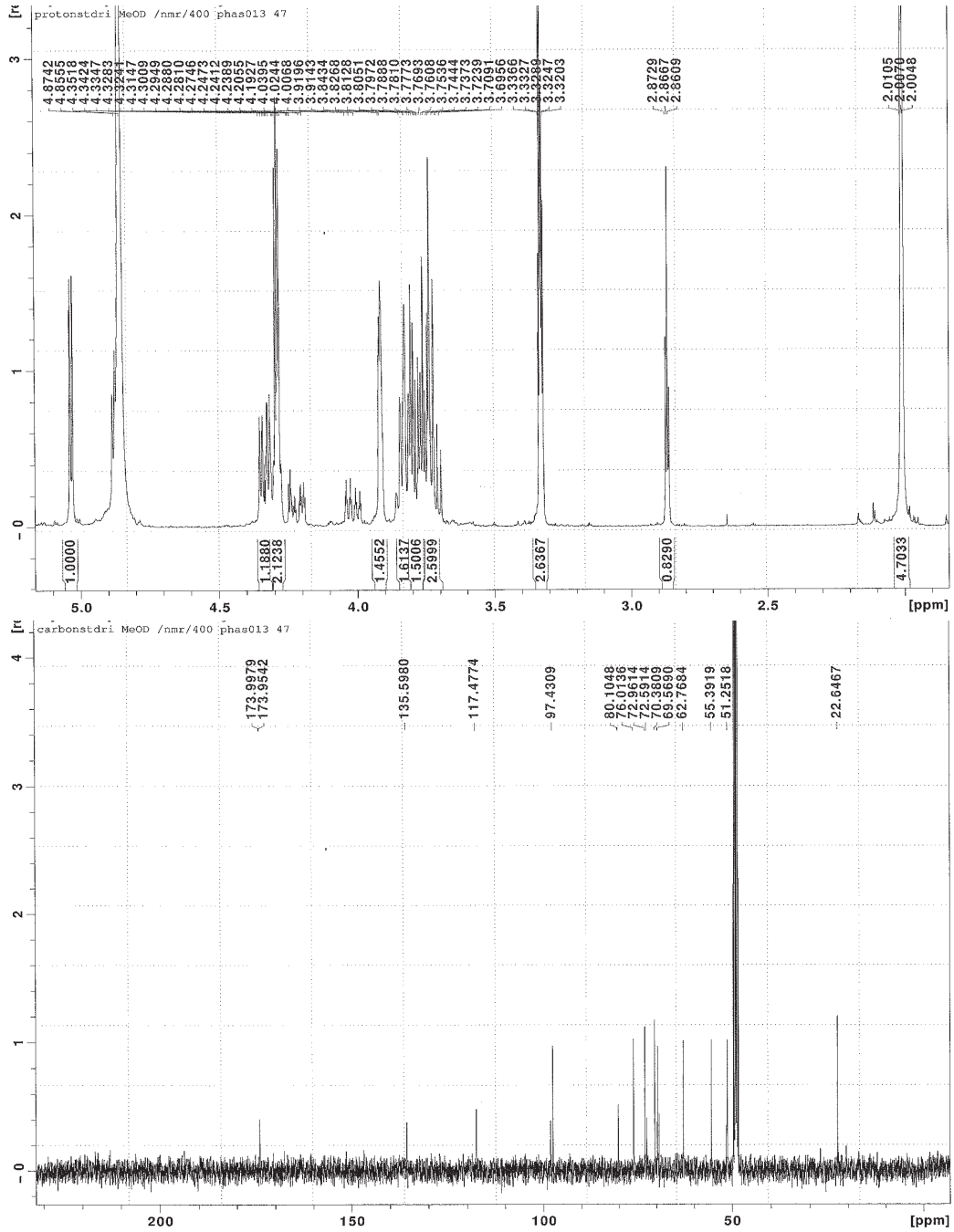

Figure 9.17: ^{1}H NMR (400 MHz, CD_3OD) and ^{13}C NMR (100 MHz, CD_3OD) of α–propargyl GalNAc **4**

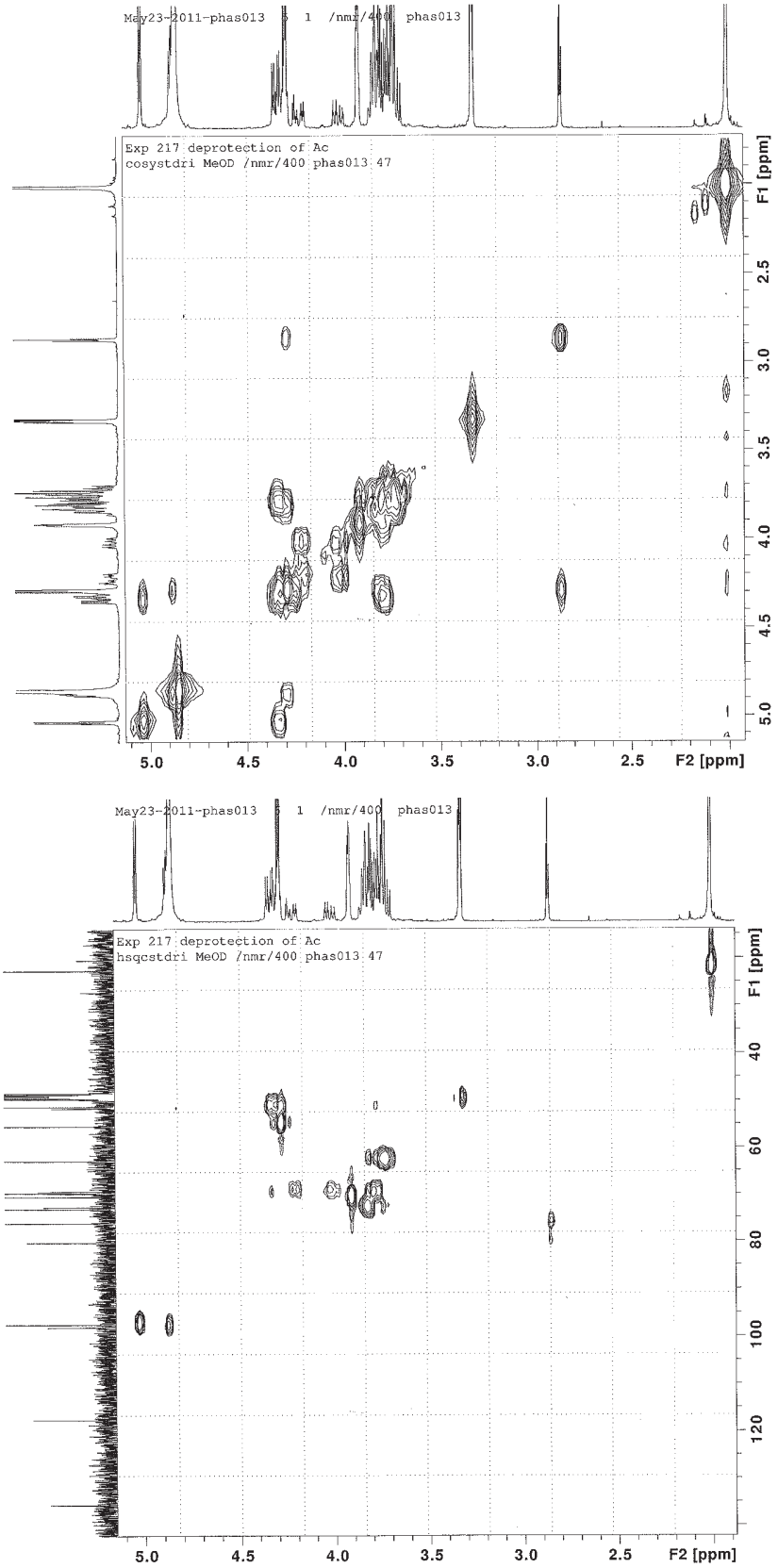

Figure 9.18: (Top) **COSY NMR (400 MHz, CD_3OD)** and (Bottom) **HSQC NMR (400 MHz and 100 MHz, CD_3OD)** of α–propargyl GalNAc **4**

(2*S*)-2-(((9*H*-fluoren-9-yl)methoxy)carbonylamino)-3-(1-deoxy-2-acet -amido-α-D-galactopyranosyl)-oxymethyl)-1*H*-1,2,3-triazol-1-yl)propanoic acid

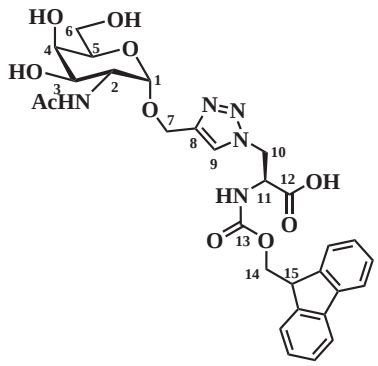

42

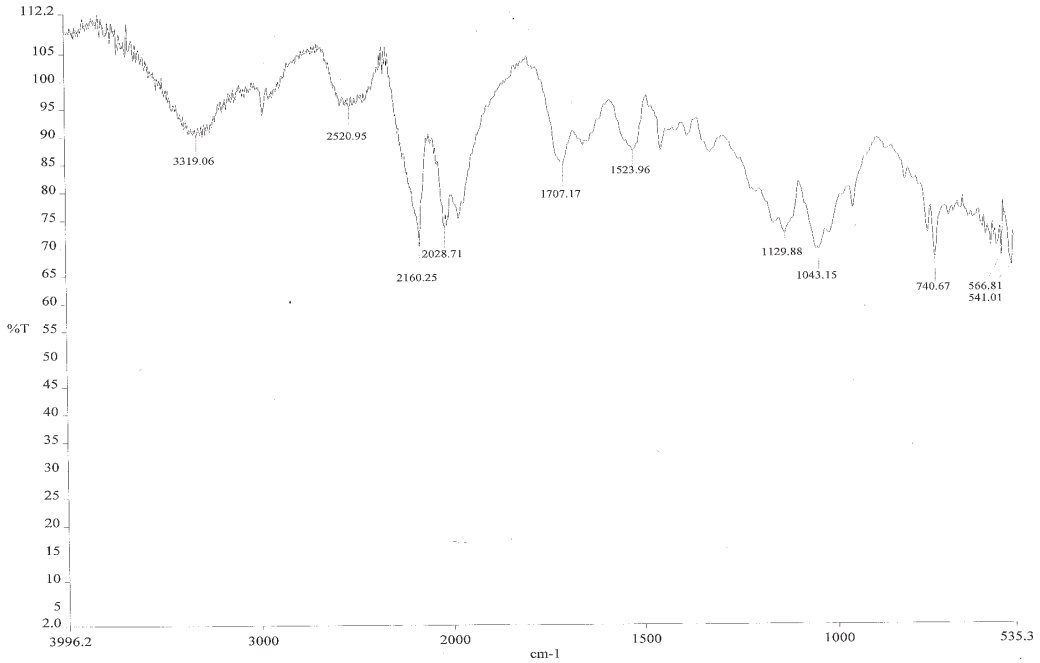

Figure 9.19: IR of de–protected click building block **42**

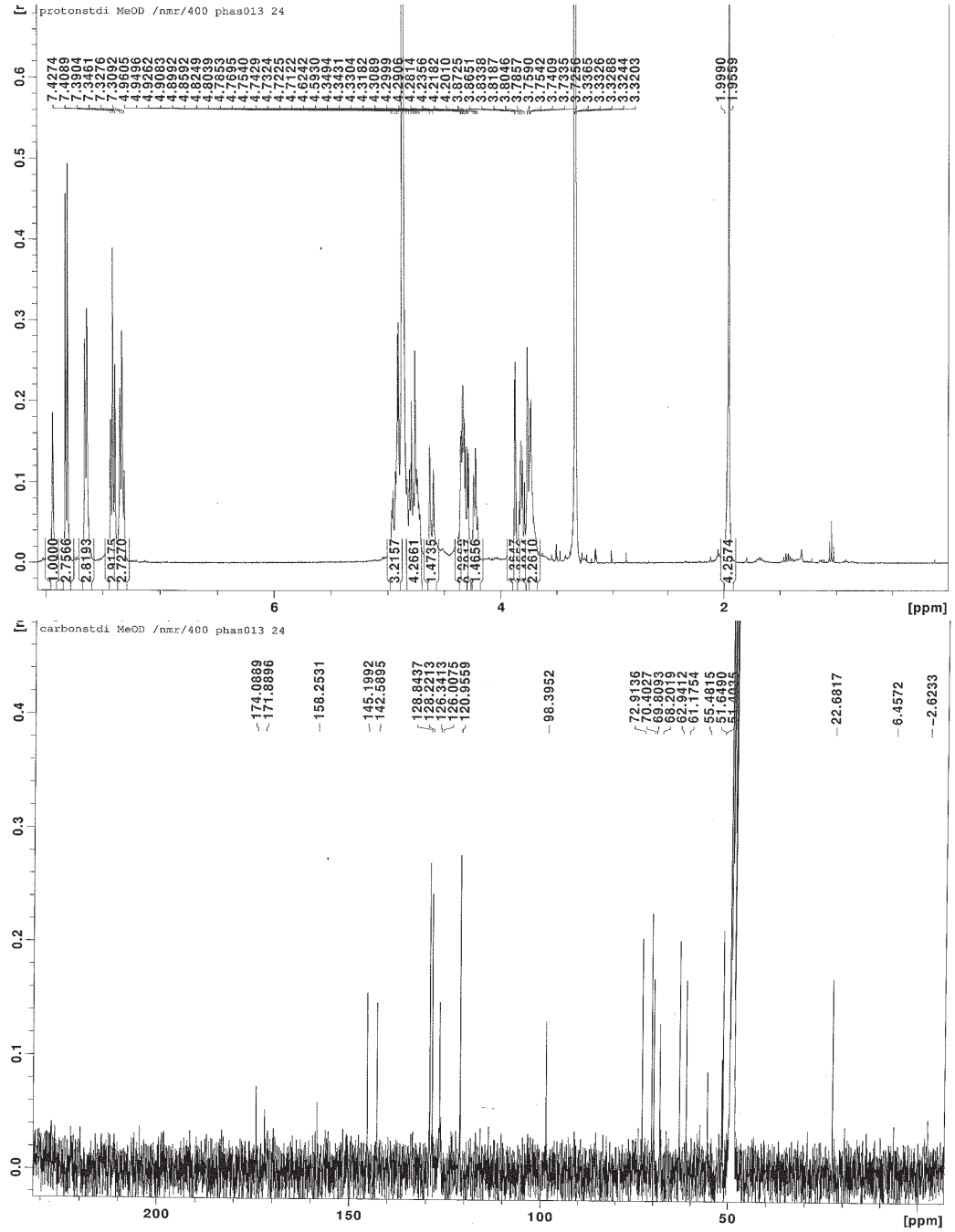

Figure 9.20: ^{1}H NMR (400 MHz, CD_3OD) and ^{13}C NMR (100 MHz, CD_3OD) of de–protected click building block **42**

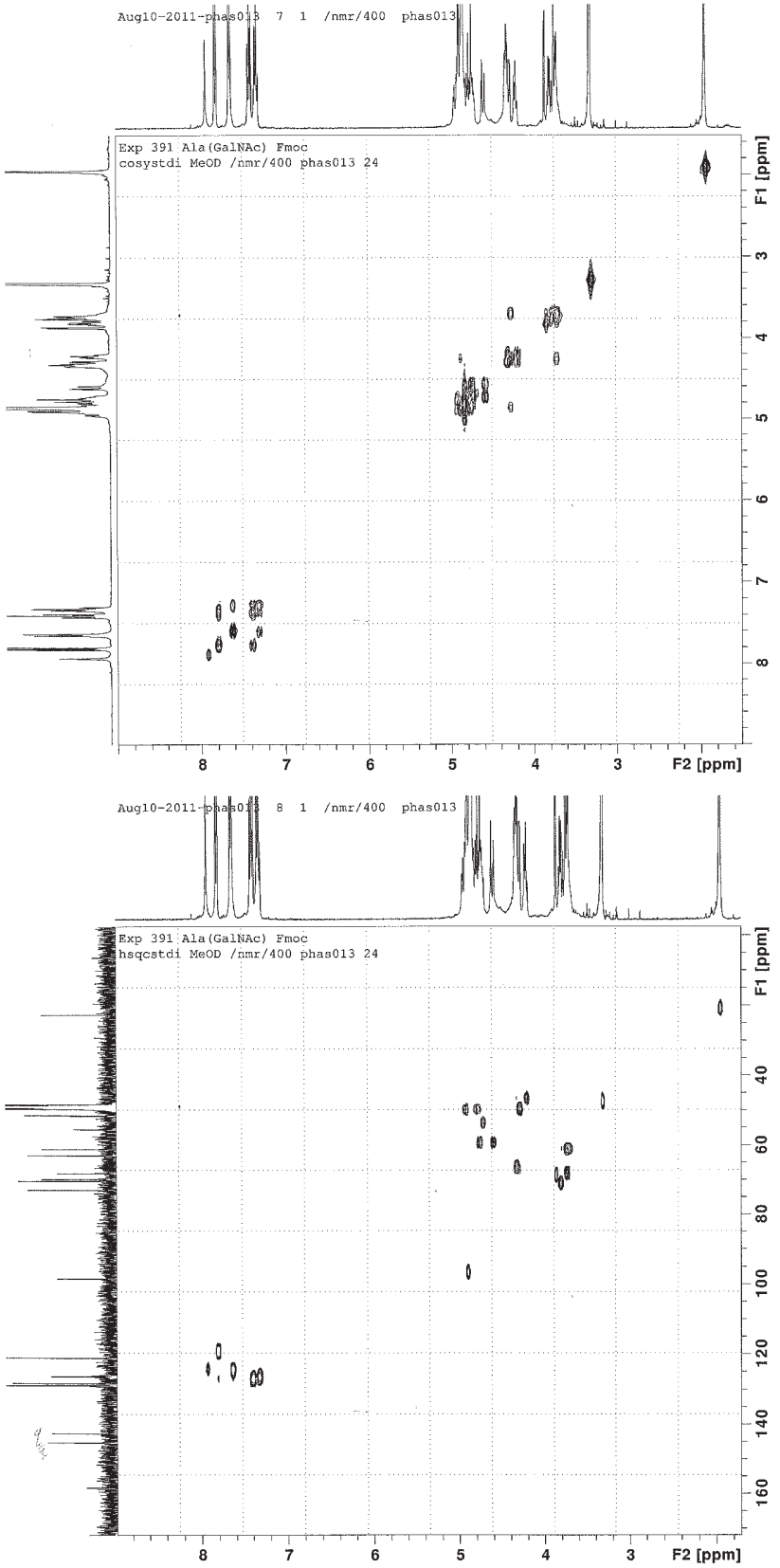

Figure 9.21: (Top) **COSY NMR (400 MHz CD_3OD)** and (Bottom) **HSQC NMR (400 MHz and 100 MHz, CD_3OD)** of de–protected click building block **42**

9.2 Thermal melt assay appendix

9.2.1 SDS–PAGE gels

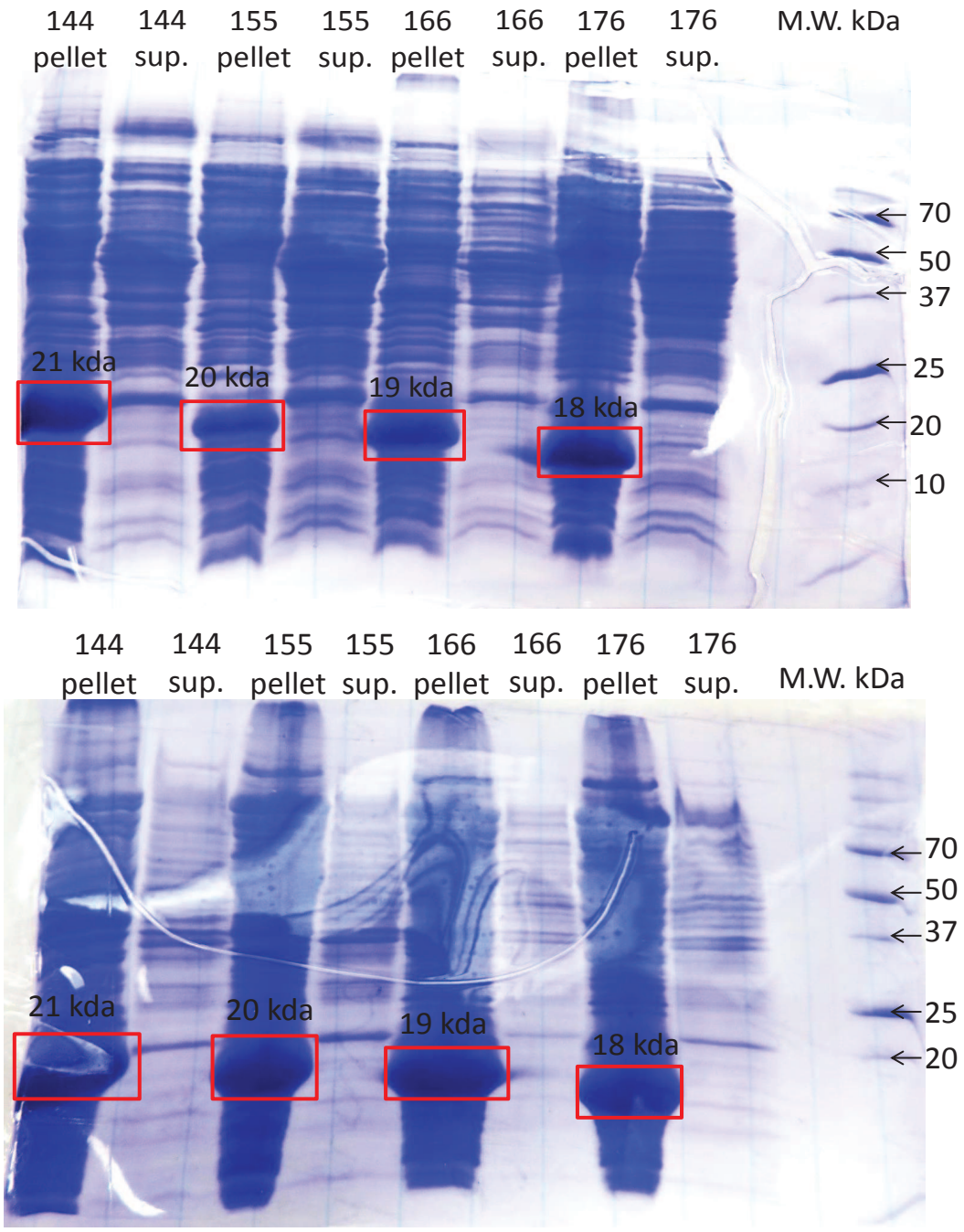

Figure 9.22: (Top) IPTG Induced expression of MGL. From left to right, MGL 144 pellet and 144 supernatant, MGL 155 pellet and 155 supernatant, MGL 166 pellet and 166 supernatant, MGL 176 pellet and 176 supernatant. (Bottom) Expression of the MGL in terrific broth. From left to right, MGL 144 pellet and 144 supernatant, MGL 155 pellet and 155 supernatant, MGL 166 pellet and 166 supernatant, MGL 176 pellet and 176 supernatant.

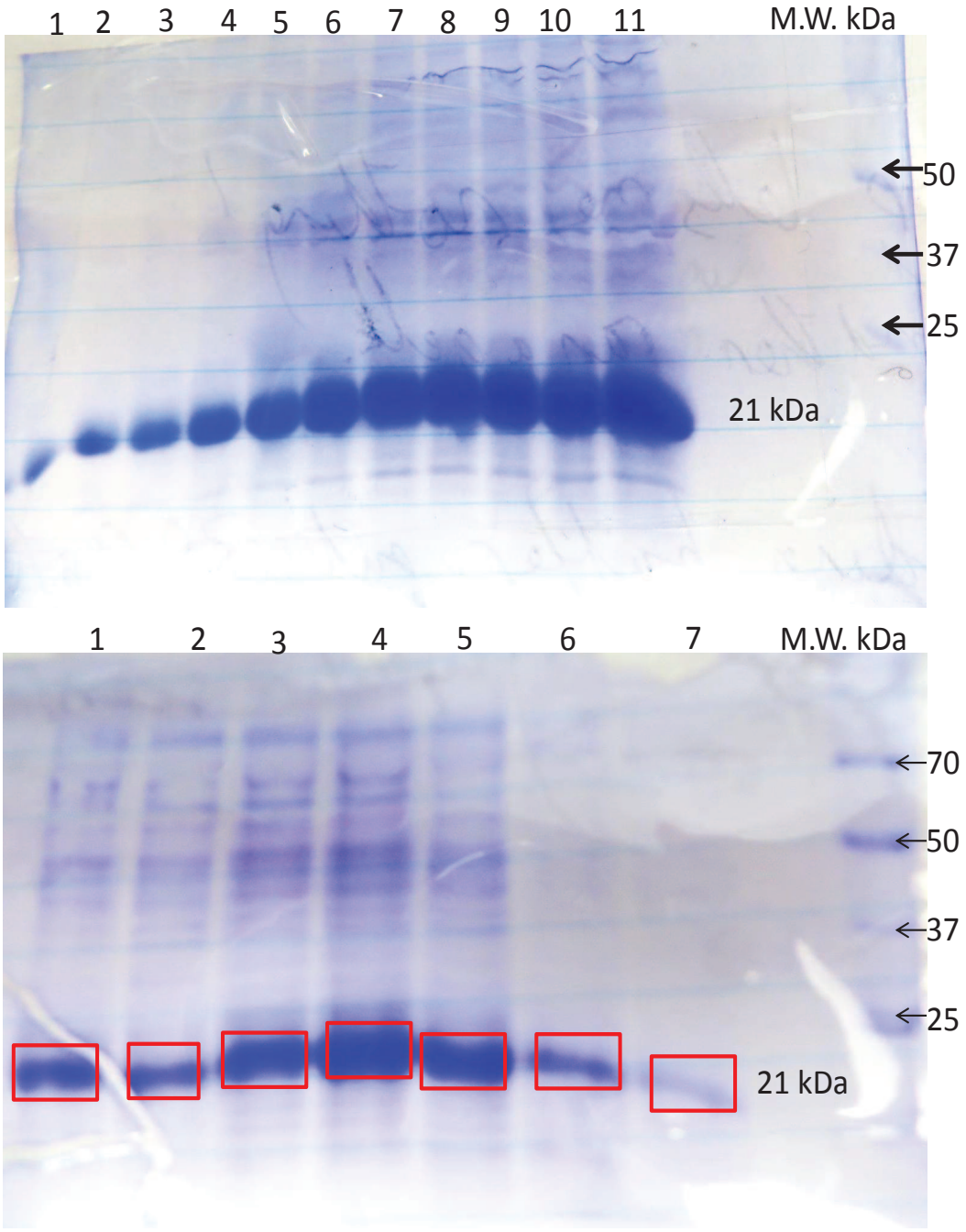

Figure 9.23: (Top) The purity of MGL 144 before size exclusion chromatography on the s75. (Bottom) The purity of MGL 144 before size exclusion chromatography on the s200.

9.3 Size exclusion chromatography traces

9.3.1 176 size exclusion chromatography trace

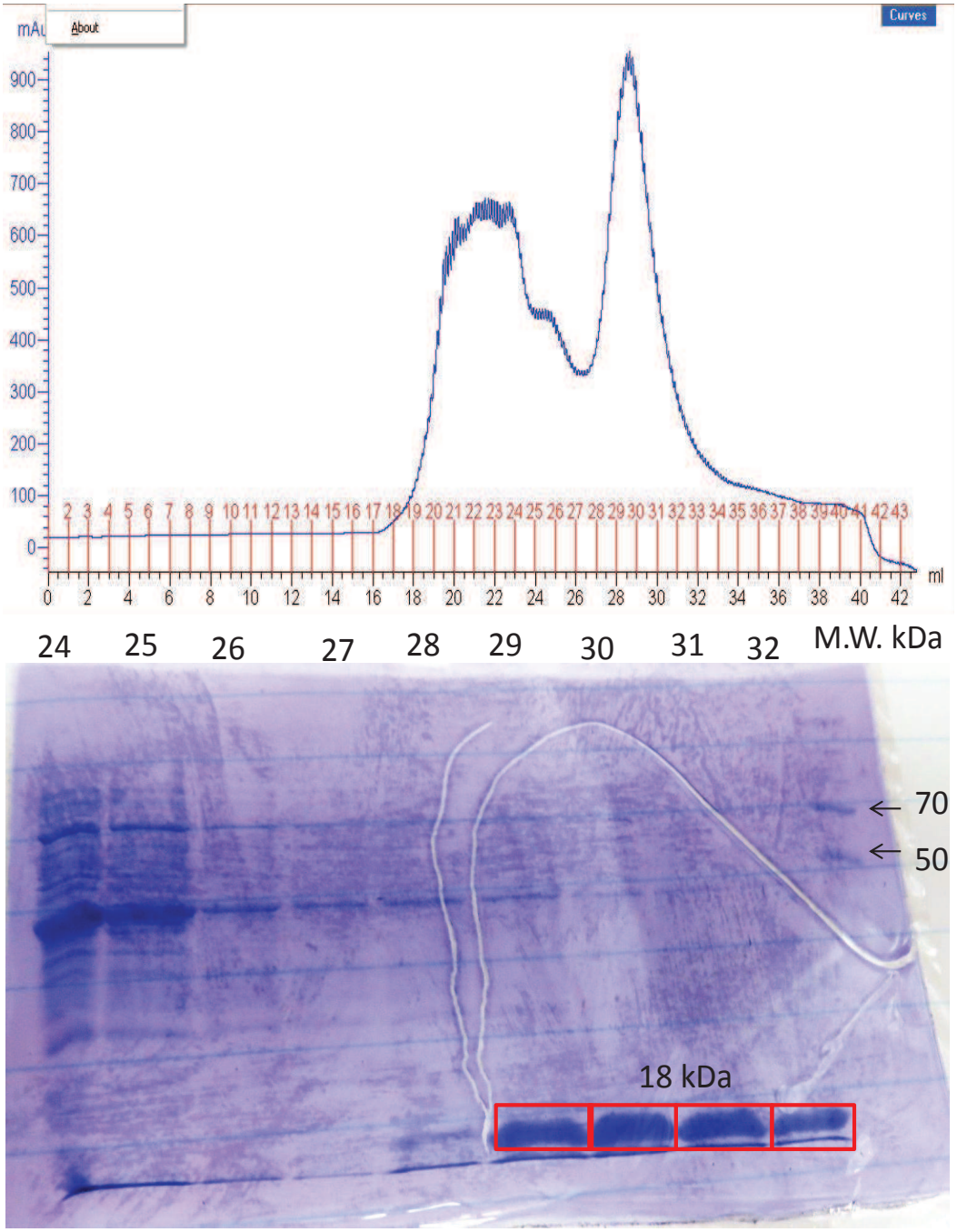

Figure 9.24: (Top) Size exclusion chromatography trace for MGL 176 purified on s75 column. (Bottom) The SDS-PAGE for the purification.

9.3.2 166 size exclusion chromatography trace

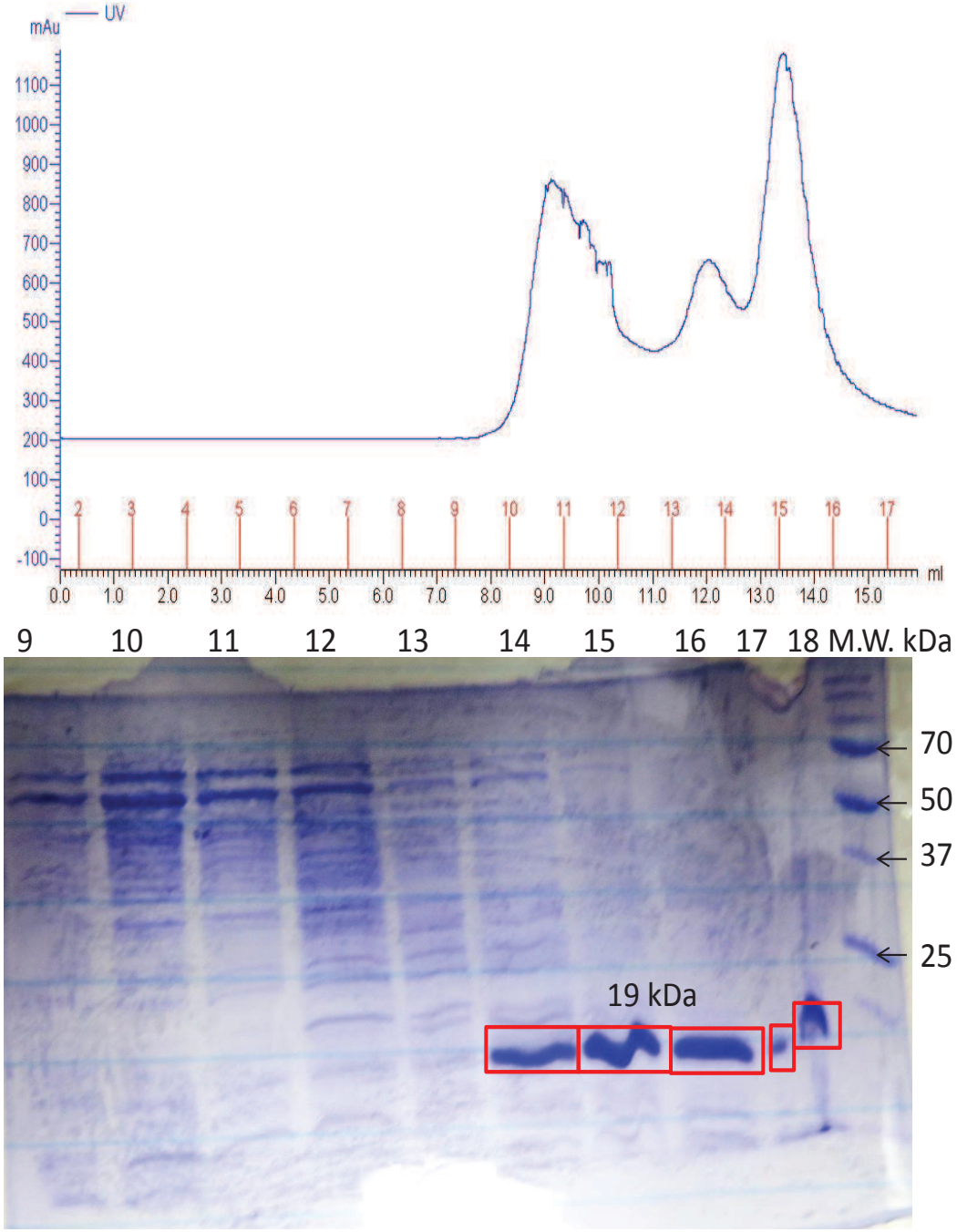

Figure 9.25: (Top) Size exclusion chromatography trace for MGL 166 purified on s75 column. (Bottom) The SDS-PAGE for the purification.

9.3.3 155 size exclusion chromatography trace

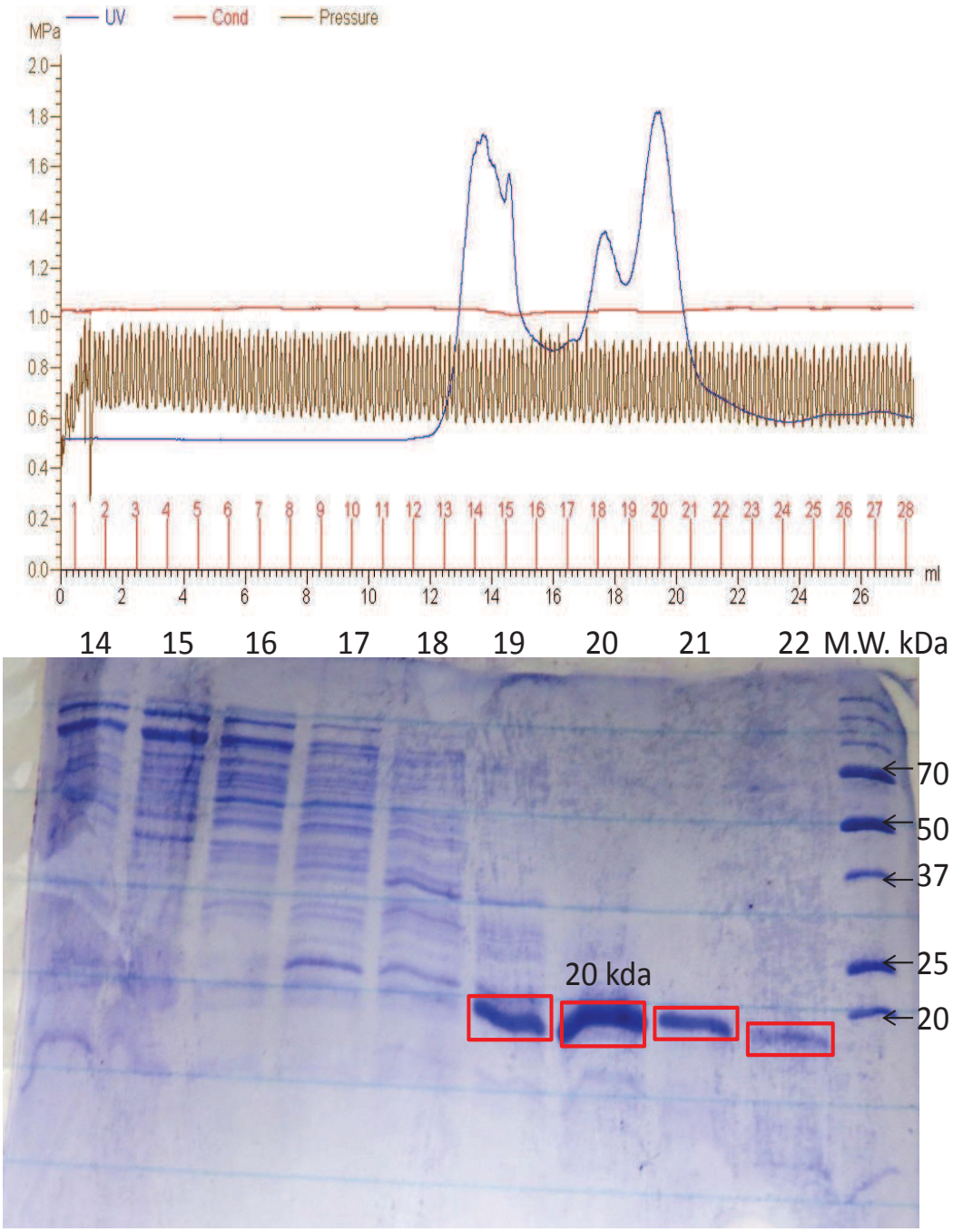

Figure 9.26: (Top) Size exclusion chromatography trace for MGL 155 purified on s75 column. (Bottom) The SDS-PAGE for the purification.

9.4 Thermal melt

9.4.1 The initial thermal melt assay

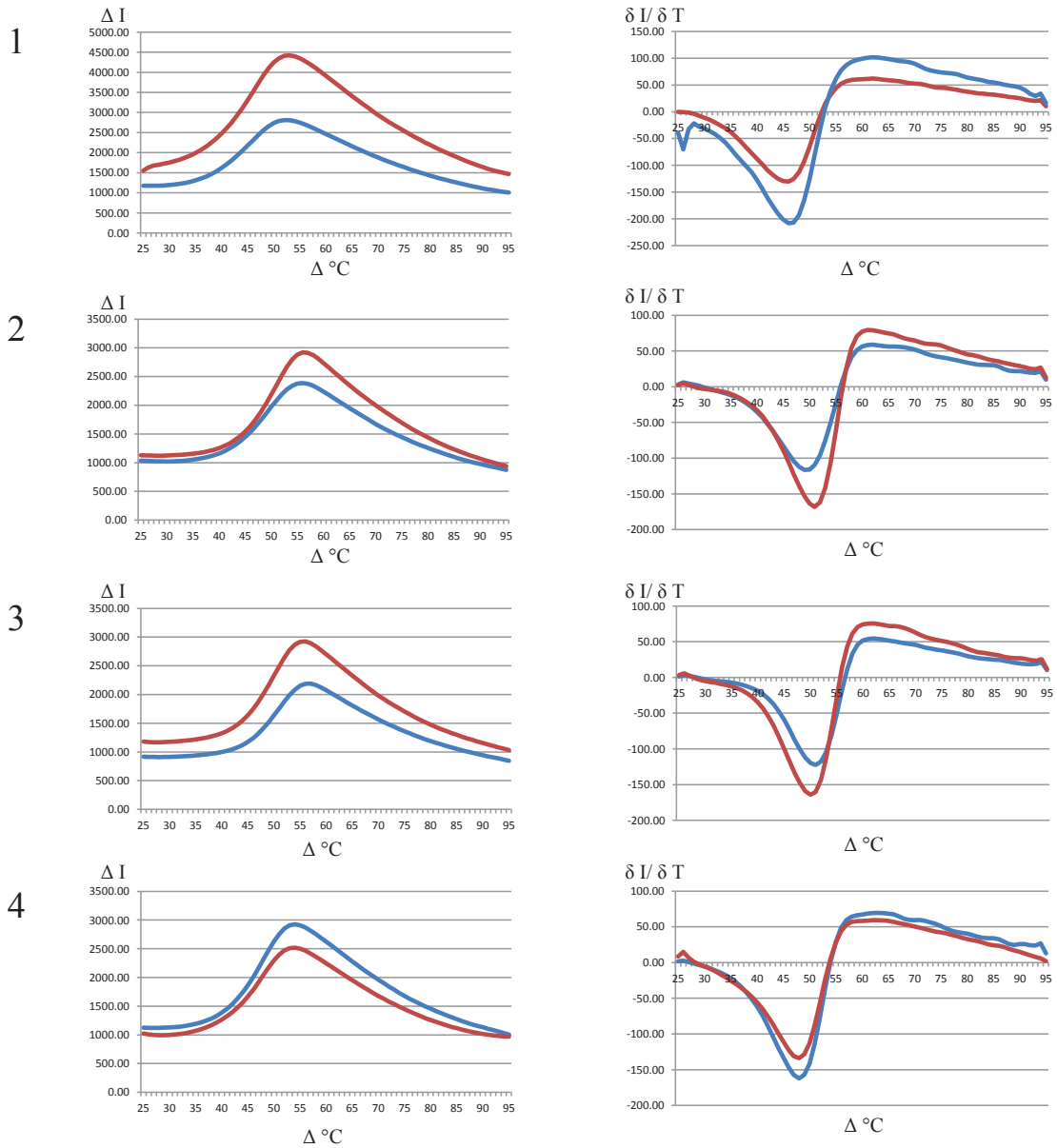

Figure 9.27: Duplicate samples for results of initial DSF experiment, thermal melt rfu (left) and differential plots (right) for MGL 176 with (1) no additive; (2) 600 μM GalNAc; (3) 300 μM GalNAc; (4) 30 μM GalNAc.

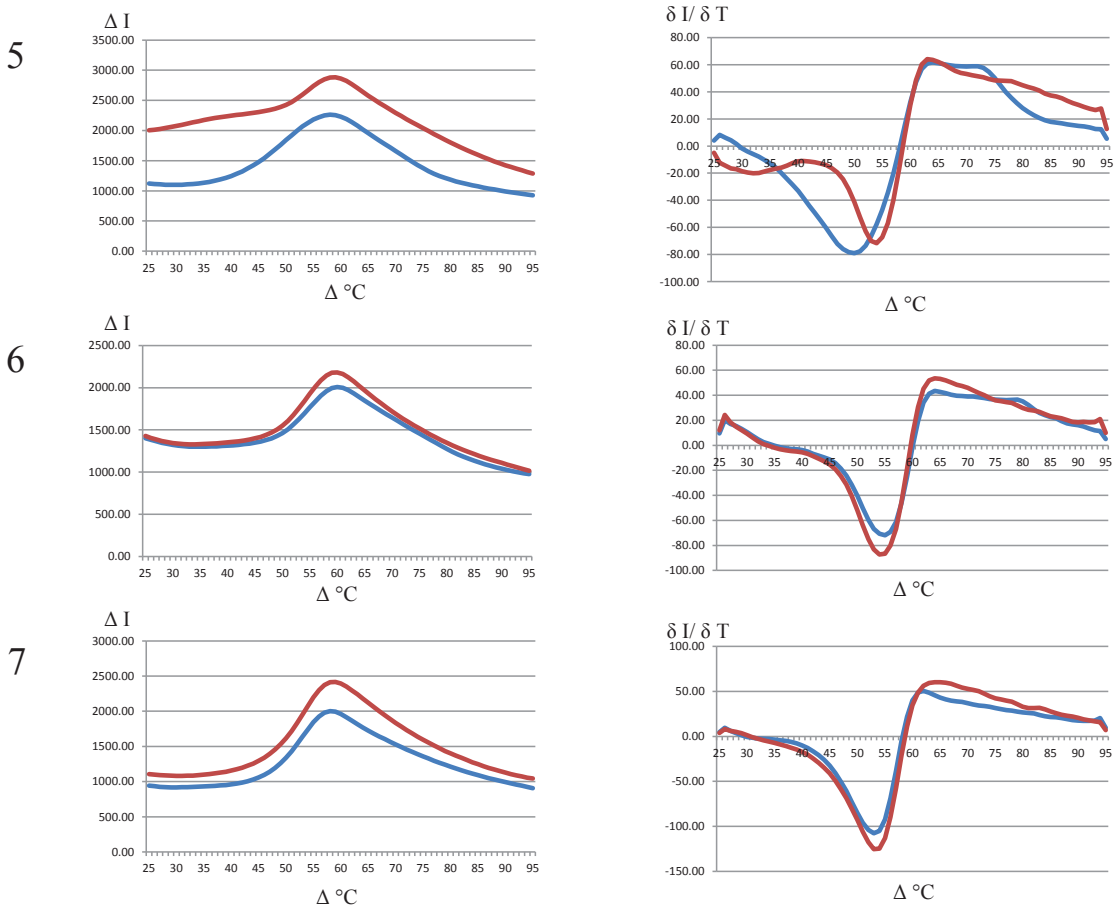

Figure 9.28: Duplicate samples for results of initial DSF experiment, thermal melt rfu (left) and differential plots (right) for MGL 176 with (5) 600 μM Dendrimer **21**; (6) 300 μM Dendrimer **21**; (7) 30 μM Dendrimer **21**.

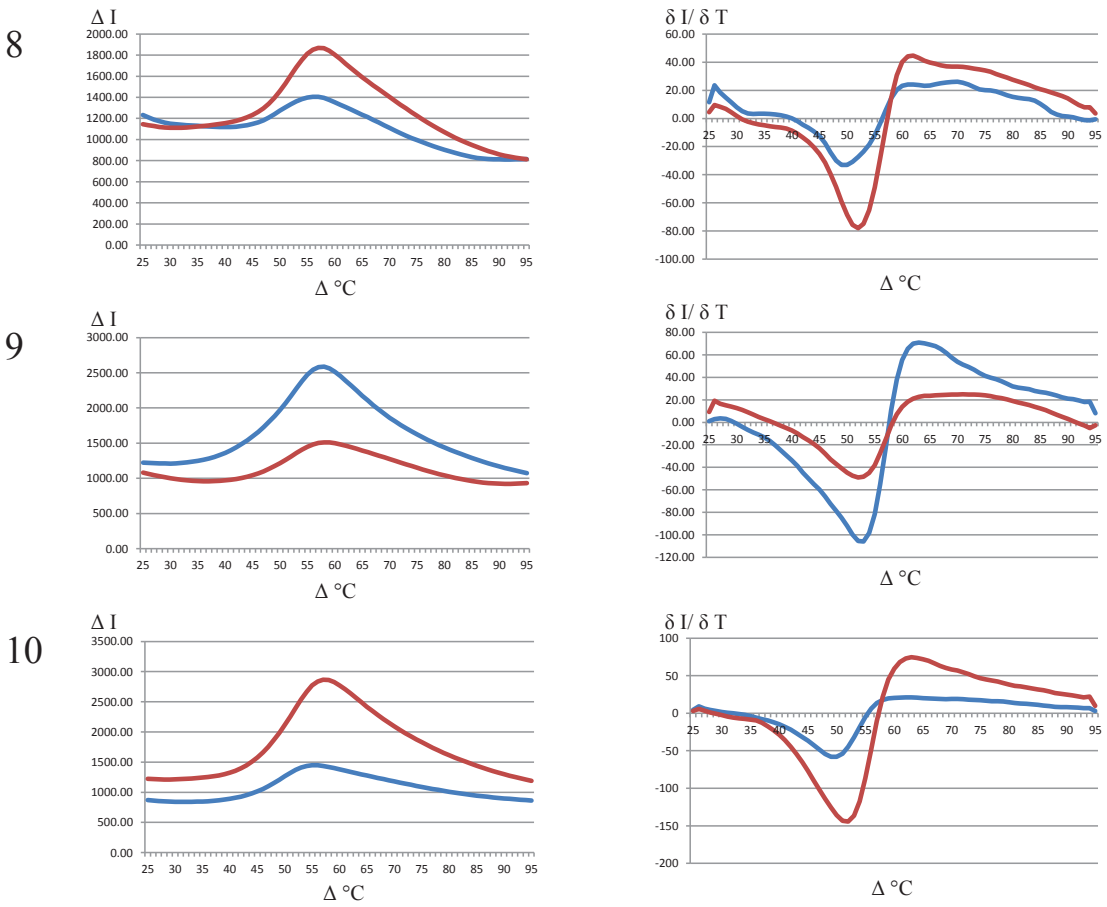

Figure 9.29: Duplicate samples for results of initial DSF experiment, thermal melt rfu (left) and differential plots (right) for MGL 176 with (8) 600 μM Dendrimer **2**; (9) 300 μM Dendrimer **2**; (10) 30 μM Dendrimer **2**.

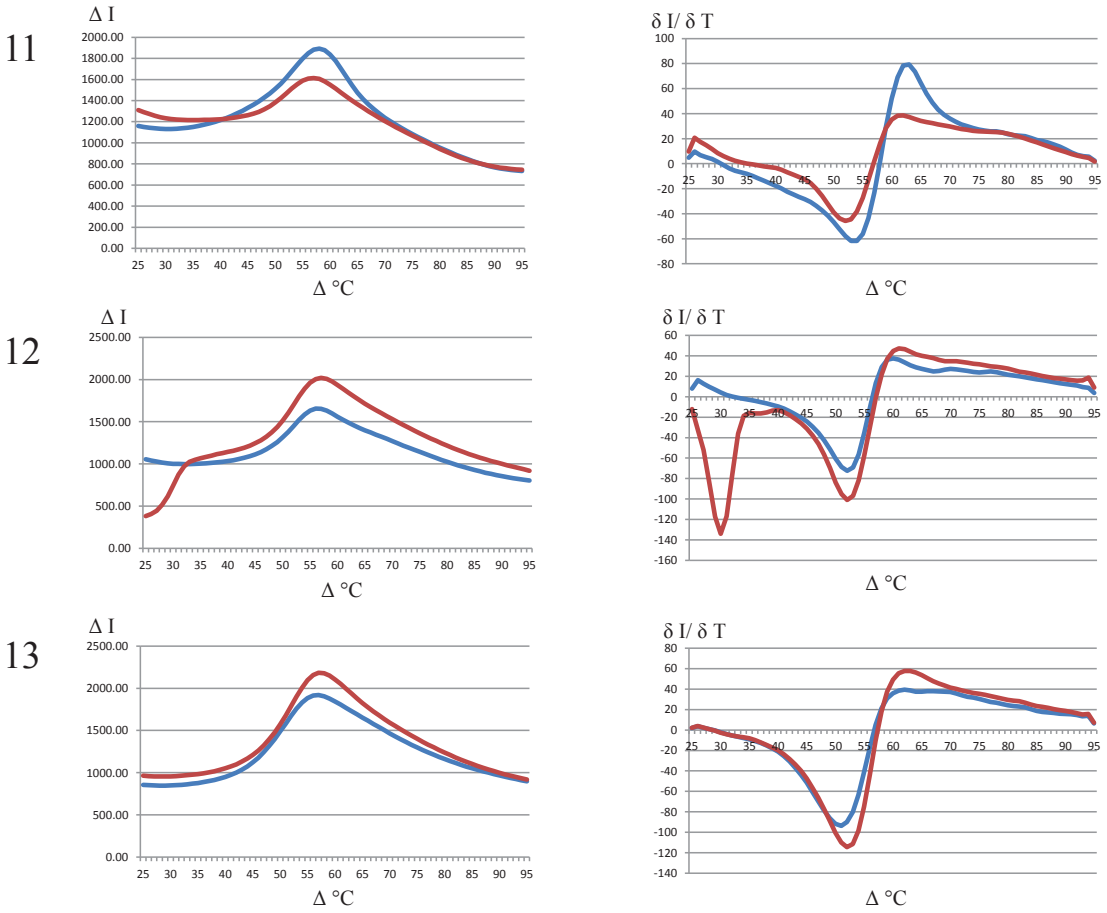

Figure 9.30: Duplicate samples for results of initial DSF experiment, thermal melt rfu (left) and differential plots (right) for MGL 176 with (11) 600 μM Dendrimer **23**; (12) 300 μM Dendrimer **23**; (13) 30 μM Dendrimer **23**.

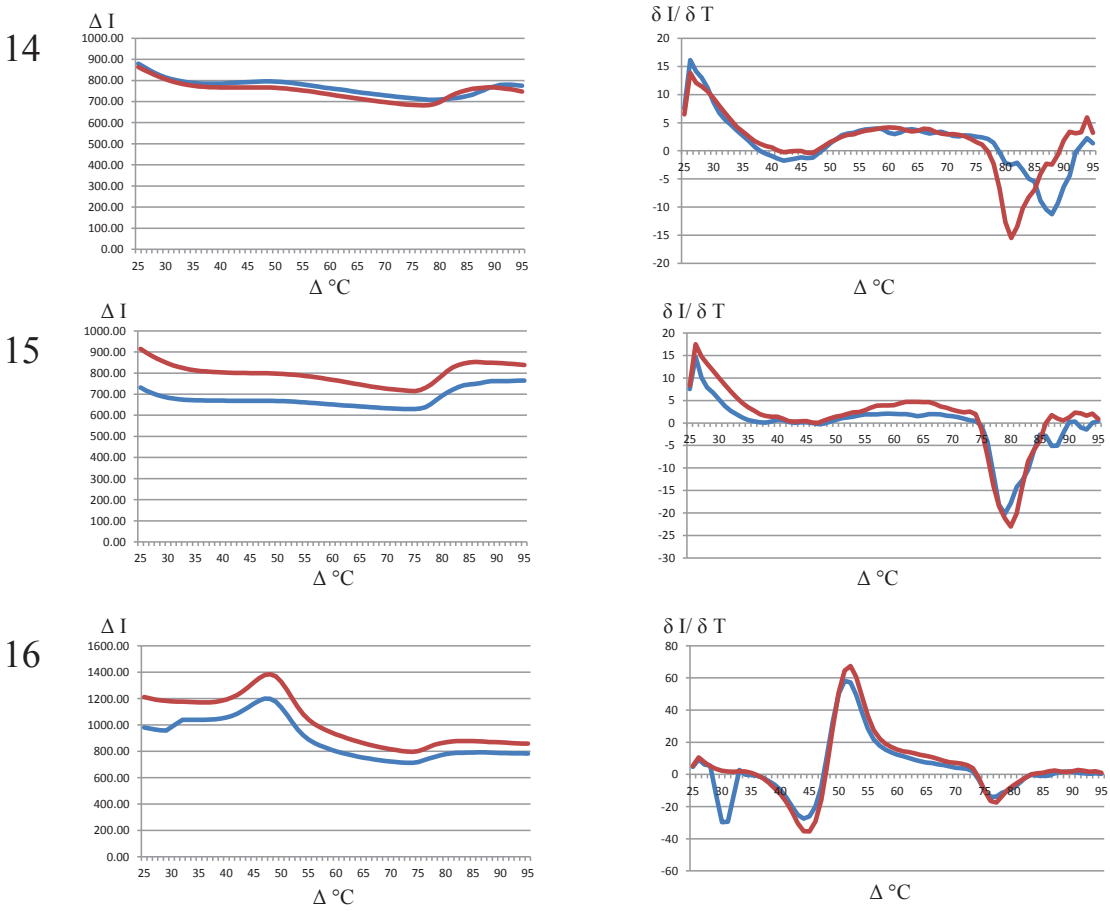

Figure 9.31: Duplicate samples for results of initial DSF experiment, thermal melt rfu (left) and differential plots (right) for MGL 176 with (14) 600 μM Dendrimer **25**; (15) 300 μM Dendrimer **25**; (16) 30 μM Dendrimer **25**.

9.4.2 Thermal melt assays titration.

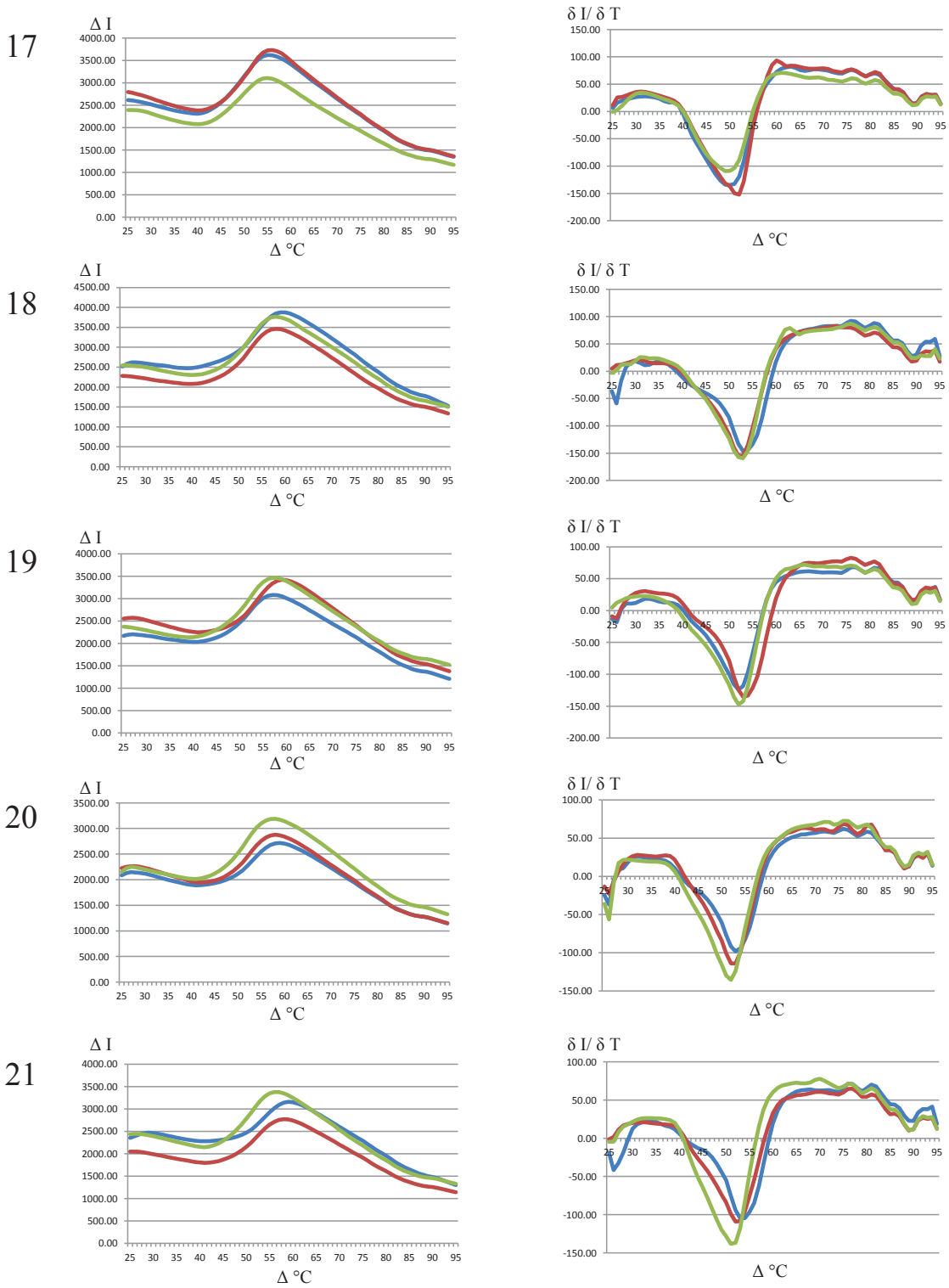

Figure 9.32: Triplicate samples for results of DSF titration experiment, thermal melt rfu (left) and differential plots (right) for MGL 176 with (17) no additive; (18) GalNAc (1 nM); (19) GalNAc (10 nM); (20) GalNAc (100 nM); (21) GalNAc (1 μM).

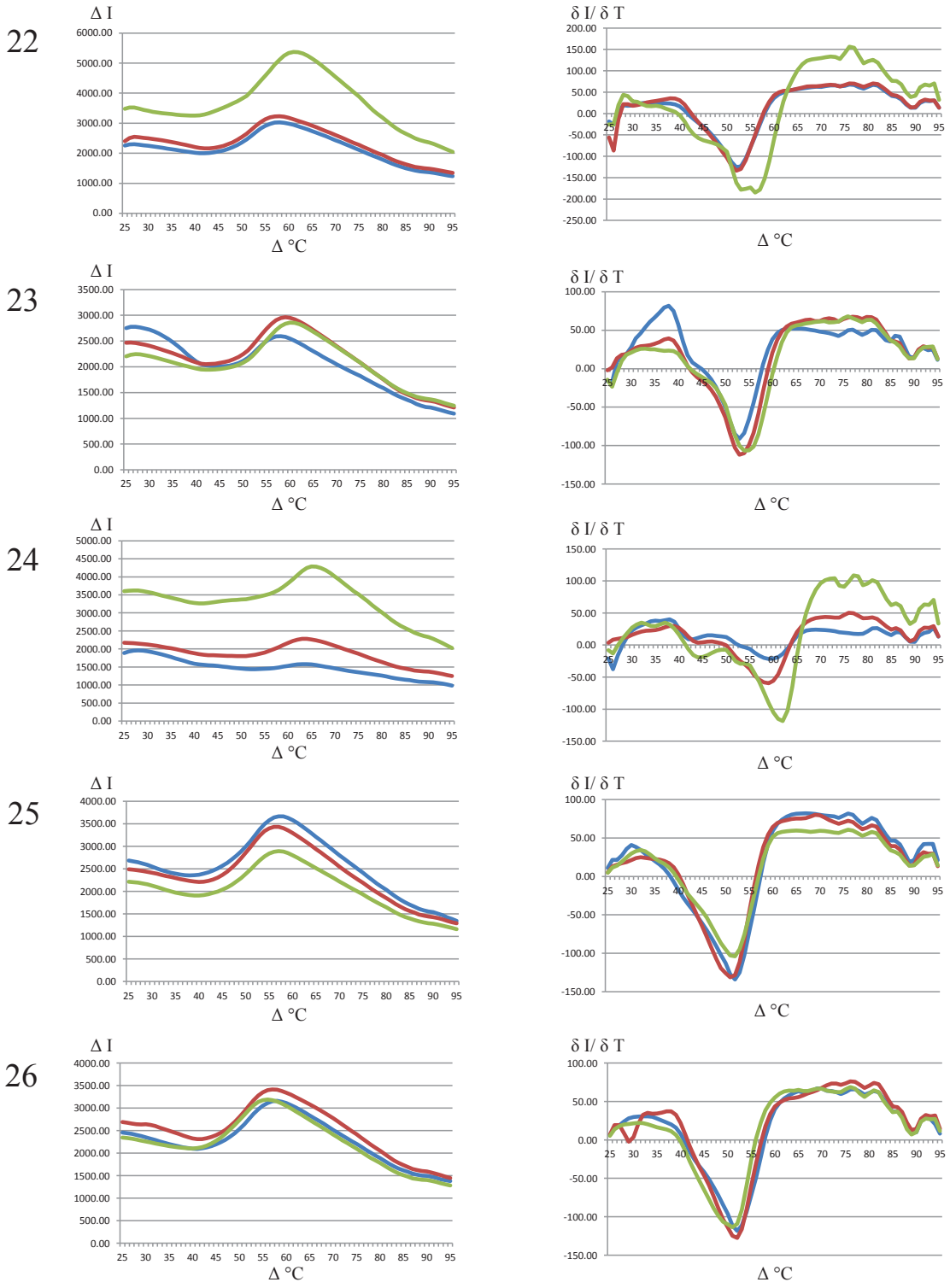

Figure 9.33: Triplicate samples for results of DSF titration experiment, thermal melt rfu (left) and differential plots (right) for MGL 176 with (22) GalNAc (10 μM); (23) GalNAc (100 μM); (24) GalNAc (1 mM); (25) Dendrimer **21**; (1 nM) (26) Dendrimer **21** (10 nM).

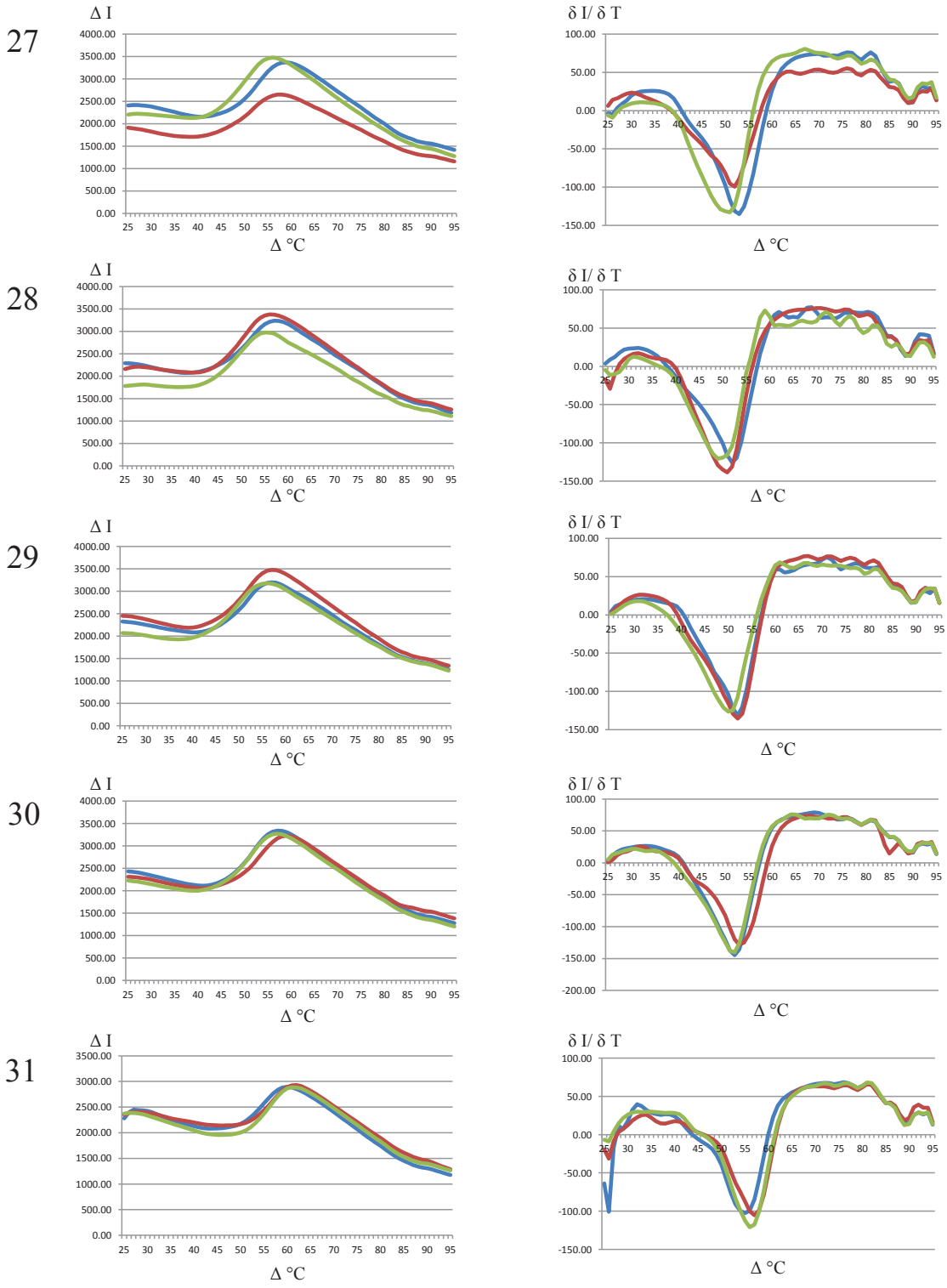

Figure 9.34: Triplicate samples for results of DSF titration experiment, thermal melt rfu (left) and differential plots (right) for MGL 176 with (27) Dendrimer **21** (100 nM); (28) Dendrimer **21** (1 μM); (29) Dendrimer **21** (10 μM); (30) Dendrimer **21** (100 μM); (31) Dendrimer **21** (1 mM).

9.4.3 Thermal melt assay of 176

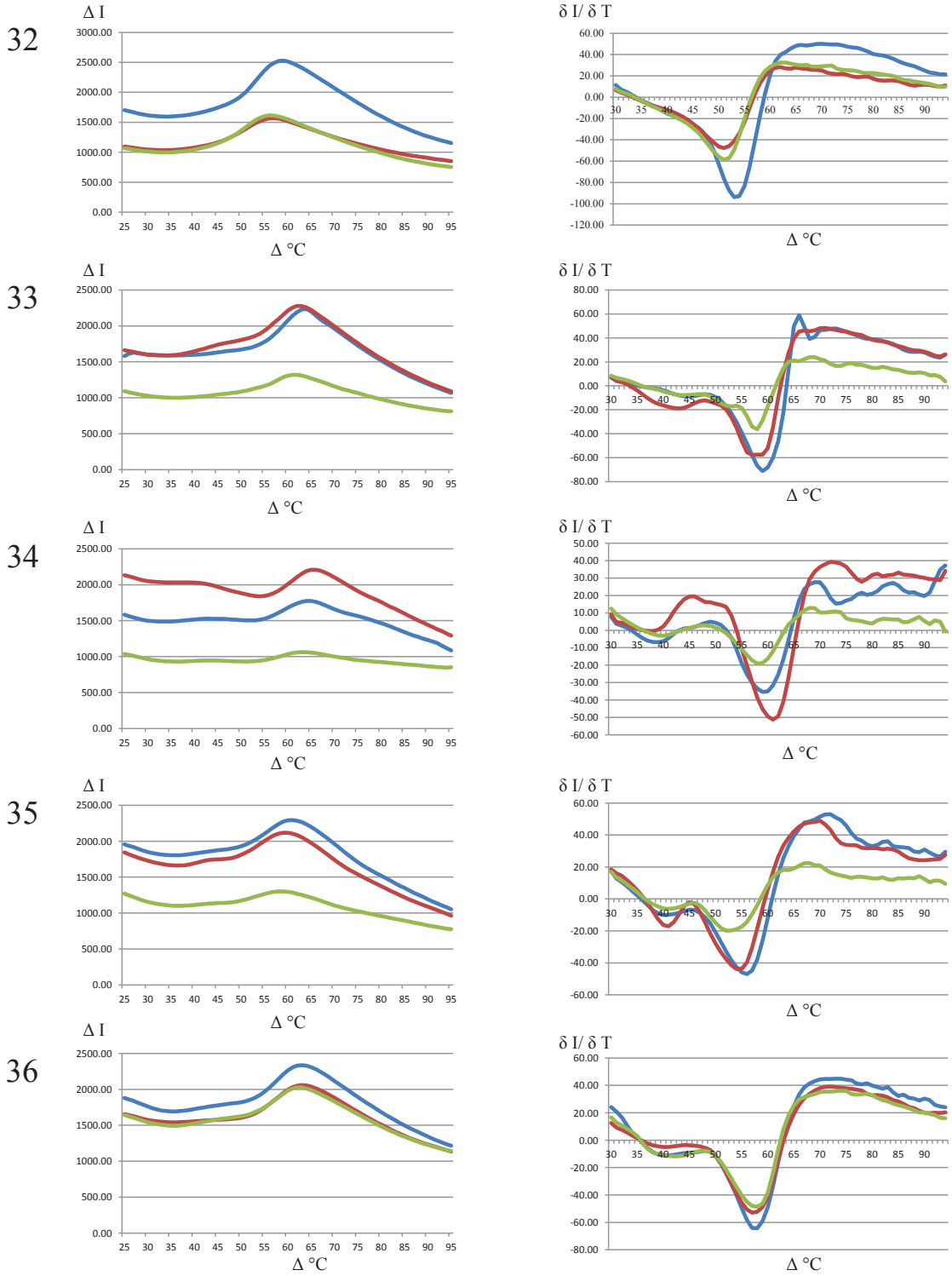

Figure 9.35: Triplicate samples for results of DSF experiment, thermal melt rfu (left) and differential plots (right) for MGL 176 with (32) no additive; (33) GalNAc (1 mM); (34) Dendrimer **21** (1mM); (35) Dendrimer **67** (1mM); (36) Dendrimer **43** (1mM).

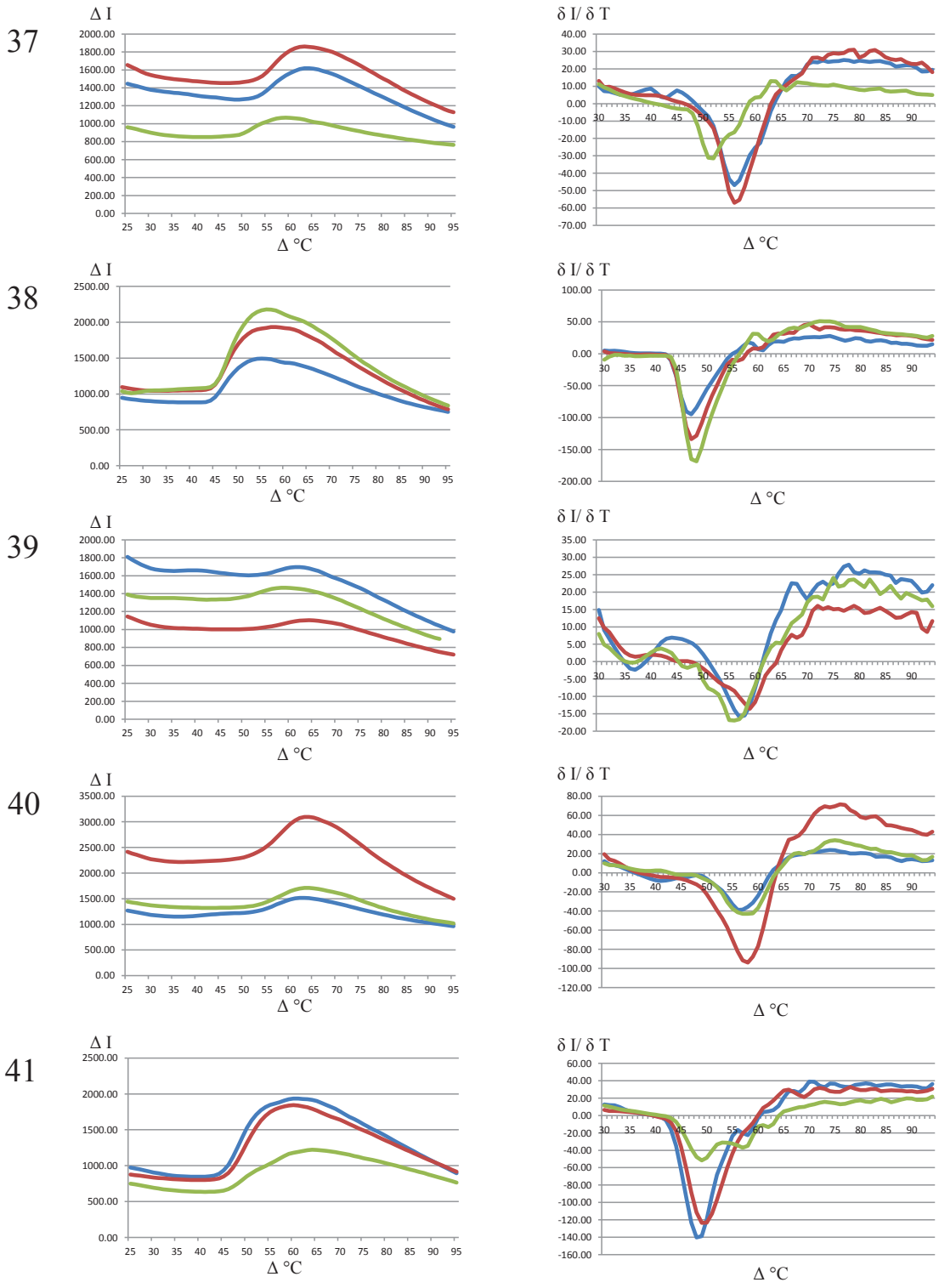

Figure 9.36: Triplicate samples for results of DSF experiment, thermal melt rfu (left) and differential plots (right) for MGL 176 with (37) Dendrimer **2** (1mM); (38) Dendrimer **45** (1 mM); (39) Dendrimer **23** (1mM); (40) Dendrimer **47** (1mM); (41) Dendrimer **25** (1mM).

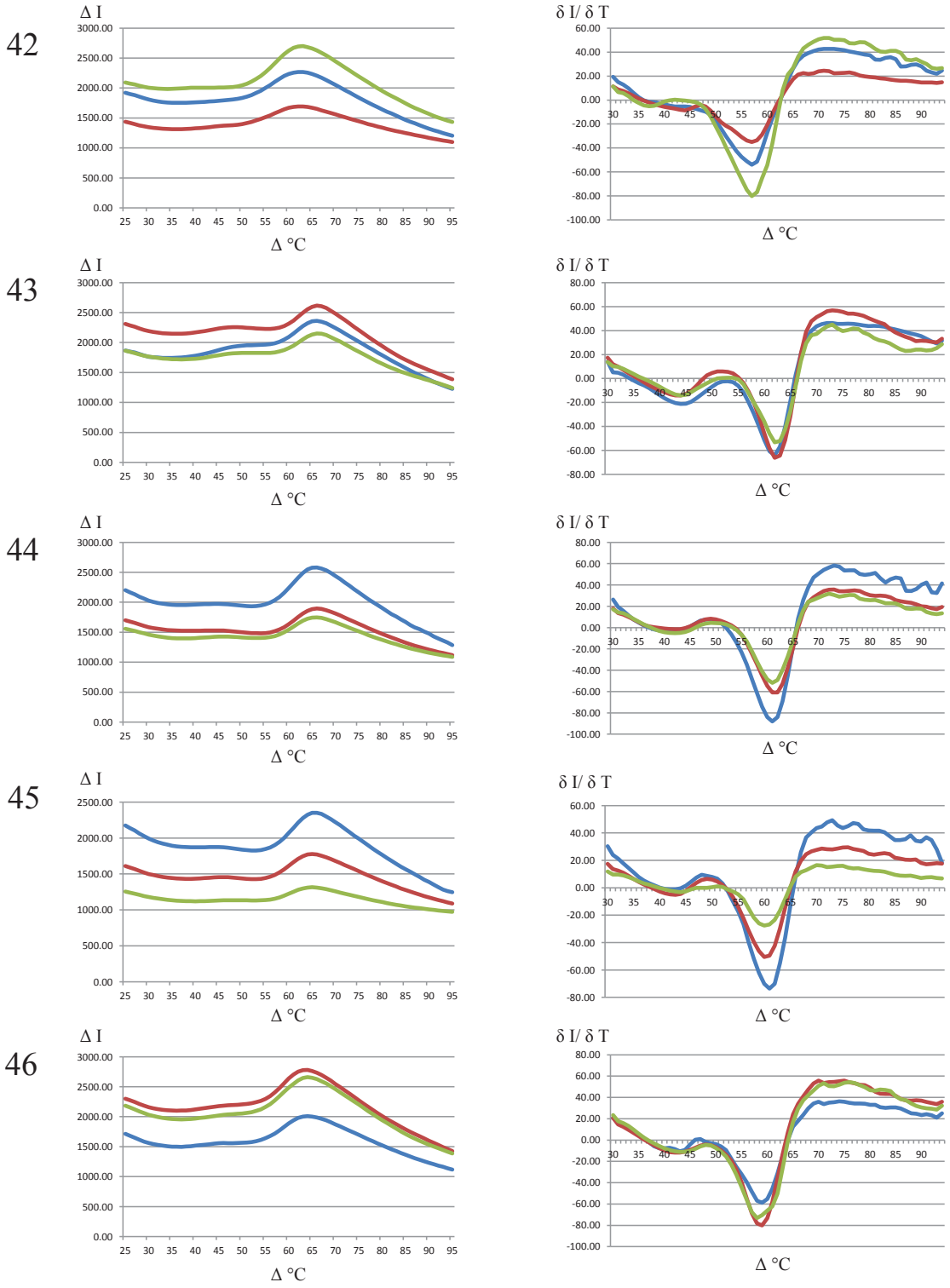

Figure 9.37: Triplicate samples for results of DSF experiment, thermal melt rfu (left) and differential plots (right) for MGL 176 with (42) Dendrimer **49** (1mM); (43) Dendrimer **51** (1 mM); (44) Dendrimer **53** (1mM); (45) Dendrimer **55** (1mM); (46) Dendrimer **57** (1mM).

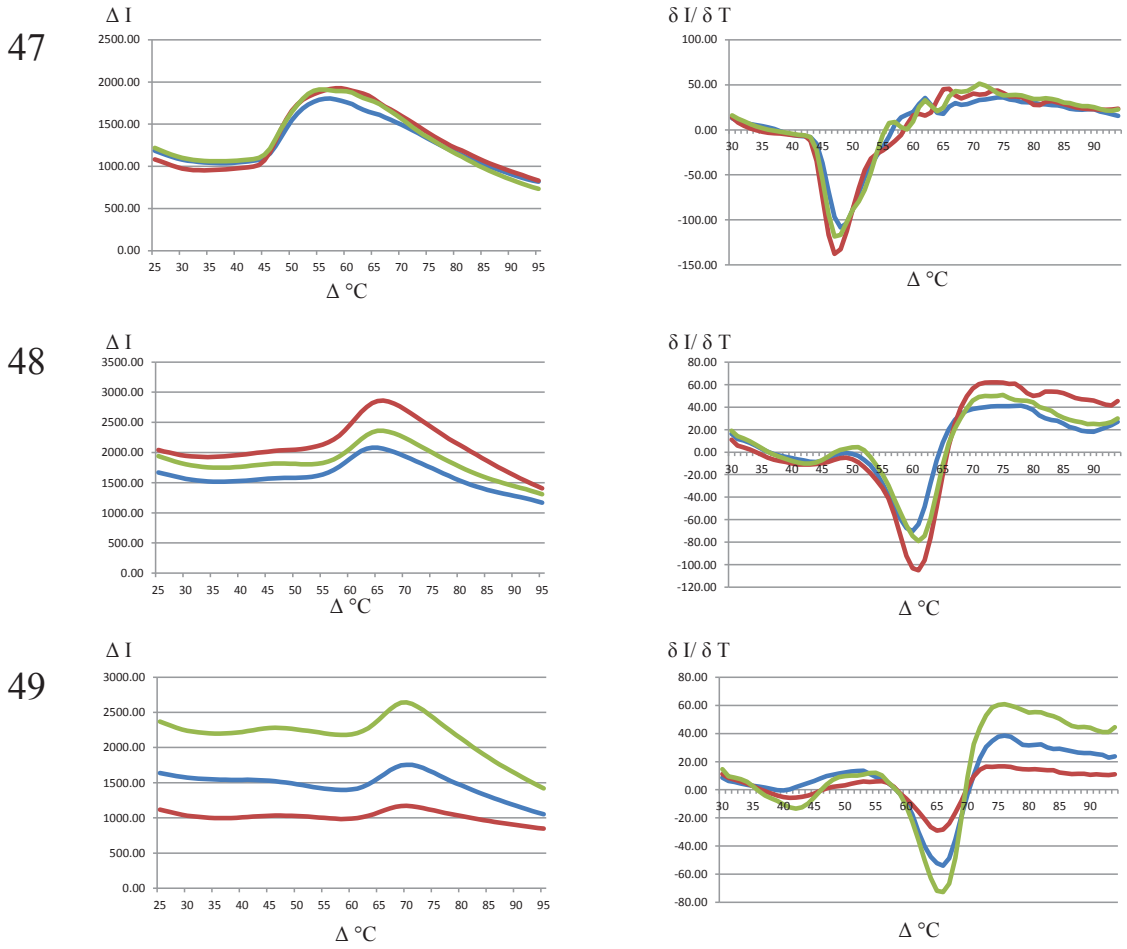

Figure 9.38: Triplicate samples for results of DSF experiment, thermal melt rfu (left) and differential plots (right) for MGL 176 with (47) Dendrimer **59** (1mM); (48) Peptide **61** (1 mM); (49) Peptide **63** (1mM).

9.4.4 Thermal melt assay of 166

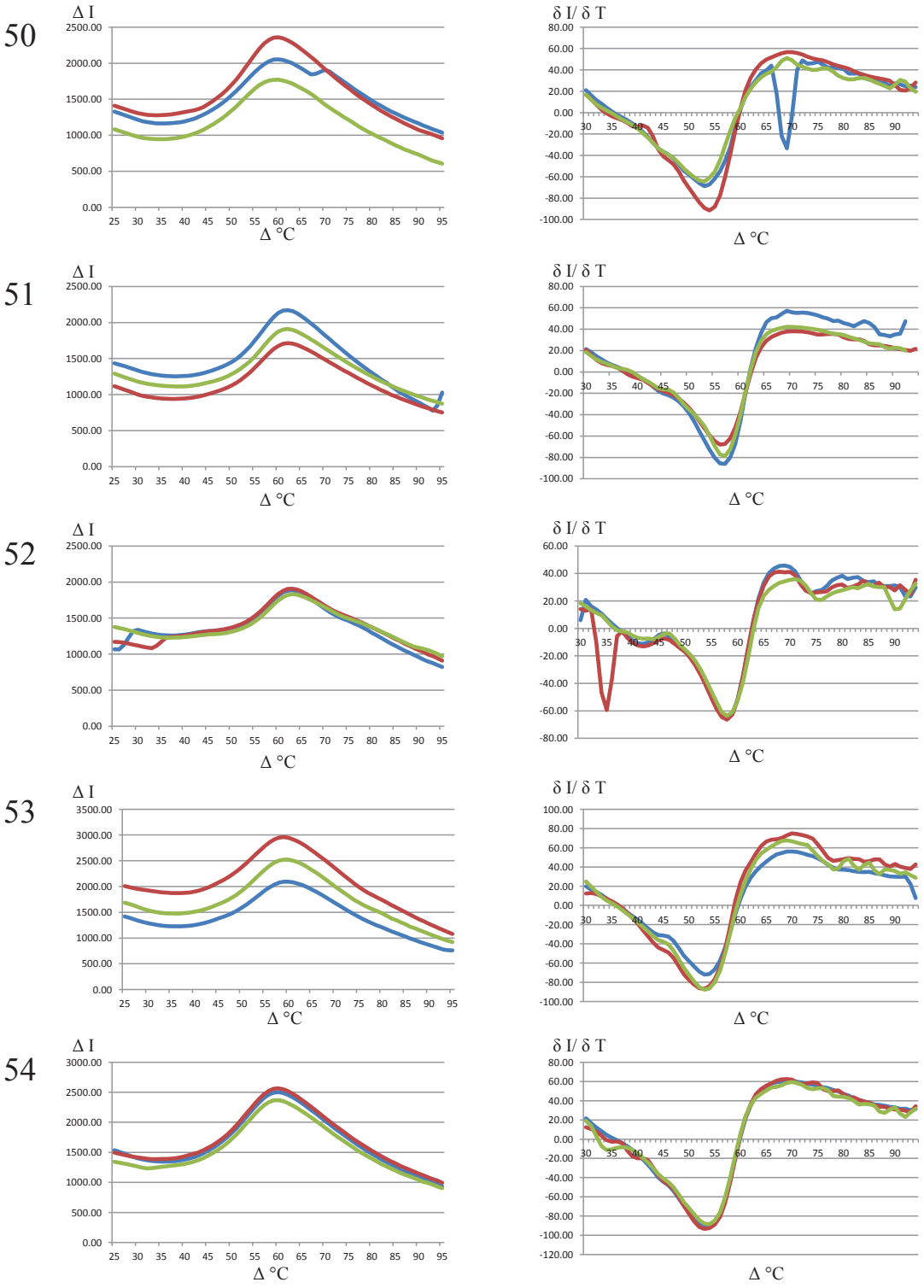

Figure 9.39: Triplicate samples for results of DSF experiment, thermal melt rfu (left) and differential plots (right) for MGL 166 with (50) no additive; (51) GalNAc (1 mM); (52) Dendrimer **21** (1mM); (53) Dendrimer **67** (1mM); (54) Dendrimer **43** (1mM).

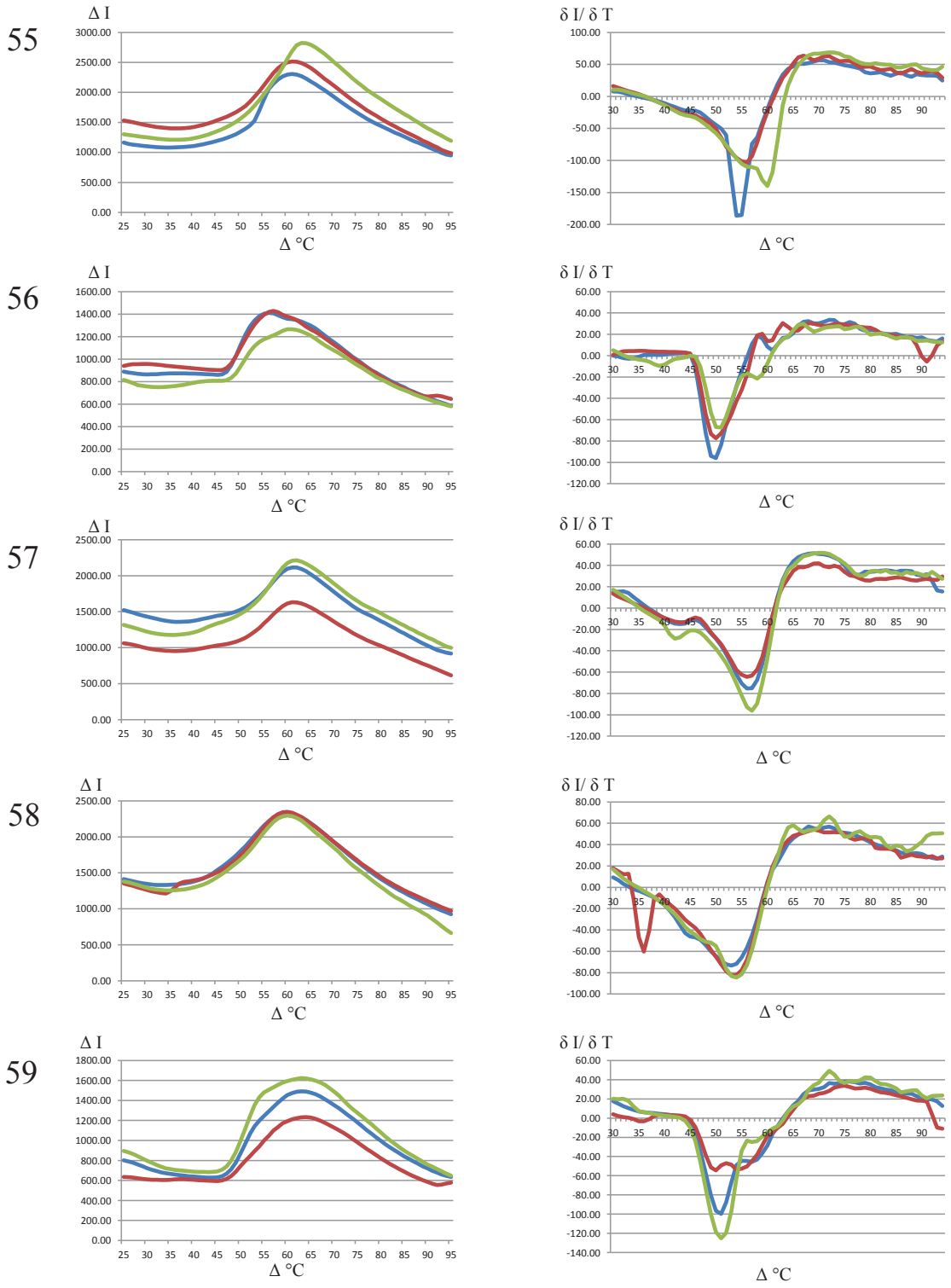

Figure 9.40: Triplicate samples for results of DSF experiment, thermal melt rfu (left) and differential plots (right) for MGL 166 with (55) Dendrimer **2** (1mM); (56) Dendrimer **45** (1 mM); (57) Dendrimer **23** (1mM); (58) Dendrimer **47** (1mM); (59) Dendrimer **25** (1mM).

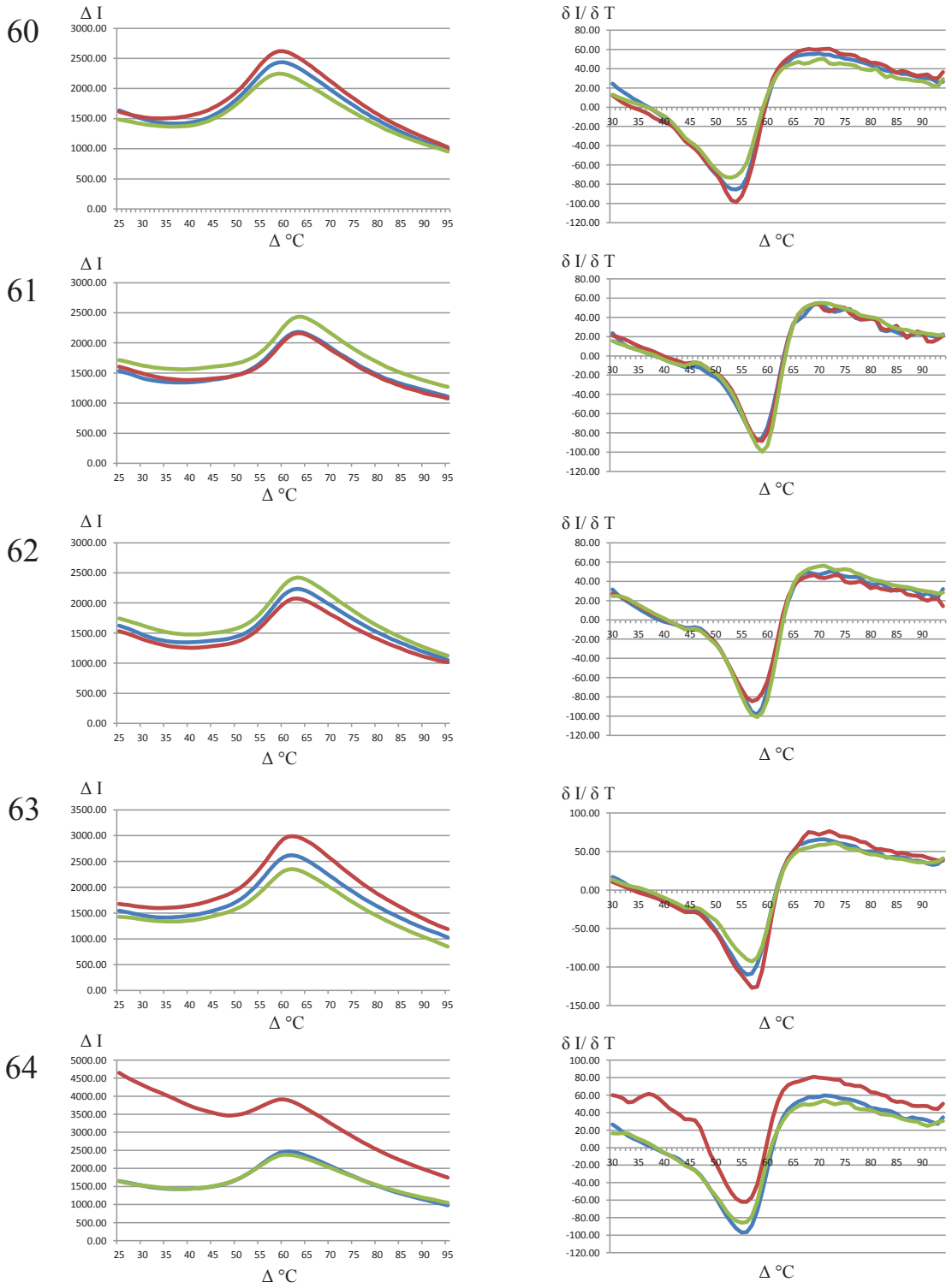

Figure 9.41: Triplicate samples for results of DSF experiment, thermal melt rfu (left) and differential plots (right) for MGL 166 with (60) Dendrimer **49** (1mM); (61) Dendrimer **51** (1 mM); (62) Dendrimer **53** (1mM); (63) Dendrimer **55** (1mM); (64) Dendrimer **57** (1mM).

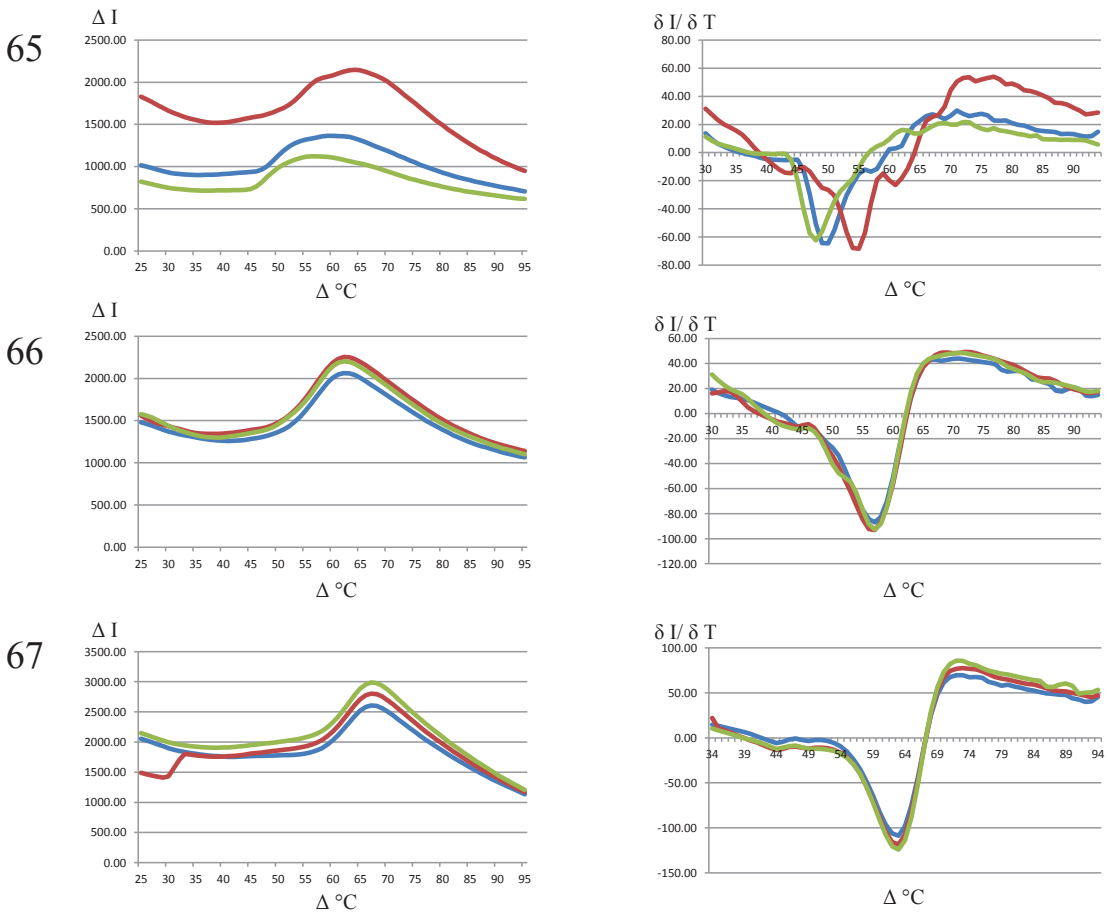

Figure 9.42: Triplicate samples for results of DSF experiment, thermal melt rfu (left) and differential plots (right) for MGL 166 with (65) Dendrimer **59** (1mM); (66) Peptide **61** (1 mM); (67) Peptide **63** (1mM).

9.4.5 Thermal melt assay of 155

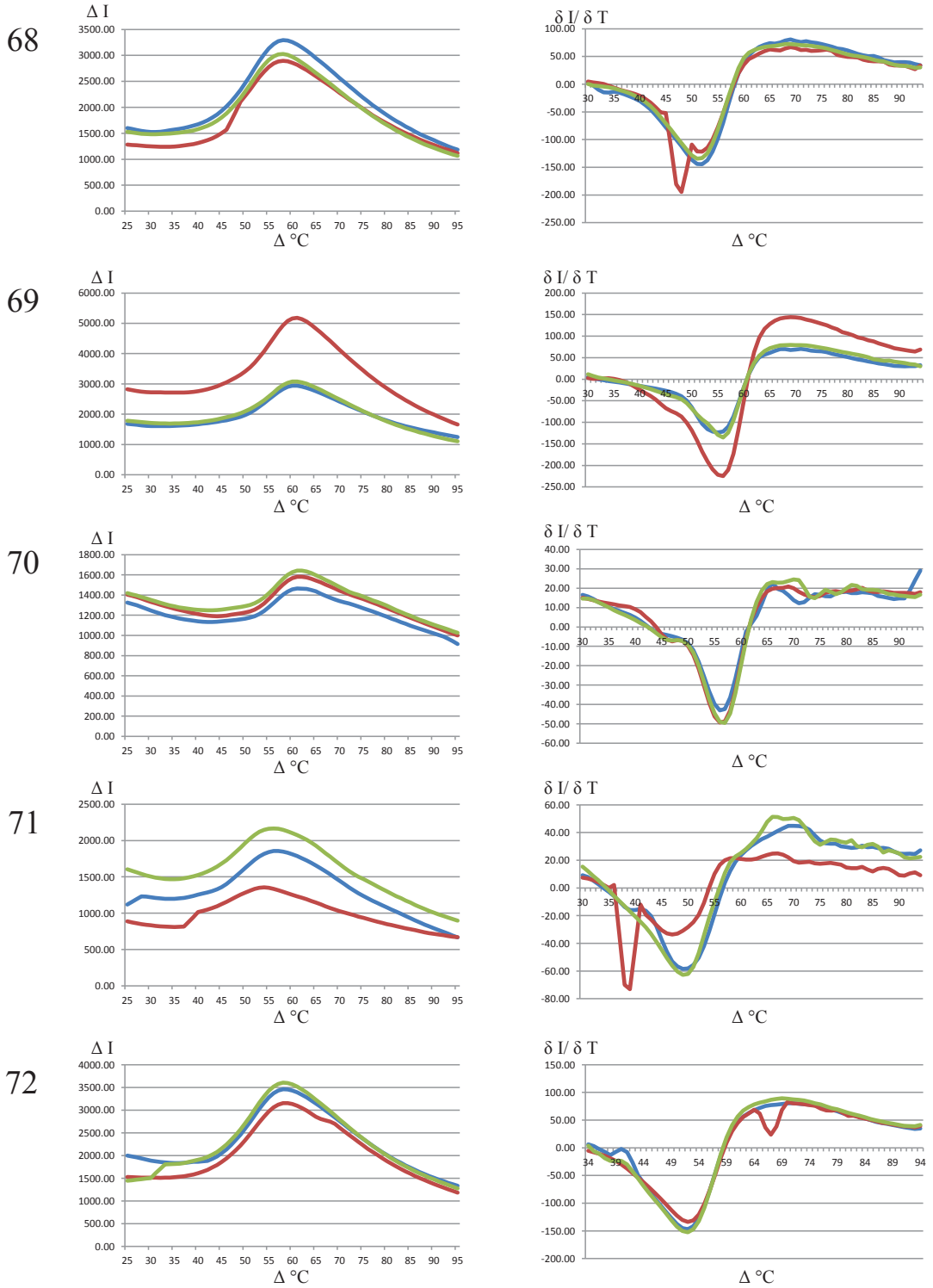

Figure 9.43: Triplicate samples for results of DSF experiment, thermal melt rfu (left) and differential plots (right) for MGL 155 with (68) no additive; (69) GalNAc (1 mM); (70) Dendrimer **21** (1mM); (71) Dendrimer **67** (1mM); (72) Dendrimer **43** (1mM).

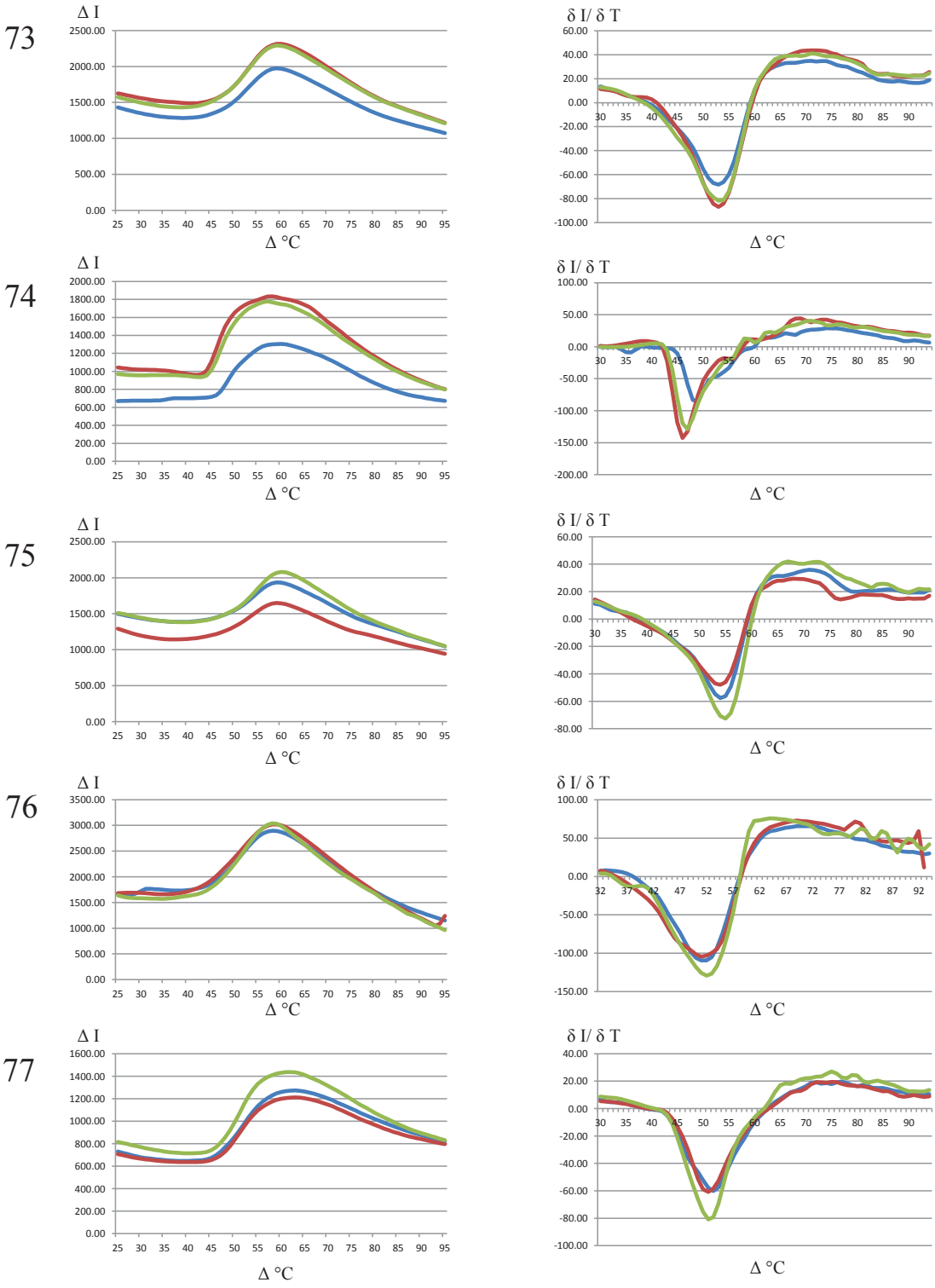

Figure 9.44: Triplicate samples for results of DSF experiment, thermal melt rfu (left) and differential plots (right) for MGL 155 with (73) Dendrimer **2** (1mM); (74) Dendrimer **45** (1 mM); (75) Dendrimer **23** (1mM); (76) Dendrimer **47** (1mM); (77) Dendrimer **25** (1mM).

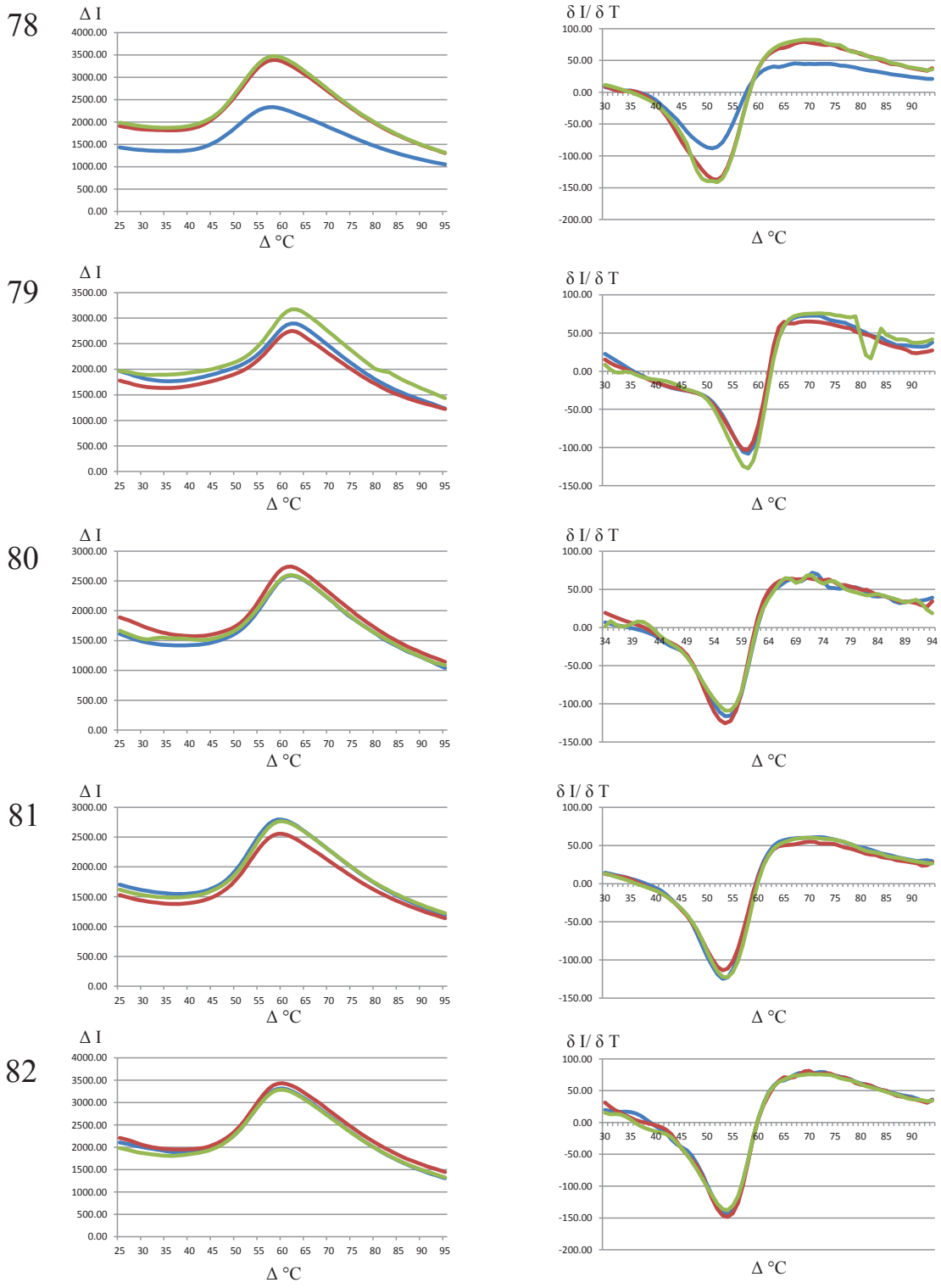

Figure 9.45: Triplicate samples for results of DSF experiment, thermal melt rfu (left) and differential plots (right) for MGL 155 with (78) Dendrimer **49** (1mM); (79) Dendrimer **51** (1 mM); (80) Dendrimer **53** (1mM); (81) Dendrimer **55** (1mM); (82) Dendrimer **57** (1mM).

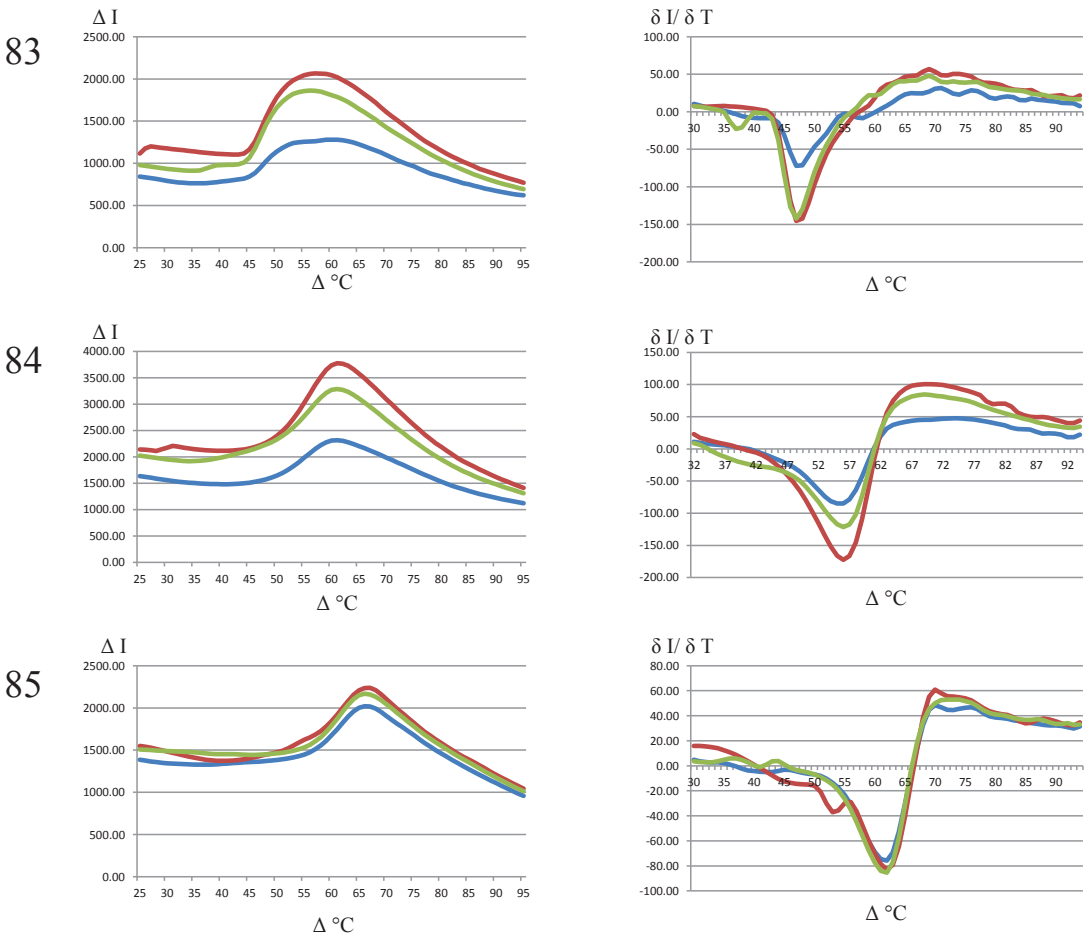

Figure 9.46: Triplicate samples for results of DSF experiment, thermal melt rfu (left) and differential plots (right) for MGL 155 with (83) Dendrimer **59** (1mM); (84) Peptide **61** (1 mM); (85) Peptide **63** (1mM).

9.4.6 Thermal melt assay of 144

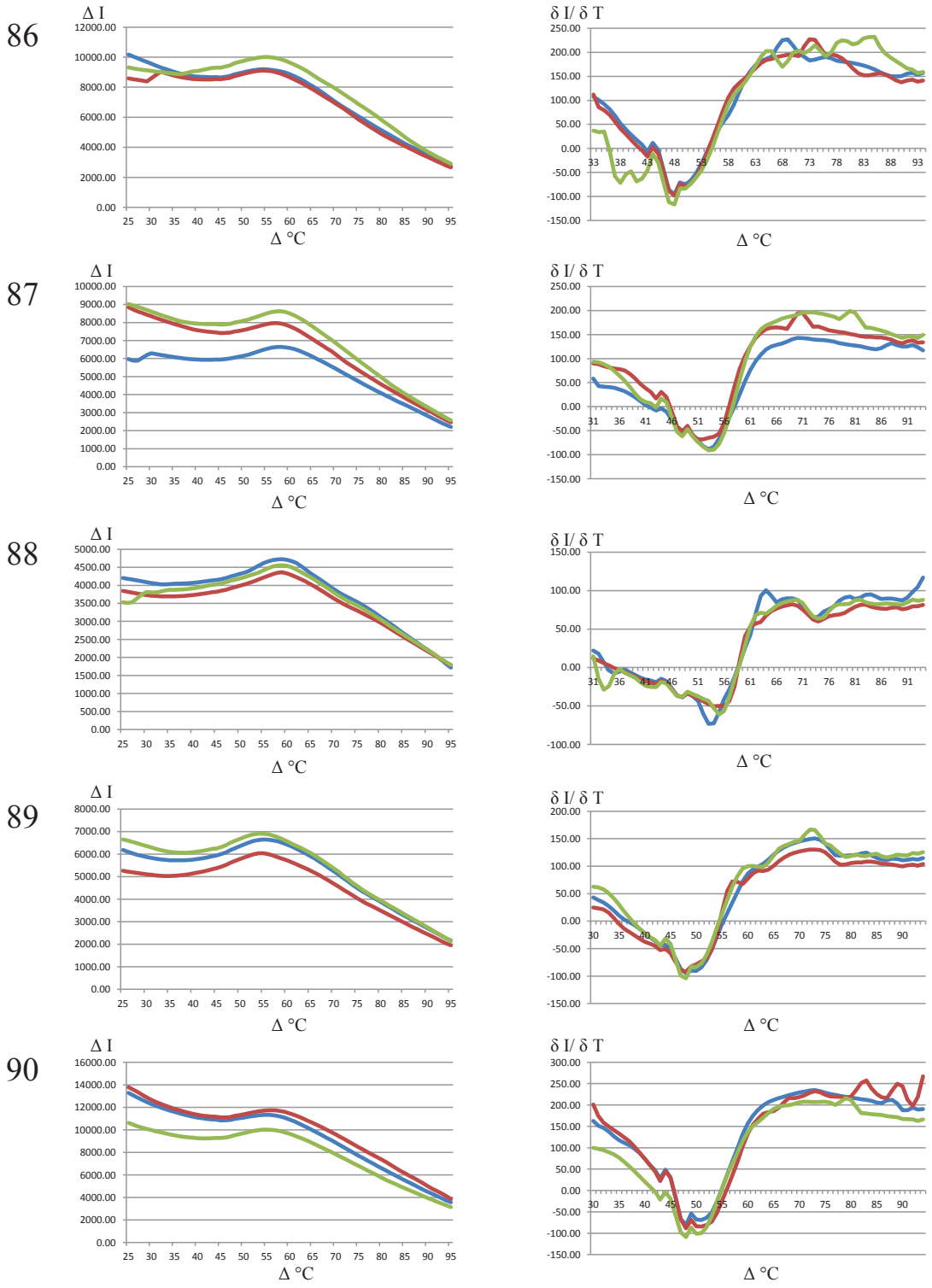

Figure 9.47: Triplicate samples for results of DSF experiment, thermal melt rfu (left) and differential plots (right) for MGL 144 with (86) no additive; (87) GalNAc (1 mM); (88) Dendrimer **21** (1mM); (89) Dendrimer **67** (1mM); (90) Dendrimer **43** (1mM).

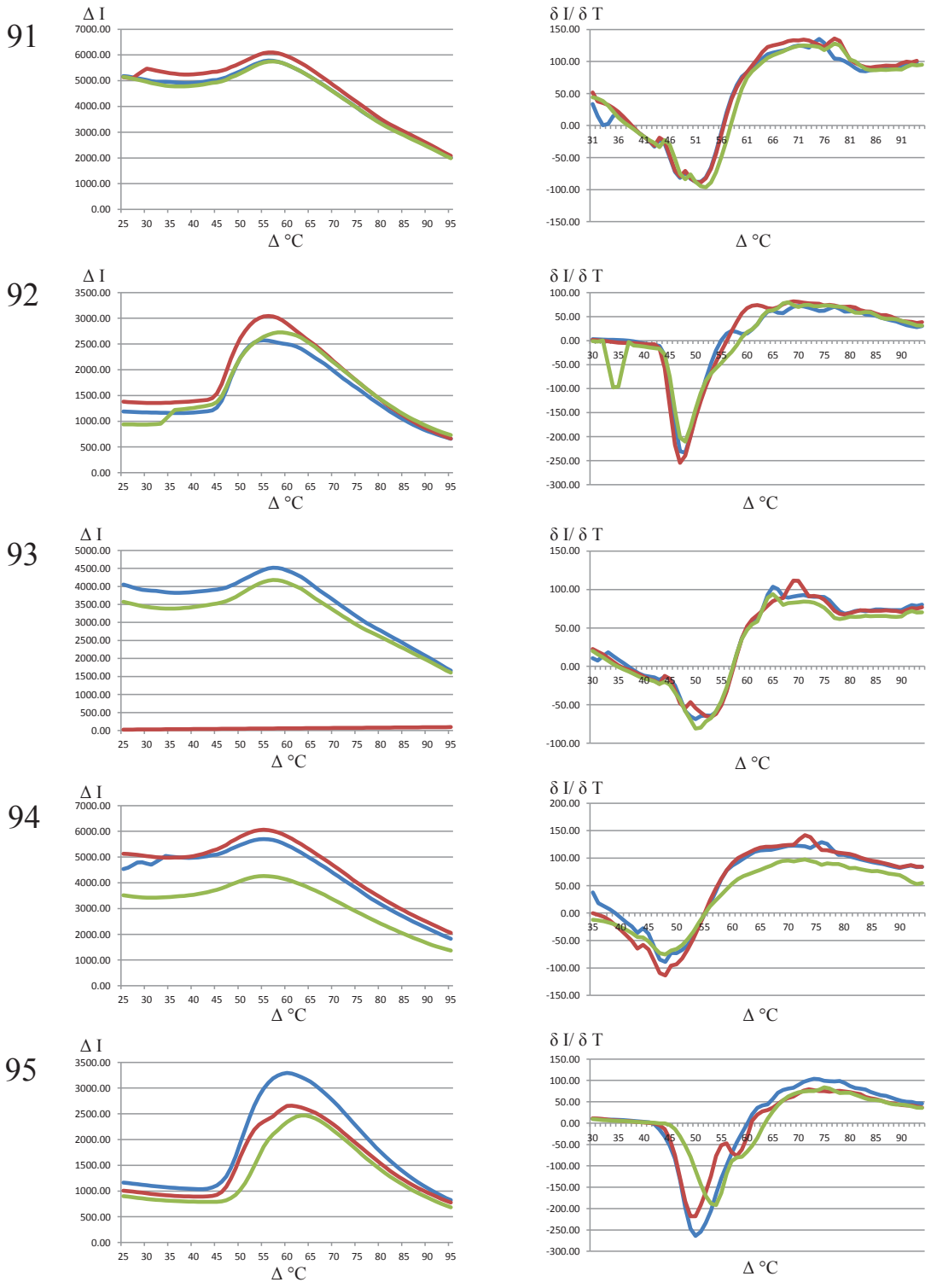

Figure 9.48: Triplicate samples for results of DSF experiment, thermal melt rfu (left) and differential plots (right) for MGL 144 with (91) Dendrimer **2** (1mM); (92) Dendrimer **45** (1 mM); (93) Dendrimer **23** (1mM); (94) Dendrimer **47** (1mM); (95) Dendrimer **25** (1mM).

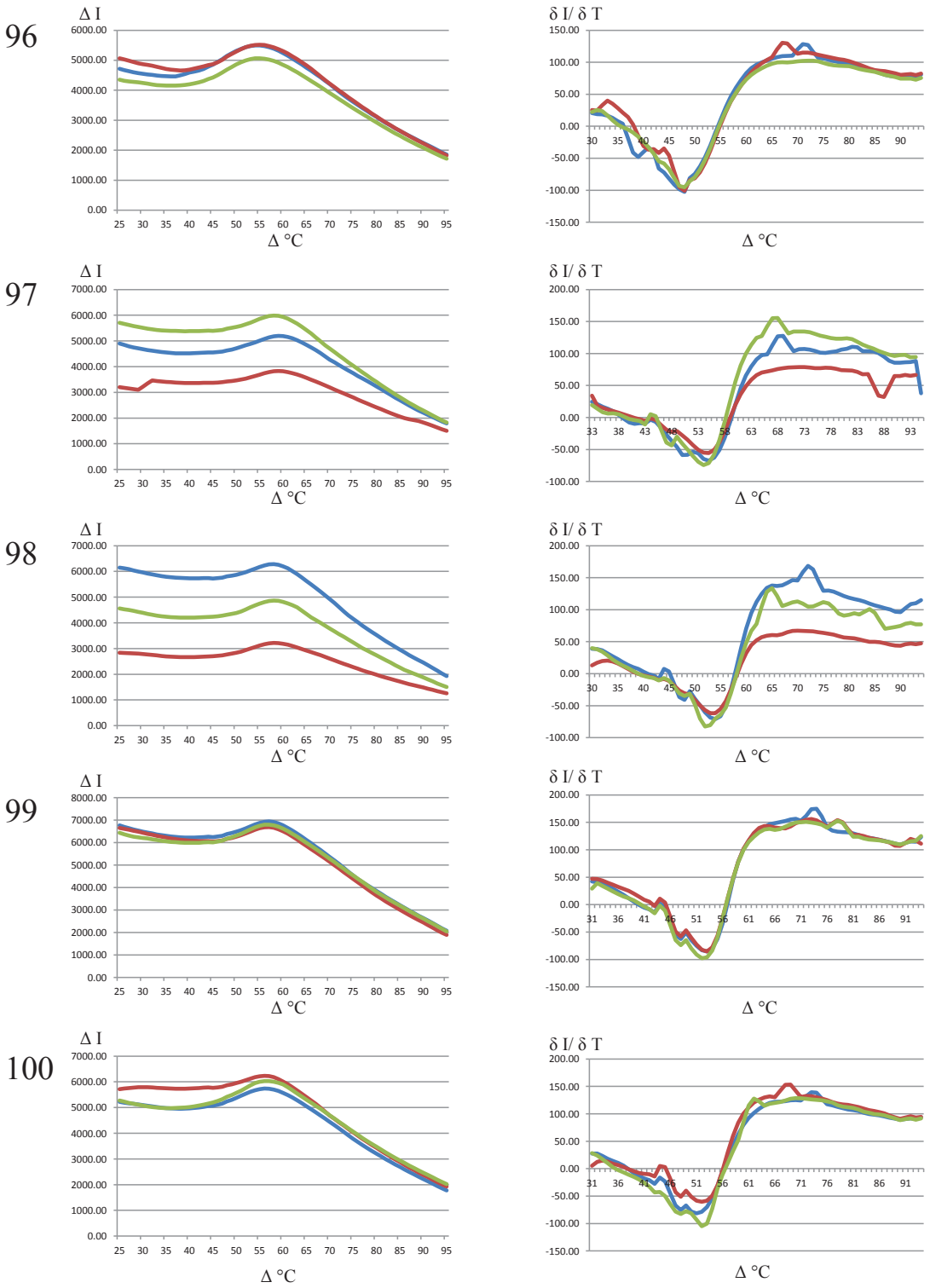

Figure 9.49: Triplicate samples for results of DSF experiment, thermal melt rfu (left) and differential plots (right) for MGL 144 with (96) Dendrimer **49** (1mM); (97) Dendrimer **51** (1 mM); (98) Dendrimer **53** (1mM); (99) Dendrimer **55** (1mM); (100) Dendrimer **57** (1mM).

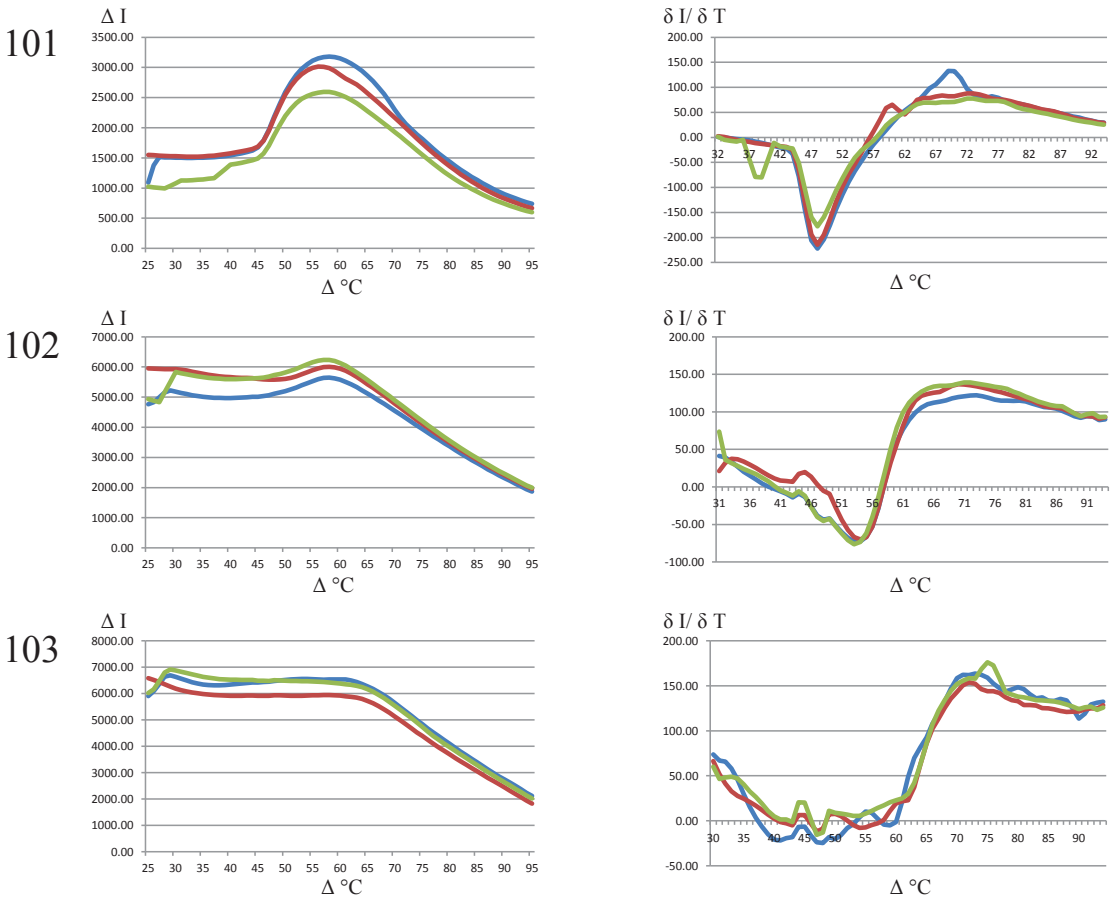

Figure 9.50: Triplicate samples for results of DSF experiment, thermal melt rfu (left) and differential plots (right) for MGL 144 with (101) Dendrimer **59** (1mM); (102) Peptide **61** (1 mM); (103) Peptide **63** (1mM).

9.5 Cell binding assay appendix

9.5.1 Cell binding assay at 0 °C

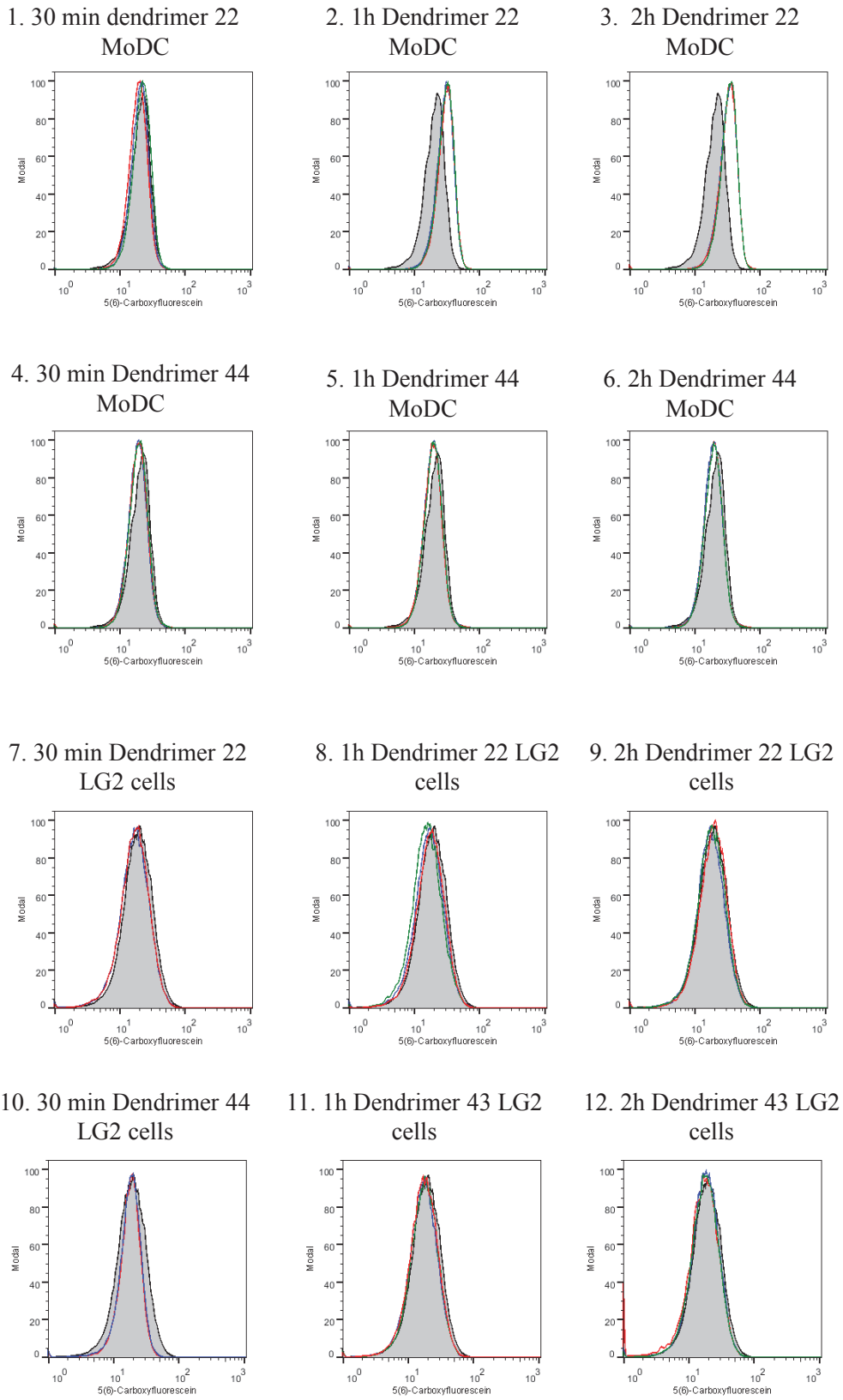

Figure 9.51: Triplicate samples for results of cell binding assay timecourse experiment at 0 °C. FACS Plots 1 to 6 for MoDC, FACS Plots 7 to 12 for LG2 cells.

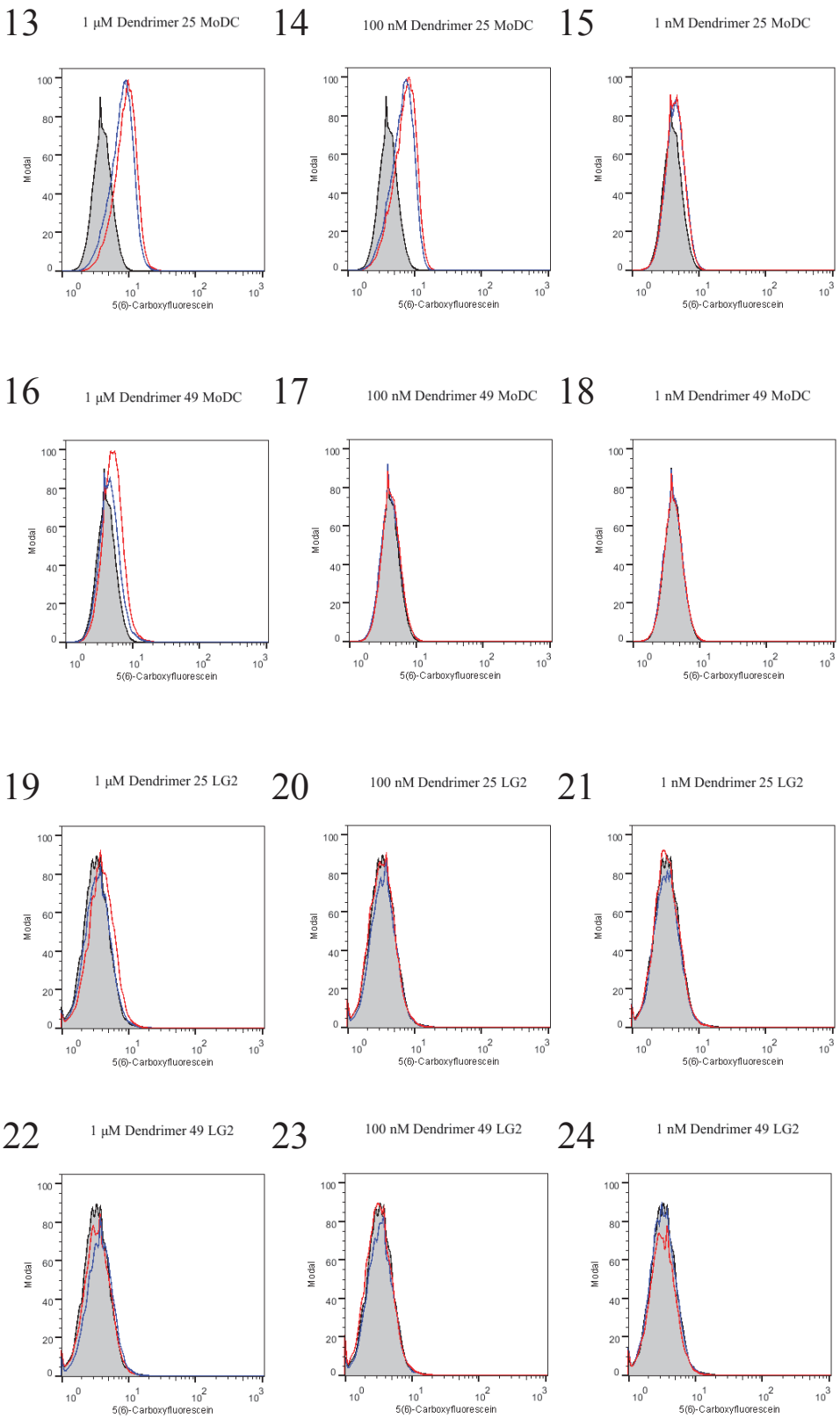

Figure 9.52: Duplicate samples for results of cell binding assay titration experiment with 1 μM, 100 nM and 1 nM concentrations at 0 °C. FACS Plots 13 to 18 for MoDC, FACS Plots 19 to 24 for LG2 cells.

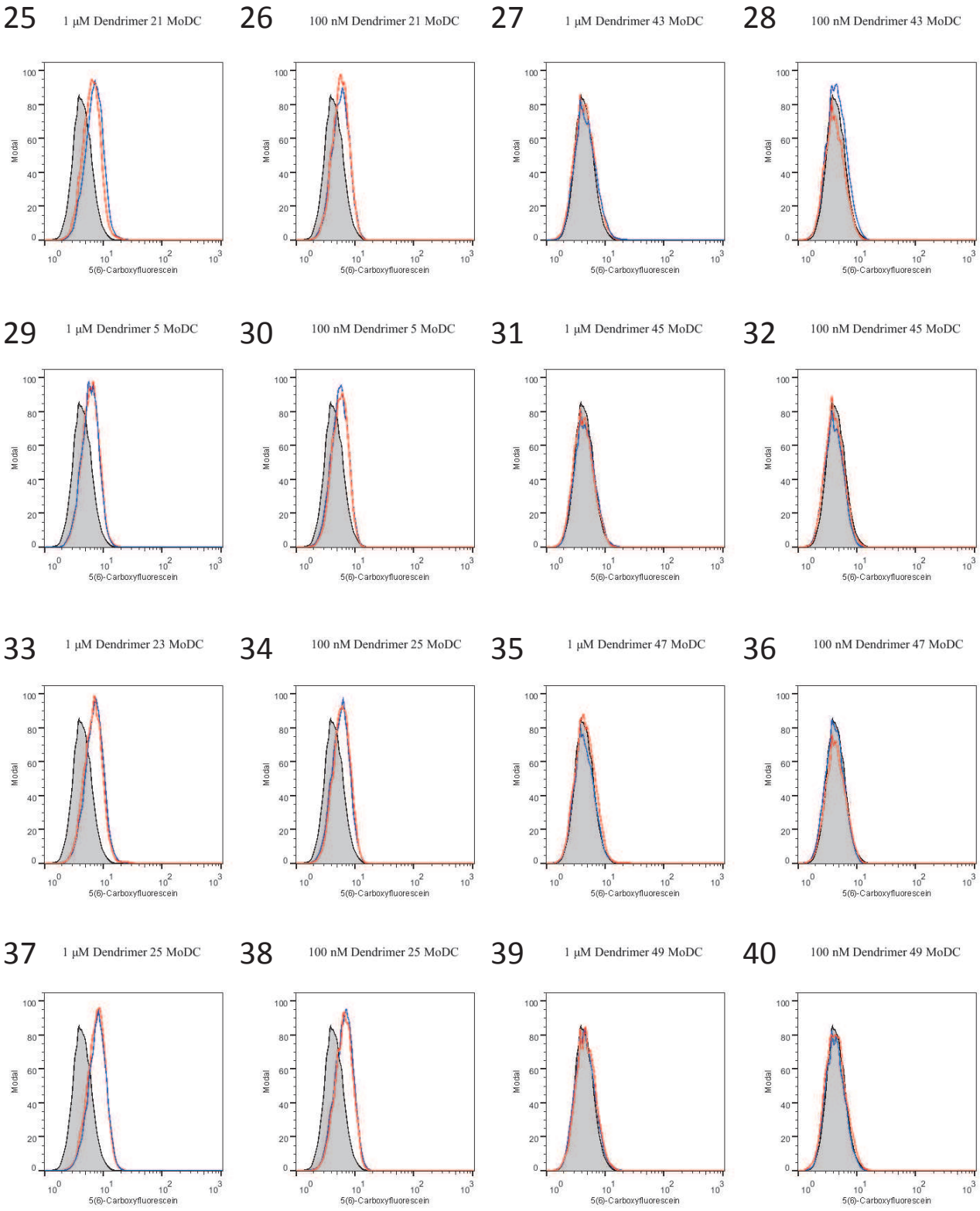

Figure 9.53: Duplicate samples for results of cell binding assay titration experiment with 1 μM, 100 nM concentrations at 0 °C. FACS Plots 25 to 40 for MoDC.

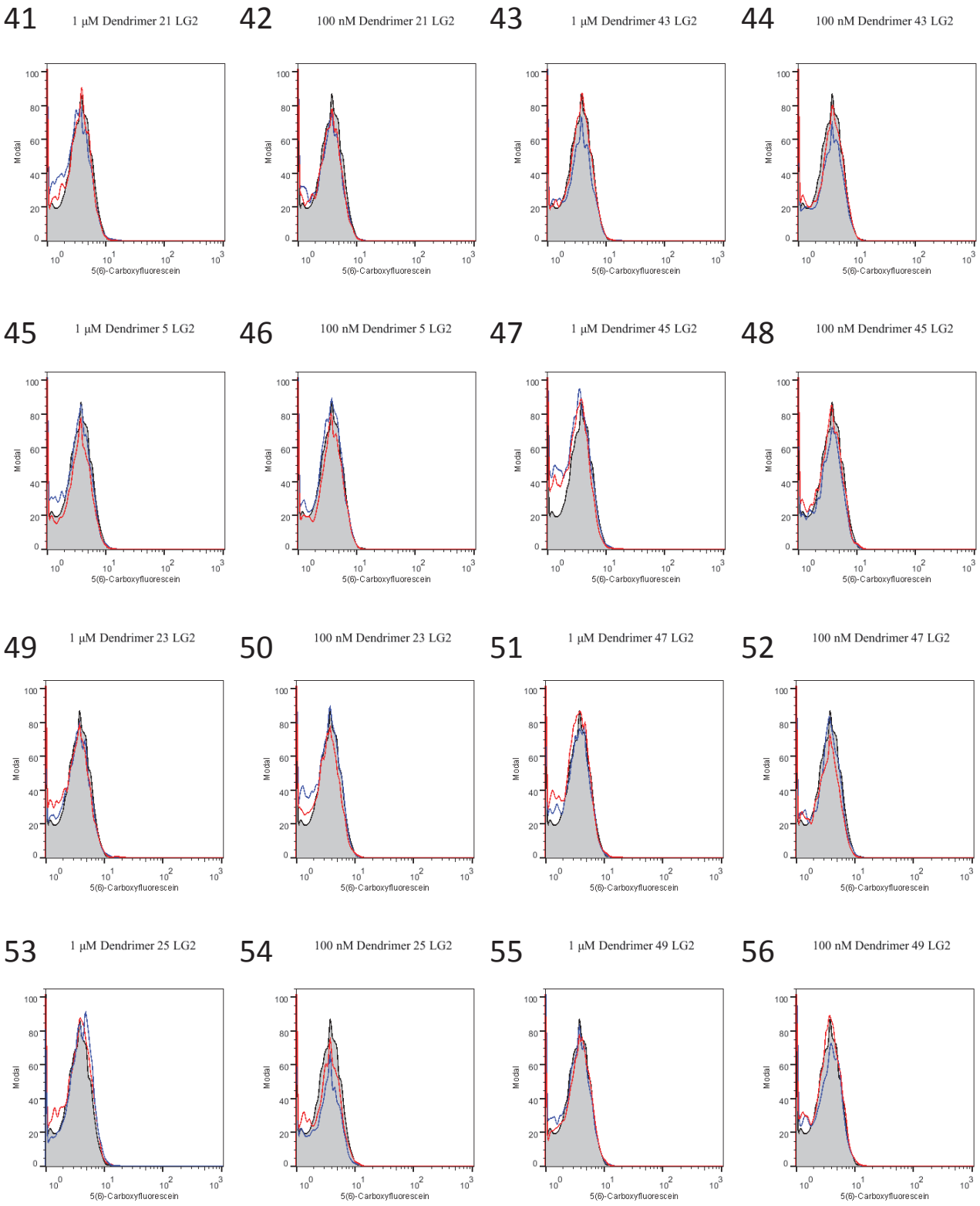

Figure 9.54: Duplicate samples for results of cell binding assay titration experiment with 1 μM, 100 nM concentrations at 0 °C. FACS Plots 41 to 56 for LG2 cells.

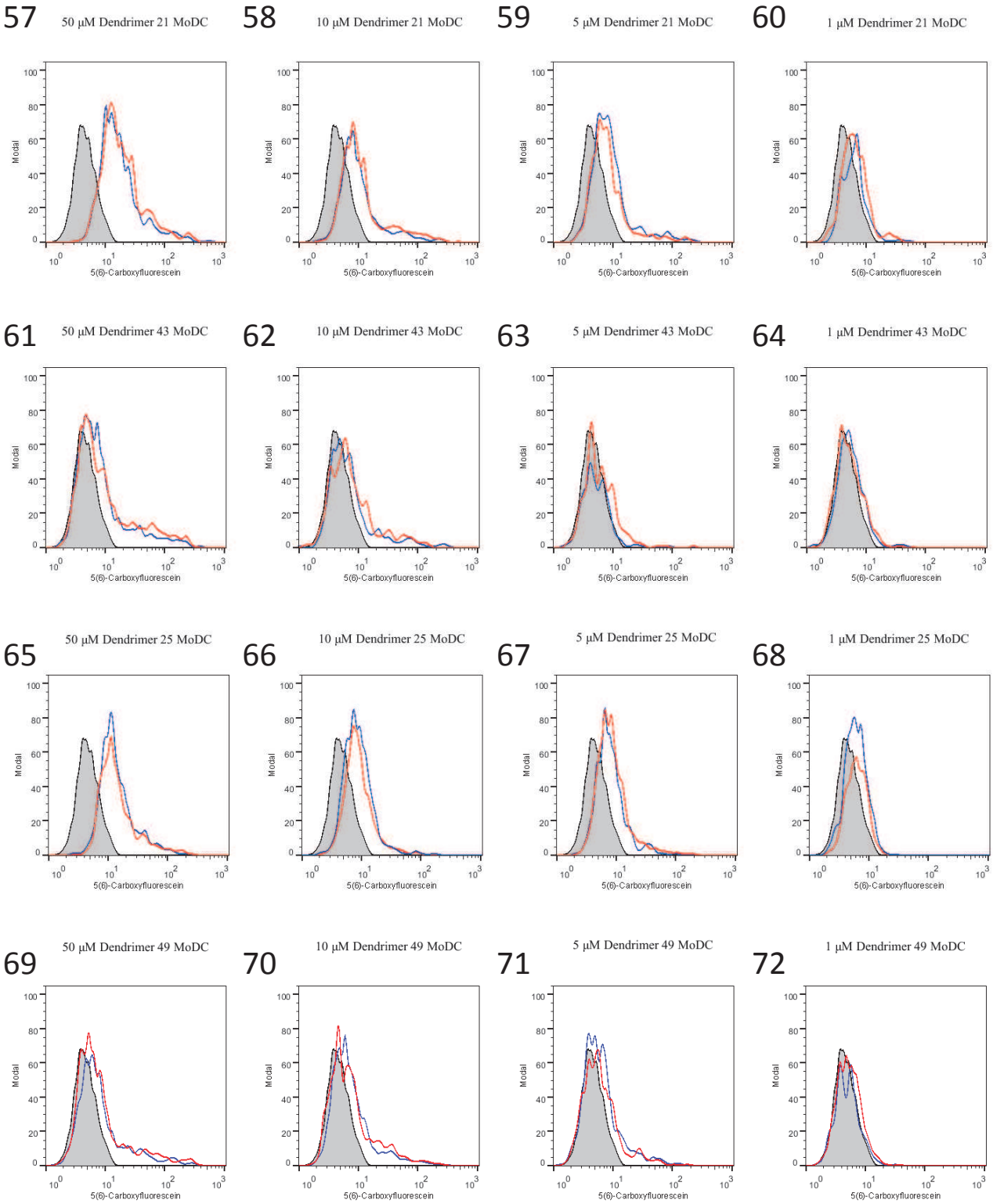

Figure 9.55: Duplicate samples for results of cell binding assay titration experiment with 50 μM, 10 μM, 5 μM and 1 μM concentrations at 0 °C for 1 h. FACS Plots 57 to 72 for MoDC cells.

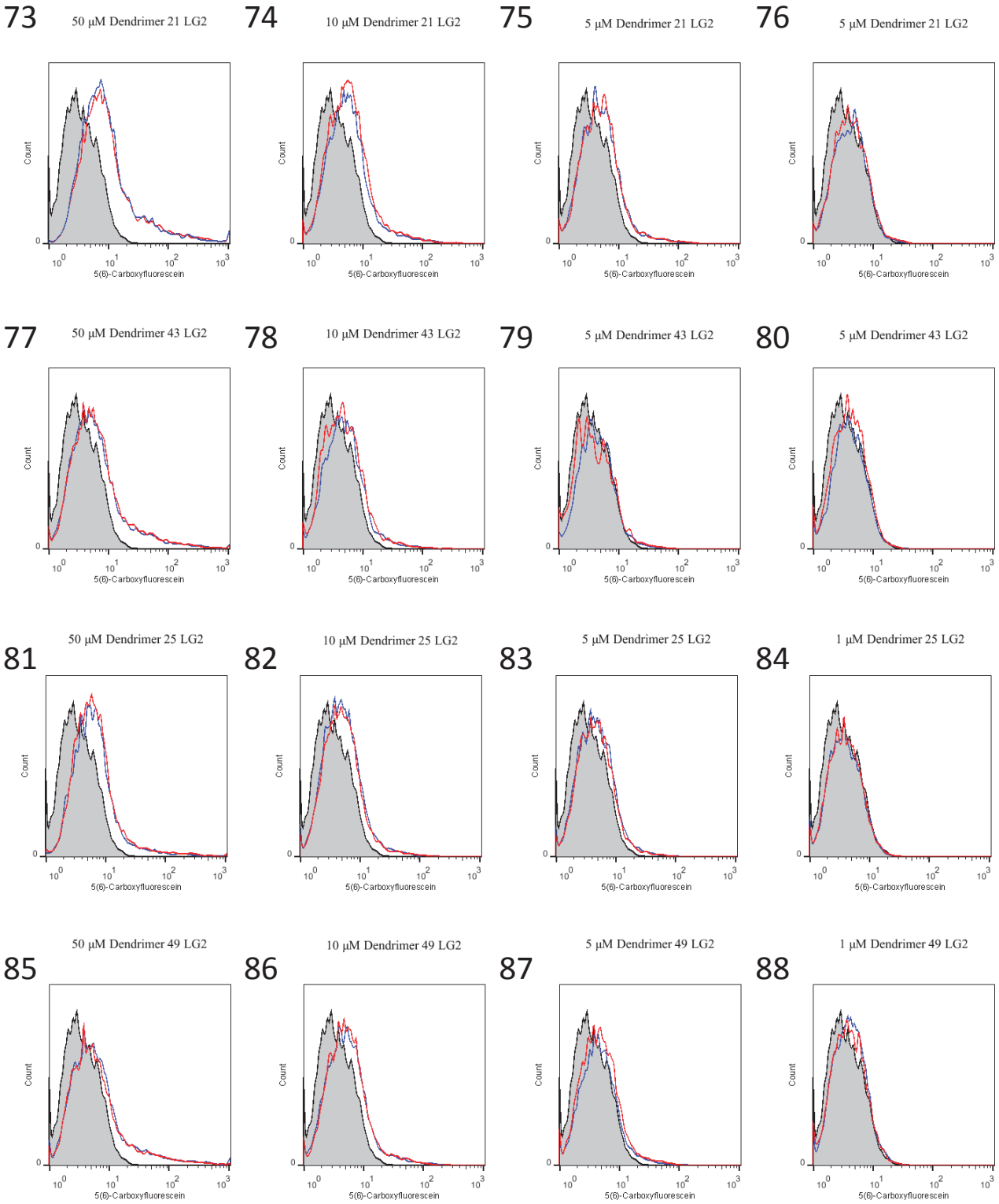

Figure 9.56: Duplicate samples for results of cell binding assay titration experiment with 50 μM, 10 μM, 5 μM and 1 μM concentrations at 0 °C for 1 h. FACS Plots 73 to 88 for LG2 cells.

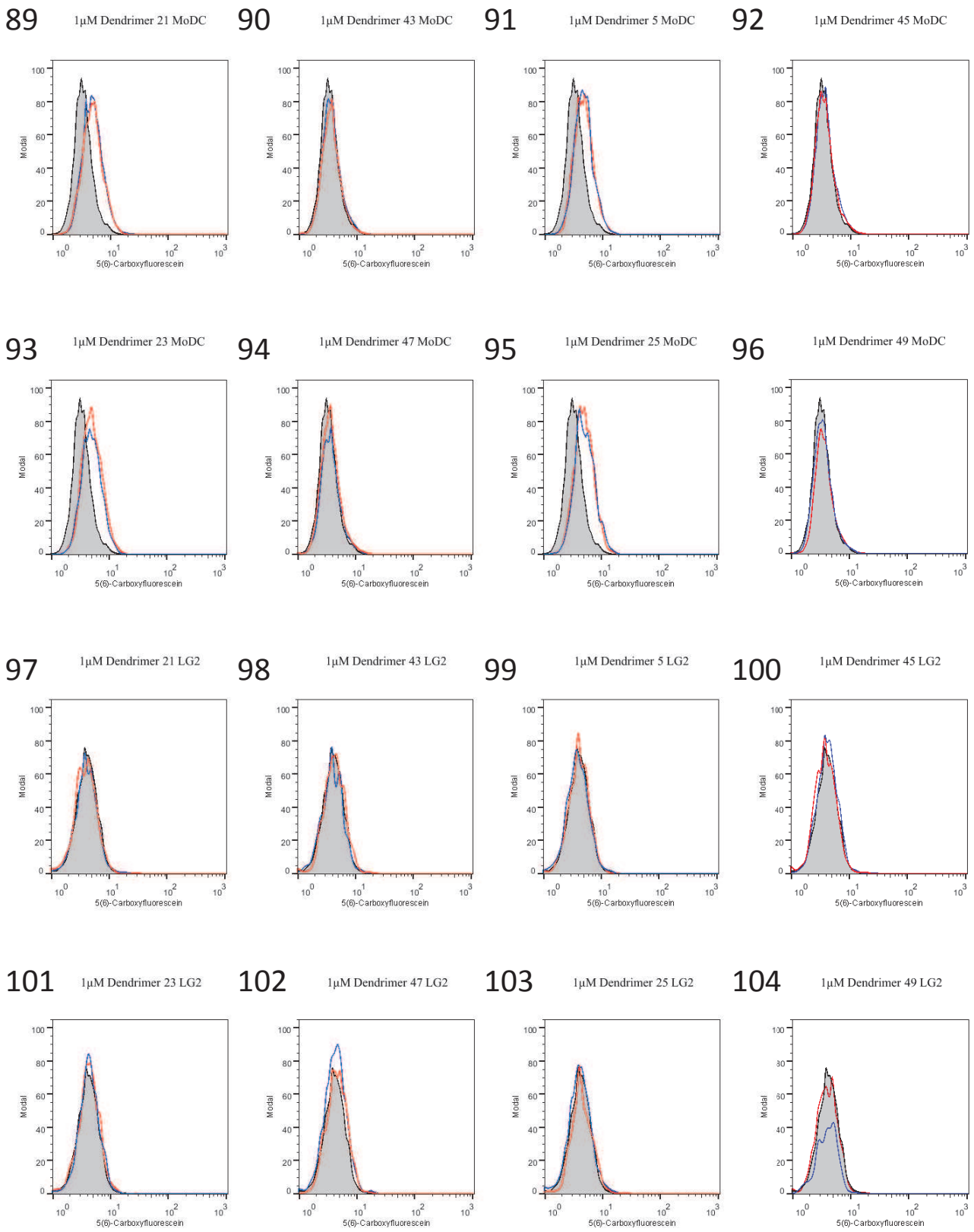

Figure 9.57: Duplicate samples for results of optimised conditions for cell binding assay titration experiment at 0 °C. FACS Plots 89 to 96 for MoDC, FACS plots 97 to 104 for LG2 cells.

9.5.2 Cell binding assay at 37 °C

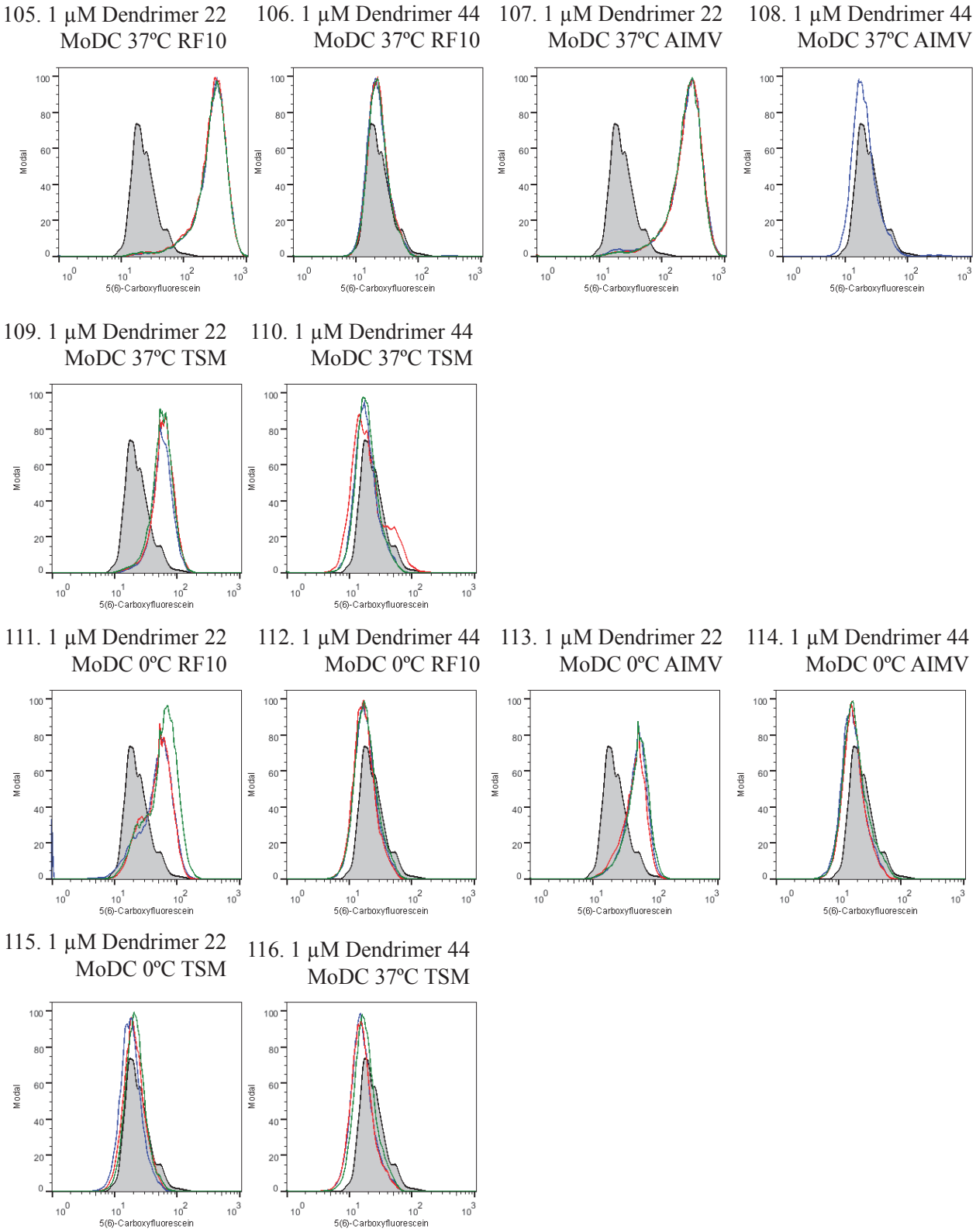

Figure 9.58: Triplicate samples for results of cell binding comparison of solvents at 0 °C and 37 °C. FACS Plots 105 to 116 for MoDC.

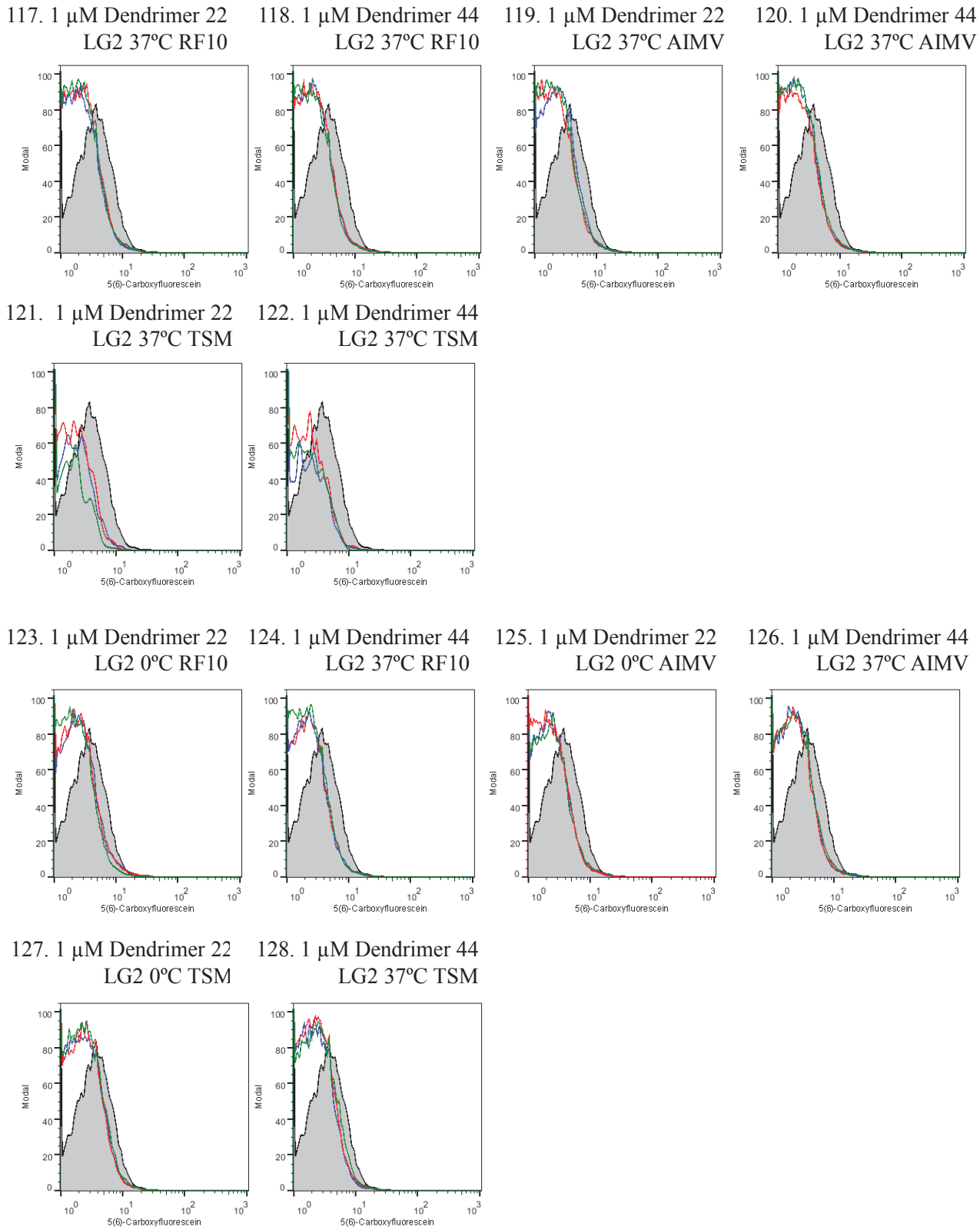

Figure 9.59: Triplicate samples for results of cell binding comparison of solvents at 0 °C and 37 °C. FACS Plots 117 to 128 for LG2 cells.

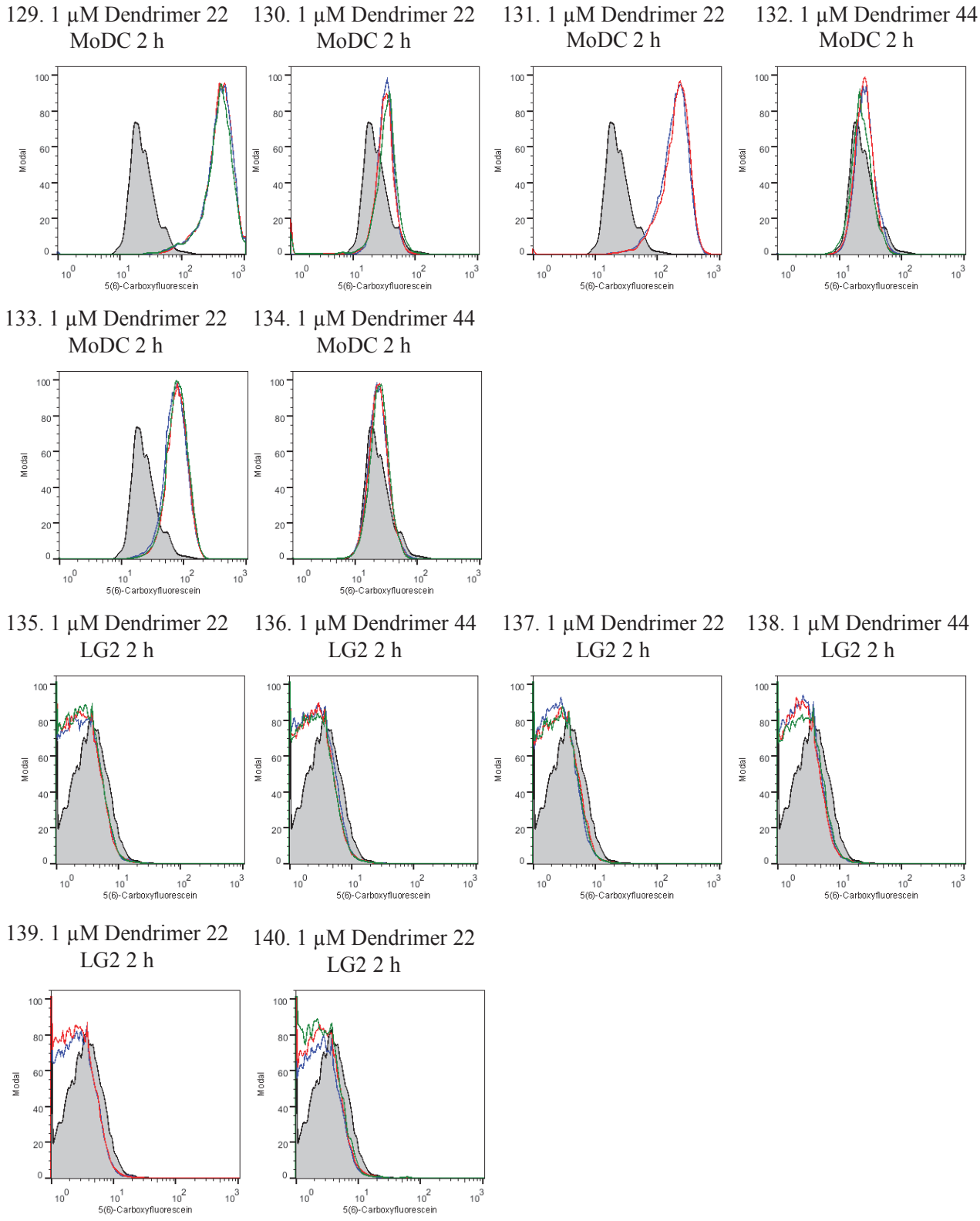

Figure 9.60: Triplicate samples for results of cell binding assay timecourse experiment at 37 °C. FACS Plots 129 to 134 for MoDC, and 135 to 140 for LG2 cells.

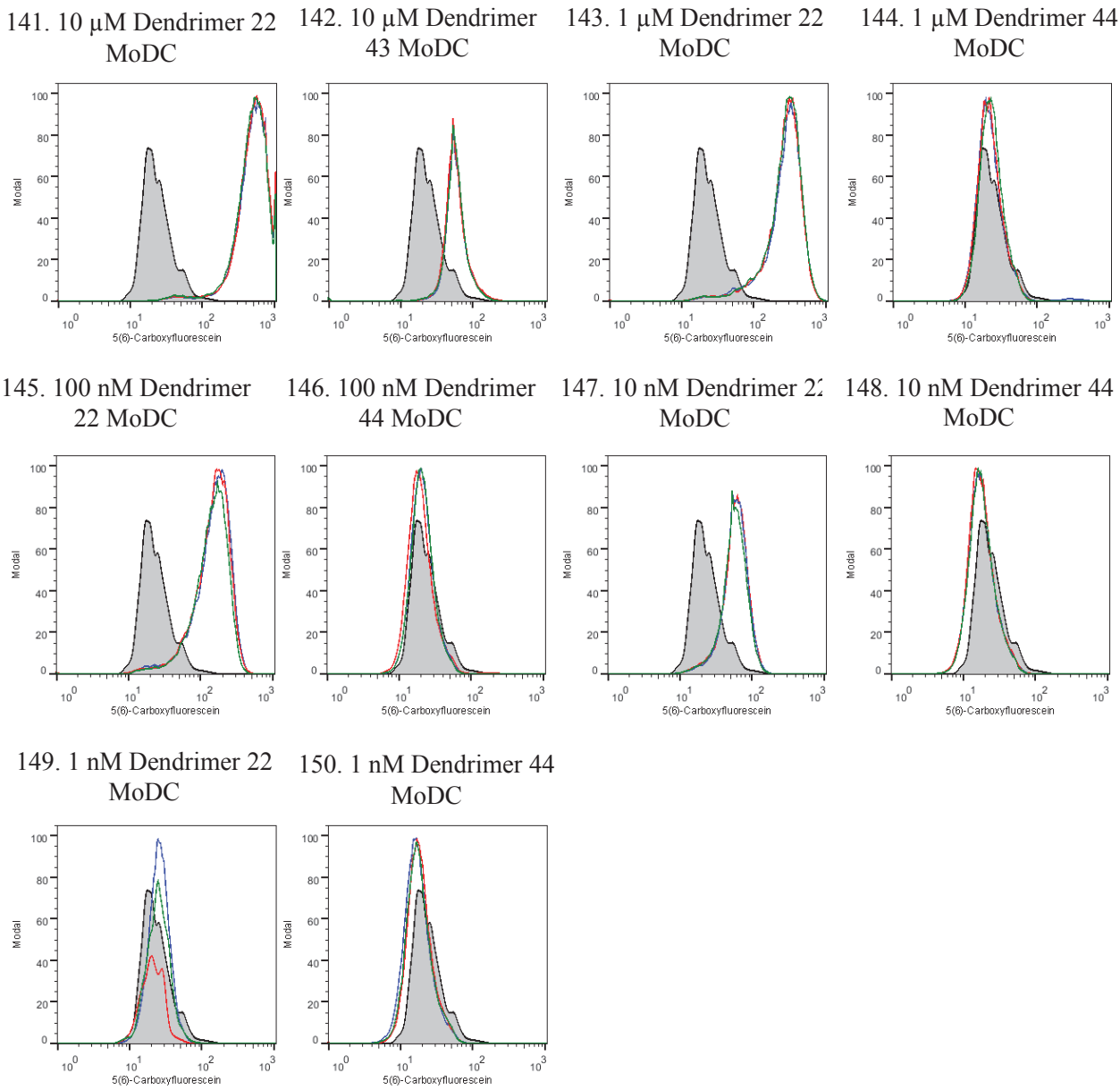

Figure 9.61: Triplicate samples for results of cell binding assay titration experiment at 37 °C. FACS Plots 141 to 150 for MoDC.

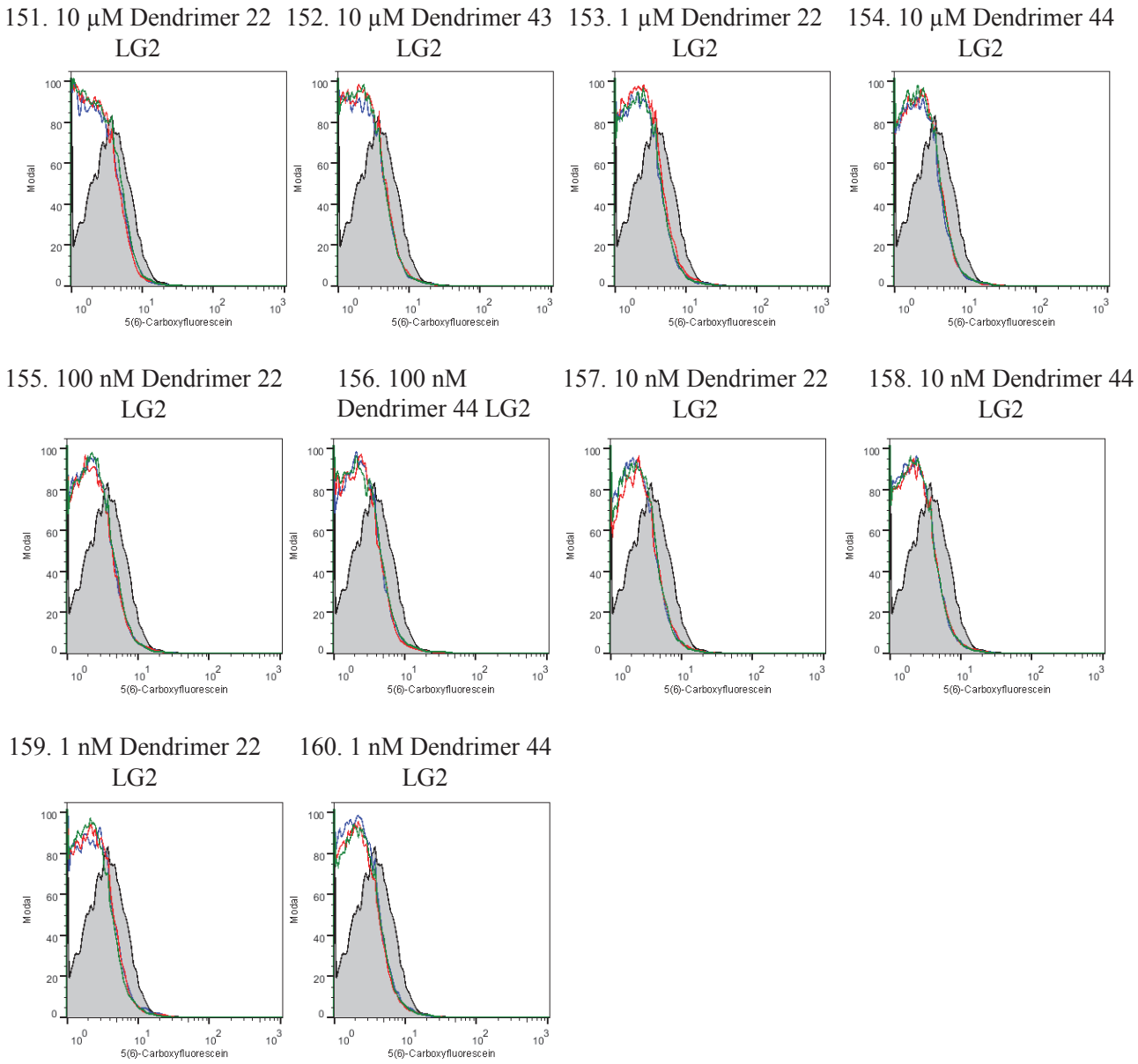

Figure 9.62: Triplicate samples for results of cell binding assay titration experiment at 37 °C. FACS Plots 151 to 160 for LG2 cells.

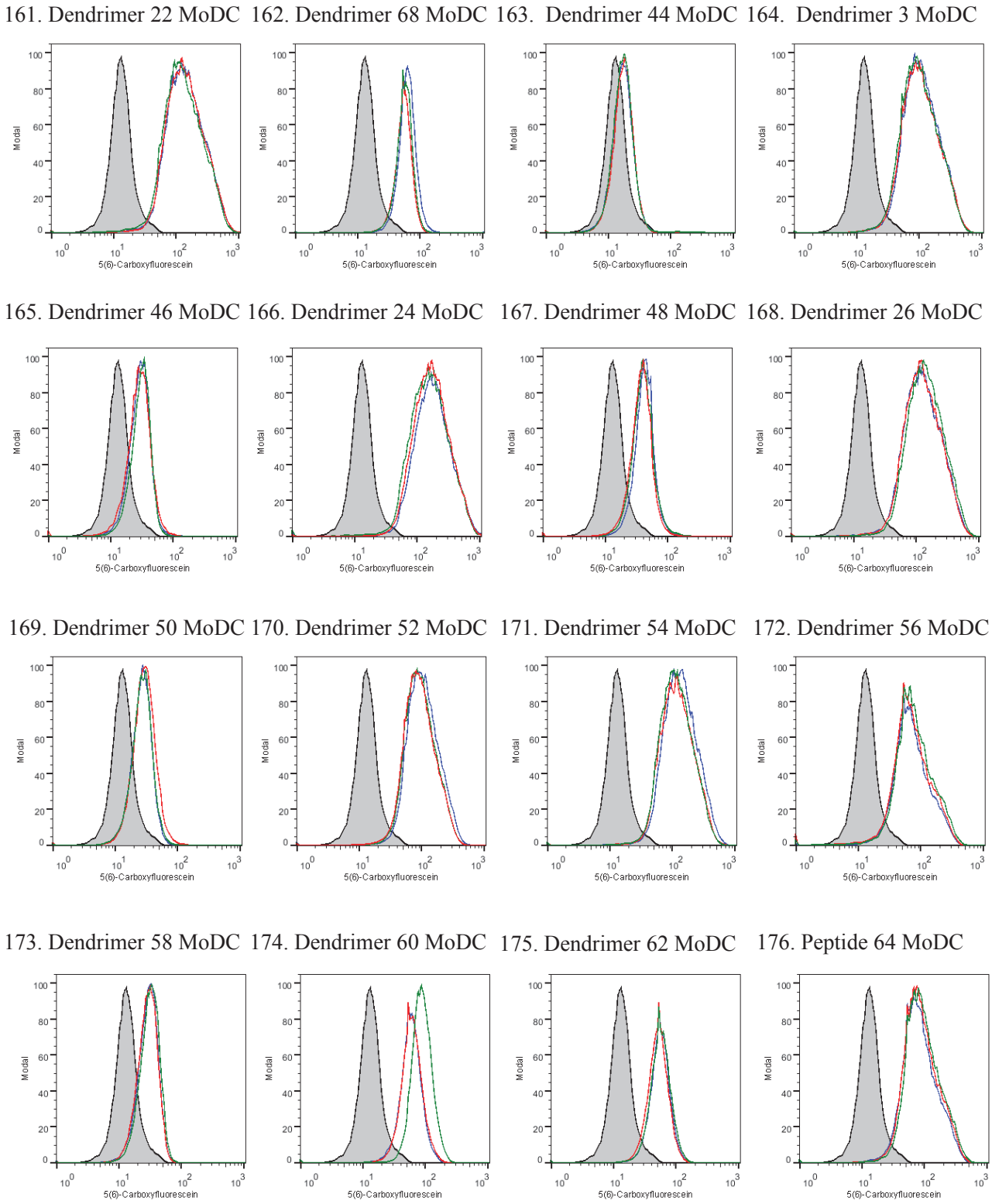

Figure 9.63: Triplicate samples for results of cell binding assay 1 h at 37 °C and 1 μM. FACS Plots 161 to 176 for MoDC.

177. Peptide 65 MoDC 178. Peptide 66 MoDC 179. MUC1 J MoDC 180. MUC1 K MoDC

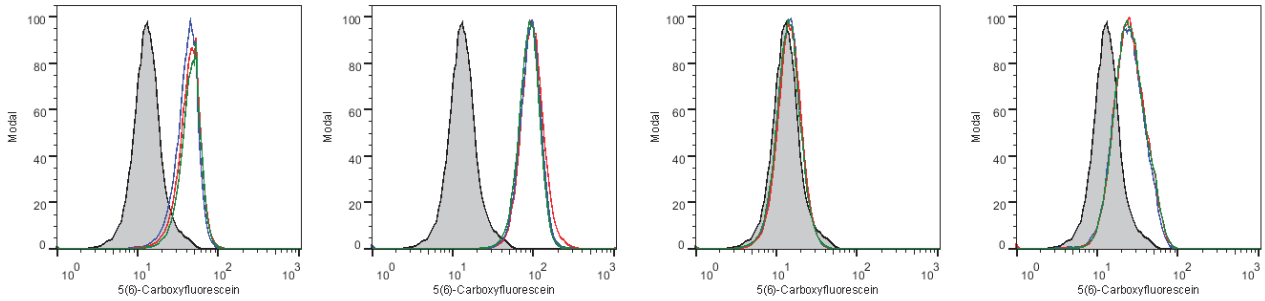

181. MUC1 L MoDC

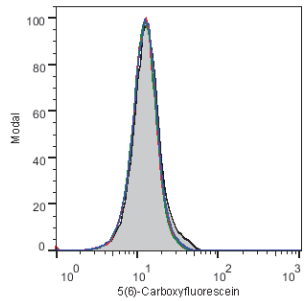

Figure 9.64: Triplicate samples for results of cell binding assay 1 h at 37 °C and 1 μM. FACS Plots 177 to 181 for MoDC.

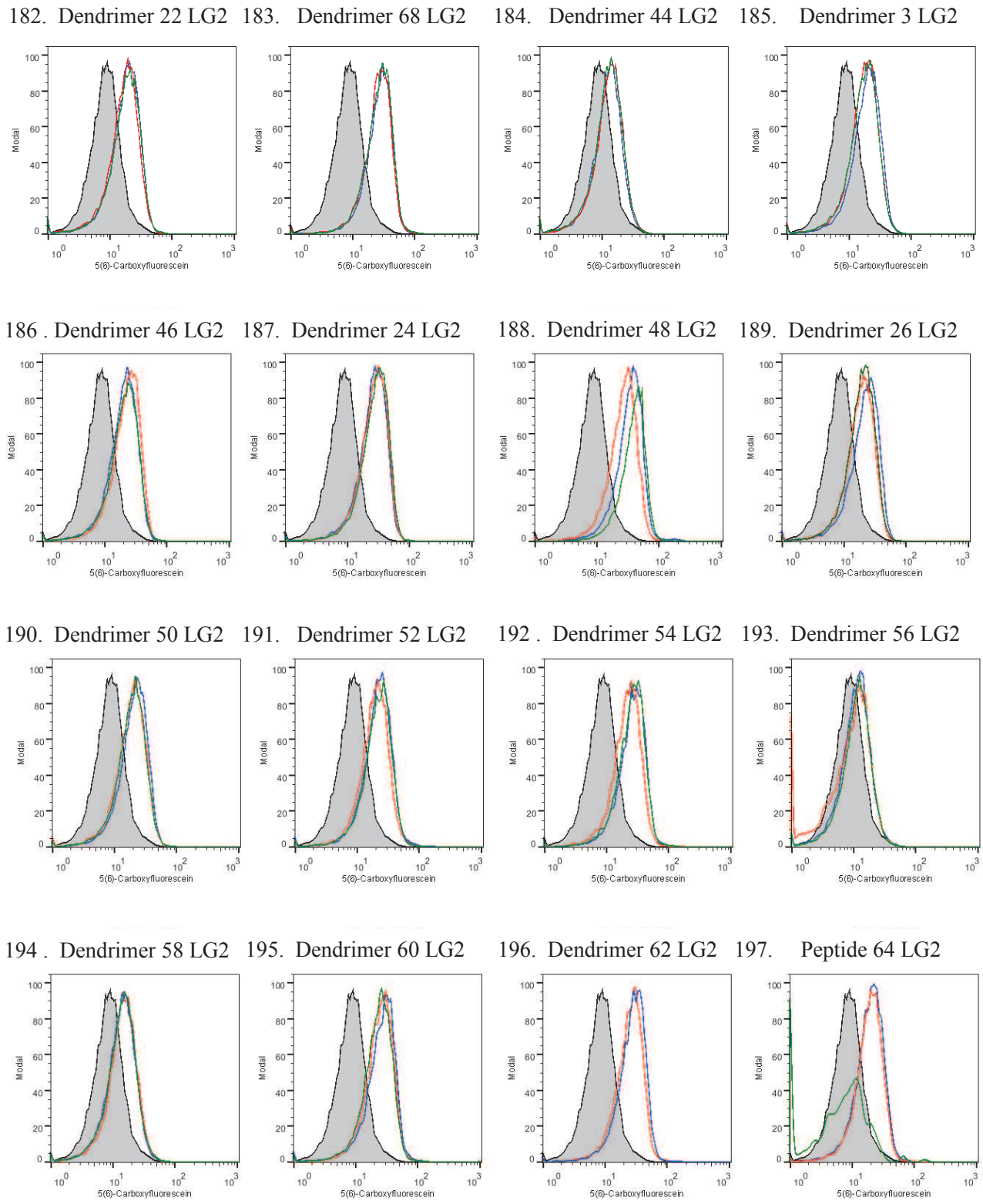

Figure 9.65: Triplicate samples for results of cell binding assay 1 h at 37 °C and 1 μM. FACS Plots 182 to 197 for LG2 cells.

198 . Peptide 65 LG2 199. Peptide 66 LG2 200. MUC1 J LG2 201. MUC1 K LG2

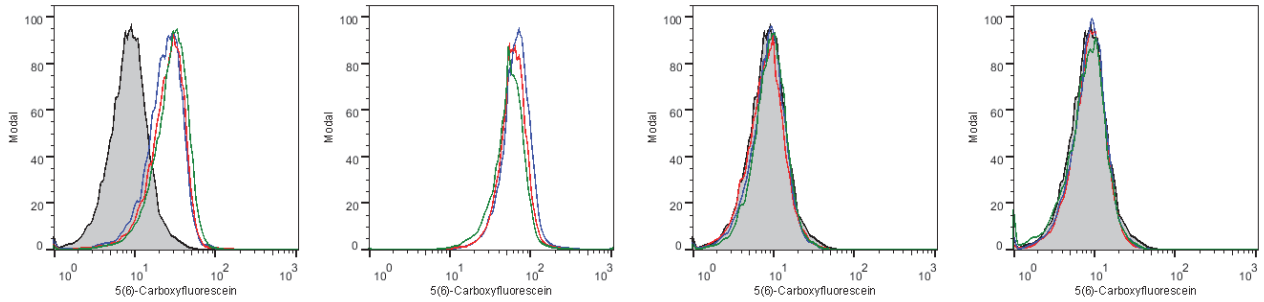

202. MUC1 L LG2

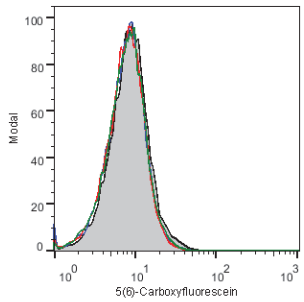

Figure 9.66: Triplicate samples for results of cell binding assay 1 h at 37 °C and 1 μM. FACS Plots 198 to 202 for LG2 cells.

9.5.3 PBMC cell binding assay performed by Dr A. Brooks appendix

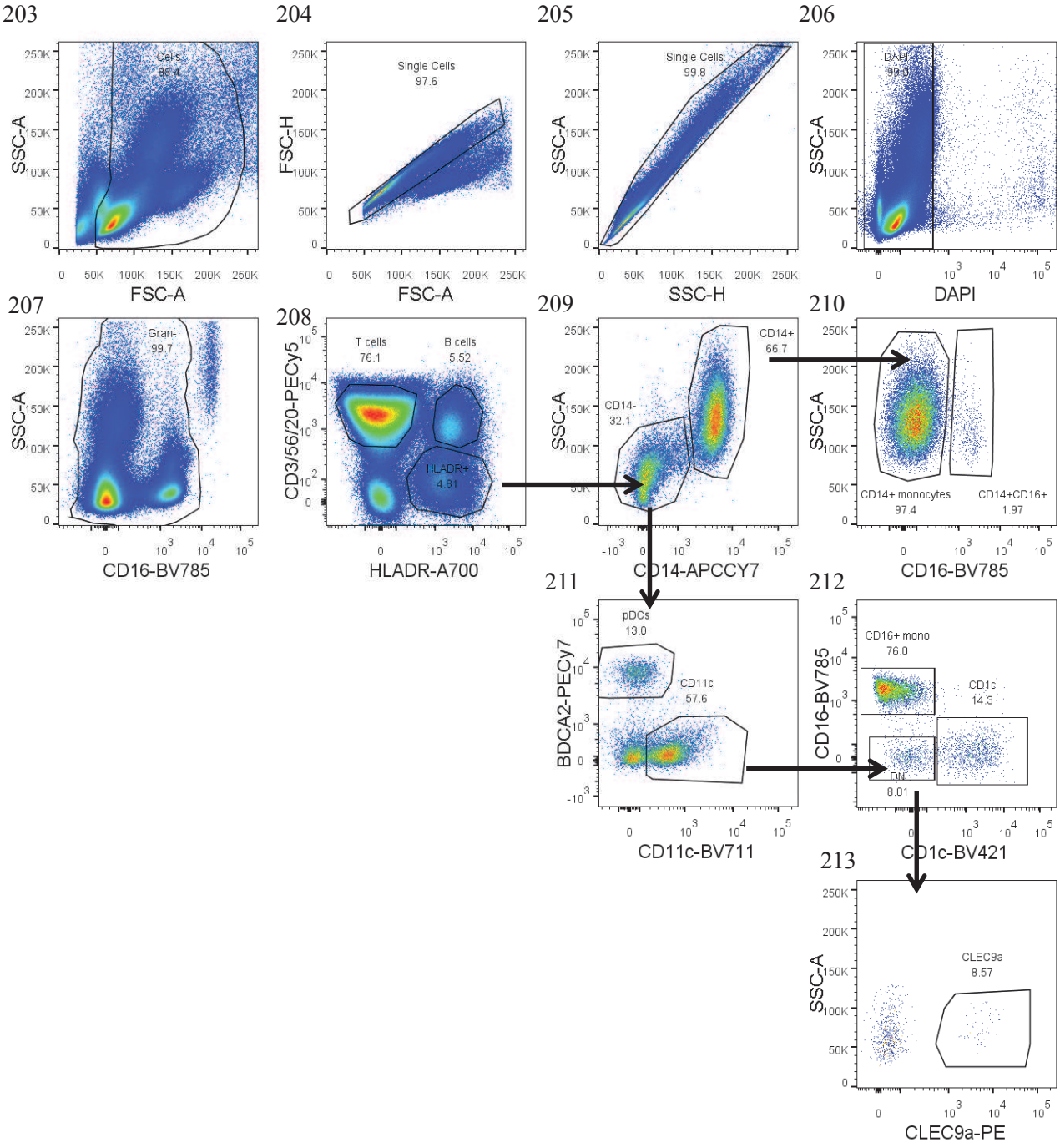

Figure 9.67: Gating strategy for identifying the different cell populations present in the PBMC cell binding assay. FACS Plots 203 to 213.

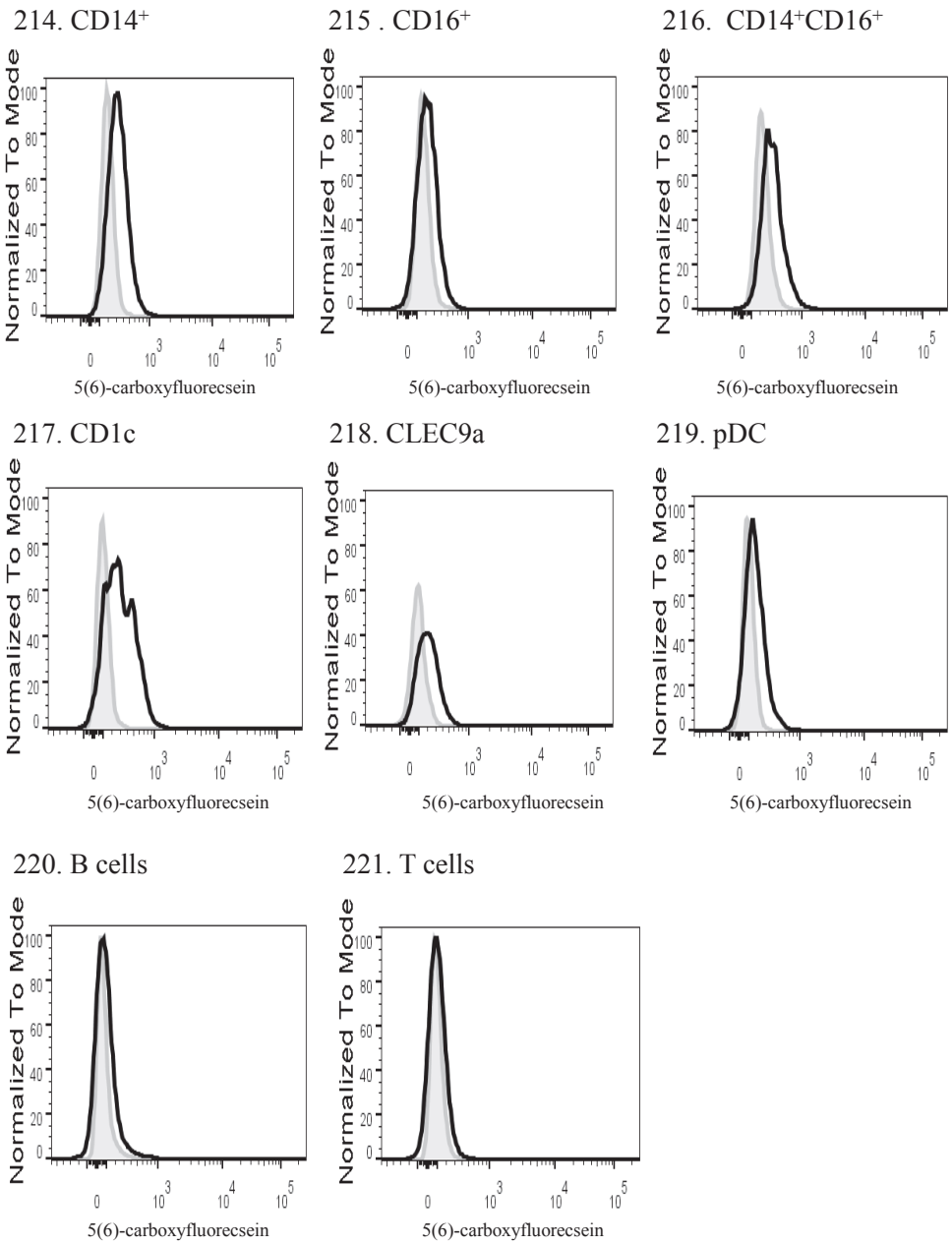

Figure 9.68: Representative FACS plots from one of four data sets of MGL expression for the different cell populations present in the PBMC cell binding assay. FACS Plots 214 to 221.

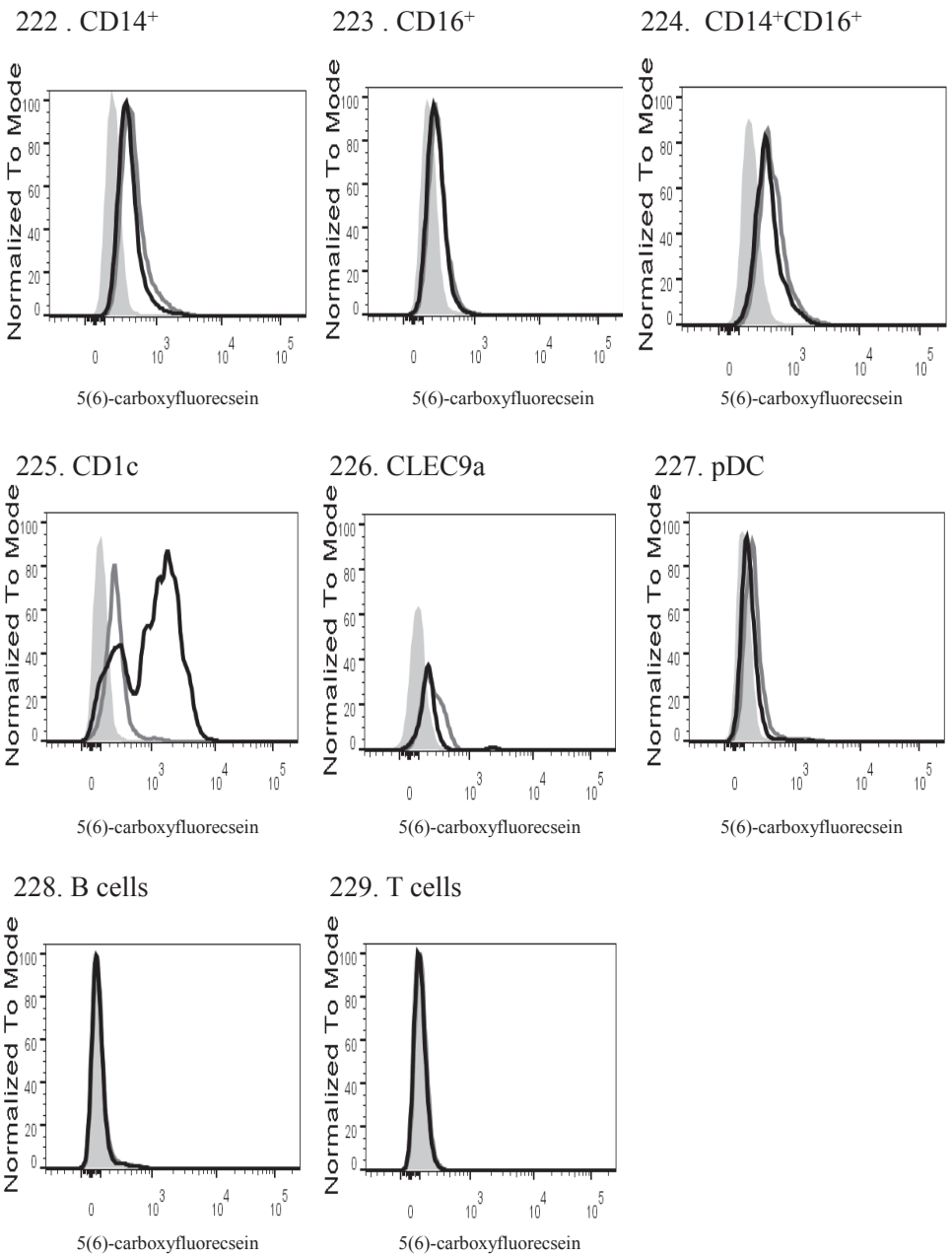

Figure 9.69: Representative FACS plots from one of four data sets of binding of the GalNAc–glycosylated generation I dendrimer **74** (black) and non–glycosylated generation II dendrimer **75** (grey) to different cell populations present in the PBMC cell binding assay. FACS Plots 222 to 229.

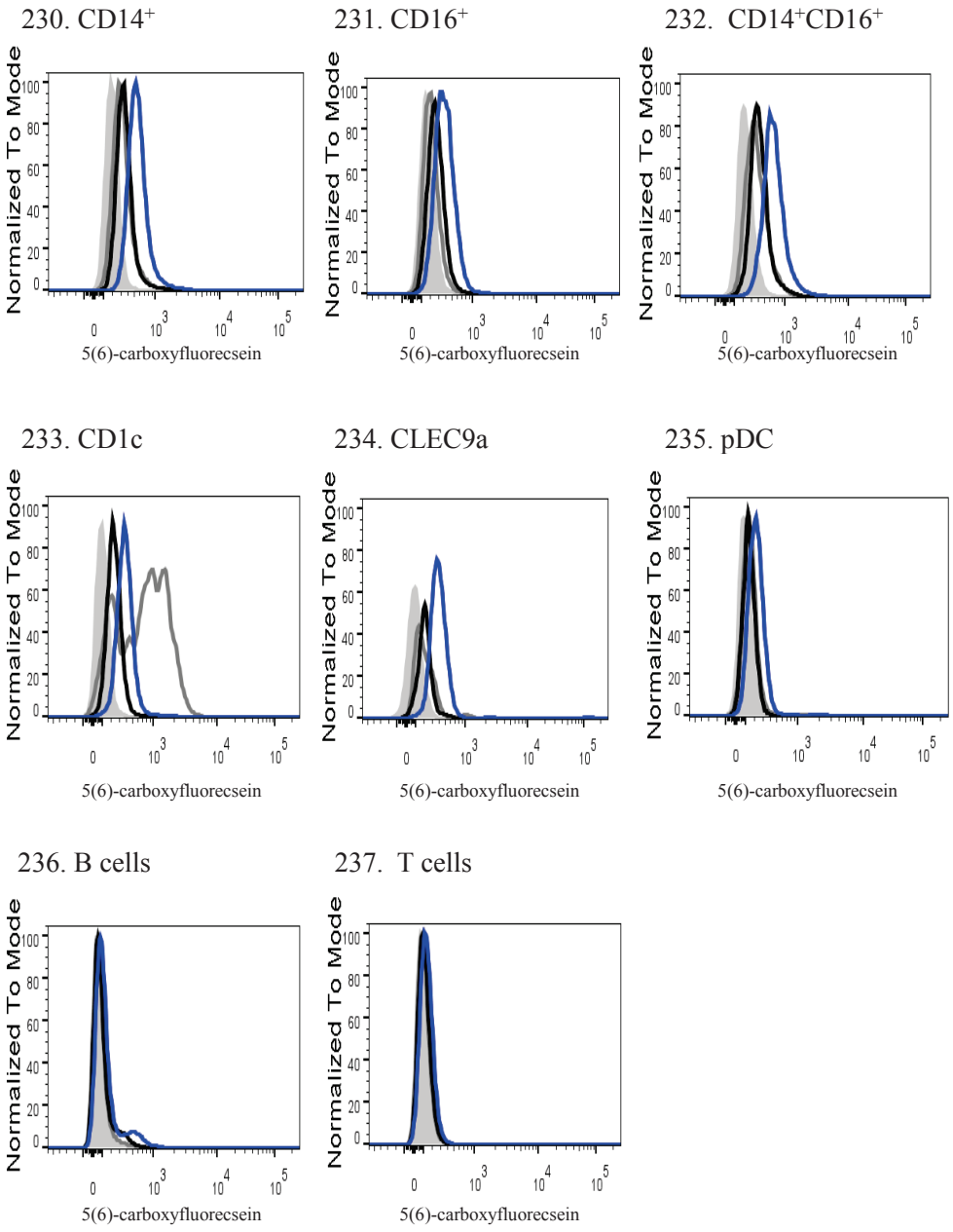

Figure 9.70: Representative FACS plots from one of four data sets of binding of the GalNAc–glycosylated generation V peptide **64** (grey) the triazole derivatised peptide **66** (blue) and the non–glycosylated peptide **65** (black) to different cell populations present in the PBMC cell binding assay. FACS Plots 230 to 237.

Bibliography

[1] Kastenmüller, W.; Kastenmüller K.; Kurts, C.; Seder, R. A. Dendritic Cell–Targeted Vaccines Hope or Hype. *Nat. Rev. Immunol.*, **2014**, *9*, 1–7.

[2] Murphy, K.; Travers, P.; Walport, M. *Janeway's Immuno Biology 7th ed.* Garland Science **2007**.

[3] Comber, J. D.; Philip, R. MHC Class I Antigen Presentation and Implications for Developing a New Generation of Therapeutic Vaccines. *Ther. Adv. Vaccine*, **2014**, *2*, 77–89.

[4] Pardoll D. M. The Blockade of Immune Checkpoints in Cancer Immunotherapy. *Nat. Rev.*, **2012**, *12*, 252–264.

[5] Eggermont, A.; Robert, C.; Soria, J. C.; Zitvogel, L. Harnessing the Immune System to Provide Long–Term Survival in Patients with Melanoma and Other Solid Tumours. *Oncoimmunology*, **2014**, *3*, e27560–1–7.

[6] Streng–Ouwehand, I.; Unger, W. W. J.; van Kooyk, Y. C–Type Lectin Receptors for Tumor Eradication: Future Directions. *Cancers*, **2011**, *3*, 3169–3188.

[7] NZ Ministry of Health. Selected cancers 2011, 2012 and 2013. http://www.health.govt.nz/publication/selected-cancers-2011-2012-2013, accessed November 3, **2014**.

[8] The World Health Organisation. Cancer. http://www.who.int/mediacentre/factsheets/fs297/en/, accessed November 3, **2014**.

[9] Cancer Research UK. Cancer survival statistics. http://www.cancerresearchuk.org/cancer-info/cancerstats/survival/england-and-wales-cancer-survival-statistics, accessed November 18, **2014**.

[10] Varki, A.; Cummings R. D.; Esko, J. D.; McEver, R. P. *Essentials of Glycobiology. 2nd edition.* Cold Spring Harbor Laboratory Press **2009**.

[11] G. Mayer. Microbiology and immunology on–line textbook. in: U.s.o medicine (ed). http://www.microbiologybook.org/book/immunol-sta.htm, accessed May 05, **2014**.

[12] van Vliet, S. J.; Saeland, E.; van Kooyk Y. Sweet Preferences of MGL: Carbohydrate Specificity and Function. *Trends in Immunol.*, **2008**, *29*, 83–90.

[13] Tokoyuni, T.; Hakomori, S.; Singhal, A. K. Synthetic Carbohydrate Vaccines Synthesis and Immunogenicity of T_N Antigen Conjugates. *Bioorg. Med. Chem.*, **1994**, *11*, 1119–1132.

[14] Jégouzo S. A.; Quintero-Martinez, A.; Ouyang, X.; dos Santos A.; Taylor, M. E.; Drickamer, K. Organization of the Extracellular Portion of the Macrophage Galactose Receptor: A Trimeric Cluster of Simple Binding Sites for N–Acetylgalactosamine. *Glycobiology*, **2013**, *23*, 853–864.

[15] Sakakura, M.; Oo–Puthinan, S.; Moriyama, C.; Kimura, T.; Moriya, J.; Irimura, T.; Shimada, I. Carbohydrate Binding Mechanism of the Macrophage Galactose–Type C–Type Lectin 1 Revealed by Saturation Transfer Experiments. *J. Bio. Chem.*, **2008**, *283*, 33665–33673.

[16] Oo–Puthinan, S.; Maenuma, K.; Sakakura, M.; Denda–Nagai, K.; Tsuiji, M.; Shimada, I.; Nakamura–Tsuruta, S.; Hirabayashi, J.; Bovin, N. V.; Irimura, T. The Amino Acids Involved in the Distinct Carbohydrate Specificities Between Macrophage Galactose–Type C–Type Lectins 1 and 2 (CD301a and b) of Mice. *Biochim. Biophys. Acta*, **2008**, *1780*, 89–100.

[17] Tsuiji, M., Fujimori, M.; Ohashi, Y.; Higashi, N.; Onami, T. M.; Hedrick, S. M.; Irimura, T. Molecular Cloning and Characterization of a Novel MouseMacrophage C–type Lectin, mMGL2, Which Has a Distinct Carbohydrate Specificity from mMGL1. *J. Bio. Chem.*, **2002**, *277*, 28892–28901.

[18] Kogelberg, H.; Feizi, T. Catalysis and Regulation Proteins Web alert. New Structural Insights Into Lectin–Type Proteins of the Immune System *Curr. Opin. Struct. Biol.*, **2001**, *11*, 635–643.

[19] Singh, S. K.; Streng–Ouwehand, I.; Litjens, M.; Kalay, H.; Saeland, E.; van Kooyk, Y. Tumour–Associated Glycan Modifications of Antigen Enhance MGL2 Dependent Uptake and MHC Class I Restricted CD8 T Cell Responses. *Int. J. Cancer*, **2011**, *128*, 1371–1383.

[20] Napoletano, C.; Rughetti, A.; Tarp, M. P. A.; Coleman, J.; Bennett, E. P.; Picco, G.; Sale, P.; Denda–Nagai K.; Irimura, T.; Mandel, U.; Clausen, H.; Frati, L.; Taylor–Papadimitriou, J.; Burchell, J.; Nuti, M. Tumor–Associated T_N–MUC1 Glycoform Is Internalized through the Macrophage Galactose–Type C–Type Lectin and Delivered to the HLA Class I and II Compartments in Dendritic Cells. *Cancer Res.* **2007**, *67*, 8358–8367.

[21] Ichii, S.; Imai, Y.; Irimura, T. Initial Steps in Lymph Node Metastasis Formation In An Experimental System: Possible Involvement of Recognition by Macrophage C–Type Lectins. *Cancer Immunol. Immunother.*, **2000**, *49*, 1–9.

[22] Da–Nagai, K.; Aida, S.; Saba, K.; Suzuki, K.; Moriyama, S.; Oo-Puthinan, S.; Tsuiji, M.; Morikawa, A.; Kumamoto, Y.; Sugiura ,D.; Distribution and Function of Macrophage

Galactose–Type C–Type Lectin 2 (MGL2/CD301b): Efficient Uptake and Presentation of Glycosylated Antigens by Dendritic Cells. *J. Biol. Chem.*, **2010**, *285*, 19193–19204.

[23] Vlad, A. M.; Muller, S.; Cudic, M.; Paulsen, H.; Otvos, L., Jr.; Hanisch, F. G.; Finn, O. J. Complex Carbohydrates are not Removed During Processing of Glycoproteins by Dendritic Cells: Processing of Tumor Antigen MUC1 Glycopeptides for Presentation to Major Histocompatibility Complex Class II–Restricted T Cells. *J. Exp. Med.*, **2002**, *196*, 1435–1446.

[24] Hanisch, F. G.; Schwientek, T.; Von Bergwelt–Baildon, M. S.; Schultze, J. L.; Finn, O. O–Linked Glycans Control Glycoprotein Processing By Antigen–Presenting Cells: A Biochemical Approach to the Molecular Aspects of MUC1 Processing by Dendritic Cells. *Eur. J. Immunol.*, **2003**, *33*, 3242–3254.

[25] Saeland, E.; van Vliet, S. J.; Bäckström, M.; van den Berg, V. C. M.; Geijtenbeek, T. B. H.; Meijer, G. A.; van Kooyk, Y. The C-Type Lectin MGL Expressed By Dendritic Cells Detects Glycan Changes on MUC1 in Colon Carcinoma. *Cancer Immunol. Immunother.* **2007**, *56*, 1225–1236.

[26] Takada, A.; Fujioka, K.; Tsuiji, M.; Morikawa, A.; Higashi, N.; Ebihara, H.; Kobasa, D.; Feldmann, H.; Irimura, T.; Kawaoka, Y. Human Macrophage C–Type Lectin Specific for Galactose and N–Acetylgalactosamine Promotes Filovirus Entry. *J. Virol.*, **2004**, *78*, 2943–2947.

[27] van Liempt, E.; van Vliet, S. J.; Engering, A.; Vallejo, J. J. G.; Bank, C. M. C.; Sanchez–Hernandez, M.; van Kooyk, Y.; van Die, I. Schistosoma Mansoni Soluble Egg Antigens Are Internalized By Human Dendritic Cells Through Multiple C–Type Lectins and Suppress TLR–Induced Dendritic Cell Activation. *Mol. Immunol.* **2007**, *44*, 2605–2615.

[28] Klaver, E. J.; Kuijk, L. M.; Laan L. C.; Kringel, H.; van Vliet, S. J.; Bouma, G.; Cummings, R. D.; Kraal, G.; van Die, I. Trichuris Suis–Induced Modulation of Human Dendritic Cell Function Is Glycan–Mediated. *Int. J. Parasitol.*, **2013**, *43*, 191–200.

[29] van Vliet, S. J.; van Liempt, E.; Saeland, E.; Aarnoudse, C. A.; Appelmelk, B.; Irimura, T.; Geijtenbeek, T. B. H.; Blixt, O.; Alvarez, R.; van Die, I.; van Kooyk, Y. Carbohydrate Profiling Reveals a Distinctive Role For the C-type Lectin MGL in the Recognition of Helminth Parasites and Tumor Antigens by Dendritic Cells. *Int. Immunol.* ***2005***, *17*, *661–669*,.

[30] Singh, S. K.; Streng-Ouwehand, I.; Litjens, M.; Weelij, D. R.; García-Vallejo, J. J.; van Vliet, S. J.; Saeland, E.; van Kooyk, Y. Characterization of Murine MGL1 and MGL2 C-Type Lectins: Distinct Glycan Specificities and Tumor Binding Properties. *Mol. Immunol.* **2009**, *46*, 1240–1249.

[31] van Sorge, N. M.; Bleumink, N. M. C.; van Vliet, S. J.; Saeland, E.; van der Pol, W. L.; van Kooyk, Y.; van Putten, J. P. M. *N*–Glycosylated Proteins And Distinct Lipooligosaccharide

Glycoforms of Campylobacter Jejuni Target the Human C–Type Lectin Receptor MGL. *Cell. Microbiol.* **2009**, *11*, 1768–1781.

[32] Niederhafner, P.; Reinis, M.; Sebestik, J.; Ježek, J. Glycopeptide Dendrimers, Part III–A Review: Use of Glycopeptide Dendrimers in Immunotherapy and Diagnosis of Cancer and Viral Diseases. *J. Pept. Sci.*, **2008**, *14*, 556–587.

[33] Amon, R.; Reuven, E. M.; Ben–Arye, S. L.; Padler–Karavani, V. Glycans In Immune Recognition And Response. *Carbohydr. Res.*, **2014**, *389*, 115–122.

[34] Danishefsky, S. J.; Allen, J. R. From the Laboratory to the Clinic: a Retrospective on Fully Synthetic Carbohydrate–Based Anticancer Vaccines [A Review]. *Angew. Chem. Int. Ed. Engl.*, **2000**, *39*, 836–863.

[35] Galonic, D. P.; Gin, D. Y. Chemical Glycosylation in the Synthesis of Glycoconjugate Antitumour Vaccines [A Review]. *Nature*, **2007**, *446*, 1000–1007.

[36] Wilson, R. M.; Danishefsky, S. J. A Vision for Vaccines Built from Fully Synthetic Tumor-Associated Antigens: From the Laboratory to the Clinic. *J. Am. Chem. Soc.*, **2013**, *135*, 14462–14472.

[37] Galan, M. C.; Dumyb, P.; Renaudet, O. Multivalent glyco(cyclo)peptides. *Chem. Soc. Rev.*, **2013**, *42*, 4599–4612.

[38] Ben–Yedidia, T.; , R. Design of Peptide and Polypeptide Vaccines. *Curr. Opin. Biotechnol.*, **1997**, *61*, 442–448.

[39] Rose, K.; Zeng, W.; Brown, L. E.; Jackson, D. C. A synthetic Peptide Based Polyoxime Vaccine Construct of High Purity and Activity. *Mol. Immunol.*, **1995**, *32*, 1031–l037.

[40] Gorse, G. J.; Keefer, M. C.; Belshe, R. B.; Matthews, T. J.; Forrest, B. D.; Hsieh, R. H.; Koff W. C.; Hanson C. V.; Dolin R.; Weinhold K. J. *et al*. A Dose–Ranging Study of a Prototype Synthetic HIV–l MN V3 Branched Peptide Vaccine. The National Institute of Allergy and Infectious Diseases AIDS Vaccine Evaluation Group. *J. infect Dis.*, **1996**, *173*, 330–339.

[41] Buhleier, E.; Wehner, E.; and Vögtle, F. Cascade–Chain Like and Nonskid–Chain–Like Syntheses of Molecular Cavity Topologies. *Synthesis*, **1978**, *2*, 155–58.

[42] Mintzer, M. A.; Grinstaff, M. W. Biomedical Applications of Dendrimers: a Tutorial. *Chem. Soc. Rev.*, **2011**, *40*, 173–190.

[43] Sadler, K.; Tam, J. P. Peptide Dendrimers: Applications and Synthesis. *Rev. Molecular Biotechnol.*, **2002**, *90*, 195–229.

[44] Heegaard, P. M. H.; Boas, U.; Sorensen N. S. Dendrimers for Vaccine and Immunostimulatory Uses. A Review. *Bioconjugate Chem.*, **2010**, *21*, 405–418.

[45] Tam, J. P. Synthetic Peptide Vaccine Design Synthesis and Properties of a High–Density Multiple Antigenic Peptide System. *Proc. Natl. Acad. Sci. U.S.A.*, **1988**, *85*, 5409–5413.

[46] Wang, R.; Charoenvit, Y.; Corradin, G.; Porrozzi, R.; Hunter, R. L.; Glenn, G.; Alving, C. R.; C, h. P.; Hoffman, S. L. Induction of Protective Polyclonal Antibodies by Immunization with a Plasmodium *Yoelii circumsporozoite* Protein Multiple Antigen Peptide Vaccine. *J. lmmunol.*, **1995**, *164*, 2764–2793.

[47] Wang, P.; Danishefsky, S. J. Promising General Solution to the Problem of Ligating Peptides and Glycopeptides. *J. Am. Chem. Soc.*, **2010**, *132*, 17045–17051.

[48] Gamblin, D. P.; Scanlan, E. M.; Davis, B. G. Glycoprotein Synthesis: An Update. *Chem. Rev.*, **2009**, *109*, 131–163.

[49] Danishefsky, S. J.; Allen, J. R. Development of Carbohydrate–Based Anticancer Vaccines. *Angew. Chem. Int. Ed.*, **2000**, *39*, 836–863.

[50] Francis, M. J. Vaccines: Recent Trends and Progress (Eds.: G. Gregoriadis, A. C. Allison, G. Poste) Plenum Press , New York, **1991**.

[51] Stroud, M. R.; Levery, S. B.; Maartensson, S.; Salyan, M. E. K.; Clausen, H.; Hakomori, S. Human Tumor-Associated Lea–Lex Hybrid Carbohydrate Antigen IV3(Gal.beta.1.fwdarw.3[Fuc.alpha.1.fwdarw.4]GlcNAc)III3FucnLc4 Defined by Monoclonal Antibody 43–9F: Enzymic Synthesis, Structural Characterization, and Comparative Reactivity with Various Antibodies. *Biochemistry*, **1994**, *33*, 10672–10680.

[52] Danishefsky, S. J.; Behar, V.; Randolph, J. T.; Lloyd, K. O. Application of the Glycal Assembly Method to the Concise Synthesis of Neoglycoconjugates of Ley and Leb Blood Group Determinants and of H–Type I and H–Type II Oligosaccharides. *J. Am. Chem. Soc.*, **1995**, *117*, 5701–5711.

[53] Kudryashov, V.; Kim, H. M.; Ragupathi, G.; Danishefsky, S. J.; Livingston, P. O.; Lloyd K. O. Immunogenicity of Synthetic Conjugates of Lewis(y) Oligosaccharide with Proteins in Mice: Towards the Design of Anticancer Vaccines. *Cancer Immunol. Immunother.*, **1998**, *45*, 281–286.

[54] Kolb, H. C.; Finn, M. G.; Sharpless, B. K. Click Chemistry: Diverse Chemical Function from a Few Good Reactions. *Angew. Chem. Int. Ed.* **2001**, *40*, 2004–2021.

[55] Hein, C.; Liu, X.; Wang, D. Click Chemistry, a Powerful Tool for Pharmaceutical Sciences. *Pharm. Res.*, **2008**, *25*, 2216–2230.

[56] Tornoe, W. C.; Christensen, C.; Medal, M. Peptidotriazoles on Solid Phase: [1,2,3]–Triazoles by Regiospecific Copper(I)–Catalyzed 1,3–Dipolar Cycloadditions of Terminal Alkynes to Azides. *J. Org. Chem.* **2002**, *67*, 3057–3064.

[57] Rostovtsev, V. V.; Green, G. L.; Fokin, V. V.; Sharpless, B. K. A Stepwise Huisgen Cycloaddition Process: Copper(I)-Catalyzed Regioselective "Ligation" of Azides and Terminal Alkynes. *Angew. Chem. Int. Ed.* **2002**, *41*, 2596–2599.

[58] Finn, M. G.; Fokin, V V. Contents. *Chem. Soc. Rev.* **2010**, *39*, 1223–1232.

[59] Tornoe, W. C.; Christensen, C.; Medal, M. Copper(I)-Catalyzed Cycloaddition Of Organic Azides And 1-iodoalkynes. *J. Org. Chem.* **2008**, *108*, 2952–3015.

[60] Wu, P.; Fokin, V. V. Catalytic Azide–Alkyne Cycloaddition: Reactivity and Applications. *Aldrichimica Acta.* **2007**, *40*, 7–17.

[61] Kolb, C. H.; Sharpless, B. K. The Growing Impact Of Click Chemistry On Drug Discovery. *Drug Discov. Today.* **2003**, *8*, 1128–1137.

[62] Hua, Y.; Flood, A. H. Click Chemistry Generates Privileged CH Hydrogen–Bonding Triazoles: The Latest Addition To Anion Supramolecular Chemistry. *Chem. Soc. Rev.* **2010**, *39*, 1262–1271.

[63] Himo, F.; Lovell, T.; Hilgraf, R.; Rostovtsev, V. V.; Noodleman, L.; Sharpless, K. B.; Fokin V. V.; Copper(I)–Catalyzed Synthesis of Azoles, DFT Study Predicts Unprecedented Reactivity and Intermediates. *J. Am. Chem. Soc.* **2005**, *127*, 210–216.

[64] Bock, V. D.; Hiemstra, H.; van Maarseveen, J. H. Cu(I)-Catalyzed Alkyne–Azide "Click" Cycloadditions From A Mechanistic And Synthetic Perspective *Eur. J. Org. Chem.* **2006**, *1*, 51–68.

[65] Sreedhar B.; Reddy, P. S. Sonochemical Synthesis of 1,4–Disubstituted 1,2,3–Triazoles in Aqueous Medium. *Synth. Commun.* **2007**, *37*, 805–812.

[66] Sreedhar B.; Reddy, P. S. Erratum Sonochemical Synthesis of 1,4–Disubstituted 1,2,3–Triazoles in Aqueous Medium. *Synth. Commun.* **2007**, *37*, 3259–3260.

[67] Baut, N. L.; Díaz, D. D. ; Punna, S.; Finn, M. G.; Brown, H. R. Study of High Glass Transition Temperature Thermosets Made From The Copper(I)–Catalyzed Azide–Alkyne Cycloaddition Reaction. *Polymer*. **2007**, *48*, 239–244.

[68] Hassane, F. S.; Frisch, B.; Schuber F. Targeted Liposomes: Convenient Coupling of Ligands to Preformed Vesicles Using "Click Chemistry". *Bioconjugate Chem.* **2006**, *17*, 849–854.

[69] Lee, B. Y.; Park, S. R.; Jeon, H. B.; Kim, K. S. A New Solvent System For Efficient Synthesis of 1,2,3–Triazoles. *Tetrahedron Lett.* **2006**, *47*, 5105–5109.

[70] Wang, Q.; Chan, T. R.; Hilgraf, R.; Fokin, V. V.; Sharpless, K. B.; Finn, M. G. Bioconjugation by Copper(I)–Catalyzed Azide–Alkyne [3 + 2] Cycloaddition. *J. Am. Chem. Soc.* **2003**, *125*, 3192–3193.

[71] Lewis, W. G.; Magallon, F. G.; Fokin, V. V.; Finn, M. G. Discovery and Characterization of Catalysts for Azide–Alkyne Cycloaddition by Fluorescence Quenching. *J. Am. Chem. Soc.* **2004**, *126*, 9152–9153.

[72] Blanco, J. L. J.; Melleta, C. O.; Fernández J. M. G. Multivalency in heterogeneous glycoenvironments: hetero–glycoclusters, glycopolymers and glycoassemblies. *Chem. Soc. Rev.*, **2013**, *42*, 4518–4531.

[73] Lee, Y. C.; Lee, R. T. Carbohydrate-Protein Interactions: Basis of Glycobiology. *Acc. Chem. Res.*, **1995**, *28*, 321–327.

[74] Lundquist J. J.;Toone E. J.; The Cluster Glycoside Effect. *Chem. Rev.*, **2002**, *102*, 555–578.

[75] Ortega–Munoz, M.; Pérez–Balderas, F.; Morales–Sanfrutos, J.; Hernández-Mateo, F.; Isac–García J.; Santoyo–González, F. Click Multivalent Heterogeneous Neoglycoconjugates âĂŞ Modular Synthesis and Evaluation of Their Binding Affinities. *Eur. J. Org. Chem.*, **2009**, *15* 2454–2473.

[76] Cendret, V.; Francois–Heude, M.; Méndez-Ardoy, A.; Moreau, V.; Fernández, J. M. G.; Djedaïni–Pilard, F. Design and Synthesis of a "Click" High–Mannose Oligosaccharide Mimic Emulating Man8 Binding Affinity Towards Con A. *Chem. Commun.*, **2012**, *48*, 3733–3735.

[77] Lee, D. J.; Yang, S. H.; Williams, G. M.; Brimble, M. A. Synthesis of Multivalent Neoglyconjugates of MUC1 by the Conjugation of Carbohydrate–Centered, Triazole–Linked Glycoclusters to MUC1 Peptides Using Click Chemistry. *J. Org. Chem.*, **2012**, *77*, 7564–7571.

[78] Kuduk, S. D.; Schwarz, J. B.; Chen, X.–T.; Glunz, P. W.; Sames, D.; Ragupathi, G.; Livingston, P. O.; Danishefsky S. J. Synthetic and Immunological Studies on Clustered Modes of Mucin–Related T_N and TF O–Linked Antigens: The Preparation of a Glycopeptide–Based Vaccine for Clinical Trials against Prostate Cancer. *J. Am. Chem. Soc.*, **1998**, *120*, 12474–12485.

[79] Chen, X. T.; Sames, D.; Danishefsky S. J. Exploration of Modalities in Building α–*O*–Linked Systems through Glycal Assembly: A Total Synthesis of the Mucin–Related F1α Antigen. *J. Am. Chem. Soc.*, **1998**, *120*, 7760–7769.

[80] Qin, Q.; Yin, Z.; Bentley, P.; Huang, X. Carbohydrate Antigen Delivery by Water Soluble Copolymers as Potential Anti–Cancer Vaccines. *Med. Chem. Commun*, **2014**, *5*, 1126–1129.

[81] Richichi, B.; Thomas, B.; Fiore, M.; Bosco, R.; Qureshi, H.; Nativi, C.; Renaudet, O.; BenMohamed L. A Cancer Therapeutic Vaccine Based On Clustered T_N–Antigen Mimetics Induces Strong Antibody–Mediated Protective Immunity. *Angew. Chem. Int. Ed.*, **2014**, *53*, 11917–11920.

[82] Tomalia, D. A.; Naylor, A. M.; Goddard, W. A. Starburst Dendrimers: Molecular–Level Control of Size, Shape, Surface Chemistry, Topology, and Flexibility from Atoms to Macroscopic Matter. *Angew. Chem. Int. Ed.* **1990**, *29*, 138–175.

[83] Ježek, J.; Velek, J.; Vepřek, P.; Velková, V.; Trnka, T.; Pecka, J.; Ledvina, M.; Vondrášek, J.; PÃśsacka, M. Solid Phase Synthesis Of Glycopeptide Dendrimers With T_N Antigenic Structure And Their Biological Activities. Part I. *J. Pept. Sci.*, **1999**, *5*, 46–55.

[84] Trauger, J. W.; Kohli, R. M.; Walsh, C. T. Cyclization of Backbone–Substituted Peptides Catalyzed by the Thioesterase Domain from the Tyrocidine Nonribosomal Peptide Synthetase. *Biochemistry*. **2001**, *40*, 7092–7098.

[85] Peptides international. mini–peg^{TM}. http://pepnet.com/ShoppingUsers/PdfDocument.aspx?-FileName=miniPEG.pdf, accessed December **2013**.

[86] Bay, S.; Lo–Man, R.; Osinaga, E.; Nakada, H.; Leclerc, C.; Cantacuzene, D. Preparation Of A Multiple Antigen Glycopeptide (MAG). *J. Peptide Res.*, **1997**, *49*, 620–625.

[87] Lo–Man, R.; Bay, S.; Vichier-Guerre, S.; Dériaud, E.; Cantacuzene, D.; Leclerc, C. A Fully Synthetic Immunogen Carrying A Carcinomaassociated Carbohydrate For Active Specific Immunotherapy. *Cancer Res.*, **1999**, *59*, 1520–1524.

[88] Paulsen, H.; Holck, J. P.; Synthese der Glycopeptide *O*–*β*–**D**–Galactopyranosyl–(1–3)–*O*–(2–Acetamido–2–Desoxy–*α*–**D**–Galactopyranosyl–(1–3)–**L**–Serin und –**L**–Threonin. *Carbohydr. Res.*, **1982**, *109*, 89–107.

[89] Paulsen, H.; Schultz, M.; Klamann, J.–D.; Waller, B.; Paal, M. Synthese Von *O*–Glycopeptid–Blocken des Glycophorins. *Liebigs Ann. Chem.*, **1985**, *10*, 2028–2048.

[90] Paulsen, H.; Adermann, K. Synthese von *O*–Glycopeptid–Sequenzen des N–Terminus von Interleukin–2. *Liebigs Ann. Chem.*, **1989**, *8*, 751–769.

[91] Lemieux, R. U.; Ratcliffe, R. M. The Azidonitration of tri–*O*–Acetyl–**D**–Galactal. *Can. J. Chem.*, **1979**, *57*, 1244–1251.

[92] Pavia, A. A.; Rocheville, J. M.; Ung, S. N. Nouvelle Méthode De Synthèse Stéréoléctive De Glycosides. Synthèse Des *α*,*α*–TréHalose, Analogues Galacto, Manno Et Autres *α*–**D**–Glycosides. *Carbohydr. Res.*, **1980**, *79*, 79–89.

[93] Lo–Man, R.; Vichier–Guerre, S.; Bay, S.; Dériaud, E.; Cantacuzene, D.; Leclerc, C. Anti–Tumor Immunity Provided By A Synthetic Multiple Antigenic Glycopeptide Displaying A Tri–T_N Glycotope. *J. Immunol.*, **2001**, *166*, 2849–2854.

[94] Lo–Man, R.; Vichier–Guerre, S.; Perraut, R.; Dériaud, E.; Huteau, V.; BenMohamed, L.; Diop, O. M.; Livingston, P. O.; Bay, S.; Leclerc, C. A Fully Synthetic Therapeutic Vaccine Candidate Targeting Carcinomaassociated T_N Carbohydrate Antigen Induces Tumor–Specific Antibodies In Nonhuman Primates. *Cancer Res.*, **2004**, *64*, 4987–4994.

[95] Marin, F. D. R.; Luquet, G.; Marie, B.; Medakovic, D. Molluscan Shell Proteins: Primary Structure, Origin, and Evolution. *Curr. Top. Dev. Biol.*, **2007**, *80*, 209–276.

[96] Baldus, S. E.; Engelmann, K.; Hanisch, F. G. MUC1 and the MUCs: a Family of Human Mucins with Impact in Cancer Biology. *Crit. Rev. Clin. Lab. Sci.*, **2004**, *41*, 189–231.

[97] Satoh, S.; Hinoda, Y.; Hayashi, T.; Burdick, M. D.; Imai, K.; Hollingsworth, M. A. Enhancement of Metastatic Properties of Pancreatic Cancer Cells by MUC1 Gene Encoding an Anti–Adhesion Molecule. *Int. J. Cancer*, **2000**, *88*, 507–518.

[98] Gendler, S. J. MUC1, the Renaissance Molecule. *J. Mammary Gland Biol. Neoplasia.*, **2001**, *6*, 339–353.

[99] Hanisch, F. G.; Muller, S. MUC1: the Polymorphic Appearance of a Human Mucin. *Glycobiology*, **2000**, *10*, 439–449.

[100] Taylor-Papadimitriou, J.; Burchell, J.; Miles, D. W.; Dalziel, M. MUC1 and Cancer. *Biochim. Biophys. Acta*, **1999**, *1455*, 301–313.

[101] Keil, S.; Claus, C.; Dippold, W.; Kunz, H. Towards the Development of Antitumor Vaccines: A Synthetic Conjugate of a Tumor-Associated MUC1 Glycopeptide Antigen and a Tetanus Toxin Epitope. *Angew. Chem. Int. Ed.*, **2001**, *40*, 366–369.

[102] Reddish, M. A.; MacLean, G. D.; Koganty, R. R.; Kan-Mitchell, J.; Jones, V.; Mitchell, M. S.; Longenecker, B. M. Anti–MUC1 Class I Restricted CTLs in Metastatic Breast Cancer Patients Immunized with a Synthetic MUC1 Peptide. *Int. J. Cancer*, **1998**, *76*, 817–823.

[103] Lee, D. J.; Mandal, K.; Harris, P. W. R.; Brimble, M. A.; Kent, S. B. H. A One–Pot Approach to Neoglycopeptides using Orthogonal Native Chemical Ligation and Click Chemistry. *Org. Lett.* **2009**, *11*, 5270–5273.

[104] Lee, D. J.; Harris, P. W. R.; Brimble M. A. Synthesis of MUC1 Neoglycopeptides Using Efficient Microwave–Enhanced Chaotrope–Assisted Click Chemistry. *Org. Biomol. Chem.*, **2011**, *9*, 1621–1626.

[105] Kershaw, M. H.; Westwood, J. A.; Darcy, P. K. Gene–Engineered T Cells For Cancer Therapy. *Nat. rev. cancer.* **2013**, *13*, 525–541.

[106] Napoletano, C.; Zizzari, I. G.; Rughetti, A.; Rahimi, H.; Irimura, T.; Clausen, H.; Wandall, H. H.; Belleudi, F.; Bellati, F.; Pierelli, L.; Frati, L.; Nuti, M. Targeting of Macrophage Galactose–Type C-Type Lectin (MGL) Induces DC Signaling and Activation. *Eur. J. Immunol.* **2012**, *42*, 936–945.

[107] Lee, R. T.; Gabius, H. J.; Lee, Y. C. The Sugar–Combining Area of the Galactose–Specific Toxic Lectin of Mistletoe Extends Beyond the Terminal Sugar Residue: Compaison with a Homologous Toxic Lectin, Ricin. *Carbohydr. Res.* **1994**, *254*, 269–276.

[108] Turnbull, W. B.; Stoddart, J. F. Design and Synthesis of Glycodendrimers. *Rev. Mol. Biotechnol.* **2002**, *90*, 231–255.

[109] Buhleier, E.; Wehner, W.; Vögtle, F. "Cascade-" and "Nonskid–Chain–Like" Syntheses of Molecular Cavity Topologies. *Synthesis*. **1978**, *2*, 155–158.

[110] Miller, N.; Williams, G. M.; Brimble, M. A. Synthesis of Fish Antifreeze Neoglycopeptides Using Microwave–Assisted "Click Chemistry". *Org. Lett.* **2009**, *11*, 2409–2412.

[111] Koskinen, A. M. P.; Valo, T.; Vihavainen, S.; Hakala, J. M. L. Synthesis of α–Helix Substituted Analogs of Calcitonin Gene–Related Peptide. *Bioorg. Med. Chem. Lett.*, **1995**, *5*, 573–578.

[112] Kaminskas, L. M.; Kota, J.; McLeod, V. M.; Kelly, B. D.; Karellas, P.; Porter, C. J. H. PEGylation of Polylysine Dendrimers Improves Absorption and Lymphatic Targeting Following SC Administration in Rats. *J. Control Release*. **2009**, *140*, 108–116.

[113] Zhou, Z.–Y.; Shi, G.–Q.; Fontaine, R.; Wei, K.; Feng, T.; Wang, F.; Wang, G.–Q.; Qu, Y.; Li, Z.–H.; Dong, Z.–J.; Zhu, H.–J.; Yang, Z.–L.; Zeng, G.; Liu, J.–K. Evidence for the Natural Toxins from the Mushroom *Trogia venenata* as a Cause of Sudden Unexpected Death in Yunnan Province, China. *Angew. Chem. Int. Ed.*, **2012**, *51*, 2368–2370.

[114] Yan, R. -B.; Yang, F.; Wu, Y.; Zhang, L.-H.; Ye, X.-S. An Efficient and Improved Procedure for Preparation of Triflyl Azide and Application in Catalytic Diazotransfer Reaction. *Tetrahedron Lett.* **2005**, *46*, 8993–8995.

[115] R. Müller. Organic chemistry portal: Synthesis of azides. `http://www.organic-chemistry.org/synthesis/diazonium/azides.shtm`, accessed March **2014**.

[116] D. Lowe. In the pipeline. `http://pipeline.corante.com/archives/2012/02/16/imidazole1sulfonyl_azide_hcl_look_out.php`, accessed February 16, **2012**.

[117] Fischer, N.; Goddard-Borger, E. D.; Greiner, R.; Klapotke, T. M.; Skelton, B. W.; Stierstorfer, J. Sensitivities of Some Imidazole-1-sulfonyl Azide Salts. *J. Org. Chem.* **2012**, *77*, 1760–1764.

[118] Goddard-Borger, E. D.; Stick, R. V. An Efficient, Inexpensive, and Shelf-Stable Diazotransfer Reagent: Imidazole–1–sulfonyl Azide Hydrochloride. *Org. Lett.* **2007**, *9*, 3797–3800.

[119] Oh, K. I.; Lee, J. H.; Joo, C.; Han, H.; Cho, M. β-Azidoalanine as an IR Probe: Application to Amyloid $\alpha\beta$(16-22) Aggregation. *J. Phys. Chem. B.* **2008**, *112*, 10352–10357.

[120] Nagel, L.; Budke, C.; Erdmann, R. S.; Dreyer, A.; Wennemers, H.; Koop, T.; Sewald, N. Influence of Sequential Modifications and Carbohydrate Variations in Synthetic AFGP Analogues on Conformation and Antifreeze Activity. *Chem. Eur. J.* **2012**, *18*, 12783–12793.

[121] Ballardie, F. W.; Capon, B.; Dearie, W. M.; Foster R. L. Neighbouring Acetamido–group Participation In Reactions Of Derivatives Of 2–acetamido–2–Deoxy–D–glucose. *Carbohydr. Res.* **1976**, *49*, 79–92.

[122] Juaristi, E.; Cuevas G. Recent Studies Of The Anomeric Effect. *Tetrahedron*. **1992**, *48*, 5019–5087.

[123] Perrin, C. L. Reverse Anomeric Effect: Fact Or Fiction? *Tetrahedron*. **1995**, *51*, 11901–11935.

[124] Wojnar, J. M.; Evans, C. W.; DeVries, A. L.; Brimble, M. A. Synthesis of an Isotopically-labelled Antarctic Fish Antifreeze Glycoprotein Probe. *Aust. J. Chem.* **2011**, *64*, 723–731.

[125] Merrifield, R. B. Synthesis and Oxidation of 2-Amino-2,3-dihydro-1H-benz[de]isoquinoline and 1,2,3,4-Tetrahydronaphtho[1,8-de][1,2]diazepine and Related Cyclic 1,2-Dibenzylhydrazines. *J. Am. Chem. Soc.* **1963**, *85*, 2149–2154.

[126] Mitchell, A. R.; Kent, S. B. H.; Engelhard M.; Merrifield, R. B.; A New Synthetic Route to Tert-Butyloxycarbonylaminoacyl-4-(Oxymethyl)phenylacetamidomethyl-Resin, an Improved Support for Solid-Phase Peptide Synthesis. *J. Org. Chem.* **1978**, *43*, 2845–2852.

[127] Kent, S. B. H. Total Chemical Synthesis of Proteins. *Chem. Soc. Rev.* **2009**, *38*, 338–351.

[128] Kaiser, E.; Colescott, R. L.; Bossinger, C. D.; Cook, P. I. Removal of Proteins From Isoelectric Focusing Media. *Anal. Biochem.* **1970**, *34*, 595–598.

[129] Isidro-Llobet, A.; Álvarez, M.; Albericio, F. Amino Acid–Protecting Groups. *Chem. Rev.* **2009**, *109*, 2455–2504.

[130] Nash, I. A.; Bycroft, B. W.; Chan, W. C. Dde – A Selective Primary Amine Protecting Group: A Facile Solid Phase Synthetic Approach to Polyamine Conjugates. *Tetrahedron Lett.* **1996**, *37*, 2625–2628.

[131] Albericio, F. Orthogonal Protecting Groups for N^{α}–Amino and C–Terminal Carboxyl Functions in Solid–Phase Peptide Synthesis. *Peptide Science.* **2000**, *55*, 123–139.

[132] Suzuki, N.;, Yamamoto, K.; Toyoshima, S.; Osawa, T.; Irimura, T. Molecular Cloning and Expression of cDNA Encoding Human Macrophage C–Type Lectin. *J. Immunol*, **1996**, *156*, 128–135.

[133] Valladeau, J.; Duvert-Frances, V.; Pin, J.–J.; Kleijmeer, M. J.; Ait-Yahia, S.; Ravel, O.; Vincent, C.; Vega Jr., F.; Helms, A.; Gorman, D.; Zurawski, S. M.; Zurawski, G.; Ford, J.; Saeland, S. Immature Human Dendritic Cells Express Asialoglycoprotein Receptor Isoforms for Efficient Receptor-Mediated Endocytosis. *J. Immunol*, **2001**, *167*, 5767–5774.

[134] Coombs, P. J.; Harrison, R.; Pemberton, S.; Quintero-Martinez, A.; Parry, S.; Haslam, S. M.; Dell, A.; Taylor M. E.; Drickamer, K. Identification of Novel Contributions to High–Affinity Glycoprotein–Receptor Interactions using Engineered Ligands. *J. Mol. Biol.*, **2010**, *396*, 685–696.

[135] UniProtKB/Swiss-Prot. Protein knowledgebase (uniprotkb). `http://www.uniprot.org/uniprot/Q8IUN9`, accessed May 05, **2014**.

[136] van Vliet, S. J.; Paessens, L. C.; Broks-van den Berg, V. C. M.; Geijtenbeek, T. B. H.; van Kooyk, Y. The C-Type Lectin Macrophage Galactose–Type Lectin Impedes Migration of Immature APCs. *J. Imunnol*, **2008**, *181*, 3148–3155.

[137] Napoletano, C.; Zizzari, I. G.; Rughetti, A.; Rahimi, H.; Irimura, T.; Clausen, H.; Wandall, H. H.; Belleudi, F.; Bellati, F.; Pierelli, L.; Frati, L.; Nuti, M. Targeting of Macrophage Galactose–Type C–Type Lectin (MGL) Induces DC Signaling and Activation. *Eur. J. Immunol.* **2012**, *42*, 936–945.

[138] Meevissen, M. H. J.; Driessen, N. N.; Smits, H. H.; Versteegh R.; van Vliet, S. J.; van Kooyk, Y.; Schramm G.; Deelder, A. M.; Haas, H.; Yazdanbakhsh, M.; Hokke, C. H. Specific Glycan Elements Determine Differential Binding of Individual Egg Glycoproteins of the Human Parasite Schistosoma Mansoni by Host C–Type Lectin Receptors. *Int. J. Parasitol.* **2012**, *42*, 269–277.

[139] Freire, T.; Zhang, X.; Dériaud, E.; Ganneau, C.; Vichier–Guerre, S.; Azria, E.; Launay, O.; Lo–Man, R.; Bay, S.; Leclerc, C. Glycosidic T_N–Based Vaccines Targeting Dermal Dendritic Cells Favor Germinal Center B–Cell Development and Potent Antibody Response in the Absence of Adjuvant. *Blood.* **2010**, *116*, 3526–3535.

[140] Lee, D. J.; Harris, P. W. R.; Kowalczyk R.; Dunbar R.; Brimble M. A. Microwave–Assisted Synthesis of Fluorescein-Labelled GalNAca1–O–Ser/Thr(T_N) Glycopeptides as Immunological Probes. *Synthesis*, **2010**, *5*, 763–769.

[141] Floyd, N.; Vijayakrishnan, B.; Koeppe, J. R.; Davis, B. G. Thiyl–Glycosylation of Olefinic Proteins: *S*–linked Glycoconjugate Synthesis. *Angew. Chem. Intl. Ed.*, **2009**, *48*, 7798–7802.

[142] Dominique, R.; Liu, B.; Das, S. K.; Roy, R. Synthesis of 'Molecular Asterisks' via Sequential Cross–Metathesis, Sonogashira and Cyclotrimerization Reactions *Synthesis*, **2000**, *6*, 862–868.

[143] The World Health Organisation. *Global Prevalence and Incidence of Selected Curable Sexually Transmitted Infections: Overview and Estimates*. Geneva **2001**.

[144] van Vliet, S. J.; Steeghs, L.; Bruijns, S. C. M.; Vaezirad, M. M.; Blok, C. S.; Busto, J. A. A.; Deken, M.; van Putten, J. P. M.; van Kooyk, Y. Variation of Neisseria Gonorrhoeae Lipooligosaccharide Directs Dendritic Cell–Induced T Helper Responses. *PLoS. Pathogens.* **2009**, *5*, 1–13.

[145] Yuita, H.; Tsuiji, M.; Tajika, Y.; Matsumoto, Y.; Hirano, K.; Suzuki, N.; Irimura, T. Retardation of removal of radiation–induced apoptotic cells in developing neural tubes in macrophage galactose–type C–type lectin–1–deficient mouse embryos. *Glycobiology*, **2005**, *15*, 1368–1375.

[146] Pretsch, E.; Bühlmann, P.; Badertscher, M. Structure Determination of Organic Compounds: Tables of Spectral Data. *U.S. Government Printing Office*, **2009**, 433.

[147] Vasella, A.; Witzig, C.; Chiara, J.–L.; Martin–Lomas, M. Convenient Synthesis of 2-Azido-2-deoxy-aldoses by Diazo Transfer. *Helv. Chim. Acta*, **1991**, *74*, 2073–2077.